

# **Chiral Carbon Nanohoops: Topology, Luminescence and Aromaticity**

**Inauguraldissertation**

zur

Erlangung der Würde eines Doktors der Philosophie

vorgelegt der

Philosophisch-Naturwissenschaftlichen Fakultät

der Universität Basel

von

**Juraj Malinčík**

2023

Genehmigt von der Philosophisch-Naturwissenschaftlichen Fakultät  
auf Antrag von

First Supervisor: Prof. Dr. Marcel Mayor

Second Supervisor: Prof. Dr. Oliver Wenger

External Expert: Prof. Dr. Max von Delius

Basel, 13.12.2022

---

Prof. Dr. Marcel Mayor

The Dean of Faculty

*Dedicated to my father*  
*Andrej Malinčik (1950 – 2021)*



## Acknowledgements

The greatest and sincerest thanks go to my supervisor, Prof. Dr. Tomáš Šolomek, for being the mentor I can look up to. Thank you for your brilliant ideas and enthusiasm about science and spending countless hours teaching me how to use a computer to obtain meaningful results. Thank you for encouraging my own scientific ideas and allowing me to pursue them. Last but not least, thank for your understanding during difficult times in my personal life and not being just a mentor to me, but a friend.

No less important thanks belong to Prof. Dr. Marcel Mayor for being my first supervisor. Thank you for allowing me to work within your group and for your willingness to solve any challenge. It was a pleasure to collaborate with such an inspiring scientist.

I would like to thank Prof. Dr. Oliver Wenger for being my second supervisor. I always appreciated your input regarding my research.

I would like to thank Prof. Dr. Max von Delius for being the external expert for my doctoral exam.

I would like to thank all my collaborators as my research would not be possible without them. Namely, I thank Prof. Araceli Campaña and Dr. Juan Mora-Fuentes for measurement of CPL, Dr. Alessandro Prescimone for XRD analysis, Prof. Dr. Daniel Häussinger and Marc-Aurèle Boillat for VT-NMR experiments, Björn Pfund for luminescence lifetime measurements and Michael Devereux for software support.

I want to thank Michael Pfeffer, Daniel Häussinger, Thomas Müntener, Daniel Joss, Pascal Rieder and Raphael Vogel for the wonderful analytical services, Andres Koller, Markus Ast, Hisni Meha and Andreas Sohler for technical support, Oliver Ilg for taking care of the chemicals and consumables, and Nathalie Plattner-Longhi and Brigitte Howald for helping me with the administration.

I would like to thank Kovida, Henrik and Nadine for proofreading parts of this dissertation.

I want to thank the past and present members of Mayor group. It was a pleasure to work within a group so deeply motivated to do science.

I would like to thank my colleagues from Šolomek group for all the fun we have had during group trips and for fruitful scientific discussions during our online meetings.

I want to thank Henrik, Laurent, Hua, Cristian, Luise, Salome and Max for creating a pleasant working atmosphere in Lab 4.

I would like to thank all my friends that have made the last four years so much fun. Only here in Basel I have learned the true meaning of the word friendship.

I would like to thank Pascal for being the best flatmate.

I would like to thank my family for supporting me in my dreams throughout my whole life. Words cannot express how grateful I am.

Lastly, I want to thank the closest to my heart. Thank you, Kovida, for motivating me to go on. I would not have written this dissertation without your constant support.



## Preface

During the course of my studies, I have worked on several projects of my own and collaborations with the groups of Prof. Marcel Mayor and Prof. Christof Sparr. Three projects of my research at the University of Basel are presented in this thesis. They all share a common topic and were selected to make for a meaningful story, while keeping the length of the thesis reasonable.

The thesis is divided into five chapters. In the first chapter, the history and the theoretical background of carbon-based materials is presented starting from graphene, followed by carbon nanotubes and nanoscrolls. Cycloparaphenylenes, also called carbon nanohoops, are discussed in more detail with a focus on their unique size-dependent properties. At the end of the chapter, the current state of research of chiral carbon nanohoops studied in this thesis is discussed. The intention of the author was to present the context and the rationale behind using carbon nanohoops as circularly polarized luminophores, which is the common topic across the projects presented in this dissertation, and to demonstrate the importance of the obtained results in this relatively young field of research.

Individual projects are presented in separate chapters starting with the design of new chiral carbon nanohoops and the goals of each project. The experimental and computational results are reported and discussed, followed by conclusions and an outlook. Furthermore, supporting information is provided for each chapter in the Appendix.

The project presented in Chapter 3 was published in *Angewandte Chemie International Edition* in July 2022<sup>[1]</sup> and is presented as published in this thesis with separate numbering of compounds, figures, schemes, tables and references. The paper is supported by a brief introduction and an outlook at the beginning and the end of the chapter, respectively.

The final chapter summarizes the major results in this thesis and draws a general outlook in the research of chiral carbon nanohoops and Möbius aromaticity.





## Table of Contents

1. Introduction .....	1
1.1. Carbon-based materials – From pencils to “nanoballs” .....	1
1.2. Graphene – The mother of all graphitic forms .....	1
1.3. Carbon nanotubes and nanoscrolls – Rolling a graphene sheet.....	4
1.4. Carbon nanohoops – Cutting up carbon nanotubes .....	8
1.4.1. Synthesis of carbon nanohoops .....	8
1.4.2. Physicochemical properties of carbon nanohoops.....	13
1.4.3. Applications of carbon nanohoops .....	19
1.4.4. Chiral carbon nanohoops.....	22
2. Spiral <i>para</i> -phenylenes.....	25
2.1. Aim of the work .....	25
2.2. Results and Discussion.....	27
2.2.1. Synthesis of <i>p</i> [9]SPP .....	27
2.2.2. Conformational analysis of [ <i>n</i> ]SPPs.....	32
2.2.3. Calculated properties of [ <i>n</i> ]SPPs.....	35
2.3. Conclusions and Outlook .....	44
3. [6,7]Helicene <i>para</i> -phenylene – A prototype chiral luminophore .....	47
3.1. Aim of the work .....	47
3.2. Circularly Polarized Luminescence in a Möbius Helicene Carbon Nanohoop .....	48
3.3. Summary and Outlook.....	55
4. [5, <i>n</i> ]Helicene <i>para</i> -phenylenes .....	59
4.1. Möbius aromaticity and anti-aromaticity .....	59
4.2. Results and Discussion.....	64
4.2.1. Synthesis of [5, <i>n</i> ]HPPs.....	64
4.2.2. Photophysical and chiroptical properties of [5,7]HPP .....	72
4.2.3. Computational investigation of [5, <i>n</i> ]HPPs.....	73
4.3. Conclusions and Outlook .....	85
5. Summary .....	87
References .....	89
Appendix .....	97
Appendix: Table of Contents .....	97



# 1. Introduction

## 1.1. Carbon-based materials – From pencils to “nanoballs”

Carbon-based materials have been in a focus of researchers for the past century mainly due to their unique physical and chemical properties that depend on their individual morphology. Two carbon allotropes, graphite and diamond, have been known to humanity since ancient times, and we may encounter them in our daily lives. While graphite is relatively soft, brittle and bendable, diamond is the hardest naturally-occurring material.

These diametrically opposed properties between allotropes of the same element emerge from the different connections between carbon atoms in their structure. Each carbon atom in the structure of diamond is connected to four other carbons (Figure 1, left), creating an infinite, three-dimensional network of  $sp^3$ -hybridized carbons. On the contrary, graphite consists of stacked crystalline layers of  $sp^2$ -hybridized carbon atoms (Figure 1, right) with van der Waals forces collectively holding the layers together. Consequently, the weak nature of van der Waals forces allows deformations of the structure by slippage or complete removal of individual layers.<sup>[2]</sup>

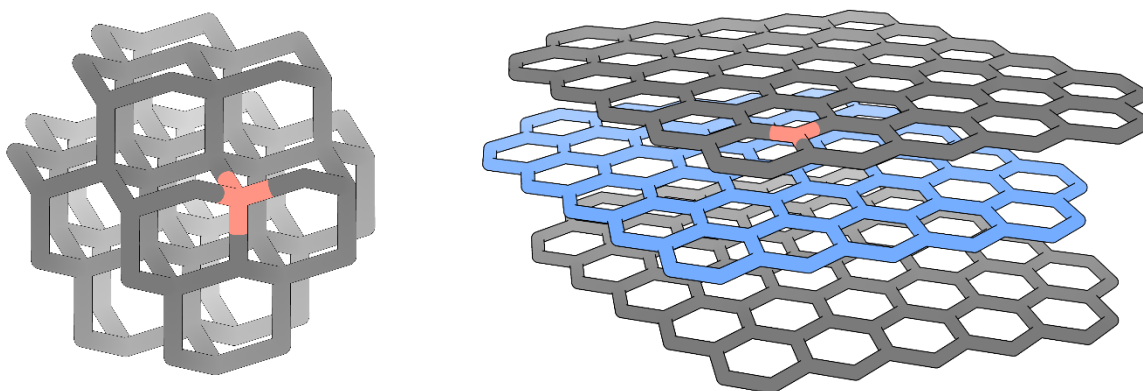


**Figure 1.** Structures of carbon allotropes: diamond (left) and graphite (right). The difference in carbon hybridization is marked in pink while graphene is marked in blue.

A single layer of carbon atoms in graphite is called graphene and it was first isolated by Novoselov and Geim in 2004.<sup>[3]</sup> The discovery of graphene has revolutionized the field of carbon-based materials with thousands of scientific works published on this topic every year<sup>[4-9]</sup> not only because of the unique properties of graphene itself, but also because of the variety of new materials one can derive from its structure.

## 1.2. Graphene – The mother of all graphitic forms

The main challenge of the first graphene synthesis was its isolation from graphite,<sup>[10]</sup> ultimately achieved by mechanical exfoliation using scotch tape.<sup>[3,11]</sup> Although this approach allows isolation of graphene in a simple way, it results in samples that contain defects. The exfoliation process is challenging to scale-up making it unlikely for commercial applications. Other top-down approaches have been developed to tackle this challenge,<sup>[6,9]</sup> including ultrasound-assisted liquid-phase exfoliation,<sup>[12,13]</sup> electrochemical exfoliation,<sup>[14,15]</sup> graphite oxide reduction<sup>[16]</sup> and the arc discharge method.<sup>[17,18]</sup> In addition, several bottom-up approaches have been developed, such as plasma etching of carbon nanotubes,<sup>[19]</sup> chemical vapor deposition (CVD),<sup>[20,21]</sup> laser-assisted synthesis<sup>[22]</sup> and pyrolysis.<sup>[23]</sup>

## 1. Introduction

While reading literature, one must be careful about what the word “graphene” refers to. It can describe a single-layer, a bilayer, a few-layer (3 to 10) or a multi-layer ( $\geq 11$ ) graphene. In this text, the term “graphene” refers to the single-layer material unless further specified. The quality of graphene material strongly impacts its properties.<sup>[6]</sup> If several graphene sheets are stacked, the material properties start to deviate from single-layer graphene and it becomes more similar to graphite as the number of layers increases. From 11 layers on, the difference of properties from bulk graphite is less than 10%.<sup>[24]</sup>

Graphene was recognized for its remarkable properties.<sup>[25,26]</sup> Single-layer and bilayer graphenes are zero-gap semiconductors while semimetallic character increases with the number of layers.<sup>[27]</sup> Graphene has high electron mobility ( $2 \times 10^5 \text{ cm}^2 \text{ V}^{-1} \text{ s}^{-1}$ ),<sup>[28,29]</sup> high thermal conductivity (around  $5 \times 10^3 \text{ W mK}^{-1}$ ),<sup>[30]</sup> is highly transparent to light ( $>95\%$  transmittance above 350 nm),<sup>[21,31]</sup> has a large surface area ( $2630 \text{ m}^2 \text{ g}^{-1}$ )<sup>[32]</sup> and is impenetrable to gases.<sup>[33]</sup> Further, it has electrocatalytic properties<sup>[34]</sup> that can be enhanced by doping.<sup>[35]</sup> Graphene is a mechanically strong material with high tensile (130 GPa) and fracture strength ( $42 \text{ N m}^{-1}$ ), and high Young’s modulus (1 TPa).<sup>[36]</sup> In fact, it is around 100 times stronger than steel.<sup>[37]</sup> Bilayer graphene is as hard as diamond despite being an ultrathin film.<sup>[38]</sup> The absence of a bandgap in graphene hampers its applications in electronics although it has high charge mobility. Nevertheless, it is a great candidate for flexible electronics because of its transparency and mechanical properties.<sup>[39]</sup>

Samples of graphene, a one-atom-thick 2D layer, can be characterized using a number of imaging and spectroscopic techniques. Thickness of the sample and corresponding number of layers can be determined with atomic force microscopy (AFM) while transmission electron microscopy (TEM) or scanning tunneling microscopy (STM) are useful for examining the morphology and the structure of the sample.<sup>[4,9,27]</sup> For example, it is possible to observe the honeycomb lattice of graphene using STM (Figure 2).<sup>[40]</sup> Raman spectroscopy has proven suitable for determination of the number of layers and presence of dopants, impurities and carbon nanostructures while having the advantage of being fast and requiring little sample preparation.<sup>[41]</sup>

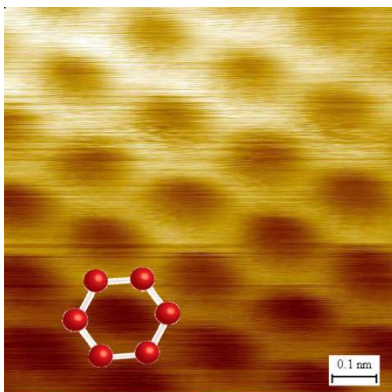


**Figure 2.** STM image of graphene. Adapted from ref.<sup>[40]</sup>.

Graphene can be covalently and non-covalently functionalized to modify its properties.<sup>[5]</sup> Opening of the bandgap is of particular interest for a transistor application. However, it is difficult to control the size and shape of graphene sheets as well as the selectivity and degree of functionalization.

When looking at the crystal structure of graphene, one can notice that all the carbon atoms are in a single plane, making it a 2D crystal. We can define cut-offs from graphene of suitable size which can be folded into different objects that can be categorized according to the number of dimensions in which the system is

periodic. For example, we can cut off a piece which can be folded into a spherical fullerene (Figure 3, left),<sup>[42]</sup> We consider this object to be 0D, since there is no periodically repeating unit in its structure. Otherwise, graphene can be rolled into a carbon nanotube (Figure 3, center)<sup>[43]</sup> or a nanoscroll,<sup>[44]</sup> or stacked into graphite (Figure 3, right), creating 1D and 3D objects, respectively. Therefore, graphene has been named by Geim and Novoselov as “the mother of all graphitic forms” as many other carbon allotropes can formally be derived from graphene.<sup>[27]</sup>

One can develop this thought experiment further and create materials, such as a Mackay crystal<sup>[45,46]</sup> (Figure 4), which is a predicted carbon allotrope that combines 8- and 6-membered rings. All these systems consist only of  $sp^2$ -hybridized carbon atoms and their substantially different properties are linked to their topology.<sup>[27]</sup>

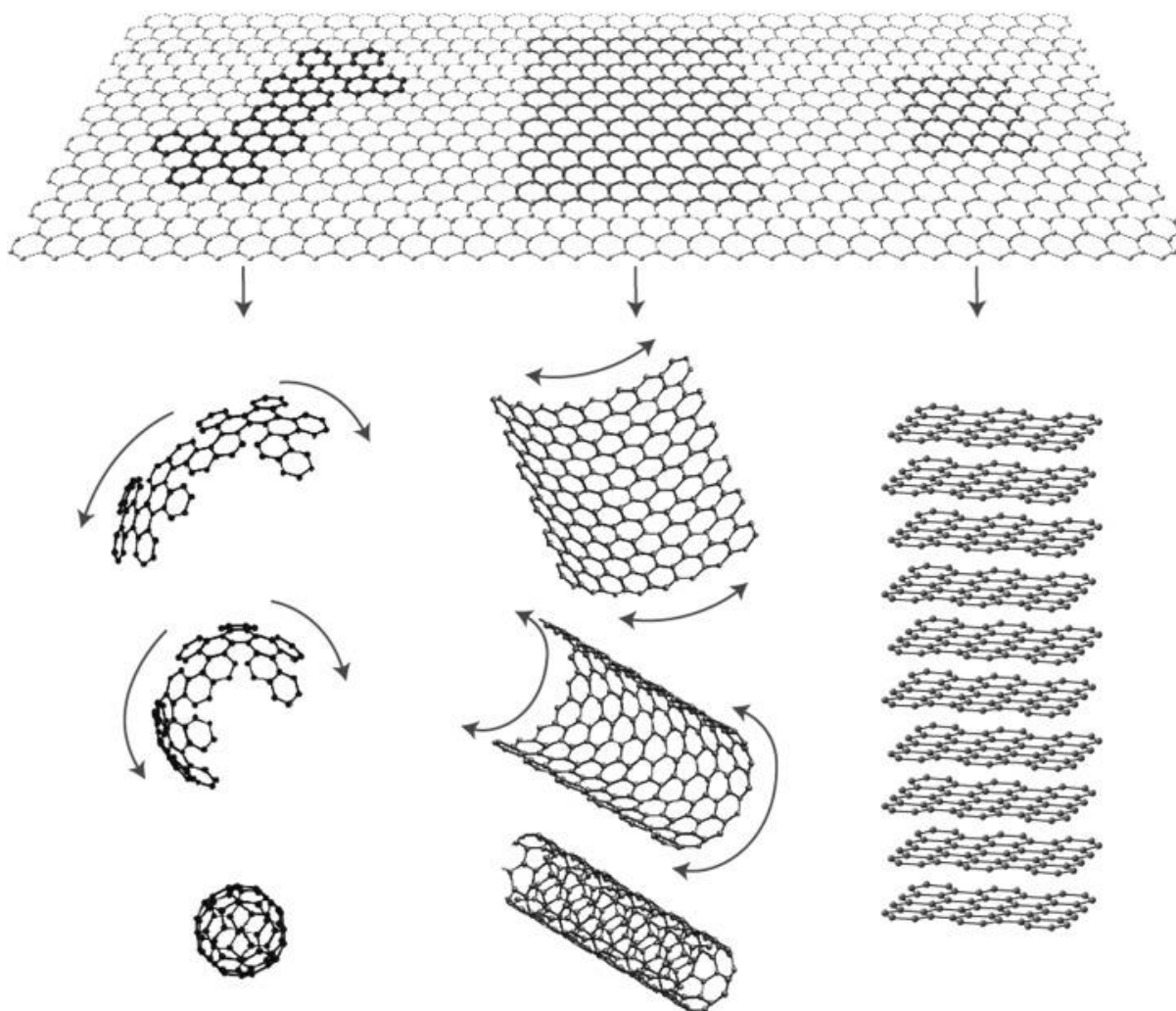


**Figure 3.** Fullerenes, carbon nanotubes and graphite formally derived from graphene, the mother of all graphitic forms. Reprinted from ref.<sup>[27]</sup> with permission from Springer Nature.

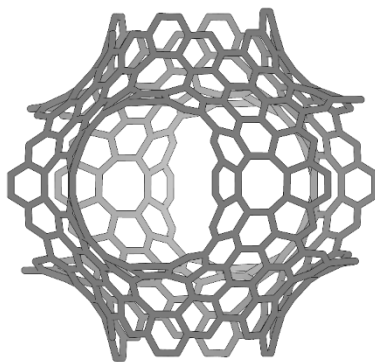


**Figure 4.** Structure of a Mackay crystal.

### 1.3. Carbon nanotubes and nanoscrolls – Rolling a graphene sheet

Graphene can be rolled up into a carbon nanotube (CNT) in infinite ways. The rolling of the sheet can be characterized by a chiral index  $(n,m)$ , where the  $n$  and  $m$  integers define the type of edge the nanotube has (Figure 5). If  $n \neq 0$  and  $m = 0$ , the graphene sheet is rolled along its zigzag edge creating a zigzag nanotube. If  $n = m$ , rolling results in an armchair nanotube, while if  $n \neq m$  but  $m \neq 0$ , a chiral nanotube is obtained. In summary, the chiral index defines both the chirality and the diameter of a CNT.

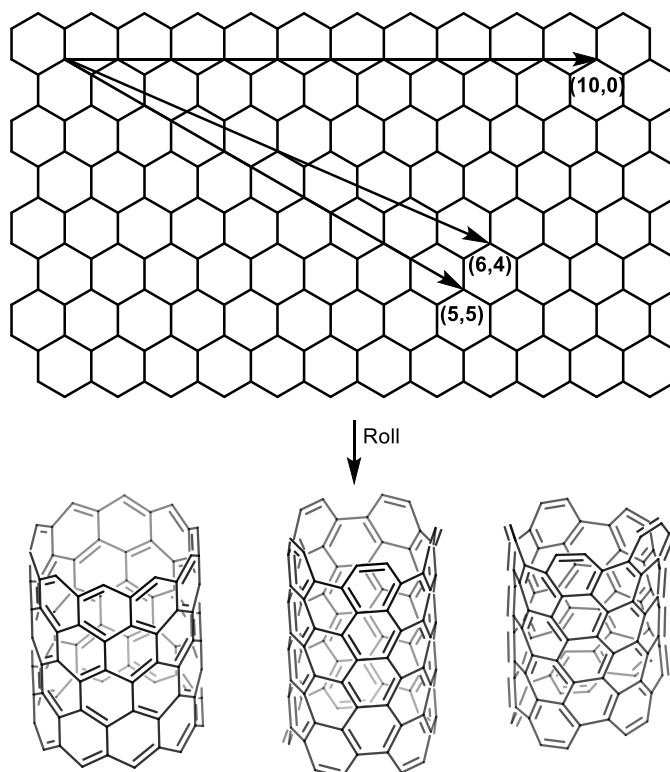


**Figure 5.** Vectors defining rolling of a graphene sheet (top); from left to right: zigzag (10,0), armchair (5,5) and chiral (6,4) carbon nanotubes (bottom).

The chirality and the diameter of the CNT (usually 0.5 to 2 nm), have a direct consequence on the material properties. CNTs for which  $|n - m| = p$ , where  $p$  is an integer divisible by three, are metallic and all the

others are semiconducting with the bandgap varying inversely in relation to the diameter. On the other hand, the ends of CNTs exhibit only a minor influence on observed properties. The ends of CNTs can be open or closed by hemispherical caps resembling a half of a fullerene structure and the number of possible caps increases with the diameter of CNTs.<sup>[47]</sup> CNTs have, similarly to graphene, strong mechanical properties with high tensile strength (up to 22 GPa)<sup>[48]</sup> and Young's modulus (up to 1 TPa).<sup>[49]</sup> These properties are also defined by the CNT's diameter and chirality. Brunauer–Emmet–Teller (BET) surface area was measured ranging from 100 to 500 m<sup>2</sup> g<sup>-1</sup>, depending on the quality of the sample. This is in contrast with the theoretical limit being half of surface area of graphene (1300 m<sup>2</sup> g<sup>-1</sup>) as formally only one side of the nanotube is accessible.<sup>[50]</sup> Thermal conductivity ranges from around 500 up to 3500 W m<sup>-1</sup> K<sup>-1</sup> depending on chirality, diameter and length of the CNTs.<sup>[51]</sup> The length of CNTs can vary from around 10 nm to 1 cm and has a much lower impact on the observed properties compared to the diameter and chirality.<sup>[52,53]</sup> Lastly, chiral nanotubes possess chiroptical properties if the sample is enriched by one of the enantiomers.<sup>[54]</sup>

It is important to note here that, until now, we have only talked about single-walled CNTs (SWCNTs) which exhibit a rather diverse morphology. However, SWCNTs of suitable diameters can be intercalated into each other, forming multi-walled CNTs (MWCNTs) which can consist of layers of different chirality. Furthermore, CNTs also tend to stack into bundles of tubes<sup>[55]</sup> and can have deformations and defects in the honeycomb lattice.<sup>[56]</sup> Since all of these factors influence the observed properties, it is crucial for their exploitation to either prepare uniform SWCNTs, or find an inexpensive and reliable method for their separation from complex mixtures that are formed during their synthesis.<sup>[57]</sup>

It is not clear who was the first to prepare CNTs<sup>[58]</sup> because the reports of tubular carbon structures go as far back as 1952.<sup>[59]</sup> Nevertheless, they were unequivocally characterized for the first time by Iijima in 1991.<sup>[43]</sup> He applied an arc discharge to graphite electrodes under argon at a low pressure to grow needles and spherical carbon structures on the cathode. TEM analysis of the needles revealed a structure of tubes of different diameters, lengths and with multiple layers. The interlayer distance was 0.34 nm, the same value as observed between the sheets in graphite. A similar carbon allotrope, carbon nanoscrolls (CNSs), was already known at this time, and Iijima demonstrated their structural difference by comparison of the electron diffraction pattern as the two appear rather similar when observed with TEM (Figure 6).

The arc discharge method was subsequently modified and scaled-up to prepare gram quantities of MWCNTs.<sup>[60]</sup> Doping the carbon electrodes with metals results in mixtures of SWCNTs of various diameters.<sup>[61,62]</sup> Additionally, laser ablation, the method developed by Kroto for the synthesis of C60 fullerene,<sup>[42]</sup> was adapted for CNT synthesis.<sup>[63–65]</sup> Both methods produce samples containing a substantial amount of undesired byproducts, necessitating subsequent purification, and are also limited in the amount of produced sample because the anode is consumed during the process as it serves as the source of carbon.<sup>[66]</sup> CVD method was utilized to synthesize SWCNTs of a single chirality using a suitable metal catalyst.<sup>[67,68]</sup> This technique employs a gas as the carbon source and is therefore suitable for a continuous production of large quantities of CNTs. However, the resulting material has usually a high density of defects and contains carbon impurities.<sup>[69–71]</sup> Although possible for all of these methods, it is difficult to find the right conditions to prepare solely SWCNTs and control their diameter, chirality and length while maintaining a low level of defects.<sup>[53,67]</sup> Purification of CNT samples can be achieved to some extent. Separation of a mixture of SWCNTs and MWCNTs with a distribution of diameters, chirality and lengths is a challenging task due to their low solubility and structural similarity, and is rather expensive.<sup>[64,72]</sup>

## 1. Introduction

The quality of CNT samples in terms of local structures, carbon impurities and nanotube defects can be evaluated by TEM or SEM imaging. The metal impurity content and the homogeneity of CNTs can be determined using thermo-gravimetric analysis (TGA).<sup>[57,72,73]</sup> Raman spectroscopy is a suitable method for the determination of the chiral index and provides semi-quantitative information about other carbon structures that might be present in the sample.<sup>[74]</sup>

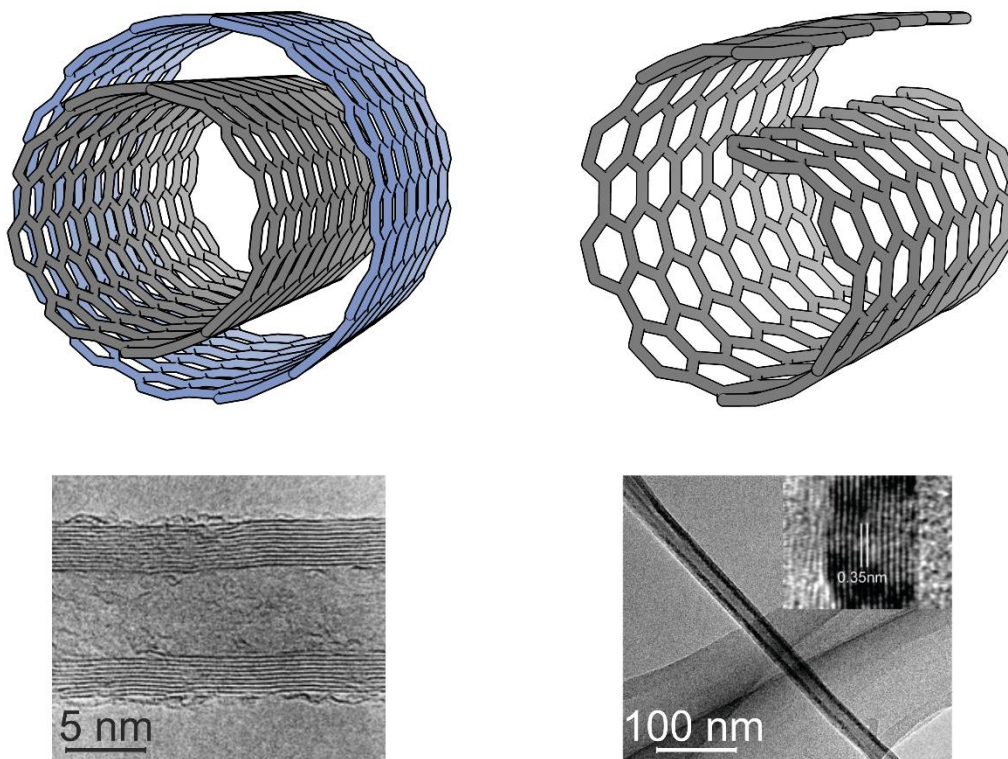


**Figure 6.** Structures (top) TEM images (bottom) of MWCNTs (left) and CNSs (right). TEM images adapted from ref.<sup>[66,75]</sup>.

Folding a planar sheet of graphene into a seamless CNT requires the curved graphene to pass through a stage where the bent graphene sheet can roll further into a nanoscroll (Figure 6) instead of making the carbon–carbon bonds between its edges. The edges of such a carbon nanoscroll (CNS) are not fused and the structure displays different properties than a SWCNT as a result of its unique shape of an Archimedean spiral (Figure 7).<sup>[76]</sup> The free edges in a carbon nanoscroll are reactive and are believed to have the ability to “bite” into the structure of the nanoscroll to close the edges, which would result in the formation of a MWCNT.<sup>[77–80]</sup>

The strain induced by bending a graphene sheet due to pyramidalization of  $sp^2$ -hybridized carbons is compensated in CNTs by formation of strong covalent carbon–carbon bonds between graphene edges. However, no covalent bonds are formed when graphene is rolled-up into a CNS. As a result, similar to graphite, the structure of a CNS is held together due to van der Waals forces between the overlapping parts of the sheet.<sup>[80–82]</sup> The inner diameter of the scroll (Figure 7,  $d = 2 r_0$ ) has to be at least 2 nm to compensate the strain energy. The stability of a CNS also depends on the dimensions of the graphene sheet and resulting chirality.<sup>[83]</sup> Molecular dynamics simulations show that for a graphene sheet of  $3.006 \times 12.146$  nm dimensions, an overlap of at least two rows of hexagons on both ends of the sheet is necessary to achieve a stable CNS.<sup>[81]</sup> These systems are still flexible because of the weak nature of van der Waals forces<sup>[84]</sup> and



allow for small guest molecules, such as hydrogen, to intercalate into the CNS.<sup>[85,86]</sup> A large surface area ( $2600 \text{ m}^2 \text{ g}^{-1}$ ) was predicted since both sides of the sheet are accessible,<sup>[87]</sup> however, the experimental BET surface areas vary from around  $200$  to  $400 \text{ m}^2 \text{ g}^{-1}$ .<sup>[88,89]</sup> The distance between the overlapping parts of the sheet (Figure 7,  $h_1$ ) is  $0.34 \text{ nm}$ , similar to graphite and MWCNTs.<sup>[44]</sup>

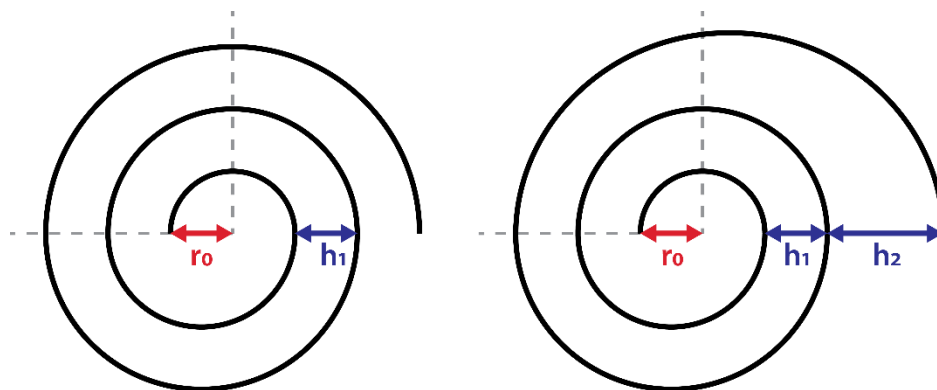


**Figure 7.** Representation of a carbon nanoscroll from the side (left) and partial unfolding (right).

Similar to CNTs, armchair, zigzag and chiral CNSs exist depending on the fold of the graphene sheet.<sup>[76]</sup> However, unlike in CNTs, different configurations may interconvert due to open edges.<sup>[81,84]</sup> This makes isolation of a uniform carbon nanoscroll material a daunting task, if possible at all. According to calculations, armchair nanoscrolls have semimetallic to metallic character with a higher conductivity than that of SWCNTs, while zigzag nanoscrolls have, on average, smaller band gaps than SWCNTs.<sup>[82]</sup>

The first CNSs were prepared and partially characterized already in 1960 by Bacon<sup>[44]</sup>, where the author refers to them as carbon whiskers prepared by arc discharge applied to graphite electrodes. Although Bacon correctly proposed their structure on the nanoscale, it was not confirmed until much later due to lack of suitable imaging techniques available at that time.<sup>[83,90,91]</sup> Even with the early electron microscopes, the CNSs were often confused with CNTs because of their structural similarity and low resolution of these devices. For instance, Shioyama and Akita referred the isolated carbon nanostructures as nanotubes, but the structure was clearly a nanoscroll.<sup>[92]</sup> Nowadays, CNSs are prepared using sonication of exfoliated graphite<sup>[93]</sup>, graphite oxide<sup>[94,95]</sup> and graphite nitrate,<sup>[96]</sup> CVD method,<sup>[97]</sup> or solvent-assisted folding of graphene sheets,<sup>[75]</sup> which can be further enhanced by microwave irradiation.<sup>[98]</sup> The quality of the synthesized CNSs varies by method with mechanical exfoliation of graphite performing the best.

It is impossible to lock a CNS to a single configuration without introduction of a clip to prevent slippage of the layers. The properties of individual configurations of CNSs could be employed in new applications. So far, CNS were used for the construction of several prototype devices. For instance, a field effect transistor device was fabricated demonstrating that the resistance of nanoscrolls decreases with increasing temperature.<sup>[75]</sup> More recent examples include single electron transistor devices,<sup>[99]</sup> supercapacitors,<sup>[100]</sup> and others.<sup>[101]</sup>

## 1.4. Carbon nano hoops – Cutting up carbon nanotubes

### 1.4.1. Synthesis of carbon nano hoops

The chirality-specific properties of SWCNTs renders their pure samples attractive for applications in electronics and sensing. The bottom-up approach uses small molecular fragments of CNTs as seeds for the growth of a chirality-specific CNT, potentially in large quantities and high quality, avoiding the tedious sample purification. Cycloparaphenylenes,  $[n]$ CPPs with  $n$  denoting the number of phenylenes, are the shortest possible cut-offs from armchair CNTs and they were termed as “carbon nano hoops” by Jasti and Bertozzi.<sup>[102]</sup> They have been envisioned as templates for bottom-up synthesis of armchair SWCNTs, while cyclacenes could be used for zigzag SWCNTs (Figure 8).<sup>[103–105]</sup> Ultimately, this hypothesis was confirmed by Itami *et al.* when they prepared a relatively uniform sample of SWCNTs using  $[9]$ CPP or  $[12]$ CPP as seeds in the CNT synthesis using the CVD method.<sup>[106]</sup> Although many attempts have been made to synthesize cyclacenes,<sup>[107]</sup> no parent cyclacene has been isolated to this date. The study of molecular fragments of CNTs can also provide more insights about the structure–property relationship for CNTs and may answer fundamental questions on topics such as aromaticity and chirality. Moreover,  $[n]$ CPPs that can be tailored with atomic precision thanks to the art of organic synthesis are of interest due to their own size-dependent optoelectronic properties, which will be discussed in more detail later in the next chapter.

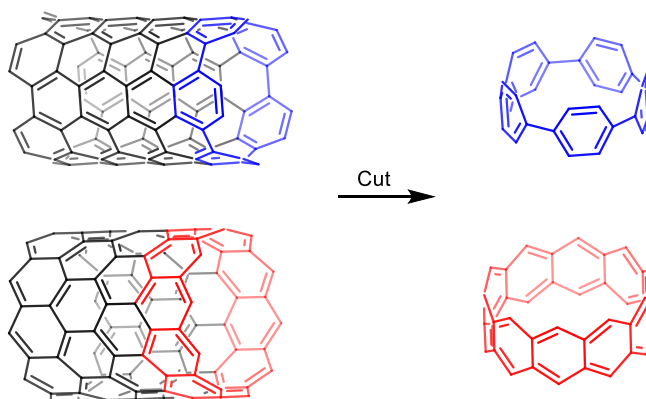


**Figure 8.**  $[5]$ CPP (top) and  $[10]$ cyclacene (bottom) as cut-offs from (5,5)- and (10,0)-CNTs respectively.

A feature common to molecular fragments of CNTs is their preservation of the radial conjugation of  $\pi$ -orbitals. The bending of the aromatic units is necessary to form a macrocycle, but it induces strain in the molecule.<sup>[108,109]</sup> To gain further insights regarding the flexibility of  $[n]$ CPPs and to estimate strain energies, the conformations of  $[n]$ CPPs were investigated by Itami *et al.* based on the two possible conformations of terphenyl (Figure 9).<sup>[110]</sup> It was found that alternating the orientation of *p*-phenylenes in  $[n]$ CPPs results in lower energy conformers. Alternating the orientation in the whole hoop is only possible for an even number of phenylenes, while for an odd number, one terphenyl unit adopts a helical orientation. The energy barriers of interconversion between such conformers are rather low and were estimated for  $[12]$ CPP to range from 3 to 10 kcal mol<sup>-1</sup> at B3LYP/6-31g(d) level of theory. These results are consistent with the <sup>1</sup>H-NMR spectrum of  $[12]$ CPP, where only one singlet is observed for all hydrogens,<sup>[102]</sup> and confirms that phenylenes rotate freely at room temperature. The strain energies were estimated via homodesmotic reactions (Scheme 1) using the lowest energy conformers and vary from 24 to 120 kcal mol<sup>-1</sup> from  $[24]$ CPP to  $[5]$ CPP, respectively.<sup>[110–112]</sup> Strain energy decreases with increasing size of the nano hoop and eventually reaches 0 at  $n = \infty$ . It is important to note that the strain energy represents a considerable barrier to overcome even for large macrocycles. Additionally, there is an entropic barrier of closing a macrocycle. In summary, formation

of carbon nano hoops is thermodynamically disfavored both by enthalpy and entropy, and is the reason why the development of synthetic strategies for strained macrocycles took a long time.

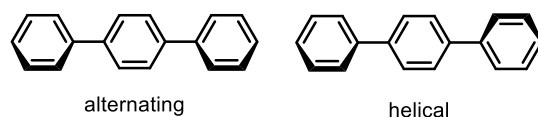
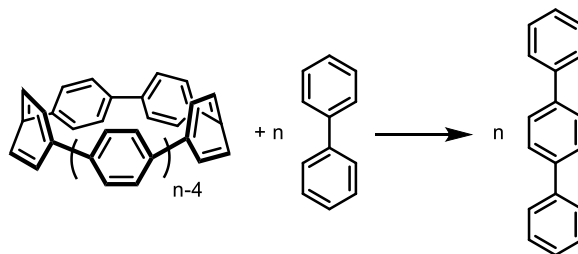


**Figure 9.** Two conformations of terphenyl.



**Scheme 1.**

One of the first to tackle the challenge was Vögtle and his group with several unsuccessful attempts (Figure 10). All of their strategies share a common concept of forming a macrocycle first and then aromatize or contract the macrocycle thereby effectively separating the entropic and enthalpic penalties into two distinct synthetic steps. Similar approach became the basis for the successful strategies developed later.<sup>[113]</sup> Although Vögtle was on the right path, it was not until 2008 when Jasti and Bertozzi realized the first successful synthesis of  $[n]$ CPPs (Figure 11). This strategy utilizes *cis*-1,4-substituted cyclohexadiene moieties which have a suitable angle ( $\sim 80^\circ$ ) to form relatively strain-free macrocycles via Suzuki-Miyaura cross-coupling which can be reduced in a subsequent step to phenylenes forming  $[n]$ CPPs. The aromatization in the latter step represents the driving force that overcomes the build-up of the molecular strain.<sup>[102]</sup> This strategy has been employed in size-selective synthesis of  $[n]$ CPPs ( $n = 5-12, 18$ ).<sup>[112, 114-116]</sup>

Soon after, other approaches to  $[n]$ CPPs emerged<sup>[117]</sup> starting with Itami group which used *cis*-1,4-substituted cyclohexanes as bent units ( $\sim 90^\circ$ ) to build macrocycles that require oxidation in the last step to convert to  $[n]$ CPPs (Figure 12),<sup>[118]</sup> similar to the attempts of Vögtle.<sup>[113]</sup>  $[n]$ CPPs of different sizes ( $n = 7-16$ ) were synthesized using this strategy,<sup>[119-122]</sup> although it is important to note that the last oxidation step provides rather low yields and is challenging to scale-up.<sup>[123]</sup>

The approach of Yamago relies on using *cis*-platinum complexes as corner units ( $\sim 90^\circ$ ) to form macrocycles in a size-selective or random manner depending on the number of phenylenes in the building blocks (Figure 12). If  $n = m$ , the synthesis is size-selective, resulting in the formation of square-shaped macrocycles. If we mix the two building blocks with different number of phenylenes ( $n \neq m$ ), a mixture of tetragonal macrocycles of various sizes is formed. Platinum macrocycles undergo mild oxidation with bromine in the last step affording  $[n]$ CPPs ( $n = 8-13$ ).<sup>[124-126]</sup> Similarly, the most recent approach of Osakada and Tsuchido uses gold complexes as corner units ( $\sim 60^\circ$ ) to create triangular macrocycles which are oxidized in the last step to afford  $[n]$ CPPs ( $n = 6, 9, 12, 15$ ).<sup>[127, 128]</sup>

## 1. Introduction

Yamago later modified the method of Jasti by replacing the robust methoxy group with an easy-to-remove triethylsilyl (TES) protecting group, although the authors offered no explanation why this particular protecting group was chosen.<sup>[129]</sup> Nevertheless, after removal of TES groups, the aromatization step requires substantially milder conditions for reduction with  $\text{H}_2\text{SnCl}_4$  instead of sodium naphthalene. This method typically provides relatively high yields, making it suitable even for the synthesis of the smallest sizes of CPPs and is the most commonly used method for  $[n]$ CPPs today.<sup>[129–131]</sup>

Substituted CPPs can also be prepared by a rhodium-catalyzed [2+2+2]cyclootrimerization of alkyne-containing macrocycles (Figure 13),<sup>[132–135]</sup> or a Diels-Alder reaction of macrocyclic dienes.<sup>[136,137]</sup>

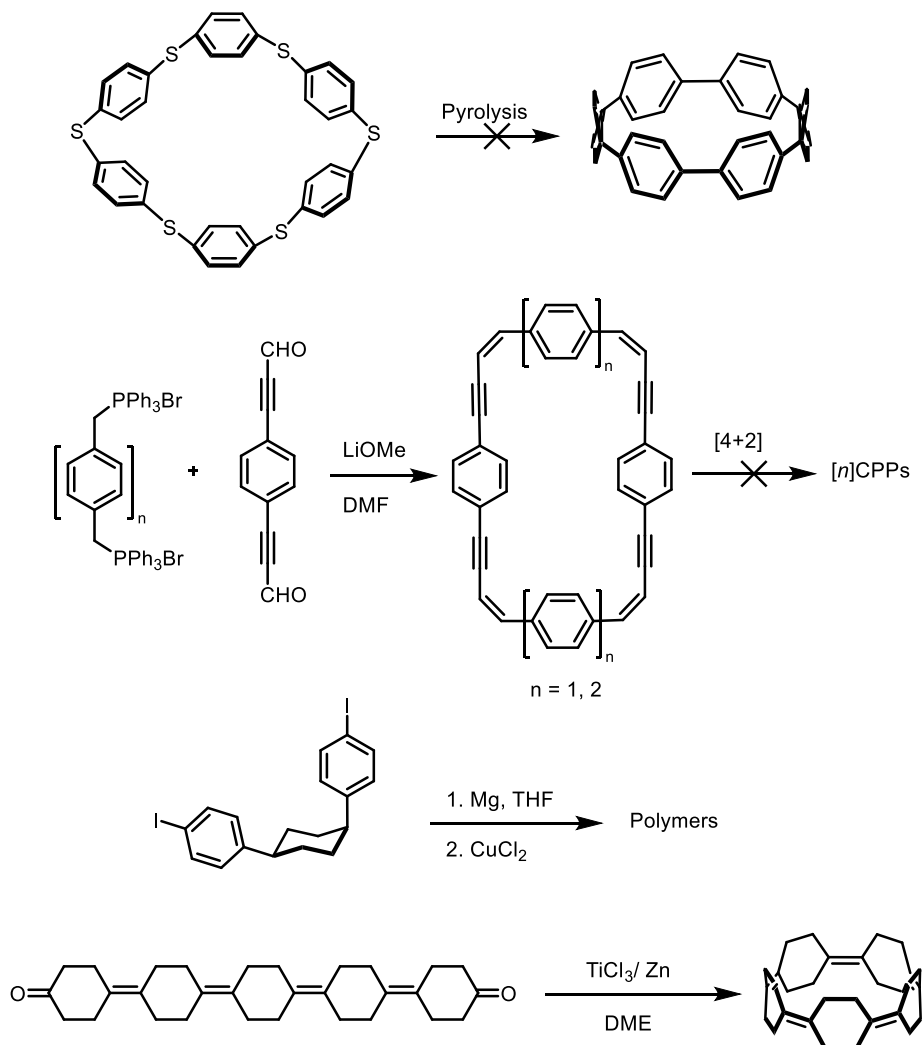


**Figure 10.** Attempts of Vögtle to synthesize  $[n]$ CPPs.<sup>[113]</sup>

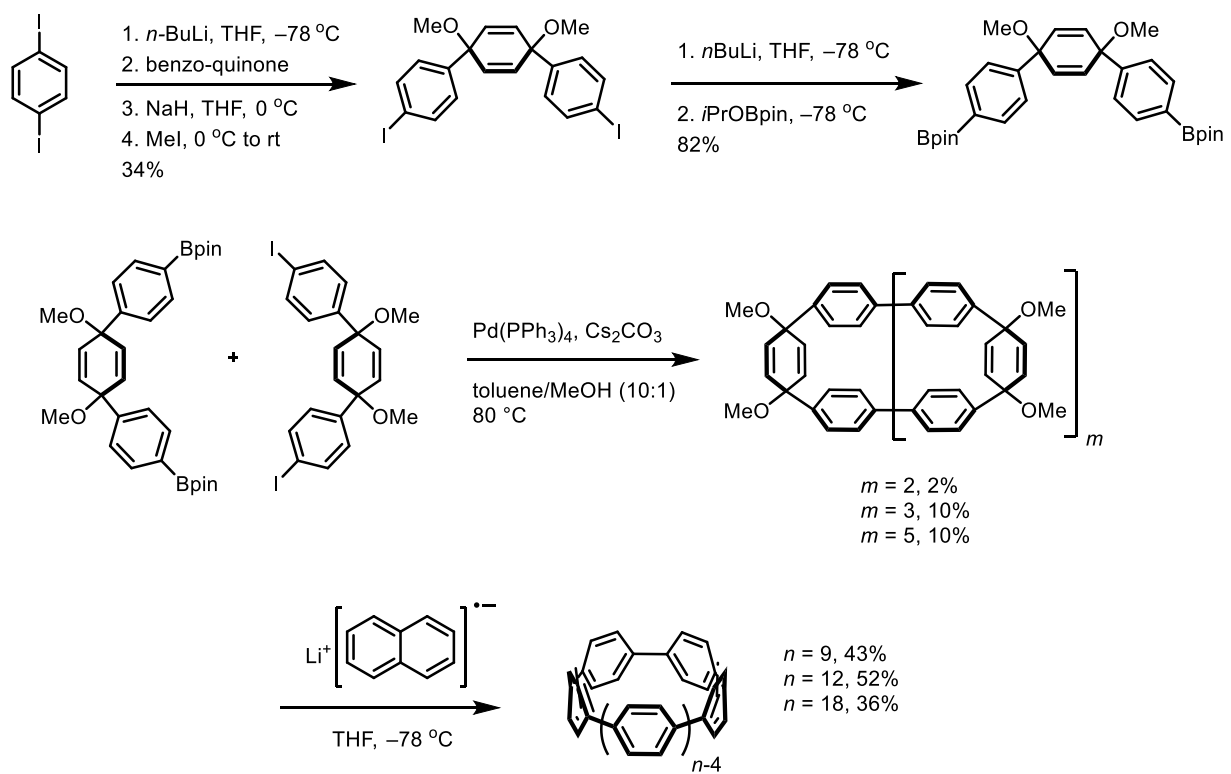


**Figure 11.** The first synthesis of  $[n]$ CPPs ( $n = 9, 12, 18$ ) by Jasti and Bertozzi.<sup>[102]</sup>

## 1. Introduction

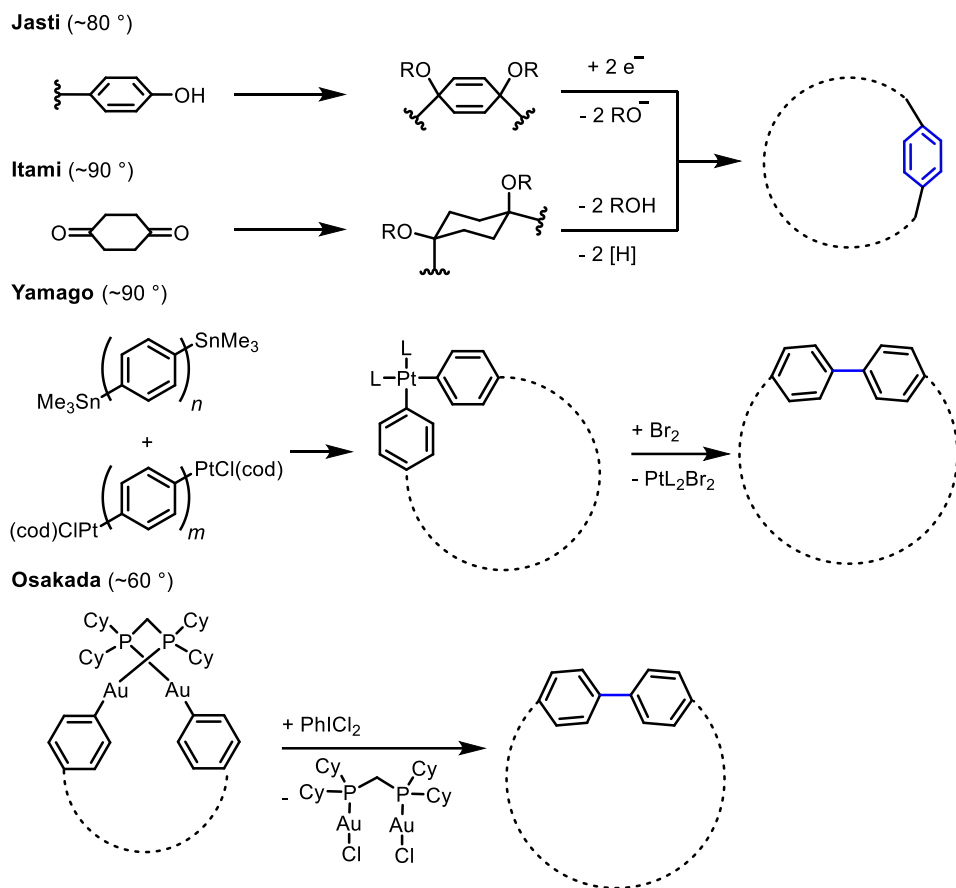


**Figure 12.** Overview of the synthetic approaches to  $[n]$ CPPs with the angles of corner units in brackets.

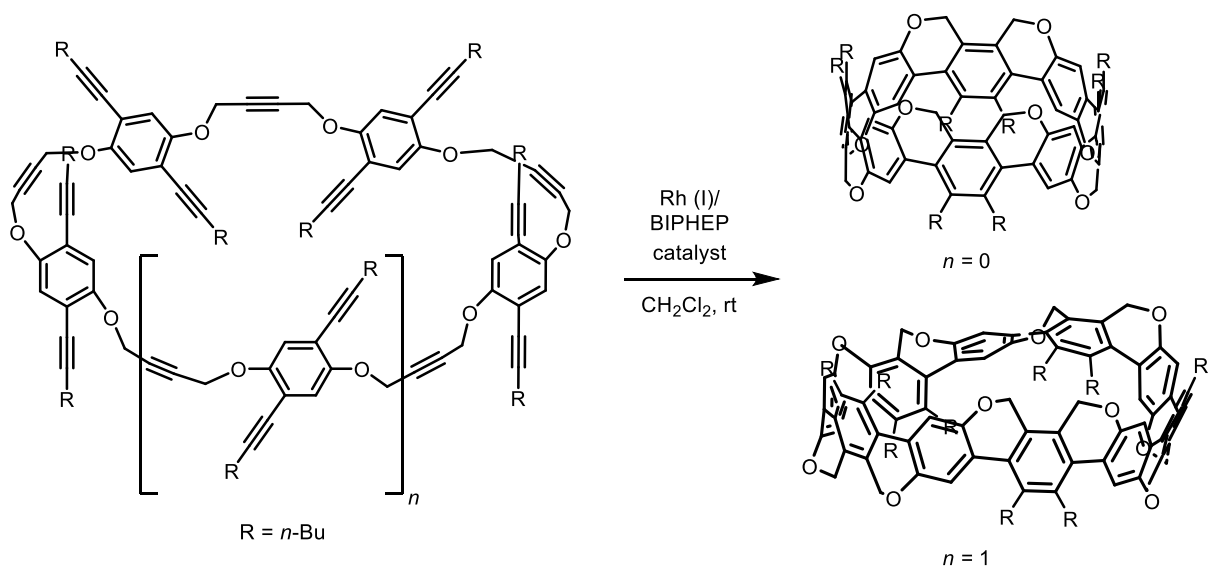


**Figure 13.** Synthesis of substituted CPPs by  $[2+2+2]$ cyclotrimerization of alkynes.

### 1.4.2. Physicochemical properties of carbon nano hoops

$[n]$ CPPs demonstrate unusual size-dependent properties as a consequence of the curvature of the  $\pi$ -system. They share common size-independent absorption maxima at around 340 nm. A large Stokes shift is observed which increases with decreasing number of phenylenes in the structure. Fluorescence quantum yields, however, decrease with the size too (Figure 14, Table 1). In fact, the smallest  $[n]$ CPPs ( $n = 5,6$ ) are non-emissive<sup>[138–140]</sup> which is in contrast to what is observed in linear systems, such as oligo-*para*-phenylenes ( $[n]$ OPPs), for which the quantum yields and red-shift of emission increase with increasing number of phenylenes.<sup>[141]</sup>

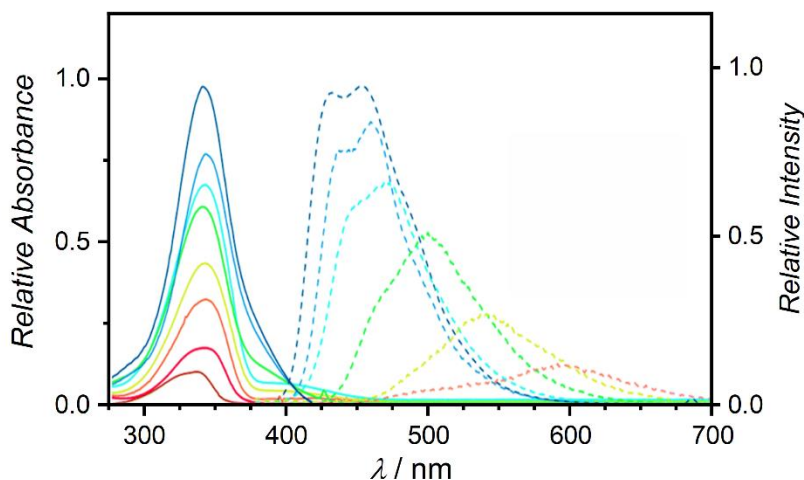


**Figure 14.** Absorption (solid) and emission (dashed) spectra of  $[n]$ CPPs ( $n = 5–12$ ). Adapted from ref.<sup>[140]</sup>

**Table 1.** Strain energies, oxidation potentials and photophysical properties of  $[n]$ CPPs.<sup>[110,112,138–140]</sup>

$[n]$ CPP	Strain / kcal mol <sup>-1</sup>	$E_{ox}$ / V	$\lambda_{abs}$ / nm	$\lambda_{em}$ / nm	$\Phi_f$	$\tau_f$ / ns
5	119	0.25, 0.46	335	-	-	-
6	96.0	0.44	340	-	-	-
7	84.0	0.55	340	587	0.007	-
8	72.2	0.59	340	533	0.084	17.6
9	65.6	0.70	340	494	0.30	10.6
10	57.7	0.74	338	466	0.46	6.6
11	53.7	0.83	340	458	0.52	3.8
12	48.1	0.85	339	450	0.66	2.7
13	45.5	-	337	446	0.72	2.0
14	41.0	-	338	443	0.89	-
15	39.2	-	339	440	0.90	-
16	35.6	-	339	438	0.88	-

The HOMO and the LUMO in  $[n]$ CPPs are delocalized over all the phenylenes in the macrocycle in a centrosymmetric fashion. As a consequence, HOMO–LUMO optical transitions are symmetry forbidden according to Laporte rule which states that for centrosymmetric molecules, like  $[n]$ CPPs, transitions between orbitals of same symmetry with respect to inversion are forbidden.<sup>[138,140]</sup> The observed size-

## 1. Introduction

independent absorption maxima at around 339 nm can be attributed to nearly degenerate HOMO–2 or HOMO–1 to LUMO and HOMO to LUMO+1 or LUMO+2 transitions which are symmetry allowed. These transitions are also responsible for the fluorescence red-shift and decrease in the emission quantum yield with decreasing size of  $[n]$ CPPs as the populated  $S_2$  and  $S_3$  states undergo fast internal conversion to geometrically relaxed  $S_1'$  state. For  $[n]$ CPPs where  $n \geq 8$ ,  $S_1'$  state breaks the symmetry due to exciton localization to a segment consisting of seven phenylenes. The symmetry-breaking induced by localization allows for the transition to the  $S_0$  state, *i.e.* the emission. For  $n \leq 7$ , the  $S_1'$  state conserves the symmetry of the  $S_0$  state and the transition stays symmetry-forbidden, hence only weak or no emission is detected (Figure 15). The decrease in the HOMO–LUMO gap with decreasing size of  $[n]$ CPPs is attributed to the reduction of the torsional angles between phenylenes as a compensation for the increase in strain energy. As a result, a more effective overlap of  $\pi$ -orbitals between individual phenylenes is achieved.<sup>[142]</sup>

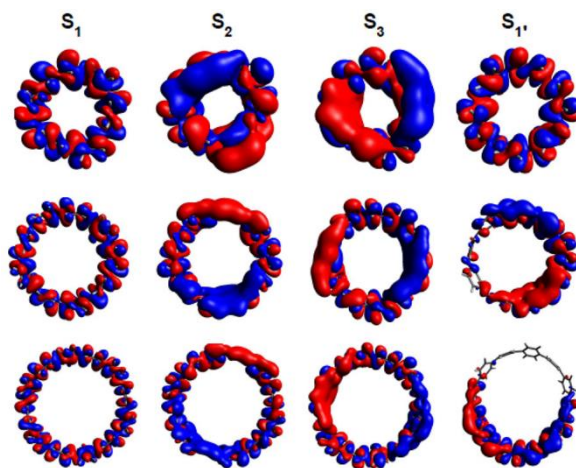


**Figure 15.** Orbital distribution of transition density for  $S_1$ ,  $S_2$ ,  $S_3$  and  $S_1'$  transitions in  $[6]$ -,  $[9]$ - and  $[12]$ -CPP (top to bottom). Red and blue color corresponds to negative and positive values of the transition density, respectively. Adapted from ref.<sup>[142]</sup>

Calculations have shown that breaking the symmetry of centrosymmetric orbitals in CPPs leads to allowed HOMO→LUMO which would result in emission even for the smallest CPPs.<sup>[143]</sup> Jasti *et al.* proved this hypothesis correct by synthesizing a series of CPPs with one of the phenylenes being connected via its *meta*-positions instead of *para*-. The resulting  $m[n]$ CPPs ( $n = 5-8, 10, 12$ ) exhibit fluorescence for all sizes (Figure 16, Table 2). Size-independent maxima at around 328 nm are attributed to HOMO–1 to LUMO and HOMO to LUMO+1 transitions while the small band shoulders or even maxima observed at longer wavelengths, red-shifting with decreasing size of the hoop, can be assigned to the HOMO→LUMO transitions.<sup>[131]</sup>



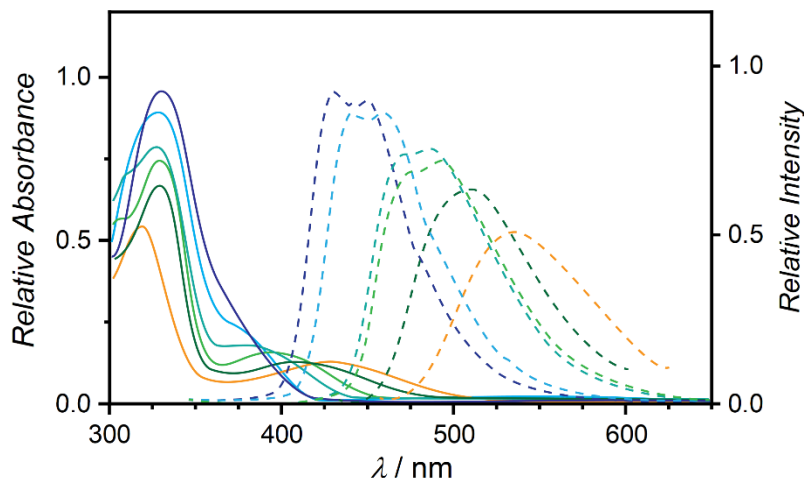
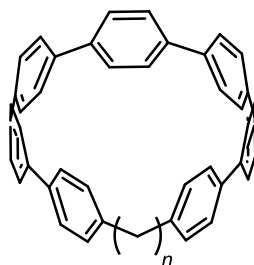


**Figure 16.** Absorption (solid) and emission (dashed) spectra of  $m[n]$ CPPs ( $n = 5-8, 10, 12$ ).<sup>[131]</sup> Redrawn from ref.<sup>[131]</sup>

**Table 2.** Strain energies, oxidation potentials and photophysical properties of  $m[n]$ CPPs.<sup>[131]</sup>

$m[n]$ CPP	Strain / kcal mol <sup>-1</sup>	$E_{\text{ox}} / \text{V}$	$\lambda_{\text{abs}} / \text{nm}$	$\lambda_{\text{em}} / \text{nm}$	$\Phi_f$	$\tau_f / \text{ns}$
5	102	0.47	316, 428	534	0.014	1.05
6	77.6	0.53	328, 410	510	0.224	2.68
7	66.4	0.67	328, 394	491	0.450	3.56
8	56.7	0.74	326, 376	484	0.595	3.41
10	51.4	0.81	328	456	0.726	2.45
12	43.3	0.88	328	429	0.769	1.78

A series of nanohoops with varying length of an alkyl chain inserted into [7]CPP was studied by Jasti *et al.* to elucidate the effect of curvature on optoelectronic properties of CPPs (Figure 17).<sup>[144]</sup> Here, both the cyclic conjugation and the symmetry are broken. Consequently, the fluorescence becomes blue-shifted with a significant increase in the intensity approaching the properties of linear oligo-*para*-phenylene ([7]OPP)<sup>[141]</sup> as the length of the tether increases. The absorption maxima are also blue-shifted indicating that the cyclic conjugation is responsible for a smaller HOMO–LUMO gap. Clearly, the increasing blue-shift in the absorption and emission with increasing length of the alkyl tether, suggests that an increasing curvature of the  $\pi$ -system, which also increases the strain, lowers the HOMO–LUMO gap.

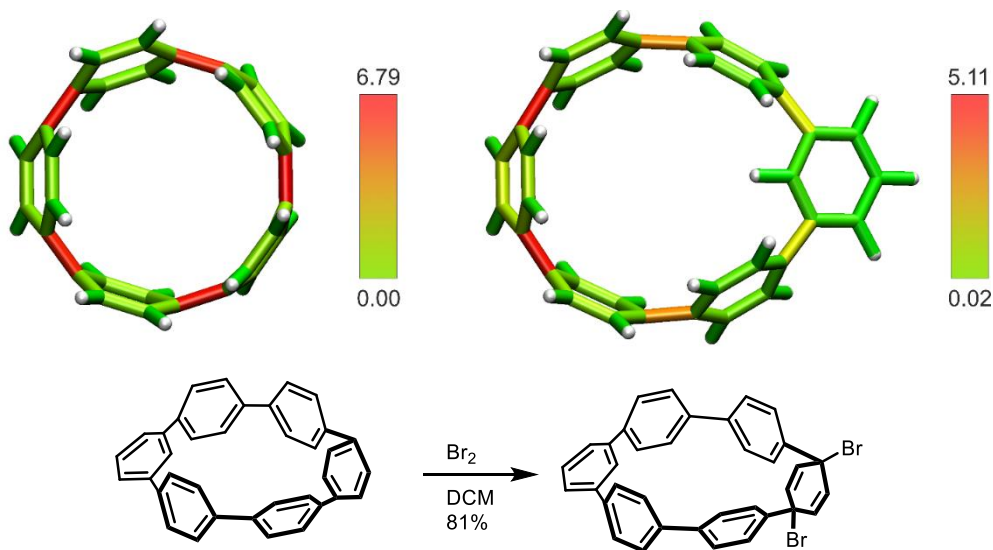


**Figure 17.** Structure of conjugation-broken  $[n]\text{CH}_2[7]$ CPPs.<sup>[144]</sup>

**Table 3.** Strain energies, oxidation potentials and photophysical properties of conjugation-broken CPPs.<sup>[141,144]</sup>

Species	$E_{\text{ox}} / \text{V}$	$\lambda_{\text{abs}} / \text{nm}$	$\lambda_{\text{em}} / \text{nm}$	$\Phi_{\text{fl}}$
[7]CPP	0.47	340	588	0.006
[1]CH <sub>2</sub> [7]CPP	0.63	321, 390	502	0.23
[3]CH <sub>2</sub> [7]CPP	0.71	319, 375	469	0.25
[7]OPP	1.00	326	408	1.00

[10]CPP and *m*[8]CPP both possess around 57 kcal mol<sup>-1</sup> of strain energy, however, they display different photophysical properties. It suggests that the strain energy alone here is an insufficient prediction tool. Furthermore, strain energy is spread unevenly in lower-symmetry systems and is localized over fewer bonds in *m*[8]CPP. Therefore, some carbon atoms are more pyramidalized than others. To access the distribution of the strain energy within carbon nano hoops, Jasti *et al.* developed a software suite, called StrainViz.<sup>[145]</sup> Contributions of perturbing individual bond lengths, valence and dihedral angles to the total strain are considered separately and can be visualized (Figure 18, top). For example, localization of the strain in the nano hoop is a powerful tool to predict the regioselectivity for CPP functionalization because the more strained parts of the molecule display higher reactivity (Figure 18, bottom).

**Figure 18.** Top: StrainViz visualization of total strain distribution (in kcal mol<sup>-1</sup>) in [5]CPP (left) and *m*[6]CPP (right). Bottom: regioselective bromination of *m*[6]CPP.<sup>[145]</sup>

In addition to curvature and symmetry, the frontier molecular orbitals (FMOs) can be manipulated by introduction of electron acceptors or electron donors into the nano hoop.<sup>[146]</sup> It is worth noting that electron-rich phenylene units can be regarded as electron donors themselves.<sup>[147]</sup> Incorporation of electron donating groups, such as thiophene, into a CPP does not significantly perturb the electronic structure of the nano hoop. On the other hand, electron acceptors can markedly lower the energy of the LUMO. If both donors and acceptors are incorporated into the structure of the nano hoop at the same time, the FMOs become localized on the *p*-phenylene units that bear the donor (HOMO) and acceptor (LUMO) moieties. This results in an increase in the HOMO and a decrease in the LUMO energies effectively lowering the HOMO–LUMO gap. If a suitable combination of donor and acceptor moieties is used, emission can theoretically reach the NIR

region.<sup>[146–149]</sup> Numerous nano hoops containing donors, acceptors, or both units were synthesized and characterized to this date (Figure 19).<sup>[146]</sup> For instance, polyaromatics,<sup>[150–152]</sup> thiophene,<sup>[153–155]</sup> dimethoxynaphthalene,<sup>[156]</sup> carbazole,<sup>[157,158]</sup> bipyridine,<sup>[159]</sup> porphyrin,<sup>[160]</sup> and other<sup>[161–163]</sup> were employed as electron donors, while pyridinium,<sup>[149,164]</sup> phthalimide,<sup>[156]</sup> anthraquinone and tetracyanoanthraquinodimethane,<sup>[147]</sup> benzothiadiazole,<sup>[165,166]</sup> and other<sup>[155,167]</sup> as electron acceptors were used.

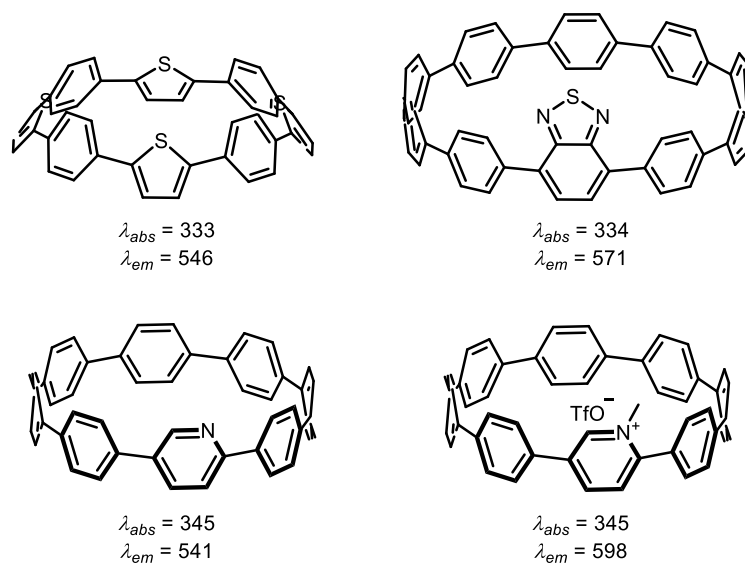


**Figure 19.** Examples of donor-acceptor nano hoops with corresponding absorption and emission wavelengths.<sup>[146]</sup>

The  $\pi$ -electrons in  $[n]$ CPPs are delocalized around the whole nano hoop and according to Hückel  $\pi$ -electron counting,<sup>[168]</sup>  $[n]$ CPPs with  $4N$   $\pi$ -electrons would be anti-aromatic if the other criteria of anti-aromaticity are met.<sup>[169]</sup> Although aromaticity can be considered a somewhat fuzzy concept with no clear definition and it cannot be quantified, there are quantifiable consequences like aromatic stabilization energy, bond length equalization and magnetic properties.<sup>[170]</sup> Aromatic stabilization energy cannot be directly measured but it is possible to estimate using quantum chemical calculations.<sup>[171]</sup> Bond length equalization can be assessed from the X-ray crystal structural analysis. This method faces difficulties with obtaining a good quality single crystal which can be challenging for relatively unstable compounds like strained carbon nano hoops. <sup>1</sup>H-NMR spectroscopy has proven invaluable in experimentally assessing aromaticity since an external magnetic field induces diatropic ring currents if the studied compound is aromatic, while paratropic currents are induced for anti-aromatic compounds.<sup>[172]</sup> Magnetically-induced ring currents in  $[n]$ CPPs ( $n = 6–11$ ) were investigated computationally.  $[n]$ CPPs ( $n = 8–11$ ) were found to have negligible ring currents and are thus non-aromatic, while [6]CPP shows a weak paratropic current rendering it slightly anti-aromatic, and [7]CPP a weak diatropic current suggesting aromaticity.<sup>[173]</sup> Yamago *et al.* synthesized a derivative of [8]CPP with an alkyl bridge connecting two parts of the nano hoop (Figure 20) to experimentally probe effect of the the magnetic currents.<sup>[157]</sup> The NMR proton resonance at  $-2.70$  ppm of the C5 methyl groups demonstrates a shielding in the center of the ring. Computational investigation of nucleus-independent chemical shifts (NICS)<sup>[174]</sup> and magnetically-induced current densities attributed the shielding to local diatropic ring currents on the inside of the ring. Local paratropic ring currents were found on the outside of the nano hoop while no global ring currents were found confirming the previous results that demonstrated the non-aromatic character of  $[n]$ CPPs ( $n \geq 8$ ). Global paratropic ring currents were observed for  $[n]$ CPPs

## 1. Introduction

( $n = 5,6$ ), however, they were too weak to be attributed to anti-aromaticity and are likely a consequence of strain and a higher quinoidal character of smaller  $[n]$ CPPs.

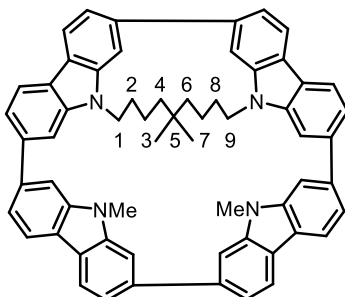


**Figure 20.** Alkyl bridged [8]CPP derivative.<sup>[157]</sup>

$[n]$ CPPs can be oxidized using  $\text{NOSbF}_6$  or  $\text{SbF}_5$  to the corresponding radical cations or dications,<sup>[175–178]</sup> or reduced using alkali metals to the corresponding radical anions, dianions or tetraanions.<sup>[179–182]</sup> Analysis of NICS values (Table 4) and induced magnetic currents revealed that dications and dianions can be regarded as aromatic by having  $(4N + 2)$   $\pi$ -electrons. Moreover, dicationic species are stable enough to obtain single crystals and analyze their crystal structures further supporting the notion of aromatic stabilization. X-ray structural analysis revealed a symmetric structure with a higher bond length alternation and lower dihedral angles than in neutral  $[n]$ CPPs indicating a higher quinoidal character with the positive charges being delocalized across the whole system.<sup>[175,177]</sup> Dications  $[n]\text{CPP}^{2+}$  are emissive with a very low quantum yield with the absorption and emission maxima shifted to near-infrared (NIR) region (Table 5).<sup>[178]</sup> Reduced  $[n]\text{CPP}^{2-}$  species have similar delocalization, however, X-ray crystallography revealed stretching of the nanohoop to an ellipsoidal shape and localization of charges on the opposite sides of the ellipse due to complexation of  $\text{K}^+$  ions in the inside of the nanohoop.<sup>[181]</sup> Upon further reduction,  $[8]\text{CPP}^{4-}$  could be isolated and analyzed revealing a high anti-aromatic character with  $4N$   $\pi$ -electrons and more pronounced elliptical stretching than that observed in the dianionic species (Figure 21).<sup>[182]</sup>

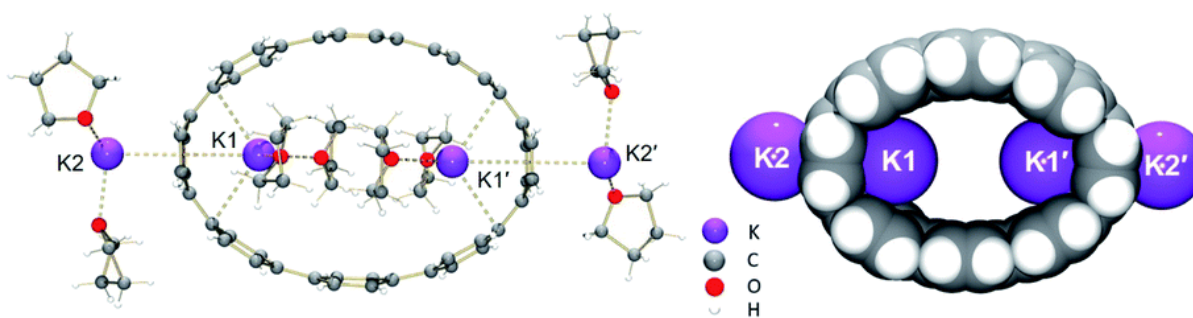


**Figure 21.** Crystal structure of  $[8]\text{CPP}^{4-}$  with  $[\text{K}(\text{THF})_2]^+$  as counter-ions. Adapted from ref.<sup>[182]</sup>

**Table 4.** NICS values in ppm in the center of the ring in  $[n]$ CPPs and corresponding dications and dianions at B3LYP/6-31g(d) level of theory.<sup>[176]</sup>

$n$	5	6	7	8	9	10
$[n]$ CPP	-1.26	-2.90	-2.52	-2.26	-1.88	-1.60
$[n]$ CPP <sup>2+</sup>	-19.63	-18.28	-16.41	-13.99	-12.30	-10.52
$[n]$ CPP <sup>2-</sup>	-16.65	-16.61	-15.47	-13.75	-12.31	-10.81

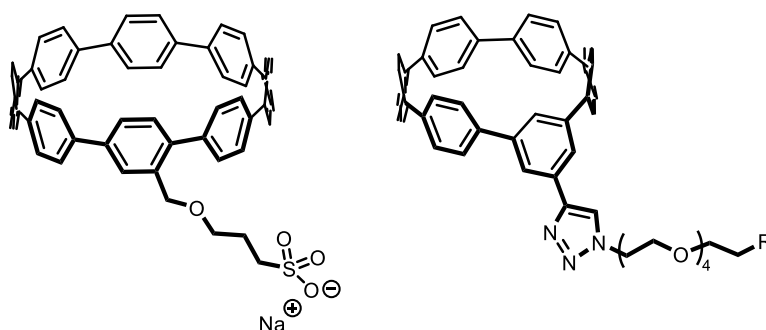
**Table 5.** Photophysical properties of  $[n]$ CPPs<sup>2+</sup>.<sup>[178]</sup>

$[n]$ CPP <sup>2+</sup>	$\lambda_{\text{abs}} / \text{nm}$	$\lambda_{\text{em}} / \text{nm}$	$\Phi_f$
5	657	664	0.00035
6	788	801	0.018
7	938	979	0.0019
8	1108	1248	0.000077
9	1308	1467	-

### 1.4.3. Applications of carbon nanohoops

The unusual size-dependent physicochemical properties of CPPs have also driven research towards their practical applications.<sup>[117,146,183]</sup> CPPs can be brightly emissive in the solid state, furthermore, the solid-state emission was shown to be very similar compared to solution in terms of brightness if CPPs were incorporated into a solid-state matrix like PMMA which makes them great candidates for solid-state optoelectronic devices. The research in this direction is still in its early stages and only prototype devices were constructed until now.<sup>[184–186]</sup>

Bright and tunable visible light emission makes them attractive as fluorophores for sensing and for imaging in a biological system because CPPs, for example, have large Stokes shifts and their curvature prevents their stacking. CPPs have proven to be biocompatible as HeLa cells were visualized using water-soluble fluorescent CPPs (Figure 22). Cells showed no cytotoxicity even after being treated with up to roughly a 10  $\mu\text{mol dm}^{-3}$  aqueous solution of CPPs.<sup>[187–189]</sup> Biocompatibility of IR emitting donor–acceptor CPPs is of particular interest due to a high penetration depth of NIR light through human tissues.<sup>[190]</sup>

**Figure 22.** Structures of biocompatible CPPs.<sup>[187,189]</sup>

## 1. Introduction

Macrocyclic nature of  $[n]$ CPPs makes them viable as hosts for guests of suitable size and renders them to be good candidates for sensors if a change in emission could be detected upon guest binding. A guest with a convex surface, such as fullerene, exhibits a high binding constant to the concave cavity of a CPP due to non-covalent interactions between the  $\pi$ -systems.<sup>[191]</sup> Specifically,  $C_{60}$  fullerene with a diameter of 0.71 nm perfectly fits into the 1.38 nm cavity of  $[10]$ CPP (Figure 23) with distance between the outer surface of fullerene and inner surface of  $[10]$ CPP being 0.34 nm, which matches the interlayer distance in graphite, MWCNTs and CNS.<sup>[192]</sup> A high binding constant of  $(2.79 \pm 0.03) \times 10^6 \text{ dm}^3 \text{ mol}^{-1}$  in toluene was determined using fluorescence-quenching experiments while no binding was observed for other  $[n]$ CPP sizes.<sup>[193]</sup> An oval-shaped  $C_{70}$  fullerene fits both into  $[10]$ CPP and  $[11]$ CPP with binding constants in toluene being  $(8.4 \pm 0.3) \times 10^4$  and  $(1.5 \pm 0.1) \times 10^5 \text{ dm}^3 \text{ mol}^{-1}$ , respectively, determined by UV/Vis titration.<sup>[194]</sup> Fullerenes  $C_{76}$ ,  $C_{78}$  and lanthanide metallofullerenes  $\text{Ln}@C_{82}$  ( $\text{Ln} = \text{La}, \text{Gd}, \text{Tm}, \text{Lu}$ ) fit into  $[11]$ CPP too with high binding constants (Table 7).<sup>[195,196]</sup> The binding constant of fullerenes can be further tuned by extension of the  $\pi$ -system<sup>[197,198]</sup> or introduction of heteroatoms into the CPP.<sup>[199]</sup> Furthermore, encapsulation of  $C_{60}$  in  $[10]$ CPP complex in a metal-organic nanocapsule forming a matryoshka complex allows regioselective functionalization of  $C_{60}$  fullerene.<sup>[200]</sup>

**Table 6.** Binding constants  $K_A$  of fullerenes and metallofullerenes with  $[11]$ CPP in toluene determined by fluorescence quenching experiments.<sup>[195,196]</sup>

Fullerene	$K_A / 10^5$
$C_{76}$	$18.2 \pm 0.6$
$C_{78}$	$14.1 \pm 0.4$
$\text{La}@C_{82}$	$30.0 \pm 2.0^a$
$\text{Gd}@C_{82}$	$18.0 \pm 1.0$
$\text{Tm}@C_{82}$	$18.0 \pm 2.0$
$\text{Lu}_2@C_{82}$	$18.0 \pm 2.0$

<sup>a</sup> Binding constant reported in dichlorobenzene.

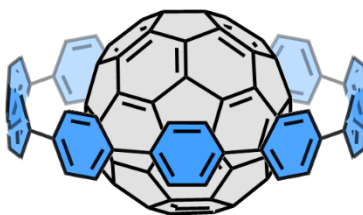


**Figure 23.** Supramolecular complex of  $C_{60}$  in  $[10]$ CPP.<sup>[193]</sup>

A porphyrin-functionalized CPP strongly binds fullerenes and azafullerenes ( $K_A > 10^5$ ) to form complexes which upon excitation produced long-lived charge separated states ( $\tau = 0.5 \mu\text{s}$ ).<sup>[201]</sup> Charge transfer complexes were also observed for  $\text{Li}^+@C_{60}$  in  $[10]$ CPP<sup>[202]</sup> and  $\text{Ln}@C_{82}$  in  $[11]$ CPP making donor-acceptor supramolecular complexes of CPPs interesting candidates for organic electronic devices.

High binding constants of fullerenes allowed synthesis of mechanically interlocked supramolecular assemblies.<sup>[191]</sup> A rotaxane using  $C_{60}$  as a binding center for  $[10]$ CPP was synthesized with functionalized  $C_{60}$  fullerenes as stoppers.<sup>[203]</sup>

Other guests bind into CPPs, too. For instance,  $\text{Cu}^I$  binds to nitrogen in aza-*m*[6]CPP and subsequent Huisgen azide-alkyne cycloaddition or Cadiot-Chodkiewicz coupling were performed inside of the

nano-hoop forming rotaxanes. The product rotaxanes exhibit a 10 to 100-fold increase of fluorescence intensity upon complexation of various metal guests which presents CPPs as viable sensors.<sup>[204]</sup> Similar strategy was also used for synthesis of CPP daisy chains<sup>[205]</sup> and catenanes.<sup>[206,207]</sup>

According to DFT,  $[n]$ CPPs which differ in size by five phenylenes show suitable fit to form a stable complex.<sup>[208,209]</sup> However, the formed  $[n]$ CPP: $[n+5]$ CPP complexes ( $n = 5-10$ ) have low association constants ranging from 50 to 750 dm<sup>3</sup> mol<sup>-1</sup> determined by <sup>1</sup>H-NMR titration.<sup>[210]</sup>

$[n]$ CPPs ( $n = 5-12$ ) were incorporated into single-molecule devices and their transport properties were measured in scanning tunneling microscope–break junction (STM–BJ) experiments.<sup>[211]</sup> Phenylenes in  $[n]$ CPPs strongly bind to gold atoms because of electron donation from a  $\pi$ -orbital on CPP to  $s$ -orbital of Au and electron back-donation from  $d$ -orbital of Au to an empty  $\pi^*$ -orbital on  $[n]$ CPP (Figure 24). Binding energies between CPPs and gold electrodes, which were calculated using DFT, decrease with an increasing size of the nano-hoop probably due to a less efficient orbital overlap between the CPP and Au as the curvature decreases. The STM–BJ experiment shows size-dependent conductance which decreases with increasing size. The authors conclude that conductance drops due to lowering of the HOMO–LUMO gap, however, we think that the drop in conductance is mainly caused by a longer conductance pathway for bigger sizes of  $[n]$ CPPs. Furthermore, the conductance of  $[n]$ CPPs is significantly higher than that of linear oligo-*para*-phenylenes at the same number of phenylenes. We find this comparison incorrect as the distance the current has to travel through an  $[n]$ OPP is twice as large as in a  $[n]$ CPP for the same number of phenylenes. Therefore, we suggest that the comparison should be done between corresponding  $[2n]$ CPPs and  $[n]$ OPPs.

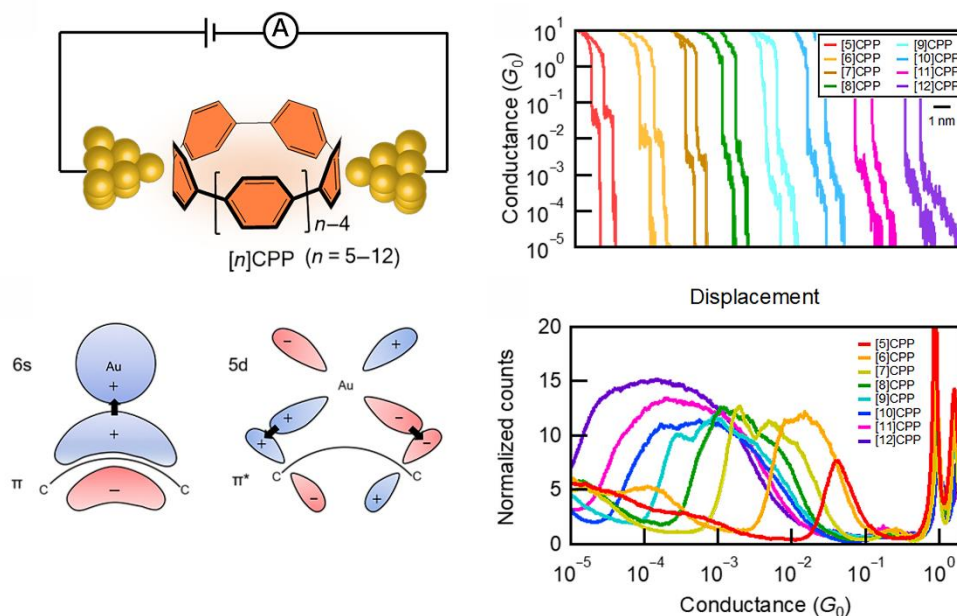


**Figure 24.** STM-BJ experiment (top) and orbital coupling between  $[n]$ CPPs and Au atoms. Adapted from ref.<sup>[211]</sup>

Lastly, the original purpose to synthesize  $[n]$ CPPs as seeds for the growth of SWCNTs<sup>[106]</sup> inspired efforts to mimic nanotube structures using supramolecular assemblies of CPPs. Columnar structures of CPPs resembling a nanotube were observed by X-ray structural analysis of carboxy-functionalized<sup>[133]</sup> and fluorinated CPPs (Figure 25).<sup>[212-215]</sup> The formation of tubular structures was attributed to hydrogen bonding and H–F interactions.

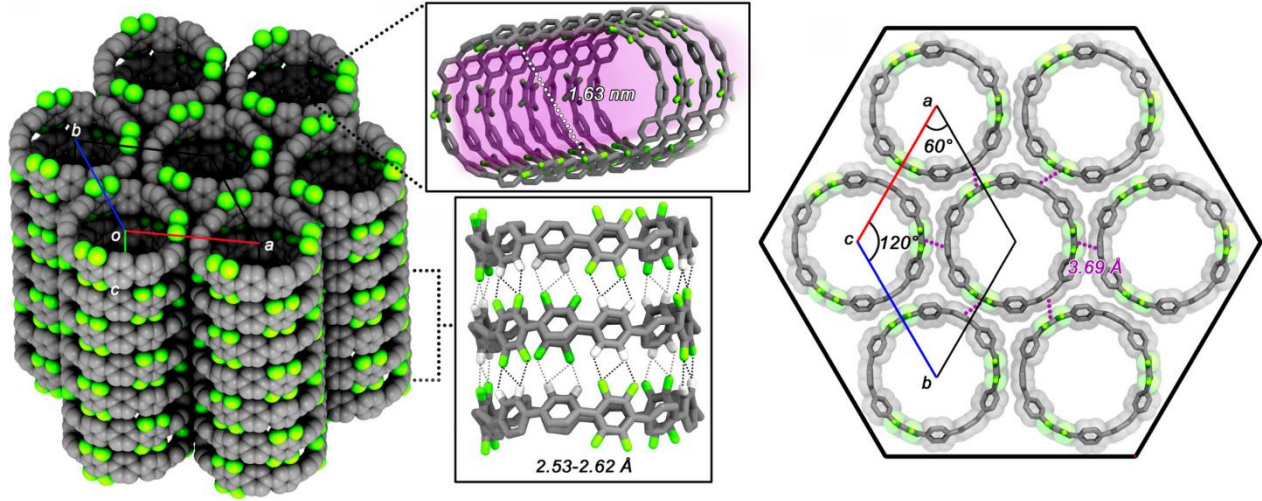


**Figure 25.** Columnar structures of fluorinated CPPs. Adapted from ref.<sup>[213]</sup>

#### 1.4.4. Chiral carbon nano hoops

Electronic circular dichroism (ECD) is a common method for determination of configuration of enantiomerically-pure chiral compounds, or enantiomeric excess.<sup>[216]</sup> Observed molar circular dichroism  $\Delta\epsilon$  can be expressed as differential absorption of left- and right-circularly polarized light by the chiral chromophore (Eq. 1):

$$\Delta\epsilon(\lambda) = \epsilon_L(\lambda) - \epsilon_R(\lambda) \quad (1)$$

where  $\epsilon_L$  and  $\epsilon_R$  are molar absorption coefficients of left- and right-circularly polarized light at a wavelength  $\lambda$ . The chiroptical response is usually evaluated by Kuhn's dissymmetry factor  $g_{abs}$ ,<sup>[217]</sup> which defines the contribution of left- or right-handed absorption to the total optical activity (Eq. 2):

$$g_{abs} = \frac{\Delta\epsilon(\lambda)}{\epsilon(\lambda)} = \frac{\epsilon_L(\lambda) - \epsilon_R(\lambda)}{\frac{1}{2}(\epsilon_L(\lambda) + \epsilon_R(\lambda))} \quad (2)$$

Circularly polarized luminescence (CPL)<sup>[216,218-223]</sup> is an emission analogous to circular dichroism and measures the difference of luminescence intensity  $\Delta I$  of left- and right-circularly polarized light by a chiral luminophore (Eq. 3):

$$\Delta I(\lambda) = I_L(\lambda) - I_R(\lambda) \quad (3)$$

where  $I_L$  and  $I_R$  are intensities of the emitted left- and right-circularly polarized light at a wavelength  $\lambda$ . Analogous to  $g_{abs}$ , luminescence dissymmetry factor  $g_{lum}$  defines the contribution of the left- or right-handed components to the total intensity of emitted light (Eq. 4):

$$g_{lum} = 2 \frac{\Delta I(\lambda)}{I(\lambda)} = 2 \frac{I_L(\lambda) - I_R(\lambda)}{I_L(\lambda) + I_R(\lambda)} \quad (4)$$

By definition, dissymmetry factors  $g_{abs}$  and  $g_{lum}$  range between  $-2$  and  $+2$ , values obtained for a perfect absorption or emission of circularly polarized light with a single handedness. CD and CPL spectroscopies both characterize electronic transitions in a molecule reflecting the structural properties of ground and excited electronic states, respectively.<sup>[218]</sup> Electronic transitions can be expressed by a rotatory strength  $R$ ,



which is a parameter dependent on the electric and magnetic transition dipole moments  $\mu$  and  $m$  and the angle  $\theta$  between them (Eq. 5):

$$R = |\mu||m| \cos \theta \quad (5)$$

The intensities of respective transitions are defined by another parameter, dipole strength  $D$ , which is also related to the transition dipole moments  $\mu$  and  $m$  (Eq. 6):

$$D = |\mu|^2 + |m|^2 \quad (6)$$

Rotatory strength  $R$  and dipole strength  $D$  then define dissymmetry factors  $g_{abs}$  and  $g_{lum}$  for ground and excited states, respectively (Eq. 7):

$$g = 4 \frac{R}{D} \quad (7)$$

Dissymmetry factors  $g_{abs}$  and  $g_{lum}$  can be predicted with a reasonable accuracy by TD-DFT quantum chemical calculations, furthermore, simulations of CD spectra are a common tool for configuration assignment of new chiral compounds.<sup>[224]</sup>

Chiral luminophores have received considerable attention in the recent years due to promising applications in optoelectronic devices where the main challenge is search of small organic chiral luminophores with high  $g_{lum}$  values. However, they are commonly found in the range of  $\sim 10^{-3}$ .<sup>[216,220,223]</sup> This means that approximately only every thousandth emitted photon is circularly polarized. Currently, small organic luminophores are outperformed by lanthanide complexes which can achieve very high  $g_{lum}$  values exceeding  $\pm 1$ .<sup>[225]</sup> Nevertheless, small organic luminophores are highly desirable because of possible tunability of emission wavelength and quantum yield by structural modification, and good processability in a device manufacturing process.

The quantum yield of emission  $\Phi_{fl}$  is also an important parameter for circularly polarized luminophores. A recent study by Mori<sup>[222]</sup> investigated the relation between  $\Phi_{fl}$  and dissymmetry factor  $g_{lum}$  because luminophores with a high quantum yield usually display low  $g_{lum}$  and *vice versa*. Rigid molecules with high  $\Phi_{fl}$  were proposed to narrow down the search since they can be fine-tuned by organic synthesis and, perhaps, reach a high  $g_{lum}$  while preserving the quantum yield.<sup>[226,227]</sup> Indeed, Isobe group reported high  $g_{lum}$  (up to 0.15) and  $\Phi_{fl}$  (0.80) for rigid cyclochrysenylene macrocycles (Figure 26).<sup>[228]</sup> However, the structure–property relationship to achieve such high  $g_{lum}$  values is not yet understood.<sup>[226,227]</sup> Therefore, systematic studies of rigid macrocycles are still vital for a development of a rational design of new chiral luminophores.

Chiral derivatives of CPPs are excellent candidates for circularly polarized luminophores considering their high quantum yield of emission.<sup>[229]</sup> A number of CPPs that incorporate polyaromatic moieties such as anthracene,<sup>[151,230]</sup> naphthalene<sup>[231]</sup> and dibenzopentalene<sup>[232,233]</sup> and other units<sup>[234–237]</sup> were synthesized, however, their CPL properties were not investigated often due to low configurational stability or low solubility.

Only a handful of chiral CPPs had their CPL properties investigated. For instance, a pentiptycene doublehoop was synthesized by the approach of Jasti, enantiomers of which were separated using HPLC with a chiral stationary phase. Dissymmetry factor  $g_{lum}$  was measured to be  $3.4 \times 10^{-3}$  with a high quantum yield of 0.63 (Figure 27).<sup>[238]</sup>

## 1. Introduction

A figure-eight CPP lemniscate was prepared similarly from a bis-carbazole macrocycle. Enantiomers were resolved using SFC with a chiral stationary phase and chiroptical properties investigated. The values of  $g_{lum}$  and  $\Phi_{\eta}$  were determined to be  $3.4 \times 10^{-3}$  and 0.36, respectively.<sup>[158]</sup>

Similar results were obtained for a binaphthyl ( $g_{lum} = 4.4 \times 10^{-3}$  and  $\Phi_{\eta} = 0.17$ )<sup>[186]</sup> and helicene-extended nano hoops ( $g_{lum} = 4.9 \times 10^{-3}$  and  $\Phi_{\eta} = 0.40$ ).<sup>[239]</sup>

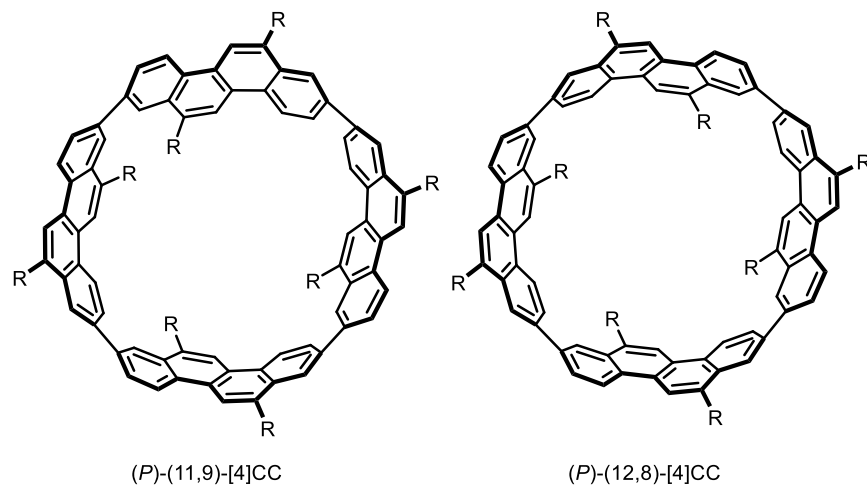


**Figure 26.** Rigid cyclochrysenylene macrocycles.<sup>[228]</sup>

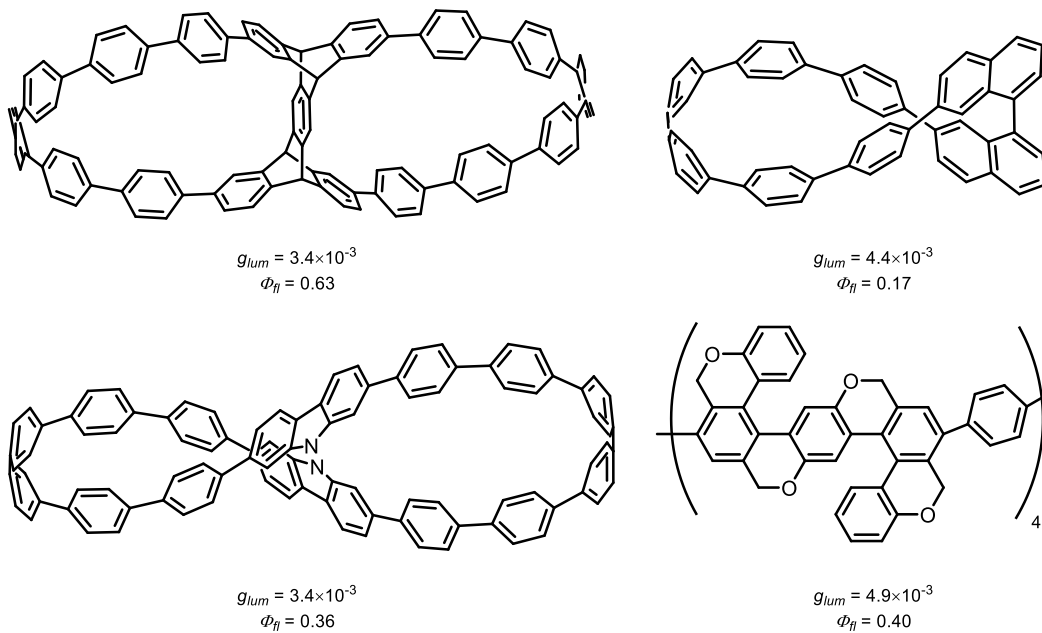


**Figure 27.** Structures of chiral carbon nano hoops and their respective  $g_{lum}$  and  $\Phi_{\eta}$ .<sup>[158,186,238,239]</sup>

## 2. Spiral *para*-phenylenes

### 2.1. Aim of the work

Small fragments of carbon nanotubes have been proposed as precursors of a bottom-up synthesis of uniform SWCNTs.<sup>[106]</sup> However, at the beginning of my PhD studies, no molecular precursors for CNSs were known. The challenge lies in the supramolecular nature of CNSs, structure of which is stabilized only by the weak van der Waals interactions. Considering the diameter of  $\sim 2$  nm for the smallest experimentally observed CNS, a molecular fragment of an armchair CNS (Figure 28, middle) of such diameter would possess strain energy of at least  $35 \text{ kcal mol}^{-1}$  because the strain energy of [16]CPP, which has a diameter of 2.2 nm, is  $35.6 \text{ kcal mol}^{-1}$ .<sup>[110]</sup> However, the van der Waals interaction between two molecules of benzene is no more than  $4 \text{ kcal mol}^{-1}$  (SCS-MP2/aug-cc-pVTZ level of theory).<sup>[240]</sup> Therefore, the interaction between terminal phenylenes would be too weak to stabilize the topology of a molecular spiral and a covalent tether, a topology clip, must be introduced to stabilize the curvature of the  $\pi$ -system (Figure 28, right).

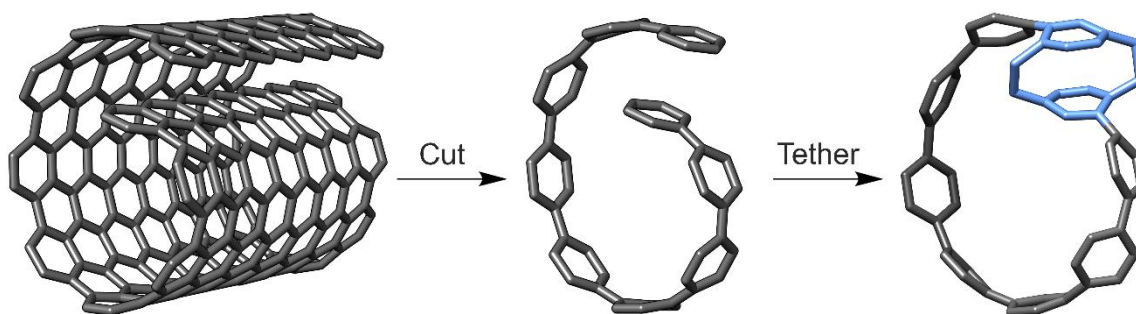


**Figure 28.** Design of armchair CNS cut-offs.

In this work, we propose a series of carbon nanohoops, which incorporate a *pseudopara*-[2.2]paracyclophane (*pPCP*) moiety into the structure of a [n]CPPs as a topology clip to create molecular representatives of armchair carbon nanoscrolls (Figure 28). We name the resulting carbon nanohoops as spiral *para*-phenylenes abbreviated as *p*[*n*]SPPs where *n* defines the number of phenylenes in the spiral and *p* denotes the *pPCP* clip. *pPCP* moiety is a good candidate for a clip because ethylene bridges are short enough to keep the edges of the spiral loop within the distance observed between the individual folds in a CNS. In fact, the distance between the benzene rings in a *pPCP* determined from X-ray structural analysis is 0.31 nm.<sup>[241]</sup> Although it is slightly shorter than the 0.34 nm found in CNSs ( $h_1$ , Figure 6), *pPCP* serves reasonably well to structurally approximate a molecular CNS. Furthermore, the chemistry of regioselective functionalization of a PCP is well explored which warrants a good synthetic accessibility of required molecular building blocks.<sup>[242]</sup>

The clip also serves to lock the chirality of the molecular CNS. Recall that the chirality in CNS is fluctuating due to a rapid equilibrium between different CNS configurations (*vide supra*). Therefore, if an [n]SPP was utilized as a template to grow an extended carbon nanostructure, a CNS, in a bottom-up approach, the covalent tether should preserve the chirality providing a uniform sample. It is necessary to point out that the structure grown from small [n]SPPs would not represent a full nanoscroll and it would rather resemble a bundle of hay opening the structure with the distance from the molecular [n]SPP template to release the strain (Figure 29).

## 2. Spiral para-phenylenes

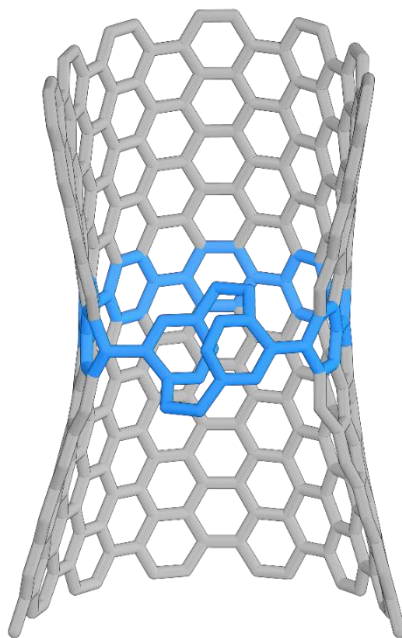


**Figure 29.** A model of a carbon nanoscroll grown using a  $p[n]$ SPP template.

We were also interested in the photophysical and chiroptical properties of  $[n]$ SPPs as they could be utilized as chiral luminophores because  $p$ PCP becomes chiral when incorporated into a macrocycle.<sup>[243]</sup> However, chiral  $p$ PCPs racemize via a rotation around single bonds connected to the PCP moiety. Racemization can be hampered by bulky substituents that have to thread through the macrocycle in order to racemize.<sup>[244]</sup>

Additionally, we have explored  $[n]$ SPPs with *pseudometa*-connection in the PCP moiety (Figure 30) to establish a clear structure–property relationship. Moreover,  $m[n]$ SPPs should not racemize because racemization would require two rotations of  $180^\circ$  of each aromatic ring in the  $m$ PCP which is thermodynamically very demanding. From now on, we will refer to the respective isomers of nano hoops as  $p[n]$ SPPs and  $m[n]$ SPPs, while the term  $[n]$ SPPs will be used generally when both isomers do not need to be distinguished.

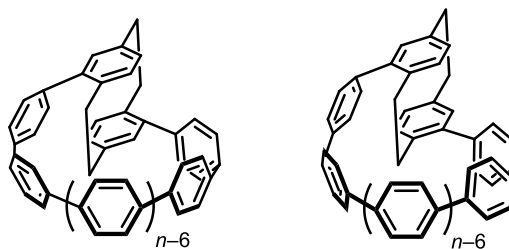


**Figure 30.** Structure of the proposed  $p[n]$ SPPs (left) and  $m[n]$ SPPs (right).

The goal of this project was to synthesize selected sizes of  $p[n]$ SPPs and  $m[n]$ SPPs, measure, and compare photophysical and chiroptical properties to theory.

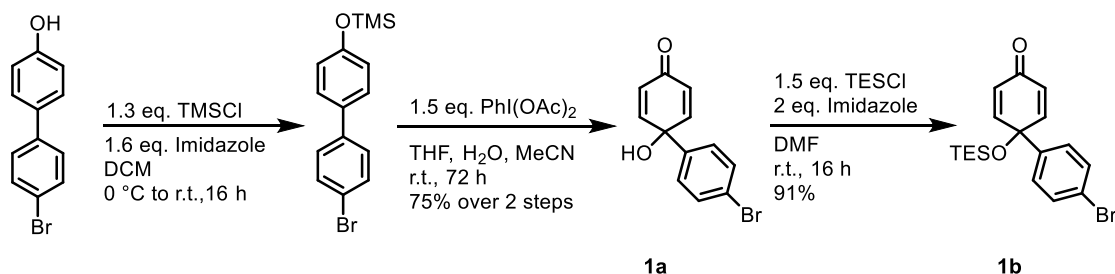
## 2.2. Results and Discussion

### 2.2.1. Synthesis of *p*[9]SPP

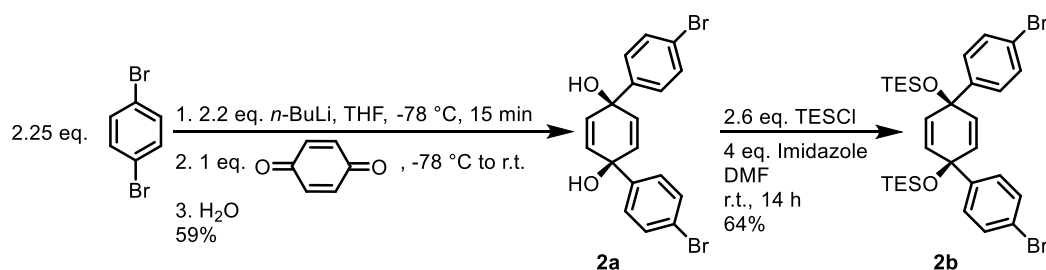
The synthetic protocols and characterization of the prepared compounds are provided in the Appendix.

We designed the synthesis of *p*[9]SPP using the approach of Jasti and Yamago.<sup>[116,130,131]</sup> The synthesis starts from commercially available 4-bromo-4'-hydroxybiphenyl which is protected with TMSCl and used without purification in the following oxidation using (diacetoxyiodo)-benzene to afford hydroxy-ketone **1a** in a 75% yield over two steps. In the next step, **1a** is treated with TESCl to afford silyl-protected building block **1b** in 91% yield (Scheme 2). A nucleophilic addition of an excess of mono-lithiated dibromo-benzene on *p*-benzoquinone affords bent building block **2a** in a 59% yield with excellent diastereoselectivity, which is treated with TESCl to afford silyl-protected building block **2b** in a 64% yield (Scheme 3).

Double-lithiation of **2b** followed by 2 equivalents of **1b** and *in situ* protection using MeI affords building block **3a** in a 71% yield. In the next step, **3a** was doubly-lithiated with *n*-BuLi followed by quenching with *i*-PrOBpin to form **3b** in an excellent 99% yield (Scheme 4). Note that the synthesis of **3b** is a part of the publication in Chapter 3 (labeled as **4**) and, therefore, its synthesis can be found in the corresponding section of the Appendix.

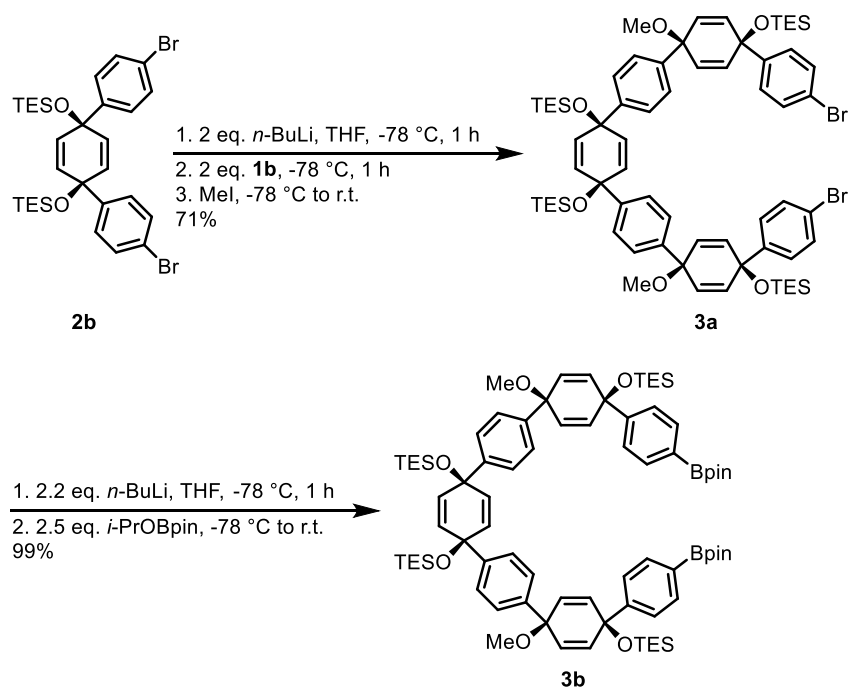


Scheme 2.



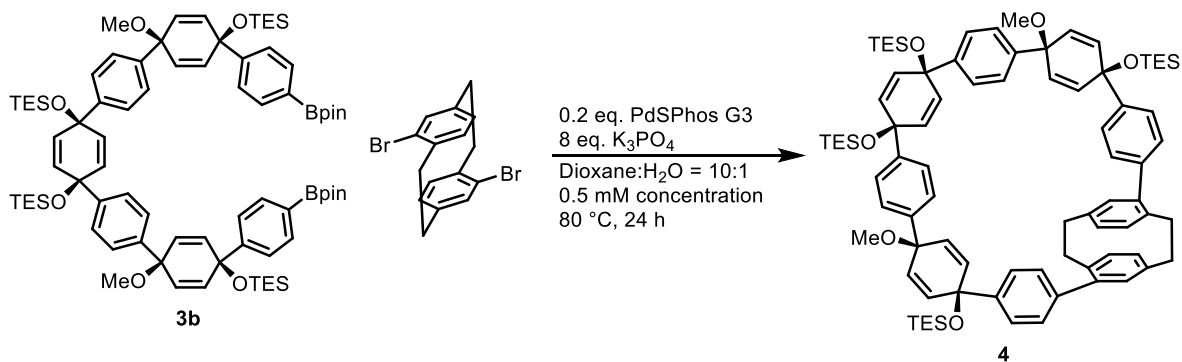
Scheme 3

## 2. Spiral para-phenylenes

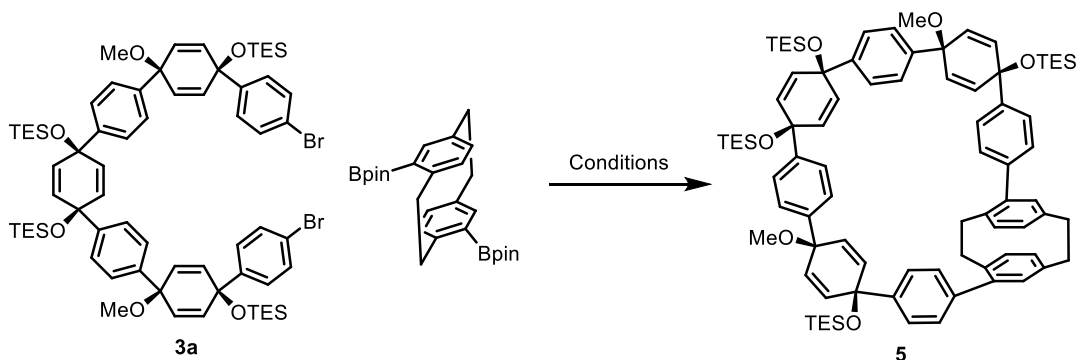


### Scheme 4.

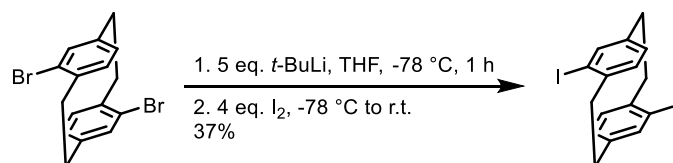
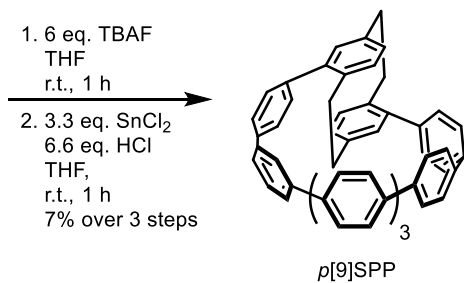
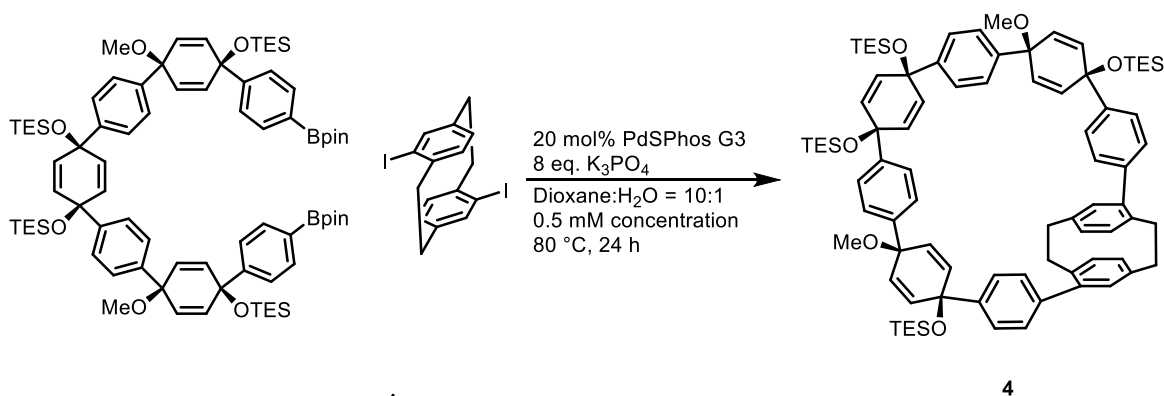
In our initial attempt to prepare *p*[9]SPP, we used a Suzuki-Miyaura cross-coupling between **3b** and literature-known *p*-dibromo-[2.2]paracyclophane.<sup>[245]</sup> We observed a deprotection of the silyl groups in **3b** followed by a decomposition of the material instead of the formation of macrocycle **4** (Scheme 5). We performed a screening of different reaction conditions that involved selected palladium catalysts, solvents, bases and temperatures for this reaction but we never managed to isolate macrocycle **4**. We also tested other position of the bromides for the cross-coupling reaction and use *m*-functionalized [2.2]paracyclophane to form a less strained macrocycle **5** (Scheme 6). All these attempts were also unfortunately unsuccessful.



### Scheme 5

**Scheme 6**

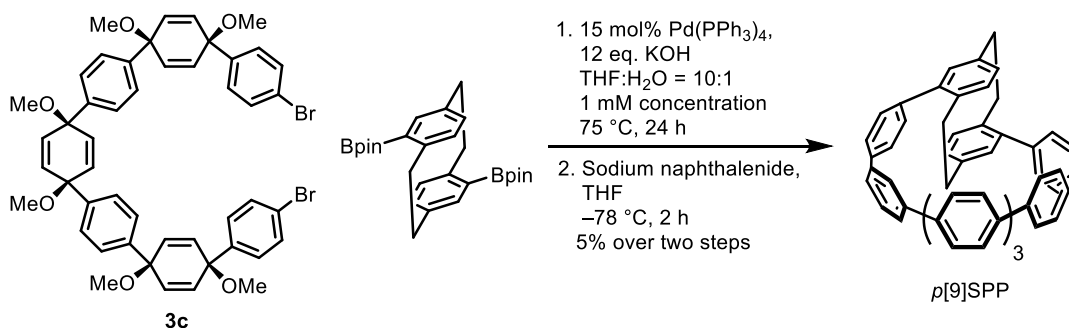
Upon replacement of bromines for iodines via a sequence of lithium-bromide exchange followed by addition of iodine (Scheme 7), the cross-coupling macrocyclization was finally successful. Macrocycle **4** was treated with 6 eq. of TBAF at room temperature and aromatized with  $\text{H}_2\text{SnCl}_4$  to obtain  $p[9]\text{SPP}$  that could be isolated in a 7% yield over three steps (Scheme 8). Our efforts to isolate macrocycle **4** before the deprotection and aromatization steps have been unsuccessful too due to a low stability of this compound, likely resulting in an overall low yield of the entire reaction sequence.

**Scheme 7****Scheme 8.**

## 2. Spiral para-phenylenes

However, at the time when our first synthesis of  $p[9]$ SPP was accomplished, the synthesis and characterization of the compound was reported by Du *et al.*<sup>[246]</sup>. This led us to reconsider the major objective of the project and to abandon the synthesis of  $[n]$ SPPs as we suspected that other groups might be performing their synthesis. Indeed, a series of nano hoops similar to  $m[n]$ SPPs with additional acetylene linkers between the phenylenes and the PCP moiety was synthesized by Jiang *et al.*<sup>[247]</sup> earlier this year.

In the synthesis of  $p[9]$ SPP, Du *et al.* used more stable bent building block **3c** (Scheme 9) to form a relatively strain-free macrocycle via a Suzuki-Miyaura cross-coupling followed by aromatization using sodium naphthalenide to afford  $p[9]$ SPP.<sup>[246]</sup> We managed to synthesize the compound using this approach, but we never managed to reach the yield of 22 % reported by Du in his original publication.

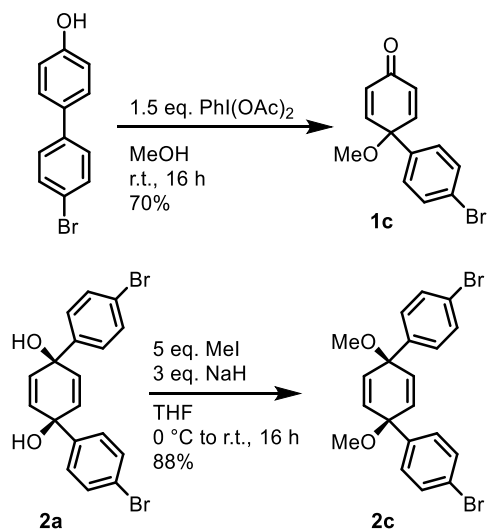


**Scheme 9.** Synthesis of  $p[9]$ SPP using the conditions published by Du *et al.*<sup>[246]</sup>

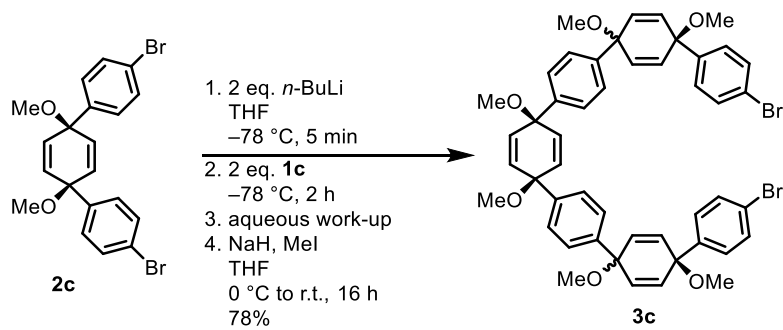
Although **3c** is a stable building block unlike **3a**, it also represents a disadvantage in the approach of Du because **3c** is always used as a mixture of diastereomers, which is clearly visible in the published <sup>1</sup>H NMR spectra. The authors did not comment that the sample of **3c** contains, in fact, other diastereomers in any of their publications where **3c** is used in the synthesis of a number of carbon nano hoops.<sup>[197,231,237,246,248]</sup> This precludes to calculate the efficiency of the macrocyclization steps because the ratio of individual diastereomers is not known. The reason that samples of **3c** are always a mixture of diastereomers arises from its synthesis that we explored in more detail and describe below.

First, compound **1c** was prepared via oxidation of 4-bromo-4'-hydroxybiphenyl using (diacetoxyiodo)-benzene in dry methanol in 70% yield while **2c** was prepared by treatment of **2a** with methyl iodide under basic conditions in 88% yield (Scheme 10). The preparation of **3c** involves two nucleophilic additions of doubly-lithiated **2c** to two units of **1c** which results in the formation of a mixture of three diastereomers in a 78% yield (Scheme 11). We performed the synthesis of **3c** and isolated the all-*cis* diastereomer using HPLC (see Appendix). This allowed us to assign the resonances of its methoxy groups in <sup>1</sup>H-NMR spectrum and assign the resonances to the other two diastereomers in the mixture (Figure 31). We could thus estimate their ratio in the mixture by comparison of the areas under the individual peaks. The mixture consists of ~8% *trans-trans*, ~25% of *cis-trans* and ~67% of *cis-cis* diastereomers. Only the latter can successfully form the desired macrocycle as described in Scheme 9.





Scheme 10



Scheme 11

## 2. Spiral para-phenylenes

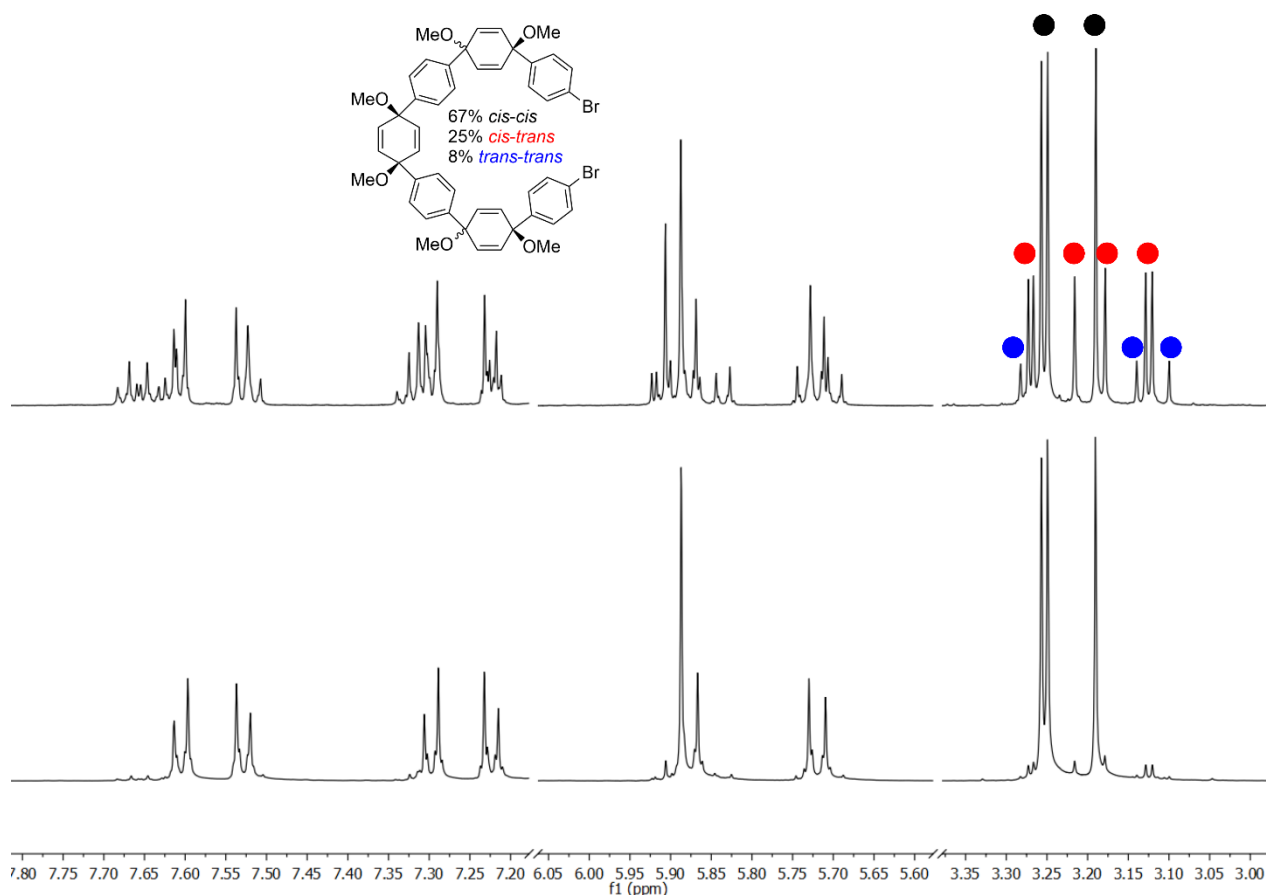


**Figure 31.** <sup>1</sup>H-NMR spectrum of mixture with assigned methoxy signals to each diastereomer (top) and cis-cis diastereomer (bottom).

At this point, we decided to further pursue only the computational part of this project as we have shifted our synthetic efforts towards the helicene carbon nano hoops described later in Chapters 3 and 4.

### 2.2.2. Conformational analysis of [*n*]SPPs

From the computational studies on [*n*]CPPs by Itami<sup>[110]</sup> and Bachrach<sup>[111]</sup> we know that the phenylene units prefer an alternating orientation to each other. This is possible for [*n*]CPPs with an odd number of phenylenes, however, a single twist in a terphenyl sub-unit is necessary (helical orientation, Figure 9) for an even number of phenylenes.

Therefore, we performed conformational analysis on *p*[*n*]SPPs and *m*[*n*]SPPs (*n* = 9,10) to determine: (a) the preferential orientation of the phenylene units relative to the PCP moiety, (b) a dependency on even or odd number of phenylenes in the nano hoops, (c) the twist localization in [*n*]SPPs if one is necessary. Thus, the differences between conformers are the orientation of phenylene units relative to the PCP moiety and to each other.

Here, we chose *p*[10]SPP as the representative example since *p*[*n*]SPPs with an even number of phenylenes cannot be arranged in an alternating fashion and at least one twist in a terphenyl sub-unit is necessary. The lowest energy conformer (Table 7 and A1, Figure 32) possessed the alternating orientation of the phenylene units relative to each other and the twist was localized at the phenylene attached directly to the PCP moiety from the inner side of the hoop (Conformer 1) rather than in the middle of the hoop (Conformer 2) or the

outer side the hoop (Conformer 3). This was also found for other sizes of  $p[n]$ SPPs with an even number of phenylenes.  $p[n]$ SPPs with an odd number of phenylenes can always be arranged in the alternating fashion (Figure 33, ) and these conformers were the lowest in energy similarly to parent  $[n]$ CPPs (Table A2).<sup>[110]</sup>

The situation was reversed in  $m[n]$ SPPs. Here, the phenylenes can alternate when  $n$  is even. Indeed, such geometries represent the lowest-energy conformers (Table A3, Figure 34, right). For an odd number of phenylenes, a twist is necessary and it is located at either side of the PCP moiety (Table A4, Figure 34, left; the twist is located on the left side). The other sizes of  $p[n]$ SPPs and  $m[n]$ SPPs were then modeled and optimized according to conformational preferences determined for the smaller nano hoops.

It is important to note that the barriers of rotation of the phenylenes in the hoops are likely to be small (3–10 kcal mol<sup>-1</sup> [12]CPP)<sup>[110]</sup> and the conformers are close in energy (Table 7). Thus, their Boltzmann distribution should be used to simulate any macroscopic properties accurately. The qualitative comparison of the properties can, however, be performed with the lowest energy conformer for each nano hoop to study the structure–property relationship.

**Table 7.** Energies  $E_{corr}$  (0 K,  $E_{el}$  + ZPVE ) and relative energies conformers of  $p[10]$ SPP. Single point energies  $E_{el}$  obtained with the cc-pVTZ basis set on D3-B3LYP/6-31g(d) geometries. Zero-point vibrational energy (ZPVE) correction is unscaled.

Conformer	$E_{corr}$ / Hartree	Relative energy / kcal mol <sup>-1</sup>
1	-2466.49249	0.00
2	-2466.49359	0.69
3	-2466.493151	0.28

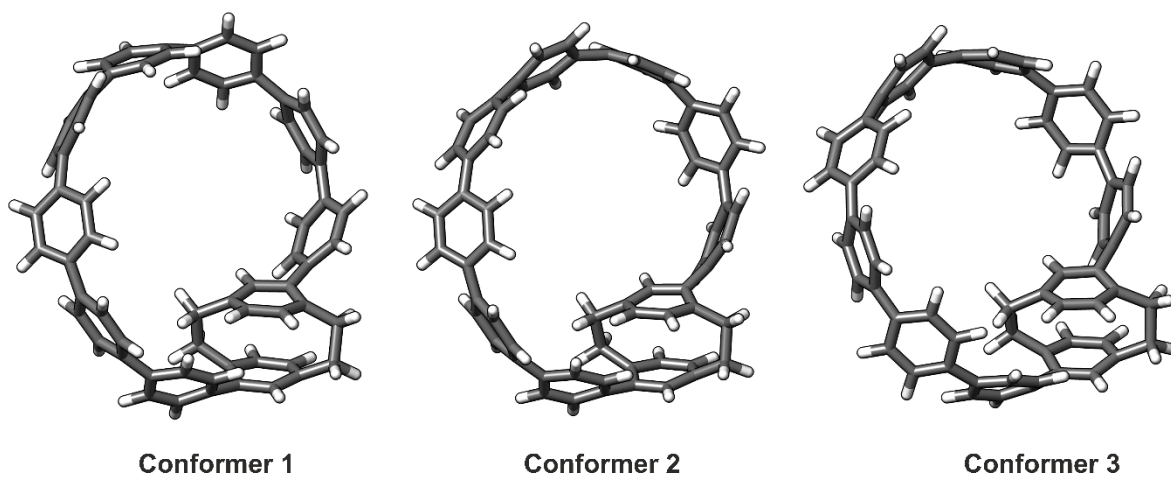


**Figure 32.** Selected conformers of  $p[10]$ SPP.

## 2. Spiral para-phenylenes

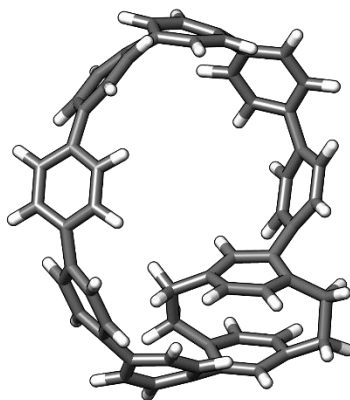


**Figure 33.** The lowest energy conformer of  $p[9]$ SPP.

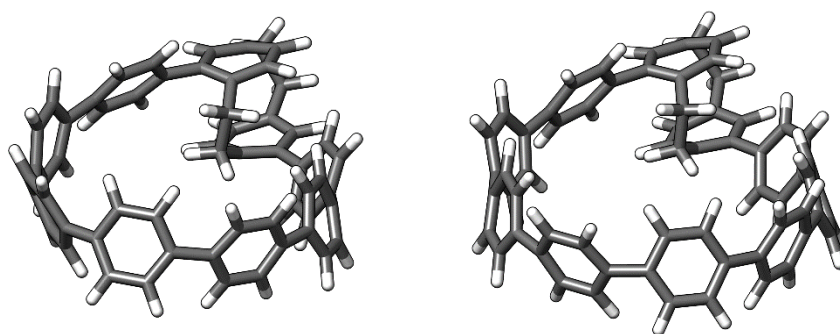
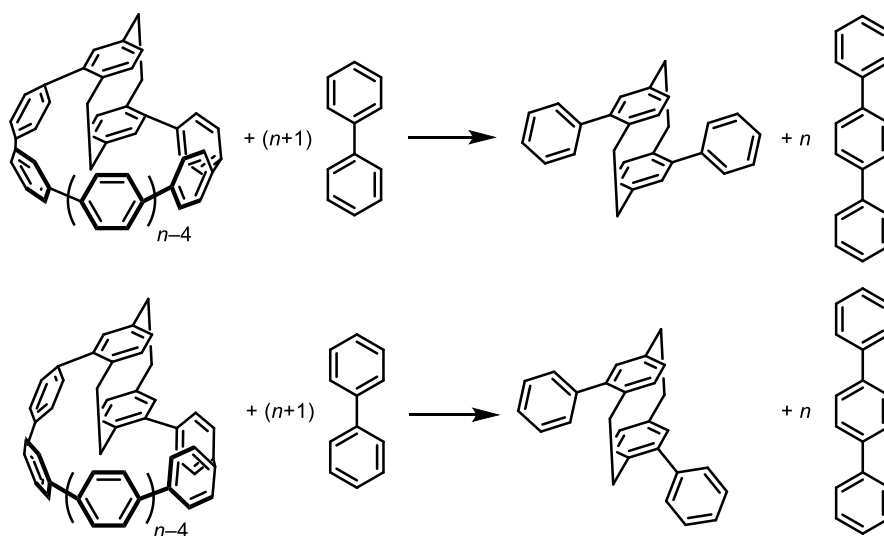


**Figure 34.** The arrangement of phenylene units in  $m[n]$ SPPs,  $n = 9$  (left), 10 (right) in the lowest-energy conformers.

### 2.2.3. Calculated properties of $[n]$ SPPs

Having found the lowest energy conformers for all molecules, we used hypothetical homodesmotic reactions (Scheme 12) to estimate the strain energy in each nano hoop (Figure 35). The strain energies were calculated to range from 35 to 100 kcal mol<sup>-1</sup> for  $p[n]$ SPPs and 27 to 73 kcal mol<sup>-1</sup> for  $m[n]$ SPPs depending on the size of the nano hoops.  $p[n]$ SPPs were found to be considerably more strained than  $m[n]$ SPPs of the same size, although this difference is less pronounced for larger sizes of  $[n]$ SPPs. Furthermore, the strain–size relationship follows a single trend in both  $p[n]$ SPPs and  $m[n]$ SPPs without observable differences between  $[n]$ SPPs with an odd or even number of phenylenes.

StrainViz calculations were used to visualize the local strain in  $p[9]$ SPP and  $m[9]$ SPP (Figure 36). The most strain is localized at the inner side of the spiral which corresponds to the localization of the twist in  $p[n]$ SPPs when  $n$  is even.  $m[n]$ SPPs have the strain energy spread more evenly across all phenylenes.



Scheme 12.

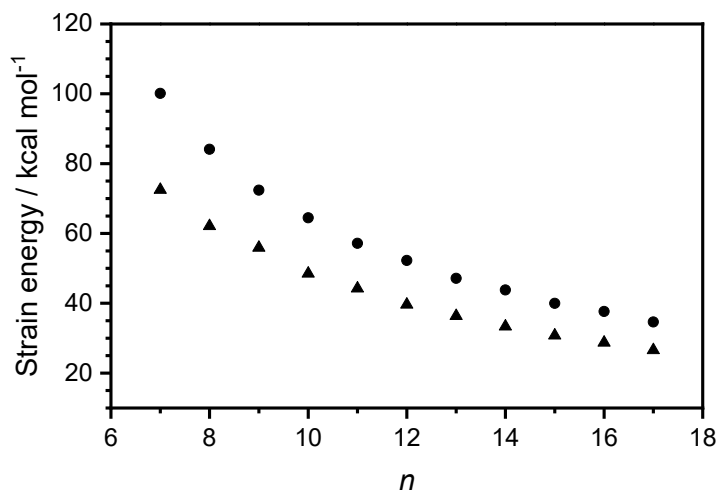


**Figure 35.** Total strain energies of  $p[n]$ SPPs (circles) and  $m[n]$ SPPs (triangles) in kcal mol<sup>-1</sup> calculated at D3-B3LYP/6-31g(d) level of theory.

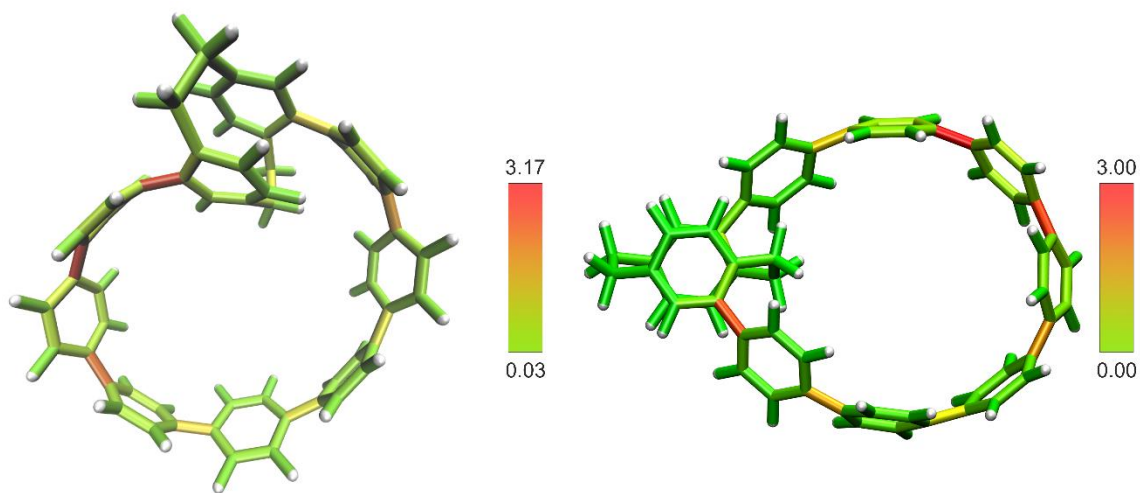


**Figure 36.** StrainViz visualization of total strain distribution (in kcal mol<sup>-1</sup>) in  $p[9]$ SPP (left) and  $m[9]$ SPP (right).

Photophysical properties are connected to the HOMO–LUMO gaps which were estimated with TD-DFT using three different density functionals, CAM-B3LYP, BMK and M06-2X with 6-31g(d) basis set. All functionals behaved consistently and provided similar results. HOMO–LUMO gaps at CAM-B3LYP/6-31g(d) level of theory (Figure 37, see Appendix Tables A5–A11 for other functionals) increase with the increasing number of phenylene units similar to  $[n]$ CPPs.<sup>[138]</sup>  $p[n]$ SPPs possess smaller HOMO–LUMO gaps than  $m[n]$ SPPs likely due to higher strain while both series display separate curves for SPPs with the odd and even number of phenylenes. The effect is more pronounced in  $m[n]$ SPPs. This result is not surprising and the same effect of the curvature on the energies of the frontier MOs (FMOs) was already identified in parent CPPs.<sup>[144,148]</sup>

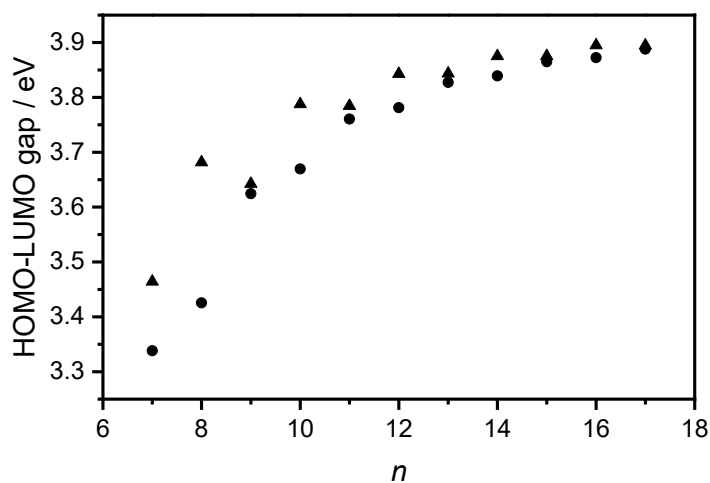


**Figure 37.** HOMO–LUMO gaps in eV for  $p$ -[ $n$ ]SPPs (circles) and  $m$ -[ $n$ ]SPPs (triangles) calculated at CAM-B3LYP/6-31g(d) level of theory.

The individual FMO energies (Figure 38) were estimated by calculating the energy of the HOMO at the CAM-B3LYP/6-31g(d) level of theory. The energy of the LUMO was estimated by addition of the HOMO–LUMO gap to the energy of the HOMO because DFT fails to provide accurate energies of unoccupied MOs.<sup>[249]</sup> The HOMO energies of  $p$ [ $n$ ]SPPs are higher than that of  $m$ [ $n$ ]SPPs likely due to higher curvature, while the LUMO energies are roughly the same in both series which causes the odd/even effect.

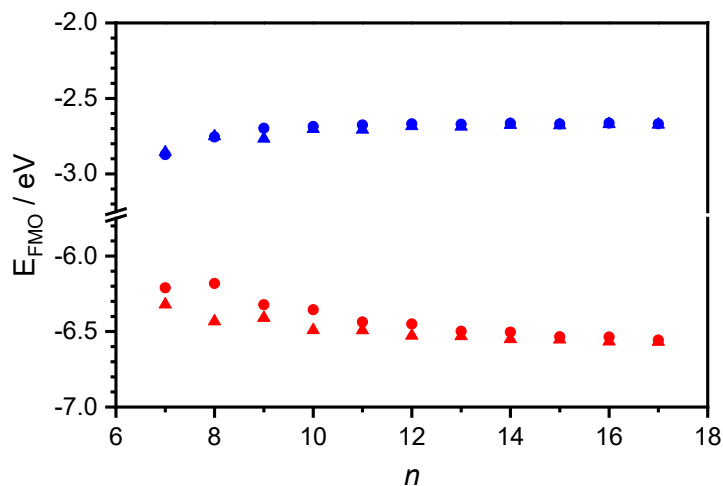


**Figure 38.** The HOMO (red) and the LUMO (blue) energies in eV for  $p$ [ $n$ ]SPPs (circles) and  $m$ [ $n$ ]SPPs (triangles) calculated at CAM-B3LYP/6-31g(d) level of theory.

## 2. Spiral para-phenylenes

Both CD and CPL can be predicted using TD-DFT on the geometries of the ground and the excited state, respectively. Oscillatory strength is an important parameter that characterizes the intensity of the transition and is related to absorption coefficient and intensity of emission.  $p[n]$ SPPs have much smaller oscillatory strengths as compared to  $m[n]$ SPPs indicating they are likely going to have smaller molar circular dichroism  $\Delta\epsilon$ . The oscillatory strengths of the transitions on the excited states are comparable for both series. We can also predict Stokes shifts by taking the difference between the energies of the first transition on the ground and the excited state (Tables A5–A16).

We used TD-DFT calculations to predict both CD and CPL and the calculations on  $Rp$ -enantiomers are presented. We calculated the absorption dissymmetry factors  $g_{abs}$  using the transition dipole moments  $\mu$  and  $m$  extracted from the TD-DFT calculations on the ground state geometries (Figure 39, see Figures A6 and A7 for other functionals).  $m[n]$ SPPs have rather similar  $g_{abs}$  values of  $0.8\text{--}2.0\times 10^{-2}$  regardless of the size, while  $p[n]$ SPPs show a stronger size-dependence with  $g_{abs} = 2.1\text{--}6.8\times 10^{-2}$ . Interestingly,  $p[n]$ SPPs with odd  $n$  show a gradual decrease of  $g_{abs}$  values with increasing size while  $p[n]$ SPPs with even  $n$  have a maximum at  $n = 12$  with a steeper decrease of  $g_{abs}$  as  $n$  increases or decreases. We hypothesize that the twist present in the even-numbered  $p[n]$ SPPs has a significant influence on the transition dipole moments  $\mu$  and  $m$  and the angle  $\theta$  between them. These quantities may be conformer-dependent and this aspect needs to be investigated in closer detail.

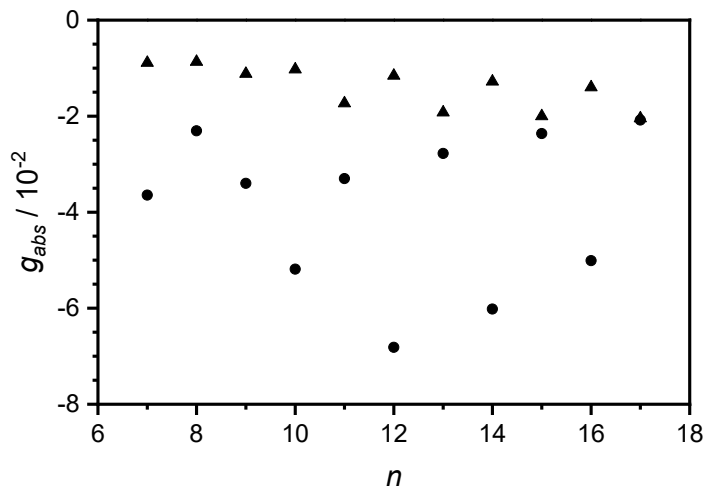


**Figure 39.** The dissymmetry factors  $g_{abs}$  for  $p[n]$ SPPs (circles) and  $m[n]$ SPPs (triangles) calculated at CAM-B3LYP/6-31g(d) level of theory.

We then optimized the geometries of the first excited states for each molecule in order to predict the properties of the circularly polarized luminescence. Luminescence dissymmetry factors  $g_{lum}$  were calculated from the corresponding  $\mu$  and  $m$  from these calculations (Figure 42, see Figures A8 and A9 for other functionals). The resulting  $g_{lum}$  values are, on average, an order of magnitude lower than the corresponding  $g_{abs}$  values.



In order to explain the significant decrease of  $g_{lum}$  compared to  $g_{abs}$ , we visualized the transition dipole moments  $\mu$  and  $m$  for selected  $p[n]$ SPPs ( $n = 9, 12, 16$ ; Figure 41) and the corresponding  $m[n]$ SPPs (Figure 42) in the ground and the first excited states. Generally, vectors  $m$  are perpendicular to the planes of the  $p[n]$ SPP and  $m[n]$ SPP macrocycles and the amplitudes gradually increase with increasing  $n$  in both states. Moreover, there is no significant change in the direction of the vectors when we compare the absorption and emission. For  $p[n]$ SPPs in the ground state, the vectors  $\mu$  are rather small as is expected because the  $S_0 \rightarrow S_1$  is only partially allowed as in  $m[n]$ CPPs. In the first excited state,  $\mu$  increases in amplitude and the vector faces away from the PCP moiety. A similar increase in  $\mu$  as well as the change in the direction are observed in  $m[n]$ SPPs when compared to the absorption.

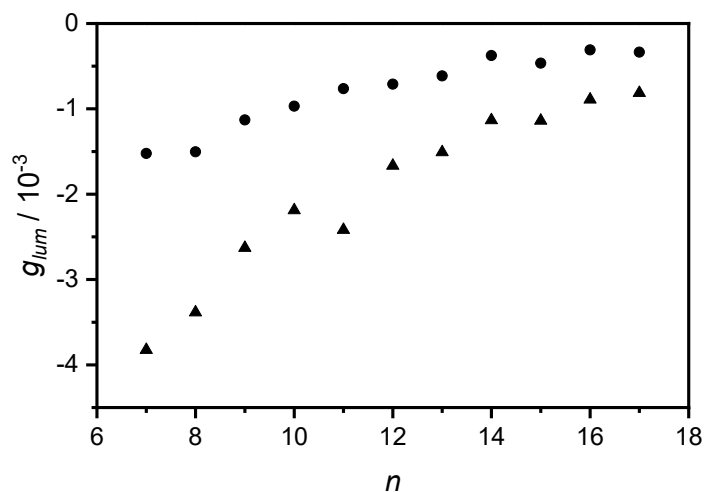


**Figure 40.** Dissymmetry factors  $g_{lum}$  for  $p[n]$ SPPs (circles) and  $m[n]$ SPPs (triangles) calculated at CAM-B3LYP/6-31g(d) level of theory.

## 2. Spiral para-phenylenes

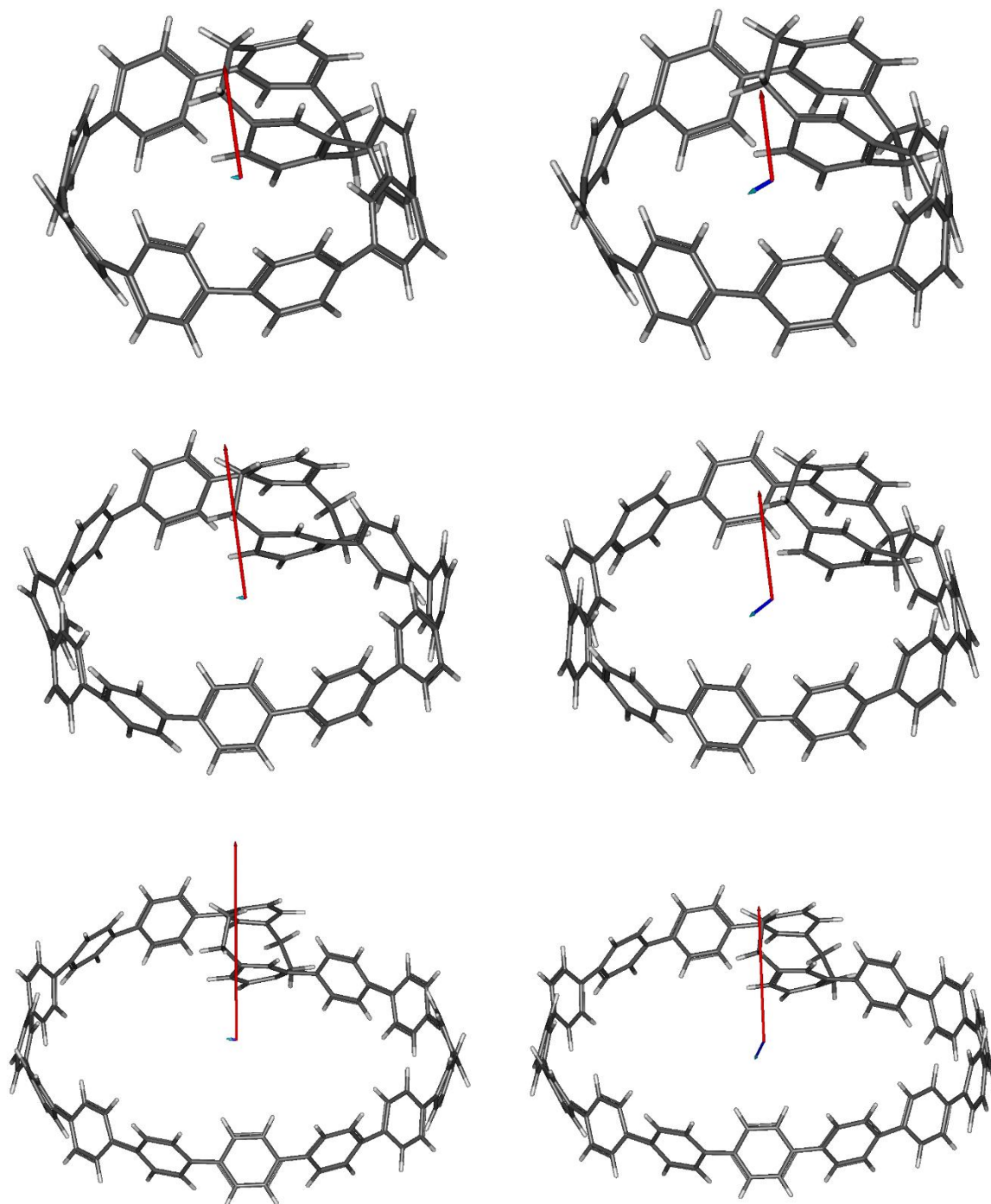


**Figure 41.** Electric (blue) and magnetic (red) transition dipole moments of the  $S_0 \rightarrow S_1$  (left) and  $S_1 \rightarrow S_0$  (right) transitions for  $p[n]$ SPPs ( $n = 9, 12, 16$ , top to bottom). The vectors were scaled up by a factor of 2 due to the small length of  $\mu$ .

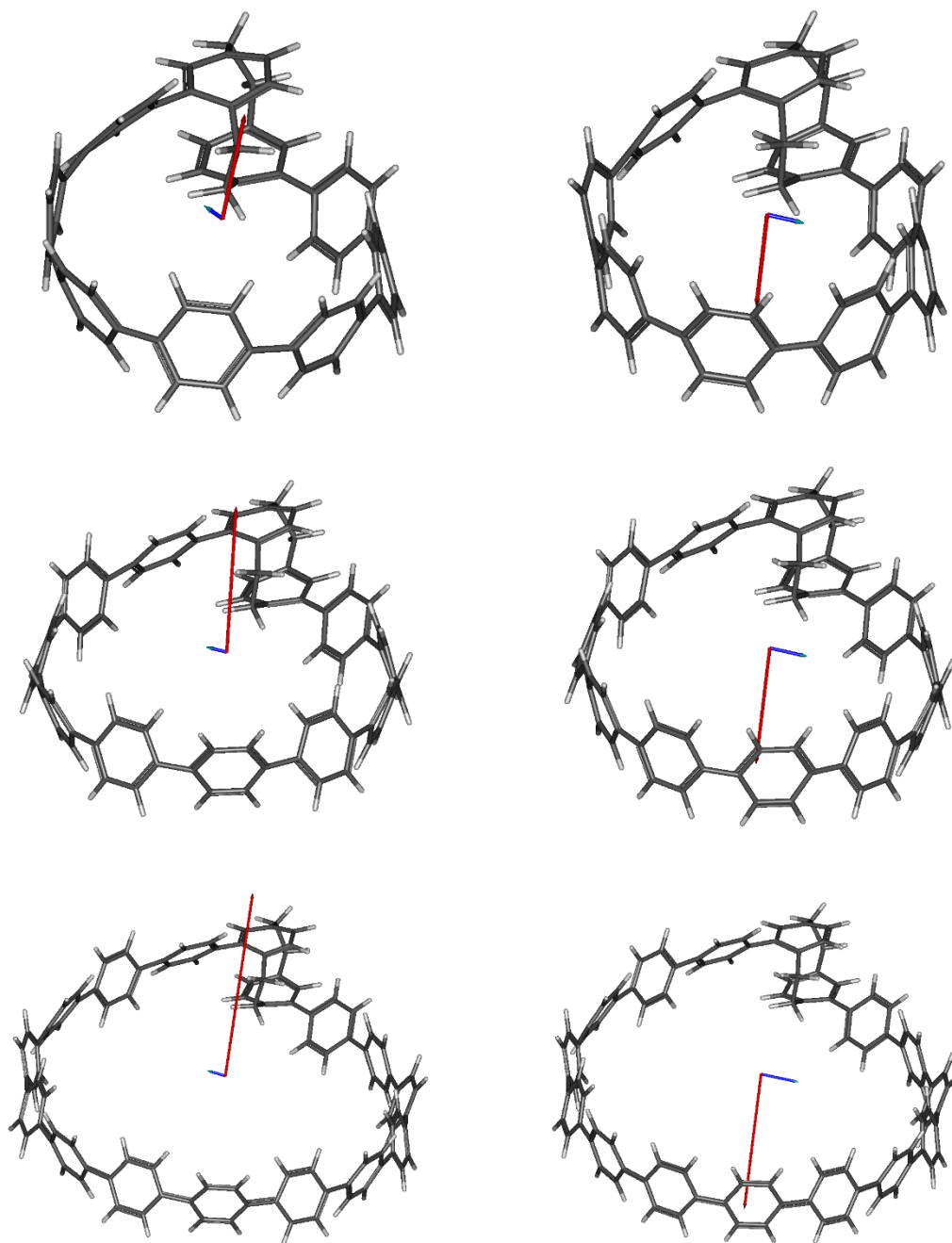


**Figure 42.** Electric (blue) and magnetic (red) transition dipole moments of the  $S_0 \rightarrow S_1$  (left) and  $S_1 \rightarrow S_0$  (right) transitions for  $m[n]$ SPPs ( $n = 9, 12, 16$ , top to bottom). The vectors were scaled up by a factor of 2 due to the small length of  $\mu$ .

The calculated  $g_{lum}$  values are much smaller than  $g_{abs}$  mainly due to the angle  $\theta$  between the electric and magnetic transition dipole moments, which got closer to  $90^\circ$  (Figure 43). Note that  $\theta = 90^\circ$  results in rotatory strength  $R$  and the corresponding  $g_{lum}$  value of 0 because  $\cos(90^\circ) = 0$  (see Eq. 5 and 7 in section 1.4.4.).

## 2. Spiral para-phenylenes

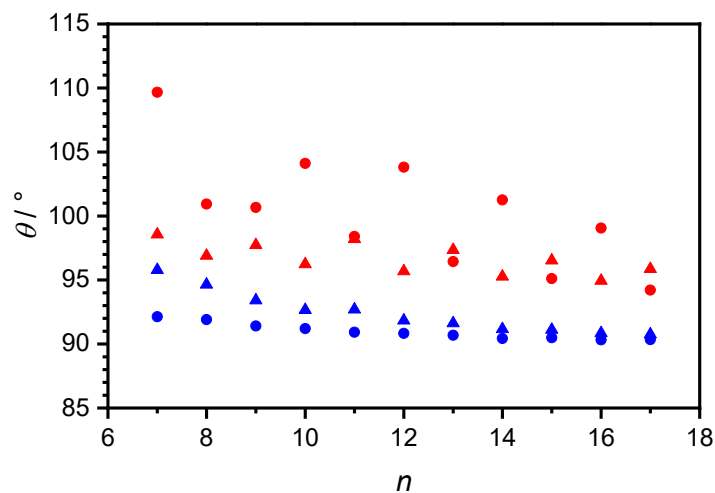


**Figure 43.** Values of angle  $\theta$  in degrees between the electric and magnetic transition dipole moments for  $p[n]$ SPPs (circles) and  $m[n]$ SPPs (triangles) in the ground (red) and the excited (blue) state calculated at CAM-B3LYP/6-31g(d) level of theory.

We have demonstrated that molecules undergo geometrical relaxation in the  $S_1$  state which influences the vectors  $\mu$  and  $m$ . When we investigate the orientation of vectors  $\mu$  in the excited states, we can notice that they always face parallel to the planarized segments of nano hoops where the excitons are localized (Figures 44–47). Generally, the excitons tend to localize at the most strained part of the molecule.

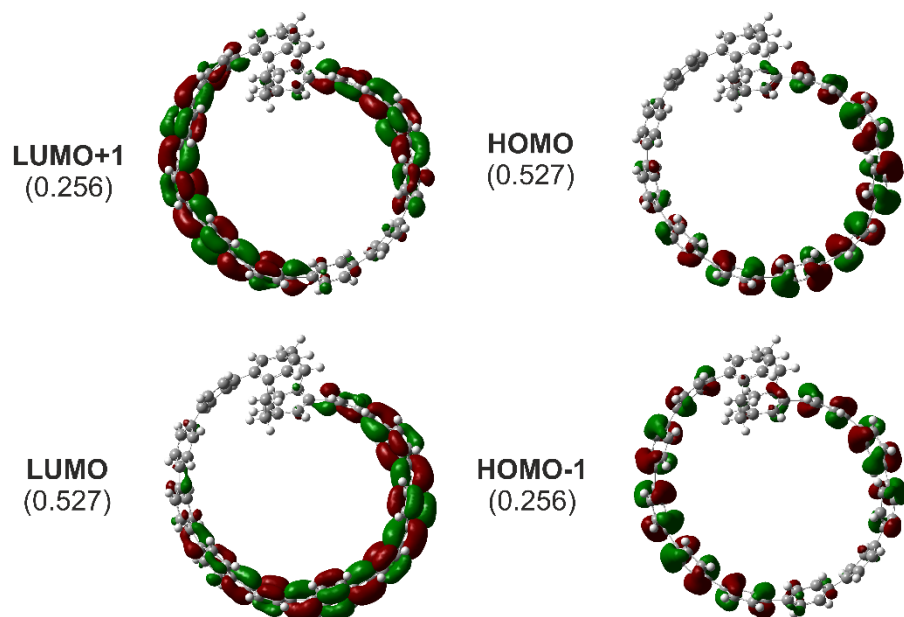


**Figure 44.** NTO of the  $S_0 \rightarrow S_1$  transition ( $E = 3.78$  eV,  $f = 0.068$ ) of  $p[12]$ SPP with their occupancies in brackets calculated at CAM-B3LYP/6-31G(d) level of theory.

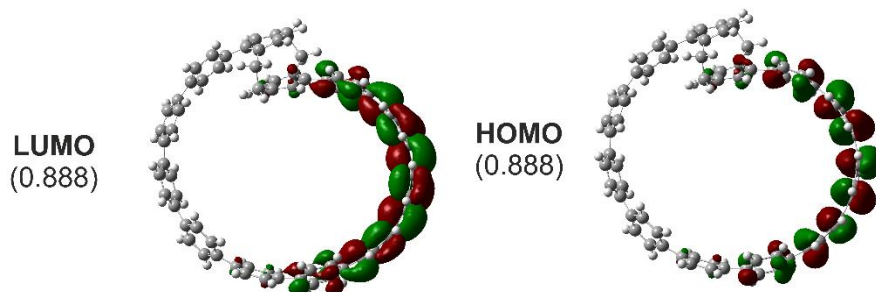


**Figure 45.** NTO of the  $S_1 \rightarrow S_0$  transition ( $E = 2.96$  eV,  $f = 0.921$ ) of  $p[12]$ SPP with their occupancies in brackets calculated at CAM-B3LYP/6-31G(d) level of theory.

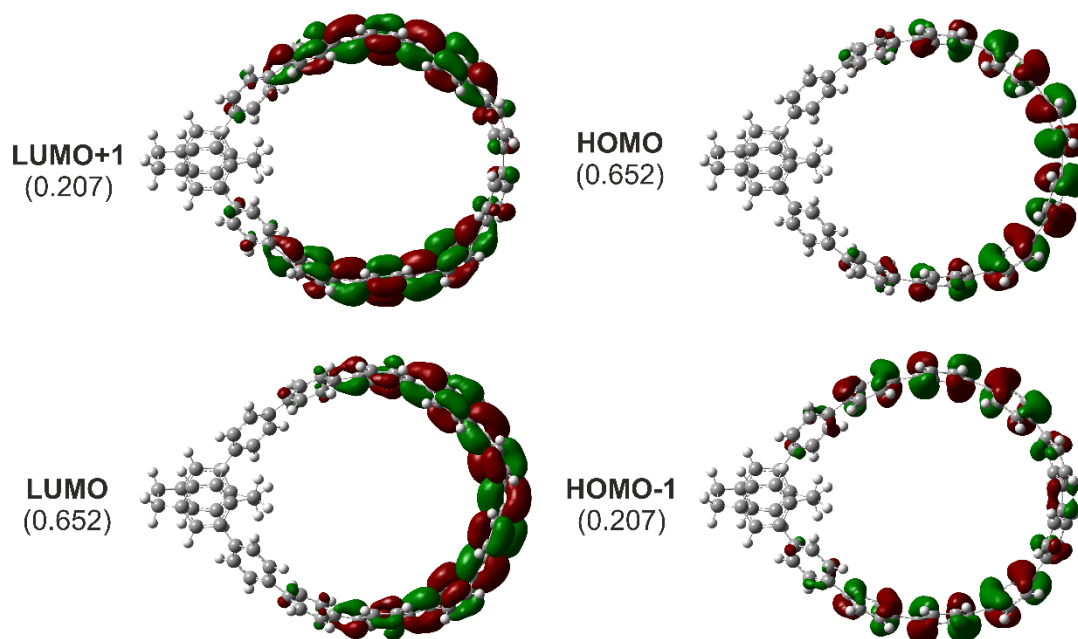


**Figure 46.** NTO of the  $S_0 \rightarrow S_1$  transition ( $E = 3.84$  eV,  $f = 0.381$ ) of  $m[12]$ SPP with their occupancies in brackets calculated at CAM-B3LYP/6-31G(d) level of theory.

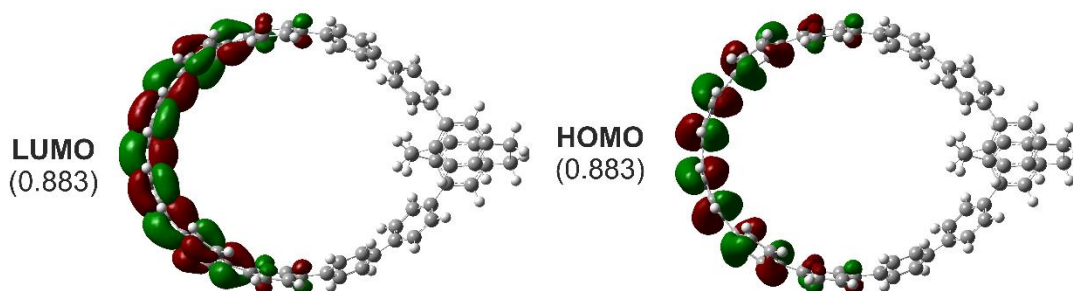


**Figure 47.** NTO of the  $S_1 \rightarrow S_0$  transition ( $E = 2.98$  eV,  $f = 0.958$ ) of  $m[12]$ SPP with their occupancies in brackets calculated at CAM-B3LYP/6-31G(d) level of theory.

### 2.3. Conclusions and Outlook

In conclusion, we have performed a conformational analysis for selected sizes of  $p[n]$ SPPs and  $m[n]$ SPPs ( $n = 9, 10$ ) to find the lowest-energy conformers. We used these results to optimize the geometries of other sizes of  $[n]$ SPPs and we calculated strain energies using homodesmotic reactions.  $p[n]$ SPPs were found to be considerably more strained than  $m[n]$ SPPs of the same size and the strain energy decreases with increasing size of the nanospiral. The most strained segment of  $p[n]$ SPPs is located on the inner side of each spiral next to the PCP moiety, which is unlike in  $m[n]$ SPPs which localize the strain on the phenylene opposite to the PCP moiety across the macrocycle. We used TD-DFT calculations to estimate the HOMO–LUMO gaps which increase with increasing size similarly to  $[n]$ CPPs. The HOMO energies of  $p[n]$ SPPs are slightly higher than those of corresponding  $m[n]$ SPPs due to higher curvature, while there is only a small influence on the LUMO energy. We calculated absorption and emission dissymmetry factors  $g_{abs}$  and  $g_{lum}$ . The massive drop in the dissymmetry factor between absorption and emission is a consequence of the geometry reorganization that planarizes a segment of five  $p$ -phenylenes in the excited state. Consequently, the direction and the amplitude of electric dipole moment vector  $\mu$  change and so does its angle  $\theta$  to the magnetic dipole moment  $m$ , diminishing value of the  $g_{lum}$ . We hypothesize that preventing the planarization may lead to high values of  $g_{lum}$  for chiral carbon nanostructures in general. Nevertheless,  $m[n]$ SPPs could be still used as circularly polarized luminophores as they are with high luminescence quantum yields due to the broken symmetry in the excitation and with configurational stability. The calculated  $g_{lum}$  values correspond well to the experimental values of acetylene-functionalized  $m[n]$ SPPs (around  $3 \times 10^{-3}$ ).<sup>[247]</sup>  $p[n]$ SPPs lack the configurational stability to allow separation of enantiomers<sup>[246]</sup> and, therefore, cannot be used as circularly polarized luminophores. However, the racemization can be prevented by steric hindrance.<sup>[244]</sup> Lastly, we would like to point out that the experimental  $g_{lum}$  could possibly be much lower if the theoretical  $g_{lum}$  of individual accessible conformers are substantially different from each other. Even so, comparison of the theoretical  $g_{lum}$  of the lowest-energy conformers offers to gain knowledge about the trends in properties as they depend on the size and curvature of the nanostructures.

As an outlook, we investigated the dissymmetry factors of  $p[12]$ SPP functionalized with bulky substituents (Figure 48) on phenylene units in order to prevent planarization in the excited state. We have chosen methyl substituents on phenylenes close to the planarization center in the excited state in **D1**, methyl substituents on every second phenylene in **D2**, methyl substituents on all phenylenes in **D3** and perfluoro-functionalization of phenylenes in **D4**.

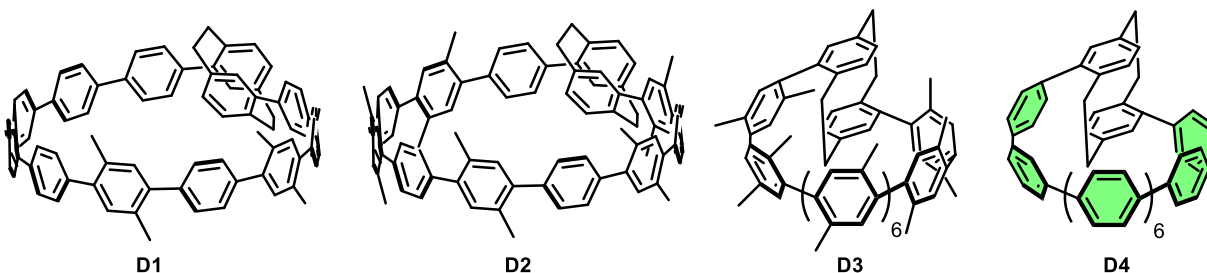


**Figure 48.** Design of  $p$ -[12]SPPs functionalized with methyl groups at the planarization center, every second phenylene, methyl groups on all phenylenes and perfluoro-phenylenes (left to right). Perfluorinated phenylenes are depicted in green.

We optimized the geometries of the ground and the first excited states for each derivative and calculated values of  $g_{abs}$  and  $g_{lum}$  (Table 8). Furthermore, we investigated the orientation and amplitudes of vectors  $\mu$

and  $m$  (Figure 49). Introduction of methyl substituents to the segment of  $p$ -phenylenes in the more curved part of the nanospiral where the planarization in the excited state takes place in **D1** proved to be insufficient because a similar geometry relaxation by planarization occurred in the less-strained part of the nanospiral. Introduction of two methyl groups on every second phenylene in **D2** sufficiently prevents the planarization in the excited state but the resulting  $g_{lum}$  value is low because the angle  $\theta$  is close to  $90^\circ$ . Introduction of two methyl groups on each phenylene in **D3** prevents the planarization in the excited state, however, the directions of  $\mu$  and  $m$  change along with a significant drop in the amplitude of  $m$  resulting low  $g_{lum}$  despite an increase in the angle  $\theta$ . Perfluoro-functionalization of the phenylenes in **D4** sufficiently prevents planarization, which was very recently confirmed in a different computational study,<sup>[250]</sup> and the corresponding values of  $g_{abs}$  and  $g_{lum}$  are close to each other. Furthermore, the amplitudes and direction of the vectors  $\mu$  and  $m$  are similar in the ground and the excited state.

**Table 8.** Dissymmetry factors and corresponding angles  $\theta$  of the first transition in the ground and the excited state of **D1–4**.

Species	$g_{abs} / 10^{-3}$	$\theta_{abs}$	$g_{lum} / 10^{-3}$	$\theta_{lum}$
<b>D1</b>	-15.3	96.66	-0.70	90.92
<b>D2</b>	-45.6	101.52	0.07	89.9
<b>D3</b>	1.2	89.06	-0.99	94.29
<b>D4</b>	-1.1	90.92	-1.12	91.65

## 2. Spiral para-phenylenes

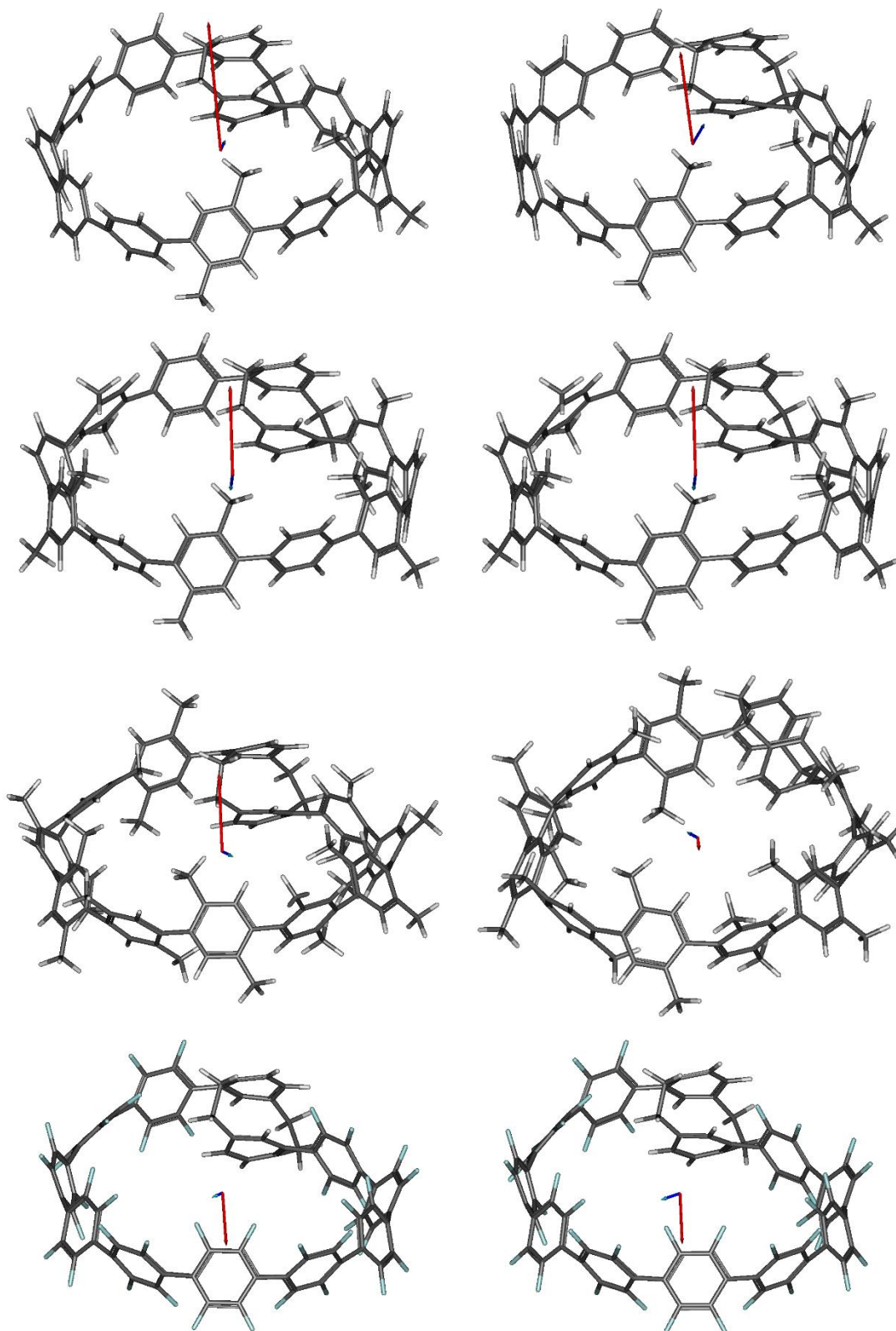


**Figure 49.** Electric (blue) and magnetic (red) transition dipole moments of the first transition in the ground (left) and excited states (right) for  $p[12]$ SPP derivatives **D1–4** (top to bottom). The vectors were scaled up by factor of 2 due to small size of electric transition dipole moments.



### 3. [6,7]Helicene *para*-phenylene – A prototype chiral luminophore

#### 3.1. Aim of the work

A number of chiral scaffolds were synthetically explored in order to achieve a high luminescence dissymmetry factor  $g_{lum}$ .<sup>[216,220]</sup> Theoretical prediction of experimental  $g_{lum}$  values using computational chemistry has proven to be rather challenging as we have demonstrated in the previous chapter. The angle  $\theta$  between transition dipole moments  $\mu$  and  $m$  and their amplitudes are sensitive to molecular geometry<sup>[226]</sup> and the resulting dissymmetry factor values can change drastically between the ground and the first excited state, for example due to a planarization of *p*-phenylenes in carbon nano hoops.

Nevertheless, carbon nano hoops possess excellent emissive properties but the chiral carbon nano hoops synthesized to this date typically have maximum  $g_{lum}$  values of  $\sim 5 \times 10^{-3}$  hampering their usage as chiral luminophores (Section 1.4.4.). We hypothesized, that an introduction of a moiety with strong chiroptical properties into  $[n]$ CPP can enhance the  $g_{lum}$  by chirality information transfer despite the planarization of the *p*-phenylene segment of the nano hoop, while ensuring a high quantum yield of fluorescence.

We chose [6]helicene as a chiral element to create a configurationally-stable chiral carbon nano hoop. It has been shown that 2,15-substituted [6]helicene derivatives can achieve high  $g_{lum}$  values<sup>[251]</sup> and have high a racemization barrier (see next section). In general, helicene carbon nano hoops produced from  $[m]$ helicene and  $[n]$ CPP are referred to as helicene *para*-phenylenes, abbreviated as  $[m,n]$ HPPs. We chose to incorporate the [6]helicene into [7]CPP resulting in a helicene carbon nano hoop [6,7]HPP (Figure 50). Seven phenylenes were chosen because the exciton localizes on seven phenylenes in  $[n]$ CPPs and a high quantum yield of emission is expected. The calculated 3D model of [6,7]HPP revealed a striking feature of the nano hoop. The  $\pi$ -system of [6,7]HPP adopts a shape of a Möbius strip, which further motivated us to test whether our initial hypotheses were correct and to validate its topology.

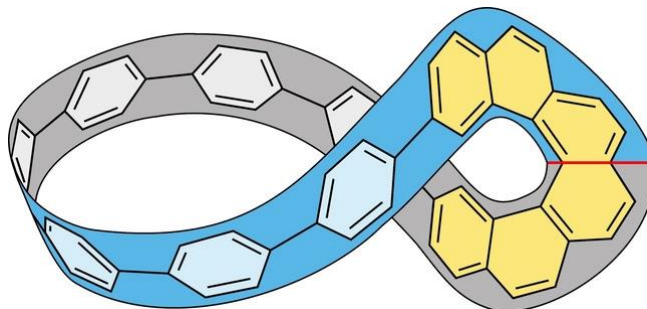


**Figure 50.** Molecular design of [6,7]HPP. Grey and blue colored stripes meeting in the helicene moiety represent that the  $\pi$ -system has only surface.

The goals of the project could thus be summarized as follows:

1. Synthesize [6,7]HPP and investigate its photophysical and chiroptical properties including CPL.
2. Validate the Möbius topology and investigate its consequences on the properties of [6,7]HPP.

### 3.2. Circularly Polarized Luminescence in a Möbius Helicene Carbon Nano hoop

The results of this study are summarized in a manuscript presented on the following pages as published in *Angewandte Chemie International Edition*<sup>[1]</sup> with separate numbering of compounds, figures, schemes, tables and references. The Supporting Information was adapted from the publication to fit the formatting of the thesis and can be found in the Appendix. My contribution to the published work is as follows: I designed and synthesized [6,7]HPP, grew the single crystals for the X-ray analysis, separated enantiomers using HPLC, measured the absorption, emission and CD spectra, investigated the optoelectronic structure by DFT calculations including the dissymmetry factors and strain energies, NMR chemical shifts and NICS values and AICD plots. Finally, I co-wrote the manuscript.

# Circularly Polarized Luminescence in a Möbius Helicene Carbon Nanoohoop\*\*

Juraj Malinčík, Sudhakar Gaikwad, Juan P. Mora-Fuentes, Marc-Aurèle Boillat, Alessandro Prescimone, Daniel Häussinger, Araceli G. Campaña, and Tomáš Šolomek\*

**Abstract:** We present the first helicene carbon nanoohoop that integrates a [6]helicene into [7]cycloparaphenylene. The [6]helicene endows the helicene carbon nanoohoop with chiroptical properties and configurational stability typical for higher helicenes, while the radially conjugated seven *para*-phenylenes largely determine the optoelectronic properties. The structure of the helicene carbon nanoohoop was unambiguously characterized by NMR, MS and X-ray analysis that revealed that it possesses a topology of a Möbius strip in the solid state and in solution. The chirality transfers from the [6]helicene to the *para*-phenylenes and leads to a pronounced circular dichroism and bright circularly polarized luminescence, which is affected by the structural topology of the nanoohoop.

**H**elicenes are polyaromatic hydrocarbons (PAHs) that consist of *ortho*-fused benzene rings adopting a helical shape.<sup>[1]</sup> Their inherent chirality and extended  $\pi$ -conjugation leads to strong electronic circular dichroism (ECD)<sup>[2]</sup> and circularly polarized luminescence (CPL).<sup>[3]</sup> Helicenes found applications in asymmetric catalysis, molecular machines, molecular recognition and sensors, polymers or in optoelec-

tronic devices.<sup>[4,5]</sup> Recently, helicenes have been used for construction of a CP-OLED device.<sup>[6]</sup> Basic all-carbon helicene emitters, however, suffer from low quantum yields of emission and require substantial synthetic modification, such as introduction of functional groups, extension of the  $\pi$ -conjugated system or doping with heteroatoms, in order to enhance their luminescence properties.<sup>[5,7-9]</sup>

[*n*]Cycloparaphenylenes ([*n*]CPPs), also known as carbon nanoohoops, are known for their unique size-dependent optoelectronic properties, which are a consequence of their curved nature and radial  $\pi$ -electron conjugation.<sup>[10-12]</sup> Unlike carbohelicenes, they display fluorescence with high quantum yields, spectrum of which shifts bathochromically with decreasing number of *p*-phenylenes. The fluorescence quantum yields also decrease with the size of CPPs and those with  $n \leq 7$  are non-fluorescent due to the forbidden nature of the  $S_1 \rightarrow S_0$  transition.<sup>[11-13]</sup> The fluorescence can be restored by replacing a phenylene ring in the structure of CPPs with PAHs lowering the molecular symmetry.<sup>[14-16]</sup> Examples of chiral carbon nanoohoops that can thereby emerge, incorporating acenes,<sup>[13,17-21]</sup> aromatic heterocycles,<sup>[22]</sup> and others,<sup>[23,24]</sup> were investigated both theoretically and experimentally. However, the individual subunits in carbon nanoohoops are connected via C–C single bonds and, therefore, have typically low enantiomerization barriers, which hampers the separation and characterization of enantiomers. Strategies to achieve configurationally stable nanoohoops by introducing a unit with an axial chirality<sup>[25-33]</sup> or by topological manipulation forming a molecular knot<sup>[34]</sup> have appeared recently. As a result, some examples displayed a promising CPL.<sup>[20,21,26,27,31-33]</sup>

Here, we investigate the first helicene carbon nanoohoop **1** (Scheme 1) with [6]helicene integrated into [7]CPP. A combination of the planar and radial  $\pi$ -conjugated units results in a Möbius topology of **1** in the solid state and in solution. Nevertheless, the properties of **1** are largely dictated by its individual subunits. The [6]helicene endows **1** with chiroptical properties and configurational stability typical for higher helicenes, while [7]CPP determines the optoelectronic properties. However, the chirality transfer from the [6]helicene leads to a pronounced circular dichroism and bright CPL. In addition, we provide experimental and theoretical evidence that also the topology in **1** affects the chiroptical response observed in the CPL.

The synthesis of **1** (Scheme 1) follows the strategy for [*n*]CPPs developed by Jasti et al.<sup>[35]</sup> We started from the commercially available 2,7-dibromonaphthalene, which was transformed to naphthalene-2,7-dicarbaldehyde via Bou-

[\*] J. Malinčík, Dr. S. Gaikwad, M.-A. Boillat, Dr. A. Prescimone, Dr. D. Häussinger, Prof. Dr. T. Šolomek  
Department of Chemistry, University of Basel  
St. Johann's-Ring 19, 4056 Basel (Switzerland)

Prof. Dr. T. Šolomek  
Department of Chemistry, Biochemistry and Pharmaceutical Sciences, University of Bern  
Freiestrasse 3, 3012 Bern (Switzerland)  
E-mail: tomas.solomek@unibe.ch

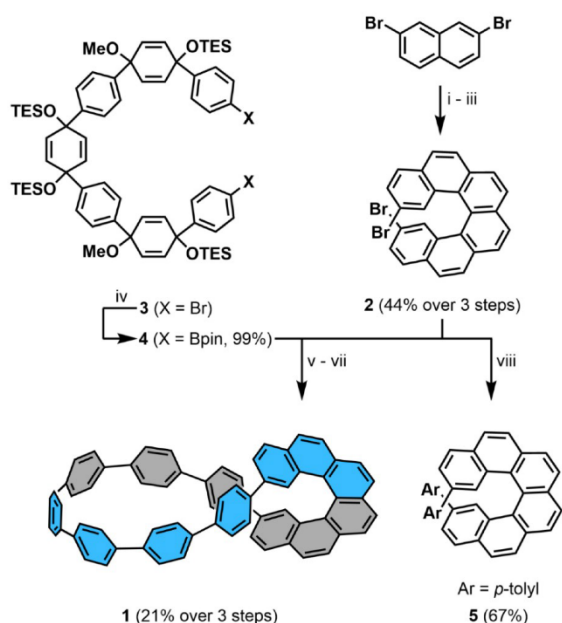
Dr. J. P. Mora-Fuentes, Prof. Dr. A. G. Campaña  
Department of Organic Chemistry, University of Granada  
Avda Fuentenueva, s/n, 18071 Granada (Spain)

J. Malinčík, Prof. Dr. T. Šolomek  
Prievidza Chemical Society  
M. Hodžu 10/16, 971 01 Prievidza (Slovakia)

[\*\*] A previous version of this manuscript has been deposited on a preprint server (<https://doi.org/10.26434/chemrxiv.13817498.v1>).

© 2022 The Authors. *Angewandte Chemie* published by Wiley-VCH GmbH. This is an open access article under the terms of the Creative Commons Attribution Non-Commercial License, which permits use, distribution and reproduction in any medium, provided the original work is properly cited and is not used for commercial purposes.

### 3. [6,7]Helicene para-phenylene



**Scheme 1.** Synthesis of compounds **1** and **5**: i) a) *n*-BuLi, THF,  $-78^{\circ}\text{C}$ , 1 h. b) DMF,  $-78^{\circ}\text{C}$  to r.t.; ii) (4-bromobenzyl)triphenylphosphonium bromide, NaH, THF, r.t., 16 h; iii) propylene oxide,  $\text{I}_2$ , toluene, *h\nu*, r.t., 4.5 h; iv) a) *n*-BuLi, THF,  $-78^{\circ}\text{C}$ , 1 h. b) *i*-PrOBpin,  $-78^{\circ}\text{C}$  to r.t.; v) Pd SPhos G3,  $\text{K}_3\text{PO}_4$ , dioxane/ $\text{H}_2\text{O}$  (10:1),  $80^{\circ}\text{C}$ , 16 h; vi) TBAF, THF, r.t., 1 h; vii)  $\text{H}_2\text{SnCl}_4$ , THF, r.t., 1 h; viii) *p*-tolueneboronic acid, Pd SPhos G3,  $\text{K}_3\text{PO}_4$ , dioxane/ $\text{H}_2\text{O}$  (10:1),  $80^{\circ}\text{C}$ , 24 h.

veault formylation<sup>[36]</sup> followed by a double Wittig reaction with (4-bromobenzyl)-triphenylphosphonium bromide and subsequent Mallory cyclization.<sup>[37]</sup> This sequence afforded 2,15-dibromo[6]helicene **2** in 44% overall yield over the three steps (Scheme S1). The synthesis of oligo-*p*-phenylene building block commenced from the previously reported compound **3**,<sup>[16]</sup> which was transformed to diboronate **4** via a double lithium–bromine exchange followed by quenching with *i*-PrOBpin in 99% yield. The double Suzuki–Miyaura cross-coupling of **2** and **4** followed by deprotection of the silyl protecting groups and subsequent reductive aromatization<sup>[38]</sup> afforded the target compound **1** in 21% yield over the three steps. So far, our attempts to isolate the intermediate macrocycle (Scheme S2) before the aromatization step have not been successful and we observed a decomposition of the material during column and gel permeation chromatographies. In order to understand the chiroptical properties of **1**, we synthesized the model [6]helicene **5** by Suzuki–Miyaura cross-coupling of *p*-tolueneboronic acid with **2** in 67% yield.

Compound **1** was characterized by high-resolution mass spectrometry and  $^1\text{H}$ ,  $^{13}\text{C}$ , and 2D NMR spectroscopies (see the Supporting Information). Yellow needle-shaped single crystals of racemic **1** were grown by layering a chlorobenzene solution with methanol under argon at room temperature. The single crystal X-ray analysis showed that **1** crystallized in monoclinic  $P2_1/n$  space group with unit cell:  $a = 18.1064(5) \text{ \AA}$ ,  $b = 12.6406(2) \text{ \AA}$ ,  $c = 23.3714(6) \text{ \AA}$ ,  $\beta = 104.885(2)^{\circ}$ ,  $\alpha = \gamma = 90^{\circ}$ . It unambiguously confirmed the

structure of **1** (Figure 1), which resembles a shape of an asymmetric figure-eight with a disordered molecule of chlorobenzene in the larger loop formed by the *p*-phenylene units.<sup>[39]</sup>

A closer inspection of the structure in the solid state reveals that **1** possesses a single non-orientable  $\pi$ -surface, i.e., it represents a structure with a Möbius topology, similar to a few previously reported carbon nano hoop derivatives.<sup>[40–44]</sup> Polycyclic aromatic hydrocarbons with Möbius topology are uncommon but have sparked particular interest because they are predicted to follow the opposite rules of aromaticity known to Hückel systems.<sup>[45–51]</sup> The synthesis of many Möbius compounds is often rather complicated, while that of **1** uses a straightforward macrocyclization of well-known building blocks. Helicene carbon nano hoops similar to **1** might thus represent worthwhile synthetic targets to study the effect of topology on the aromaticity if the Möbius topology was conserved also in a solution. Therefore, we studied the conformational dynamics of **1** via variable-temperature (VT)  $^1\text{H}$  NMR spectroscopy and DFT calculations.

Broadening of  $^1\text{H}$  NMR signals at 7.5 ppm at room temperature (Figure 2) suggests that **1** interconverts between at least two conformers. Therefore, we conducted a conformational search using DFT to identify possible conformations that could be reached by rotation of individual *p*-phenylene units in **1**. We located conformations with the Hückel topology, which are, however, predicted to be  $>5 \text{ kcal mol}^{-1}$  higher in energy than the conformer with the Möbius topology (Figures 2 and S16, Table S3) that matches the solid-state structure of **1**. The conformers in the two topologies differ in the orientation of the two *p*-phenylene rings (**A**, Table 1) attached directly to the [6]helicene unit. Nevertheless, the energy proximity of the Möbius and the Hückel conformations in **1** suggests that they can interconvert rapidly in a solution on the NMR time scale. In order to confirm these results, we cooled a sample of **1** in THF- $d_6$  (Figures 2 and S58) and TCE- $d_2$  (Figure S52) to support our findings from the DFT calculations. The sharp resonance at 6.34 ppm for *ortho*-protons in the pair of *p*-phenylenes **A** adjacent to [6]helicene broadens upon decreasing the temperature and splits into two individual resonances that can be observed at 168 K at 5.38 and 7.29 ppm (Figures S57–S62). We determined the coalescence temperature  $T_c = 190 \text{ K}$  and  $\Delta G^{\ddagger} = (8.0 \pm 0.12) \text{ kcal mol}^{-1}$  for their chemical

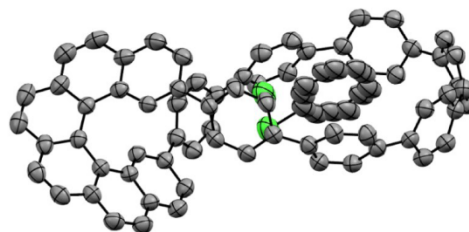


**Figure 1.** X-ray analysis of *rac*-**1** crystal (*M*-enantiomer is displayed). The thermal ellipsoids are shown at the 50% probability level.

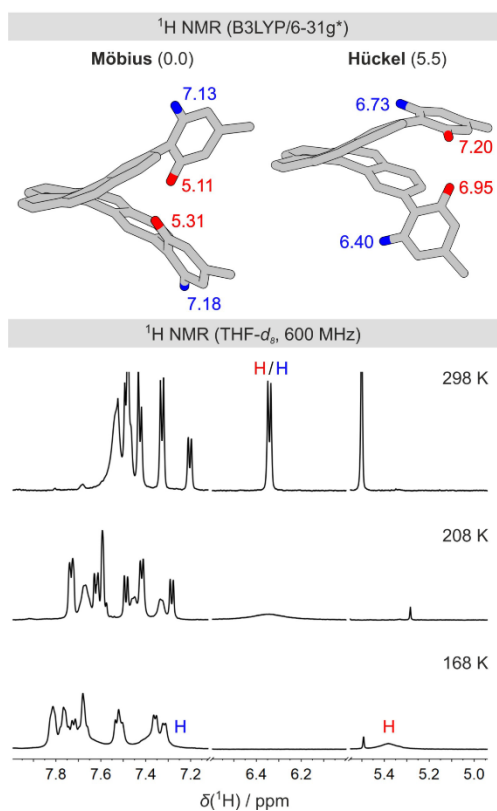


**Figure 2.** (top) Segment of the structure of the Möbius (left) and Hückel (right) conformations of **1** with the calculated  $^1\text{H}$  chemical shifts (in ppm) and (bottom) selected spectra from VT  $^1\text{H}$  NMR experiments of **1** in  $\text{THF-}d_8$ .

**Table 1:** Photophysical properties of **1**, **5**, [6]helicene,<sup>[52]</sup> *m*[8]CPP,<sup>[16]</sup> and [10]CPP.<sup>[12]</sup> Strain denotes the strain energy calculated for individual compounds (see text and the Supporting Information). Pairs of individual *p*-phenylene rings in **1** are marked with capital letters. The strain energy stored in individual C–C bonds in **1** increases with the depth of the hue of the red color.

Compound	$\lambda_{em}$ / nm	$\Phi_{fl}$	$\tau_{fl}$ / ns	Strain / kcal mol $^{-1}$
<b>1</b>	490	0.645	4.4	55.4
<b>5</b>	425	0.047	-	-
[6]Helicene	423	0.041	14.5	-
<i>m</i> [8]CPP	484	0.60	3.4	56.7
[10]CPP	466	0.65	6.6	57.7

exchange. These results are in very good accord with the chemical shifts of 5.3 and 7.1 ppm, respectively, obtained from DFT calculations for the Möbius conformer. The NMR rotation barrier also agrees well with the computed

value of 5.7–7.8 kcal mol $^{-1}$  (Table S3). In addition, the DFT calculations predict that the chemical shifts for the same proton resonances differ markedly in the Hückel conformers. Our results demonstrate that **1** possesses stable Möbius topology both in the solid state and in a solution with less than 1% of **1** in its possible Hückel conformations in the latter. In our case, compound **1**, however, cannot display global Möbius aromaticity because there is an odd number of  $\pi$  electrons in the conjugation path due to the connection of the [6]helicene unit to the *p*-phenylene segment (see Supporting Information). Nevertheless, the stable Möbius topology in related helicene nano hoops makes these compounds attractive to investigate non-linear optical properties as proposed recently by Lu et al. for topologically less stable Möbius phenanthroline carbon nano hoops.<sup>[42]</sup>

We observed the coalescence also for other proton resonances in **1**. We determined the  $T_c = 248$  K and  $\Delta G^\ddagger = (11.4 \pm 0.12)$  kcal mol $^{-1}$  for the protons at 7.36 and 7.69 ppm (*p*-phenylenes **B**, Table 1), while the rotation of the two remaining *p*-phenylene rings (**C** and **D**) required heating of the NMR sample above room temperature (Figure S52). However, the comparable chemical shifts of the protons in these rings prevented us from determining the exact coalescence temperatures. Nevertheless, we observed that the individual rotational barriers increase with the distance of the *p*-phenylene from the [6]helicene unit (**D** > **C** > **B** > **A**) and correlate with the distribution of the strain energy within the *p*-phenylenes half-loop in **1** (Table 1 and Figure S15). Thus, a higher strain stored in the C–C single bonds connecting the *p*-phenylene rings corresponds to a higher activation free energy of rotation around these bonds. We calculated the strain energy in **1** using StrainViz software,<sup>[53]</sup> and the homodesmotic reaction depicted in Scheme S3. We obtained the total strain energies (Table 1) of 55.6 kcal mol $^{-1}$  and 55.4 kcal mol $^{-1}$ , respectively, that compare well to those found for *m*[8]CPP (56.7 kcal mol $^{-1}$ )<sup>[16]</sup> or [10]CPPs (57.7 kcal mol $^{-1}$ )<sup>[54]</sup> although our values neglect part of the strain in the [6]helicene moiety in **1**.

The absorption and emission spectra (Figure 3) of **1** show that its electronic structure differs to that of the [6]helicene **5**. Unlike the vibronically-resolved fluorescence

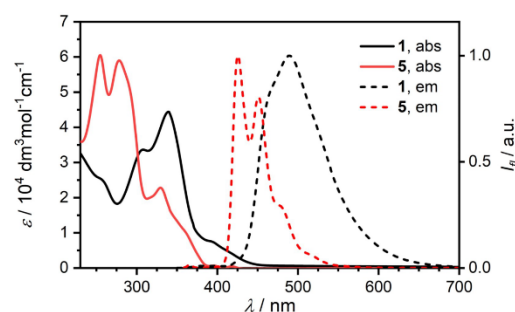


**Figure 3.** Absorption and emission spectra of **1** (black,  $\lambda_{exc} = 339$  nm) and **5** (red,  $\lambda_{exc} = 330$  nm) in  $\text{CH}_2\text{Cl}_2$ .

### 3. [6,7]Helicene *para*-phenylene

spectrum of **5**, the room temperature emission of **1** is nearly featureless with the emission maximum shifted bathochromically to  $\lambda_{\text{em}} = 490$  nm. The band maximum changes marginally with the polarity of the solvent (Figures S4 and S5). The inspection of the natural transition orbitals (NTOs, Figures S19–S22) of the first two electronic transitions shows that the lowest energy transitions are spatially decoupled but close in energy with a low oscillator strength.

The  $S_0 \rightarrow S_1$  is localized in the [6]helicene unit, while the more intense  $S_0 \rightarrow S_2$  transition in the curved *p*-phenylene segment. This agrees well with the absorption spectra measured for **1** and **5** ( $\approx 400$  nm absorption onset, Figure 3). It is expected that the excitation localized in the *p*-phenylene segment will possess a larger reorganization energy when compared to the [6]helicene unit due to a larger release of molecular strain and will likely become the lowest excited state upon geometry relaxation. As a result, the fluorescence characteristic for the CPPs could be observed. Indeed, not only the weak  $S_0 \rightarrow S_1$  absorption at  $\approx 400$  nm and the absorption maximum at 339 nm in **1** match well those in *m*[8]CPP,<sup>[11,16]</sup> the luminescence spectrum, quantum yield (64.5%) and the excited state lifetime (4.44 ns, Figures S7 and S8) compare well (Table 1), too. The similarity of the data collected for **1** and *m*[8]CPP<sup>[16]</sup> can be understood by the comparable curvature (and strain) in these two compounds (Figure S14). Thus, embedding a helicene unit into a CPP augments the emission properties of the helicene.<sup>[52]</sup>

We then investigated the chiroptical properties that the [6]helicene as a stereogenic element induces in **1**. Because our synthesis uses racemic 2,15-dibromo[6]helicene, we first separated the enantiomers of **1** using HPLC equipped with a chiral stationary phase (Figure S1). The measured ECD spectra of the isolated enantiomers appear as mirror images (Figure 4, top) and we assigned the *M*- and *P*- configurations to the respective enantiomers by TD-DFT calculations (Figures S28–S32). The ECD spectra of the individual enantiomers of **1** and **5** display the Cotton bands with the same signs at comparable wavelengths for the intense electronic transitions ( $< 390$  nm). This shows that the chiroptical response in these transitions is dominated by the [6]helicene unit. Comparison of the onset of the ECD spectra, however, reveals that the sign of the weak Cotton band in **1** is opposite to that in **5**. This transition is dominantly localized on the [6]helicene (Figure S19). Indeed, the sign of the transition agrees with the TD-DFT calculations (Table S4) and shows that extending the two phenyls into a closed loop swaps the sign of the Cotton band.

In addition, the chirality transfer from the [6]helicene induces a circularly polarized luminescence (CPL) of the *p*-phenylene segment in the enantiomers of **1** (Figure 4 and S10) that display the CPL of opposite signs. Notably, the signs of the CPL spectra were opposite to the signs of the longest wavelength CD signal, suggesting again a significant geometry reorganization in the excited state. The observed dissymmetry factor  $|g_{\text{lum}}| = 2.2 \times 10^{-3}$  is comparable to that measured for parent [6]helicene ( $\approx 1 \times 10^{-3}$ )<sup>[6]</sup> and other simple helicene derivatives.<sup>[3]</sup> Figure-of-eight molecules with two helicene units possess  $g_{\text{lum}}$  values that are an order of

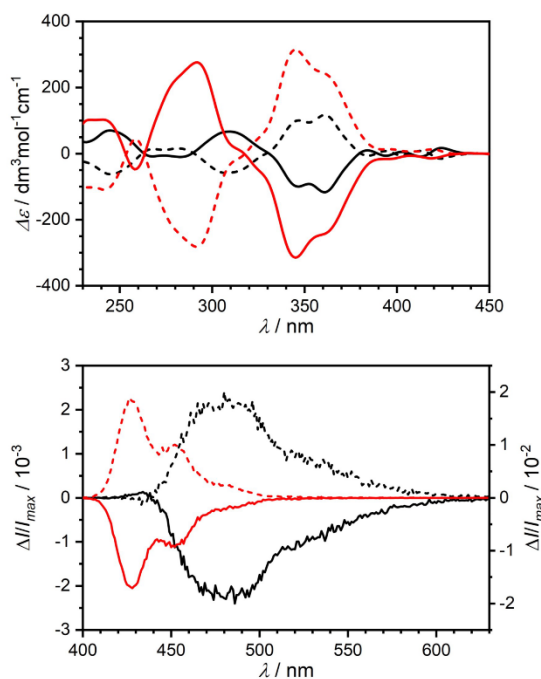


**Figure 4.** (top) Electronic circular dichroism and (bottom) circularly polarized luminescence spectra of **1** (black, left scale,  $\lambda_{\text{exc}} = 370$  nm) and **5** (red, right scale  $\lambda_{\text{exc}} = 345$  nm) in  $\text{CH}_2\text{Cl}_2$ . (*M*- and *P*-enantiomers are depicted in solid and dashed lines, respectively.

magnitude higher but with a commensurate decrease in their luminescence quantum yield.<sup>[55,56]</sup> Surprisingly, we determined the  $|g_{\text{lum}}| \approx 2 \times 10^{-2}$  in **5** (Figure S13). Crassous and Favereau et al. reported recently that the presence of electron-donating<sup>[6]</sup> or electron-withdrawing<sup>[57]</sup> substituents in the 2,15 positions of [6]helicene results in a similar enhancement of the  $|g_{\text{lum}}|$  values due to chiral exciton coupling. It is curious that one can achieve a similar effect with two simple tolyl substituents that do not strongly perturb the electronic structure of the [6]helicene and in which a strong exciton coupling is missing. Nevertheless, the combination of the high fluorescence quantum yield and the  $|g_{\text{lum}}|$  value makes nanohoop **1** a superior CPL emitter in comparison to the simple helicenes and even **5** with a  $\approx 10$ -fold enhanced  $g_{\text{lum}}$ . This can be demonstrated with the values of CPL brightness  $B_{\text{CPL}}$ ,<sup>[58,59]</sup> which are 63 and 21 for **1** and **5**, respectively.

We note that a weak, curious CPL signal with the opposite sign of  $g_{\text{lum}}$  can be observed at 435 nm. This weak emission suggests that there might be an additional excited state that contributes to the CPL but is not distinguished in the linear fluorescence at room (Figure 3) or low temperature (Figure S9). Excitation spectra (Figure S6) recorded at different emission wavelengths do not show a presence of additional species. The energy of this transition suggests that it could originate from the [6]helicene unit. We optimized the lowest-energy excited states from the Franck–Condon geometry of both the Möbius and Hückel conformers of **1** (Figure S16) using TD-DFT to understand the origin of this

additional spectral feature in CPL. Geometry relaxation in  $\mathbf{1}_{\text{Möbius}}$  fully localizes the excitation in the  $S_1$  state to the *p*-phenylenes (Figure S23), in agreement with our expectation of larger geometry reorganization associated with their curvature in  $\mathbf{1}$ . We do not see any appreciable contribution from the helicene unit in the  $S_1$  state, which confirms a full chirality information transfer from the helicene and reinforces that the luminescence of  $\mathbf{1}$  resembles that in *m*[8]CPP. The calculated sign and value of the  $g_{\text{lum}}$  also match the experiment (Table S5 and Figure 4). However, the  $S_1$  state NTOs in  $\mathbf{1}_{\text{Hückel}}$  show a full localization of the excitation to the [6]helicene (Figure S25). This transition is predicted to be blue-shifted and the sign of the  $g_{\text{lum}}$  for this putative emission corresponds to the weak signal in the experimental CPL spectrum. Rotation of *p*-phenylenes  $\mathbf{A}$  (Table 1) in the excited state is slow compared to the excited state lifetime. Therefore, the intensity of the signal, missing in the linear fluorescence spectrum, must reflect the Boltzmann distribution of the two topologically different conformers in the ground state at room temperature. The  $\approx 5$  kcal mol<sup>-1</sup> difference at 298 K corresponds to  $\approx 5000:1$  ratio of  $\mathbf{1}_{\text{Möbius}}:\mathbf{1}_{\text{Hückel}}$  in the ground state. Assuming similar absorption coefficients and  $\Phi_{\text{fl}}$ , the value of  $g_{\text{lum}}$  in  $\mathbf{1}_{\text{Hückel}}$  would need to be markedly higher than that in  $\mathbf{1}_{\text{Möbius}}$  to be experimentally observable. Indeed, the TD-DFT calculations show  $g_{\text{lum}} = -1.23 \times 10^{-2}$ , a 5-fold enhancement from that in  $\mathbf{1}_{\text{Möbius}}$ . Therefore, the ratio of the experimental intensities is expected to be  $\approx 1000:1$ . Integrating the two bands in the CPL spectrum (Figure 4) yields a ratio of  $\approx 100:1$ , which is in reasonable agreement considering the assumptions of the model and the initial population ratio estimated by DFT. We thus tentatively attribute the weak signal in the CPL spectrum to the  $S_1 \rightarrow S_0$  fluorescence of the topologically distinct  $\mathbf{1}_{\text{Hückel}}$ . The change in the topology in  $\mathbf{1}_{\text{Möbius}}$  lifts the Möbius twist/writhe and necessarily breaks the conjugation between the [6]helicene and the CPP segment, effectively localizing the excitation to the former subunit. As a result, the emission is shifted and the sign of the  $g_{\text{lum}}$  reverted in comparison to  $\mathbf{1}_{\text{Möbius}}$  but also to  $\mathbf{5}$ . It will be interesting to find a system where the two topologically distinct conformations are closer in energy and can interconvert faster to provide additional support to our hypothesis.

Finally, we investigated the configurational stability of  $\mathbf{1}$ . [6]Helicene possesses a high configurational stability<sup>[60,61]</sup> with a barrier to enantiomerization of 35 kcal mol<sup>-1</sup> (DFT: 35–38 kcal mol<sup>-1</sup>, Table S2). Our calculations predict that the presence of the *p*-phenylene loop increases this barrier in  $\mathbf{1}$  to  $\approx 38$ –44 kcal mol<sup>-1</sup>, rendering  $\mathbf{1}$  even more persistent to racemization. This observation is consistent with the concept of persistent chirality of figure-of-eight geometries that involve helicenes.<sup>[55,56]</sup> Although the chiroptical response of  $\mathbf{1}$  ( $\Delta\epsilon$ , Figure 4) is approximately third of that of  $\mathbf{5}$ , our results confirm that the [6]helicene unit endows  $\mathbf{1}$  with similar configurational stability.

In conclusion, we developed a strategy to enhance the luminescence properties of [6]helicene by integrating it into curved [7]cycloparaphenylene, creating a helicene carbon nanohoop  $\mathbf{1}$ . The enantiomers of  $\mathbf{1}$  displayed the chiroptical properties and configurational stability typical for

[6]helicene, while the presence of curved *p*-phenylene segment provided the optoelectronic properties comparable to *m*[8]cycloparaphenylene, such as emission of blue-green light with a high quantum yield. We showed, by a combination of X-ray analysis, variable-temperature NMR experiments and DFT calculations that the helicene carbon nanohoop  $\mathbf{1}$  possesses a stable Möbius topology in the solid state and in solution. In addition, the chirality transfer from the [6]helicene induces a bright circularly polarized luminescence in  $\mathbf{1}$ . Finally, we observe that a minor, topologically distinct Hückel conformer of  $\mathbf{1}$  displays a different chiroptical response in CPL. Extension of helicene systems with curved *p*-phenylene segments thus proves to be an efficient strategy to improve the emissive properties of helicenes and chiroptical properties of carbon nanohoops at the same time.

### Acknowledgements

We thank Prof. Dr. M. Mayor and the University of Basel for the invaluable support of our research and the SciCore facilities for computational resources. We thank T. Pastierik and Prof. Dr. M. Juríček for their help with the synthesis of [6]helicene and helpful discussions, M. Meyer and B. Pfund for photochemical measurements. This project received funding from the European Research Council (ERC) under the European Union's Horizon 2020 research and innovation programme (Grant Agreements No. 949397 and 677023), the Swiss National Science Foundation (SNSF, PZ00P2\_174175, CRSK-2\_190341) and the Project PGC2018-101181-B-I00 funded by MCIN/AEI/ 10.13039/501100011033 FEDER “Una manera de hacer Europa”. Open access funding provided by Universität Bern.

### Conflict of Interest

The authors declare no conflict of interest.

### Data Availability Statement

The data that support the findings of this study are available in the Supporting Information of this article.

**Keywords:** Chirality · Circularly Polarized Luminescence · Cycloparaphenylenes · Helicenes · Molecular Nanocarbons · Möbius Topology

- [1] R. H. Martin, *Angew. Chem. Int. Ed. Engl.* **1974**, *13*, 649–660; *Angew. Chem.* **1974**, *86*, 727–738.
- [2] Y. Nakai, T. Mori, Y. Inoue, *J. Phys. Chem. A* **2012**, *116*, 7372–7385.
- [3] W.-L. Zhao, M. Li, H.-Y. Lu, C.-F. Chen, *Chem. Commun.* **2019**, *55*, 13793–13803.
- [4] Y. Shen, C.-F. Chen, *Chem. Rev.* **2012**, *112*, 1463–1535.
- [5] M. Gingras, *Chem. Soc. Rev.* **2013**, *42*, 1051–1095.

### 3. [6,7]Helicene para-phenylene

- [6] K. Dhbaibi, L. Abella, S. Meunier-Della-Gatta, T. Roisnel, N. Vanthuyne, B. Jamoussi, G. Pieters, B. Racine, E. Quesnel, J. Autschbach, J. Crassous, L. Favereau, *Chem. Sci.* **2021**, *12*, 5522–5533.
- [7] E. Vander Donckt, J. Nasielski, J. R. Greenleaf, J. B. Birks, *Chem. Phys. Lett.* **1968**, *2*, 409–410.
- [8] H. Kubo, T. Hirose, K. Matsuda, *Org. Lett.* **2017**, *19*, 1776–1779.
- [9] K. Dhbaibi, L. Favereau, J. Crassous, *Chem. Rev.* **2019**, *119*, 8846–8953.
- [10] M. Fujitsuka, C. Lu, T. Iwamoto, E. Kayahara, S. Yamago, T. Majima, *J. Phys. Chem. A* **2014**, *118*, 4527–4532.
- [11] Y. Segawa, A. Fukazawa, S. Matsuura, H. Omachi, S. Yamaguchi, S. Irle, K. Itami, *Org. Biomol. Chem.* **2012**, *10*, 5979–5984.
- [12] E. R. Darzi, R. Jasti, *Chem. Soc. Rev.* **2015**, *44*, 6401–6410.
- [13] R. Daengngern, C. Camacho, N. Kungwan, S. Irle, *J. Phys. Chem. A* **2018**, *122*, 7284–7292.
- [14] B. M. Wong, J. W. Lee, *J. Phys. Chem. Lett.* **2011**, *2*, 2702–2706.
- [15] R. Franklin-Mergarejo, D. O. Alvarez, S. Tretiak, S. Fernandez-Alberti, *Sci. Rep.* **2016**, *6*, 31253.
- [16] T. C. Lovell, C. E. Colwell, L. N. Zakharov, R. Jasti, *Chem. Sci.* **2019**, *10*, 3786–3790.
- [17] H. Omachi, Y. Segawa, K. Itami, *Org. Lett.* **2011**, *13*, 2480–2483.
- [18] J. Wang, G. Zhuang, Q. Huang, Y. Xiao, Y. Zhou, H. Liu, P. Du, *Chem. Commun.* **2019**, *55*, 9456–9459.
- [19] P. Della Sala, C. Talotta, M. De Rosa, A. Soriente, S. Geremia, N. Hickey, P. Neri, C. Gaeta, *J. Org. Chem.* **2019**, *84*, 9489–9496.
- [20] J. Wang, H. Shi, S. Wang, X. Zhang, P. Fang, Y. Zhou, G.-L. Zhuang, X. Shao, P. Du, *Chem. Eur. J.* **2022**, *28*, e202103828.
- [21] J. Wang, G. Zhuang, M. Chen, D. Lu, Z. Li, Q. Huang, H. Jia, S. Cui, X. Shao, S. Yang, P. Du, *Angew. Chem. Int. Ed.* **2020**, *59*, 1619–1626; *Angew. Chem.* **2020**, *132*, 1636–1643.
- [22] E. R. Darzi, E. S. Hirst, C. D. Weber, L. N. Zakharov, M. C. Lonergan, R. Jasti, *ACS Cent. Sci.* **2015**, *1*, 335–342.
- [23] E. P. Jackson, T. J. Sisto, E. R. Darzi, R. Jasti, *Tetrahedron* **2016**, *72*, 3754–3758.
- [24] Y. Wu, G. Zhuang, S. Cui, Y. Zhou, J. Wang, Q. Huang, P. Du, *Chem. Commun.* **2019**, *55*, 14617–14620.
- [25] L.-H. Wang, N. Hayase, H. Sugiyama, J. Nogami, H. Uekusa, K. Tanaka, *Angew. Chem. Int. Ed.* **2020**, *59*, 17951–17957; *Angew. Chem.* **2020**, *132*, 18107–18113.
- [26] K. Sato, M. Hasegawa, Y. Nojima, N. Hara, T. Nishiuchi, Y. Imai, Y. Mazaki, *Chem. Eur. J.* **2021**, *27*, 1323–1329.
- [27] K. Senthilkumar, M. Kondratowicz, T. Lis, P. J. Chmielewski, J. Cybińska, J. L. Zafra, J. Casado, T. Vives, J. Crassous, L. Favereau, M. Stępień, *J. Am. Chem. Soc.* **2019**, *141*, 7421–7427.
- [28] T. A. Schaub, E. A. Prantl, J. Kohn, M. Bursch, C. R. Marshall, E. J. Leonhardt, T. C. Lovell, L. N. Zakharov, C. K. Brozek, S. R. Waldvogel, S. Grimme, R. Jasti, *J. Am. Chem. Soc.* **2020**, *142*, 8763–8775.
- [29] M. Hermann, D. Wassy, J. Kohn, P. Seitz, M. U. Betschart, S. Grimme, B. Esser, *Angew. Chem. Int. Ed.* **2021**, *60*, 10680–10689; *Angew. Chem.* **2021**, *133*, 10775–10784.
- [30] D. Wassy, M. Hermann, J. S. Wössner, L. Frédéric, G. Pieters, B. Esser, *Chem. Sci.* **2021**, *12*, 10150–10158.
- [31] M. Krzeszewski, H. Ito, K. Itami, *J. Am. Chem. Soc.* **2022**, *144*, 862–871.
- [32] J. He, M. Yu, M. Pang, Y. Fan, Z. Lian, Y. Wang, W. Wang, Y. Liu, H. Jiang, *Chem. Eur. J.* **2022**, *28*, e202103832.
- [33] J. Nogami, Y. Nagashima, K. Miyamoto, A. Muranaka, M. Uchiyama, K. Tanaka, *Chem. Sci.* **2021**, *12*, 7858–7865.
- [34] Y. Segawa, M. Kuwayama, Y. Hijikata, M. Fushimi, T. Nishihara, J. Pirillo, J. Shirasaki, N. Kubota, K. Itami, *Science* **2019**, *365*, 272–276.
- [35] R. Jasti, J. Bhattacharjee, J. B. Neaton, C. R. Bertozzi, *J. Am. Chem. Soc.* **2008**, *130*, 17646–17647.
- [36] V. Církva, P. Jakubík, T. Strašák, J. Hrbáč, J. Sýkora, I. Císařová, J. Vacek, J. Žádný, J. Storch, *J. Org. Chem.* **2019**, *84*, 1980–1993.
- [37] J. M. Fox, D. Lin, Y. Itagaki, T. Fujita, *J. Org. Chem.* **1998**, *63*, 2031–2038.
- [38] V. K. Patel, E. Kayahara, S. Yamago, *Chem. Eur. J.* **2015**, *21*, 5742–5749.
- [39] Deposition Number 2178271 contains the supplementary crystallographic data for this paper. These data are provided free of charge by the joint Cambridge Crystallographic Data Centre and Fachinformationszentrum Karlsruhe Access Structures service.
- [40] Y.-Y. Fan, D. Chen, Z.-A. Huang, J. Zhu, C.-H. Tung, L.-Z. Wu, H. Cong, *Nat. Commun.* **2018**, *9*, 3037.
- [41] S. Nishigaki, Y. Shibata, A. Nakajima, H. Okajima, Y. Masumoto, T. Osawa, A. Muranaka, H. Sugiyama, A. Hori-kawa, H. Uekusa, H. Koshino, M. Uchiyama, A. Sakamoto, K. Tanaka, *J. Am. Chem. Soc.* **2019**, *141*, 14955–14960.
- [42] Z. Liu, T. Lu, *J. Phys. Chem. C* **2020**, *124*, 7353–7360.
- [43] K. Li, Z. Xu, J. Xu, T. Weng, X. Chen, S. Sato, J. Wu, Z. Sun, *J. Am. Chem. Soc.* **2021**, *143*, 20419–20430.
- [44] Z.-L. Qiu, D. Chen, Z. Deng, K.-S. Chu, Y.-Z. Tan, J. Zhu, *Sci. China Chem.* **2021**, *64*, 1004–1008.
- [45] E. Heilbronner, *Tetrahedron Lett.* **1964**, *5*, 1923–1928.
- [46] H. S. Rzepa, *Chem. Rev.* **2005**, *105*, 3697–3715.
- [47] D. Ajami, O. Oeckler, A. Simon, R. Herges, *Nature* **2003**, *426*, 819–821.
- [48] R. Herges, *Chem. Rev.* **2006**, *106*, 4820–4842.
- [49] Z. S. Yoon, A. Osuka, D. Kim, *Nat. Chem.* **2009**, *1*, 113–122.
- [50] G. Naulet, L. Sturm, A. Robert, P. Dechambenoit, F. Röhrich, R. Herges, H. Bock, F. Durola, *Chem. Sci.* **2018**, *9*, 8930–8936.
- [51] X. Jiang, J. D. Laffoon, D. Chen, S. Pérez-Estrada, A. S. Danis, J. Rodríguez-López, M. A. Garcia-Garibay, J. Zhu, J. S. Moore, *J. Am. Chem. Soc.* **2020**, *142*, 6493–6498.
- [52] J. B. Birks, D. J. S. Birch, E. Cordemans, E. Vander Donckt, *Chem. Phys. Lett.* **1976**, *43*, 33–36.
- [53] C. E. Colwell, T. W. Price, T. Stauch, R. Jasti, *Chem. Sci.* **2020**, *11*, 3923–3930.
- [54] Y. Segawa, H. Omachi, K. Itami, *Org. Lett.* **2010**, *12*, 2262–2265.
- [55] A. Robert, G. Naulet, H. Bock, N. Vanthuyne, M. Jean, M. Giorgi, Y. Carissan, C. Aroulanda, A. Scalabre, E. Pouget, F. Durola, Y. Coquerel, *Chem. Eur. J.* **2019**, *25*, 14364–14369.
- [56] H. Kubo, D. Shimizu, T. Hirose, K. Matsuda, *Org. Lett.* **2020**, *22*, 9276–9281.
- [57] K. Dhbaibi, L. Favereau, M. Srebro-Hooper, C. Quinton, N. Vanthuyne, L. Arrico, T. Roisnel, B. Jamoussi, C. Poriel, C. Cabanetos, J. Autschbach, J. Crassous, *Chem. Sci.* **2020**, *11*, 567–576.
- [58] L. Arrico, L. Di Bari, F. Zinna, *Chem. Eur. J.* **2021**, *27*, 2920–2934.
- [59] Y. Nagata, T. Mori, *Front. Chem.* **2020**, *8*, 448.
- [60] R. H. Martin, M.-J. Marchant, *Tetrahedron Lett.* **1972**, *13*, 3707–3708.
- [61] J. Barroso, J. L. Cabellos, S. Pan, F. Murillo, X. Zarate, M. A. Fernandez-Herrera, G. Merino, *Chem. Commun.* **2018**, *54*, 188–191.

Manuscript received: June 13, 2022

Accepted manuscript online: July 20, 2022

Version of record online: August 4, 2022



### 3.3. Summary and Outlook

We demonstrated the synthesis of [6,7]HPP, its spectroscopic and crystallographic characterization complemented by computational investigation of the electronic structure. [6,7]HPP is a configurationally-stable chiral luminophore with a high quantum yield of 65% and moderate luminescence dissymmetry factor of  $2.2 \times 10^{-3}$ . The measured brightness of CPL ( $B_{CPL}$ ) 63 is relatively high compared to other chiral carbon nanostructures and superior to other known [6]helicene derivatives. Furthermore, we showed that a curious CPL signal at 435 nm with opposite sign of  $g_{lum}$  emerges from the emission of a higher energy conformer of [6,7]HPP with Hückel topology. This unexpected result demonstrates that the handedness of CPL could be controlled by topology of the luminophore and that reliable prediction of accurate  $g_{lum}$  is a delicate task.

The results of X-ray crystal structure analysis and VT-NMR spectroscopy, which revealed that [6,7]HPP possesses Möbius topology, motivated us to investigate whether the molecule or its oxidized or reduced forms (Section 1.4.2) could display a global Möbius aromaticity (see section 4.1. for the theoretical background). A common computational method to investigate magnetically-induced currents that can validate the aromaticity of a compound is the anisotropy of the induced current density (AICD) plot.<sup>[252]</sup> AICD can visualize delocalization of electrons through  $\pi$ - and  $\sigma$ -sigma bonds or even through space. Current density vectors can then be mapped onto the AICD surface after defining the direction of the external magnetic field  $B_0$  that induces magnetic currents observable in the molecule. The result depends on the relative orientation of the molecule with respect to the  $B_0$  vector. If the direction of the induced magnetic current vectors follows the left- or right-hand rule, the currents are called diatropic and paratropic, respectively. For example, a planar aromatic system, such as benzene, requires a perpendicular orientation of the  $B_0$  vector relative to the ring plane to induce a diatropic magnetic current. Möbius aromatic compounds, on the other hand, require the  $B_0$  vector to be perpendicular to the  $C_2$  axis of symmetry of the molecule.<sup>[253]</sup> For example, Möbius aromatic [16]annulene displays an induced diatropic current (Figure 51) when the  $B_0$  vector is  $(-1,0,0)$ .

We tested many different orientations of [6,7]HPP, [6,7]HPP<sup>2+</sup>, [6,7]HPP<sup>4+</sup> and [6,7]HPP<sup>2-</sup> with respect to the external magnetic field  $B_0$  using the AICD method, but we have never observed any global magnetic currents (Figure 52), despite a full electron delocalization across the whole macrocycle. We thus conclude that neutral [6,7]HPP and its oxidized or reduced forms are globally non-aromatic, although individual phenylenes and the helicene display induced local diatropic currents and are locally aromatic.

Investigation of the NICS values in [6,7]HPP, [6,7]HPP<sup>2+</sup> and [6,7]HPP<sup>2-</sup> further confirmed the non-aromatic character (Figure 53) of the investigated compounds as only a weak shielding is observed in the cavity of [6,7]HPP which increases upon oxidation or reduction. We attribute the increase to the planarization of phenylene units in the ionic helicene hoops that lead to a higher shielding inside the cavity by local magnetic fields on the individual phenylene units. We hypothesize that the primary reason for the observed non-aromaticity are the electron delocalization paths with only an odd number of carbon atoms within the [6]helicene. This always results in the delocalization of an odd number of  $\pi$ -electrons around the helicene nanostructure unlike the even number of electrons required formally by the Hückel rules to comprise an aromatic or an anti-aromatic system (Figure 54).

As an outlook, we suggest that helicene carbon nanostructures that provide an even number of electrons in the delocalization pathway are synthesized and investigated computationally to understand their aromaticity. This can be achieved by incorporating [ $m$ ]helicenes where  $m$  is an odd number (Figure 54), into helicene

### 3. [6,7]Helicene para-phenylene

carbon nanohoops. In addition, we propose that switching between the two conformations of different topologies upon an external stimuli could create a new type of molecular CPL switches.

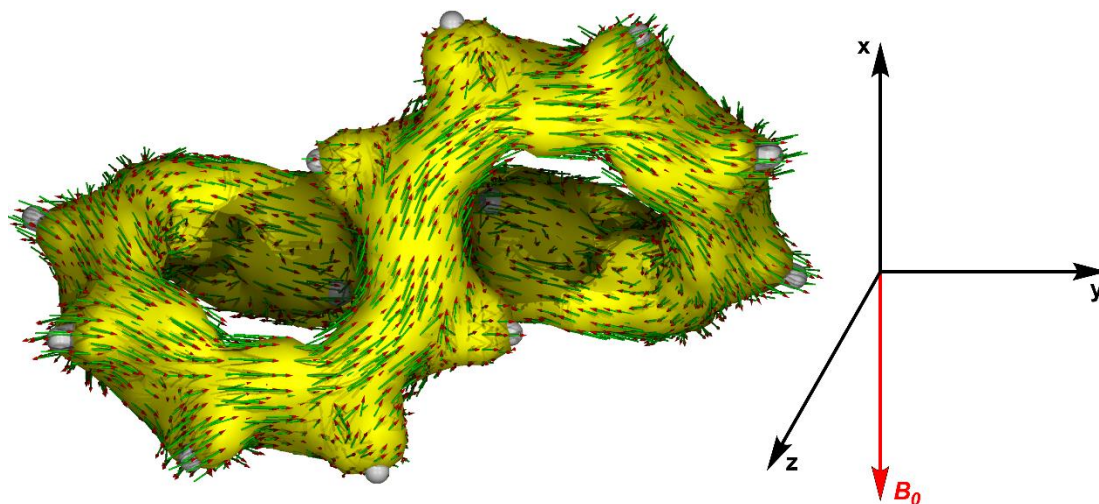


**Figure 51.** AICD plot of [16]annulene with induced current density vectors in external magnetic field  $B_0$  (-1,0,0)

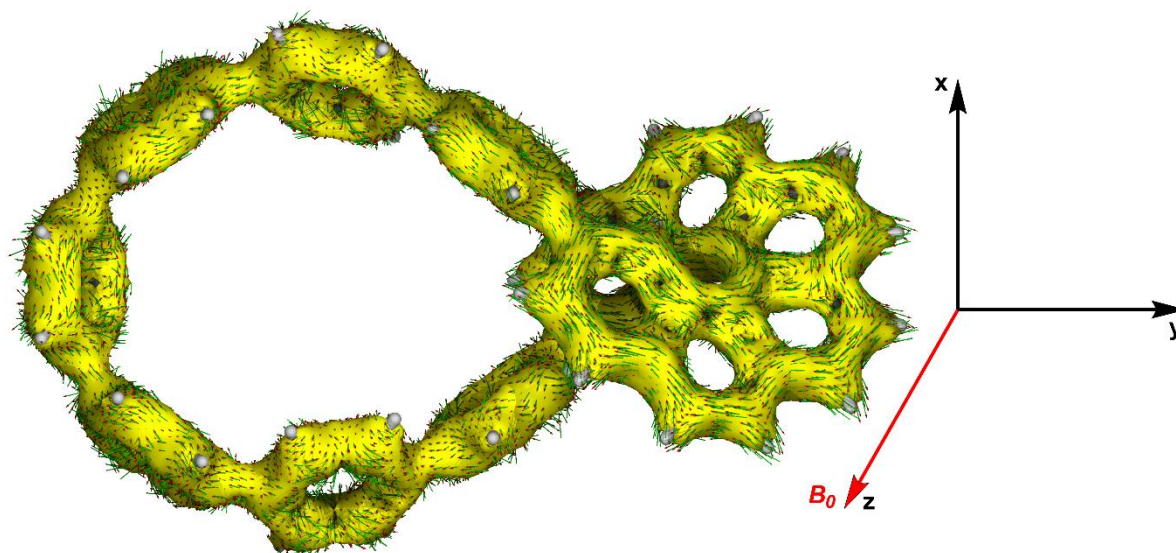


**Figure 52.** AICD plot of [6,7]HPP with induced current density vectors in external magnetic field  $B_0$  (0,0,1)

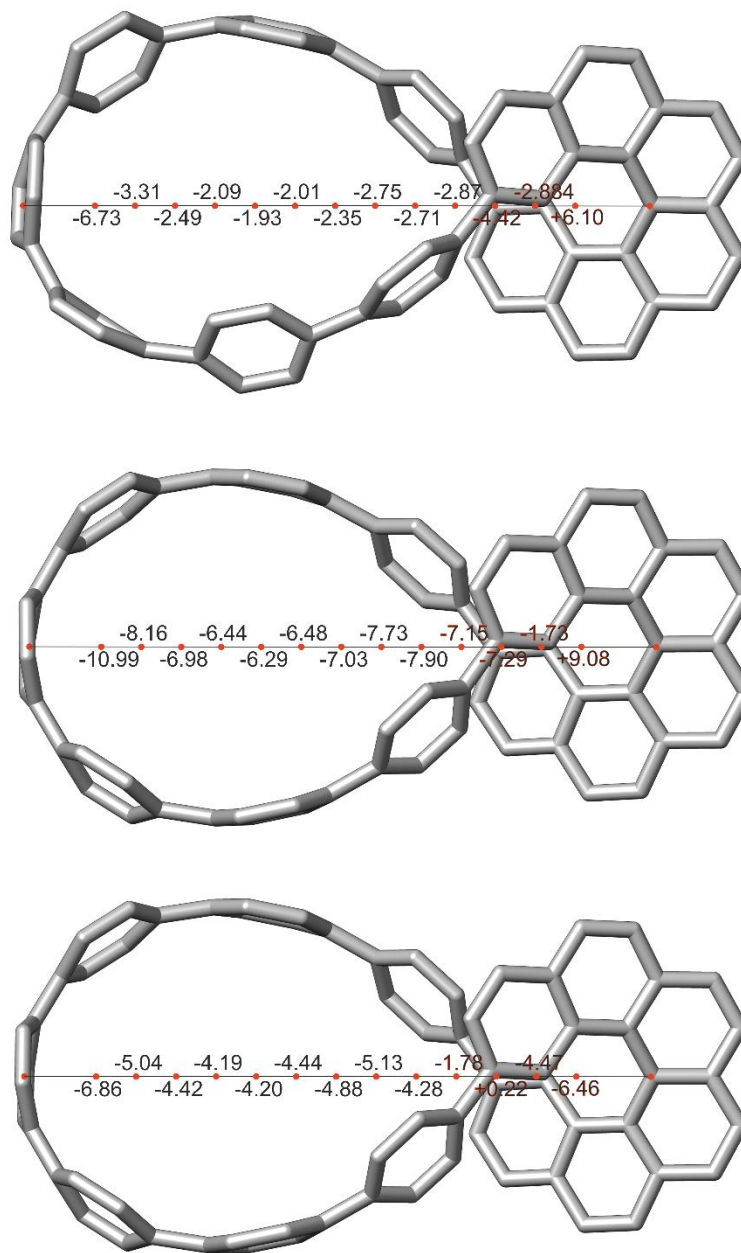


**Figure 53.** NICS values across the cavity of [6,7]HPP, [6,7]HPP<sup>2+</sup> and [6,7]HPP<sup>2-</sup> (top to bottom).

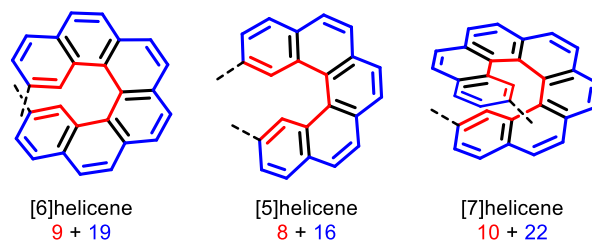


**Figure 54.** Inner (red) and outer (blue) conjugation pathways across [m]helicenes.



## 4. [5,*n*]Helicene *para*-phenylenes

### 4.1. Möbius aromaticity and anti-aromaticity

Aromaticity is a key concept in organic chemistry describing stabilization of cyclic conjugated system of  $(4N + 2)$   $\pi$ -electrons with benzene being the prototypical aromatic compound with six  $\pi$ -electrons.<sup>[168]</sup> On the other hand,  $4N$   $\pi$ -electron cyclic conjugated systems possess a low stability because they require electrons to be distributed among two (nearly) degenerate MOs that leads to electronic configuration with unpaired electrons. Such systems are referred to as anti-aromatic. However, the same  $4N$   $\pi$ -electrons can be distributed into doubly occupied MOs stabilizing the system like in benzene if the cyclic conjugated system is twisted into a Möbius strip (Figure 55). Such systems were termed Möbius aromatic in 1964 by Heilbronner who derived this concept based on Hückel theory.<sup>[254]</sup> If a compound with Möbius topology has  $(4N + 2)$   $\pi$ -electrons, a similar destabilization is observed as for Hückel  $4N$   $\pi$ -electron systems and such compounds are termed as Möbius anti-aromatic.<sup>[255]</sup>

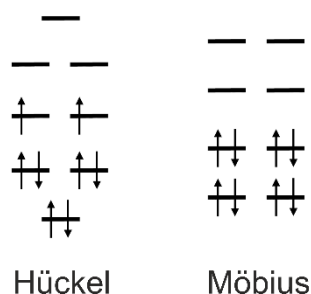
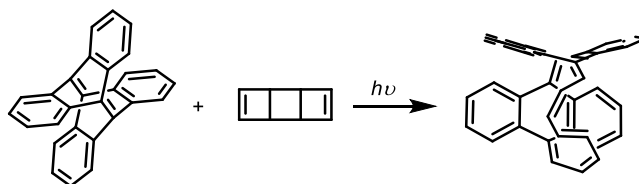


**Figure 55.** Molecular orbital diagrams for [8]annulene with  $4N$   $\pi$ -electrons of Hückel (left) and Möbius (right) topology.

The consequences of Möbius aromaticity are difficult to quantify in the same way as traditional Hückel aromaticity. X-ray crystal structures can determine the bond-length equalization which is an unambiguous proof. The first Möbius aromatic compound was synthesized only in 2003 by Herges *et al.*<sup>[256]</sup> by a photochemical [2+2]cycloaddition of tetrahydrodianthracene and *syn*-tricyclooctadiene resulting in a mixture of five isomers of [16]annulene derivative which were separated using HPLC. The Möbius  $C_2$  symmetric isomer (Scheme 13) exhibits higher bond-length equalization in the X-ray crystal structure than other isomers and thereby has higher aromatic character, which supports the predictions of Heilbronner.



**Scheme 13.**

The design of Herges combines linearly- and radially-conjugated synthons to create the twist required to obtain a Möbius topology. Pyramidalization of  $sp^2$ -carbons, and therefore strain, is necessary to achieve radial conjugation and, consequently, Möbius topology.<sup>[253]</sup> Aside from [*n*]annulenes, several other structural motifs were demonstrated experimentally to adopt Möbius topology such as porphyrinoids<sup>[253,257–259]</sup> and helicene trimers.<sup>[260,261]</sup> Radially-conjugated nanohoops seem to be the perfect candidates for design

#### 4. [5,m]Helicene para-phenylenes

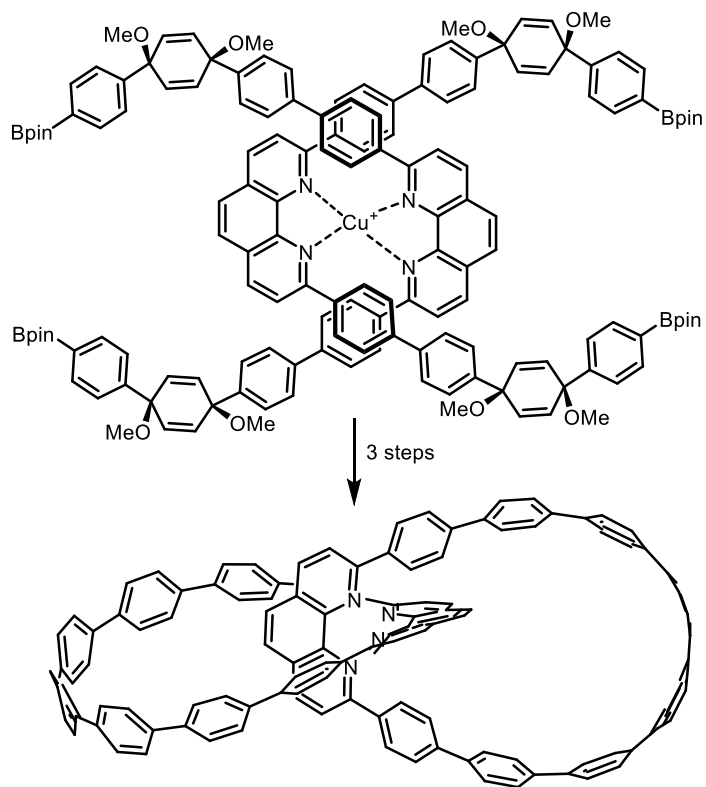
of Möbius systems which was demonstrated by the synthesis of such compounds in the recent years.<sup>[206,262–264]</sup>

A catenane consisting of nanohoops containing two phenanthrolines that served as the template was synthesized by Cong *et al.* in 2018 by macrocyclization of a preorganized copper(I) complex by a two-fold Jasti oxidative coupling, subsequent removal of copper(I) ions and aromatization (Scheme 14).<sup>[206]</sup> The individual nanohoops in the catenane adopt a Möbius topology, while the nanohoop alone displays a Hückel topology. The twist necessary to achieve the Möbius topology is likely an effect of steric repulsion between nanohoops in the catenane. The delocalization of  $\pi$ -electrons across the whole macrocycle was confirmed by an AICD plot (Figure 56), however, only local induced diatropic currents in the phenanthroline and phenylene rings were observed. The hoops in the catenane are thus globally non-aromatic. The effect of a Möbius topology in phenanthroline nanohoops of different sizes was further investigated using DFT calculations revealing slightly lower hyper-polarizability for Möbius conformers.<sup>[265]</sup>

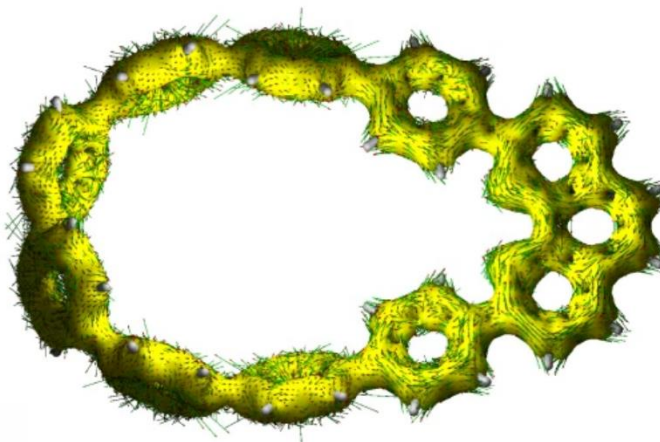
Another Möbius-shaped carbon nanohoop was synthesized by Tanaka *et al.* in 2019 via rhodium-catalyzed [2+2+2]cyclootrimerization to a belt structure along a [10]CPP core (Scheme 15). Calculated NICS values revealed only a minor shielding in the center of the nanohoop and a weak conjugation between the phenylenes was observed in an AICD plot rendering this compound globally non-aromatic.<sup>[262]</sup>

In April 2021, 3*m*[12]CPP was synthesized by Tan *et al.* via the approach of Itami (Figure 57) and its structure was confirmed by single-crystal X-ray diffraction (XRD) revealing the Möbius topology of its  $\pi$ -system. AICD plot showed delocalization  $\pi$ -electrons around the whole macrocycle but only local induced diatropic currents were observed in phenylene rings. Moreover, the conjugation pathway has an odd number of carbons which already disqualifies the compound being globally aromatic.<sup>[263]</sup>

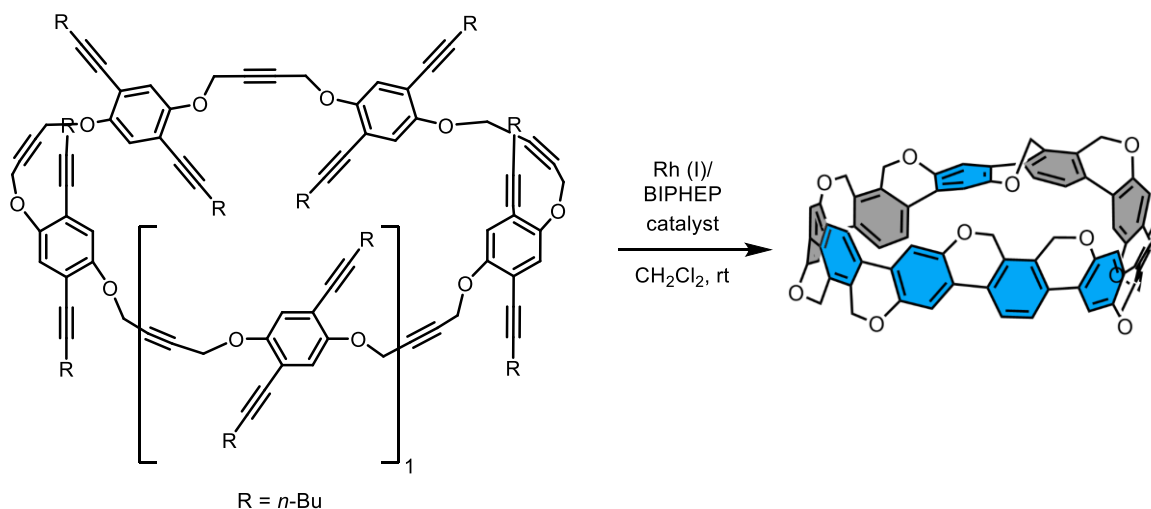
Lastly, in November 2021, an anthraquinodimethane-based (AQD) double nanohoop (Figure 58) was synthesized by Sun *et al.* using the approach of Jasti. It was oxidized by magic blue to a dication and the structures of both the neutral AQD nanohoop and the dication were confirmed by single-crystal XRD.<sup>[264]</sup> High bond-length equalization was observed in the dication with Hückel topology and magnetic deshielding in the cavity of each nanohoop was calculated but the authors do not state numerical NICS values. A ground state diradical of the AQD nanohoop was investigated using DFT. Unlike the crystal structure, DFT calculations showed a doubly twisted geometry with a Möbius topology for the oxidized nanohoop. The authors claim that there is a global paratropic current observable in the AICD plot of both the dication and the diradical and conclude that they are globally Hückel and Möbius anti-aromatic, respectively. We examined the published AICD plot (Figure 58), however, we have observed no global currents as the authors draw them. They also do not state the direction of the external magnetic field which is crucial for determination of the direction of the current. We can see only locally induced currents in the phenylene rings and AQD moiety and only a weak electron delocalization across the macrocycles which contradicts the conclusion of global anti-aromaticity in either topology. We conclude here that the AQD nanohoop is, in fact, globally non-aromatic.



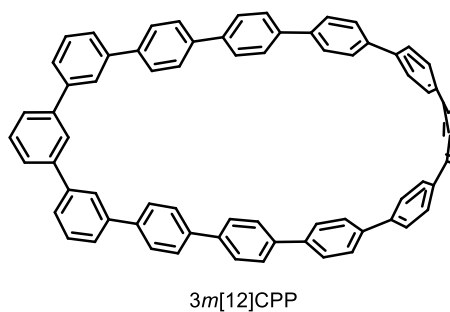
Scheme 14.

Figure 56. AICD plot of a phenanthroline carbon nano hoop in Möbius topology.<sup>[206]</sup>

#### 4. [5,m]Helicene para-phenylenes



**Scheme 15.** The synthesis of a Möbius-shaped [10]CPP. Different sides of the  $\pi$ -system in the individual phenylenes are depicted in blue and grey, respectively, to illustrate Möbius topology.



**Figure 57.** Structure of  $3m[12]\text{CPP}$ .

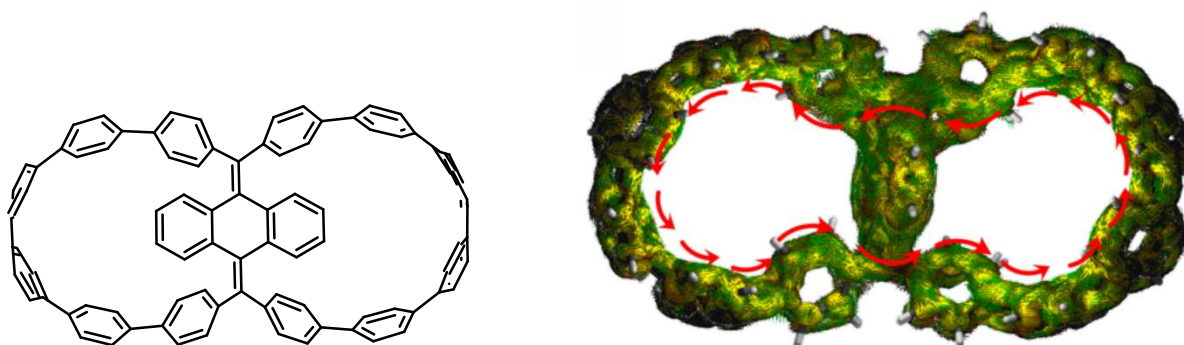


**Figure 58.** Structure of anthraquinodimethane-based doublehoop (left) and the AICD plot of its dication diradical.<sup>[264]</sup> The red arrows visualize a non-existent induced magnetic current.

In Chapter 3, we presented that incorporation of a single helicene moiety into a CPP scaffold provides helicene carbon nano hoops that possess a stable Möbius topology.

In this work, we designed and attempted the synthesis of a series of [5,*n*]HPPs (Figure 59) in order to elucidate the effect of topology on the observed properties and to assess the aromaticity [5,*n*]HPPs and their oxidized and reduced forms. Moreover, we were interested, at which size of [*n*]CPP used formally in [5,*n*]HPPs, if any, would the photophysical properties cease to parallel the *m*[*n*]CPP and emerge from the



[5]helicene unit. That would allow us to find the limit of using helicene nano hoops as chiral luminophores. Therefore, the goals of this project can be defined as follows:

1. Synthesize a series of [5,*n*]HPPs (*n* = 6,7,9) and investigate their photophysical and chiroptical properties including CPL.
2. Establish a structure–property relationship regarding the size of the nano hoops.
3. Investigate the aromaticity of [5,*n*]HPP, [5,*n*]HPP<sup>2+</sup> and [5,*n*]HPP<sup>2-</sup> species.

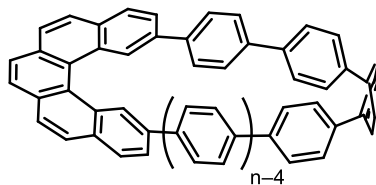


**Figure 59.** Molecular structures of [5,*n*]HPPs (*n* = 6,7,9).

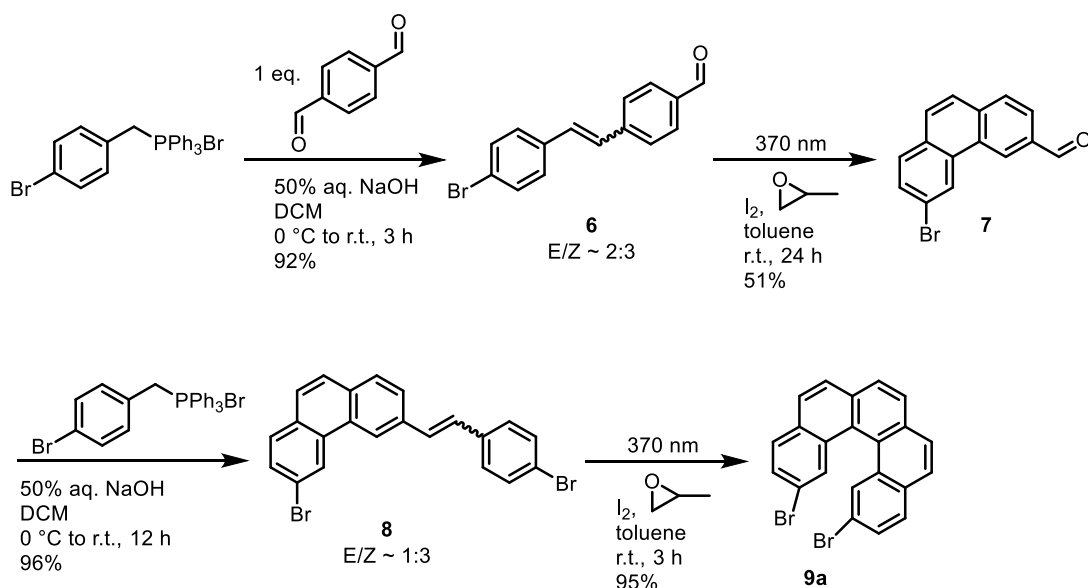
## 4.2. Results and Discussion

### 4.2.1. Synthesis of [5,*n*]HPPs

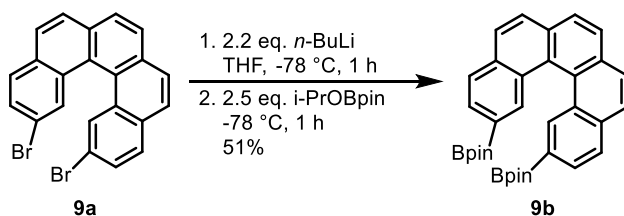
The synthetic protocols and characterization of the prepared compounds are provided in the Appendix.

We designed the synthesis of [5,*n*]HPPs using the approach of Jasti from a literature-known 2,13-dibromo-[5]helicene **9a**.<sup>[266]</sup> In the first step, terephthalaldehyde reacted with (4-bromobenzyl)-triphenylphosphonium bromide in a Wittig olefination to afford alkene **6** as a mixture of diastereomers in a 92% yield (Scheme 16). Both diastereomers of **6** underwent photochemical Mallory cyclization to afford phenanthrene **7** in a moderate 51% yield which was treated with (4-bromobenzyl)-triphenylphosphonium bromide in another Wittig olefination to afford alkene **8** as a mixture of diastereomers in an excellent 96% yield. Finally, 2,13-dibromo-[5]helicene **9a** is prepared in an excellent 95% yield by a photochemical Mallory cyclization of both diastereomers of **8**. Helicene **9a** was subsequently treated with *n*-BuLi followed by the addition of *i*-PrOBpin to afford diboronate **9b** in a moderate yield of 51% (Scheme 17).

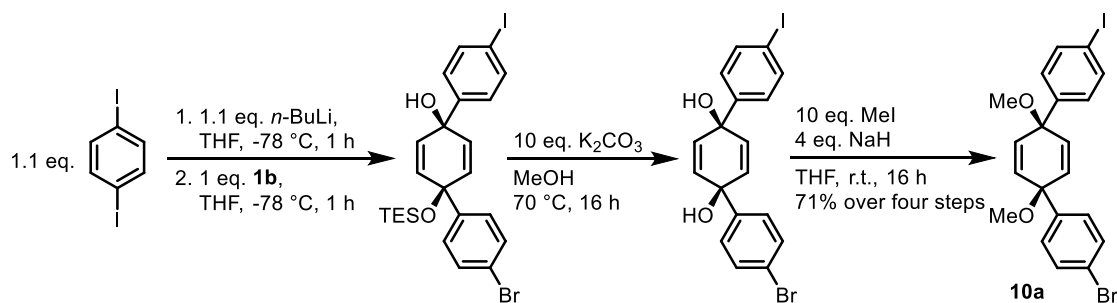
Building block **10a** was prepared diastereoselectively via a novel strategy (Scheme 18). Starting with a mono-lithiation of 1,4-diiodobenzene forming 4-iodophenyllithium which undergoes a diastereoselective nucleophilic addition to the silylated ketone **1b**. In the following steps, the silyl group is deprotected using K<sub>2</sub>CO<sub>3</sub> in boiling methanol and both free hydroxyl groups are protected using MeI to afford **10a** in 71% over four steps. We tried to perform a Suzuki-Miyaura cross-coupling of **9b** and **10a** (Scheme 19) using various conditions, but we never managed to exceed the yield of 26% for the building block **11a**. For preparation of [5,6]HPP, we would need high quantities of **11a**, while this reaction was also difficult to upscale as a substantial amount of polymers were formed even at low concentrations. We concluded that the C–Br bond in **10a** is too reactive under the cross-coupling reaction conditions even at room temperature.



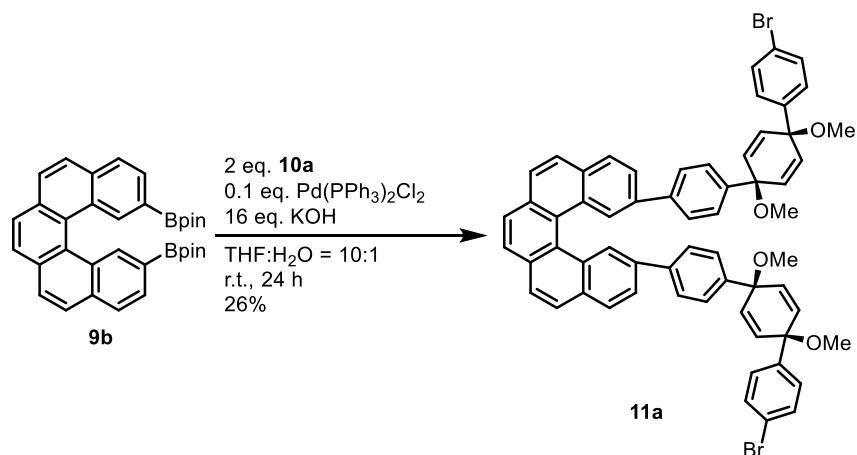
Scheme 16.



Scheme 17.



Scheme 18.



Scheme 19.

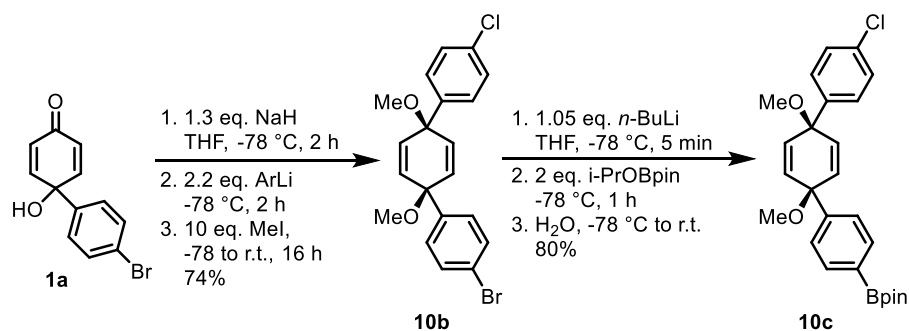
We decided to use a combination of less reactive halogens by first exchanging bromine in 1-bromo-4-chlorobenzene for lithium followed by a nucleophilic addition of the formed mono-lithiated species to deprotonated ketone **1a** and protecting the newly-formed diol with MeI. As a result, the building block **10b** was isolated in 81% yield. Mono-lithiation of **10b** followed by the addition of *i*-PrOBpin afforded the boronate **10c** in 80% yield (Scheme 20).

A key intermediate **11b** was prepared from **9a** using Suzuki-Miyaura cross-coupling with **10c** in a good yield of 80% (Scheme 21). We tried to directly cyclize intermediate **11b** to a macrocycle using Yamamoto homo-coupling. However, no conversion of the starting material was observed under standard reaction conditions likely due to a low reactivity of the C–Cl bonds (Scheme 22).

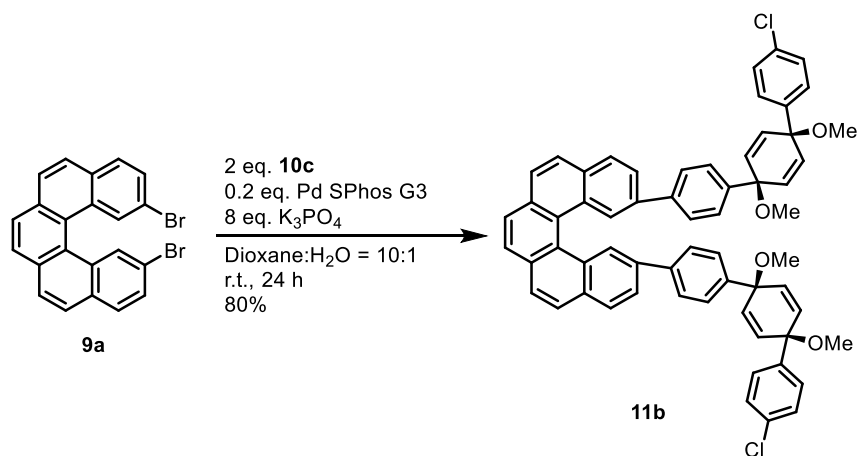
Therefore, we used Miyaura borylation to convert **11b** to the boronate **11c** which was used without any further purification in an oxidative homo-coupling macrocyclization developed by Jasti *et al.*<sup>[267]</sup> After the macrocyclization (Scheme 23), we observed the molecular peak of the desired macrocycle **12** (Figure 60).

#### 4. [5,m]Helicene para-phenylenes

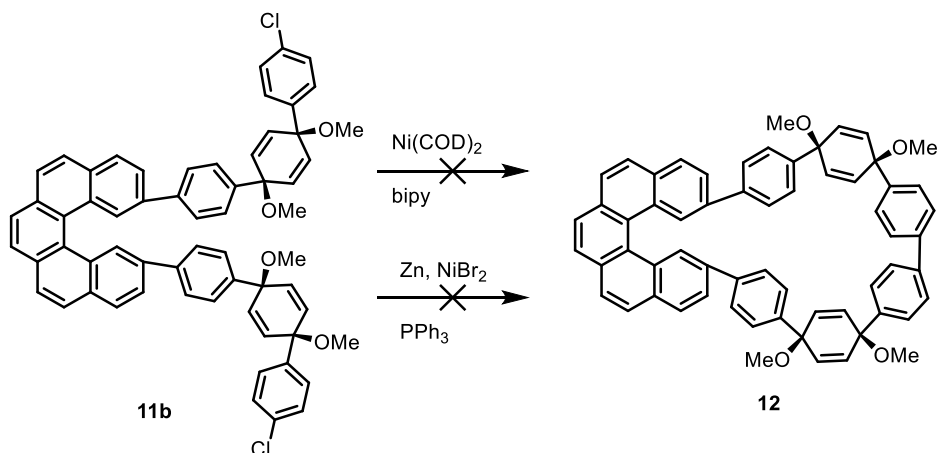
So far, this reaction sequence was performed only on an analytical scale and the reductive aromatization to prepare [5,6]HPP will require a considerably larger amount of **12** that will be synthesized after further screening of the reaction conditions and upscaling. Nevertheless, based on the previous experience with [6,7]HPP and *p*[9]SPP, it should be possible to aromatize macrocycle **12** using sodium naphthalenide or  $\text{H}_2\text{SnCl}_4$  (Scheme 24).



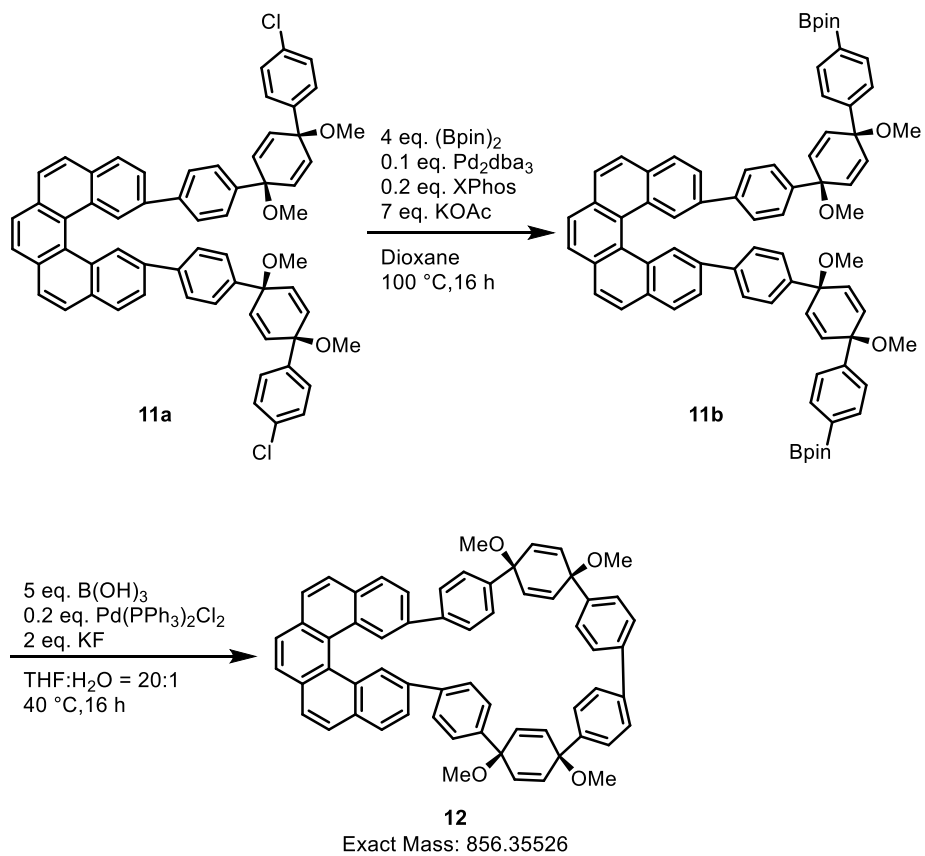
**Scheme 20.**



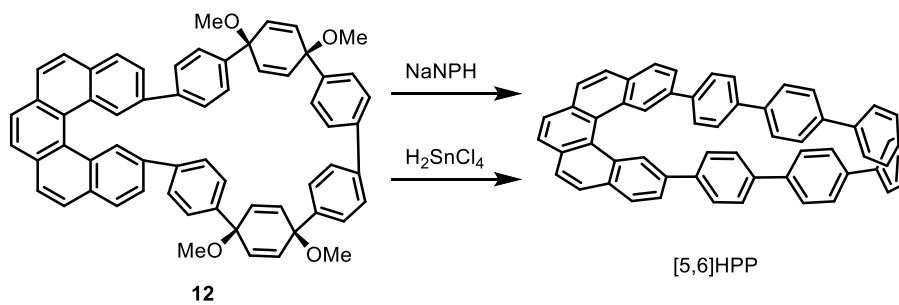
**Scheme 21.**



**Scheme 22.**



Scheme 23.



Scheme 24.

#### 4. [5,m]Helicene para-phenylenes

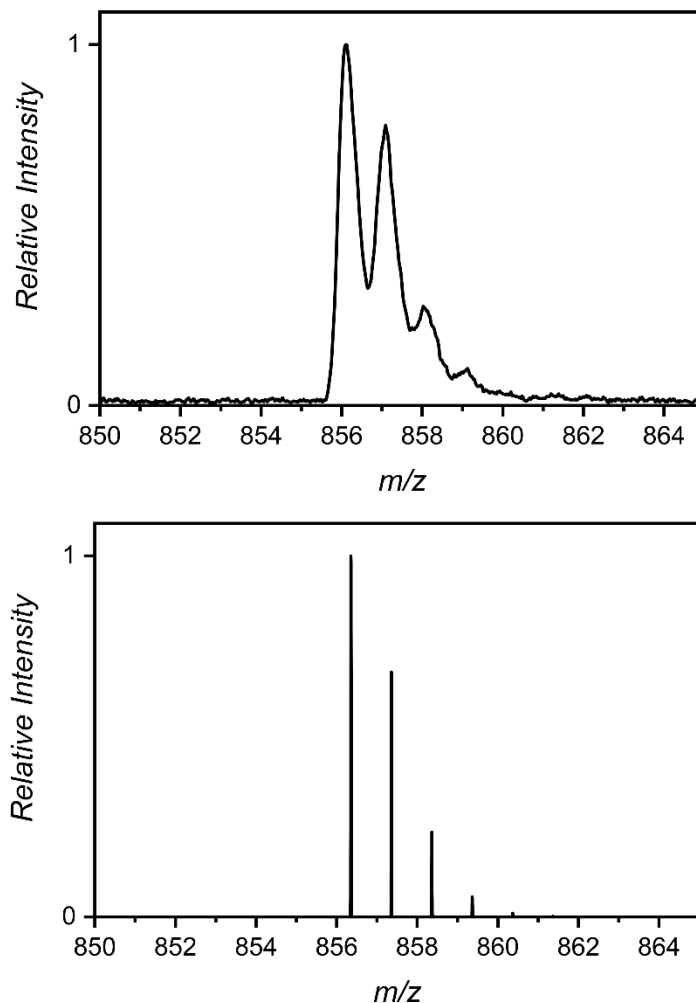
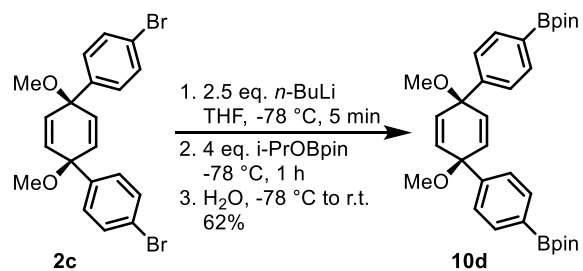
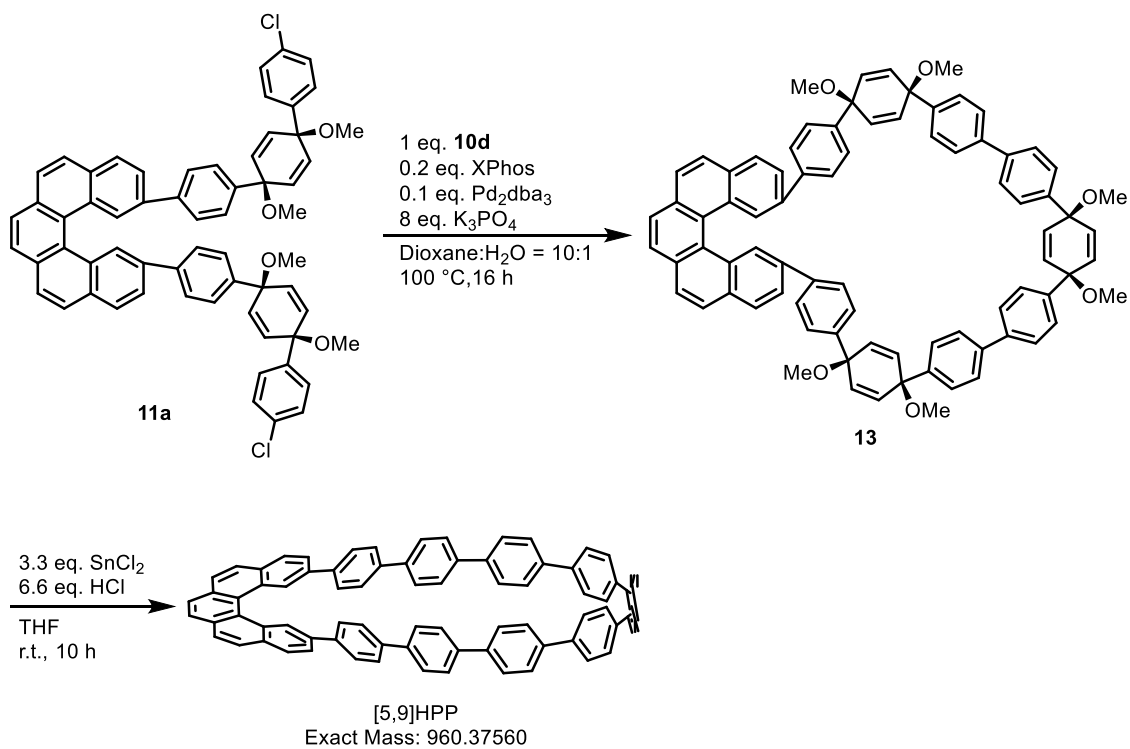


**Figure 60.** Normalized MALDI-MS spectrum of macrocycle **12** (top) with simulated isotope pattern (bottom).

Intermediate **11b** could be used to synthesize the larger [5,9]HPP. First, **2c** undergoes double lithiation followed by addition of *i*-PrOBpin to afford **10d** in a 62% yield (Scheme 25). Suzuki-Miyaura cross-coupling of **11b** and building block **10d** afforded a compounds mixture (Scheme 26), which contained the macrocycle **13** (see Appendix) together with a number of unidentified side-products. The mixture proved to be very challenging to separate. We therefore managed to partially purify macrocycle **13** using several consecutive column chromatography and gel permeation chromatography (GPC) steps. Nevertheless, we treated the partially impure fraction containing macrocycle **13** with  $\text{H}_2\text{SnCl}_4$  to attempt aromatization. Indeed, as expected, a bright blue fluorescence of the products mixture was observed, likely originating from [5,9]HPP. Furthermore, we observed the presence of [5,9]HPP in the reaction mixture with MALDI-MS (Figure 61). However, isolation of [5,9]HPP from the complex mixture has been unsuccessful so far even after a series of column chromatography and GPC purifications steps. We injected the pre-purified sample of [5,9]HPP to HPLC with a chiral stationary phase to test whether we could separate enantiomers from presumably minor impurities but we observed separation into at least six different peaks (Figure 62). Further screening of macrocyclization conditions is required to prepare **13** in a cleaner fashion.



Scheme 25



Scheme 26.

4. [5,m]Helicene para-phenylenes

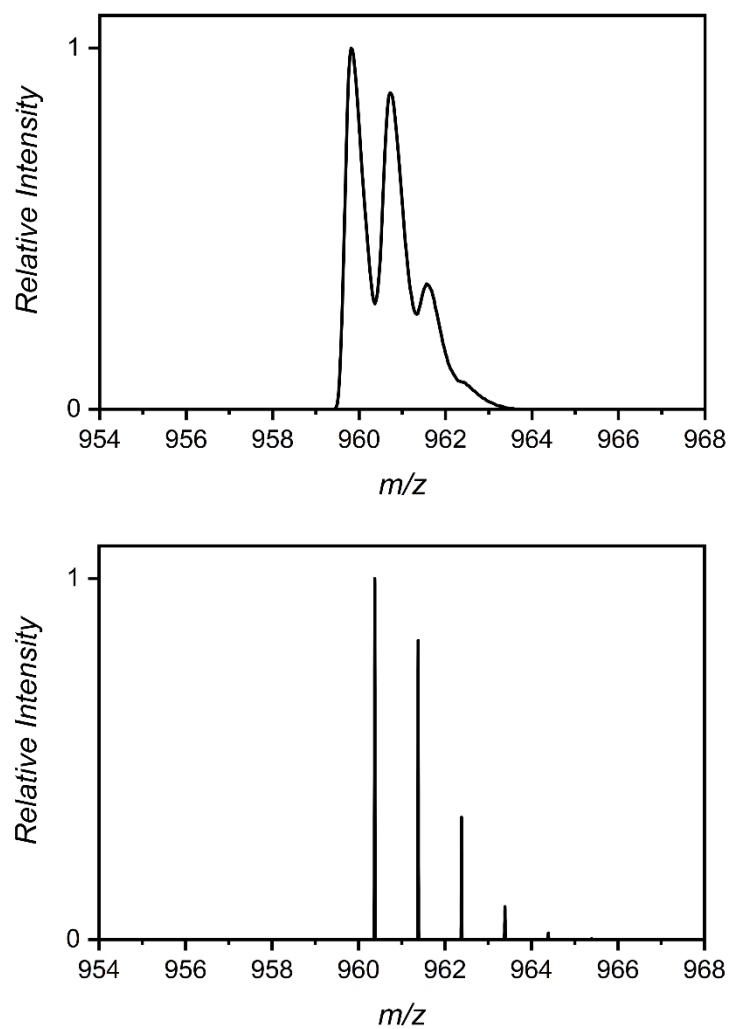


**Figure 61.** Normalized MALDI-MS spectrum of [5,9]HPP (top) with simulated isotope pattern (bottom).



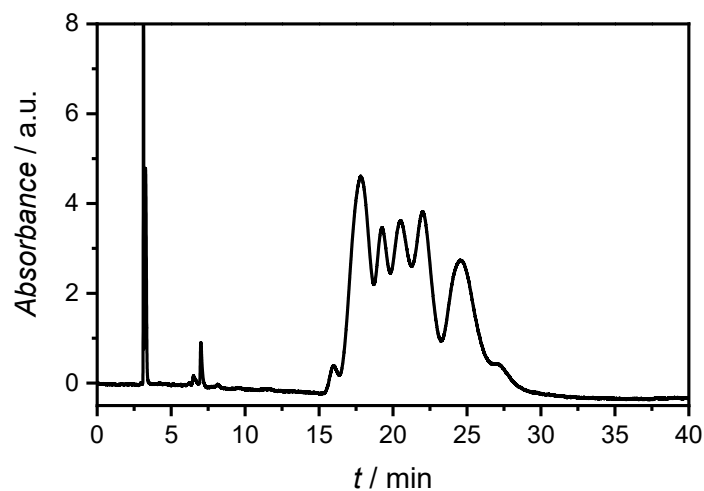
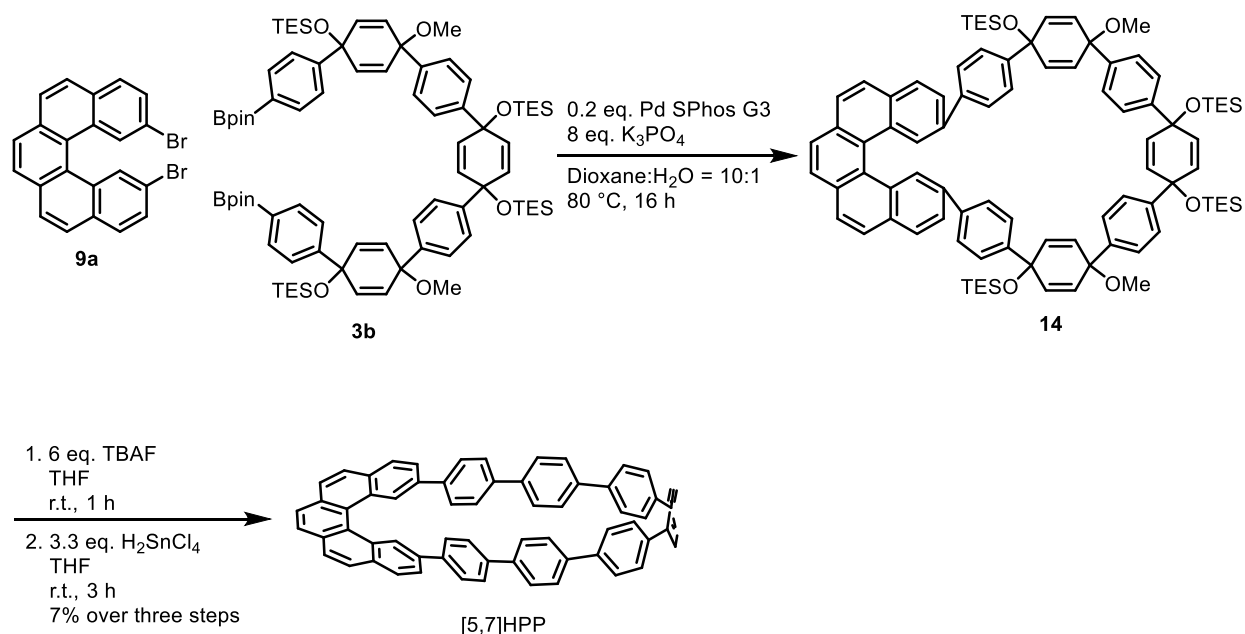


**Figure 62.** HPLC chromatogram (column: IG, flow: 1 mL min<sup>-1</sup>, eluent: DCM/hexane = 40/60) of pre-purified [5,9]HPP.

Finally, helicene **9a** and building block **3b** were reacted under Suzuki-Miyaura cross-coupling conditions to afford macrocycle **14**. Similar to the synthesis of [6,7]HPP, the intermediate macrocycle **14** proved to be too unstable to isolate. Therefore, we deprotected the TES groups with TBAF and performed a reductive aromatization using H<sub>2</sub>SnCl<sub>4</sub> directly without isolation of any intermediates. Indeed, a bright green fluorescence of the reaction mixture was observed upon addition of H<sub>2</sub>SnCl<sub>4</sub> indicating formation of [5,7]HPP. After work-up, [5,7]HPP was isolated using a single column chromatography purification step in a low yield of 7% over three steps (Scheme 27). We confirmed the structure of [5,7]HPP using NMR and HR-MS, which can be found in the Appendix (Figures A25-26).

#### 4. [5,m]Helicene para-phenylenes



Scheme 27.

#### 4.2.2. Photophysical and chiroptical properties of [5,7]HPP

We measured the absorption, emission and excitation spectra of [5,7]HPP (Figure 63) to assess its optoelectronic properties and compare them to those of [6,7]HPP. An absorption maximum observed at 338 nm was attributed to HOMO-1→LUMO and HOMO→LUMO+1 transitions and that at around 400 nm to the HOMO→LUMO transition (Figure A32). Fluorescence spectrum shows a broad visible light emission with a maximum at 498 nm with a 46% quantum yield. Both absorption and emission properties are similar to [6,7]HPP but [5,7]HPP has a lower quantum yield likely due to higher curvature of the *p*-phenylene segment<sup>[144]</sup> as [5]helicene has similar photophysics to [6]helicene.<sup>[268]</sup>

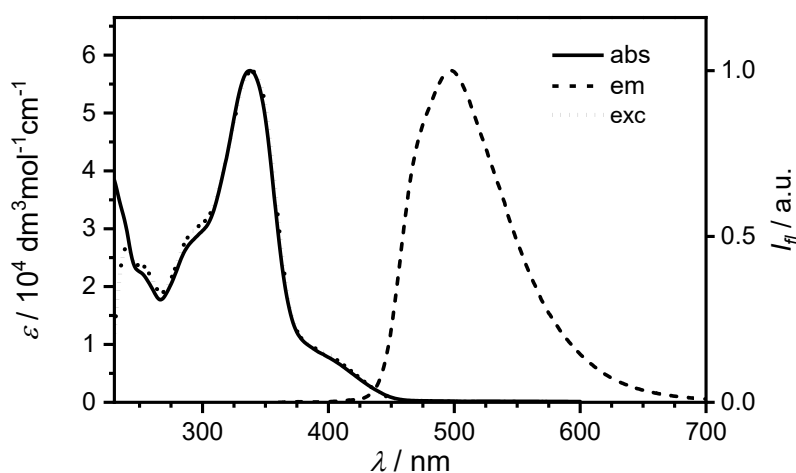
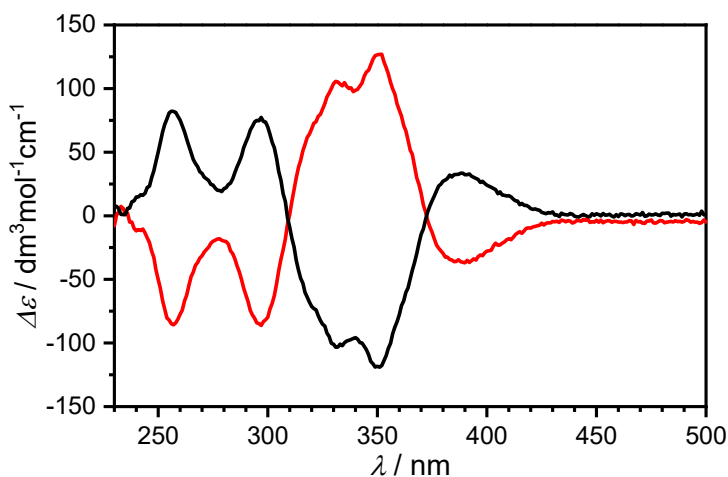


Figure 63. Absorption (solid), excitation (dotted) and emission (dashed) spectra of [5,7]HPP.

We separated the enantiomers using HPLC with a chiral stationary phase (Figure A29) and measured the CD spectra of the individual enantiomers (Figure 64). Their absolute configuration was assigned by a comparison with CD spectra calculated by TD-DFT (Figures A33 and A34). The corresponding experimental absorption dissymmetry factor  $g_{abs} = 3.9 \times 10^{-3}$  is somewhat lower than that of [6,7]HPP with  $g_{abs} = 6.5 \times 10^{-3}$ . Investigation of the transition dipole moments  $\mu$  and  $m$  shows that the angle  $\theta$  is significantly lower in [5,7]HPP than it is in [6,7]HPP (Table 9, Figure A35) although the amplitudes of  $\mu$  and  $m$  are higher. The molar circular dichroism  $\Delta\varepsilon$  of [5,7]HPP is around half of [6,7]HPP demonstrating less efficient chirality transfer from the helicene onto *p*-phenylene segment of the nanohoop. So far, we have not managed to investigate CPL of [5,7]HPP but it will be measured by our collaborators in the near future.



**Figure 64.** CD spectra of *M*- (red) and *P*-enantiomer (black) of [5,7]HPP.

**Table 9.** Calculated electric ( $\mu$ ) and magnetic ( $m$ ) transition dipole moments, the angles  $\theta$  and calculated dissymmetry factor ( $g_{abs}$ ) values for the  $S_0 \rightarrow S_1$  transition of [*m*,7]HPPs at CAM-B3LYP/6-31g(d) level of theory.

[ <i>m</i> ,7]HPP	$ \mu  / 10^{-18}$ esu·cm	$ m  / 10^{-20}$ erg·G <sup>-1</sup>	$\theta / ^\circ$	$g_{abs} / 10^{-2}$
5	2.92	8.31	107	-3.5
6	1.67	3.07	161	-7.2

#### 4.2.3. Computational investigation of [5,*n*]HPPs

We performed conformational analysis on [5,*n*]HPPs ( $n = 6,7,9$ ) with different orientations of phenylene units relative to the helicene moiety to identify the lowest-energy conformer for each molecule. Alternating orientation of the phenylenes is possible in both odd- and even-numbered [5,*n*]HPPs. We calculated the strain energies using StrainViz (Table 10) and visualized their distribution in the structures of [5,*n*]HPPs (Figure 65). The strain energy in [5,7]HPP was calculated to be around 5 kcal mol<sup>-1</sup> lower than that in

#### 4. $[5,m]$ Helicene para-phenylenes

$[6,7]$ HPP, while the strain distribution is comparable and the phenylene opposite to the helicene moiety is the most distorted phenylene in the nanohoop.

**Table 10.** Total strain energies of  $[n]$ HPPs in  $\text{kcal mol}^{-1}$  calculated at D3-B3LYP/6-31g(d) level of theory using StrainViz.

$n$	Strain energy / $\text{kcal mol}^{-1}$
6	55.1
7	50.4
9	41.0

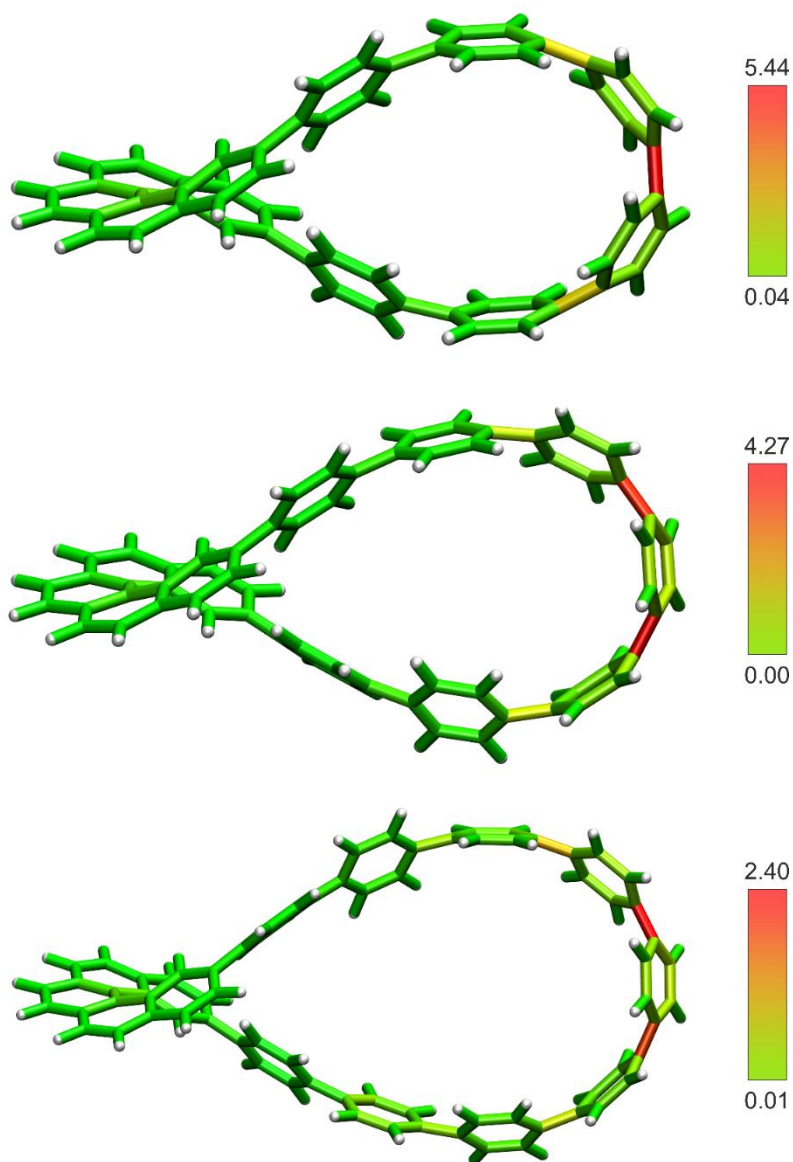


**Figure 65.** StrainViz visualization of total strain distribution (in  $\text{kcal mol}^{-1}$ ) in  $[5,n]$ HPPs ( $n = 6,7,9$ , top to bottom).

In order to investigate the aromaticity of [5,*n*]HPPs, [5,*n*]HPPs<sup>2+</sup> and [5,*n*]HPPs<sup>2-</sup> (*n* = 6,7) we calculated NICS values in the interior of the macrocycles. The points were selected to lie on a line that connects the center of the C–C bond in the bay of [5]helicene and the center of the bond between phenylenes (*n* = 6) or of the opposite phenylene ring (*n* = 7). Initially, the NICS values were calculated at B3LYP/6-31g(d) level of theory (Figures 66 and 67). Neutral [5,6]HPP showed only a slightly negative values suggesting rather a global non-aromatic character of the helicene nanohoop. However, removing two electrons and reoptimizing the geometry of [5,6]HPP<sup>2+</sup> resulted in extremely high positive NICS values of 517–912. Reduction by two electrons to obtain [5,6]HPP<sup>2-</sup> and [5,7]HPP<sup>2-</sup> showed a similar effect with large positive NICS values of 41–78 and 170–344, respectively. Highly positive NICS values are normally observed for anti-aromatic species. However, such extreme values are typically observed for radical species or lanthanide metal complexes and not for a closed-shell organic molecule. Surprisingly, oxidation of [5,7]HPP by two electrons resulted in high negative NICS values of –57 to –38 suggesting a global Möbius aromaticity. These results suggested that the oxidized and reduced [5,*n*]HPPs might be diradicaloids and the treatment of their electronic structure by B3LYP assuming a closed-shell Kohn-Sham wavefunction might be inaccurate.

A similar conclusion can be obtained by analysis of the AICD plots of the individual species. Neutral [5,*n*]HPPs revealed delocalization of electrons across the whole macrocycle but only a presence of local induced diatropic currents is visible. Therefore, these molecules are globally non-aromatic, which is consistent with the computed NICS values. AICD plot of [5,*n*]HPPs<sup>2+</sup> and [5,*n*]HPPs<sup>2-</sup> display an unusual delocalization of electrons around the macrocycles (Figures 68 and 69). Interestingly, [5,6]HPP<sup>2+</sup> shows markedly stronger delocalization than [5,6]HPP<sup>2-</sup>, while both species exhibit a global diatropic current across the whole system suggesting that both are globally Möbius aromatic. This is in stark contrast to the computed NICS values. On the other hand, [5,7]HPP<sup>2+</sup> also shows a global diatropic current consistent with the computed negative NICS values inside the cavity. Both results point at a global Möbius aromaticity. [5,7]HPP<sup>2-</sup> shows a global paratropic current in accord with the NICS values. The species is thus predicted to be globally Möbius anti-aromatic.

The conjugation pathways across [5,6]HPP<sup>2+</sup> and [5,6]HPP<sup>2-</sup> have 32 carbon atoms with 30 and 34  $\pi$ -electrons, respectively, which matches the  $(4N + 2)$   $\pi$ -electron rule of Möbius anti-aromaticity (Figure 70, left). [5,7]HPP<sup>2+</sup> and [5,7]HPP<sup>2-</sup> have 36 carbons in the conjugation pathway with 34 and 38  $\pi$ -electrons, respectively, and both species fit  $(4N + 2)$   $\pi$ -electron rule of Möbius anti-aromaticity (Figure 70, right).

The results obtained by B3LYP are puzzling not only due to the extremely high NICS values inside of [5,*n*]HPPs<sup>2+/-</sup> but also because a change of 4 electrons should preserve the aromaticity or anti-aromaticity of the system. However, the NICS calculations and the AICD plots of [5,7]HPP<sup>2+/-</sup> suggest otherwise. All the evidence rather points to a failure of the used functional to treat the electronic structure of the molecules accurately.

4.  $[5,m]$ Helicene para-phenylenes

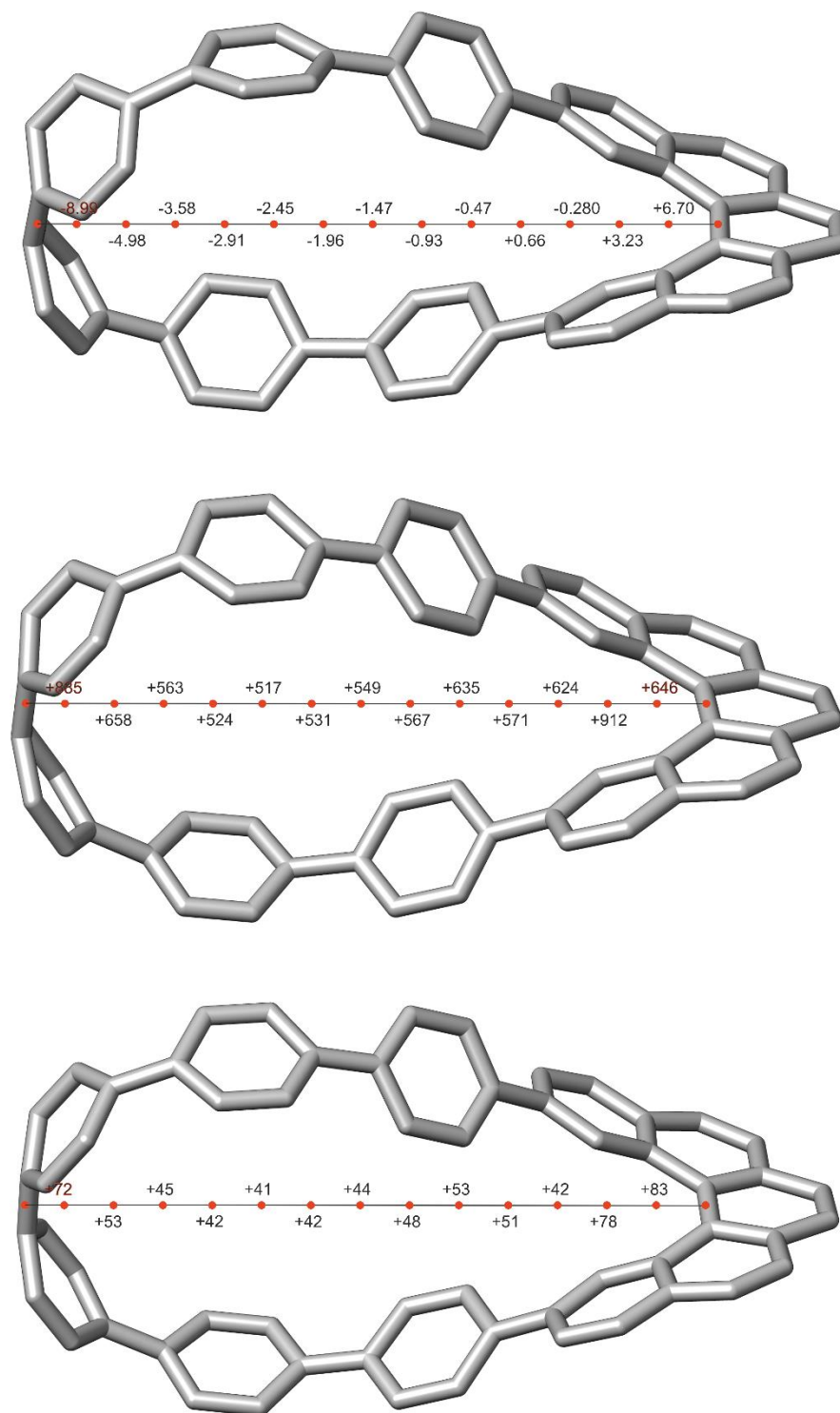


**Figure 66.** NICS values inside cavities of [5,6]HPP, [5,6]HPP<sup>2+</sup> and [5,6]HPP<sup>2-</sup> (top to bottom) at B3LYP/6-31g(d) level of theory.

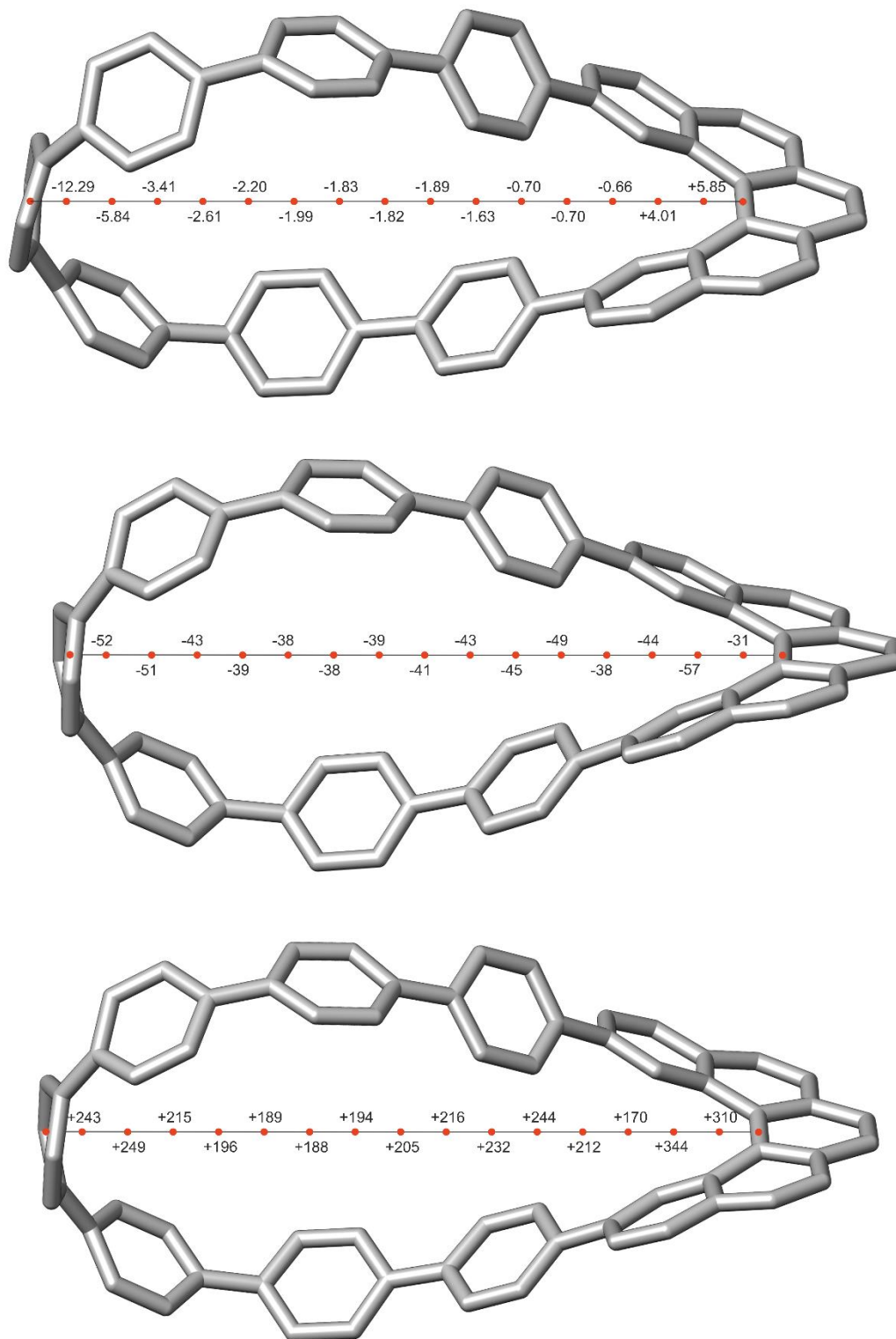


**Figure 67.** NICS values inside cavities of [5,7]HPP, [5,7]HPP<sup>2+</sup> and [5,7]HPP<sup>2-</sup> (top to bottom) at B3LYP/6-31g(d) level of theory.

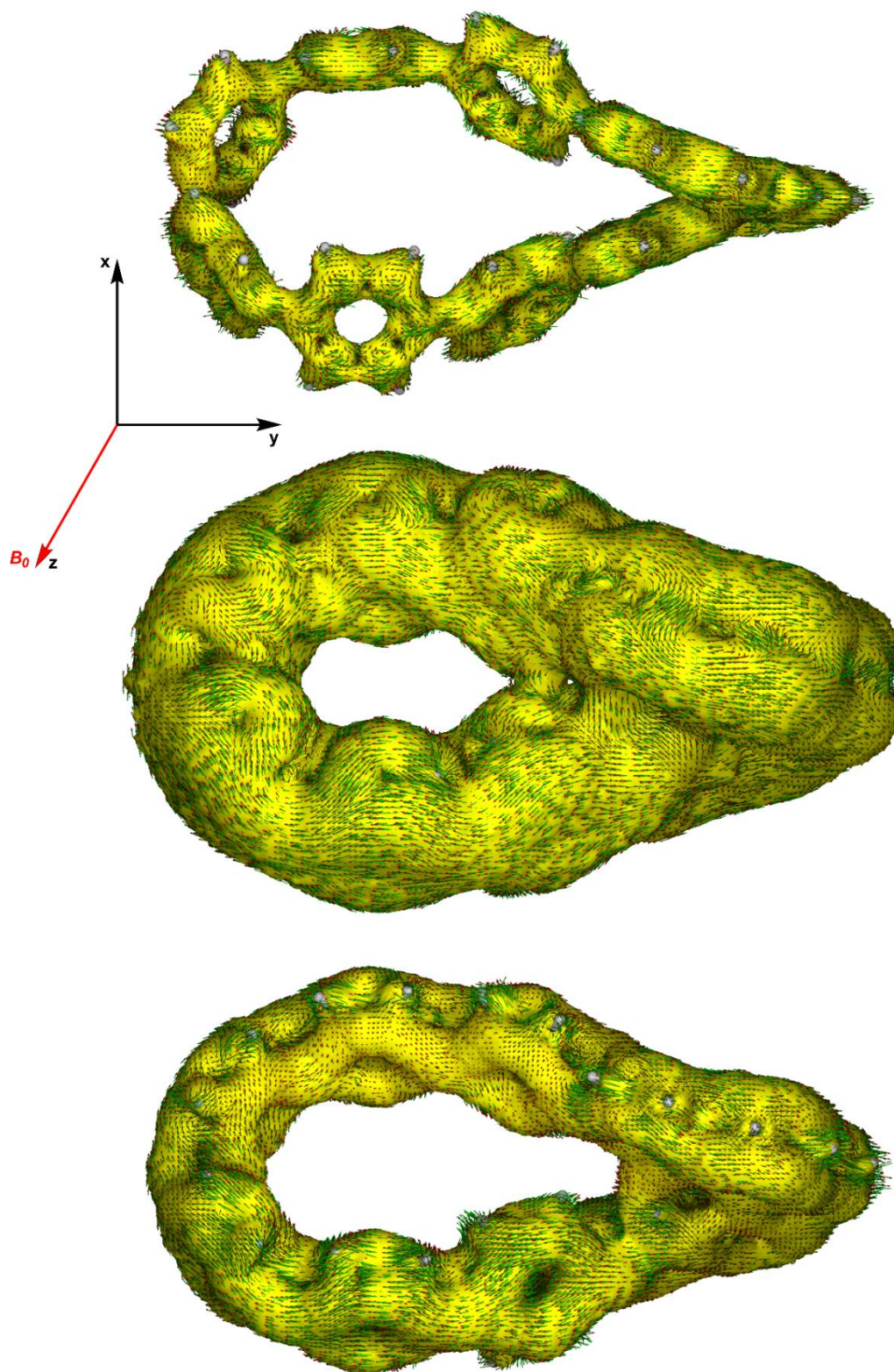


**Figure 68.** AICD plot (isosurface value 0.05) of [5,6]HPP, [5,6]HPP<sup>2+</sup> and [5,6]HPP<sup>2-</sup> (top to bottom) at B3LYP/6-31g(d) level of theory.



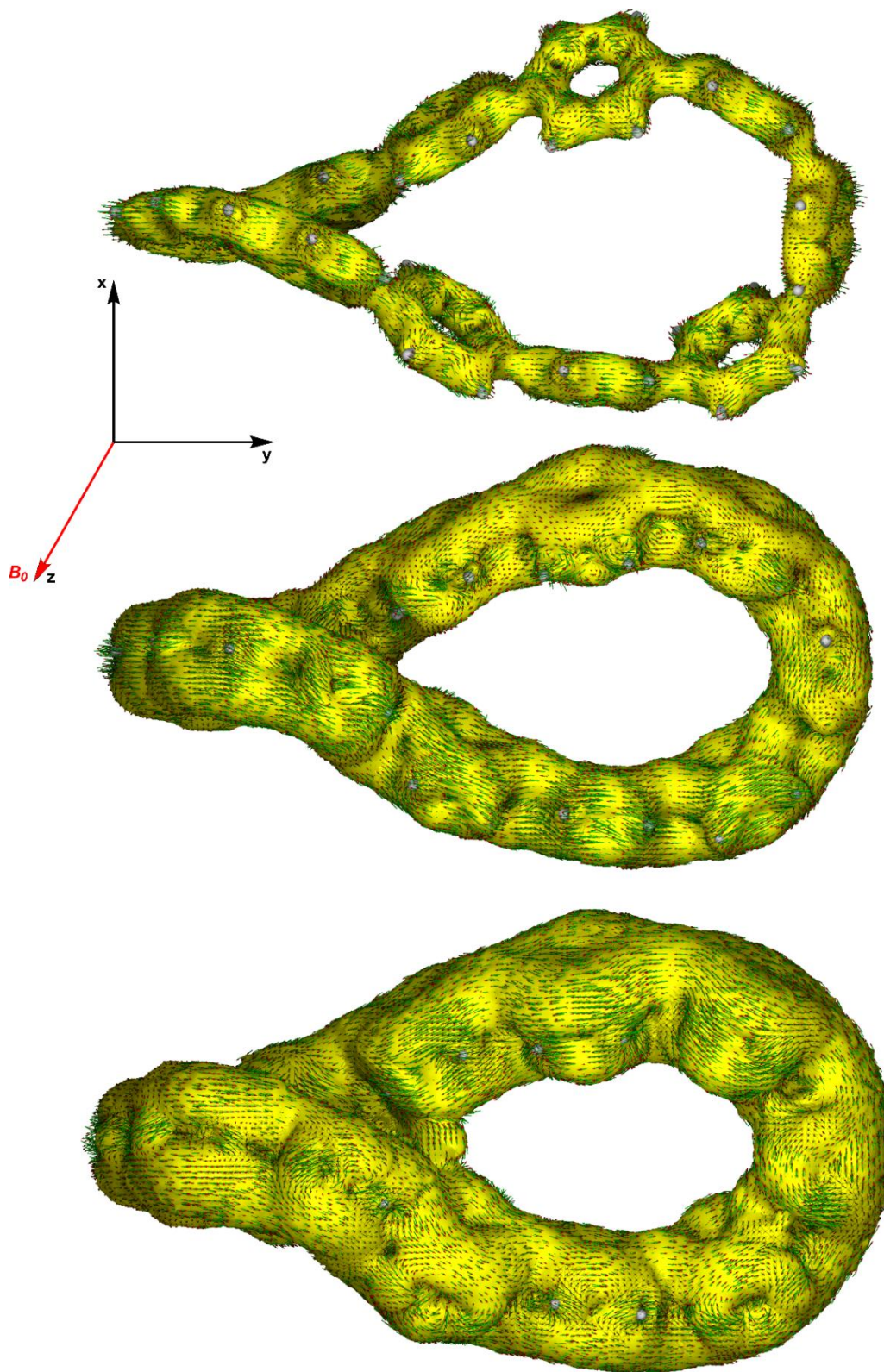


**Figure 69.** AICD plot (isosurface value 0.05) of [5,7]HPP, [5,7]HPP<sup>2+</sup> and [5,7]HPP<sup>2-</sup> (top to bottom) at B3LYP/6-31g(d) level of theory.

#### 4. [5,m]Helicene para-phenylenes

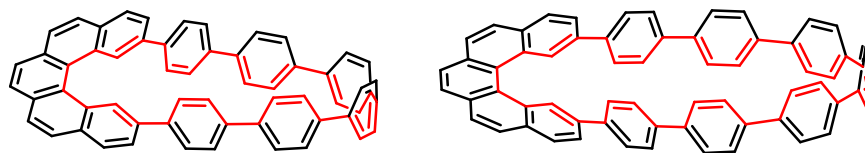


**Figure 70.** Conjugation pathway across [5,6]HPP (left) and [5,7]HPP (right).

We investigated the stability of the closed-shell B3LYP wavefunction used in all studied ionic species and we have discovered an instability due to restriction of the spin symmetry in the closed-shell SCF solution. Upon wavefunction reoptimization, the value of the  $\hat{S}^2$  operator was 0.2287 due to a slight admixture of the triplet state into the ground state wavefunction. This suggests that the studied ionic species may be better described as ground state diradicaloids. The use of the closed-shell B3LYP Kohn-Sham wavefunction therefore restricted its flexibility to treat the systems correctly, which could explain the calculated high NICS values. Therefore, we recalculated the NICS values and AICD plots for [5,6]HPP<sup>2+</sup> using M06-2X functional, which includes more Hartree-Fock exchange than B3LYP and is known to provide a more balanced description of organic diradicaloids.<sup>[269–273]</sup> The resulting NICS values were now positive for both [5,*n*]HPPs<sup>2+</sup> and [5,*n*]HPPs<sup>2-</sup> suggesting Möbius anti-aromaticity (Figure 71). Moreover, global paratropic current can be observed across the whole Möbius-shaped  $\pi$ -system confirming global anti-aromaticity in both [5,*n*]HPPs<sup>2+</sup> and [5,*n*]HPPs<sup>2-</sup> ( $n = 6,7$ ).

Upon observation of global anti-aromaticity in dication and dianions, we performed calculation of a NICS value and AICD plot for [5,6]HPP<sup>4-</sup> as we expected for it to be aromatic with  $4N$   $\pi$ -electrons. We calculated NICS value of  $-8.3$  in the cavity and a global diatropic current can be observed in the AICD plot (Figure 74) confirming that [5,6]HPP<sup>4-</sup> is globally Möbius aromatic as expected by applying simple  $\pi$ -electron count in comparison with the doubly-reduced [5,6]HPP<sup>2-</sup>.

Nevertheless, caution must be exercised when using DFT methods in similar cases. Indeed, we tested the stability of the wavefunctions obtained by the M06-2X functional and we have found out that they are unstable with respect to breaking the spin symmetry, too. Therefore, as an example, we tested calculating the NICS values and AICD plots for [5,6]HPP<sup>2+</sup> with a broken-symmetry (BS) B3LYP wavefunction. We first used the BS-B3LYP to reoptimize the geometry of [5,6]HPP<sup>2+</sup> and then performed the calculations with an external magnetic field as the perturbation (NMR calculation). We obtained NICS value of  $-19.6$  in the center of the dicationic helicene nano hoop cavity and a global diatropic current was observed using AICD plot (Figure 75) suggesting that [5,6]HPP<sup>2+</sup> is, in fact, globally Möbius aromatic. Also, the conjugation pathway now only leads through the outer part of the helicene moiety (Figure 76) unlike what we observed in the spin-restricted B3LYP or M06-2X calculations.

Clearly, one must use DFT in this case cautiously and additional calculations testing a wider variety of functionals and, ideally, multireference methods such as CASSCF is necessary to shed more light into the issues with predicting the global (anti)aromaticity of [5,*n*]HPP<sup>x+/-</sup>, where  $x = 2,4$ . In addition, chemical oxidation and reduction of [5,*n*]HPP after their successful synthesis must be performed and the corresponding ions crystallized for XRD analysis to validate the theoretical predictions.

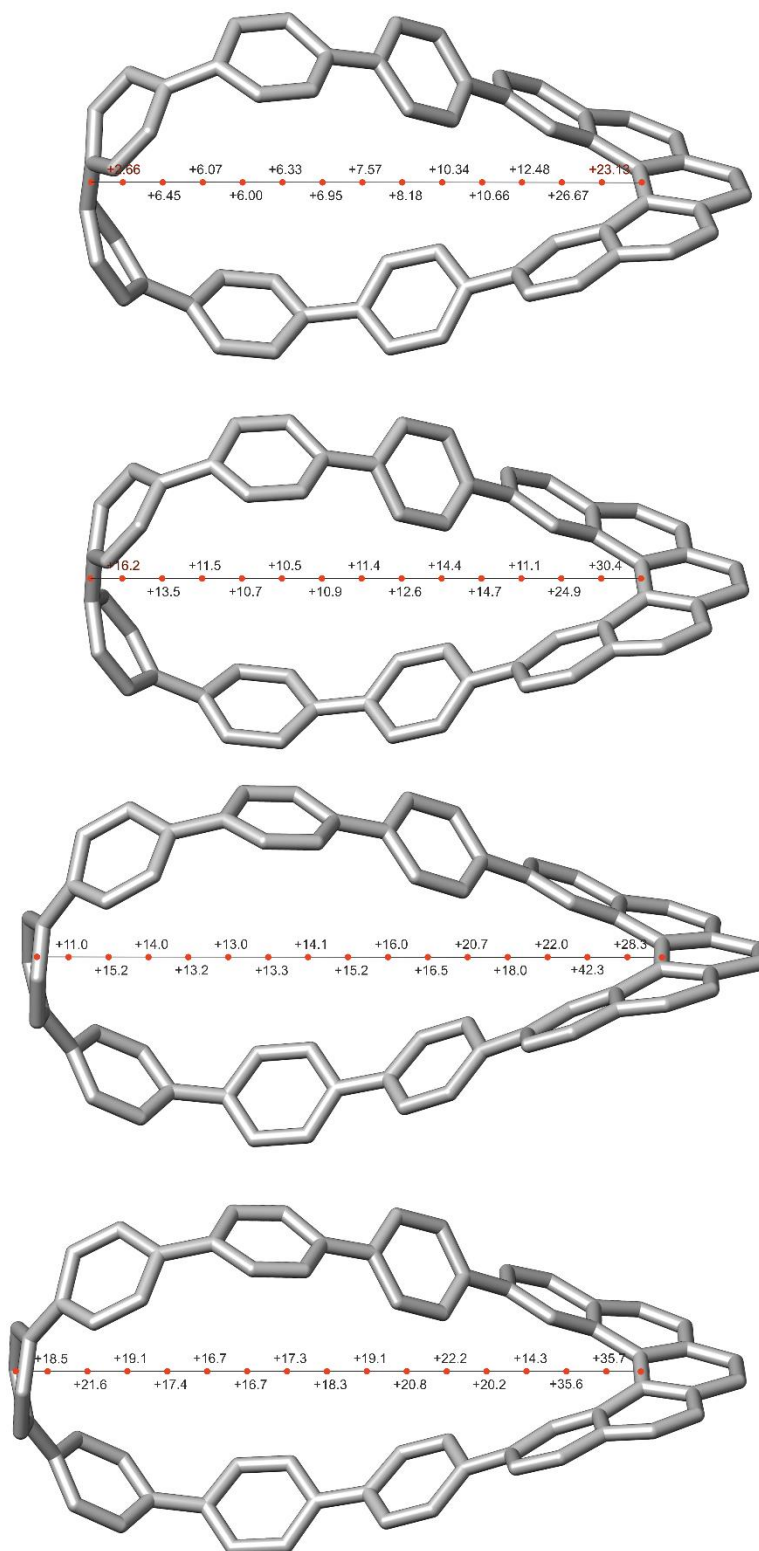


**Figure 71.** NICS values inside the cavity of  $[5,6]$ HPP $^{2+}$ ,  $[5,6]$ HPP $^{2-}$ ,  $[5,7]$ HPP $^{2+}$  and  $[5,7]$ HPP $^{2-}$  (top to bottom) at M06-2X/6-31g(d) level of theory.

4.  $[5,m]$ Helicene para-phenylenes

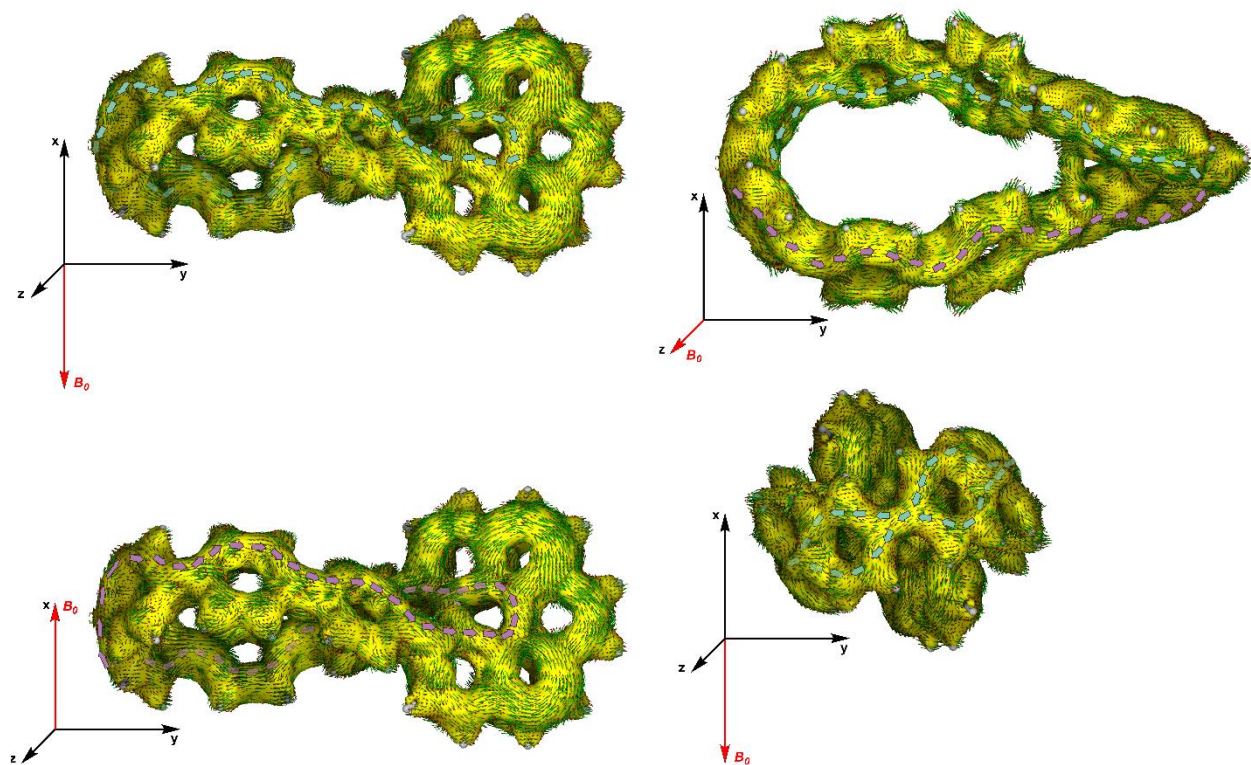


**Figure 72.** AICD plot (isosurface value 0.05) of [5,6]HPP<sup>2+</sup> at M06-2X/6-31g(d) level of theory.

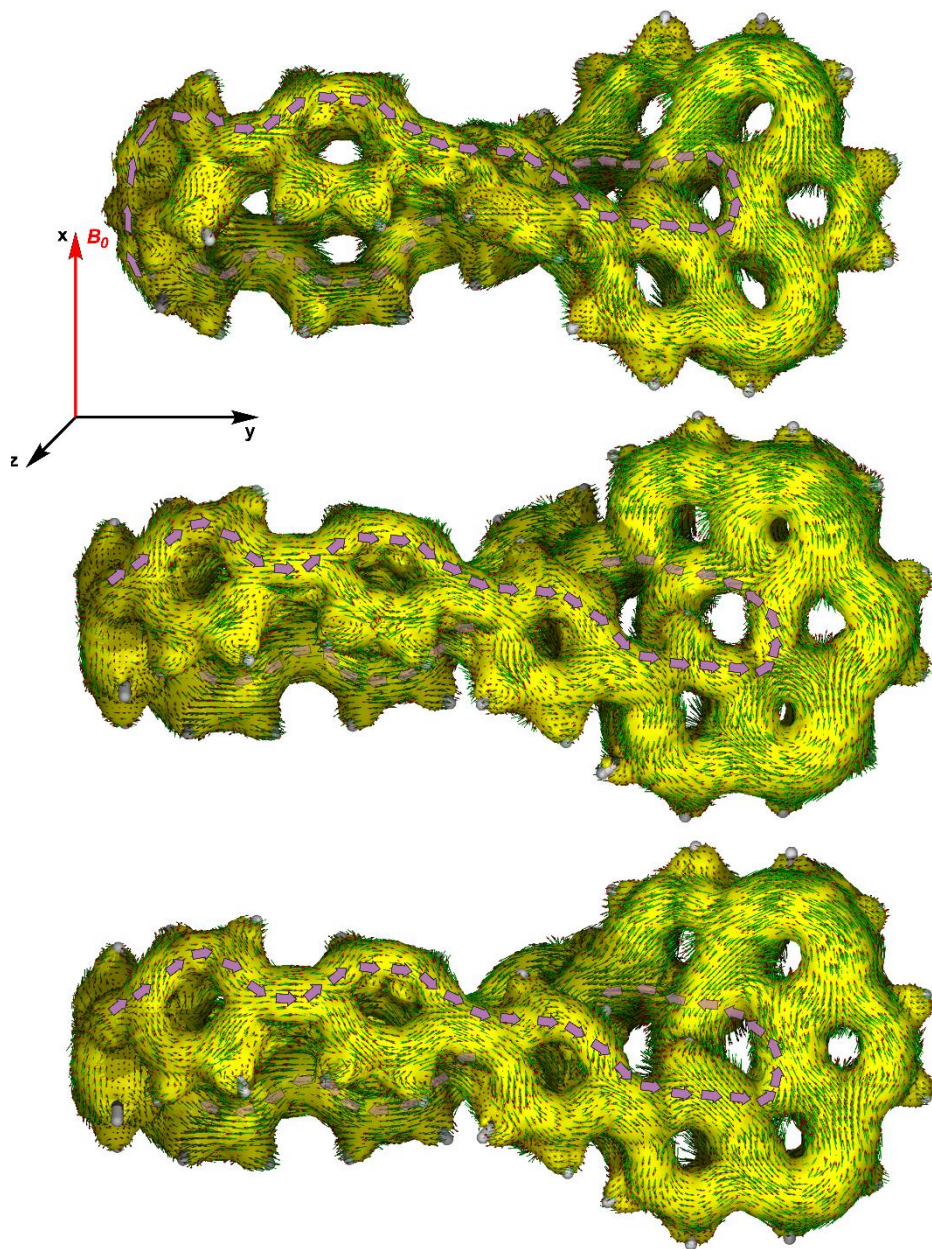


**Figure 73.** AICD plot (isosurface value 0.05) of  $[5,6]\text{HPP}^{2-}$ ,  $[5,7]\text{HPP}^{2+}$  and  $[5,7]\text{HPP}^{2-}$  (top to bottom) at M06-2X/6-31g(d) level of theory.

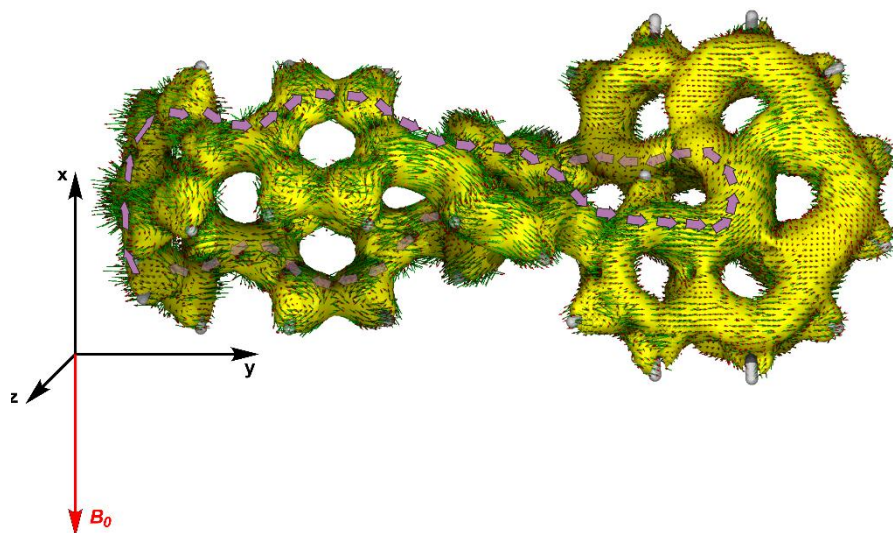


**Figure 74.** AICD plot (isosurface value 0.05) of [5,6]HPP<sup>4+</sup> at M06-2X/6-31g(d) level of theory.

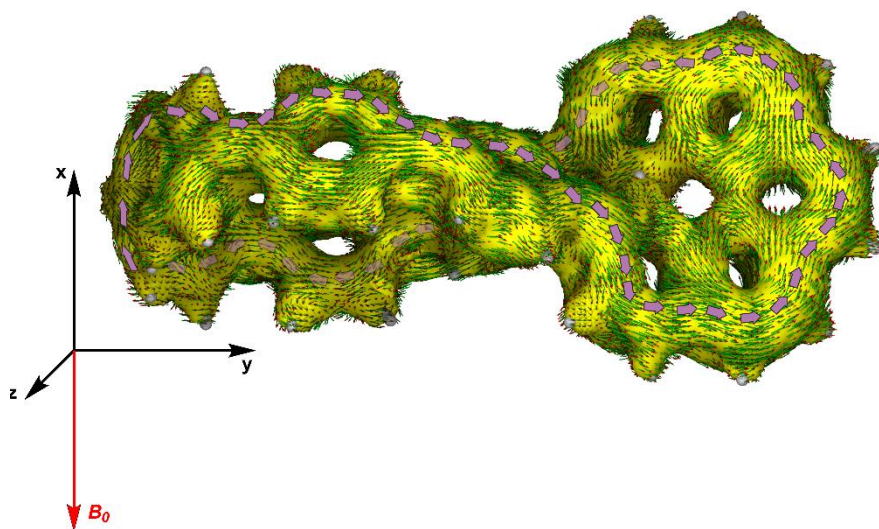


**Figure 75.** AICD plot (isosurface value 0.05) of re-optimized [5,6]HPP<sup>2+</sup> at U-B3LYP/6-31g(d) level of theory.

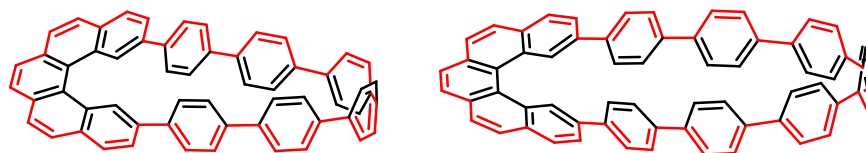


**Figure 76.** Outer conjugation pathway across [5,6]HPP (left) and [5,7]HPP (right).

### 4.3. Conclusions and Outlook

In conclusion, we have designed a series of [5,*n*]HPPs ( $n = 6,7,9$ ) to investigate the aromaticity in [*m,n*]HPPs with an even-number of carbon atoms in the conjugation pathway. We managed to synthesize and characterize [5,7]HPP using NMR and HR-MS. Unfortunately, we were not yet able to isolate [5,6]HPP and [5,9]HPP before submission of this dissertation, however, we have observed the formation of [5,9]HPP using MALDI-MS and we synthesized **11c**, a key precursor in the synthesis of [5,6]HPP. We determined that [5,7]HPP is emissive with a high quantum yield of 46%. Enantiomers were separated using chiral HPLC and we have assigned the configuration of respective enantiomers via comparison of experimental and calculated CD spectra. [5,7]HPP has weaker chiroptical properties than [6,7]HPP with absorption dissymmetry factor  $g_{abs} = 3.9 \times 10^{-3}$ .

Furthermore, we have investigated the electronic structure of the designed molecules using DFT. We have performed conformational analysis to find the lowest-energy conformers and calculated strain energies for each molecule which decrease with as the size of the nano hoop increases. To address the aromaticity of the designed compounds, we calculated the NICS values inside of the cavities of [5,*n*]HPPs ( $n = 6,7$ ) and their respective dication and dianion. AICD plots and NICS values of neutral molecules confirmed their global non-aromatic character, while dication and dianion showed unusually large NICS values, typically not observed in closed-shell systems. Moreover, the number of delocalized electrons in the system, the sign and the values of NICS, and the direction of induced currents in the system showed contradictory results. We hypothesized that the origin of this discrepancy is a diradicaloid character of the studied species. The NICS values and directions of induced currents were found to be consistent when calculated with M06-2X suggesting global anti-aromaticity of the dication and dianion. However, the restricted M06-2X wavefunctions displayed instability, too. Allowing for more flexibility in the wavefunction by removing the orbital spin symmetries, UB3LYP, provided reasonable NICS values and AICD plots for [5,6]HPP<sup>2+</sup> test case, i.e., the negative NICS value in the cavity and a global diatropic current. Therefore, one could conclude that [5,6]HPP<sup>2+</sup> is globally Möbius aromatic. Nevertheless, we strongly emphasize the importance of confirming these results experimentally and with better theoretical methods because the DFT methods in general might be unreliable in this case.

As an outlook, we suggest to complete the synthesis of all designed [5,*n*]HPPs and generate their respective dianion and dication via chemical reduction and oxidation, respectively. The magnetic properties of these species can be studied by NMR, while X-ray crystal structures would characterize the bonding parameters. These experimental results are vital for a conclusive assessment of aromaticity and anti-aromaticity. Additionally, further investigation of the electronic structures of ionic species and assessment of the diradicaloid character are crucial for drawing a clear structure–property relationship. Lastly, measurement of circularly polarized luminescence of these species could elaborate on the unusual sign change of the luminescence dissymmetry factor  $g_{lum}$  between different conformers as observed for [6,7]HPP described in Chapter 3.





## 5. Summary

Carbon-based materials experienced a rapid evolution in the past 30 years starting with the discovery of CNTs in 1991. The unique properties of SWCNTs inspired researchers to explore strategies for their size-exclusive synthesis. The bottom-up approach uses molecular fragments of CNTs as seeds for their chirality-specific growth. The fragments preserve the radial conjugation of  $\pi$ -orbitals leading to unusual properties. Specifically, carbon nanohoops as molecular fragments of armchair SWCNTs possess unique size-dependent visible light emission tunable by structural modification. However, the curved nature of carbon nanohoops induces strain which renders their synthesis a challenging task.

In Chapter 1, a brief overview of the history, synthesis, properties and applications of graphene, CNTs, CNSs and carbon nanohoops was presented in order to highlight the importance of this relatively young research topic. Synthetic strategies that overcome entropy and the build-up of strain were presented in more detail followed by structure–property relationships. Carbon nanohoops are promising luminophores with a high quantum yield of emission, however, they are typically achiral which prevents their utilization as emitters of circularly polarized light.

In Chapter 2, spiral carbon nanohoops as molecular fragments of CNSs were envisioned. Two series of spiral *para*-phenylenes,  $p[n]$ SPPs and  $m[n]$ SPPs, were designed utilizing a [2.2]paracyclophane moiety as a clip to prevent their spiral structures from unfolding. Moreover, the [2.2]paracyclophane renders  $[n]$ SPPs chiral making them great candidates for chiral luminophores. Although the challenging synthesis of  $p[9]$ SPP was successful, the same target compound was published by a different group during the course of the study. Therefore, the synthesis of  $[n]$ SPPs was abandoned and the focus turned to theoretical description of  $[n]$ SPPs to establish a clear structure–property relationship. Conformational analysis of  $[n]$ SPPs using DFT was performed to find the lowest-energy conformers which were used for prediction of optical properties. Several trends of properties that depend on the size and [2.2]paracyclophane connectivity were identified. HOMO–LUMO gap decreases with an increasing size of  $[n]$ SPP similarly to  $[n]$ CPPs. Strain energy was found to be higher in  $p[n]$ SPPs than in  $m[n]$ SPPs with the difference diminishing with increasing size. Special attention was paid to the chiroptical properties which required geometry optimization of the first excited state of  $[n]$ SPPs. TD-DFT on the ground and the first excited state geometries were used to obtain electric and magnetic transition dipole moments that were used for absorption and emission dissymmetry factors calculation. Relatively high values of absorption dissymmetry factor have been determined in  $[n]$ SPPs, although only  $p[n]$ SPPs showed size-dependence with a maximum for  $g_{\text{abs}}$  in  $p[12]$ SPP. The dissymmetry factor drops markedly for emission. This was rationalized by planarization of the most strained segment of the nanohoop which critically affects the angle between the electric and the magnetic transition dipole moments. In the outlook of the chapter, consequences of preventing the planarization on resulting dissymmetry factor was explored.

In Chapter 3, a new class of chiral carbon nanohoops was designed using [6]helicene as chirality-inducing element. A prototype helicene *para*-phenylene, [6,7]HPP was synthesized and its structure was confirmed using X-ray structural analysis. The crystal structure revealed that [6,7]HPP possessed a Möbius topology in the solid state.  $^1\text{H}$  NMR experiments at low temperature confirmed that the Möbius topology of [6,7]HPP is preserved in solution. Consequences of topology on properties were explored with a special emphasis on aromaticity. [6,7]HPP was proved to be an emitter of circularly polarized light with a high CPL brightness. An unusual effect of topology was found as the sign of CPL emission was opposite for Möbius and Hückel topologies of the compound. In the outlook of the chapter, we have investigated the aromaticity of

## 5. Summary

corresponding oxidized and reduced species of [6,7]HPP using calculation of NICS values and AICD plots. Global non-aromatic character for all species was confirmed.

In Chapter 4, a new series of [ $m,n$ ]HPPs was designed to investigate the aromaticity of helicene nano hoops that could not be tested in [6,7]HPP and its oxidized and reduced forms. [5]helicene was selected because it has an even number of carbon atoms between positions 2 and 13 required to connect it to a segment of *para*-phenylenes. [ $5,n$ ]HPPs ( $n = 6,7,9$ ) were targeted and their synthesis was attempted. The synthesis of [5,7]HPP using the same strategy as for [6,7]HPP was successful and its structure confirmed using NMR and HR-MS. A key intermediate for the synthesis of [5,6]HPP was isolated although its synthesis has not yet been accomplished. Formation of [5,9]HPP was proven using mass spectrometry, however, its isolation from a complex mixture was unsuccessful so far. Optical and chiroptical properties of the synthesized [5,7]HPP were investigated and compared to [6,7]HPP. [5,7]HPP has a higher curvature than [6,7]HPP which leads to a decrease in the luminescence quantum yield. The chiroptical properties of [5,7]HPP are also less pronounced than those of [6,7]HPP mainly due to a large difference in the angle between the transition dipole moments. Finally, aromaticity of [ $5,n$ ]HPPs ( $n = 6,7$ ) and their oxidized and reduced forms was investigated using calculation of NICS values and AICD plots. The neutral species were confirmed to be globally non-aromatic. Unusually large NICS values were calculated in both oxidized and reduced forms and global induced diatropic and paratropic currents were observed in AICD plots. Instability of the used wavefunctions was identified as the reason for such results indicating that oxidized and reduced forms of [ $5,n$ ]HPPs might be ground state diradicals. Indeed, negative NICS values in the cavity of [5,6]HPP<sup>2+</sup> were calculated when treated as a diradical and a global diatropic current was observed in an AICD plot rendering [5,6]HPP<sup>2+</sup> globally Möbius aromatic.

In this dissertation, we have explored the synthesis and properties of structurally diverse carbon nano hoops and we made several unexpected discoveries. We have gained insights about the chiroptical properties of chiral carbon nano hoops, their topology and its connection to aromaticity.

## References

- [1] J. Malinčič, S. Gaikwad, J. P. Mora-Fuentes, M.-A. Boillat, A. Prescimone, D. Häussinger, A. G. Campaña, T. Šolomek, *Angew. Chem. Int. Ed.* **2022**, *61*, e202208591.
- [2] D. D. L. Chung, *J. Mater. Sci.* **2002**, *37*, 1475–1489.
- [3] K. S. Novoselov, A. K. Geim, S. V. Morozov, D. Jiang, Y. Zhang, S. V. Dubonos, I. V. Grigorieva, A. A. Firsov, *Science* **2004**, *306*, 666–669.
- [4] C. N. R. Rao, A. K. Sood, K. S. Subrahmanyam, A. Govindaraj, *Angew. Chem. Int. Ed.* **2009**, *48*, 7752–7777.
- [5] K. P. Loh, Q. Bao, P. K. Ang, J. Yang, *J. Mater. Chem.* **2010**, *20*, 2277–2289.
- [6] K. S. Novoselov, V. I. Fal'ko, L. Colombo, P. R. Gellert, M. G. Schwab, K. Kim, *Nature* **2012**, *490*, 192–200.
- [7] J. K. Wassei, R. B. Kaner, *Acc. Chem. Res.* **2013**, *46*, 2244–2253.
- [8] D. Goyal, R. K. Dang, T. Goyal, K. K. Saxena, K. A. Mohammed, S. Dixit, *Materials* **2022**, *15*, 6241.
- [9] F. Zhang, K. Yang, G. Liu, Y. Chen, M. Wang, S. Li, R. Li, *Compos. Part Appl. Sci. Manuf.* **2022**, *160*, 107051.
- [10] X. Lu, M. Yu, H. Huang, R. S. Ruoff, *Nanotechnology* **1999**, *10*, 269–272.
- [11] K. S. Novoselov, D. Jiang, F. Schedin, T. J. Booth, V. V. Khotkevich, S. V. Morozov, A. K. Geim, *Proc. Natl. Acad. Sci.* **2005**, *102*, 10451–10453.
- [12] X. Gu, Y. Zhao, K. Sun, C. L. Z. Vieira, Z. Jia, C. Cui, Z. Wang, A. Walsh, S. Huang, *Ultrason. Sonochem.* **2019**, *58*, 104630.
- [13] Y. Hernandez, V. Nicolosi, M. Lotya, F. M. Blighe, Z. Sun, S. De, I. T. McGovern, B. Holland, M. Byrne, Y. K. Gun'Ko, J. J. Boland, P. Niraj, G. Duesberg, S. Krishnamurthy, R. Goodhue, J. Hutchison, V. Scardaci, A. C. Ferrari, J. N. Coleman, *Nat. Nanotechnol.* **2008**, *3*, 563–568.
- [14] C.-Y. Su, A.-Y. Lu, Y. Xu, F.-R. Chen, A. N. Khlobystov, L.-J. Li, *ACS Nano* **2011**, *5*, 2332–2339.
- [15] Y. Zhang, Y. Xu, R. Liu, *Carbon* **2021**, *176*, 157–167.
- [16] T. D. Dao, H. M. Jeong, *Mater. Res. Bull.* **2015**, *70*, 651–657.
- [17] C. Wu, G. Dong, L. Guan, *Phys. E Low-Dimens. Syst. Nanostructures* **2010**, *42*, 1267–1271.
- [18] G.-W. Cheng, K. Chu, J. S. Chen, J. T. H. Tsai, *Superlattices Microstruct.* **2017**, *104*, 258–265.
- [19] L. Jiao, L. Zhang, X. Wang, G. Diankov, H. Dai, *Nature* **2009**, *458*, 877–880.
- [20] S. Cai, X. Chen, P. Liu, H. Zhou, S. Fu, K. Xu, S. Chen, D. Liang, *J. Mater. Eng. Perform.* **2020**, *29*, 2248–2255.
- [21] S. Bae, H. Kim, Y. Lee, X. Xu, J.-S. Park, Y. Zheng, J. Balakrishnan, T. Lei, H. Ri Kim, Y. I. Song, Y.-J. Kim, K. S. Kim, B. Özyilmaz, J.-H. Ahn, B. H. Hong, S. Iijima, *Nat. Nanotechnol.* **2010**, *5*, 574–578.
- [22] R. Ye, D. K. James, J. M. Tour, *Acc. Chem. Res.* **2018**, *51*, 1609–1620.
- [23] H. Zhang, F. Ding, H. Li, F. Qu, H. Meng, H. Gu, *Mater. Lett.* **2019**, *244*, 171–174.
- [24] B. Partoens, F. M. Peeters, *Phys. Rev. B* **2006**, *74*, 075404.
- [25] Y. Zhang, Y.-W. Tan, H. L. Stormer, P. Kim, *Nature* **2005**, *438*, 201–204.
- [26] K. S. Novoselov, A. K. Geim, S. V. Morozov, D. Jiang, M. I. Katsnelson, I. V. Grigorieva, S. V. Dubonos, A. A. Firsov, *Nature* **2005**, *438*, 197–200.
- [27] A. K. Geim, K. S. Novoselov, *Nat. Mater.* **2007**, *6*, 183–191.
- [28] K. I. Bolotin, K. J. Sikes, Z. Jiang, M. Klima, G. Fudenberg, J. Hone, P. Kim, H. L. Stormer, *Solid State Commun.* **2008**, *146*, 351–355.
- [29] A. S. Mayorov, R. V. Gorbachev, S. V. Morozov, L. Britnell, R. Jalil, L. A. Ponomarenko, P. Blake, K. S. Novoselov, K. Watanabe, T. Taniguchi, A. K. Geim, *Nano Lett.* **2011**, *11*, 2396–2399.
- [30] A. A. Balandin, S. Ghosh, W. Bao, I. Calizo, D. Teweldebrhan, F. Miao, C. N. Lau, *Nano Lett.* **2008**, *8*, 902–907.
- [31] R. R. Nair, P. Blake, A. N. Grigorenko, K. S. Novoselov, T. J. Booth, T. Stauber, N. M. R. Peres, A. K. Geim, *Science* **2008**, *320*, 1308–1308.
- [32] M. D. Stoller, S. Park, Y. Zhu, J. An, R. S. Ruoff, *Nano Lett.* **2008**, *8*, 3498–3502.
- [33] J. S. Bunch, S. S. Verbridge, J. S. Alden, A. M. van der Zande, J. M. Parpia, H. G. Craighead, P. L. McEuen, *Nano Lett.* **2008**, *8*, 2458–2462.
- [34] N. G. Shang, P. Papakonstantinou, M. McMullan, M. Chu, A. Stamboulis, A. Potenza, S. S. Dhesi, H. Marchetto, *Adv. Funct. Mater.* **2008**, *18*, 3506–3514.

## References

- [35] L. Wang, Z. Sofer, M. Pumera, *ACS Nano* **2020**, *14*, 21–25.
- [36] C. Lee, X. Wei, J. W. Kysar, J. Hone, *Science* **2008**, *321*, 385–388.
- [37] E. J. Pavlina, C. J. Van Tyne, *J. Mater. Eng. Perform.* **2008**, *17*, 888–893.
- [38] Y. Gao, T. Cao, F. Cellini, C. Berger, W. A. de Heer, E. Tosatti, E. Riedo, A. Bongiorno, *Nat. Nanotechnol.* **2018**, *13*, 133–138.
- [39] H. Jang, Y. J. Park, X. Chen, T. Das, M.-S. Kim, J.-H. Ahn, *Adv. Mater.* **2016**, *28*, 4184–4202.
- [40] E. Stolyarova, K. T. Rim, S. Ryu, J. Maultzsch, P. Kim, L. E. Brus, T. F. Heinz, M. S. Hybertsen, G. W. Flynn, *Proc. Natl. Acad. Sci.* **2007**, *104*, 9209–9212.
- [41] A. C. Ferrari, *Solid State Commun.* **2007**, *143*, 47–57.
- [42] H. W. Kroto, J. R. Heath, S. C. O'Brien, R. F. Curl, R. E. Smalley, *Nature* **1985**, *318*, 162–163.
- [43] S. Iijima, *Nature* **1991**, *354*, 56–58.
- [44] R. Bacon, *J. Appl. Phys.* **1960**, *31*, 283–290.
- [45] A. L. Mackay, H. Terrones, *Nature* **1991**, *352*, 762–762.
- [46] M. Tagami, Y. Liang, H. Naito, Y. Kawazoe, M. Kotani, *Carbon* **2014**, *76*, 266–274.
- [47] M. S. Dresselhaus, G. Dresselhaus, R. Saito, *Carbon* **1995**, *33*, 883–891.
- [48] F. Li, H. M. Cheng, S. Bai, G. Su, M. S. Dresselhaus, *Appl. Phys. Lett.* **2000**, *77*, 3161–3163.
- [49] N. Yao, V. Lordi, *J. Appl. Phys.* **1998**, *84*, 1939–1943.
- [50] W. Chen, L. Duan, D. Zhu, *Environ. Sci. Technol.* **2007**, *41*, 8295–8300.
- [51] E. Pop, D. Mann, Q. Wang, K. Goodson, H. Dai, *Nano Lett.* **2006**, *6*, 96–100.
- [52] M. C. Hersam, *Nat. Nanotechnol.* **2008**, *3*, 387–394.
- [53] H. Dai, *Acc. Chem. Res.* **2002**, *35*, 1035–1044.
- [54] A. Yokoyama, M. Yoshida, A. Ishii, Y. K. Kato, *Phys. Rev. X* **2014**, *4*, 011005.
- [55] R. S. Ruoff, J. Tersoff, D. C. Lorents, S. Subramoney, B. Chan, *Nature* **1993**, *364*, 514–516.
- [56] S. Iijima, C. Brabec, A. Maiti, J. Bernholc, *J. Chem. Phys.* **1996**, *104*, 2089–2092.
- [57] P.-X. Hou, C. Liu, H.-M. Cheng, *Carbon* **2008**, *46*, 2003–2025.
- [58] M. Monthieux, V. L. Kuznetsov, *Carbon* **2006**, *44*, 1621–1623.
- [59] L. Radushkevich, V. áM Lukyanovich, *Zurn Fis. Chim* **1952**, *26*, 88–95.
- [60] T. W. Ebbesen, P. M. Ajayan, *Nature* **1992**, *358*, 220–222.
- [61] S. Iijima, T. Ichihashi, *Nature* **1993**, *363*, 603–605.
- [62] D. S. Bethune, C. H. Kiang, M. S. de Vries, G. Gorman, R. Savoy, J. Vazquez, R. Beyers, *Nature* **1993**, *363*, 605–607.
- [63] A. Thess, R. Lee, P. Nikolaev, H. Dai, P. Petit, J. Robert, C. Xu, Y. H. Lee, S. G. Kim, A. G. Rinzler, D. T. Colbert, G. E. Scuseria, D. Tománek, J. E. Fischer, R. E. Smalley, *Science* **1996**, *273*, 483–487.
- [64] A. G. Rinzler, J. Liu, H. Dai, P. Nikolaev, C. B. Huffman, F. J. Rodríguez-Macías, P. J. Boul, A. H. Lu, D. Heymann, D. T. Colbert, R. S. Lee, J. E. Fischer, A. M. Rao, P. C. Eklund, R. E. Smalley, *Appl. Phys. A* **1998**, *67*, 29–37.
- [65] Y. Zhang, S. Iijima, *Appl. Phys. Lett.* **1999**, *75*, 3087–3089.
- [66] E. T. Thostenson, Z. Ren, T.-W. Chou, *Compos. Sci. Technol.* **2001**, *61*, 1899–1912.
- [67] X. Wei, S. Li, W. Wang, X. Zhang, W. Zhou, S. Xie, H. Liu, *Adv. Sci.* **2022**, *9*, 2200054.
- [68] F. Yang, X. Wang, D. Zhang, J. Yang, D. Luo, Z. Xu, J. Wei, J.-Q. Wang, Z. Xu, F. Peng, X. Li, R. Li, Y. Li, M. Li, X. Bai, F. Ding, Y. Li, *Nature* **2014**, *510*, 522–524.
- [69] Z. F. Ren, Z. P. Huang, J. W. Xu, J. H. Wang, P. Bush, M. P. Siegal, P. N. Provencio, *Science* **1998**, *282*, 1105–1107.
- [70] H. M. Cheng, F. Li, G. Su, H. Y. Pan, L. L. He, X. Sun, M. S. Dresselhaus, *Appl. Phys. Lett.* **1998**, *72*, 3282–3284.
- [71] P. Nikolaev, M. J. Bronikowski, R. K. Bradley, F. Rohmund, D. T. Colbert, K. A. Smith, R. E. Smalley, *Chem. Phys. Lett.* **1999**, *313*, 91–97.
- [72] S. K. Pillai, S. S. Ray, M. Moodley, *J. Nanosci. Nanotechnol.* **2007**, *7*, 3011–3047.
- [73] M. E. Itkis, D. E. Perea, R. Jung, S. Niyogi, R. C. Haddon, *J. Am. Chem. Soc.* **2005**, *127*, 3439–3448.
- [74] P. C. Eklund, J. M. Holden, R. A. Jishi, *Carbon* **1995**, *33*, 959–972.
- [75] X. Xie, L. Ju, X. Feng, Y. Sun, R. Zhou, K. Liu, S. Fan, Q. Li, K. Jiang, *Nano Lett.* **2009**, *9*, 2565–2570.
- [76] E. Perim, L. D. Machado, D. S. Galvao, *Front. Mater.* **2014**, *1*.
- [77] S. Amelineckx, D. Bernaerts, X. B. Zhang, G. Van Tendeloo, J. Van Landuyt, *Science* **1995**, *267*, 1334–1338.
- [78] M. Quintana, M. Grzelczak, K. Spyrou, M. Calvaresi, S. Bals, B. Kooi, G. Van Tendeloo, P. Rudolf, F. Zerbetto, M. Prato, *J. Am. Chem. Soc.* **2012**, *134*, 13310–13315.
- [79] S. Berber, D. Tománek, *Phys. Rev. B* **2004**, *69*, 233404.
- [80] M. Calvaresi, M. Quintana, P. Rudolf, F. Zerbetto, M. Prato, *ChemPhysChem* **2013**, *14*, 3447–3453.

- [81] S. F. Braga, V. R. Coluci, S. B. Legoas, R. Giro, D. S. Galvão, R. H. Baughman, *Nano Lett.* **2004**, *4*, 881–884.
- [82] Y. Chen, J. Lu, Z. Gao, *J. Phys. Chem. C* **2007**, *111*, 1625–1630.
- [83] O. Zhou, R. M. Fleming, D. W. Murphy, C. H. Chen, R. C. Haddon, A. P. Ramirez, S. H. Glarum, *Science* **1994**, *263*, 1744–1747.
- [84] M. M. Zaeri, S. Ziaei-Rad, *RSC Adv.* **2014**, *4*, 22995–23001.
- [85] S. F. Braga, V. R. Coluci, R. H. Baughman, D. S. Galvão, *Chem. Phys. Lett.* **2007**, *441*, 78–82.
- [86] G. Mpourmpakis, E. Tylianakis, G. E. Froudakis, *Nano Lett.* **2007**, *7*, 1893–1897.
- [87] V. R. Coluci, S. F. Braga, R. H. Baughman, D. S. Galvão, *Phys. Rev. B* **2007**, *75*, 125404.
- [88] P. Yadav, S. Warule, J. Jog, S. Ogale, *Solid State Commun.* **2012**, *152*, 2092–2095.
- [89] B. Zheng, Z. Xu, C. Gao, *Nanoscale* **2016**, *8*, 1413–1420.
- [90] V. P. Dravid, X. Lin, Y. Wang, X. K. Wang, A. Yee, J. B. Ketterson, R. P. H. Chang, *Science* **1993**, *259*, 1601–1604.
- [91] D. Roy, E. Angeles-Tactay, R. J. C. Brown, S. J. Spencer, T. Fry, T. A. Dunton, T. Young, M. J. T. Milton, *Chem. Phys. Lett.* **2008**, *465*, 254–257.
- [92] H. Shioyama, T. Akita, *Carbon* **2003**, *41*, 179–181.
- [93] L. M. Viculis, J. J. Mack, R. B. Kaner, *Science* **2003**, *299*, 1361–1361.
- [94] F. Zeng, Y. Kuang, Y. Wang, Z. Huang, C. Fu, H. Zhou, *Adv. Mater.* **2011**, *23*, 4929–4932.
- [95] Z. Xu, B. Zheng, J. Chen, C. Gao, *Chem. Mater.* **2014**, *26*, 6811–6818.
- [96] M. V. Savoskin, V. N. Mochalin, A. P. Yaroshenko, N. I. Lazareva, T. E. Konstantinova, I. V. Barsukov, I. G. Prokofiev, *Carbon* **2007**, *45*, 2797–2800.
- [97] A. L. Chuvilin, V. L. Kuznetsov, A. N. Obratsov, *Carbon* **2009**, *47*, 3099–3105.
- [98] J. Zheng, H. Liu, B. Wu, Y. Guo, T. Wu, G. Yu, Y. Liu, D. Zhu, *Adv. Mater.* **2011**, *23*, 2460–2463.
- [99] V. Khademhosseini, D. Dideban, M. T. Ahmadi, H. Heidari, *Molecules* **2022**, *27*, 301.
- [100] F. Zeng, Y. Kuang, G. Liu, R. Liu, Z. Huang, C. Fu, H. Zhou, *Nanoscale* **2012**, *4*, 3997–4001.
- [101] H. Liu, T. Le, L. Zhang, M. Xu, *J. Mater. Sci. Mater. Electron.* **2018**, *29*, 18891–18904.
- [102] R. Jasti, J. Bhattacharjee, J. B. Neaton, C. R. Bertozzi, *J. Am. Chem. Soc.* **2008**, *130*, 17646–17647.
- [103] E. H. Fort, L. T. Scott, *J. Mater. Chem.* **2011**, *21*, 1373–1381.
- [104] R. Jasti, C. R. Bertozzi, *Chem. Phys. Lett.* **2010**, *494*, 1–7.
- [105] Y. Segawa, A. Yagi, K. Matsui, K. Itami, *Angew. Chem. Int. Ed.* **2016**, *55*, 5136–5158.
- [106] H. Omachi, T. Nakayama, E. Takahashi, Y. Segawa, K. Itami, *Nat. Chem.* **2013**, *5*, 572–576.
- [107] T.-H. Shi, M.-X. Wang, *CCS Chem.* **2020**, *3*, 916–931.
- [108] M. R. Golder, R. Jasti, *Acc. Chem. Res.* **2015**, *48*, 557–566.
- [109] T. J. Sisto, R. Jasti, *Synlett* **2012**, *2012*, 483–489.
- [110] Y. Segawa, H. Omachi, K. Itami, *Org. Lett.* **2010**, *12*, 2262–2265.
- [111] S. M. Bachrach, D. Stück, *J. Org. Chem.* **2010**, *75*, 6595–6604.
- [112] P. J. Evans, E. R. Darzi, R. Jasti, *Nat. Chem.* **2014**, *6*, 404–408.
- [113] R. Friederich, M. Nieger, F. Vögtle, *Chem. Ber.* **1993**, *126*, 1723–1732.
- [114] T. J. Sisto, M. R. Golder, E. S. Hirst, R. Jasti, *J. Am. Chem. Soc.* **2011**, *133*, 15800–15802.
- [115] J. Xia, R. Jasti, *Angew. Chem. Int. Ed.* **2012**, *51*, 2474–2476.
- [116] E. R. Darzi, T. J. Sisto, R. Jasti, *J. Org. Chem.* **2012**, *77*, 6624–6628.
- [117] S. E. Lewis, *Chem. Soc. Rev.* **2015**, *44*, 2221–2304.
- [118] H. Takaba, H. Omachi, Y. Yamamoto, J. Bouffard, K. Itami, *Angew. Chem. Int. Ed.* **2009**, *48*, 6112–6116.
- [119] H. Omachi, S. Matsuura, Y. Segawa, K. Itami, *Angew. Chem. Int. Ed.* **2010**, *49*, 10202–10205.
- [120] Y. Segawa, P. Šenel, S. Matsuura, H. Omachi, K. Itami, *Chem. Lett.* **2011**, *40*, 423–425.
- [121] Y. Ishii, Y. Nakanishi, H. Omachi, S. Matsuura, K. Matsui, H. Shinohara, Y. Segawa, K. Itami, *Chem. Sci.* **2012**, *3*, 2340–2345.
- [122] F. Sibbel, K. Matsui, Y. Segawa, A. Studer, K. Itami, *Chem. Commun.* **2013**, *50*, 954–956.
- [123] J. Malinčík, *Pers. Discuss. Author Hideto Ito Memb. Itami Group ISNA-19 Conf.* **2022**.
- [124] S. Yamago, Y. Watanabe, T. Iwamoto, *Angew. Chem. Int. Ed.* **2010**, *49*, 757–759.
- [125] E. Kayahara, Y. Sakamoto, T. Suzuki, S. Yamago, *Org. Lett.* **2012**, *14*, 3284–3287.
- [126] T. Iwamoto, Y. Watanabe, Y. Sakamoto, T. Suzuki, S. Yamago, *J. Am. Chem. Soc.* **2011**, *133*, 8354–8361.
- [127] Y. Tsuchido, R. Abe, T. Ide, K. Osakada, *Angew. Chem. Int. Ed.* **2020**, *59*, 22928–22932.
- [128] Y. Yoshigoe, Y. Tanji, Y. Hata, K. Osakada, S. Saito, E. Kayahara, S. Yamago, Y. Tsuchido, H. Kawai, *JACS Au* **2022**, *2*, 1857–1868.
- [129] E. Kayahara, V. K. Patel, S. Yamago, *J. Am. Chem. Soc.* **2014**, *136*, 2284–2287.
- [130] V. K. Patel, E. Kayahara, S. Yamago, *Chem. – Eur. J.* **2015**, *21*, 5742–5749.

## References

- [131] T. C. Lovell, C. E. Colwell, L. N. Zakharov, R. Jasti, *Chem Sci* **2019**, *10*, 3786–3790.
- [132] A.-F. Tran-Van, E. Huxol, J. M. Basler, M. Neuburger, J.-J. Adjizian, C. P. Ewels, H. A. Wegner, *Org. Lett.* **2014**, *16*, 1594–1597.
- [133] Y. Miyauchi, K. Johmoto, N. Yasuda, H. Uekusa, S. Fujii, M. Kiguchi, H. Ito, K. Itami, K. Tanaka, *Chem. – Eur. J.* **2015**, *21*, 18900–18904.
- [134] J. Volkmann, D. Kohrs, F. Bernt, H. A. Wegner, *Eur. J. Org. Chem.* **2022**, *2022*, e202101357.
- [135] D. Kohrs, J. Becker, H. A. Wegner, *Chem. – Eur. J.* **2022**, *28*, e202104239.
- [136] C. Huang, Y. Huang, N. G. Akhmedov, B. V. Popp, J. L. Petersen, K. K. Wang, *Org. Lett.* **2014**, *16*, 2672–2675.
- [137] S. Li, C. Huang, H. Thakellapalli, B. Farajidizaji, B. V. Popp, J. L. Petersen, K. K. Wang, *Org. Lett.* **2016**, *18*, 2268–2271.
- [138] Y. Segawa, A. Fukazawa, S. Matsuura, H. Omachi, S. Yamaguchi, S. Irle, K. Itami, *Org. Biomol. Chem.* **2012**, *10*, 5979–5984.
- [139] M. Fujitsuka, D. W. Cho, T. Iwamoto, S. Yamago, T. Majima, *Phys. Chem. Chem. Phys.* **2012**, *14*, 14585–14588.
- [140] E. R. Darzi, R. Jasti, *Chem. Soc. Rev.* **2015**, *44*, 6401–6410.
- [141] M. Banerjee, R. Shukla, R. Rathore, *J. Am. Chem. Soc.* **2009**, *131*, 1780–1786.
- [142] L. Adamska, I. Nayyar, H. Chen, A. K. Swan, N. Oldani, S. Fernandez-Alberti, M. R. Golder, R. Jasti, S. K. Doorn, S. Tretiak, *Nano Lett.* **2014**, *14*, 6539–6546.
- [143] R. Franklin-Mergarejo, D. O. Alvarez, S. Tretiak, S. Fernandez-Alberti, *Sci. Rep.* **2016**, *6*, 31253.
- [144] P. Li, T. J. Sisto, E. R. Darzi, R. Jasti, *Org. Lett.* **2014**, *16*, 182–185.
- [145] C. E. Colwell, T. W. Price, T. Stauch, R. Jasti, *Chem. Sci.* **2020**, *11*, 3923–3930.
- [146] M. Hermann, D. Wassy, B. Esser, *Angew. Chem. Int. Ed.* **2021**, *60*, 15743–15766.
- [147] T. Kuwabara, J. Orii, Y. Segawa, K. Itami, *Angew. Chem. Int. Ed.* **2015**, *54*, 9646–9649.
- [148] T. C. Lovell, K. G. Fosnacht, C. E. Colwell, R. Jasti, *Chem. Sci.* **2020**, *11*, 12029–12035.
- [149] E. R. Darzi, E. S. Hirst, C. D. Weber, L. N. Zakharov, M. C. Lonergan, R. Jasti, *ACS Cent. Sci.* **2015**, *1*, 335–342.
- [150] A. Yagi, G. Venkataramana, Y. Segawa, K. Itami, *Chem. Commun.* **2013**, *50*, 957–959.
- [151] Z.-A. Huang, C. Chen, X.-D. Yang, X.-B. Fan, W. Zhou, C.-H. Tung, L.-Z. Wu, H. Cong, *J. Am. Chem. Soc.* **2016**, *138*, 11144–11147.
- [152] P. Li, B. M. Wong, L. N. Zakharov, R. Jasti, *Org. Lett.* **2016**, *18*, 1574–1577.
- [153] H. Thakellapalli, B. Farajidizaji, T. W. Butcher, N. G. Akhmedov, B. V. Popp, J. L. Petersen, K. K. Wang, *Org. Lett.* **2015**, *17*, 3470–3473.
- [154] H. Ito, Y. Mitamura, Y. Segawa, K. Itami, *Angew. Chem. Int. Ed.* **2015**, *54*, 159–163.
- [155] H. Thakellapalli, S. Li, B. Farajidizaji, N. N. Baughman, N. G. Akhmedov, B. V. Popp, K. K. Wang, *Org. Lett.* **2017**, *19*, 2674–2677.
- [156] S. Nishigaki, M. Fukui, H. Sugiyama, H. Uekusa, S. Kawauchi, Y. Shibata, K. Tanaka, *Chem. – Eur. J.* **2017**, *23*, 7227–7231.
- [157] Y. Kuroda, Y. Sakamoto, T. Suzuki, E. Kayahara, S. Yamago, *J. Org. Chem.* **2016**, *81*, 3356–3363.
- [158] K. Senthilkumar, M. Kondratowicz, T. Lis, P. J. Chmielewski, J. Cybińska, J. L. Zafrá, J. Casado, T. Vives, J. Crassous, L. Favereau, M. Stepień, *J. Am. Chem. Soc.* **2019**, DOI 10.1021/jacs.9b01797.
- [159] K. Matsui, Y. Segawa, K. Itami, *Org. Lett.* **2012**, *14*, 1888–1891.
- [160] Y. Xu, S. Gsänger, M. B. Minameyer, I. Imaz, D. Maspoeh, O. Shyshov, F. Schwer, X. Ribas, T. Drewello, B. Meyer, M. von Delius, *J. Am. Chem. Soc.* **2019**, *141*, 18500–18507.
- [161] B. Farajidizaji, H. Thakellapalli, S. Li, C. Huang, N. N. Baughman, N. G. Akhmedov, B. V. Popp, J. L. Petersen, K. K. Wang, *Chem. – Eur. J.* **2016**, *22*, 16420–16424.
- [162] E. Kayahara, X. Zhai, S. Yamago, *Can. J. Chem.* **2017**, *95*, 351–356.
- [163] M. Chen, K. S. Unikela, R. Ramalakshmi, B. Li, C. Darrigan, A. Chrostowska, S.-Y. Liu, *Angew. Chem. Int. Ed.* **2021**, *60*, 1556–1560.
- [164] J. M. V. Raden, E. R. Darzi, L. N. Zakharov, R. Jasti, *Org. Biomol. Chem.* **2016**, *14*, 5721–5727.
- [165] T. C. Lovell, Z. R. Garrison, R. Jasti, *Angew. Chem. Int. Ed.* **2020**, *59*, 14363–14367.
- [166] Z.-L. Qiu, C. Tang, X.-R. Wang, Y.-Y. Ju, K.-S. Chu, Z.-Y. Deng, H. Hou, Y.-M. Liu, Y.-Z. Tan, *Angew. Chem.* **2020**, *132*, 21054–21058.
- [167] M. Ball, Y. Zhong, B. Fowler, B. Zhang, P. Li, G. Etkin, D. W. Paley, J. Decatur, A. K. Dalsania, H. Li, S. Xiao, F. Ng, M. L. Steigerwald, C. Nuckolls, *J. Am. Chem. Soc.* **2016**, *138*, 12861–12867.
- [168] E. Hückel, *Z. Für Phys.* **1931**, *70*, 204–286.
- [169] V. I. Minkin, *Pure Appl. Chem.* **1999**, *71*, 1919–1981.

- [170] M. K. Cyrański, T. M. Krygowski, A. R. Katritzky, P. von R. Schleyer, *J. Org. Chem.* **2002**, *67*, 1333–1338.
- [171] M. Jirásek, M. Rickhaus, L. Tejerina, H. L. Anderson, *J. Am. Chem. Soc.* **2021**, *143*, 2403–2412.
- [172] H. Fliegl, D. Sundholm, S. Taubert, J. Jusélius, W. Klopper, *J. Phys. Chem. A* **2009**, *113*, 8668–8676.
- [173] S. Taubert, D. Sundholm, F. Pichierri, *J. Org. Chem.* **2010**, *75*, 5867–5874.
- [174] P. von R. Schleyer, C. Maerker, A. Dransfeld, H. Jiao, N. J. R. van Eikema Hommes, *J. Am. Chem. Soc.* **1996**, *118*, 6317–6318.
- [175] E. Kayahara, T. Kouyama, T. Kato, H. Takaya, N. Yasuda, S. Yamago, *Angew. Chem. Int. Ed.* **2013**, *52*, 13722–13726.
- [176] N. Toriumi, A. Muranaka, E. Kayahara, S. Yamago, M. Uchiyama, *J. Am. Chem. Soc.* **2015**, *137*, 82–85.
- [177] E. Kayahara, T. Kouyama, T. Kato, S. Yamago, *J. Am. Chem. Soc.* **2016**, *138*, 338–344.
- [178] Y. Masumoto, N. Toriumi, A. Muranaka, E. Kayahara, S. Yamago, M. Uchiyama, *J. Phys. Chem. A* **2018**, *122*, 5162–5167.
- [179] A. V. Zabula, A. S. Filatov, J. Xia, R. Jasti, M. A. Petrukhina, *Angew. Chem. Int. Ed.* **2013**, *52*, 5033–5036.
- [180] S. N. Spisak, Z. Wei, E. Darzi, R. Jasti, M. A. Petrukhina, *Chem. Commun.* **2018**, *54*, 7818–7821.
- [181] Z. Zhou, Z. Wei, T. A. Schaub, R. Jasti, M. A. Petrukhina, *Chem. Sci.* **2020**, *11*, 9395–9401.
- [182] A. Yu. Rogachev, Z. Zhou, S. Liu, Z. Wei, T. A. Schaub, R. Jasti, M. A. Petrukhina, *Chem. Sci.* **2021**, *12*, 6526–6535.
- [183] E. J. Leonhardt, R. Jasti, *Nat. Rev. Chem.* **2019**, *3*, 672–686.
- [184] N. Ozaki, H. Sakamoto, T. Nishihara, T. Fujimori, Y. Hijikata, R. Kimura, S. Irle, K. Itami, *Angew. Chem. Int. Ed.* **2017**, *56*, 11196–11202.
- [185] P. D. Sala, N. Buccheri, A. Sanzone, M. Sassi, P. Neri, C. Talotta, A. Rocco, V. Pinchetti, L. Beverina, S. Brovelli, C. Gaeta, *Chem. Commun.* **2019**, *55*, 3160–3163.
- [186] K. Sato, M. Hasegawa, Y. Nojima, N. Hara, T. Nishiuchi, Y. Imai, Y. Mazaki, *Chem. – Eur. J.* **2021**, *27*, 1323–1329.
- [187] B. M. White, Y. Zhao, T. E. Kawashima, B. P. Branchaud, M. D. Pluth, R. Jasti, *ACS Cent. Sci.* **2018**, *4*, 1173–1178.
- [188] H. Tang, Z. Gu, C. Li, Z. Li, W. Wu, X. Jiang, *Biomater. Sci.* **2019**, *7*, 2552–2558.
- [189] T. C. Lovell, S. G. Bolton, J. P. Kenison, J. Shangguan, C. E. Otteson, F. Civitci, X. Nan, M. D. Pluth, R. Jasti, *ACS Nano* **2021**, *15*, 15285–15293.
- [190] M. V. Padalkar, N. Pleshko, *Analyst* **2015**, *140*, 2093–2100.
- [191] Y. Xu, M. von Delius, *Angew. Chem. Int. Ed.* **2020**, *59*, 559–573.
- [192] J. Xia, J. W. Bacon, R. Jasti, *Chem. Sci.* **2012**, *3*, 3018–3021.
- [193] T. Iwamoto, Y. Watanabe, T. Sadahiro, T. Haino, S. Yamago, *Angew. Chem. Int. Ed.* **2011**, *50*, 8342–8344.
- [194] T. Iwamoto, Y. Watanabe, H. Takaya, T. Haino, N. Yasuda, S. Yamago, *Chem. – Eur. J.* **2013**, *19*, 14061–14068.
- [195] Y. Nakanishi, H. Omachi, S. Matsuura, Y. Miyata, R. Kitaura, Y. Segawa, K. Itami, H. Shinohara, *Angew. Chem. Int. Ed.* **2014**, *53*, 3102–3106.
- [196] T. Iwamoto, Z. Slanina, N. Mizorogi, J. Guo, T. Akasaka, S. Nagase, H. Takaya, N. Yasuda, T. Kato, S. Yamago, *Chem. – Eur. J.* **2014**, *20*, 14403–14409.
- [197] Q. Huang, G. Zhuang, H. Jia, M. Qian, S. Cui, S. Yang, P. Du, *Angew. Chem. Int. Ed.* **2019**, *58*, 6244–6249.
- [198] Y. Yang, S. Huangfu, S. Sato, M. Juriček, *Org. Lett.* **2021**, *23*, 7943–7948.
- [199] F. Schwer, S. Zank, M. Freiberger, R. Kaur, S. Frühwald, C. C. Robertson, A. Görling, T. Drewello, D. M. Guldi, M. von Delius, *Org. Mater.* **2022**, *4*, 7–17.
- [200] E. Ubasart, O. Borodin, C. Fuertes-Espinosa, Y. Xu, C. García-Simón, L. Gómez, J. Juanhuix, F. Gándara, I. Imaz, D. MasPOCH, M. von Delius, X. Ribas, *Nat. Chem.* **2021**, *13*, 420–427.
- [201] Y. Xu, B. Wang, R. Kaur, M. B. Minameyer, M. Bothe, T. Drewello, D. M. Guldi, M. von Delius, *Angew. Chem. Int. Ed.* **2018**, *57*, 11549–11553.
- [202] H. Ueno, T. Nishihara, Y. Segawa, K. Itami, *Angew. Chem. Int. Ed.* **2015**, *54*, 3707–3711.
- [203] Y. Xu, R. Kaur, B. Wang, M. B. Minameyer, S. Gsänger, B. Meyer, T. Drewello, D. M. Guldi, M. von Delius, *J. Am. Chem. Soc.* **2018**, *140*, 13413–13420.
- [204] J. M. Van Raden, B. M. White, L. N. Zakharov, R. Jasti, *Angew. Chem. Int. Ed.* **2019**, *58*, 7341–7345.
- [205] J. M. Van Raden, N. N. Jarenwattananon, L. N. Zakharov, R. Jasti, *Chem. – Eur. J.* **2020**, *26*, 10205–10209.
- [206] Y.-Y. Fan, D. Chen, Z.-A. Huang, J. Zhu, C.-H. Tung, L.-Z. Wu, H. Cong, *Nat. Commun.* **2018**, *9*, 3037.
- [207] Y. Segawa, M. Kuwayama, Y. Hijikata, M. Fushimi, T. Nishihara, J. Pirillo, J. Shirasaki, N. Kubota, K. Itami, *Science* **2019**, *365*, 272–276.
- [208] S. Fomine, M. G. Zolotukhin, P. Guadarrama, *J. Mol. Model.* **2012**, *18*, 4025–4032.
- [209] S. M. Bachrach, Z.-C. Zayat, *J. Org. Chem.* **2016**, *81*, 4559–4565.

## References

- [210] S. Hashimoto, T. Iwamoto, D. Kurachi, E. Kayahara, S. Yamago, *ChemPlusChem* **2017**, *82*, 1015–1020.
- [211] Y. Lv, J. Lin, K. Song, X. Song, H. Zang, Y. Zang, D. Zhu, *Sci. Adv.* **2021**, *7*, eabk3095.
- [212] S. Hashimoto, E. Kayahara, Y. Mizuhata, N. Tokitoh, K. Takeuchi, F. Ozawa, S. Yamago, *Org. Lett.* **2018**, *20*, 5973–5976.
- [213] E. J. Leonhardt, J. M. Van Raden, D. Miller, L. N. Zakharov, B. Alemán, R. Jasti, *Nano Lett.* **2018**, *18*, 7991–7997.
- [214] J. M. Van Raden, E. J. Leonhardt, L. N. Zakharov, A. Pérez-Guardiola, A. J. Pérez-Jiménez, C. R. Marshall, C. K. Brozek, J. C. Sancho-García, R. Jasti, *J. Org. Chem.* **2020**, *85*, 129–141.
- [215] H. Shudo, M. Kuwayama, M. Shimasaki, T. Nishihara, Y. Takeda, N. Mitoma, T. Kuwabara, A. Yagi, Y. Segawa, K. Itami, *Nat. Commun.* **2022**, *13*, 3713.
- [216] H. Tanaka, Y. Inoue, T. Mori, *ChemPhotoChem* **2018**, *2*, 386–402.
- [217] W. Kuhn, *Trans. Faraday Soc.* **1930**, *26*, 293–308.
- [218] J. P. Riehl, F. S. Richardson, *Chem. Rev.* **1986**, *86*, 1–16.
- [219] M. Wakabayashi, S. Yokojima, T. Fukaminato, K. Shiino, M. Irie, S. Nakamura, *J. Phys. Chem. A* **2014**, *118*, 5046–5057.
- [220] E. M. Sánchez-Carnerero, A. R. Agarrabeitia, F. Moreno, B. L. Maroto, G. Muller, M. J. Ortiz, S. de la Moya, *Chem. – Eur. J.* **2015**, *21*, 13488–13500.
- [221] G. Longhi, E. Castiglioni, J. Koshoubu, G. Mazzeo, S. Abbate, *Chirality* **2016**, *28*, 696–707.
- [222] Y. Nagata, T. Mori, *Front. Chem.* **2020**, *8*.
- [223] Y. Deng, M. Wang, Y. Zhuang, S. Liu, W. Huang, Q. Zhao, *Light Sci. Appl.* **2021**, *10*, 76.
- [224] P. L. Polavarapu, C. L. Covington, *Chirality* **2014**, *26*, 539–552.
- [225] F. Zinna, L. Di Bari, *Chirality* **2015**, *27*, 1–13.
- [226] T. M. Fukunaga, C. Sawabe, T. Matsuno, J. Takeya, T. Okamoto, H. Isobe, *Angew. Chem. Int. Ed.* **2021**, *60*, 19097–19101.
- [227] Y. Onaka, S. Tanaka, A. Kobayashi, T. Matsuno, H. Isobe, *Tetrahedron Lett.* **2022**, *96*, 153774.
- [228] S. Sato, A. Yoshii, S. Takahashi, S. Furumi, M. Takeuchi, H. Isobe, *Proc. Natl. Acad. Sci.* **2017**, *114*, 13097–13101.
- [229] R. Daengngern, C. Camacho, N. Kungwan, S. Irlle, *J. Phys. Chem. A* **2018**, *122*, 7284–7292.
- [230] L. Guo, X. Yang, H. Cong, *Chin. J. Chem.* **2018**, *36*, 1135–1138.
- [231] J. Wang, G. Zhuang, Q. Huang, Y. Xiao, Y. Zhou, H. Liu, P. Du, *Chem. Commun.* **2019**, *55*, 9456–9459.
- [232] M. Hermann, D. Wassy, J. Kohn, P. Seitz, M. U. Betschart, S. Grimme, B. Esser, *Angew. Chem. Int. Ed.* **2021**, *60*, 10680–10689.
- [233] J. S. Wössner, J. Kohn, D. Wassy, M. Hermann, S. Grimme, B. Esser, *Org. Lett.* **2022**, *24*, 983–988.
- [234] P. Della Sala, C. Talotta, M. De Rosa, A. Soriente, S. Geremia, N. Hickey, P. Neri, C. Gaeta, *J. Org. Chem.* **2019**, *84*, 9489–9496.
- [235] T. A. Schaub, E. A. Prantl, J. Kohn, M. Bursch, C. R. Marshall, E. J. Leonhardt, T. C. Lovell, L. N. Zakharov, C. K. Brozek, S. R. Waldvogel, S. Grimme, R. Jasti, *J. Am. Chem. Soc.* **2020**, *142*, 8763–8775.
- [236] L.-H. Wang, N. Hayase, H. Sugiyama, J. Nogami, H. Uekusa, K. Tanaka, *Angew. Chem. Int. Ed.* **2020**, *59*, 17951–17957.
- [237] X. Zhang, H. Shi, G. Zhuang, S. Wang, J. Wang, S. Yang, X. Shao, P. Du, *Angew. Chem. Int. Ed.* **2021**, *60*, 17368–17372.
- [238] W. Xu, X.-D. Yang, X.-B. Fan, X. Wang, C.-H. Tung, L.-Z. Wu, H. Cong, *Angew. Chem. Int. Ed.* **2019**, *58*, 3943–3947.
- [239] J. Nogami, Y. Nagashima, K. Miyamoto, A. Muranaka, M. Uchiyama, K. Tanaka, *Chem. Sci.* **2021**, *12*, 7858–7865.
- [240] M. Piacenza, S. Grimme, *ChemPhysChem* **2005**, *6*, 1554–1558.
- [241] S. Grimme, *Chem. – Eur. J.* **2004**, *10*, 3423–3429.
- [242] Z. Hassan, E. Spuling, D. M. Knoll, S. Bräse, *Angew. Chem. Int. Ed.* **2020**, *59*, 2156–2170.
- [243] K. J. Weiland, N. Münch, W. Gschwind, D. Häussinger, M. Mayor, *Helv. Chim. Acta* **2019**, *102*, e1800205.
- [244] K. J. Weiland, T. Brandl, K. Atz, A. Prescimone, D. Häussinger, T. Šolomek, M. Mayor, *J. Am. Chem. Soc.* **2019**, *141*, 2104–2110.
- [245] N. V. Vorontsova, V. I. Rozenberg, E. V. Sergeeva, E. V. Vorontsov, Z. A. Starikova, K. A. Lyssenko, H. Hopf, *Chem. – Eur. J.* **2008**, *14*, 4600–4617.
- [246] Y. Wu, G. Zhuang, S. Cui, Y. Zhou, J. Wang, Q. Huang, P. Du, *Chem. Commun.* **2019**, *55*, 14617–14620.
- [247] J. He, M. Yu, M. Pang, Y. Fan, Z. Lian, Y. Wang, W. Wang, Y. Liu, H. Jiang, *Chem. – Eur. J.* **2022**, *28*, e202103832.



- [248] J. Wang, H. Shi, S. Wang, X. Zhang, P. Fang, Y. Zhou, G.-L. Zhuang, X. Shao, P. Du, *Chem. – Eur. J.* **2022**, *28*, e202103828.
- [249] G. Zhang, C. B. Musgrave, *J. Phys. Chem. A* **2007**, *111*, 1554–1561.
- [250] S. Chen, X. Miao, H. Zhou, C. Peng, R. Zhang, X. Han, *J. Phys. Chem. A* **2022**, *126*, 7452–7459.
- [251] K. Dhbaibi, L. Abella, S. Meunier-Della-Gatta, T. Roisnel, N. Vanthuynne, B. Jamoussi, G. Pieters, B. Racine, E. Quesnel, J. Autschbach, J. Crassous, L. Favereau, *Chem. Sci.* **2021**, *12*, 5522–5533.
- [252] D. Geuenich, K. Hess, F. Köhler, R. Herges, *Chem. Rev.* **2005**, *105*, 3758–3772.
- [253] R. Herges, *Chem. Rev.* **2006**, *106*, 4820–4842.
- [254] E. Heilbronner, *Tetrahedron Lett.* **1964**, *5*, 1923–1928.
- [255] H. S. Rzepa, *Chem. Rev.* **2005**, *105*, 3697–3715.
- [256] D. Ajami, O. Oeckler, A. Simon, R. Herges, *Nature* **2003**, *426*, 819–821.
- [257] Z. S. Yoon, A. Osuka, D. Kim, *Nat. Chem.* **2009**, *1*, 113–122.
- [258] M. Stępień, N. Sprutta, L. Latos-Grażyński, *Angew. Chem. Int. Ed.* **2011**, *50*, 4288–4340.
- [259] T. Tanaka, A. Osuka, *Chem. Rev.* **2017**, *117*, 2584–2640.
- [260] G. Naulet, L. Sturm, A. Robert, P. Dechambenoit, F. Röhrich, R. Herges, H. Bock, F. Durola, *Chem. Sci.* **2018**, *9*, 8930–8936.
- [261] X. Jiang, J. D. Laffoon, D. Chen, S. Pérez-Estrada, A. S. Danis, J. Rodríguez-López, M. A. Garcia-Garibay, J. Zhu, J. S. Moore, *J. Am. Chem. Soc.* **2020**, *142*, 6493–6498.
- [262] S. Nishigaki, Y. Shibata, A. Nakajima, H. Okajima, Y. Masumoto, T. Osawa, A. Muranaka, H. Sugiyama, A. Horikawa, H. Uekusa, H. Koshino, M. Uchiyama, A. Sakamoto, K. Tanaka, *J. Am. Chem. Soc.* **2019**, *141*, 14955–14960.
- [263] Z.-L. Qiu, D. Chen, Z. Deng, K.-S. Chu, Y.-Z. Tan, J. Zhu, *Sci. China Chem.* **2021**, *64*, 1004–1008.
- [264] K. Li, Z. Xu, J. Xu, T. Weng, X. Chen, S. Sato, J. Wu, Z. Sun, *J. Am. Chem. Soc.* **2021**, *143*, 20419–20430.
- [265] Z. Liu, T. Lu, *J. Phys. Chem. C* **2020**, *124*, 7353–7360.
- [266] S. Jhulki, A. K. Mishra, T. J. Chow, J. N. Moorthy, *Chem. – Eur. J.* **2016**, *22*, 9375–9386.
- [267] E. R. Darzi, B. M. White, L. K. Loventhal, L. N. Zakharov, R. Jasti, *J. Am. Chem. Soc.* **2017**, *139*, 3106–3114.
- [268] M. Gingras, *Chem. Soc. Rev.* **2013**, *42*, 1051–1095.
- [269] Z. Mou, K. Uchida, T. Kubo, M. Kertesz, *J. Am. Chem. Soc.* **2014**, *136*, 18009–18022.
- [270] P. Ravat, T. Šolomek, M. Rickhaus, D. Häussinger, M. Neuburger, M. Baumgarten, M. Juriček, *Angew. Chem. Int. Ed.* **2016**, *55*, 1183–1186.
- [271] Z. Mou, T. Kubo, M. Kertesz, *Chem. – Eur. J.* **2015**, *21*, 18230–18236.
- [272] Z. Mou, M. Kertesz, *Chem. – Eur. J.* **2018**, *24*, 6140–6147.
- [273] T. Šolomek, P. Ravat, Z. Mou, M. Kertesz, M. Juriček, *J. Org. Chem.* **2018**, *83*, 4769–4774.



# Appendix

## Table of Contents

Appendix .....	97
Table of Contents .....	97
A.1. SI Spiral cycloparaphenylenes.....	99
A.1.1. Experimental part .....	99
General remarks .....	99
Synthetic procedures .....	99
A.1.2. DFT calculations .....	107
Conformational analysis.....	107
TD-DFT.....	108
A.1.3. XYZ atomic coordinates.....	118
A.2. SI [6,7]Helicene <i>para</i> -phenylene .....	137
A.2.1. Experimental Part .....	138
General Remarks .....	138
Synthesis Overview .....	139
Synthetic Procedures .....	140
X-ray analysis.....	143
HPLC Separations .....	144
Optical Properties .....	145
Circularly Polarized Luminescence.....	149
A.2.2. DFT Calculations.....	152
Strain Calculations .....	152
Frontier Molecular Orbitals.....	156
Natural Transition Orbitals.....	157
CD Spectra .....	161
Dissymmetry Factors Calculation .....	165
NICS Values.....	166
A.2.3. NMR Spectra .....	168
A.2.4. HR-MS Spectra .....	189
A.2.5. XYZ Atomic Coordinates.....	192
A.3. SI [5, <i>n</i> ]Helicene <i>para</i> -phenylenes.....	199
A.3.1. Experimental part .....	199

*Appendix*

General remarks .....	199
Synthetic procedures .....	199
HPLC.....	218
Optical properties .....	219
A.4.2. DFT calculations .....	220
TD-DFT.....	221
A.4.3. XYZ atomic coordinates.....	223
A.4. References .....	227
A.5. List of abbreviations.....	229

## A.1. SI Spiral cycloparaphenylenes

### A.1.1. Experimental part

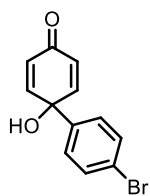
#### General remarks

All commercially available chemicals were purchased from Acros, Alfa Aesar, Apollo Scientific, Fluorochem and Sigma-Aldrich and used without further purification. Anhydrous solvents were purchased from Acros and stored over molecular sieves (4 Å). Column chromatography was performed on silica gel P60 (40–63 μm) from SilicycleTM. Celite® 545 (0.02–0.1 mm) from Supelco was used. Automated flash chromatography was performed using Biotage Isolera One. TLC was performed with silica gel 60 F254 aluminium plates purchased from Merck. High resolution mass spectra (HRMS) were measured on a maXisTM4G instrument from Bruker for HR-ESI-ToF MS. NMR experiments were performed on Bruker Avance III NMR spectrometers operating at 400, 500 or 600 MHz proton frequencies. The instruments were equipped with a direct-observe 5 mm BBFO smart probe (400 and 500 MHz). All probes were equipped with actively shielded z-gradients (10 A). The chemical shifts are reported in ppm relative to tetramethylsilane or referenced to residual solvent peak and the *J* values are given in Hz (±0.1 Hz). Standard Bruker pulse sequences were used, and the data was processed on Topspin 3.6 (Bruker) using twofold zero-filling in the indirect dimension.

#### Synthetic procedures

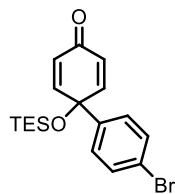
**3a** and intermediates **1** and **2** were prepared according to modified procedures by Jasti *et al.* and Yamago *et al.* and their spectral data matches literature.<sup>[1–3]</sup> We would like to note here that we have had difficulties reproducing the synthesis of compound **3a** as described in literature, and we had to optimize this reaction to prepare it in a large scale. *pseudopara*-Dibromo-[2.2]paracyclophane was prepared according to procedure by Hopf *et al.*<sup>[4]</sup> We first tried to synthesize *pseudopara*-diiodo-[2.2]paracyclophane using a procedure by Lützen *et al.*<sup>[5]</sup> but never observed any conversion when using *n*-BuLi.

#### 1a



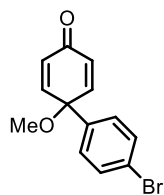
4-Bromo-4'-hydroxybiphenyl (51.1 g; 205 mmol; 1.00 eq.) and imidazole (22.3 g; 328 mmol; 1.60 eq.) were suspended in dry DCM (300 mL). The reaction was cooled down to 0 °C. TMSCl (34.8 mL; 267 mmol; 1.30 eq.) was added dropwise over period of 15 min. The reaction was stirred for 16 h at r.t. and quenched with sat. aq. NaHCO<sub>3</sub> (100 mL). The phases were separated and the aqueous phase was extracted with DCM (50 mL). Combined organic phases were washed with sat. aq. NaHCO<sub>3</sub> (100 mL) and with brine (2 times 100 mL). The organic phase was dried with Na<sub>2</sub>SO<sub>4</sub> and the volatiles were evaporated. Crude product (64.9 g) was used without further purification. THF (480 mL), H<sub>2</sub>O (210 mL) and MeCN (120 mL) were mixed in a 2 L flask. TMS protected 4-bromo-4'-hydroxybiphenyl (34.1 g; 106 mmol; 1.00 eq.) and (diacetoxyiodo)benzene (52.3 g; 159 mmol; 1.50 eq.) were added to the reaction mixture alternatively as solids during 30 min. Color changed from colorless to yellow to red during the addition. After the addition was finished, the reaction was stirred for 72 h at r.t.. The reaction mixture was concentrated on rotavap and treated with EtOAc (200 mL) and sat. aq. NaHCO<sub>3</sub> (200 mL). The phases were separated and the aqueous phase was extracted with EtOAc (4 times 50 mL). The combined organic phases were washed with brine (50 mL) and dried with Na<sub>2</sub>SO<sub>4</sub>. The volatiles were evaporated. The crude product was dissolved in boiling chloroform (approximately 300 mL) and petrolether (approximately 300 mL) was added until precipitation started. The mixture was left to cool down to r.t. over 16 h. The resulting solid was filtered off and washed with petrolether to afford **1a** as a pale yellow solid (21.1 g; 75%).

<sup>1</sup>H-NMR (400 MHz, CDCl<sub>3</sub>, 298 K, δ/ppm): 7.51 (d, *J* = 8.7, 2H), 7.35 (d, *J* = 8.8, 2H), 6.85 (d, *J* = 10.1, 2H), 6.25 (d, *J* = 10.1, 2H), 2.38 (br s, 1H).

**1b**

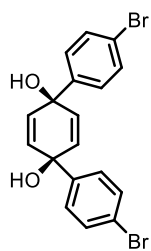
**1a** (8.99 g; 33.9 mmol; 1.00 eq.) and imidazole (4.62 g; 67.8 mmol; 2.00 eq.) were dissolved in dry DMF (50 mL). TESCOI (8.53 mL; 50.9 mmol; 1.50 eq.) was added dropwise and the reaction was stirred for 16 h at r.t.. The reaction was quenched with sat. aq. NaHCO<sub>3</sub> (150 mL) and extracted with EtOAc (3 times 50 mL). The organic layer was washed with sat. aq. NaHCO<sub>3</sub> (50 mL), H<sub>2</sub>O (50 mL) and brine (50 mL), and dried with Na<sub>2</sub>SO<sub>4</sub>. Volatiles were evaporated. Crude product was purified using automated flash chromatography (SiO<sub>2</sub>, 10% EtOAc in cyclohexane). The product was isolated as a yellow viscous liquid (11.7 g; 91%).

<sup>1</sup>H-NMR (400 MHz, CDCl<sub>3</sub>, 298 K, δ/ppm): 7.47 (d, *J* = 8.6, 2H), 7.31 (d, *J* = 8.6, 2H), 6.79 (d, *J* = 10.1, 2H), 6.23 (d, *J* = 10.0, 2H), 0.97 (t, *J* = 7.9, 9H), 0.65 (q, *J* = 7.7, 9H).

**1c**

4-Bromo-4'-hydroxybiphenyl (5.1 g; 20.5 mmol; 1.00 eq.) and (diacetoxyiodo)benzene (8.4 g; 25.6 mmol; 1.25 eq.) were added to a dry flask filled with Ar and placed in an ice-water bath. Dry MeOH (100 mL) was added through a cannula and the reaction was let to warm up to r.t. and stirred for 48 h. The reaction mixture was poured into H<sub>2</sub>O (250 mL), extracted with EtOAc (3 times 50 ml) and dried with Na<sub>2</sub>SO<sub>4</sub>. Volatiles were evaporated. Crude product was purified using automated flash chromatography (SiO<sub>2</sub>, 10% EtOAc in cyclohexane). The product was isolated as a slightly yellow solid (4.26 g; 74%).

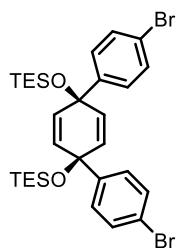
<sup>1</sup>H NMR (250 MHz, CDCl<sub>3</sub>) δ 7.48 (d, *J* = 8.7, 2H), 7.33 (d, *J* = 8.7, 2H), 6.74 (d, *J* = 10.2, 2H), 6.41 (d, *J* = 10.2, 2H), 3.42 (s, 3H).

**2a**

A round-bottom flask was charged with 1,4-dibromobenzene (5.01 g; 20.8 mmol; 2.25 eq.) and dry THF (35 mL) was added. The solution was cooled down to -78 °C. *n*-BuLi (2.44 M; 8.34 mL; 20.3 mmol; 2.20 eq.) was added dropwise and the reaction was stirred for 15 min at -78 °C. A solution of *p*-benzoquinone (1.00 g; 9.25 mmol; 1.00 eq.) in dry THF (5 mL) was added via cannula and the reaction was stirred and left to warm to r.t. over 16 h. H<sub>2</sub>O (50 mL) was added and the resulting mixture was extracted with EtOAc (3 times 25 mL). Combined organic phases were washed with brine (25 mL) and dried with Na<sub>2</sub>SO<sub>4</sub>. Volatiles were evaporated. Crude product was purified using automated flash chromatography (SiO<sub>2</sub>, 0% to 10% to 100% EtOAc in cyclohexane). The product was isolated as yellow solid (2.31 g; 59%).

<sup>1</sup>H-NMR (400 MHz, CDCl<sub>3</sub>, 298 K, δ/ppm): 7.44 (d, *J* = 8.6, 4H), 7.23 (d, *J* = 8.7, 4H), 5.94 (s, 4H), 3.96 (br s, 2H).

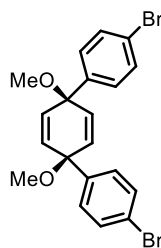
## 2b



**2a** (950 mg; 2.25 mmol; 1.00 eq.) and imidazole (613 mg; 9.00 mmol; 4 eq.) were dissolved in dry DMF (20 mL) and TESCO (0.99 mL; 5.85 mmol; 2.60 eq.) was added. The reaction was stirred for 14 h at r.t.. The reaction was quenched with sat. aq. NaHCO<sub>3</sub> (25 mL). The resulting mixture was diluted with H<sub>2</sub>O (50 mL) and extracted with EtOAc (3 times 15 mL). Combined organic phases were washed with brine (25 mL) and dried with Na<sub>2</sub>SO<sub>4</sub>. Volatiles were evaporated. Crude product was purified using automated flash chromatography (SiO<sub>2</sub>, 0% to 10% DCM in cyclohexane). The product was isolated as colorless oil (943 mg; 64%).

<sup>1</sup>H-NMR (400 MHz, CDCl<sub>3</sub>, 298 K,  $\delta$ /ppm): 7.39 (d,  $J$  = 8.6, 4H), 7.17 (d,  $J$  = 8.6, 4H), 5.95 (s, 4H), 0.92 (t,  $J$  = 7.9, 18H), 0.59 (q,  $J$  = 7.9, 12H).

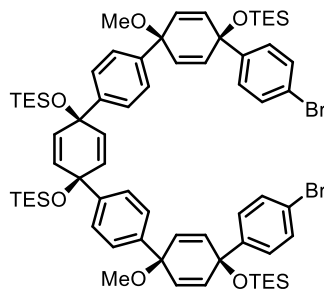
## 2c



NaH (1.89 g; 60% in oil; 47.2 mmol; 4 eq.) was weighed in a dry flask and dry THF (25 mL) was added. The suspension was cooled down to 0 °C and a solution of **2a** (4.98 g; 11.8 mmol; 1 eq.) in dry THF (25 mL) was added through a cannula over 10 min. The reaction was stirred at 0 °C for 30 min and MeI (8.4 mL; 59.0 mmol; 5 eq.) was added. The reaction was warmed up to r.t. and stirred for 16 h. The reaction was poured into H<sub>2</sub>O (100 mL), extracted with EtOAc (3 times 25 mL) and dried with Na<sub>2</sub>SO<sub>4</sub>. Volatiles were evaporated and the crude product was purified using automated flash chromatography (SiO<sub>2</sub>, 15% EtOAc in petrolether). The product was isolated as a white solid (2.42 g; 46%).

<sup>1</sup>H-NMR (400 MHz, CDCl<sub>3</sub>, 298 K,  $\delta$ /ppm): 7.39 (d,  $J$  = 8.6, 4H), 7.17 (d,  $J$  = 8.6, 4H), 5.95 (s, 4H), 0.92 (t,  $J$  = 7.9, 18H), 0.59 (q,  $J$  = 7.9, 12H).

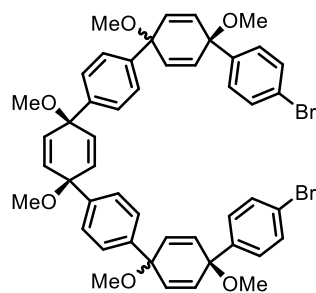
## 3a



**2b** (820 mg; 1.26 mmol; 1.00 eq.) was dissolved in dry THF (10 mL) and cooled down to -78 °C. *n*-BuLi (1.6 M; 1.61 mL; 2.58 mmol; 2.05 eq.) was added dropwise and the reaction was stirred for 1 h at -78 °C. A solution of **1b** (908 mg; 2.39 mmol; 1.90 eq.) in dry THF (2 mL) was added via syringe and the reaction was stirred for 1 h at -78 °C. MeI (0.78 mL; 12.6 mmol; 10.0 eq.) was added and the reaction was stirred and left to warm to r.t. over 16 h. H<sub>2</sub>O (50 mL) was added and the resulting mixture was extracted with EtOAc (3 times 25 mL). Combined organic phases were washed with brine (25 mL) and dried with Na<sub>2</sub>SO<sub>4</sub>. Volatiles were evaporated. Crude product was purified using automated flash chromatography (SiO<sub>2</sub>, 0% to 10% to 100% ethyl acetate in cyclohexane). The product was isolated as a yellow solid (1.14 g; 71%).

<sup>1</sup>H-NMR (400 MHz, CDCl<sub>3</sub>, 298 K,  $\delta$ /ppm): 7.34 (d,  $J$  = 8.6, 4H), 7.31 (d,  $J$  = 8.6, 4H), 7.26 (d,  $J$  = 8.6, 4H), 7.16 (d,  $J$  = 8.6, 4H), 6.09 (d,  $J$  = 10.2, 4H), 5.99 (d,  $J$  = 10.3, 4H), 5.96 (s, 4H), 3.36 (s, 6H), 1.00-0.90 (m, 36H), 0.71-0.56 (m, 24H).

## 3c

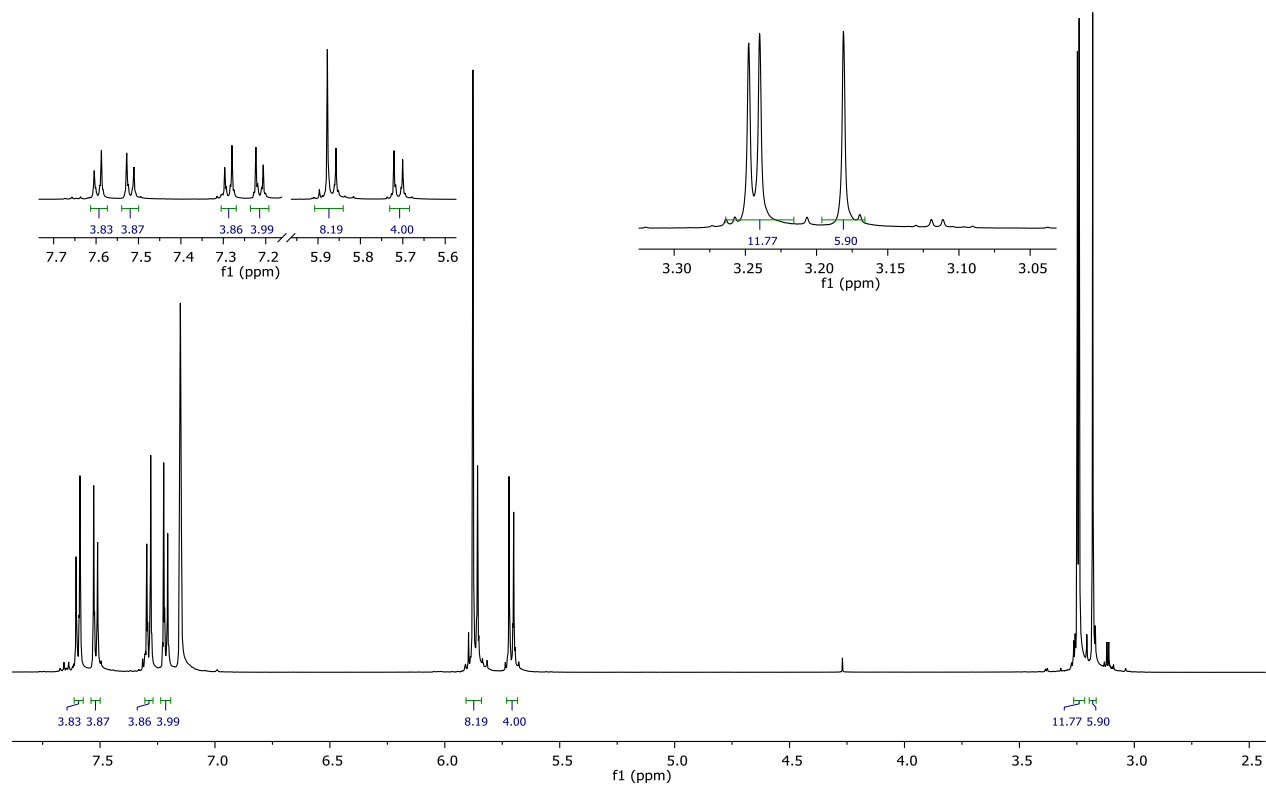


**2c** (1.01 g; 2.24 mmol; 1.00 eq.) was dissolved in dry THF (50 mL) and cooled down to  $-78\text{ }^{\circ}\text{C}$ . *n*-BuLi (2 mL; 2.41 M in hexanes; 2.1 eq.) was added dropwise and the reaction was stirred for 15 min at  $-78\text{ }^{\circ}\text{C}$ . A solution of **1c** (1.28 g; 4.59 mmol; 2.05 eq.) in dry THF (5 mL) was added via syringe and the reaction was stirred for 2 h at  $-78\text{ }^{\circ}\text{C}$ . The reaction was quenched with  $\text{H}_2\text{O}$  (50 mL) and the resulting mixture was extracted with EtOAc (3 times 25 mL), washed with brine (25 mL) and dried with  $\text{Na}_2\text{SO}_4$ . Volatiles were evaporated. The crude was dissolved in THF (10 mL) and cooled to  $0\text{ }^{\circ}\text{C}$ . NaH (358 mg; 60% in oil; 8.96 mmol; 4 eq.) was added and stirred for 30 min at  $0\text{ }^{\circ}\text{C}$ . MeI (1.3 mL; 9.18 mmol; 4.1 eq.) was added and the reaction was warmed up to r.t. and stirred for 16 h. The reaction was poured into  $\text{H}_2\text{O}$  (100 mL), extracted with EtOAc (3 times 25 ml) and dried with  $\text{Na}_2\text{SO}_4$ . Volatiles were evaporated and the crude product was purified using automated flash chromatography ( $\text{SiO}_2$ , 10% EtOAc in cyclohexane). The mixture of diastereomers was isolated as a white fluffy solid (1.54 g; 78% as a mixture of diastereomers).

The all-*cis* diastereomer was isolated using HPLC with a chiral stationary phase (IG column, eluent: DCM/heptane 30/70).

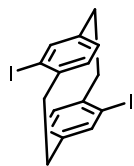
**$^1\text{H-NMR}$**  (400 MHz,  $\text{CDCl}_3$ , 298 K,  $\delta/\text{ppm}$ ): 7.60 (d,  $J = 8.6\text{ Hz}$ , 4H), 7.52 (d,  $J = 8.5\text{ Hz}$ , 4H), 7.29 (d,  $J = 8.6\text{ Hz}$ , 4H), 7.21 (d,  $J = 8.7\text{ Hz}$ , 4H), 5.88 (s, 4H), 5.87 (d,  $J = 10.1\text{ Hz}$ , 4H), 5.71 (d,  $J = 10.2\text{ Hz}$ , 4H), 3.25 (s, 6H), 3.24 (s, 6H), 3.18 (s, 6H).

$^1\text{H-NMR}$  (500 MHz,  $\text{CDCl}_3$ )  $\delta$  7.60 (d,  $J = 8.6\text{ Hz}$ , 1H), 7.52 (d,  $J = 8.5\text{ Hz}$ , 1H), 7.29 (d,  $J = 8.6\text{ Hz}$ , 1H), 7.21 (d,  $J = 8.7\text{ Hz}$ , 1H), 5.87 (d,  $J = 10.1\text{ Hz}$ , 3H), 5.71 (d,  $J = 10.2\text{ Hz}$ , 1H), 3.25 (s, 2H), 3.24 (s, 2H), 3.18 (s, 2H).



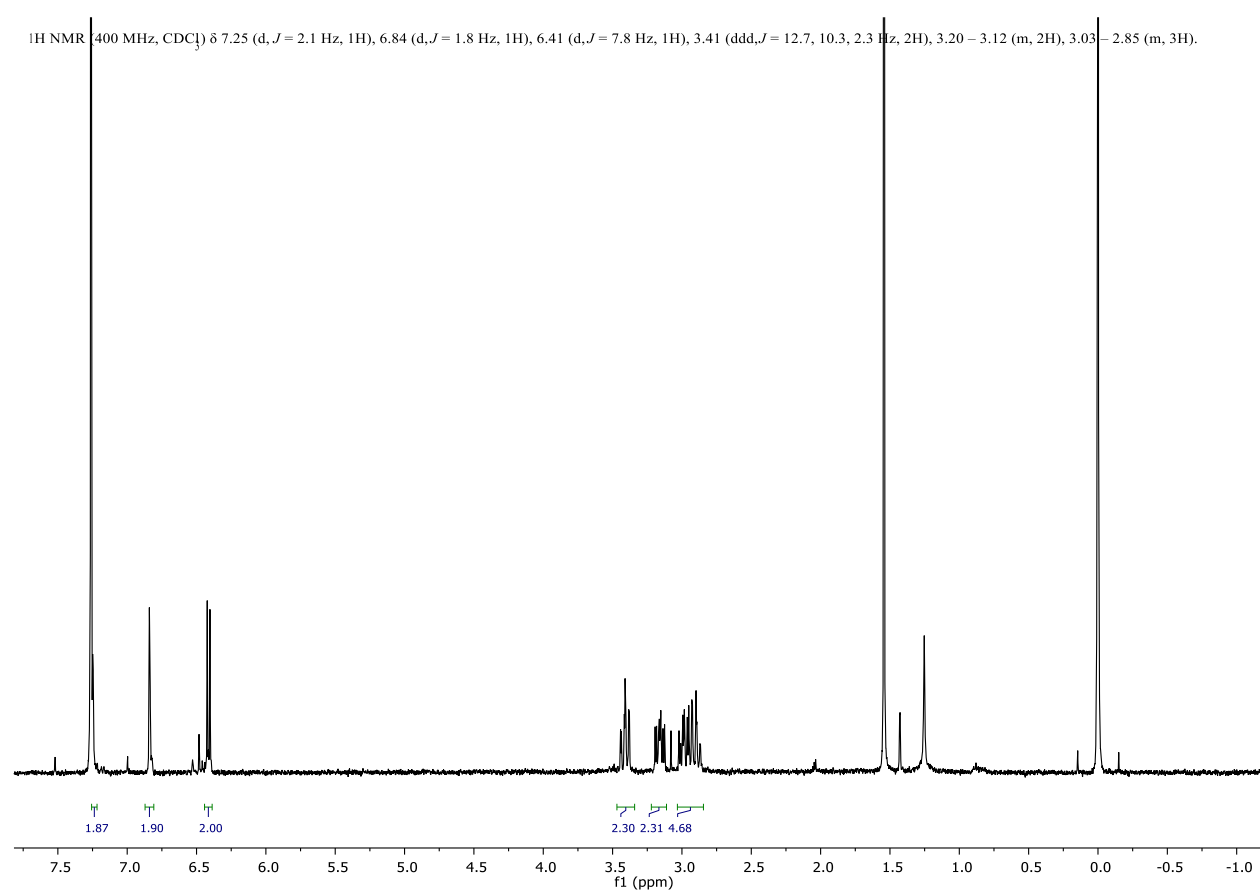
**Figure A1.**  $^1\text{H-NMR}$  (500 MHz,  $\text{CDCl}_3$ , 298 K) spectrum of all-*cis* **3c**.



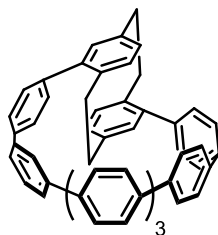
*pseudopara*-Diiodo-[2.2]paracyclophane

*pseudopara*-Dibromo-[2.2]paracyclophane (98 mg; 0.268 mmol; 1 eq.) was dissolved in dry THF (40 mL) in a Schlenk flask and the solution was cooled to  $-78\text{ }^{\circ}\text{C}$ . *t*-BuLi (0.7 mL; 1.6M in pentane; 5 eq.) was added dropwise and the reaction was stirred for 2 h.  $\text{I}_2$  was added as a solid and the reaction was left to stir at  $-78\text{ }^{\circ}\text{C}$  for 2 h after which it was warmed up to r.t. and quenched with sat. aq.  $\text{Na}_2\text{S}_2\text{O}_3$  (20 mL). The resulting mixture was extracted with DCM (3 times 25 mL) and dried with  $\text{Na}_2\text{SO}_4$ . The crude product was purified via re-crystallization from cyclohexane to afford *pseudopara*-diiodo-[2.2]paracyclophane as a white crystalline solid (46 mg; 37%).

$^1\text{H-NMR}$  (400 MHz,  $\text{CDCl}_3$ , 298 K,  $\delta/\text{ppm}$ ): 7.25 (d,  $J = 2.1$ , 2H), 6.84 (d,  $J = 1.8$ , 2H), 6.41 (d,  $J = 7.8$ , 2H), 3.41 (ddd,  $J = 12.7, 10.3, 2.3$ , 2H), 3.20 – 3.12 (m, 2H), 3.03 – 2.85 (m, 4H).



**Figure A2.**  $^1\text{H-NMR}$  (500 MHz,  $\text{CDCl}_3$ , 298 K) spectrum of *pseudopara*-diiodo-[2.2]paracyclophane.

*p*[9]SPP

*pseudopara*-Diiodo-[2.2]paracyclophane (10 mg; 0.021 mmol; 1.00 eq.) and **3b** (33 mg; 0.024 mmol; 1.1 eq.) were added to a Schlenk flask. Dioxane (40 mL) and H<sub>2</sub>O (4 mL) were added and the solution was degassed by bubbling with Ar for 1 h. K<sub>3</sub>PO<sub>4</sub> (37 mg; 0.174 mmol; 8 eq.) and Pd SPhos G3 (3 mg; 0.004 mmol; 0.2 eq.) were added and the degassing was continued for another 20 min. The Schlenk flask was sealed and placed into a preheated oil bath (80 °C). The reaction was stirred at 80 °C for 24 h, cooled down and filtered through celite. The flask and celite were washed with DCM,

volatiles evaporated and the crude containing intermediate **4** was dried in vacuo. A resulting waxy solid was dissolved in THF (0.5 mL) and TBAF (131 μL; 1M in THF) was added. The resulting solution was stirred at r.t. for 1 h and H<sub>2</sub>O (1 mL) was added to quench the reaction. THF was removed under reduced pressure (160 mbar; 40 °C) to precipitate a yellowish solid which was filtered off and washed with DCM (2 times 1 mL). Resulting white solid was dissolved in THF (1 mL) and a solution of H<sub>2</sub>SnCl<sub>4</sub> (0.58 mL; 127 mM in THF; 3.3 eq.) was added. Color of the reaction mixture changed from colorless to yellow and strong blue-green fluorescence was observed under irradiation (365 nm). The reaction was stirred for 1 h and quenched with 10% aq. NaOH (1 mL), diluted with H<sub>2</sub>O (10 mL) and extracted with DCM (4 times 5 mL). The organic phase was washed with brine (10 mL) and dried with Na<sub>2</sub>SO<sub>4</sub>. Volatiles were evaporated and the crude product was purified by first passing its DCM solution through a short pad of silica followed by size-exclusion chromatography (SX3, DCM) to afford *p*[9]SPP as a yellow solid. The spectral data matches that of published by Du *et al.*<sup>[6]</sup>

<sup>1</sup>H-NMR (500 MHz, CDCl<sub>3</sub>, 298 K, δ/ppm): 7.71 (dd, *J* = 8.7, 2.2 Hz, 2H), 7.57 (dd, *J* = 8.7, 2.0 Hz, 2H), 7.53 (d, *J* = 8.3 Hz, 2H), 7.48 (dd, *J* = 8.6, 2.2 Hz, 2H), 7.47 – 7.40 (m, 18H), 7.17 (dd, *J* = 8.5, 2.0 Hz, 2H), 6.29 (d, *J* = 7.8 Hz, 2H), 6.25 (d, *J* = 1.8 Hz, 2H), 6.17 (dd, *J* = 7.8, 1.8 Hz, 2H), 3.37 (ddd, *J* = 13.7, 8.7, 4.9 Hz, 2H), 2.78 (ddd, *J* = 14.1, 9.2, 5.4 Hz, 2H), 2.36 (ddd, *J* = 13.5, 9.1, 4.9 Hz, 2H), 1.86 (ddd, *J* = 13.5, 8.6, 5.4 Hz, 2H).

HRMS (ESI, +): *m/z* calcd. for C<sub>58</sub>H<sub>42</sub>Ag [M+Ag]<sup>+</sup>: 845.2332, found: 845.2326.

$^1\text{H}$  NMR (500 MHz,  $\text{CDCl}_3$ )  $\delta$  7.71 (dd,  $J = 8.7, 2.2$  Hz, 1H), 7.57 (dd,  $J = 8.7, 2.0$  Hz, 1H), 7.53 (d,  $J = 8.3$  Hz, 2H), 7.48 (dd,  $J = 8.6, 2.2$  Hz, 1H), 7.47 – 7.40 (m, 7H), 7.17 (dd,  $J = 8.5, 2.0$  Hz, 1H), 6.29 (d,  $J = 7.8$  Hz, 1H), 6.25 (d,  $J = 1.8$  Hz, 1H), 6.17 (dd,  $J = 7.8, 1.8$  Hz, 1H), 3.37 (ddd,  $J = 13.7, 8.7, 4.9$  Hz, 1H), 2.78 (ddd,  $J = 14.1, 9.2, 5.4$  Hz, 1H), 2.36 (ddd,  $J = 13.5, 9.1, 4.9$  Hz, 1H), 1.86 (ddd,  $J = 13.5, 8.6, 5.4$  Hz, 1H).

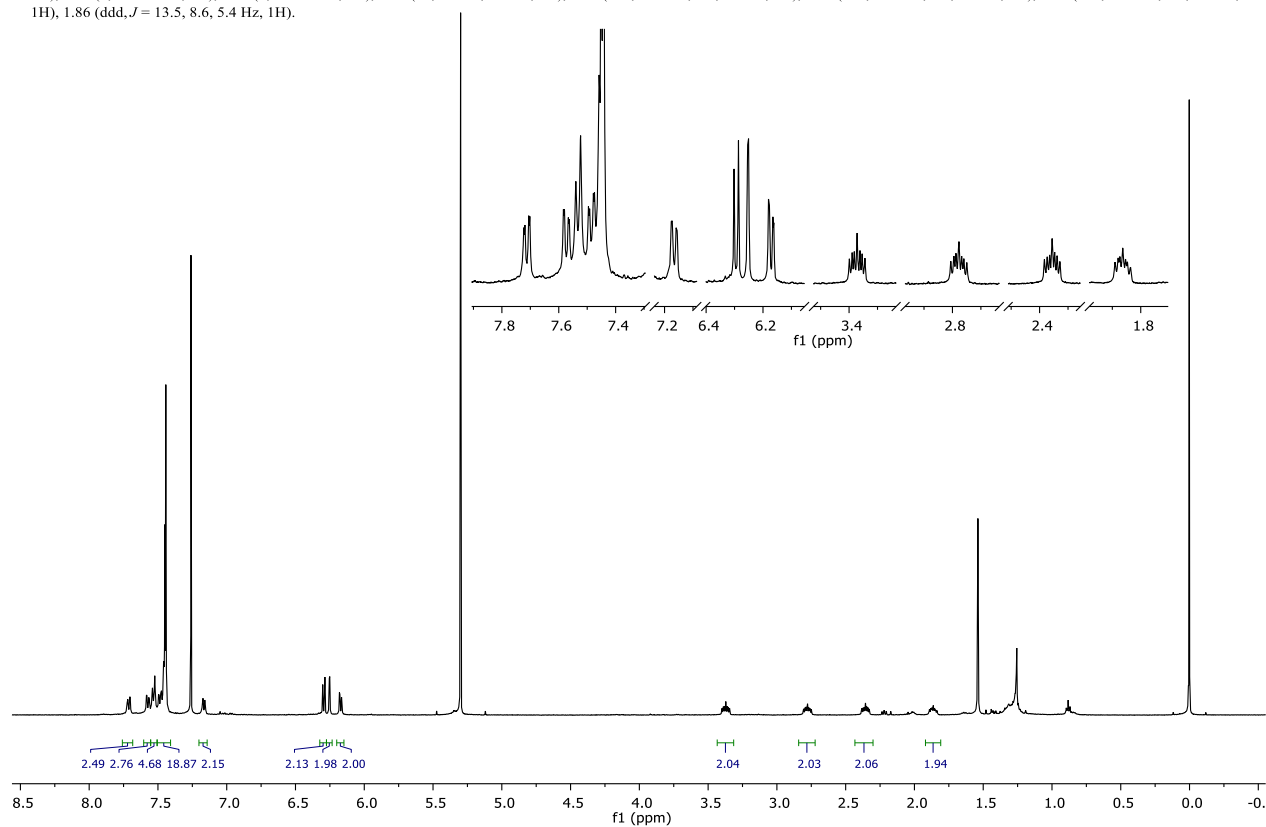


**Figure A3.**  $^1\text{H}$ -NMR (500 MHz,  $\text{CDCl}_3$ , 298 K) spectrum of  $p[9]\text{SPP}$ .

## High Resolution Mass Spectrometry Report

Sample Name Jurai Malincik / MAJ-190  
Comment 10 ug / mL in MeOH, analyzed in  
MeOH+AgNO<sub>3</sub> (1mM)

Instrument maXis 4G  
Method 23 Direct\_pos\_higher.m

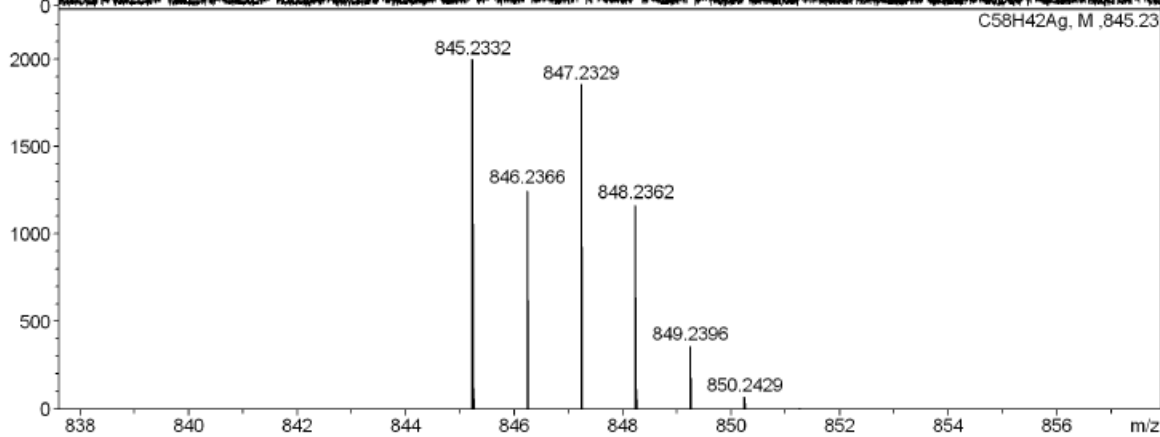
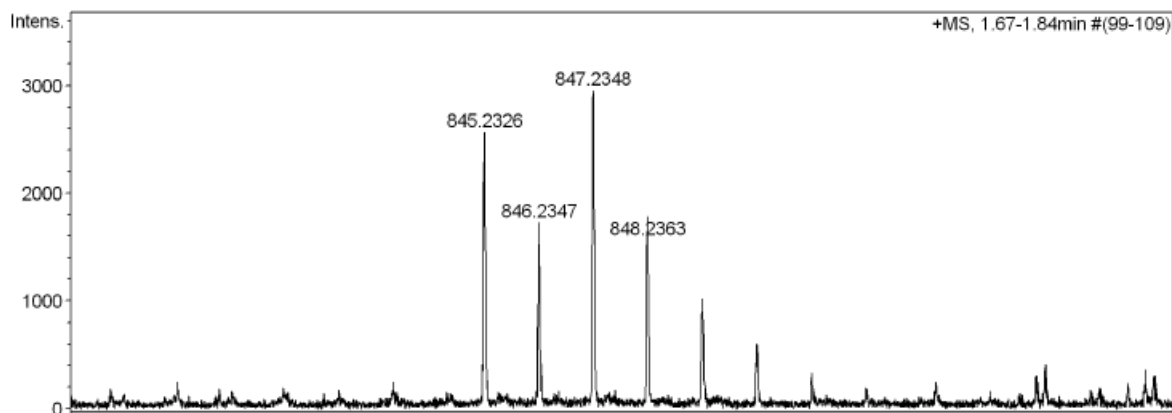
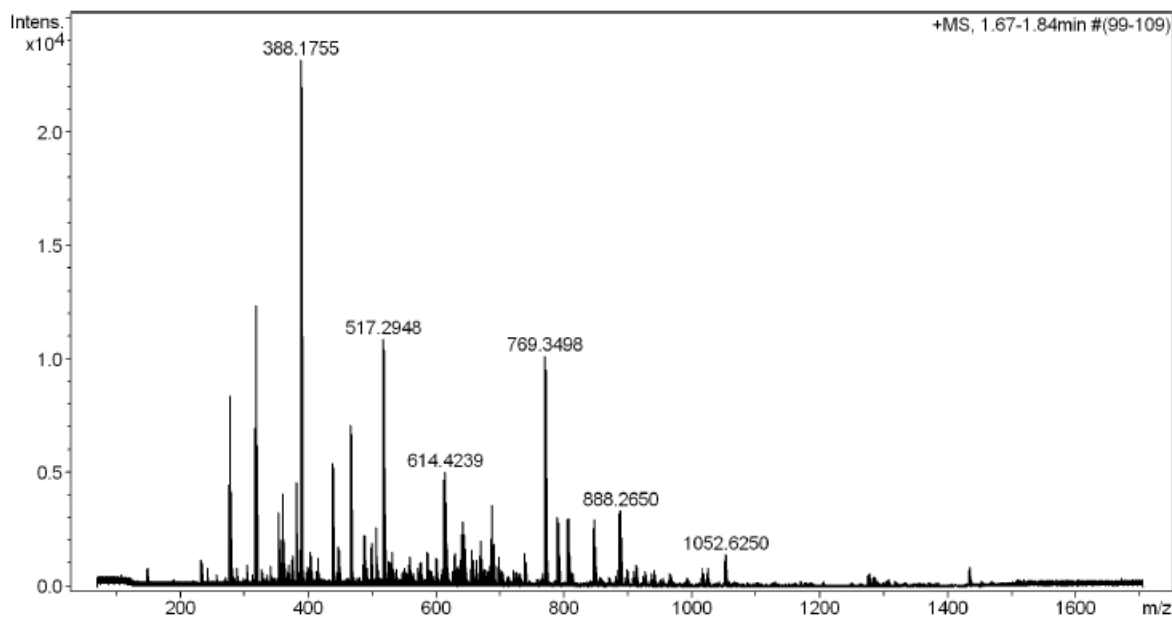


Figure A4. HR-MS (ESI, +) spectrum of  $p[9]SPP [M+Ag]^+$ .

### A.1.2. DFT calculations

Calculations were performed with Gaussian 09<sup>[7]</sup> (release D.01) software. Molecular geometries were optimized at B3LYP/6-31g(d) level of theory with Grimme's D3 dispersion correction. Stationary points were confirmed by a subsequent vibrational frequencies calculations. All vibrational frequencies were real for minima at the potential energy surface. SuperFine integration grid was used in all calculations. The single point energies were then calculated at D3-B3LYP/ cc-pVTZ level of theory. Excited state geometries were optimized at CAM-B3LYP/6-31g(d) level of theory with the ground state geometry being the starting point. Electric and magnetic transition dipole moment vectors were extracted from a TD-DFT calculation run on geometries of the ground and the excited state.

We would like to note here that the result of a StrainViz calculation is strongly dependent on the input geometries of molecular fragments. We do not in the Appendix as it would multiply the number of pages this document would have.

### Conformational analysis

Conformational analysis was performed on *p*[10]SPP, *p*[9]SPP, *m*[10]SPP and *m*[9]SPP. Potential candidates for global minima were chosen by a random search using Avogadro software at MMFF94 level of theory.<sup>[8]</sup> Conformers were then optimized using DFT and compared according to their relative energies which are summarized in Tables A1–A4.

**Table A1.** Energies  $E_{corr}$  (0 K,  $E_{el} + ZPVE$ ) and relative energies conformers of *p*[10]SPP. Single point energies  $E_{el}$  obtained with the cc-pVTZ basis set on D3-B3LYP/6-31g(d) geometries. Zero-point vibrational energy (ZPVE) correction is unscaled.

Conformer	$E_{corr}$ / Hartree	Relative energy / kcal mol <sup>-1</sup>
1	-2466.49249	0
2	-2466.49359	0.6901
3	-2466.493151	0.2755
4	-2466.49249	0.6903
5	-2466.492534	0.6629
6	-2466.49315	0.2762

**Table A2.** Energies  $E_{corr}$  (0 K,  $E_{el} + ZPVE$ ) and relative energies conformers of *p*[9]SPP. Single point energies  $E_{el}$  obtained with the cc-pVTZ basis set on D3-B3LYP/6-31g(d) geometries. Zero-point vibrational energy (ZPVE) correction is unscaled.

Conformer	$E_{corr}$ / Hartree	Relative energy / kcal mol <sup>-1</sup>
1	-2235.4188	0
2	-2235.418086	0.4479

**Table A3.** Energies  $E_{corr}$  (0 K,  $E_{el} + ZPVE$ ) and relative energies conformers of  $m[10]$ SPP. Single point energies  $E_{el}$  obtained with the cc-pVTZ basis set on D3-B3LYP/6-31g(d) geometries. Zero-point vibrational energy (ZPVE) correction is unscaled.

Conformer	$E_{corr}$ / Hartree	Relative energy / kcal mol <sup>-1</sup>
1	-2466.520066	0
2	-2466.513171	4.326
3	-2466.513529	4.102

**Table A4.** Energies  $E_{corr}$  (0 K,  $E_{el} + ZPVE$ ) and relative energies conformers of  $m[9]$ SPP. Single point energies  $E_{el}$  obtained with the cc-pVTZ basis set on D3-B3LYP/6-31g(d) geometries. Zero-point vibrational energy (ZPVE) correction is unscaled

Conformer	$E_{corr}$ / Hartree	Relative energy / kcal mol <sup>-1</sup>
1	-2235.446072	0
2	-2235.444407	1.045
3	-2235.444408	1.044

## TD-DFT

The calculations were performed for the ( $R_P$ )-enantiomers.

**Table A5.** Calculated electric ( $\mu$ ) and magnetic ( $m$ ) transition dipole moments, rotatory strengths ( $R$ , velocity form), dipole strengths ( $D$ ) and calculated dissymmetry factor ( $g_{abs}$ ) values for the  $S_0 \rightarrow S_1$  transition of  $p[n]$ SPPs at CAM-B3LYP/6-31g(d) level of theory.

$p[n]$ SPP	$E$ / eV	$f$	$ \mu  / 10^{-18}$ esu·cm	$ m  / 10^{-20}$ erg·G <sup>-1</sup>	$\theta / ^\circ$	$R / 10^{-40}$ esu erg cm G <sup>-1</sup>	$D / 10^{-36}$ esu <sup>2</sup> cm <sup>2</sup> erg <sup>2</sup> G <sup>-2</sup>	$g_{abs} / 10^{-2}$
7	3.338	0.061	2.19	5.88	109.67	-439	4.82	-3.65
8	3.425	0.0733	2.38	7.26	100.93	-325	5.65	-2.31
9	3.625	0.0576	2.05	9.52	100.67	-357	4.20	-3.40
10	3.670	0.0614	2.10	11.35	104.11	-574	4.43	-5.19
11	3.761	0.0817	2.39	13.72	98.4	-474	5.75	-3.30
12	3.781	0.0679	2.18	15.82	103.81	-811	4.76	-6.82
13	3.827	0.1216	2.89	18.20	96.44	-584	8.41	-2.78
14	3.839	0.0996	2.62	20.55	101.26	-1036	6.89	-6.02
15	3.865	0.17	3.41	22.99	95.11	-688	11.65	-2.36
16	3.873	0.1454	3.15	25.55	99.06	-1248	9.97	-5.01
17	3.888	0.2228	3.89	28.08	94.21	-791	15.19	-2.08

**Table A6.** Calculated electric ( $\mu$ ) and magnetic ( $m$ ) transition dipole moments, rotatory strengths ( $R$ , velocity form), dipole strengths ( $D$ ) and calculated dissymmetry factor ( $g_{abs}$ ) values for the  $S_0 \rightarrow S_1$  transition of  $p[n]$ SPPs at BMK/6-31g(d) level of theory.

$p[n]$ SPP	$E /$ eV	$f$	$ \mu  / 10^{-18}$ esu·cm	$ m  / 10^{-20}$ erg·G <sup>-1</sup>	$\theta / ^\circ$	$R / 10^{-40}$ esu erg cm G <sup>-1</sup>	$D / 10^{-36}$ esu <sup>2</sup> cm <sup>2</sup> erg <sup>2</sup> G <sup>-2</sup>	$g_{abs} / 10^{-2}$
7	3.226	0.0669	2.34	5.65	107.8	-405	5.47	-2.96
8	3.309	0.0646	2.27	7.06	101.1	-305	5.15	-2.37
9	3.504	0.0601	2.13	9.17	99.71	-323	4.53	-2.85
10	3.548	0.0624	2.15	10.96	103.18	-529	4.65	-4.55
11	3.639	0.0879	2.52	13.21	97.67	-437	6.39	-2.74
12	3.658	0.0742	2.31	15.25	102.61	-756	5.37	-5.62
13	3.705	0.1294	3.03	17.53	95.91	-538	9.24	-2.33
14	3.716	0.1078	2.77	19.80	100.46	-976	7.69	-5.08
15	3.742	0.179	3.55	22.14	94.76	-641	12.66	-2.02
16	3.749	0.1542	3.29	24.61	98.49	-1175	10.91	-4.31
17	3.765	0.2322	4.03	27.07	93.93	-736	16.34	-1.80

**Table A7.** Calculated electric ( $\mu$ ) and magnetic ( $m$ ) transition dipole moments, rotatory strengths ( $R$ , velocity form), dipole strengths ( $D$ ) and calculated dissymmetry factor ( $g_{abs}$ ) values for the  $S_0 \rightarrow S_1$  transition of  $p[n]$ SPPs at M06-2X/6-31g(d) level of theory.

$p[n]$ SPP	$E /$ eV	$f$	$ \mu  / 10^{-18}$ esu·cm	$ m  / 10^{-20}$ erg·G <sup>-1</sup>	$\theta / ^\circ$	$R / 10^{-40}$ esu erg cm G <sup>-1</sup>	$D / 10^{-36}$ esu <sup>2</sup> cm <sup>2</sup> erg <sup>2</sup> G <sup>-2</sup>	$g_{abs} / 10^{-2}$
7	3.339	0.0634	2.24	6.11	109.12	-469	5.01	-3.75
8	3.424	0.0704	2.33	7.58	101.08	-349	5.43	-2.58
9	3.622	0.0576	2.05	9.92	100.52	-379	4.20	-3.61
10	3.666	0.0612	2.10	11.85	103.99	-614	4.42	-5.56
11	3.757	0.0823	2.40	14.30	98.26	-505	5.80	-3.49
12	3.777	0.0685	2.19	16.51	103.66	-872	4.81	-7.25
13	3.823	0.1222	2.90	18.99	96.42	-632	8.46	-2.99
14	3.835	0.0997	2.62	21.45	101.23	-1120	6.90	-6.49
15	3.861	0.1702	3.41	24.00	95.06	-740	11.68	-2.53
16	3.868	0.1445	3.14	26.67	99	-1343	9.92	-5.41
17	3.884	0.2224	3.89	29.33	94.17	-851	15.19	-2.24

**Table A8.** Calculated electric ( $\mu$ ) and magnetic ( $m$ ) transition dipole moments, rotatory strengths ( $R$ , velocity form), dipole strengths ( $D$ ) and calculated dissymmetry factor ( $g_{abs}$ ) values for the  $S_0 \rightarrow S_1$  transition of  $m[n]$ SPPs at CAM-B3LYP/6-31g(d) level of theory.

$m[n]$ SPP	$E /$ eV	$f$	$ \mu  / 10^{-18}$ esu·cm	$ m  / 10^{-20}$ erg·G <sup>-1</sup>	$\theta / ^\circ$	$R / 10^{-40}$ esu erg cm G <sup>-1</sup>	$D / 10^{-36}$ esu <sup>2</sup> cm <sup>2</sup> erg <sup>2</sup> G <sup>-2</sup>	$g_{abs} / 10^{-2}$
7	3.464	0.2085	3.98	5.88	98.56	-353	15.9	-0.89
8	3.682	0.2498	4.23	7.60	96.9	-389	17.9	-0.87
9	3.643	0.2676	4.40	9.15	97.73	-542	19.4	-1.12
10	3.788	0.3159	4.69	11.13	96.23	-564	22.0	-1.03
11	3.785	0.264	4.29	13.09	98.2	-797	18.4	-1.73
12	3.843	0.3809	5.11	15.05	95.69	-756	26.2	-1.16
13	3.844	0.3038	4.57	17.31	97.35	-1003	20.9	-1.92
14	3.875	0.442	5.48	19.35	95.27	-964	30.1	-1.28
15	3.876	0.3546	4.91	21.85	96.53	-1208	24.2	-2.00
16	3.895	0.5007	5.82	23.98	94.94	-1187	34.0	-1.40
17	3.895	0.4086	5.26	26.70	95.86	-1418	27.7	-2.05

**Table A9.** Calculated electric ( $\mu$ ) and magnetic ( $m$ ) transition dipole moments, rotatory strengths ( $R$ , velocity form), dipole strengths ( $D$ ) and calculated dissymmetry factor ( $g_{abs}$ ) values for the  $S_0 \rightarrow S_1$  transition of  $m[n]$ SPPs at BMK/6-31g(d) level of theory.

$m[n]$ SPP	$E /$ eV	$f$	$ \mu  / 10^{-18}$ esu·cm	$ m  / 10^{-20}$ erg·G <sup>-1</sup>	$\theta / ^\circ$	$R / 10^{-40}$ esu erg cm G <sup>-1</sup>	$D / 10^{-36}$ esu <sup>2</sup> cm <sup>2</sup> erg <sup>2</sup> G <sup>-2</sup>	$g_{abs} / 10^{-2}$
7	3.370	0.2065	4.02	5.77	98.42	-342	16.2	-0.85
8	3.577	0.2443	4.24	7.40	96.88	-376	18.0	-0.84
9	3.528	0.2621	4.43	8.88	97.53	-513	19.6	-1.05
10	3.671	0.3086	4.71	10.77	96.09	-534	22.2	-0.96
11	3.663	0.2585	4.31	12.64	98	-752	18.6	-1.61
12	3.722	0.3725	5.14	14.53	95.6	-719	26.4	-1.09
13	3.720	0.297	4.59	16.69	97.24	-953	21.1	-1.81
14	3.753	0.4322	5.51	18.66	95.2	-918	30.4	-1.21
15	3.752	0.3457	4.93	21.07	96.45	-1149	24.3	-1.89
16	3.772	0.4913	5.86	23.12	94.82	-1120	34.4	-1.30
17	3.771	0.3983	5.28	25.75	95.74	-1337	27.9	-1.92



**Table A10.** Calculated electric ( $\mu$ ) and magnetic ( $m$ ) transition dipole moments, rotatory strengths ( $R$ , velocity form), dipole strengths ( $D$ ) and calculated dissymmetry factor ( $g_{abs}$ ) values for the  $S_0 \rightarrow S_1$  transition of  $m[n]$ SPPs at M06-2X/6-31g(d) level of theory

$m[n]$ SPP	$E /$ eV	$f$	$ \mu  / 10^{-18}$ esu·cm	$ m  / 10^{-20}$ erg·G <sup>-1</sup>	$\theta / ^\circ$	$R / 10^{-40}$ esu erg cm G <sup>-1</sup>	$D / 10^{-36}$ esu <sup>2</sup> cm <sup>2</sup> erg <sup>2</sup> G <sup>-2</sup>	$g_{abs} / 10^{-2}$
7	3.470	0.2087	3.98	6.15	98.43	-377	15.9	-0.95
8	3.684	0.2487	4.22	7.95	96.9	-421	17.8	-0.94
9	3.641	0.2668	4.40	9.56	97.65	-581	19.3	-1.20
10	3.786	0.3148	4.68	11.63	96.2	-607	21.9	-1.11
11	3.781	0.2616	4.27	13.67	98.15	-855	18.3	-1.87
12	3.840	0.3797	5.11	15.73	95.69	-821	26.1	-1.26
13	3.839	0.2995	4.54	18.10	97.43	-1095	20.6	-2.12
14	3.872	0.4408	5.48	20.23	95.26	-1044	30.1	-1.39
15	3.871	0.3498	4.88	22.84	96.56	-1310	23.9	-2.19
16	3.891	0.4991	5.82	25.06	94.93	-1287	33.9	-1.52
17	3.890	0.4018	5.22	27.91	95.85	-1526	27.3	-2.23

**Table A11.** Calculated electric ( $\mu$ ) and magnetic ( $m$ ) transition dipole moments, rotatory strengths ( $R$ , velocity form), dipole strengths ( $D$ ) and calculated dissymmetry factor ( $g_{lum}$ ) values for the  $S_1 \rightarrow S_0$  transition of  $p[n]$ SPPs at CAM-B3LYP/6-31g(d) level of theory.

$p[n]$ SPP	$E /$ eV	$f$	$ \mu  / 10^{-18}$ esu·cm	$ m  / 10^{-20}$ erg·G <sup>-1</sup>	$\theta / ^\circ$	$R / 10^{-40}$ esu erg cm G <sup>-1</sup>	$D / 10^{-36}$ esu <sup>2</sup> cm <sup>2</sup> erg <sup>2</sup> G <sup>-2</sup>	$g_{lum} / 10^{-3}$
7	2.299	0.1651	4.35	4.40	92.13	-72	18.93	-1.52
8	2.565	0.2703	5.27	5.90	91.91	-104	27.79	-1.50
9	2.716	0.4106	6.31	7.25	91.41	-113	39.87	-1.13
10	2.820	0.5735	7.32	8.52	91.2	-130	53.63	-0.97
11	2.897	0.7475	8.25	9.82	90.92	-130	68.05	-0.76
12	2.961	0.9208	9.06	11.17	90.83	-146	82.01	-0.71
13	3.018	1.0965	9.79	12.57	90.69	-147	95.83	-0.61
14	3.044	1.3046	10.63	13.42	90.43	-106	113.04	-0.38
15	3.088	1.4542	11.14	15.29	90.49	-144	124.19	-0.47
16	3.111	1.645	11.81	16.45	90.32	-108	139.45	-0.31
17	3.131	1.8014	12.32	17.76	90.34	-127	151.76	-0.33

**Table A12.** Calculated electric ( $\mu$ ) and magnetic ( $m$ ) transition dipole moments, rotatory strengths ( $R$ , velocity form), dipole strengths ( $D$ ) and calculated dissymmetry factor ( $g_{lum}$ ) values for the  $S_1 \rightarrow S_0$  transition of  $p[n]$ SPPs at BMK/6-31g(d) level of theory.

$m[n]$ SPP	$E /$ eV	$f$	$ \mu  / 10^{-18}$ esu·cm	$ m  / 10^{-20}$ erg·G <sup>-1</sup>	$\theta / ^\circ$	$R / 10^{-40}$ esu erg cm G <sup>-1</sup>	$D / 10^{-36}$ esu <sup>2</sup> cm <sup>2</sup> erg <sup>2</sup> G <sup>-2</sup>	$g_{lum} / 10^{-3}$
7	2.242	0.1489	4.19	4.48	92.02	-66	17.52	-1.51
8	2.489	0.2501	5.15	5.92	91.98	-105	26.50	-1.59
9	2.633	0.3878	6.23	7.24	91.52	-119	38.85	-1.22
10	2.733	0.55	7.28	8.50	91.25	-133	53.08	-1.01
11	2.806	0.7246	8.25	9.79	90.97	-136	68.11	-0.80
12	2.866	0.8983	9.09	11.12	90.87	-152	82.67	-0.74
13	2.919	1.0746	9.85	12.49	90.75	-159	97.08	-0.66
14	2.945	1.2862	10.73	13.34	90.5	-122	115.19	-0.42
15	2.986	1.4361	11.26	15.17	90.5	-148	126.86	-0.47
16	3.006	1.6298	11.96	16.31	90.31	-104	142.99	-0.29
17	3.026	1.7911	12.49	17.61	90.33	-125	156.11	-0.32

**Table A13.** Calculated electric ( $\mu$ ) and magnetic ( $m$ ) transition dipole moments, rotatory strengths ( $R$ , velocity form), dipole strengths ( $D$ ) and calculated dissymmetry factor ( $g_{lum}$ ) values for the  $S_1 \rightarrow S_0$  transition of  $p[n]$ SPPs at M06-2X/6-31g(d) level of theory.

$m[n]$ SPP	$E /$ eV	$f$	$ \mu  / 10^{-18}$ esu·cm	$ m  / 10^{-20}$ erg·G <sup>-1</sup>	$\theta / ^\circ$	$R / 10^{-40}$ esu erg cm G <sup>-1</sup>	$D / 10^{-36}$ esu <sup>2</sup> cm <sup>2</sup> erg <sup>2</sup> G <sup>-2</sup>	$g_{lum} / 10^{-3}$
7	2.309	0.1609	4.29	4.62	92.06	-75	18.38	-1.63
8	2.569	0.2657	5.22	6.18	91.9	-111	27.27	-1.64
9	2.719	0.4067	6.28	7.59	91.44	-124	39.45	-1.26
10	2.822	0.5712	7.31	8.92	91.17	-138	53.39	-1.03
11	2.898	0.7476	8.25	10.29	90.91	-140	68.05	-0.82
12	2.960	0.9222	9.06	11.70	90.82	-156	82.16	-0.76
13	3.016	1.0995	9.80	13.16	90.7	-162	96.15	-0.67
14	3.042	1.3117	10.66	14.06	90.44	-118	113.72	-0.42
15	3.086	1.4623	11.18	16.01	90.47	-151	124.99	-0.48
16	3.108	1.6557	11.85	17.22	90.3	-111	140.51	-0.31
17	3.128	1.816	12.37	18.60	90.32	-133	153.15	-0.35

**Table A14.** Calculated electric ( $\mu$ ) and magnetic ( $m$ ) transition dipole moments, rotatory strengths ( $R$ , velocity form), dipole strengths ( $D$ ) and calculated dissymmetry factor ( $g_{lum}$ ) values for the  $S_1 \rightarrow S_0$  transition of  $m[n]$ SPPs at CAM-B3LYP/6-31g(d) level of theory.

$m[n]$ SPP	$E /$ eV	$f$	$ \mu  / 10^{-18}$ esu·cm	$ m  / 10^{-20}$ erg·G <sup>-1</sup>	$\theta / ^\circ$	$R / 10^{-40}$ esu erg cm G <sup>-1</sup>	$D / 10^{-36}$ esu <sup>2</sup> cm <sup>2</sup> erg <sup>2</sup> G <sup>-2</sup>	$g_{lum} / 10^{-3}$
7	2.640	0.313	5.59	5.21	95.78	-299	31.3	-3.83
8	2.728	0.4068	6.27	6.49	94.64	-333	39.3	-3.38
9	2.786	0.5329	7.10	7.80	93.41	-332	50.4	-2.63
10	2.860	0.6659	7.84	9.21	92.66	-336	61.4	-2.19
11	2.929	0.766	8.30	10.65	92.7	-417	69.0	-2.42
12	2.980	0.9581	9.21	11.97	91.84	-353	84.8	-1.67
13	2.996	1.1136	9.90	13.28	91.62	-370	98.0	-1.51
14	3.053	1.2815	10.52	14.79	91.16	-313	110.7	-1.13
15	3.073	1.4181	11.03	16.13	91.12	-346	121.7	-1.14
16	3.102	1.5934	11.64	17.54	90.85	-302	135.5	-0.89
17	3.122	1.7367	12.11	18.96	90.75	-298	146.7	-0.81

**Table A15.** Calculated electric ( $\mu$ ) and magnetic ( $m$ ) transition dipole moments, rotatory strengths ( $R$ , velocity form), dipole strengths ( $D$ ) and calculated dissymmetry factor ( $g_{lum}$ ) values for the  $S_1 \rightarrow S_0$  transition of  $m[n]$ SPPs at BMK/6-31g(d) level of theory.

$m[n]$ SPP	$E /$ eV	$f$	$ \mu  / 10^{-18}$ esu·cm	$ m  / 10^{-20}$ erg·G <sup>-1</sup>	$\theta / ^\circ$	$R / 10^{-40}$ esu erg cm G <sup>-1</sup>	$D / 10^{-36}$ esu <sup>2</sup> cm <sup>2</sup> erg <sup>2</sup> G <sup>-2</sup>	$g_{lum} / 10^{-3}$
7	2.587	0.3145	5.66	5.21	95.85	-304	32.1	-3.80
8	2.659	0.4022	6.32	6.46	94.75	-340	39.9	-3.41
9	2.707	0.5247	7.15	7.75	93.54	-343	51.1	-2.68
10	2.771	0.6539	7.89	9.14	92.77	-348	62.2	-2.23
11	2.831	0.7468	8.34	10.54	92.85	-435	69.6	-2.50
12	2.882	0.9401	9.27	11.87	91.93	-366	86.0	-1.70
13	2.896	1.0939	9.98	13.17	91.72	-390	99.6	-1.57
14	2.951	1.2643	10.63	14.65	91.24	-333	113.0	-1.18
15	2.970	1.4018	11.16	15.99	91.18	-363	124.5	-1.17
16	2.998	1.5807	11.79	17.36	90.9	-318	139.1	-0.92
17	3.016	1.7251	12.28	18.78	90.78	-311	150.9	-0.82

**Table A16.** Calculated electric ( $\mu$ ) and magnetic ( $m$ ) transition dipole moments, rotatory strengths ( $R$ , velocity form), dipole strengths ( $D$ ) and calculated dissymmetry factor ( $g_{lum}$ ) values for the  $S_1 \rightarrow S_0$  transition of  $m[n]$ SPPs at M06-2X/6-31g(d) level of theory.

$m[n]$ SPP	$E /$ eV	$f$	$ \mu  / 10^{-18}$ esu·cm	$ m  / 10^{-20}$ erg·G <sup>-1</sup>	$\theta / ^\circ$	$R / 10^{-40}$ esu erg cm G <sup>-1</sup>	$D / 10^{-36}$ esu <sup>2</sup> cm <sup>2</sup> erg <sup>2</sup> G <sup>-2</sup>	$g_{lum} / 10^{-3}$
7	2.651	0.3145	5.59	5.46	95.72	-322	31.3	-4.11
8	2.735	0.4064	6.26	6.79	94.6	-358	39.2	-3.66
9	2.790	0.5326	7.09	8.16	93.39	-358	50.3	-2.84
10	2.861	0.6653	7.83	9.64	92.63	-361	61.3	-2.35
11	2.928	0.7652	8.30	11.14	92.72	-455	68.9	-2.64
12	2.979	0.9604	9.22	12.53	91.84	-384	85.0	-1.81
13	2.994	1.1165	9.92	13.90	91.64	-407	98.4	-1.65
14	3.051	1.2872	10.55	15.47	91.17	-345	111.3	-1.24
15	3.071	1.4263	11.07	16.88	91.11	-373	122.5	-1.22
16	3.099	1.6046	11.68	18.35	90.85	-326	136.6	-0.96
17	3.119	1.7494	12.16	19.84	90.76	-328	148.0	-0.89

**Table A17.** Calculated electric ( $\mu$ ) and magnetic ( $m$ ) transition dipole moments, rotatory strengths ( $R$ , velocity form), dipole strengths ( $D$ ) and calculated dissymmetry factor ( $g_{abs}$ ) values for the  $S_0 \rightarrow S_1$  transition of **D1–4** at CAM-B3LYP/6-31g(d) level of theory.

Species	$E /$ eV	$f$	$ \mu  / 10^{-18}$ esu·cm	$ m  / 10^{-20}$ erg·G <sup>-1</sup>	$\theta / ^\circ$	$R / 10^{-40}$ esu erg cm G <sup>-1</sup>	$D / 10^{-36}$ esu <sup>2</sup> cm <sup>2</sup> erg <sup>2</sup> G <sup>-2</sup>	$g_{abs} / 10^{-2}$
<b>D1</b>	3.917	0.3195	4.64	15.40	96.66	-823	21.53	-1.53
<b>D2</b>	4.197	0.1122	2.66	15.54	101.52	-806	7.08	-4.56
<b>D3</b>	4.493	0.3846	4.75	8.91	89.06	67	22.58	0.12
<b>D4</b>	4.118	0.2082	3.65	6.43	90.92	-36	13.33	-0.11

**Table A18.** Calculated electric ( $\mu$ ) and magnetic ( $m$ ) transition dipole moments, rotatory strengths ( $R$ , velocity form), dipole strengths ( $D$ ) and calculated dissymmetry factor ( $g_{lum}$ ) values for the  $S_1 \rightarrow S_0$  transition of **D1–4** at CAM-B3LYP/6-31g(d) level of theory.

Species	$E /$ eV	$f$	$ \mu  / 10^{-18}$ esu·cm	$ m  / 10^{-20}$ erg·G <sup>-1</sup>	$\theta / ^\circ$	$R / 10^{-40}$ esu erg cm G <sup>-1</sup>	$D / 10^{-36}$ esu <sup>2</sup> cm <sup>2</sup> erg <sup>2</sup> G <sup>-2</sup>	$g_{lum} / 10^{-3}$
<b>D1</b>	3.048	1.2006	10.19	11.21	90.92	-182	103.87	-0.70
<b>D2</b>	3.158	1.0217	9.24	9.79	89.9	15	85.31	0.07
<b>D3</b>	1.551	0.1239	4.59	1.52	94.29	-52	21.06	-0.99
<b>D4</b>	3.215	0.4462	6.05	6.11	91.65	-103	36.61	-1.12

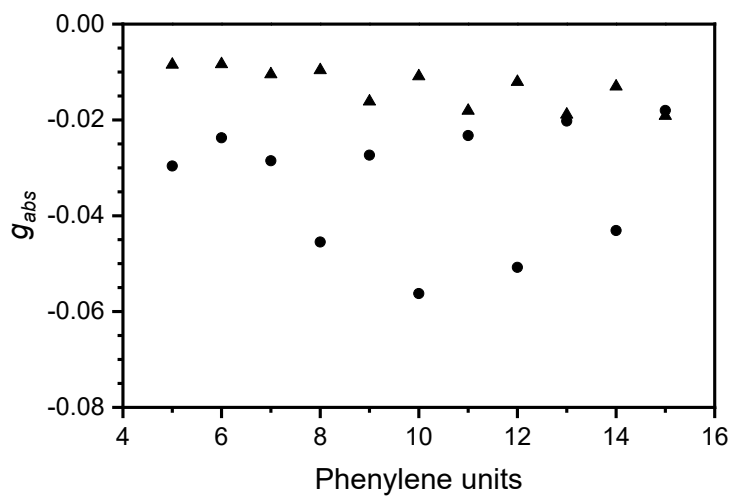


**Figure A5.** Dissymmetry factors  $g_{abs}$  for  $p[n]$ SPPs (circles) and  $m[n]$ SPPs (triangles) calculated at BMK/6-31g(d)level of theory.

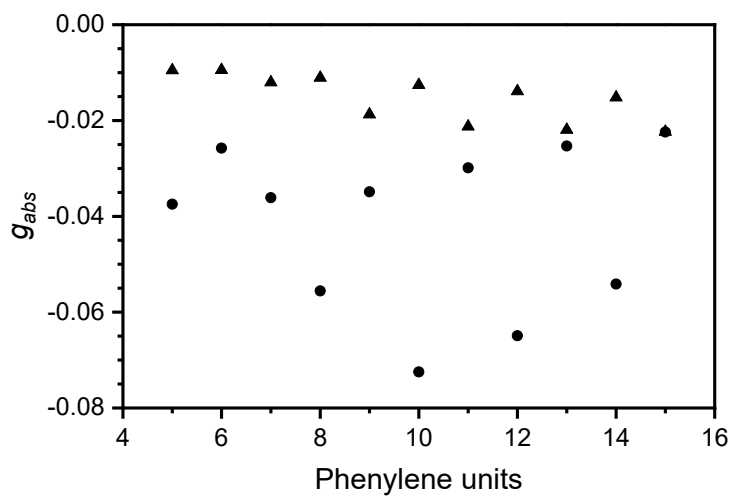


**Figure A6.** Dissymmetry factors  $g_{abs}$  for  $p[n]$ SPPs (circles) and  $m[n]$ SPPs (triangles) calculated at M06-2X/6-31g(d)level of theory.

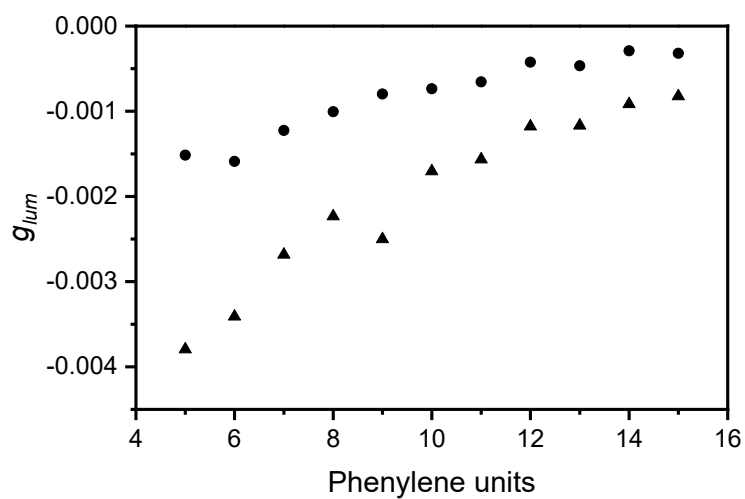


**Figure A7.** Dissymmetry factors  $g_{lum}$  for  $p[n]$ SPPs (circles) and  $m[n]$ SPPs (triangles) calculated at BMK /6-31g(d) level of theory.

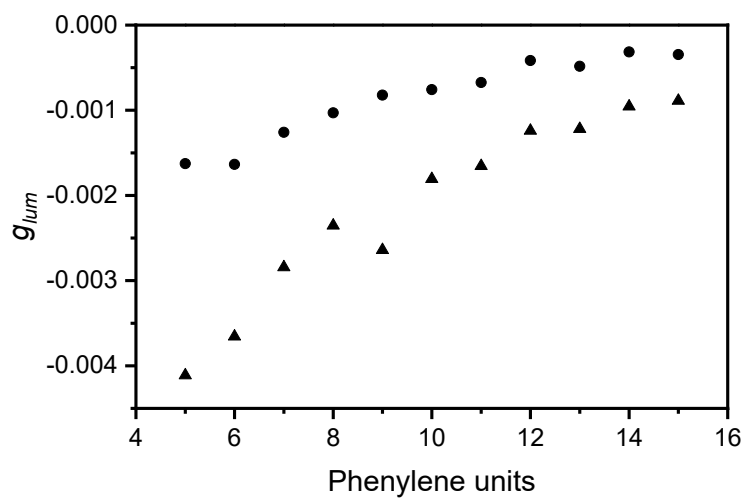


**Figure A8.** Dissymmetry factors  $g_{lum}$  for  $p[n]$ SPPs (circles) and  $m[n]$ SPPs (triangles) calculated at M06-2X/6-31g(d) level of theory.

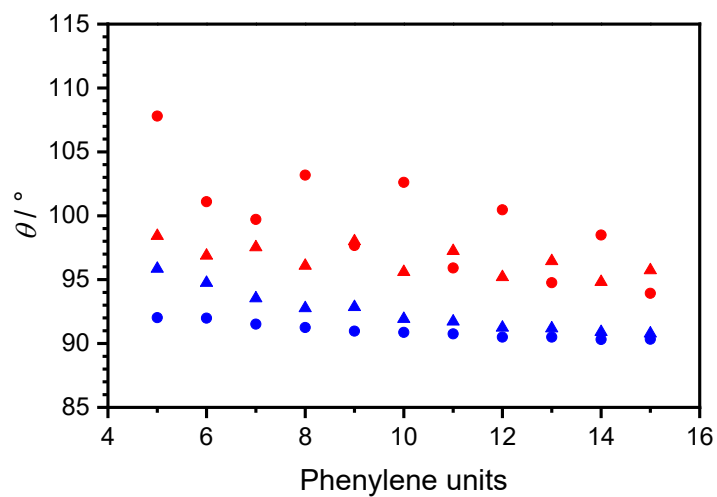


**Figure A9.** Values of angle  $\theta$  in degrees between the electric and magnetic transition dipole moments for  $p[n]$ SPPs (circles) and  $m[n]$ SPPs (triangles) in the ground (red) and the excited (blue) state calculated at BMK/6-31g(d) level of theory.

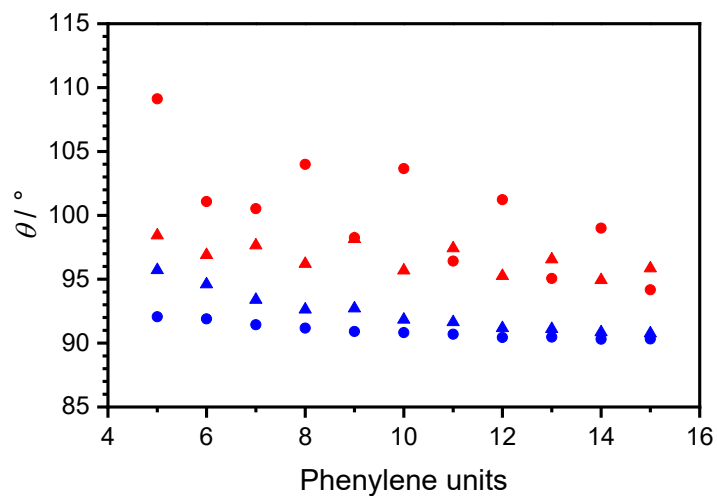


**Figure A10.** Values of angle  $\theta$  in degrees between the electric and magnetic transition dipole moments for  $p[n]$ SPPs (circles) and  $m[n]$ SPPs (triangles) in the ground (red) and the excited (blue) state calculated at M06-2X/6-31g(d) level of theory.









Table of numerical values with 4 columns and 20 rows.

p[10]SPP conformer 4

E = -2467.39699797

Table of numerical values for conformer 4, with 4 columns and 880 rows.

p[10]SPP conformer 5

E = -2467.39588059

Table of numerical values for conformer 5, with 4 columns and 880 rows.

p[10]SPP conformer 6

E = -2467.3964719

Table of numerical values for conformer 6, with 4 columns and 140 rows.

Table of numerical values on the right side of the page, with 4 columns and 880 rows.

p[11]SPP ground state

E = -2698.55221444

Table of numerical values for ground state, with 4 columns and 150 rows.





Appendix

p[14]SPP ground state E = -3392.00396185

Table with 3 columns: index, value, value. Rows 1-100 of the p[14]SPP ground state energy spectrum.

Table with 3 columns: index, value, value. Rows 101-200 of the p[14]SPP ground state energy spectrum.

p[14]SPP excited state E = -3388.83982525

Table with 3 columns: index, value, value. Rows 1-100 of the p[14]SPP excited state energy spectrum.

Table with 3 columns: index, value, value. Rows 1-100 of the p[15]SPP ground state energy spectrum.

p[15]SPP ground state E = -3623.15352467

Table with 3 columns: index, value, value. Rows 1-100 of the p[15]SPP ground state energy spectrum.











conformer 2

E = -2236.26666280

Table of energy levels for conformer 2, listing atom types (C, H), atom IDs, and their corresponding energy values in Hartrees.

m[9]SPP

conformer 3

E = -2236.26666310

Table of energy levels for m[9]SPP conformer 3, listing atom types (C, H), atom IDs, and their corresponding energy values in Hartrees.

Table of energy levels for m[10]SPP conformer 1 excited state, listing atom types (C, H), atom IDs, and their corresponding energy values in Hartrees.

m[10]SPP

conformer 1

ground state

E = -2467.42353374

Table of energy levels for m[10]SPP conformer 1 ground state, listing atom types (C, H), atom IDs, and their corresponding energy values in Hartrees.

m[10]SPP

conformer 1

excited state

E = -2465.11407184

Table of energy levels for m[10]SPP conformer 1 excited state, listing atom types (C, H), atom IDs, and their corresponding energy values in Hartrees.













C	8.50606	0.00756	-0.79233
H	8.21171	-1.00944	-0.22854
H	7.71950	-0.67571	-1.12104
C	8.50606	-0.00758	0.79242
H	7.71950	0.67569	1.12112
H	8.21719	-1.00946	1.12363
C	9.62944	2.79559	1.13831
H	8.60987	3.01759	2.07000
C	9.77341	3.72125	0.10180
C	7.73257	4.07959	1.93599
H	8.49808	2.32767	2.90075
C	8.88352	4.78093	-0.04279
H	10.57313	3.59352	-0.52380
C	7.83146	4.96407	0.85721
H	6.92325	4.19949	2.64945
H	9.00202	5.47042	-0.87372
C	9.62943	-2.79561	-1.13829
H	9.77341	-3.72130	-2.10080
H	8.60986	-3.01758	-2.06997
C	8.88351	-4.78098	0.04276
H	10.57313	-3.59337	0.62108
C	7.73255	-4.07957	-1.93598
H	8.49806	-2.32763	-2.90070
C	7.83145	-4.96408	-0.85723
H	9.00202	-5.47049	0.87367
H	6.92323	-4.19945	-2.64945
C	6.76740	5.97746	0.65838
C	6.15844	6.13511	-0.58889
H	6.24448	6.70122	-1.79419
C	5.01405	6.90635	-0.73322
H	6.53799	5.57909	-1.44085
C	5.10920	7.48242	1.58644
H	6.72701	6.63663	2.70483
C	4.43912	7.56076	0.26060
H	4.51465	6.93390	-1.69642
H	4.72409	8.02522	2.44380
C	3.09766	8.18303	0.25108
C	2.20272	8.09483	1.32212
C	2.62800	8.75432	-0.93662
H	0.88231	8.49216	1.19024
H	2.52372	7.63577	2.25125
C	1.30281	9.14333	-1.07200
H	3.30658	8.88470	-1.77410
C	0.39219	8.98515	-0.02207
H	0.19795	8.19771	2.13202
H	0.96579	9.56712	-2.01333
C	6.76738	-5.97747	-0.65842
C	6.24445	-6.70120	-1.79424
C	6.15843	-6.13515	0.58885
C	5.10917	-7.48220	-1.58651
H	6.24448	-6.70122	-1.79419
C	5.01404	-6.90639	0.73317
H	6.53799	-5.57916	1.44082
C	4.43910	-7.56077	-0.26066
H	4.72405	-8.02518	-2.44388
H	4.51464	-6.93396	-1.69642
C	3.09763	-8.18304	-0.25115
C	2.20268	-8.09481	-1.32219
C	2.62798	-8.75435	0.93654
C	0.88228	-8.49214	-1.19030
H	2.52368	-7.63573	-2.25131
C	1.30279	-9.14336	-1.07192
H	3.30656	-8.88475	1.77401
C	0.39216	-8.98516	0.02200
H	0.19791	-8.33467	-2.01808
H	0.96577	-9.56717	2.01324
C	-3.08313	-9.05624	-0.36672
C	-3.08253	-8.69643	-1.45026
C	-3.25709	9.57978	0.76678
C	-1.70080	8.75770	-1.36586
H	-3.53664	8.27403	-2.34063
C	-1.87572	9.63637	-0.85209
H	-3.85419	9.92901	1.60334
C	-1.06582	9.17906	-0.19344
H	-1.10279	8.38623	-2.19213
H	-1.41376	10.02527	1.75488
H	-12.19964	-3.15403	2.39851
H	-10.58775	-4.45033	2.46746
H	-10.58547	-0.85254	2.21622
H	-12.57028	-1.12680	2.08766
C	-12.23326	-2.70180	1.41338
C	-12.60901	-1.39078	1.30841
C	-10.44536	-5.05039	1.57681
C	-12.48389	1.55091	1.09476
H	-8.92568	-6.19136	2.51844
H	-11.91489	3.41758	1.89578
C	-11.88657	-3.47231	0.27514
C	-9.49497	-6.04591	1.60669
H	-12.64066	-0.71407	0.05077
C	-12.11436	2.86427	0.98548
C	-11.12800	-4.70899	0.38349
C	-12.64066	0.71110	-0.05069
H	-11.46297	5.41511	1.64182
H	-7.90300	-7.11288	2.51979
C	-12.11440	-2.86424	-0.98542
C	-12.48392	-1.55098	-1.09469
H	-9.79220	7.16095	1.57757
C	-10.89546	5.55724	0.72886
C	-7.35928	-8.14039	1.57704
C	-9.15883	-6.78290	0.45453
C	-11.88656	3.47233	-0.27508
C	-10.89549	-5.55721	-0.72882
H	-5.66323	-9.07061	2.47766
H	-9.94610	6.55192	0.69261
H	-11.91494	-3.41756	-1.89572
H	-12.57032	-1.12677	-2.08758
C	-12.60903	1.39080	-1.30833
C	-6.08883	-8.68653	1.55560
C	-11.12799	4.70901	-0.38344
C	-7.94674	-7.60671	-1.61612
C	-9.94613	-6.55190	-0.69259
C	-12.23328	2.70182	-1.41331
H	-11.46302	-5.41508	-1.64178
H	-12.85470	0.85257	-2.21614
H	-9.15892	-6.78291	-0.45452
H	-5.66344	-9.07007	2.47742
C	-10.44555	5.05100	-1.57677
H	-9.79225	-7.16092	-1.57755
H	-7.23256	-7.58822	-0.78395
H	-12.19967	3.15405	-2.39845
C	-9.49497	6.04592	-1.60667
C	-3.89315	-9.05624	0.36667
C	-5.06277	-8.30343	-0.80250
H	-10.58775	4.45034	-2.46742
H	-7.63689	-7.35116	-1.70392
H	-8.92569	-6.19136	-2.51842
H	-5.40988	-8.30980	-1.73601
C	-3.25712	-9.57977	-0.76685
H	-3.85423	-9.92898	-1.60341
H	-3.53665	-8.27406	2.34059
H	-1.10280	-8.38626	2.19207
H	-1.30824	-8.69645	1.45021
C	-1.70082	-8.75773	1.36580
C	-1.06584	-9.17906	0.19337
C	-1.87576	-9.63796	-0.85228

**$m[17]SPP$**   
**ground state**  
 **$E = -4085.4630602$**

H	-1.41380	-10.02523	-1.75497
H	-7.35120	-7.63689	-1.70391
H	-5.40984	-8.30983	1.73597
C	-7.23253	7.58884	0.78394
C	-5.96273	8.30344	0.80248
C	-7.94762	7.60672	-0.41612
C	-5.33439	8.73308	-0.37416
C	-7.35927	8.14407	-1.57705
C	-6.08881	8.68652	-1.55564
H	-7.90299	8.11287	-2.51580
H	-5.66322	9.07060	-2.47770
C	-12.69059	1.13593	-1.02527
C	-13.42963	-0.05269	-0.95624
C	-12.79332	-1.22258	-1.38312
C	-11.40587	-1.24073	-1.10045
C	-10.62856	-0.10263	-1.30446
C	-11.30298	1.14067	-1.22197
C	-14.72649	-0.11205	-0.17571
C	-14.53893	-0.75742	1.27553
C	-13.10809	-0.67817	1.76647
C	-12.51760	0.55244	2.07144
C	-11.13890	0.71051	1.94016
C	-10.31513	-0.34268	1.52711
C	-10.86312	-1.64857	1.57109
C	-12.25478	-1.78534	1.66609
C	-9.98991	-2.93566	1.39642
C	-10.29759	-3.89577	0.52769
C	-9.41674	-4.96251	0.34978
C	-8.19458	-5.01774	1.03991
C	-7.90977	-3.97851	1.94358
C	-8.78789	-2.91813	2.11966
C	-7.18602	-6.07746	0.80022
C	-6.37835	-6.55164	1.85027
C	-5.30970	-7.40588	1.60654
C	-5.00120	-7.83463	0.30377
C	-5.86057	-7.42886	-0.73192
C	-6.92737	-6.56789	-0.48867
C	-3.73997	-8.56822	0.04209
C	-2.97846	-8.28314	-1.10424
C	-1.69514	-8.79494	-1.26270
C	-1.11116	-9.61223	-0.28012
C	-1.90533	-9.97022	0.82285
C	-3.19117	-9.46226	0.97872
C	0.33326	-9.93593	-0.34870
C	1.12564	-9.84921	0.80831
C	2.51287	-9.90752	0.73676
C	3.17384	-10.06121	-0.49426
C	2.37668	-10.25123	0.80252
C	0.98840	-10.18616	-1.56688
C	4.63931	-9.85386	-0.57885
C	5.50502	-10.18616	0.47874
C	6.82411	-9.74320	0.49691
C	7.33699	-8.35650	-0.95353
C	6.50802	-8.71922	-1.65367
C	5.18841	-9.15656	-1.66869
C	8.62490	-8.22502	-0.42760
C	8.97319	-7.62279	0.79315
C	10.00668	-6.69585	0.86902
C	10.74414	-6.33159	-0.27088
C	10.47598	-7.02721	-1.46366
C	9.43745	-7.95012	-1.54140
C	11.61044	-5.12891	-0.23442
C	12.28975	-4.72548	0.92936
C	12.83869	-3.45117	0.33810
C	12.73842	-2.52460	-0.01455
C	12.17231	-2.97322	-1.21999
C	11.61955	-4.24416	-1.32658
C	13.00942	-1.07890	0.16874
C	-12.61605	-0.44559	1.36058
C	12.55859	0.94053	1.45285
C	12.89091	1.75786	0.35880
C	13.40818	1.12633	-0.78662
C	13.46402	-0.26083	-0.88055
C	12.50373	3.18894	0.36524
C	12.48054	3.96029	1.54109
C	11.83410	5.19063	1.58441
C	11.17784	5.70675	0.45300
C	11.30485	4.99207	-0.75038
C	11.95136	3.76247	-0.79301
C	10.22309	6.83792	0.63782
C	9.37238	6.95644	1.64542
C	8.27487	7.81038	1.62489
C	7.97724	8.58457	0.49064
C	8.96466	8.55597	-0.57316
C	9.99477	7.70227	-0.55233
C	6.65944	9.23925	0.36978
C	5.97750	9.78919	1.47239
C	4.63819	10.15872	1.38569
C	3.91273	9.99306	0.19248
C	4.61774	9.53711	-0.93474
C	5.95561	9.17095	-0.84913
C	2.43738	10.12484	0.13411
C	1.77257	10.50899	-1.04411
C	0.39307	10.38074	-1.16693
C	-0.38603	9.87026	-0.11416
C	0.26470	9.58806	1.09835
C	1.64536	9.70954	1.21856
C	-1.80459	9.48836	-0.30757
C	-2.19598	8.85108	-1.49702
C	-3.46253	8.29605	-1.63358
C	-4.40434	8.35913	-0.59173
C	-4.03889	9.06623	0.58774
C	-2.76647	9.61348	0.70912
C	-5.67207	7.59656	-0.68973
C	-6.29685	7.36345	-1.92815
C	-7.36190	6.47680	-2.04308
C	-7.86235	5.79460	-0.92171
C	-7.30082	6.09580	0.32934
C	-6.22527	6.97183	0.44167
C	-8.85605	4.70325	-1.05934
C	-9.90443	4.51840	-0.14403
C	-10.73528	3.38901	-0.21678
C	-10.53060	2.40826	-2.19203
C	-9.52290	2.63109	-2.14570
C	-8.70553	3.75280	-2.08379
C	-9.05206	-0.00602	0.74549
C	-9.20218	-0.29762	-0.80809
C	-6.43970	8.73437	-1.71787
H	4.08760	9.37779	-1.86907
H	4.14068	10.56423	-2.26257
H	2.34742	10.89409	-1.88188
H	2.12481	9.38985	-2.13928
H	-0.08914	10.66374	-2.09879
H	-0.30875	9.18046	1.92764

**$m[17]SPP$**   
**excited state**  
 **$E = -4081.6600300$**

H	-12.85618	1.15281	-0.97541

# Appendix

C	13.27959	-0.35018	1.37596
C	13.19144	1.01229	1.46269
C	13.17308	1.84167	0.30462
C	13.46819	1.18339	-0.92542
C	13.55241	-0.17774	-1.01473
C	12.71955	3.20663	0.35612
C	12.48409	3.88869	1.58131
C	11.76670	5.05882	1.63183
C	11.23176	5.65507	0.46743
C	11.60237	5.06794	-0.76181
C	12.31808	3.89691	-0.81850
C	10.22141	6.70774	0.52147
C	9.39490	6.85295	1.65198
C	8.26843	7.65170	1.62483
C	7.90024	8.35806	0.47046
C	8.78749	8.31200	-0.61669
C	9.91442	7.51445	-0.59266
C	6.56493	8.97419	0.36457
C	5.87962	9.47838	1.47881
C	4.54324	9.83543	1.39931
C	3.82639	9.70384	0.20358
C	4.53529	9.28855	-0.92918
C	5.87111	8.93504	-0.85186
C	2.35372	9.84307	0.14500
C	1.69531	10.24732	-1.02225
C	0.31761	10.14919	-1.13925
C	-0.46289	9.64879	-0.09186
C	0.18455	9.33624	1.10686
C	1.56276	9.42920	1.22201
C	-1.89398	9.31228	-0.27603
C	-2.31619	8.71373	-1.46658
C	-3.59686	8.20210	-1.59683
C	-4.51631	8.27246	-0.54575
C	-4.11899	8.94397	0.61657
C	-2.83788	9.44756	0.75052
C	-5.80418	7.54334	-0.63874
C	-6.45651	7.35947	-1.86263
C	-7.53960	6.50150	-1.97654
C	-8.02431	5.80045	-0.86835
C	-7.43045	6.05261	0.37093
C	-6.34004	6.90238	0.48231
C	-9.03455	4.72468	-1.00992
C	-10.04670	4.51769	-0.06982
C	-10.87308	3.40202	-0.14100
C	-10.70706	-2.44304	-1.14416
C	-9.73998	2.69209	-2.12365
C	-8.92244	3.80801	-2.06007
C	-9.20092	-0.13785	0.72907
C	-9.36821	-0.27098	-0.83901
H	6.36037	8.53378	-1.73320
H	4.01020	9.15736	-1.86966
H	4.04094	10.20933	-2.28628
H	2.27287	10.62840	-1.85874
H	2.03945	9.09327	2.13724
H	-0.16168	10.45071	-2.06577
H	-0.59115	8.93303	1.93413
H	7.60734	7.65463	2.48536
H	8.57760	8.90298	-1.50287
H	9.58135	6.24938	2.53328
H	10.56607	7.50316	-1.45996
H	-2.55079	9.94751	1.67208
H	-1.60512	8.57543	-2.27482
H	-4.82275	9.05929	1.43492
H	-3.86191	7.67076	-2.50501
H	-6.10089	7.88452	-2.74367
H	-5.84992	7.00876	1.44476
H	-8.01170	6.36208	-2.94845
H	-7.77777	5.51398	1.24730
H	-10.18051	5.23202	0.73735
H	-8.14681	3.94604	-2.80697
H	-11.63623	3.25517	0.61673
H	-9.61723	1.98096	-2.93469
H	-10.86296	1.52337	2.02840
H	-12.81229	-2.94691	1.46441
H	-11.28510	-4.00774	-0.15079
H	-8.72819	-2.29229	2.82156
H	-9.70415	-5.86505	-0.44038
H	-7.12117	-4.11514	2.49774
H	6.39925	9.57987	2.42658
H	-6.67459	-6.32931	2.82534
H	-7.53221	-6.25364	-1.37209
H	-4.70620	-7.71388	2.39906
H	-5.60879	-7.71134	-1.79080
H	-3.33107	-7.43570	-1.83456
H	-3.69978	-9.68654	1.79461
H	-1.03882	-8.23873	-2.10076
H	-1.39551	-10.47816	1.53475
H	0.51448	-9.99751	-2.48085
H	0.72027	-9.41826	1.75948
H	2.95898	-10.05840	-2.59093
H	3.15772	-9.45803	1.65086
H	5.19140	-10.38100	1.36054
H	4.65077	-8.58199	-2.49503
H	7.51059	-9.62184	1.38858
H	6.96404	-7.83451	-2.47513
H	9.19696	-8.01229	-2.53121
H	8.63307	-7.70665	1.71380
H	11.07679	-6.49176	-2.39581
H	10.49348	-6.17748	1.86101
H	12.26045	-5.11661	1.92538
H	11.79798	-4.57046	-2.32429
H	13.29550	-2.95421	2.09262
H	12.83751	-2.42138	-2.16889
H	13.19436	-0.92750	2.28878
H	13.76131	-0.62032	-1.98200
H	13.04124	1.45281	2.44110
H	13.61298	1.76914	-1.82600
H	12.85792	3.47288	2.50993
H	12.48733	3.44913	-1.79020
H	11.59837	5.52609	2.59660
H	11.23407	5.49241	-1.68917
H	-13.49965	-2.11767	-1.48305
H	-11.06706	-2.13258	-1.76295
H	-15.36887	-0.48759	1.96159
H	-14.95672	-1.96026	1.09693
H	-15.65432	-0.66017	-0.70194
H	-15.24061	0.86240	0.07053
H	-8.65592	0.41832	-1.29809
H	-9.06489	-1.28146	-1.12870
H	-8.33133	-0.73579	1.01081
H	-8.95897	0.90385	0.95948
H	-13.28200	1.22241	2.27853
H	-13.35458	2.08806	-0.73025

## A.2. SI [6,7]Helicene *para*-phenylene

### Circularly Polarized Luminescence in a Möbius Helicene Carbon Nano hoop

Juraj Malinčík,<sup>[a,d]</sup> Sudhakar Gaikwad,<sup>[a]</sup> Juan P. Mora-Fuentes,<sup>[c]</sup> Marc-Aurèle Boillat,<sup>[a]</sup> Alessandro Prescimone,<sup>[a]</sup> Daniel Häussinger,<sup>[a]</sup> Araceli G. Campaña,<sup>[c]</sup> and Tomáš Šolomek\*<sup>[a,b,d]</sup>

---

[a] Department of Chemistry, University of Basel, St. Johann's-Ring 19, 4056 Basel, Switzerland.

[b] Department of Chemistry, Biochemistry and Pharmaceutical Sciences, University of Bern, Freiestrasse 3, 3012 Bern, Switzerland.

[c] Department of Organic Chemistry, University of Granada, Avda Fuentenueva, s/n, 18071 Granada, Spain.

[d] Prievidza Chemical Society, M. Hodžu 10/16, 971 01 Prievidza, Slovakia.

E-mail: tomas.solomek@unibe.ch

## Supporting Information

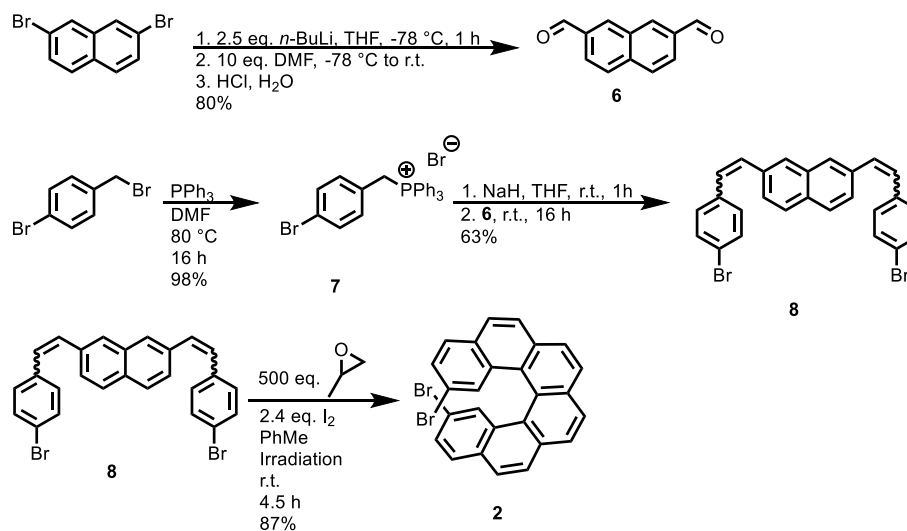
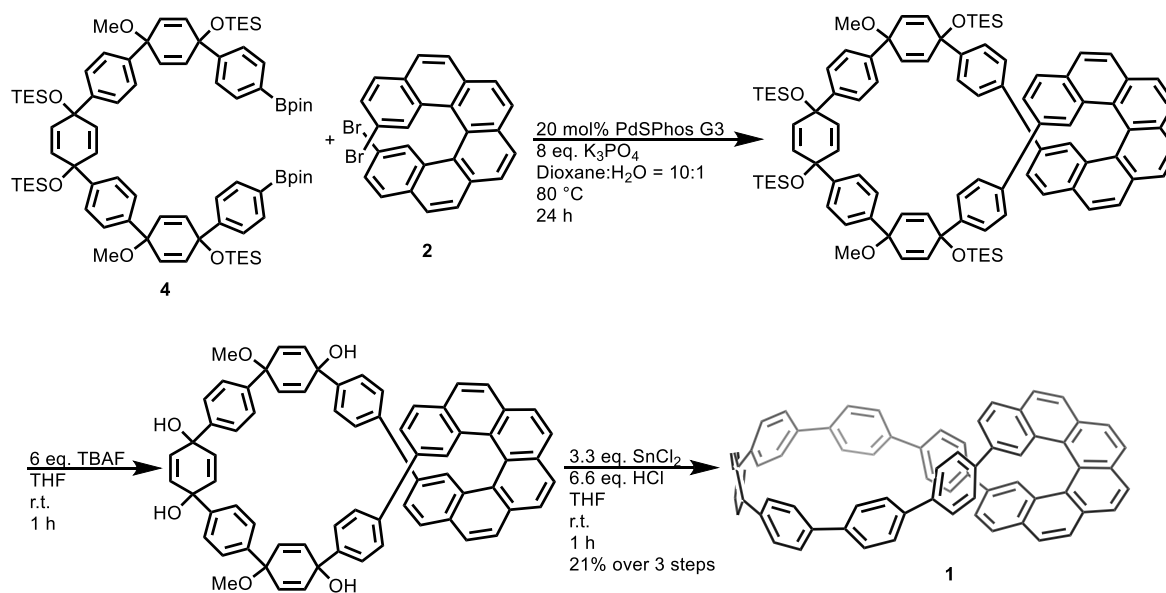
## A.2.1. Experimental Part

### General Remarks

**Materials:** All commercially available chemicals were purchased from Acros, Alfa Aesar, Apollo Scientific, Fluorochem and Sigma-Aldrich and used without further purification. Anhydrous solvents were purchased from Acros and stored over molecular sieves (4 Å). THF was dried by distillation over sodium and benzophenone under Ar and used fresh. Concentration of organolithium reagents was determined via titration prior to use. Molecular sieves were dried at 300 °C and 1 mbar over 24 h in Büchi Glass Oven B-585. Column chromatography was performed on silica gel P60 (40–63 µm) from Silicycle™. Celite® 545 (0.02–0.1 mm) from Supelco was used. Automated flash chromatography was performed using Biotage Isolera One. TLC was performed with silica gel 60 F254 aluminium plates purchased from Merck. High resolution mass spectra (HRMS) were measured on a maX-is™4G instrument from Bruker for HR-ESI-ToF MS. UV-Vis absorption were measured using Jasco V-770 with Jasco ETCR-762 Peltier thermostatted cell holder at 25 °C in 1 cm cuvette. Excitation and emission spectra were recorded using Jasco FP-8600 with Jasco ETC-815 Peltier thermostatted cell holder at 25 °C in 1 cm cuvette. Circular dichroism was measured using Jasco J-1500 with Jasco PTC-517 Peltier thermostatted cell holder at 25 °C in 1 cm cuvette. Time-correlated single photon counting (TCSPC)-based emission lifetime measurements were performed on a LifeSpec II spectrometer (Edinburgh Instruments) employing a picosecond pulsed diode laser (ca. 60 ps pulse width). Hamamatsu absolute photoluminescence quantum yield spectrometer C11347 Quantaaurus-QY was used for quantum yield measurement. Circularly polarized luminescence (CPL) was recorded in an Olis DSM172 spectrophotometer equipped with a xenon lamp of 150 W.

**Nuclear magnetic resonance:** NMR experiments were performed on Bruker Avance III NMR spectrometers operating at 400, 500 or 600 MHz proton frequencies. The instruments were equipped with a direct-observe 5 mm BBFO smart probe (400 and 500 MHz), an indirect-detection 5 mm BBI probe (600 MHz). All probes were equipped with actively shielded z-gradients (10 A). The chemical shifts are reported in ppm relative to tetramethylsilane or referenced to residual solvent peak and the J values are given in Hz ( $\pm 0.1$  Hz). Standard Bruker pulse sequences were used, and the data was processed on Topspin 3.6 (Bruker) using twofold zero-filling in the indirect dimension. Variable temperature experiments were performed in 1,1,2,2-tetrachloro-ethane- $d_2$  ( $\delta^1\text{H} = 6.00$  ppm) between 368 K and 228 K or in tetrahydrofuran- $d_8$  ( $\delta^1\text{H} = 3.58$  ppm) between 298 K and 168 K. As far as possible, the temperature was calibrated by either a glycerol (high T) or a methanol (low T) sample and showed accuracy within  $\pm 0.2$  K. Compound **1** was characterized at slow exchange conditions (168 K) by  $^1\text{H}$ , cosy, roesy ( $t_{\text{mix}} = 200$  ms) and noesy ( $t_{\text{mix}} = 1$  s) experiments and in fast exchange (368 K) by  $^1\text{H}$ , cosy, noesy ( $t_{\text{mix}} = 1$  s), hsqc and hmbc spectra. The coalescence was quantitatively extracted for the exchanging proton pairs at 5.38 and 7.29 ppm yielding  $T_c$  of 190 K and  $\Delta G^\ddagger$  of  $33.3 \pm 0.5$  kJ mol $^{-1}$  for the p-phenylene ring adjacent to the helicene. For the proximal p-phenylene ring we determined  $T_c$  of 248 K and  $\Delta G^\ddagger$  of  $47.7 \pm 0.5$  kJ mol $^{-1}$  for the protons at 7.36 and 7.69 ppm.

## Synthesis Overview

Scheme S1. Synthesis of 11,15-dibromo[6]helicene **2**.Scheme S2. Synthesis of **1**.

## Synthetic Procedures

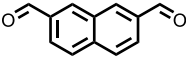
Literature known compound **8** was prepared via a different than published route. Compound **8** was converted to compound **2** via a modified procedure by Fujita<sup>[9]</sup> and bent building **3** was prepared via procedure by Jasti.<sup>[3]</sup>

**Synthesis:** All reactions were performed under Ar atmosphere. Oxygen or water sensitive reactions were performed using Schlenk techniques with anhydrous solvents in glassware, which was dried in an oven at 130 °C for 24 h and cooled down to room temperature under stream of Ar prior to use.

**Organolithium reagent titration:** Phenanthroline (0.1 mg) was dissolved in dry THF (5 mL) and the solution was cooled to 0 °C. Organolithium reagent (2 mL) was added via syringe. Dry propan-2-ol was added dropwise via syringe until color of solution changed from yellow to colorless. The experiment was repeated 3 times.

**H<sub>2</sub>SnCl<sub>4</sub> preparation:** SnCl<sub>2</sub>·2H<sub>2</sub>O (147 mg; 138 μmol) was suspended in THF (5 mL) and 37% aqueous HCl (100 μL) was added and the resulting mixture was stirred for 30 min and used fresh.

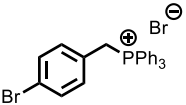
### Naphthalene-2,7-dicarbaldehyde (**6**)

 2,7-Dibromonaphthalene (2.00 g; 6.99 mmol; 1.00 eq.) was dissolved in dry THF (100 mL) and cooled to -78 °C. *n*-BuLi (2.5 M; 7.0 mL; 17.5 mmol; 2.50 eq.) was added dropwise and the reaction was stirred for 1 h at -78 °C. DMF (5.5 mL; 69.9 mmol; 10 eq.) was added and the reaction was stirred and left to warm to room temperature over 16 h. 5% aqueous HCl (50 mL) was added and resulting mixture was stirred for 15 min at room temperature and concentrated on rotavap to 1/3 of the volume. DCM (25 mL) was added. The phases were separated and the aqueous phase was extracted with DCM (3 times 25 mL). The combined organic phases were washed with brine (25 mL) and dried with Na<sub>2</sub>SO<sub>4</sub>. Volatiles were evaporated. The crude product was purified by automated flash silica gel chromatography (50% DCM in cyclohexane). The product was isolated as a white solid (1.03 g; 80%).

<sup>1</sup>H-NMR (400 MHz, CDCl<sub>3</sub>, 298 K, δ/ppm): 10.22 (s, 2H), 8.52 (dt, <sup>4</sup>*J* = 1.5 Hz, <sup>5</sup>*J* = 0.8 Hz, 2H), 8.13 (dd, <sup>3</sup>*J*<sub>HH</sub> = 8.6 Hz, <sup>4</sup>*J*<sub>HH</sub> = 1.5 Hz, 2H), 8.03 (d, <sup>3</sup>*J*<sub>HH</sub> = 8.2 Hz, 2H).

Spectral data matches the literature-reported values.<sup>[10]</sup>

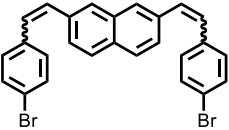
### (4-Bromobenzyl)triphenylphosphonium bromide (**7**)

 A round-bottom flask was charged with 4-bromobenzyl bromide (3.00 g; 12.0 mmol, 1.00 eq.) and triphenylphosphine (4.31 g; 16.4 mmol; 1.37 eq.) and dry DMF (10 mL) was added. The reaction was stirred for 16 h at 80 °C. DMF was removed on rotavap and the residue was suspended in toluene and sonicated for 5 min. The solid was filtered off and washed with toluene and dried in high vacuum. The product was isolated as a white solid (6.03 g; 98%).

<sup>1</sup>H-NMR (400 MHz, CDCl<sub>3</sub>, 298 K, δ/ppm): 7.83-7.74 (m, 9H), 7.69-7.61 (m, 6H), 7.26-7.23 (m, 2H), 7.05 (dd, <sup>3</sup>*J*<sub>HH</sub> = 8.5 Hz, <sup>4</sup>*J*<sub>HH</sub> = 2.6 Hz, 2H), 5.53 (d, <sup>3</sup>*J*<sub>HH</sub> = 14.6 Hz, 2H).

Spectral data matches the literature-reported values.<sup>[11]</sup>

### 2,7-bis(4-Bromostyryl)naphthalene (**8**)

 NaH (60% in oil; 587 mg; 14.7 mmol; 3.00 eq.) was suspended in dry THF (100 mL) and cooled to 0 °C. **7** (5.26 g; 10.3 mmol; 2.11 eq.) was added and the reaction was stirred for 10 min at 0 °C and for 2 h at room temperature. Color of the reaction mixture changed from white to orange. **6** (901 mg; 4.89 mmol; 1.00 eq.) was added and the color of reaction mixture changed from orange back to white. The reaction was stirred for 16 h at room temperature. At

this point, the color of reaction mixture was back to orange. The reaction was quenched with H<sub>2</sub>O (50 mL), concentrated on rotavap to 1/3 of the volume and extracted with DCM (5 times 50 mL). Combined organic phases were washed with brine (50 mL) and dried with Na<sub>2</sub>SO<sub>4</sub>. Volatiles were evaporated. Crude product was purified by automated flash silica gel chromatography (10% DCM in cyclohexane). A mixture of *Z,Z*- and *Z,E*-isomer was isolated as a yellow solid (1.50 g; 63%).

*Z,Z* product:

<sup>1</sup>H-NMR (500 MHz, CDCl<sub>3</sub>, 298 K, δ/ppm): 7.60 (d, <sup>3</sup>J<sub>HH</sub> = 8.5 Hz, 4H), 7.34 (d, <sup>3</sup>J<sub>HH</sub> = 8.5 Hz, 4H), 7.28 (dd, <sup>3</sup>J<sub>HH</sub> = 8.3 Hz, <sup>4</sup>J<sub>HH</sub> = 1.7 Hz, 2H), 7.14 (d, <sup>3</sup>J<sub>HH</sub> = 8.2 Hz, 4H), 6.76 (d, <sup>3</sup>J<sub>HH</sub> = 12.1 Hz, 2H), 6.59 (d, <sup>3</sup>J<sub>HH</sub> = 12.1 Hz, 2H).

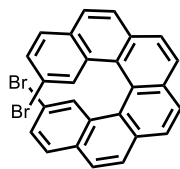
<sup>13</sup>C-NMR (126 MHz, CDCl<sub>3</sub>, 298 K, δ/ppm): 136.07, 134.77, 133.48, 131.81, 131.41, 130.82, 130.61, 129.40, 128.05, 127.47, 126.95, 121.13.

*Z,E* product

<sup>1</sup>H-NMR (500 MHz, CDCl<sub>3</sub>, 298 K, δ/ppm): 7.76 (d, <sup>3</sup>J<sub>HH</sub> = 8.5 Hz, 1H), 7.72 (s, 1H), 7.71 – 7.67 (m, 2H), 7.65 (d, <sup>3</sup>J<sub>HH</sub> = 8.5 Hz, 1H), 7.50 (d, <sup>3</sup>J<sub>HH</sub> = 8.5 Hz, 2H), 7.42 (d, <sup>3</sup>J<sub>HH</sub> = 8.4 Hz, 2H), 7.34 (d, <sup>3</sup>J<sub>HH</sub> = 8.5 Hz, 2H), 7.29 (dd, <sup>3</sup>J<sub>HH</sub> = 8.7 Hz, <sup>4</sup>J<sub>HH</sub> = 1.7 Hz, 1H), 7.25 – 7.12 (m, 4H), 6.78 (d, <sup>3</sup>J<sub>HH</sub> = 12.2 Hz, 1H), 6.60 (d, <sup>3</sup>J<sub>HH</sub> = 12.2 Hz, 1H).

Spectral data matches the literature-reported values.<sup>[9]</sup>

### 11,14-Dibromo[6]helicene (2)

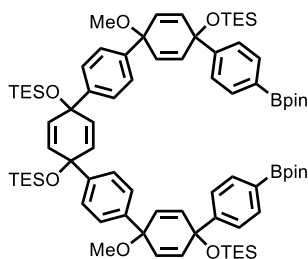


8 (300 mg; 612 μmol; 1.00 eq.) was dissolved in toluene (1.4 L) and iodine (373 mg; 1.47 mmol; 2.40 eq.) was added and the solution was degassed by bubbling with Ar for 45 min. Propylene oxide (21.4 mL; 306 mmol; 500 eq.) was added and degassing was further continued for 15 min. The reaction mixture was irradiated with 150 W medium-pressure mercury lamp for 4.5 h. Volatiles were evaporated. Crude product was purified by column chromatography (DCM). The product was isolated as yellow solid (260 mg; 87%).

<sup>1</sup>H-NMR (400 MHz, CDCl<sub>3</sub>, 298 K, δ/ppm): 8.04 (d, <sup>3</sup>J<sub>HH</sub> = 8.2 Hz, 2H), 8.00 (d, <sup>3</sup>J<sub>HH</sub> = 8.2 Hz, 2H), 7.96 (d, <sup>3</sup>J<sub>HH</sub> = 8.5 Hz, 2H), 7.91 (d, <sup>3</sup>J<sub>HH</sub> = 8.5 Hz, 2H), 7.74 (d, <sup>3</sup>J<sub>HH</sub> = 8.5 Hz, 2H), 7.71 (d, <sup>4</sup>J<sub>HH</sub> = 1.9 Hz, 2H), 7.39 (dd, <sup>3</sup>J<sub>HH</sub> = 8.5 Hz, <sup>4</sup>J<sub>HH</sub> = 2.0 Hz, 2H).

Spectral data matches the literature-reported values.<sup>[9]</sup>

### Compound 4

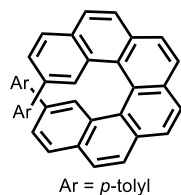


3 (1.61 g; 1.26 mmol; 1.00 eq.) was dissolved in dry THF (30 mL) and the solution was cooled to -78 °C. *n*-BuLi (2.6 M; 1.1 mL; 2.77 mmol; 2.20 eq.) was added dropwise and the reaction was stirred for 1 h at -78 °C, *i*-PrOBpin (0.65 mL; 3.15 mmol; 2.5 eq.) was added and the reaction was stirred and left to warm to room temperature over 16 h. H<sub>2</sub>O (50 mL) and brine (50 mL) were added and the resulting mixture was extracted with EtOAc (3 times 50 mL). The combined organic phases were washed with brine (50 mL) and dried with Na<sub>2</sub>SO<sub>4</sub>. Volatiles were evaporated. The crude product isolated as a white amorphous solid (1.71 g) and used without further purification.

<sup>1</sup>H-NMR (400 MHz, CDCl<sub>3</sub>, 298 K, δ/ppm): 7.70 (d, <sup>3</sup>J<sub>HH</sub> = 8.2 Hz, 4H), 7.33 (d, <sup>3</sup>J<sub>HH</sub> = 8.2 Hz, 4H), 7.33-7.25 (m, 8H), 6.12 (d, <sup>3</sup>J<sub>HH</sub> = 10.2 Hz, 4H), 5.97 (s, 4H), 5.94 (d, <sup>3</sup>J<sub>HH</sub> = 10.2 Hz, 4H), 3.34 (s, 6H), 1.32 (s, 24H), 1.00-0.90 (m, 36H), 0.71-0.55 (m, 24H).

<sup>13</sup>C-NMR (126 MHz, CDCl<sub>3</sub>, 298 K, δ/ppm): 149.08, 145.60, 142.31, 135.37, 134.83, 131.58, 129.27, 126.18, 126.07, 125.14, 83.82, 74.55, 72.13, 71.39, 52.10, 25.00, 7.20, 6.68, 6.61.

HRMS (ESI, +): *m/z* calcd. for C<sub>80</sub>H<sub>118</sub>B<sub>2</sub>NaO<sub>10</sub>Si<sub>4</sub> [M+Na]<sup>+</sup>: 1395.7905, found: 1395.7896; C<sub>80</sub>H<sub>118</sub>B<sub>2</sub>KO<sub>10</sub>Si<sub>4</sub> [M+K]<sup>+</sup>: 1411.7644, found: 1411.7626.

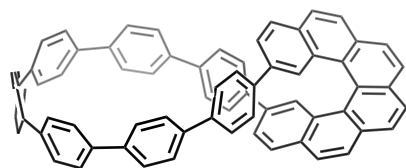
**11,14-Di-*p*-tolyl[6]helicene (5)**

2 (22.0 mg; 45.2  $\mu\text{mol}$ ; 1.00 eq.) and *p*-tolueneboronic acid (12.9 mg; 94.9  $\mu\text{mol}$ ; 2.10 eq.) were weighted in a Schlenk flask and dissolved in dioxane (20 mL) and H<sub>2</sub>O (2 mL). The resulting solution was degassed by bubbling with Ar for 1 h. K<sub>3</sub>PO<sub>4</sub> (76.8 mg; 362  $\mu\text{mol}$ ; 8.00 eq.) and SPhos Pd G3 (3.5 mg; 4.52  $\mu\text{mol}$ ; 0.1 eq.) were added and the degassing was further continued for 20 min. The Schlenk flask was sealed and placed into an oil bath pre-heated to 80 °C. The reaction was stirred for 24 h at 80 °C. The reaction mixture was filtered through celite, the flask and celite were rinsed with DCM and the volatiles were evaporated. The crude product was purified by column chromatography (10% DCM in cyclohexane). The product was isolated as a white solid (15.5 mg; 67%)

<sup>1</sup>H-NMR (400 MHz, CDCl<sub>3</sub>, 298 K,  $\delta$ /ppm): 8.10 (d, <sup>4</sup>*J*<sub>HH</sub> = 1.8 Hz, 2H), 8.04 (d, <sup>3</sup>*J*<sub>HH</sub> = 8.5 Hz, 2H), 7.99 (d, <sup>3</sup>*J*<sub>HH</sub> = 8.0 Hz, 2H), 7.98 (d, <sup>3</sup>*J*<sub>HH</sub> = 8.0 Hz, 2H), 7.97 (d, <sup>3</sup>*J*<sub>HH</sub> = 8.5 Hz, 2H), 7.94 (d, <sup>3</sup>*J*<sub>HH</sub> = 8.2 Hz, 2H), 7.48 (dd, <sup>3</sup>*J*<sub>HH</sub> = 8.2 Hz, <sup>4</sup>*J*<sub>HH</sub> = 1.8 Hz, 2H), 6.98 (d, <sup>3</sup>*J*<sub>HH</sub> = 7.8 Hz, 4H), 6.66 (d, <sup>3</sup>*J*<sub>HH</sub> = 7.8 Hz, 4H), 2.28 (s, 6H).

<sup>13</sup>C-NMR (126 MHz, CDCl<sub>3</sub>, 298 K,  $\delta$ /ppm): 138.20, 138.11, 136.53, 133.29, 131.83, 131.36, 130.05, 128.83, 128.38, 127.99, 127.42, 127.31, 127.15, 127.13, 126.60, 126.46, 125.50, 124.21, 20.96.

HRMS (ESI, +): *m/z* calcd. for C<sub>40</sub>H<sub>28</sub>Ag [M+Ag]<sup>+</sup>: 615.1236, found: 615.1253.

**[6]Helicene nanohoop (1)**

2 (50.0 mg; 103  $\mu\text{mol}$ ; 1.00 eq.) and 4 (156 mg; 113  $\mu\text{mol}$ ; 1.10 eq.) were weighted in a Schlenk flask and dissolved in dioxane (100 mL) and H<sub>2</sub>O (10 mL). The resulting solution was degassed by bubbling with Ar for 1 h. K<sub>3</sub>PO<sub>4</sub> (175 mg; 824  $\mu\text{mol}$ ; 8.00 eq.) and SPhos Pd G3 (16.1 mg; 20.6  $\mu\text{mol}$ ; 0.2 eq.) were added and the degassing was further continued for 30 min. The Schlenk flask was sealed and placed into an oil bath pre-heated to 80 °C. The reaction was stirred for 16 h at 80 °C. The reaction mixture was filtered through celite, the flask and celite were rinsed with DCM and the volatiles were evaporated and crude product dried in high vacuum. The residue was dissolved in dry THF (2.5 mL) and TBAF (1 M in THF; 0.62 mL; 618  $\mu\text{mol}$ ; 6.00 eq.) was added and the reaction was stirred for 1 h at room temperature and quenched with H<sub>2</sub>O (5 mL). The resulting mixture was concentrated on rotavap (40 °C; 160 mbar). Formed precipitate was filtered off, washed with DCM (2 times 5 mL) and dried in high vacuum. The residue was dissolved in THF (10 mL) and H<sub>2</sub>SnCl<sub>4</sub> (127 mM in THF; 2.8 mL; 356  $\mu\text{mol}$ ; 3.45 eq.) was added. The reaction was stirred for 1 h at room temperature and quenched with 10% aqueous NaOH (2.5 mL). The resulting mixture was diluted with H<sub>2</sub>O (25 mL) and extracted with DCM (6 times 25 mL). The combined organic phases were washed with brine (25 mL) and dried with Na<sub>2</sub>SO<sub>4</sub>. Volatiles were evaporated. The crude product was purified by column chromatography (50% toluene in *n*-heptane). The product was isolated as yellow solid (18.4 mg; 21%).

<sup>1</sup>H-NMR (600 MHz, TCE-d<sub>2</sub>, 368 K,  $\delta$ /ppm): 8.25 (s, 2H), 8.11-8.07 (m, 10H), 7.57-7.50 (m, 16H), 7.49 (d, <sup>3</sup>*J*<sub>HH</sub> = 8.4 Hz, 4H), 7.37 (d, <sup>3</sup>*J*<sub>HH</sub> = 8.4 Hz, 4H), 7.21 (dd, <sup>3</sup>*J*<sub>HH</sub> = 8.3 Hz, <sup>4</sup>*J*<sub>HH</sub> = 1.4 Hz, 2H), 6.42 (d, <sup>3</sup>*J*<sub>HH</sub> = 8.4 Hz, 4H).

See section NMR spectra for assignment of the chemical shifts (in particular Figures S47 and S53).

HRMS (ESI, +): *m/z* calcd. for C<sub>68</sub>H<sub>42</sub>Ag [M+Ag]<sup>+</sup>: 965.2332, found: 965.2330.



## X-ray analysis

Single crystals were grown from chlorobenzene solution of racemic **1** (~1.5 mmol/L) by layering with methanol in an NMR tube under argon at room temperature. The grown crystals had an appearance of yellow needles. A suitable crystal with dimensions  $0.37 \times 0.23 \times 0.13 \text{ mm}^3$  was selected and mounted on a mylar loop in perfluoroether oil on a STOE STADIVARI Cu diffractometer. The crystal was kept at a steady  $T = 150 \text{ K}$  during data collection. The structure was solved with the **ShelXT** 2018/2 solution program<sup>[12]</sup> using dual methods and by using **Olex2** 1.3 as the graphical interface<sup>[13]</sup>. The model was refined with **ShelXL** 2018/3<sup>[14]</sup> using full matrix least squares minimisation on  $F^2$ .

**Crystal Data.**  $\text{C}_{71.3}\text{H}_{44.75}\text{Cl}_{0.55}$ ,  $M_r = 920.92$ , monoclinic,  $P2_1/n$  (No. 14),  $a = 18.1064(5) \text{ \AA}$ ,  $b = 12.6406(2) \text{ \AA}$ ,  $c = 23.3714(6) \text{ \AA}$ ,  $\beta = 104.885(2)^\circ$ ,  $\alpha = \gamma = 90^\circ$ ,  $V = 5169.6(2) \text{ \AA}^3$ ,  $T = 150 \text{ K}$ ,  $Z = 4$ ,  $Z' = 1$ ,  $m(\text{Cu K}\alpha) = 0.764$ , 44419 reflections measured, 9660 unique ( $R_{\text{int}} = 0.0743$ ) which were used in all calculations. The final  $wR_2$  was 0.2743 (all data) and  $R_I$  was 0.1170 ( $I \geq 2 \sigma(I)$ ).

Crystal data has been deposited to the Cambridge Crystallographic Database with CCDC number 2178271 containing the supplementary crystallographic data for this paper. These data can be obtained free of charge from The Cambridge Crystallographic Data Centre.

## HPLC Separations

Enantiomers of **1** (4 mg in 5 mL of eluent) and **5** (8 mg in 5 mL of eluent) were separated using HPLC with chiral stationary phase (Chiralpak IG column 250x30 mm, particle size 5  $\mu\text{m}$ , 15 mL min<sup>-1</sup>, DCM/*n*-heptane (1:1)).

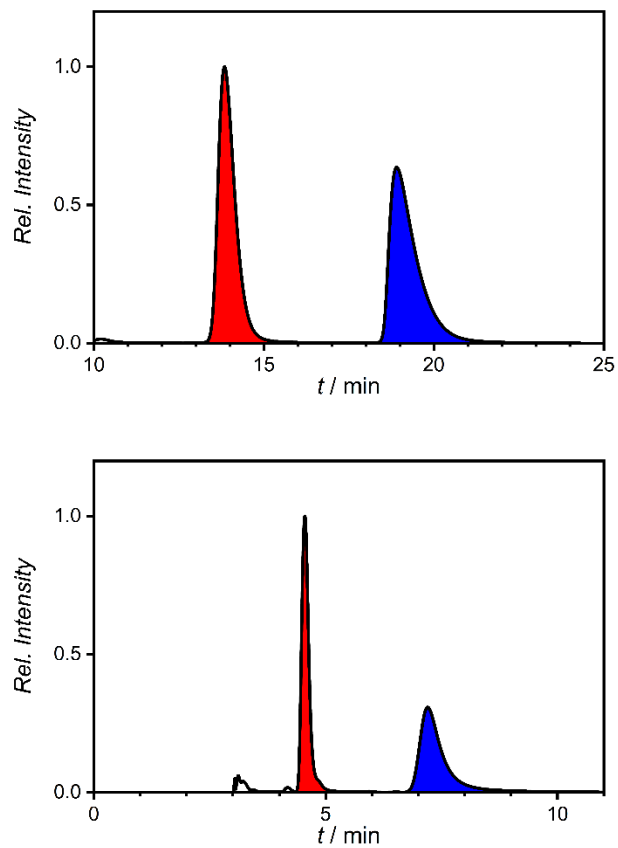


**Figure S1.** HPLC chromatogram of **1** (top) and **5** (bottom) with (*M*)-enantiomers (red) eluting first followed by (*P*)-enantiomers (blue).

## Optical Properties

We investigated the photophysical properties of **1** and **5**. Quantum yield of **1** in  $\text{CH}_2\text{Cl}_2$  was determined to be 58.74% and 64.52% respectively before and after degassing (excitation at 339 nm, observed emission at 490 nm).

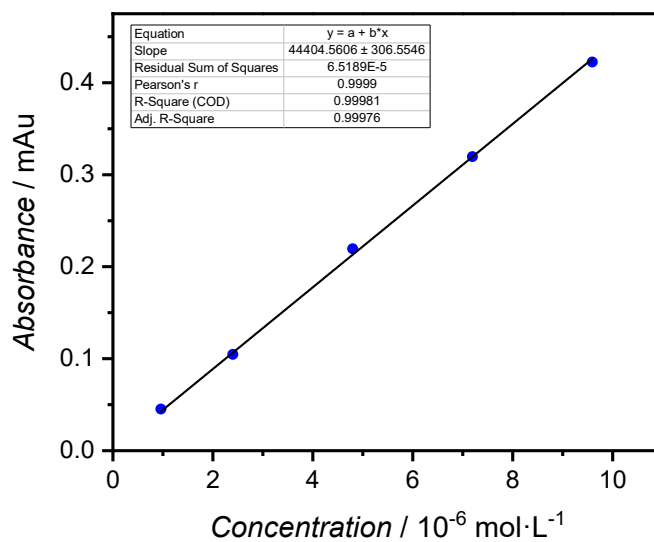


**Figure S2.** Graph of absorbance as a function of concentration of **1** in  $\text{CH}_2\text{Cl}_2$ .

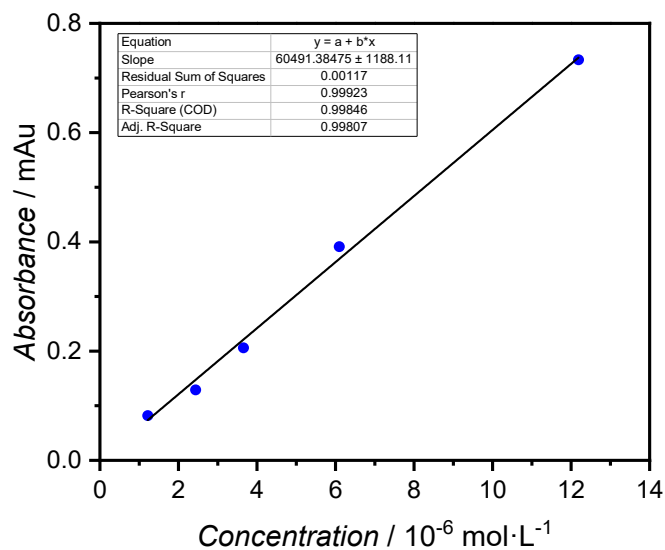


**Figure S3.** Graph of absorbance as a function of concentration of **5** in  $\text{CH}_2\text{Cl}_2$ .

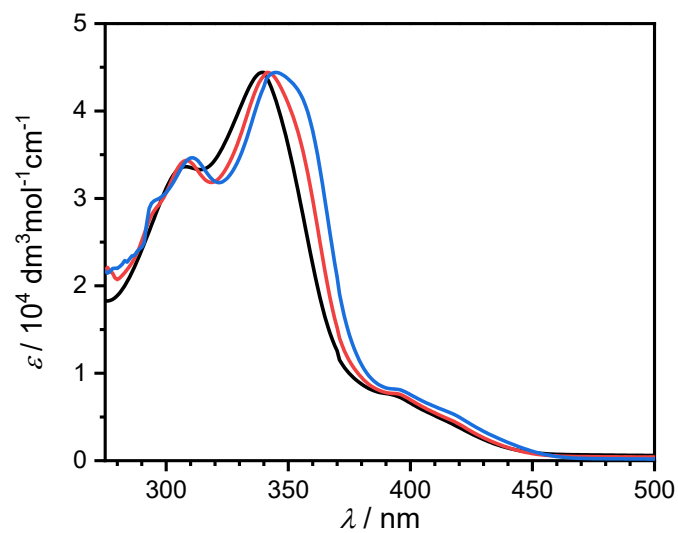


**Figure S4.** Absorption spectra of **1** in CH<sub>2</sub>Cl<sub>2</sub> (black), toluene (red) and benzonitrile (blue).

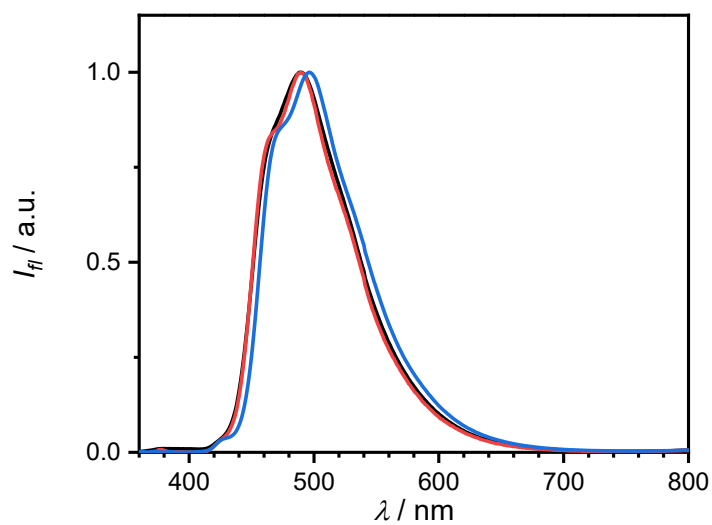


**Figure S5.** Emission spectra of **1** with excitation at 338 nm in CH<sub>2</sub>Cl<sub>2</sub> (black), toluene (red) and benzonitrile (blue).

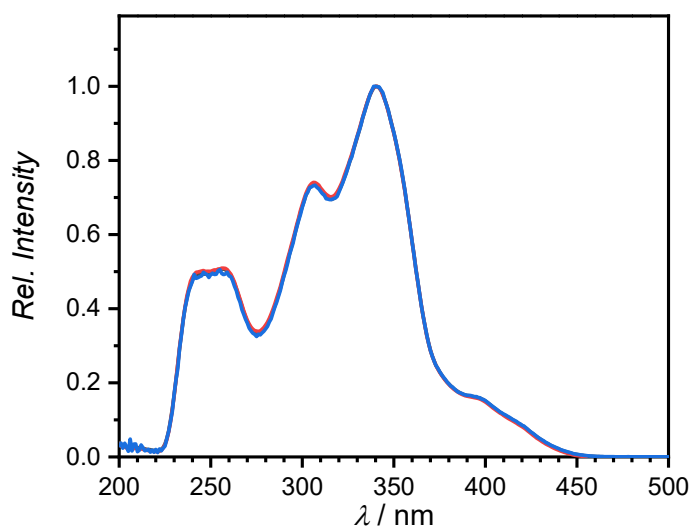


**Figure S6.** Normalized excitation spectra of **1** with observed emissions at 495 nm (black), 465 nm (red) and 600 nm (blue) in CH<sub>2</sub>Cl<sub>2</sub>.

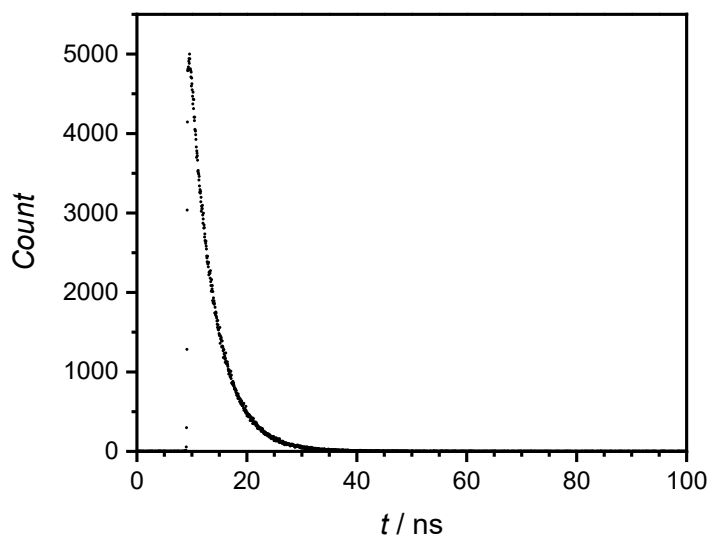


**Figure S7.** Lifetime measurement of **1**, excitation at 405 nm and detection at 490 nm in CH<sub>2</sub>Cl<sub>2</sub>.

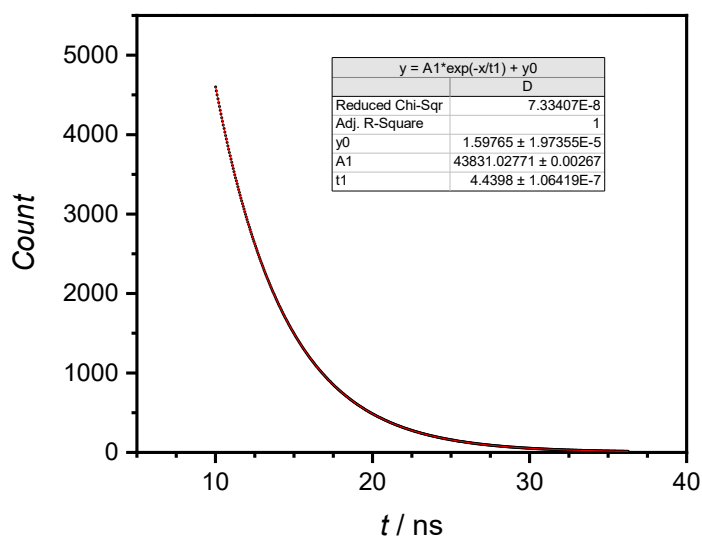


**Figure S8.** Lifetime measurement of **1** in  $\text{CH}_2\text{Cl}_2$ , excitation at 405 nm and detection at 490 nm with a fitted curve.

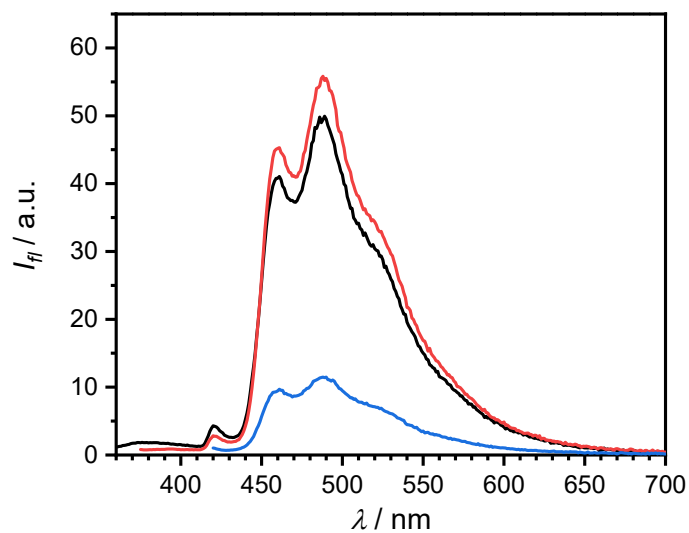


**Figure S9.** Fluorescence spectra of **1** in 2-MeTHF at 77 K with excitation at 339 nm (black), 355 nm (red) and 405 nm (blue). Peak at 420 nm is a scattering artifact.

## Circularly Polarized Luminescence

### 11,14-Di-*p*-tolyl[6]helicene (**5**)

The spectra were recorded at ca.  $2.25 \times 10^{-5}$  M (for *P* and *M*) and were investigated in dichloromethane. For CPL measurements, a fixed wavelength of 355 nm (for *M*) and 345 nm (for *P*) provided by a Lamp source and 1.0 s of integration time were selected, the CPL calculated is an average spectra calculated after 100 scans.

### [6]Helicene nanohoop (**1**)

The spectra were recorded at ca.  $2.25 \times 10^{-5}$  M (for *M*) and ca.  $3.18 \times 10^{-5}$  M (for *P*) and were investigated in dichloromethane. For CPL measurements, a fixed wavelength of 370 nm (for *M* and *P*) provided by a Lamp source and 1.0 s of integration time were selected, the CPL calculated is an average spectra calculated after 100 scans.

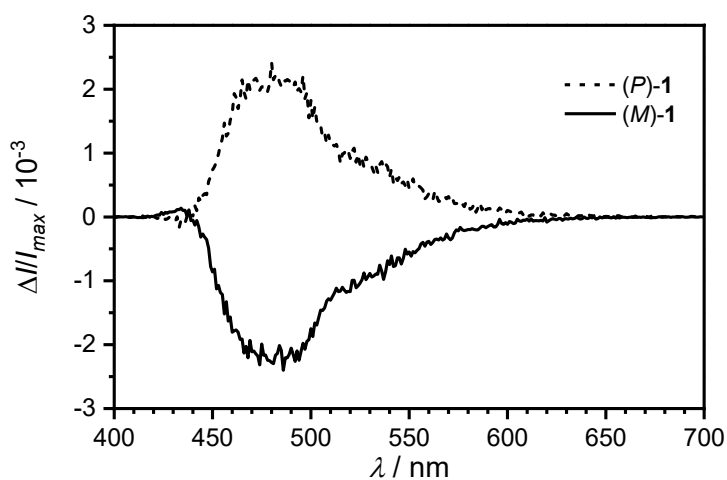


**Figure S10.** Circularly polarized luminescence spectra of **1** in  $\text{CH}_2\text{Cl}_2$  ( $\lambda_{exc} = 370$  nm).

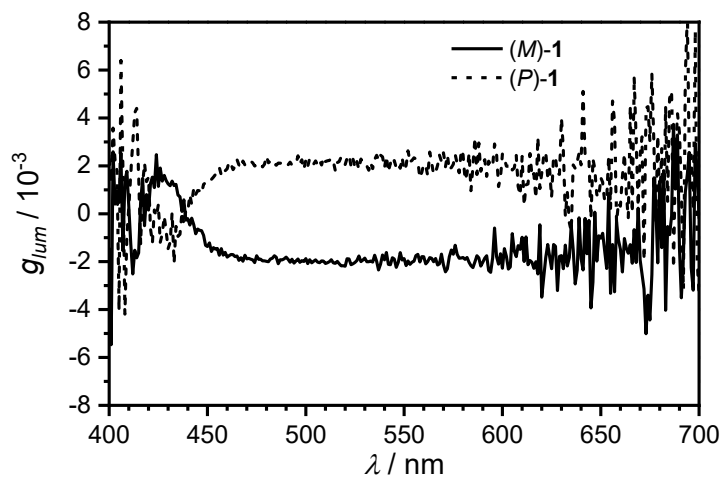


**Figure S11.** Dissymmetry factor plot of circularly polarized luminescence spectra of **1** in  $\text{CH}_2\text{Cl}_2$  ( $\lambda_{exc} = 370$  nm).

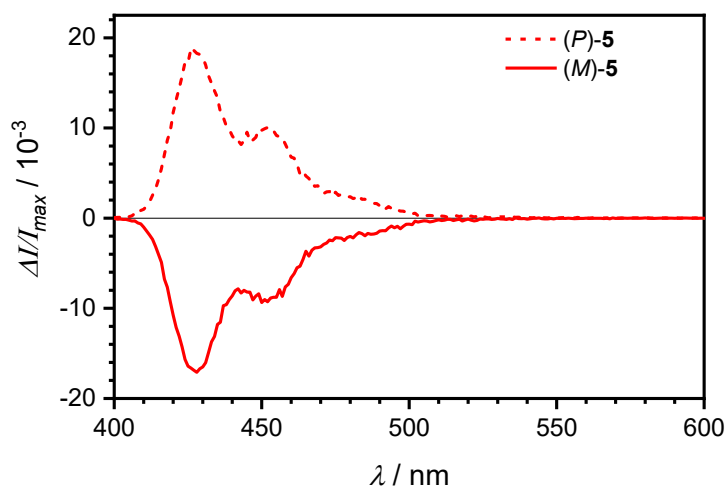


**Figure S12.** Circularly polarized luminescence spectra of **5** in  $\text{CH}_2\text{Cl}_2$  ( $\lambda_{exc} = 370$  nm).



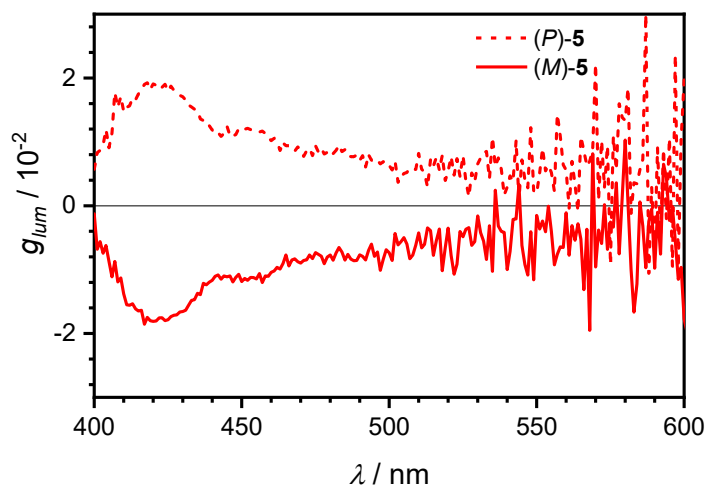


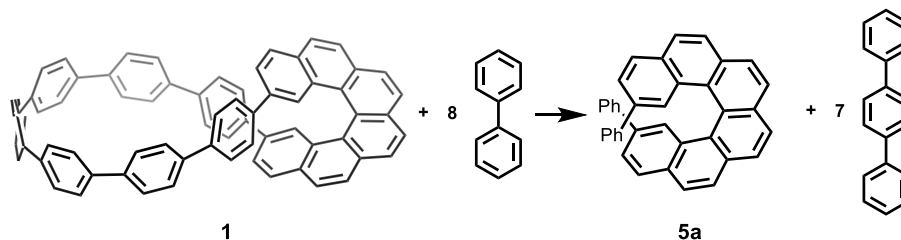
**Figure S13.** Dissymmetry factor plot of circularly polarized luminescence spectra of **5** in  $\text{CH}_2\text{Cl}_2$  ( $\lambda_{exc} = 370$  nm).

### A.2.2. DFT Calculations

Calculations were performed with Gaussian 09<sup>[7]</sup> (release D.01) suite of electronic structure programs. The geometries of the potential energy minima or transition states were optimized at D3-B3LYP/6-31G(d) level of theory. The nature of the stationary points was confirmed by a subsequent frequency calculation. UltraFine integration grid was used in all calculations. The nature of the transition states was verified by following the IRC path to connect the respective energy minima. Due to low force constants of the reaction coordinate, the IRC paths did not converge to the corresponding energy minima. Therefore, the last point of the IRC path was optimized calculating the full Hessian matrix in each optimization step to make sure that the optimization converged to the correct energy minimum. The single point energies were then calculated with a number of DFT functionals using cc-pVTZ basis set. NMR chemical shifts (referenced to TMS) and NICS values were calculated using GIAO at B3LYP/6-31G(d)/gas phase level of theory.

### Strain Calculations

Strain energy was estimated via a homodesmotic reaction (Scheme S3). Single point energies were calculated on D3-B3LYP/cc-pVTZ level of theory and corrected by unscaled zero-point vibrational energy (ZPVE) correction from D3-B3LYP/6-31G(d). Strain energy was estimated to be 55.4 kcal mol<sup>-1</sup>.



**Scheme S3.** Homodesmotic reaction used for total strain energy calculation.

**Table S1.** Thermochemistry of the homodesmotic reaction shown in Scheme S3.

Compound	ZPVE / Hartree	$E_{el}$ / Hartree	$E_{corr}^a$ / Hartree	$E_{corr}^a$ / kcal mol <sup>-1</sup>
<b>1-B<sub>Möbius</sub></b>	0.882079	-2617.539105	-2616.657026	-1641977.142
<b>5a</b>	0.497848	-1463.106891	-1462.609043	-917801.0695
<b>biphenyl</b>	0.182137	-463.4811803	-463.2990433	-290724.551
<b>terphenyl</b>	0.263352	-694.624577	-694.361225	-435718.2651

<sup>a</sup> Energies (0K,  $E_{el}$  + ZPVE) obtained with the cc-pVTZ basis set on D3-B3LYP/6-31G(d) geometries. Zero-point vibrational energy (ZPVE) correction is unscaled.

Additionally, we calculated strain energy using program StrainViz, recently developed by Jasti group.<sup>[15]</sup> 8 fragments were produced from D3-B3LYP/6-31G(d) optimized geometry of (*P*)-**1** in **B<sub>Möbius</sub>** conformation and used as an input for StrainViz. We obtained a total strain of 55.6 kcal mol<sup>-1</sup>, which is comparable to strain obtained via homodesmotic reaction.

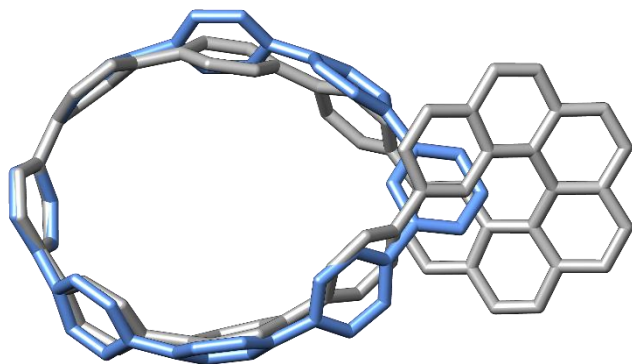


**Figure S14.** Overlay of the optimized structures of (*P*)-**1** in  $B_{\text{Möbius}}$  conformation (grey) and *m*[8]CPP (blue).

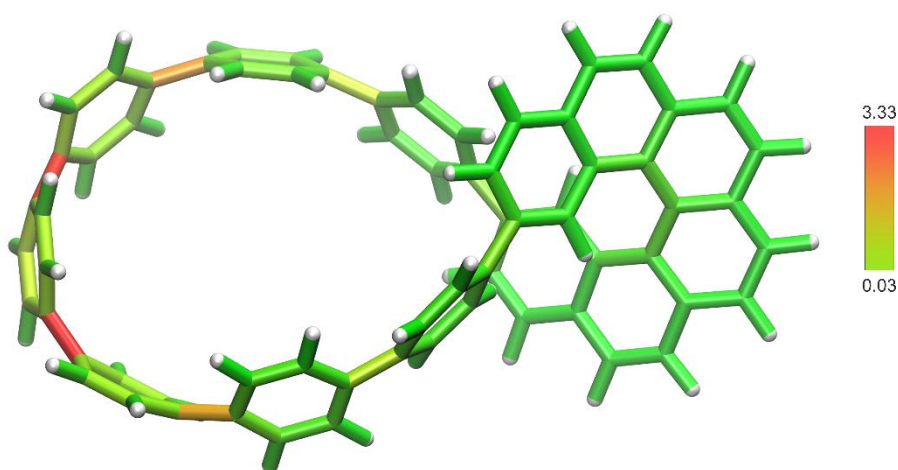


**Figure S15.** Total strain visualization of **1** in  $B_{\text{Möbius}}$  conformation by StrainViz. Green = 0.03 kcal mol<sup>-1</sup>, red = 3.33 kcal mol<sup>-1</sup>.

**Table S2.** DFT-calculated activation energies of enantiomerization of **1** and [6]helicene.

Compound	Energy <sup>a</sup> / kcal mol <sup>-1</sup>					
	B3LYP	BMK	M06-2X	M06L	B97D	PBE0
<b>1</b>	39.6	43.5	41.3	38.8	37.4	39.6
[6]helicene	36.5	37.8	37.9	37.0	35.0	36.7

<sup>a</sup> Energies (0K,  $E_{el}$  + ZPVE) obtained with the cc-pVTZ basis set on D3-B3LYP/6-31G(d) geometries. Zero-point vibrational energy (ZPVE) correction is unscaled.

**Table S3.** DFT-calculated energies of different conformers<sup>a</sup> of **1** and the transition states that interconvert them.

Conformer / transition state	Relative Energy <sup>b</sup> / kcal mol <sup>-1</sup>					
	B3LYP	BMK	M06-2X	M06L	B97D	PBE0
<b>A</b> <sub>Möbius</sub>	0.0	0.0	0.0	0.0	0.0	0.0
<b>B</b> <sub>Möbius</sub>	0.1	-0.2	0.1	-1.0	-0.5	0.1
<b>C</b> <sub>Hückel</sub>	5.3	5.8	5.5	3.8	4.6	5.3
<b>D</b> <sub>Hückel</sub>	5.0	6.6	5.3	5.2	5.4	5.1
<b>TS</b> <sup>c</sup> [ <b>A</b> → <b>A</b> ]	5.9	7.8	6.0	6.5	6.5	5.7
<b>TS</b> [ <b>A</b> → <b>B</b> ]	1.5	1.8	1.7	0.8	1.6	1.5
<b>TS</b> [ <b>A</b> → <b>C</b> ]	6.7	7.3	7.0	5.4	6.4	6.9
<b>TS</b> [ <b>B</b> → <b>D</b> ]	5.1	6.8	5.4	5.0	5.6	5.2

<sup>a</sup> Structures of the individual conformers and transition states are in Figure S16. <sup>b</sup> Energies (0K,  $E_{el}$  + ZPVE) with relative to conformer **A** obtained with the cc-pVTZ basis set on D3-B3LYP/6-31G(d) geometries. Zero-point vibrational energy (ZPVE) correction is unscaled. <sup>c</sup> Transition state of full phenyl **A** (see Table 1 in the manuscript and Figure S16) rotation resulting in the proton exchange as observed in the VT <sup>1</sup>H NMR experiments (see Figure 2 in the manuscript and Figure S59).

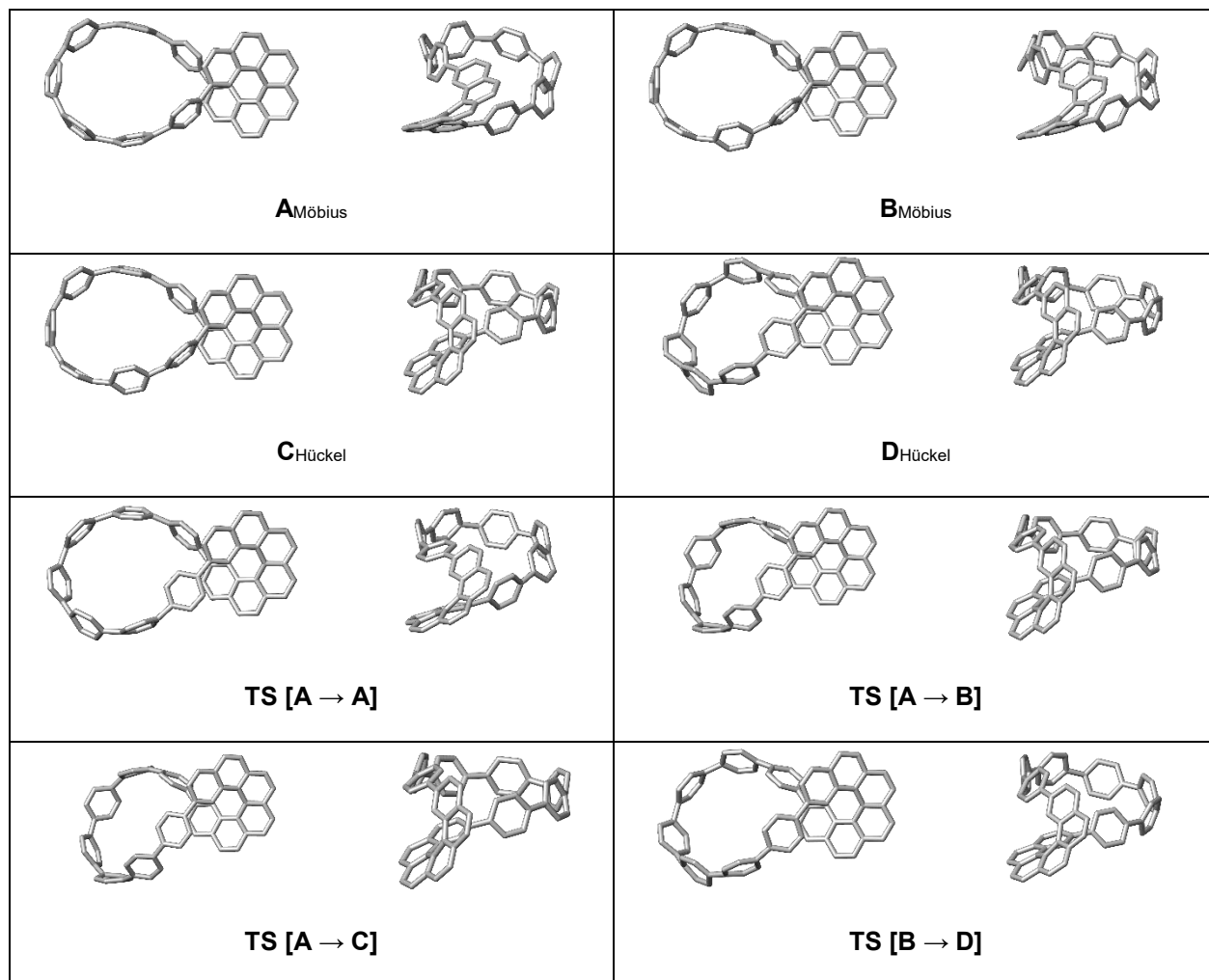


**Figure S16.** Structures of the individual conformers and transition states in **1** that interconvert them.

## Frontier Molecular Orbitals

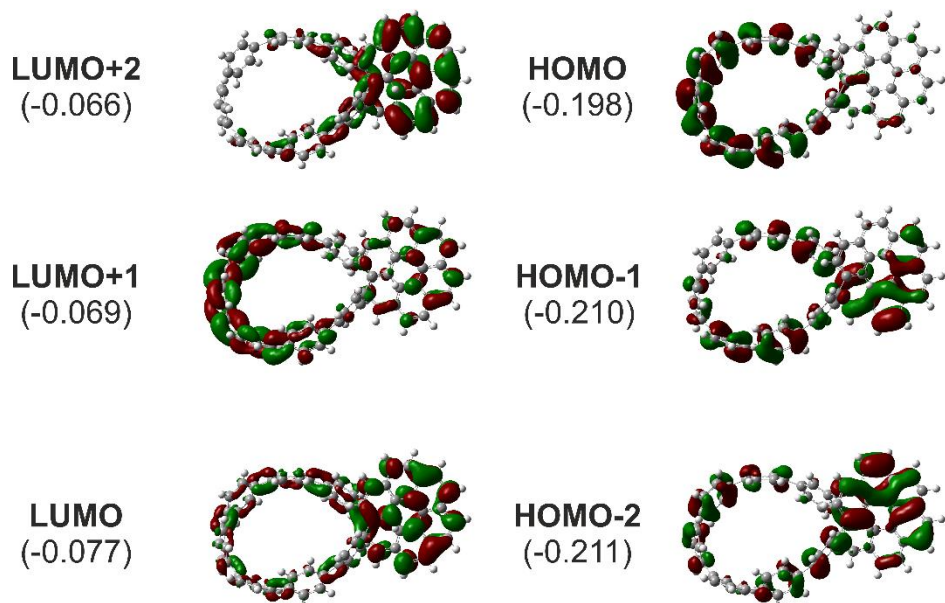


**Figure S17.** Frontier molecular (canonical) orbitals of **1** in  $B_{\text{Möbius}}$  conformation (see Figure S16) with their energies in eV in brackets calculated at D3-B3LYP/6-31G(d) level of theory.

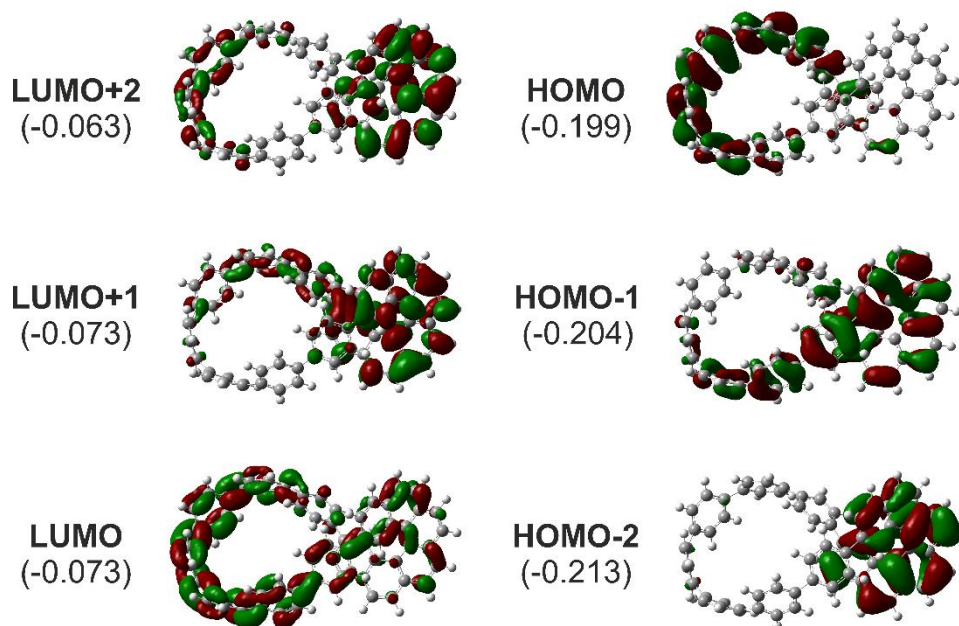


**Figure S18.** Frontier molecular (canonical) orbitals of **1** in  $C_{\text{Hückel}}$  conformation (see Figure S16) with their energies in eV in brackets calculated at D3-B3LYP/6-31G(d) level of theory.

## Natural Transition Orbitals

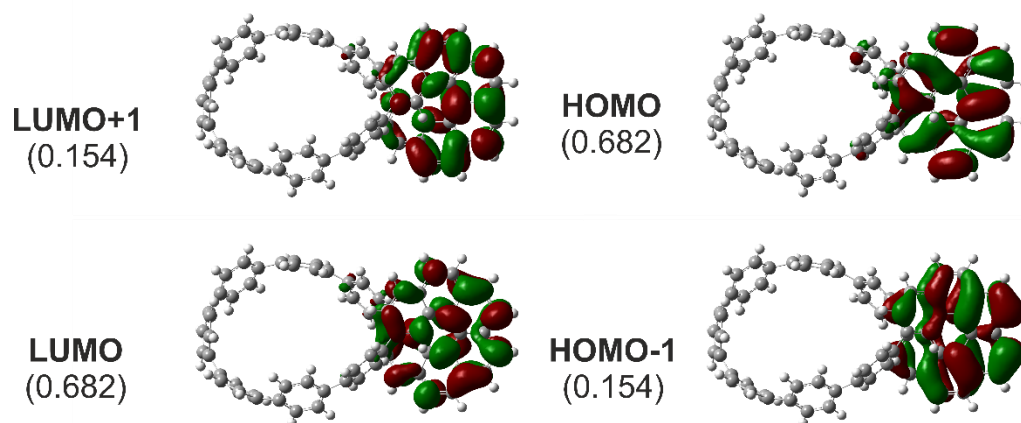


**Figure S19.** NTO of the  $S_0 \rightarrow S_1$  transition ( $E = 3.48$  eV,  $f = 0.098$ ) of **1** in  $\mathbf{B}_{\text{Möbius}}$  conformation (see Figure S16) with their occupancies in brackets calculated at TD-CAM-B3LYP/6-31G(d) level of theory.

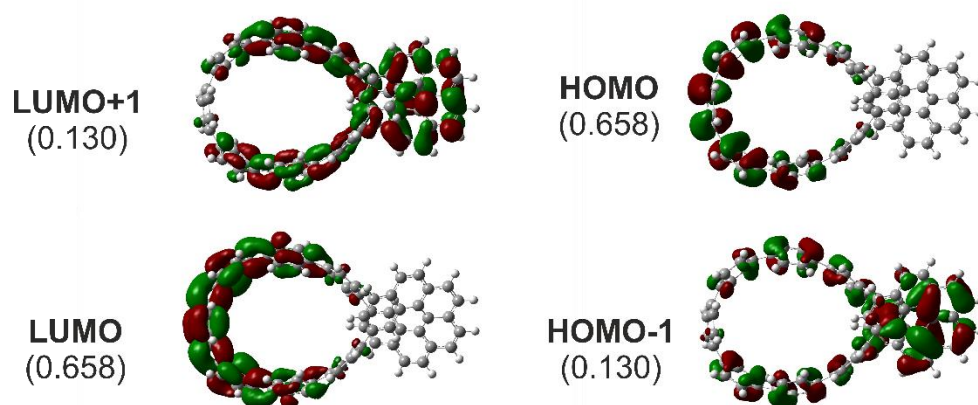


**Figure S20.** NTO of the  $S_0 \rightarrow S_2$  transition ( $E = 3.56$  eV,  $f = 0.152$ ) of **1** in  $\mathbf{B}_{\text{Möbius}}$  conformation (see Figure S16) with their occupancies in brackets calculated at TD-CAM-B3LYP/6-31G(d) level of theory.

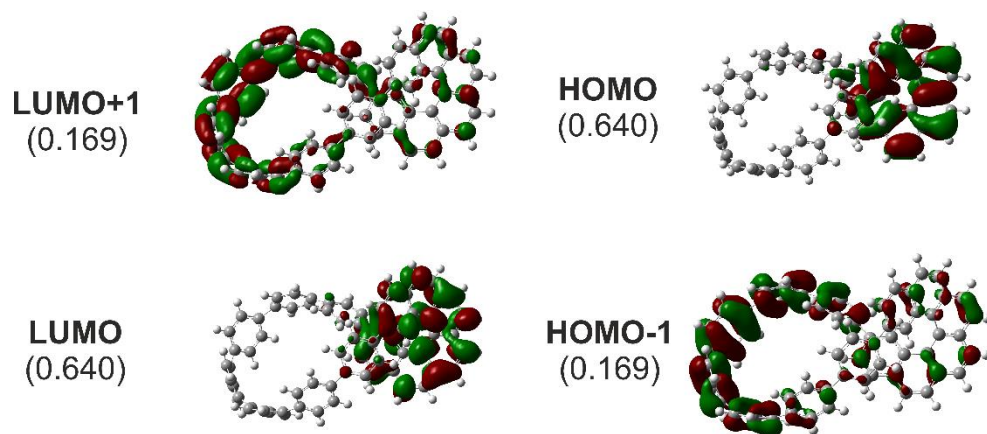


**Figure S21.** NTO of the  $S_0 \rightarrow S_1$  transition ( $E = 3.48$  eV,  $f = 0.054$ ) of **1** in  $C_{\text{Hückel}}$  conformation (see Figure S16) with their occupancies in brackets calculated at TD-CAM-B3LYP/6-31G(d) level of theory.

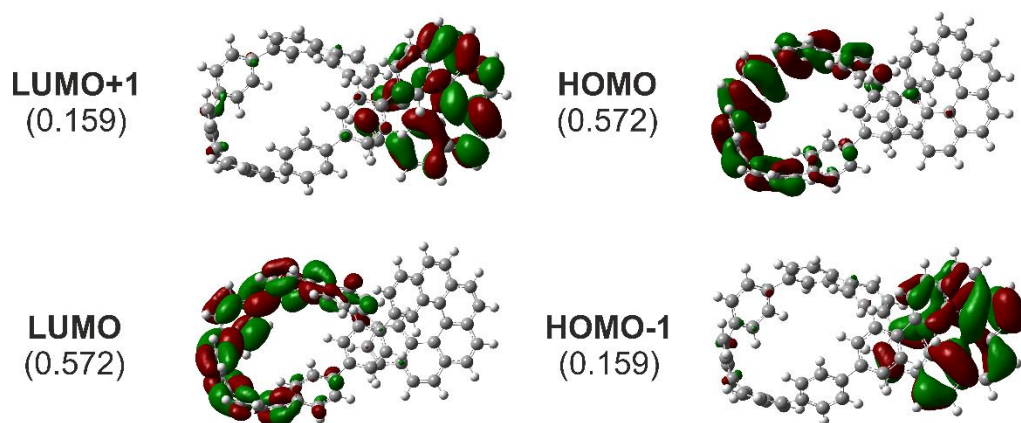


**Figure S22.** NTO of the  $S_0 \rightarrow S_2$  transition ( $E = 3.57$  eV,  $f = 0.152$ ) of **1** in  $C_{\text{Hückel}}$  conformation (see Figure S16) with their occupancies in brackets calculated at TD-CAM-B3LYP/6-31G(d) level of theory.



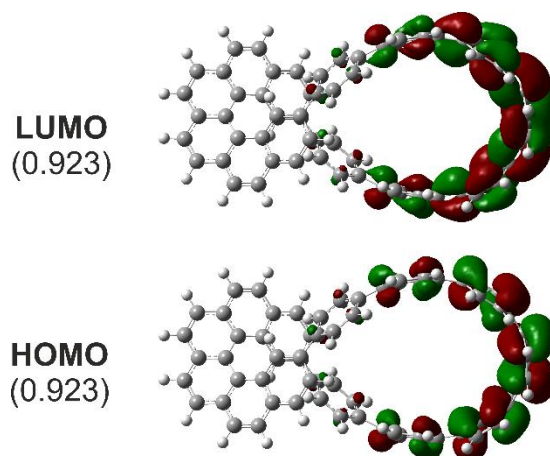


**Figure S23.** NTO of the  $S_0 \rightarrow S_1$  transition ( $E = 2.65$  eV,  $f = 0.466$ ) of the optimized 1<sup>st</sup> excited state geometry reached from **1** in  $\mathbf{B}_{\text{Möbius}}$  conformation with their occupancies in brackets calculated at TD-CAM-B3LYP/6-31G(d) level of theory.

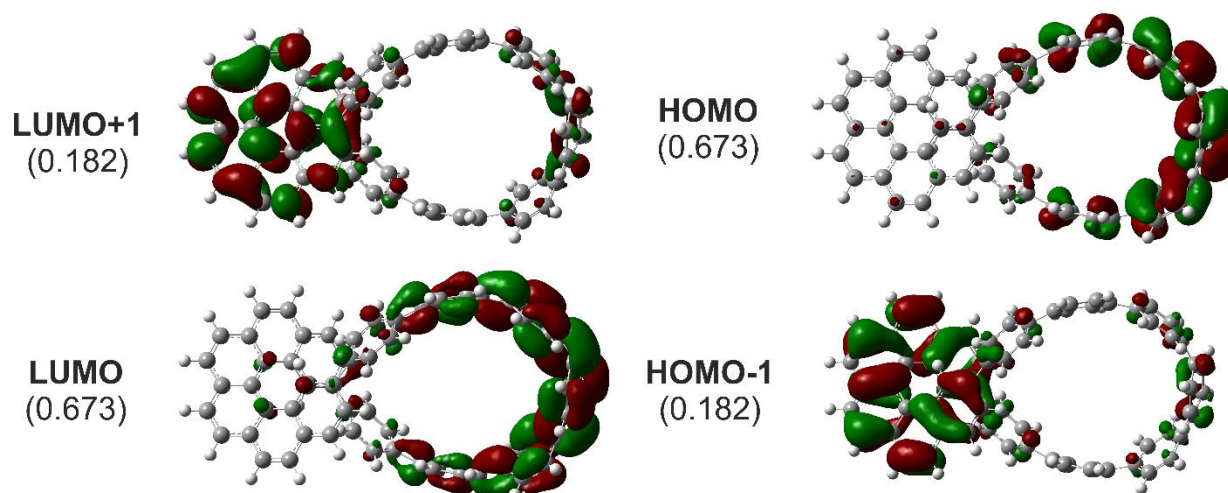


**Figure S24.** NTO of the  $S_0 \rightarrow S_1$  transition ( $E = 3.32$  eV,  $f = 0.215$ ) of the optimized 2<sup>nd</sup> excited state geometry reached from **1** in  $\mathbf{B}_{\text{Möbius}}$  conformation with their occupancies in brackets calculated at TD-CAM-B3LYP/6-31G(d) level of theory.

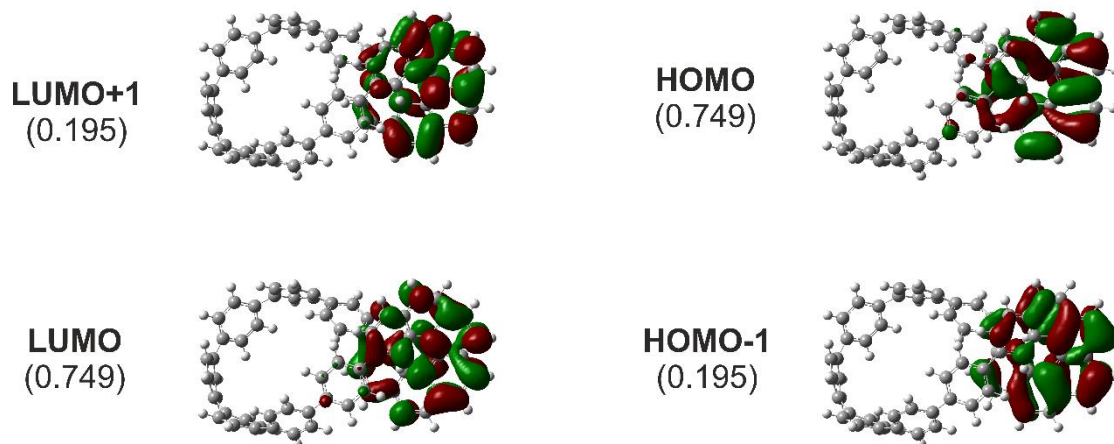


**Figure S25.** NTO of the  $S_0 \rightarrow S_1$  transition ( $E = 3.30$  eV,  $f = 0.029$ ) of the optimized 1<sup>st</sup> excited state geometry reached from **1** in  $C_{\text{Hückel}}$  conformation with their occupancies in brackets calculated at TD-CAM-B3LYP/6-31G(d) level of theory.

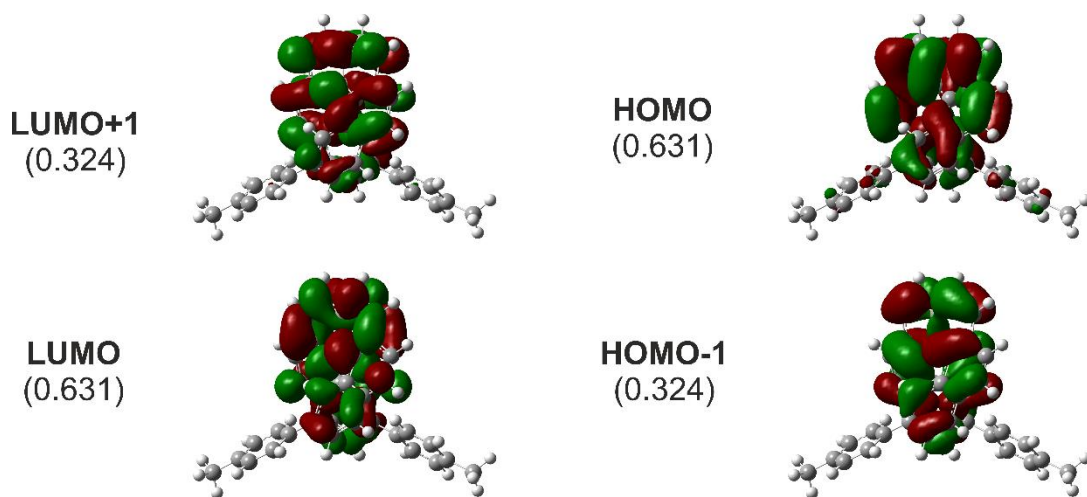


**Figure S26.** NTO of the  $S_0 \rightarrow S_1$  transition ( $E = 3.32$  eV,  $f = 0.0102$ ) of the optimized 1<sup>st</sup> excited state geometry of **5** with their occupancies in brackets calculated at TD-CAM-B3LYP/6-31G(d) level of theory.

## CD Spectra

The absolute configurations of respective enantiomers of **1** and **5** were assigned by comparison of the calculated and measured CD spectra.  $\mathbf{B}_{\text{Möbius}}$  conformation of **1** was used. The spectra were obtained using TD-CAM-B3LYP method with 6-31G(d) basis set calculating first 75 singlet excitations. Solvent effects were simulated using PCM model. The ECD spectra were compared using SpecDis (release 1.71).<sup>[16]</sup> Empirical vibrational broadening of 0.2 eV was used and the calculated spectra were shifted by  $-0.3$  eV. The velocity form of the rotatory strength was used. A good agreement of experimental and calculated data was observed.

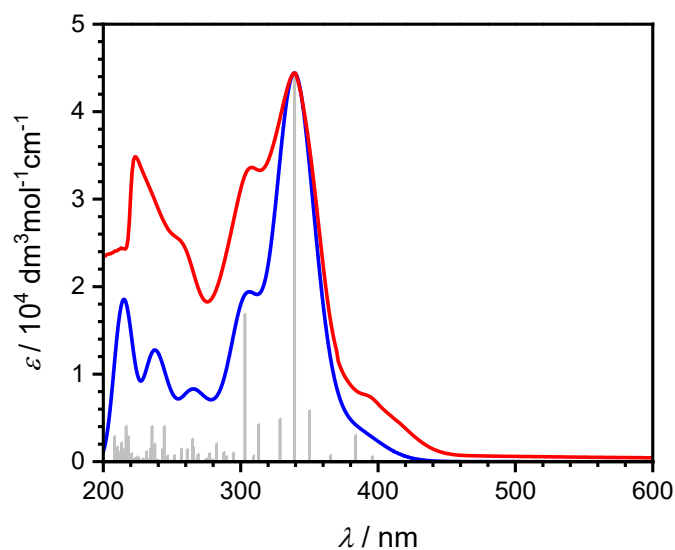


**Figure S27.** Experimental (red) and calculated (blue) UV-Vis spectra of **1** with excitation transitions (grey lines) in DCM.

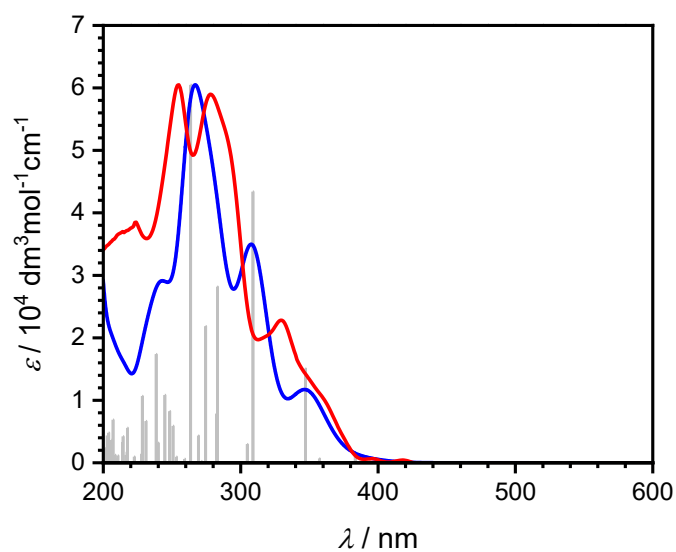


**Figure S28.** Experimental (red) and calculated (blue) UV-Vis spectra of **5** with excitation transitions (grey lines) in DCM.

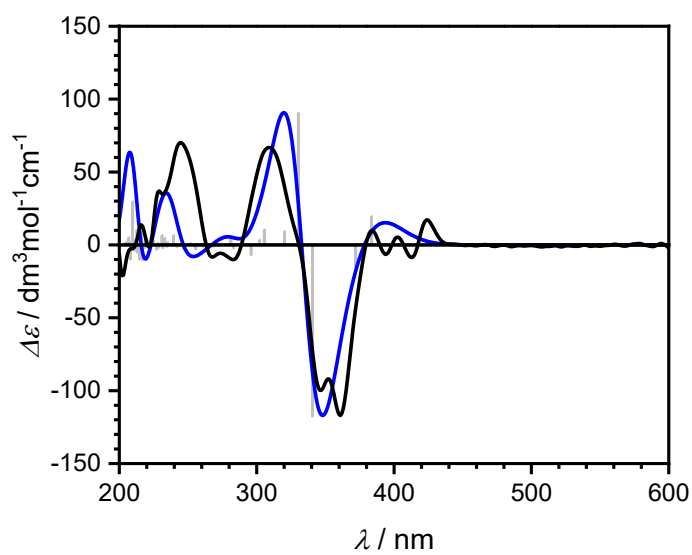


**Figure S29.** Experimental (black) and calculated (blue) CD spectra of (*M*)-**1** with excitation transitions (grey lines) in DCM.

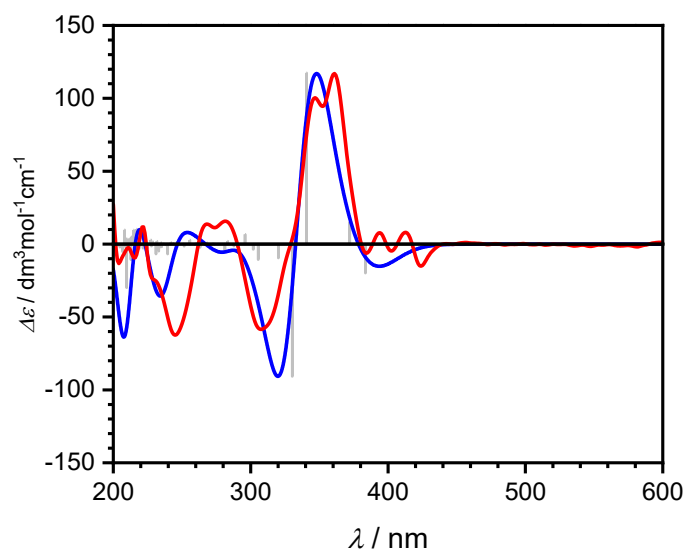


**Figure S30.** Experimental (red) and calculated (blue) CD spectra of (*P*)-**1** with excitation transitions (grey lines) in DCM.

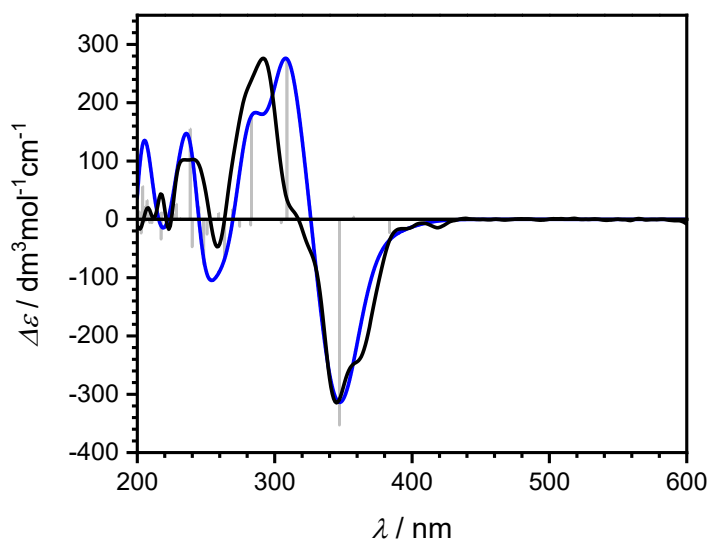


**Figure S31.** Experimental (black) and calculated (blue) CD spectra of (*M*)-**5** with excitation transitions (grey lines) in DCM.

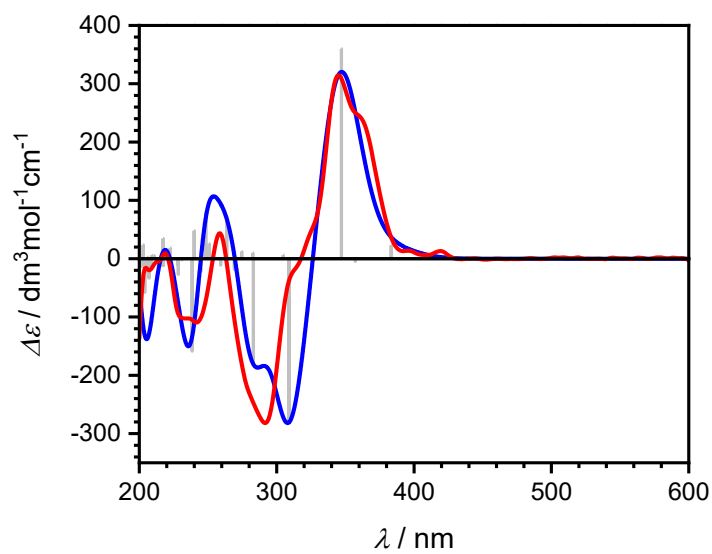


**Figure S32.** Experimental (red) and calculated (blue) CD spectra of (*P*)-**5** with excitation transitions (grey lines) in DCM.

### Dissymmetry Factors Calculation

Electric and magnetic transition dipole moment vectors were extracted from a TD-DFT calculation run on geometries of ground, 1st excited and 2nd excited states. Excited state geometries were optimized at CAM-B3LYP/6-31g\* level of theory. Compound H6(H)<sub>2</sub> was previously studied by Favereau *et al.*<sup>[17]</sup>

**Table S4.** Calculated electric ( $\mu$ ) and magnetic ( $m$ ) transition dipole moments for ground state geometries ( $\mathbf{B}_{\text{Möbius}}$ , and  $\mathbf{C}_{\text{Hückel}}$  conformations in **1**; see Figure S16), rotatory strengths ( $R$ , velocity form), dipole strengths ( $D$ ) and calculated dissymmetry factor ( $g_{\text{abs}}$ ) values.

Compound (Transition)	$E / \text{eV}$	$f$	$ \mu  / 10^{-19}$ esu·cm	$ m  / 10^{-21}$ erg·G <sup>-1</sup>	$\theta / ^\circ$	$R / 10^{-40}$ esu erg cm G <sup>-1</sup>	$D / 10^{-37}$ esu <sup>2</sup> cm <sup>2</sup> erg <sup>2</sup> G <sup>-2</sup>	$g_{\text{abs}} / 10^{-3}$
<i>P</i> - <b>1</b> - $\mathbf{B}_{\text{Möbius}}$ (S <sub>0</sub> – S <sub>1</sub> )	3.533	0.0374	16.71	30.75	160.81	–502.0532	27.93	–71.89
<i>P</i> - <b>1</b> - $\mathbf{B}_{\text{Möbius}}$ (S <sub>0</sub> – S <sub>2</sub> )	3.631	0.1900	37.15	81.72	82.63	388.3042	138.0	11.25
<i>P</i> - <b>1</b> - $\mathbf{C}_{\text{Hückel}}$ (S <sub>0</sub> – S <sub>1</sub> )	3.482	0.0544	20.30	40.22	116.71	–376.6444	41.22	–36.55
<i>P</i> - <b>5</b> (S <sub>0</sub> – S <sub>1</sub> )	3.534	0.0183	11.69	12.37	51.36	90.9635	13.66	26.64
<i>P</i> - <b>H6(H)</b> <sub>2</sub> (S <sub>0</sub> – S <sub>1</sub> )	3.535	0.0044	5.713	5.634	45.12	23.7512	3.264	29.11

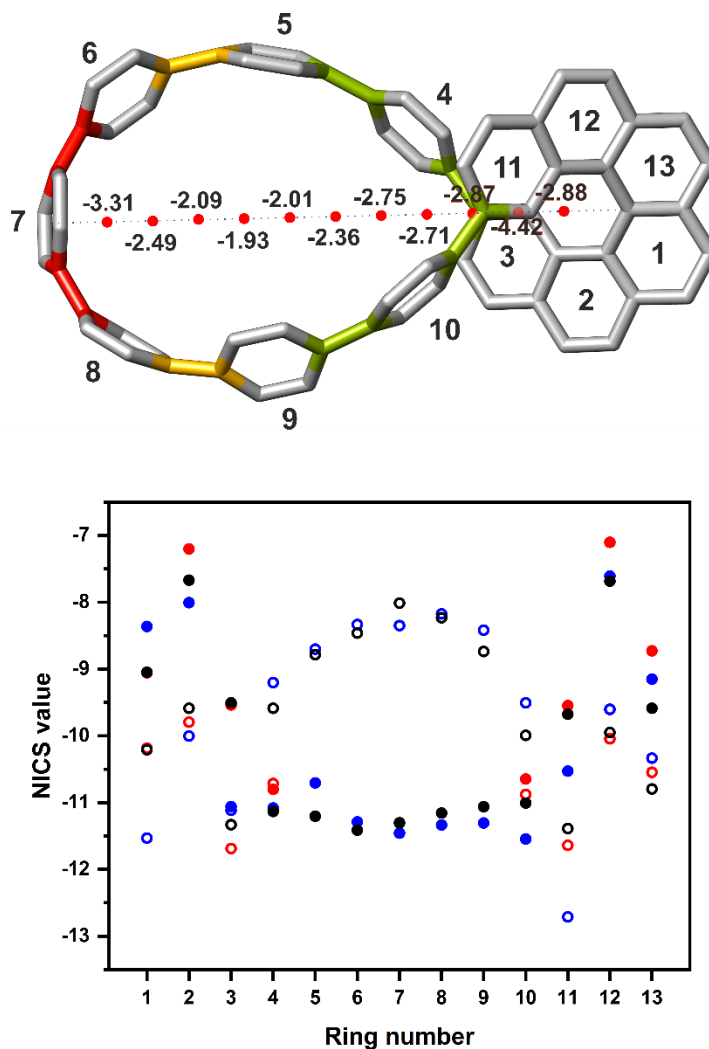
**Table S5.** Calculated electric ( $\mu$ ) and magnetic ( $m$ ) transition dipole moments for the S<sub>0</sub>→S<sub>1</sub> transition in the optimized 1<sup>st</sup> and 2<sup>nd</sup> excited state geometries, rotatory strengths ( $R$ , velocity form), dipole strengths ( $D$ ) and calculated dissymmetry factor<sup>a</sup> ( $g_{\text{lum}}$ ) values.

Geometry (Excited state)	$E / \text{eV}$	$f$	$ \mu  / 10^{-19}$ esu·cm	$ m  / 10^{-21}$ erg·G <sup>-1</sup>	$\theta / ^\circ$	$R / 10^{-40}$ esu erg cm G <sup>-1</sup>	$D / 10^{-37}$ esu <sup>2</sup> cm <sup>2</sup> erg <sup>2</sup> G <sup>-2</sup>	$g_{\text{lum}} / 10^{-3}$
<i>P</i> - <b>1</b> - $\mathbf{B}_{\text{Möbius}}$ (1st)	2.651	0.4660	68.09	77.08	86.67	307.2451	463.7	2.651
<i>P</i> - <b>1</b> - $\mathbf{B}_{\text{Möbius}}$ (2nd)	3.325	0.2150	57.59	74.14	105.58	–832.6916	331.8	–10.04
<i>P</i> - <b>1</b> - $\mathbf{C}_{\text{Hückel}}$ (1st)	3.304	0.0287	15.14	22.06	101.95	–70.6948	22.92	–12.34
<i>P</i> - <b>5</b> (1st)	3.316	0.0102	9.002	8.351	57	41.4194	8.105	20.44
<i>P</i> - <b>H6(H)</b> <sub>2</sub> (1st)	3.537	0.0082	7.814	7.163	47.08	39.3359	6.106	25.77

<sup>a</sup>The dissymmetry factor  $g_{\text{abs}}$  for the S<sub>0</sub>→S<sub>1</sub> transition can be regarded as the  $g_{\text{lum}}$  for the S<sub>1</sub>→S<sub>0</sub> transition in the same geometry.

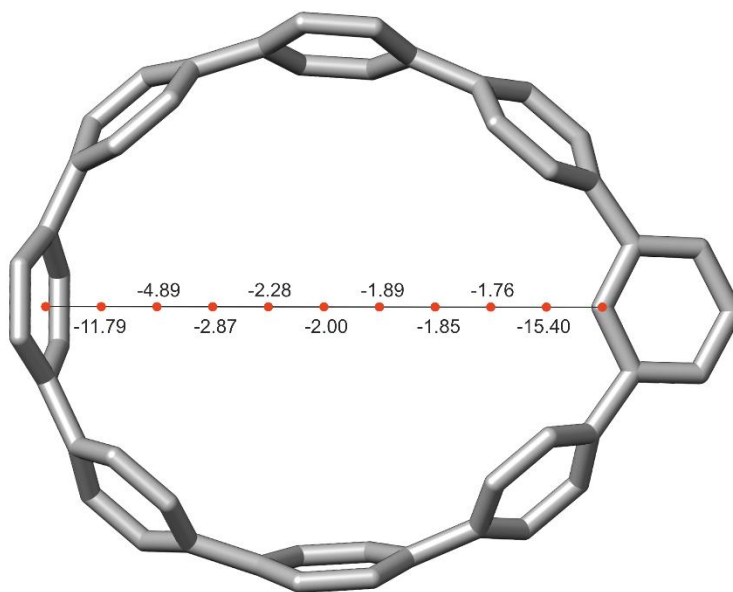
## NICS Values

Although macrocycles with Möbius topology may display a global Möbius aromaticity, in our case, there is an odd number of  $sp^2$ -hybridized carbon atoms in the path between the two positions in the [6]helicene unit, via which the *p*-phenylene half-loop is connected. This is in agreement with our calculations of the nucleus-independent chemical shifts (NICS, Figure S33) that show only small differences in NICS(1) values for individual aromatic rings between the Möbius and Hückel conformations of **1**. Similarly, the NICS values calculated in the inner void of **1** parallel to those found in *m*[8]CPP (Figure S34) and their values demonstrate a global non-aromatic character of these macrocycles. Both the NICS values and the strain energies reinforce our conclusion that compounds similar to **1** preserve the properties of *m*[*n*]CPPs due to their structural similarity.



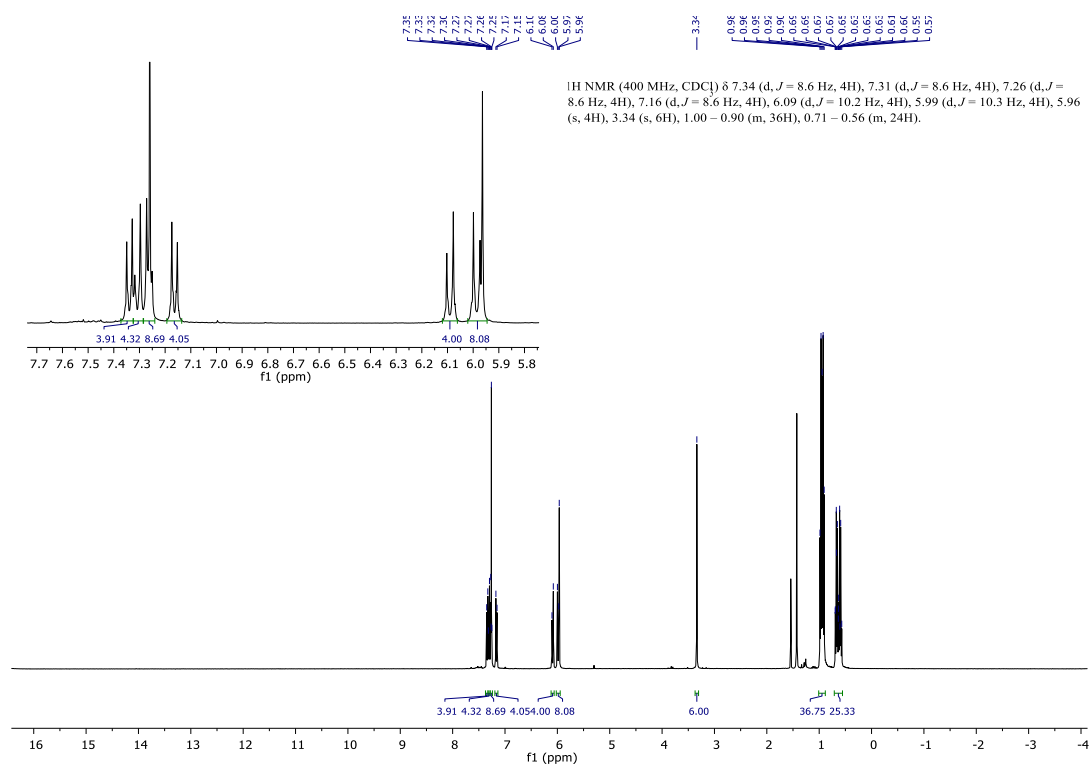
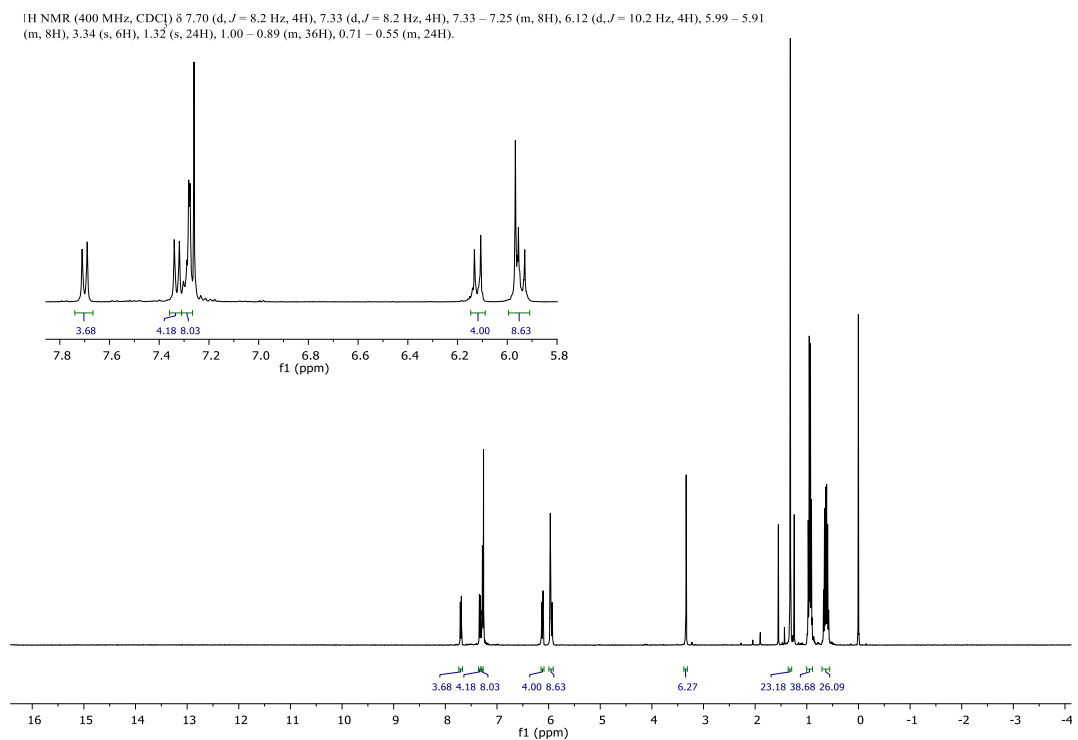
**Figure S33.** NICS values (*top*) calculated for selected points (red dots) in the interior of **1** and NICS(1) values (*bottom*; macrocycle **1** interior: full circles, exterior: empty circles) calculated for the  $B_{\text{Möbius}}$  (black) and  $C_{\text{Hückel}}$  (blue) conformations of **1** and for **5** (red).





**Figure S34.** NICS values calculated for selected points (red dots) in the interior of *m*[8]CPP.

## A.2.3. NMR Spectra

Figure S35.  $^1\text{H-NMR}$  (400 MHz,  $\text{CDCl}_3$ , 298 K) spectrum of **3**.Figure S36.  $^1\text{H-NMR}$  (400 MHz,  $\text{CDCl}_3$ , 298 K) spectrum of **4**.

$^{13}\text{C}$  NMR (126 MHz,  $\text{CDCl}_3$ )  $\delta$  149.08, 145.60, 142.31, 135.37, 134.83, 131.58, 129.27, 126.18, 126.07, 125.14, 83.82, 74.55, 72.13, 71.39, 52.10, 25.00, 7.20, 6.68, 6.61.

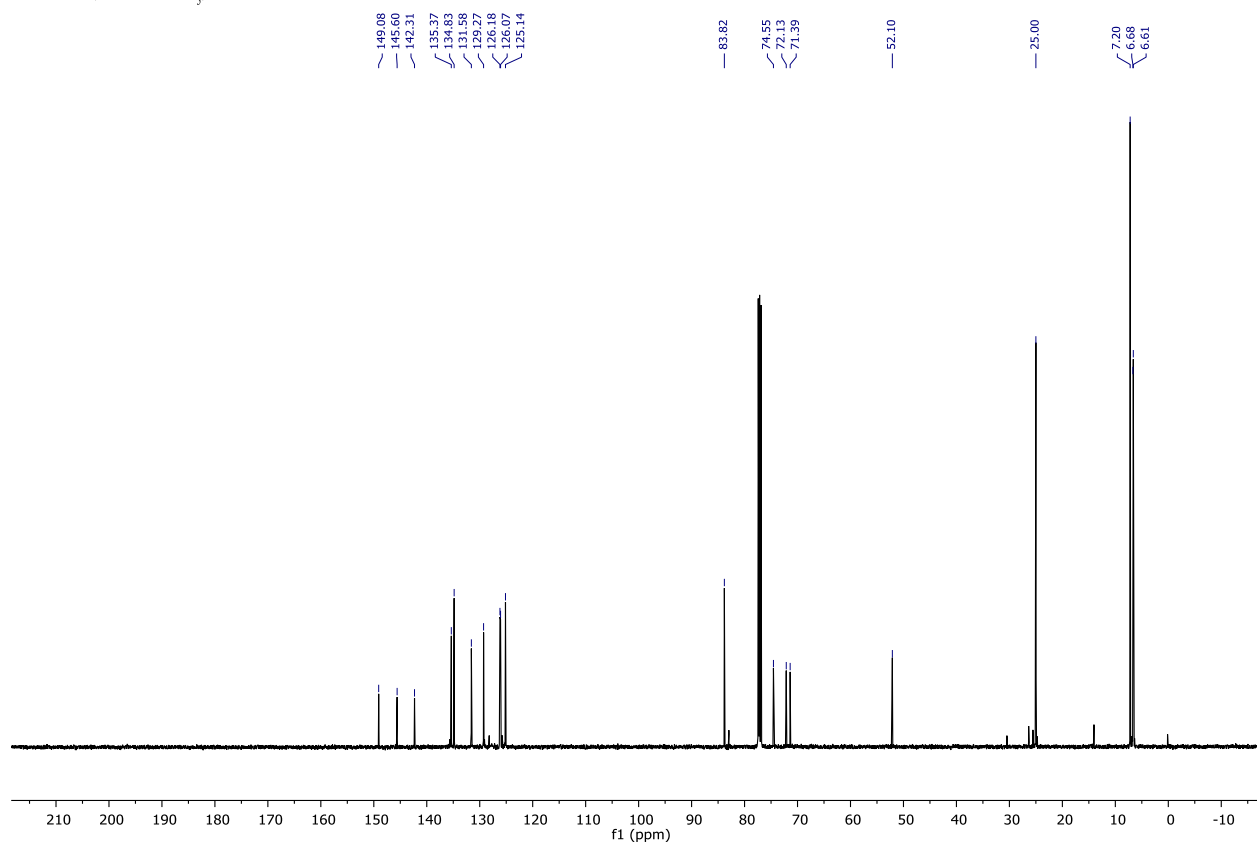


**Figure S37.**  $^{13}\text{C}\{^1\text{H}\}$ -NMR (126 MHz,  $\text{CDCl}_3$ , 298 K) spectrum of **4**.

$^1\text{H}$  NMR (400 MHz,  $\text{CDCl}_3$ )  $\delta$  10.22 (s, 2H), 8.54 – 8.49 (m, 2H), 8.13 (dd,  $J = 8.6, 1.5$  Hz, 2H), 8.03 (d,  $J = 8.2$  Hz, 2H).

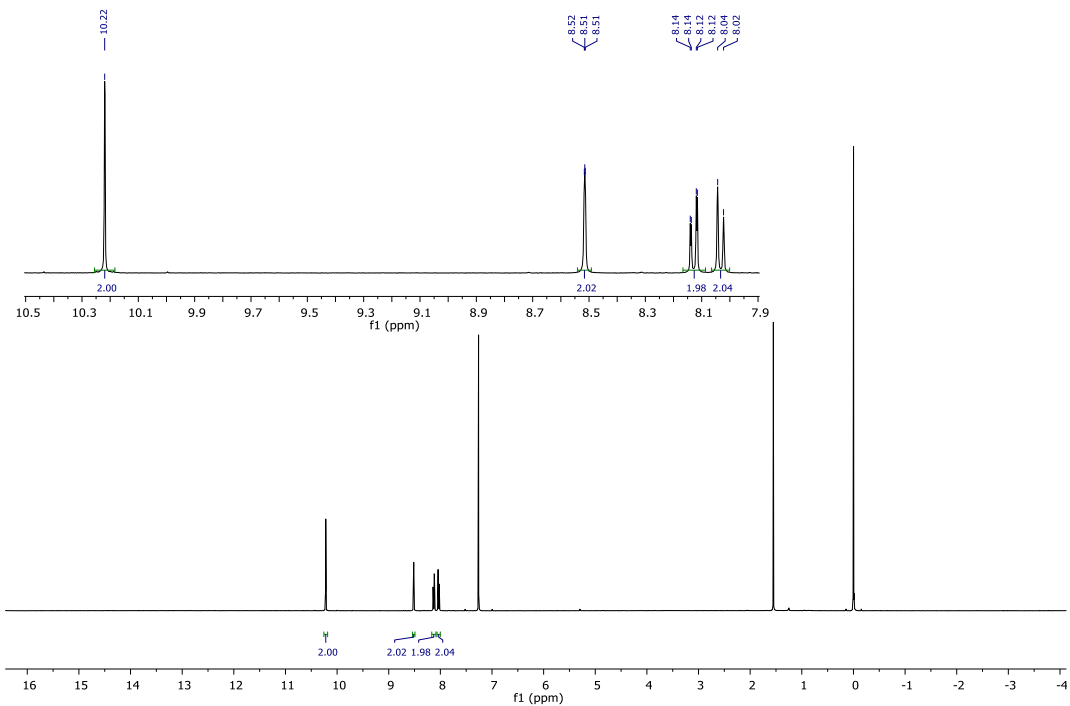


**Figure S38.**  $^1\text{H}$ -NMR (400 MHz,  $\text{CDCl}_3$ , 298 K) spectrum of **6**.

$^1\text{H}$  NMR (400 MHz,  $\text{CDCl}_3$ )  $\delta$  7.83 – 7.74 (m, 9H), 7.69 – 7.61 (m, 6H), 7.26 – 7.23 (m, 2H), 7.05 (dd,  $J = 8.5, 2.6$  Hz, 2H), 5.53 (d,  $J = 14.6$  Hz, 2H).

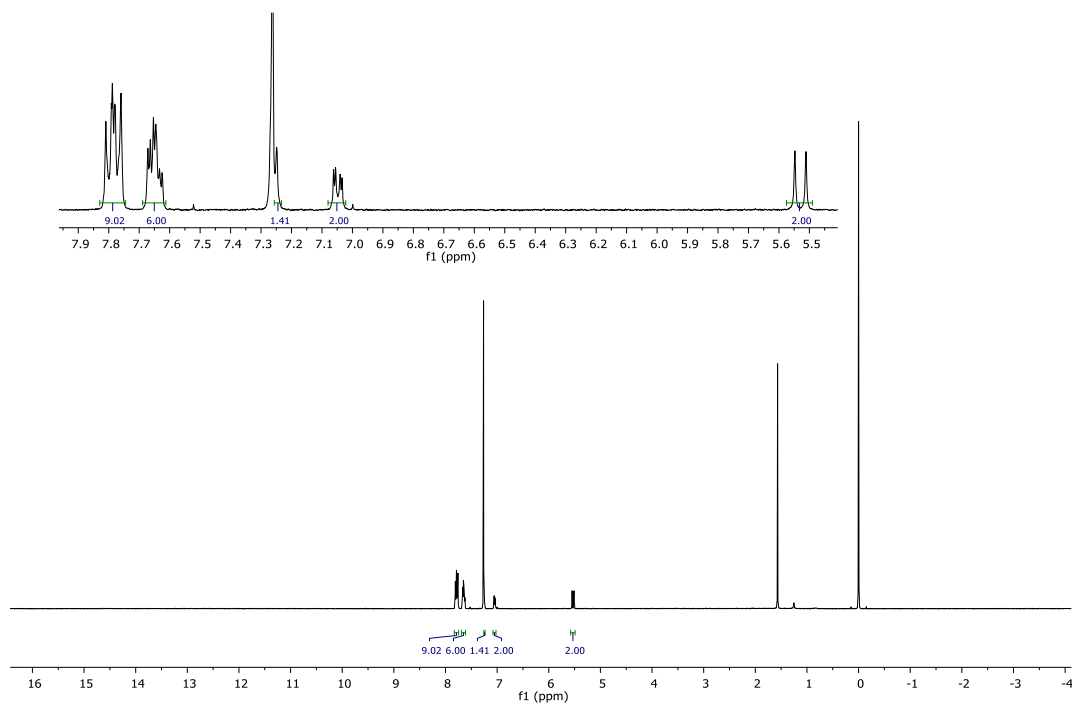


Figure S39.  $^1\text{H}$ -NMR (400 MHz,  $\text{CDCl}_3$ , 298 K) spectrum of **7**.

$^1\text{H}$  NMR (500 MHz,  $\text{CDCl}_3$ )  $\delta$  7.60 (d,  $J = 8.5$  Hz, 4H), 7.34 (d,  $J = 8.5$  Hz, 4H), 7.28 (dd,  $J = 8.3, 1.7$  Hz, 2H), 7.14 (d,  $J = 8.2$  Hz, 4H), 6.76 (d,  $J = 12.1$  Hz, 2H), 6.59 (d,  $J = 12.2$  Hz, 2H).

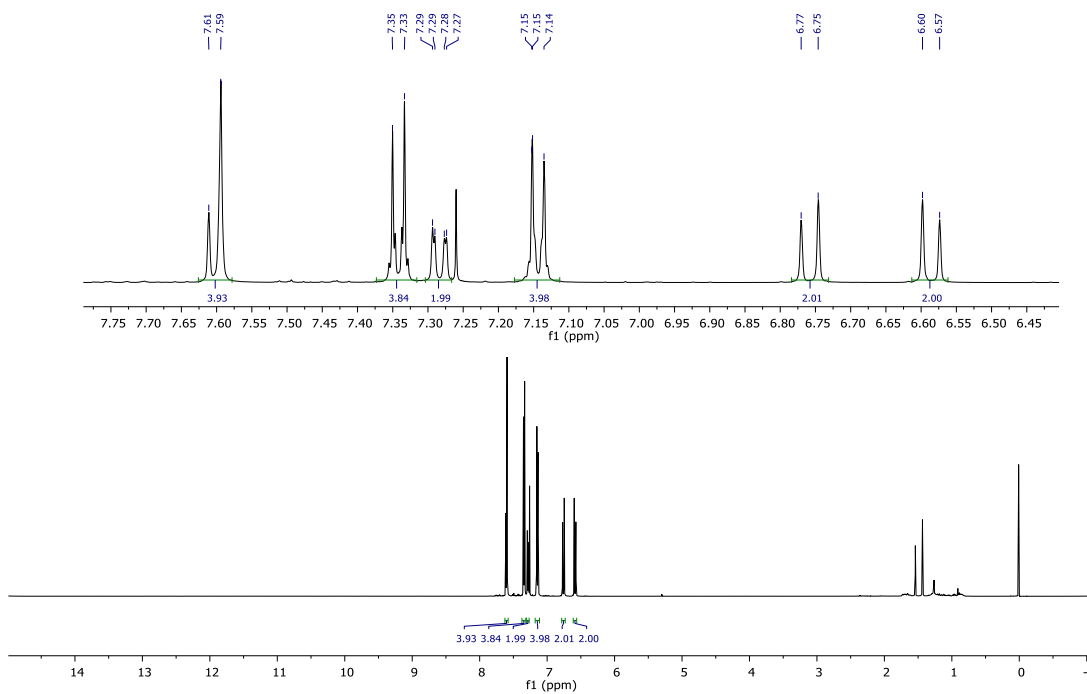
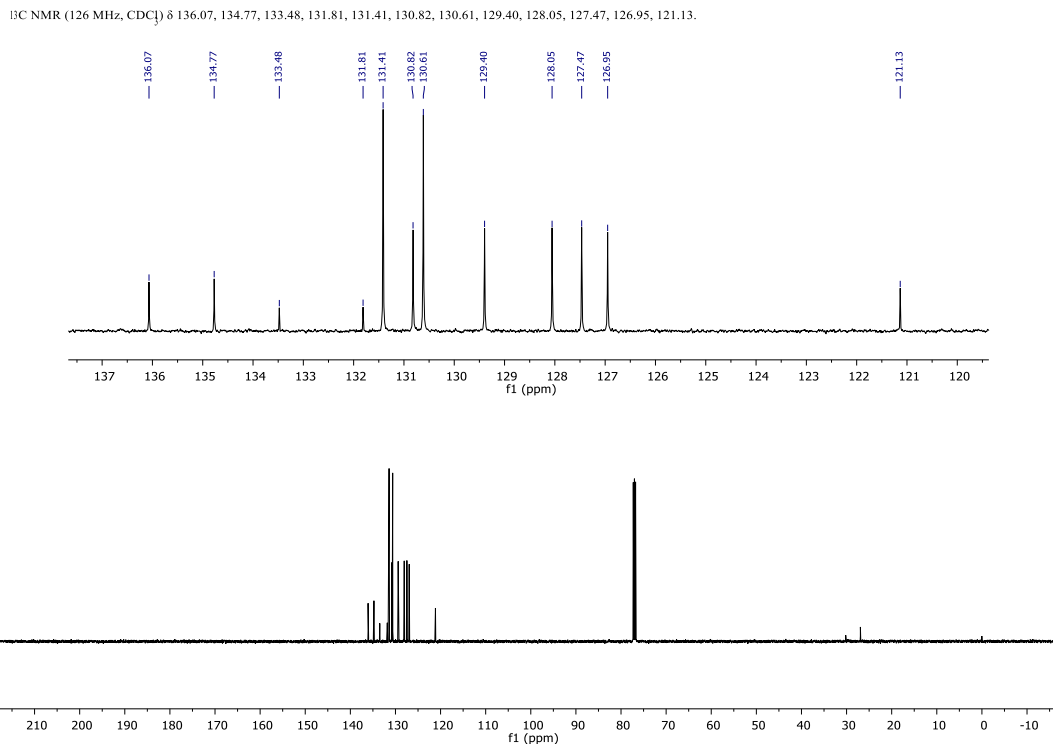
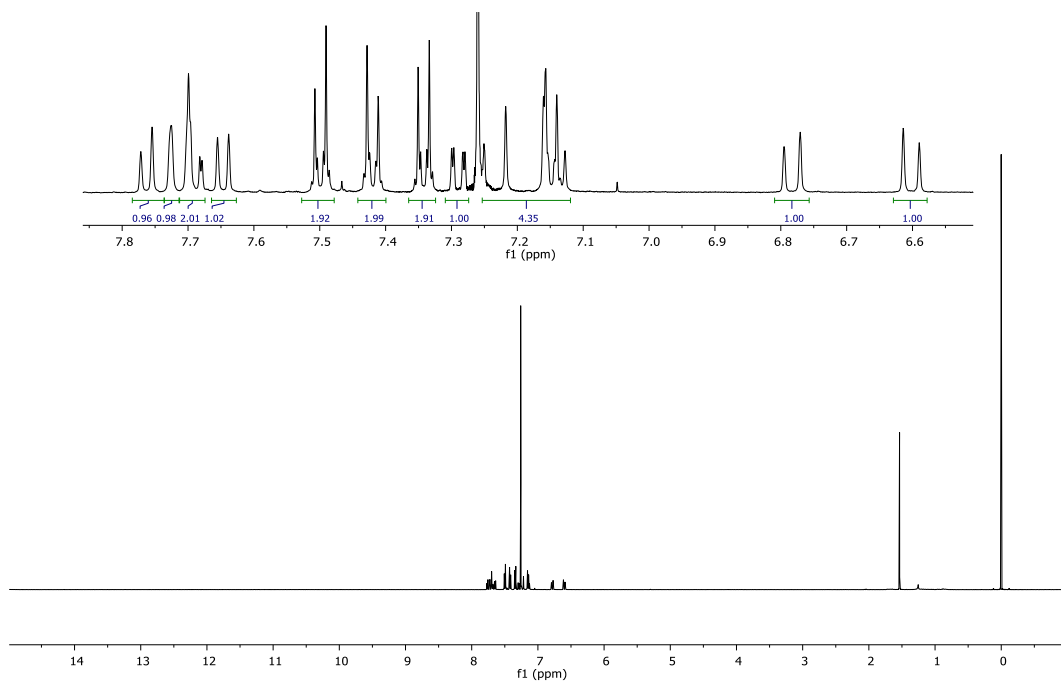


Figure S40.  $^1\text{H}$ -NMR (500 MHz,  $\text{CDCl}_3$ , 298 K) spectrum of (*Z,Z*)-**8**.



**Figure S41.**  $^{13}\text{C}\{^1\text{H}\}$ -NMR (126 MHz,  $\text{CDCl}_3$ , 298 K) spectrum of (*Z,Z*)-**8**.

$^1\text{H}$  NMR (500 MHz,  $\text{CDCl}_3$ )  $\delta$  7.76 (d,  $J = 8.5$  Hz, 1H), 7.72 (s, 1H), 7.71 – 7.67 (m, 2H), 7.65 (d,  $J = 8.5$  Hz, 1H), 7.50 (d,  $J = 8.5$  Hz, 2H), 7.42 (d,  $J = 8.4$  Hz, 2H), 7.34 (d,  $J = 8.5$  Hz, 2H), 7.29 (dd,  $J = 8.7, 1.7$  Hz, 1H), 7.25 – 7.12 (m, 4H), 6.78 (d,  $J = 12.2$  Hz, 1H), 6.60 (d,  $J = 12.2$  Hz, 1H).



**Figure S42.**  $^1\text{H}$ -NMR (500 MHz,  $\text{CDCl}_3$ , 298 K) spectrum of (*Z,E*)-**8**.

$^1\text{H}$  NMR (400 MHz,  $\text{CDCl}_3$ )  $\delta$  8.06 – 7.98 (m, 4H), 7.98 – 7.90 (m, 4H), 7.74 (d,  $J = 8.5$  Hz, 2H), 7.71 (d,  $J = 1.9$  Hz, 2H), 7.39 (dd,  $J = 8.5, 2.0$  Hz, 2H).

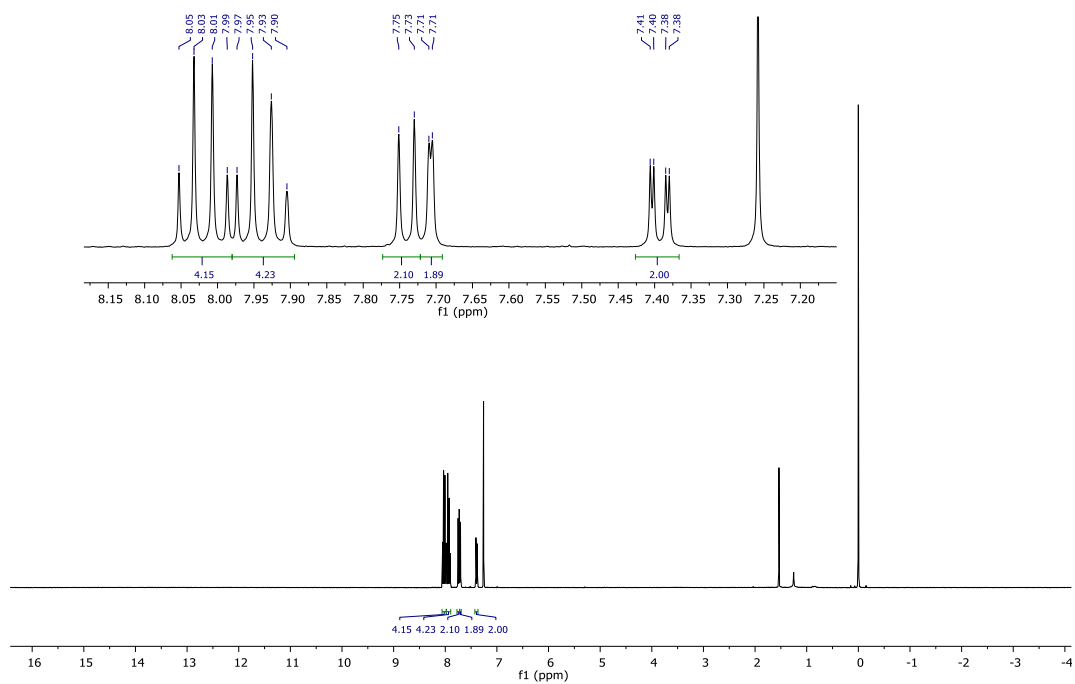


Figure S43.  $^1\text{H}$ -NMR (400 MHz,  $\text{CDCl}_3$ , 298 K) spectrum of **2**.

$^1\text{H}$  NMR (500 MHz,  $\text{CDCl}_3$ )  $\delta$  8.10 (d,  $J = 1.8$  Hz, 2H), 8.04 – 7.95 (m, 8H), 7.94 (d,  $J = 8.2$  Hz, 2H), 7.48 (dd,  $J = 8.2, 1.8$  Hz, 2H), 6.98 (d,  $J = 7.8$  Hz, 4H), 6.66 (d,  $J = 8.1$  Hz, 4H), 2.28 (s, 6H).

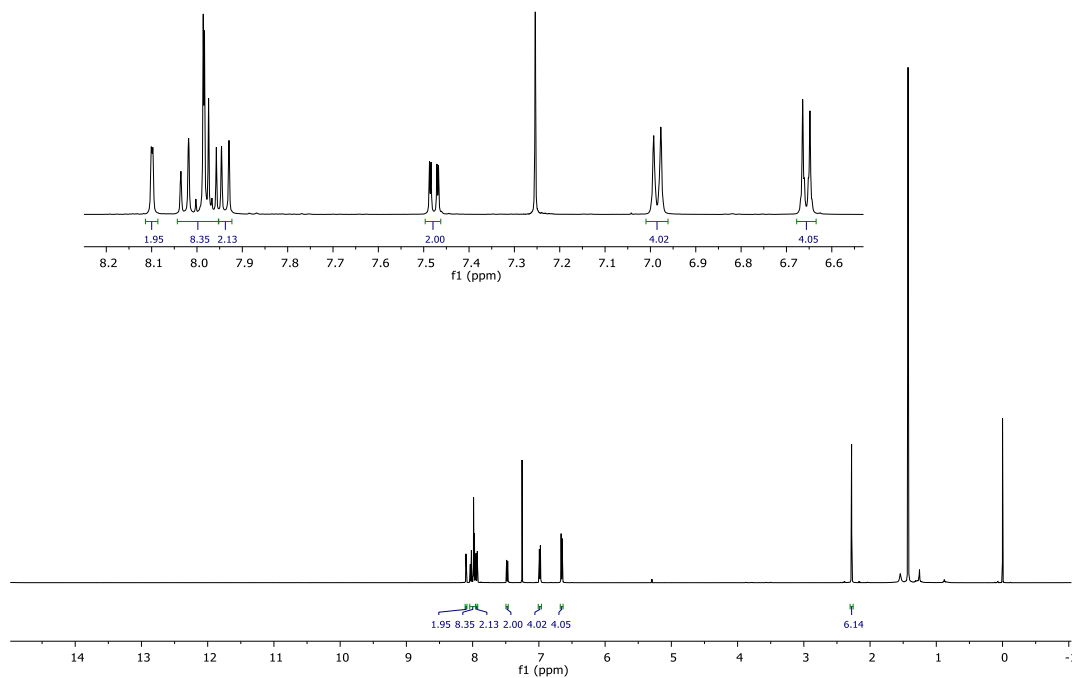


Figure S44.  $^1\text{H}$ -NMR (500 MHz,  $\text{CDCl}_3$ , 298 K) spectrum of **5**.

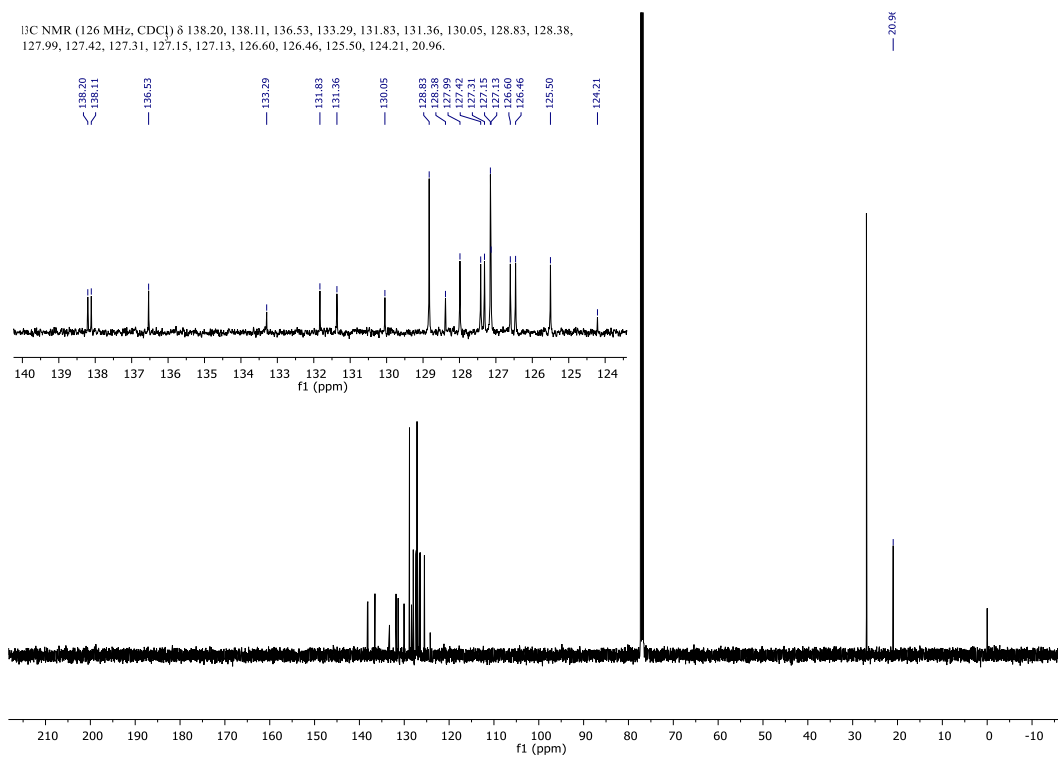


Figure S45.  $^{13}\text{C}\{^1\text{H}\}$ -NMR (126 MHz,  $\text{CDCl}_3$ , 298 K) spectrum of **5**.

$^1\text{H}$  NMR (500 MHz,  $\text{CDCl}_3$ )  $\delta$  8.13 (d,  $J = 1.6$  Hz, 2H), 8.06 – 7.98 (m, 10H), 7.59 – 7.43 (m, 8H), 7.43 – 7.35 (m, 8H), 7.32 (d,  $J = 8.2$  Hz, 4H), 7.26 (d,  $J = 8.6$  Hz, 4H), 7.17 (dd,  $J = 8.3, 1.7$  Hz, 2H), 6.31 (d,  $J = 8.5$  Hz, 4H).

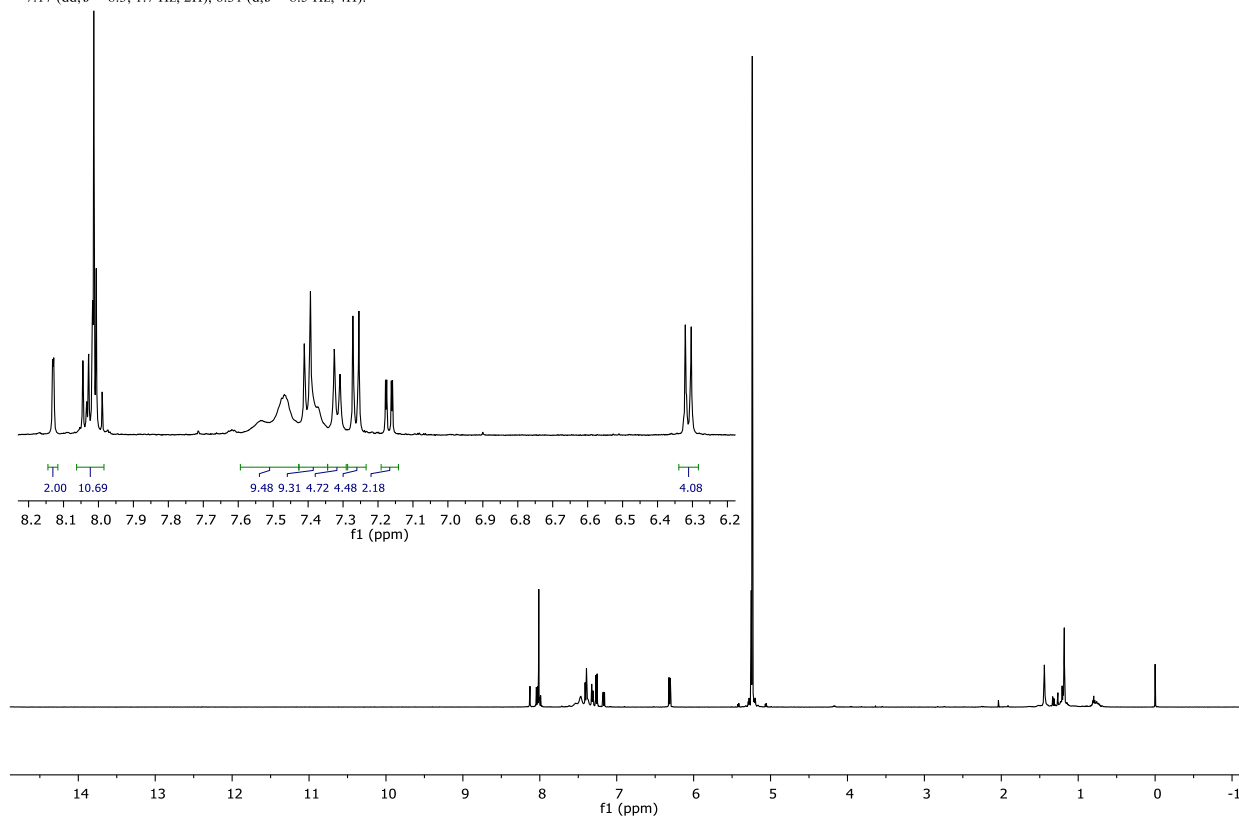


Figure S46.  $^1\text{H}$ -NMR (500 MHz,  $\text{CD}_2\text{Cl}_2$ , 298 K) spectrum of **1**.

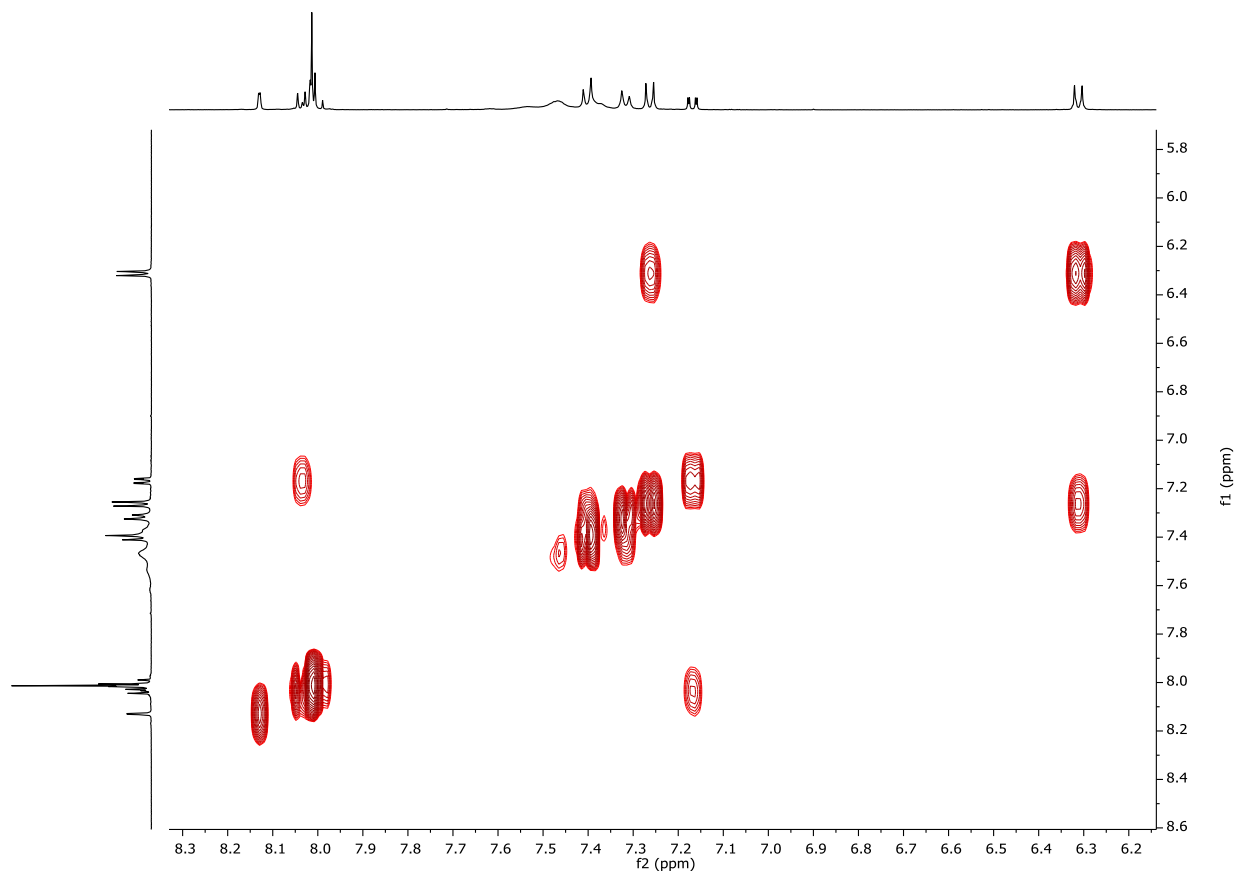
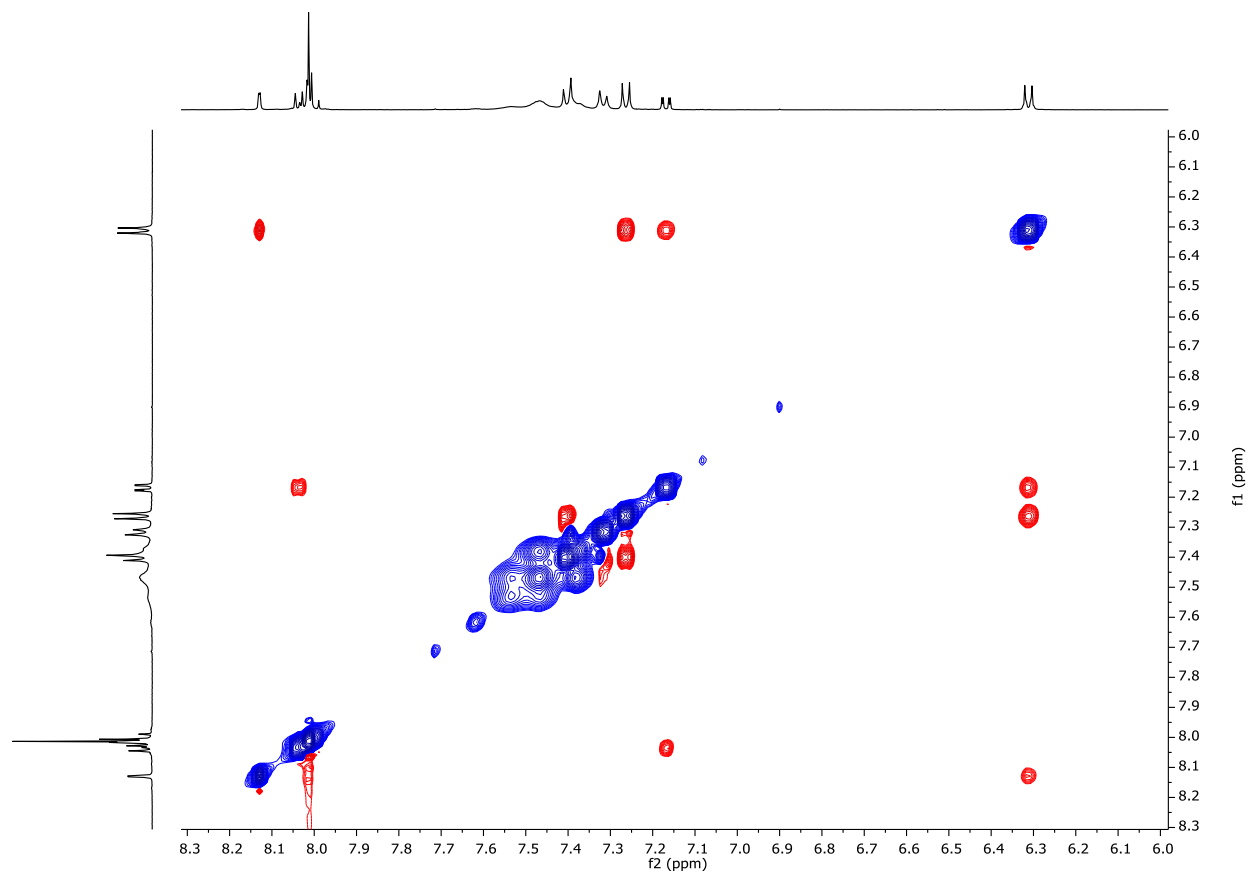


Figure S47. Aromatic region of the  $^1\text{H}$ - $^1\text{H}$  COSY spectrum of compound **1** (11.7 T,  $\text{CD}_2\text{Cl}_2$ , 298 K).





**Figure S48.** Aromatic region of the <sup>1</sup>H–<sup>1</sup>H NOESY spectrum of compound **1** (11.7 T, CD<sub>2</sub>Cl<sub>2</sub>, 298 K).

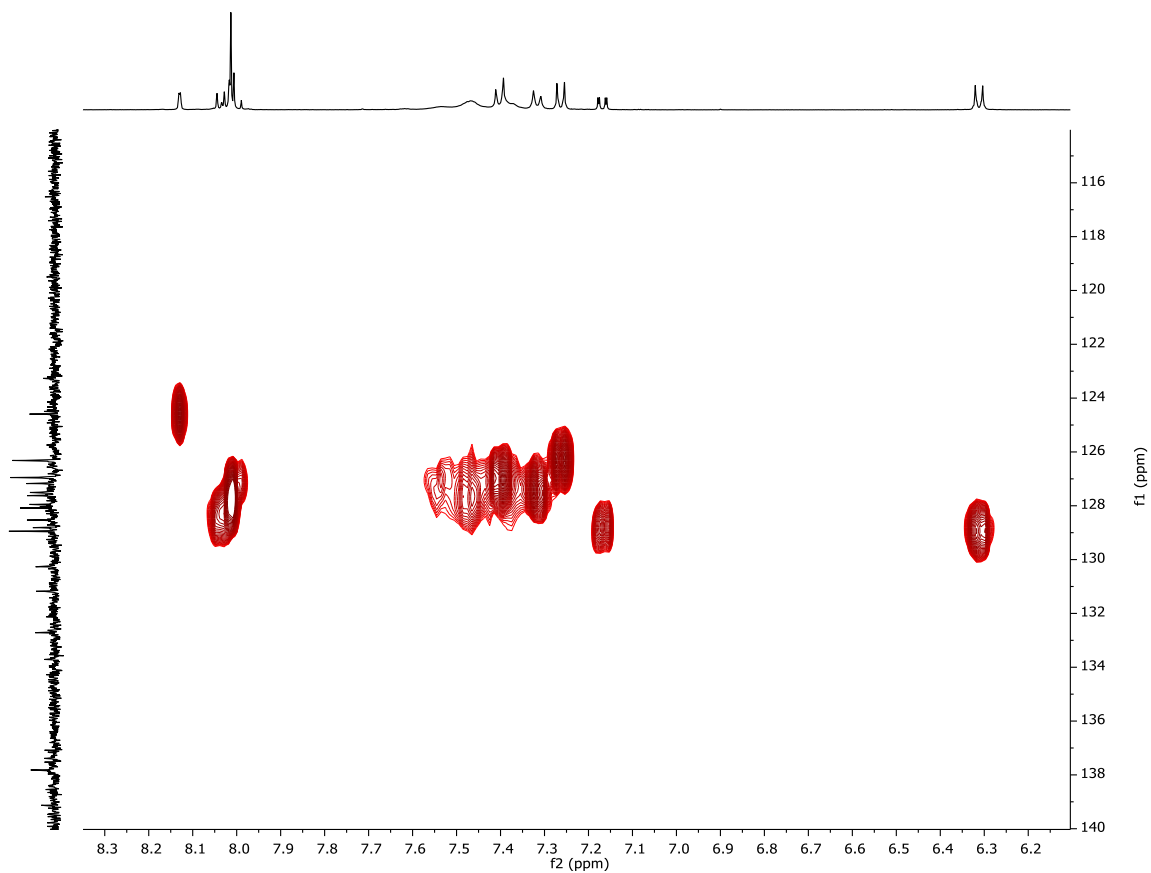
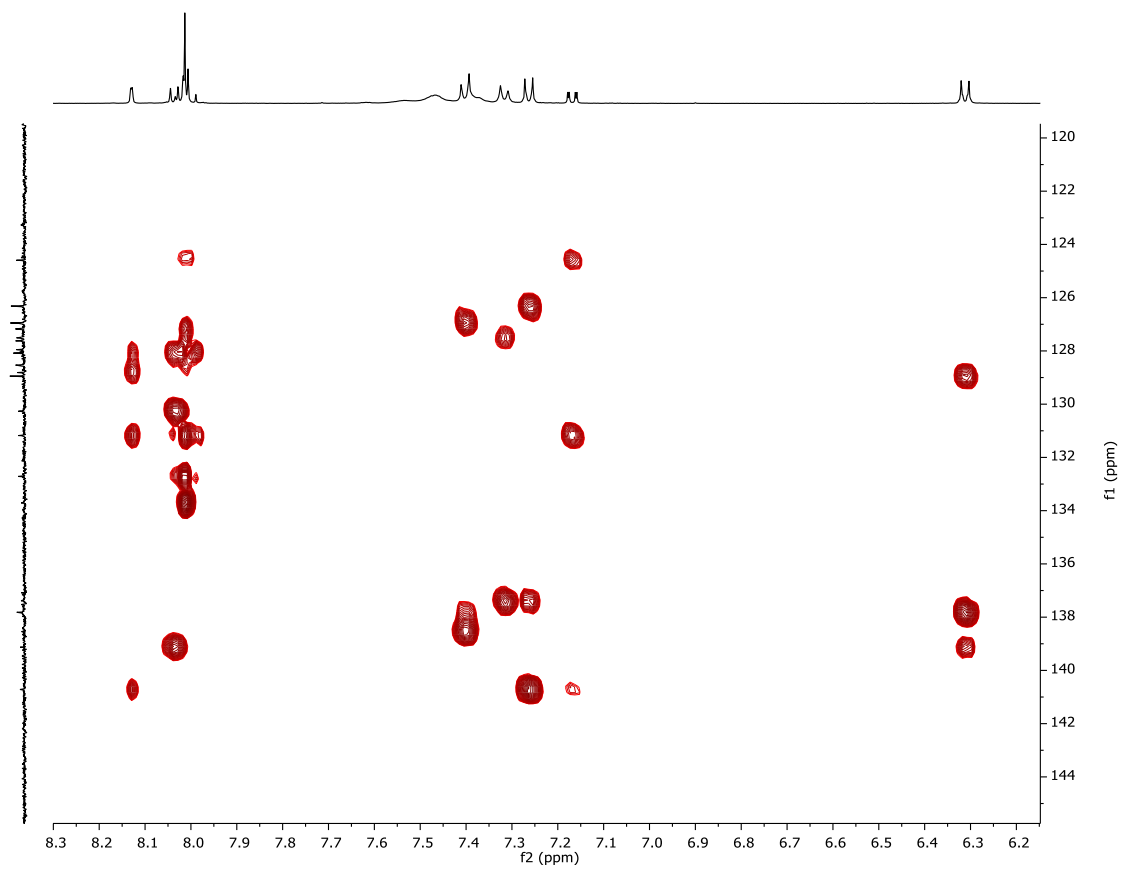


Figure S49. Aromatic region of the  $^1\text{H}$ - $^{13}\text{C}$  HSQC spectrum of compound **1** (11.7 T,  $\text{CD}_2\text{Cl}_2$ , 298 K).



**Figure S50.** Aromatic region of the  $^1\text{H}$ - $^{13}\text{C}$  HMBC spectrum of compound **1** (11.7 T,  $\text{CD}_2\text{Cl}_2$ , 298 K).

Appendix

$^1\text{H}$  NMR (600 MHz, TCE)  $\delta$  8.25 (s, 2H), 8.13 – 8.06 (m, 10H), 7.58 – 7.50 (m, 8H), 7.49 (d,  $J = 8.6$  Hz, 2H), 7.37 (d,  $J = 8.4$  Hz, 4H), 7.21 (dd,  $J = 8.3, 1.7$  Hz, 2H), 6.46 – 6.40 (m, 4H).

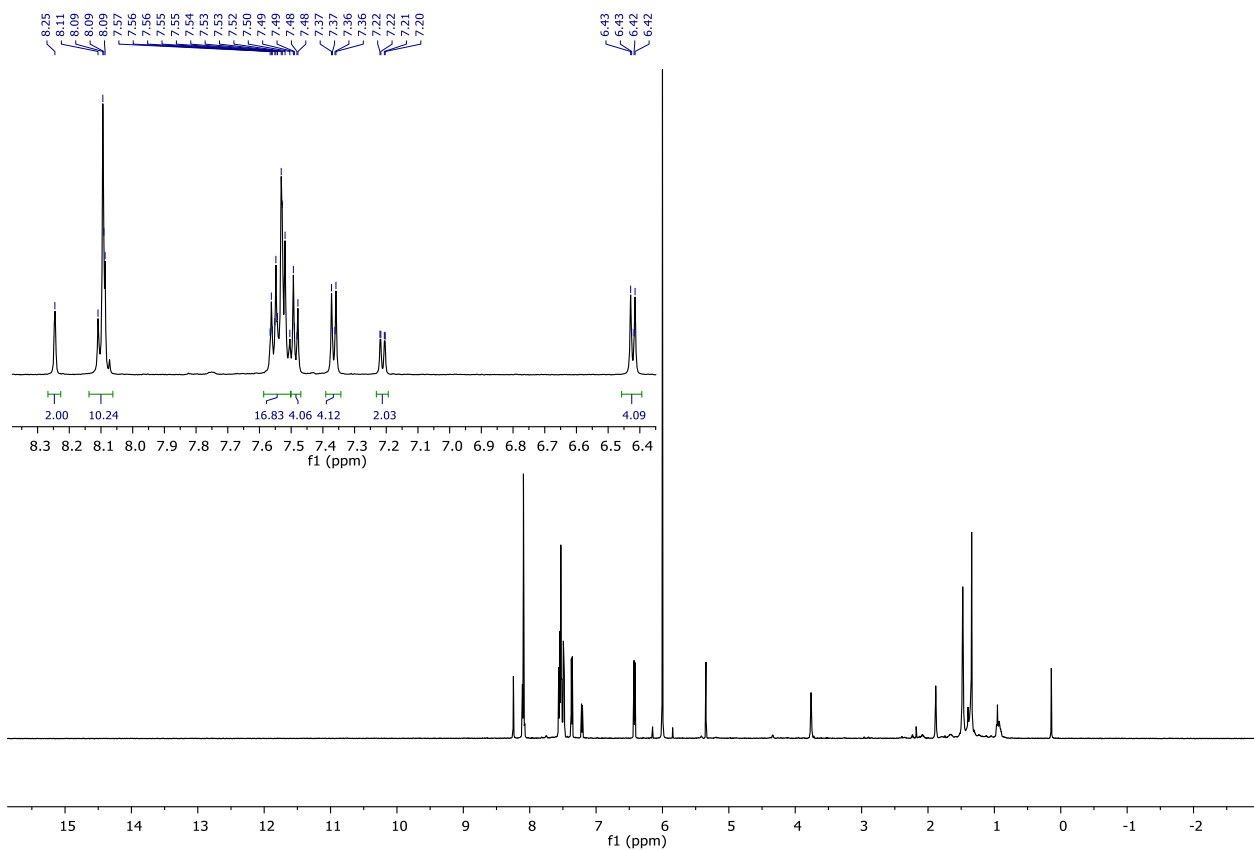


**Figure S51.**  $^1\text{H}$ -NMR (600 MHz, TCE- $d_2$ , 368 K) spectrum of **1**.

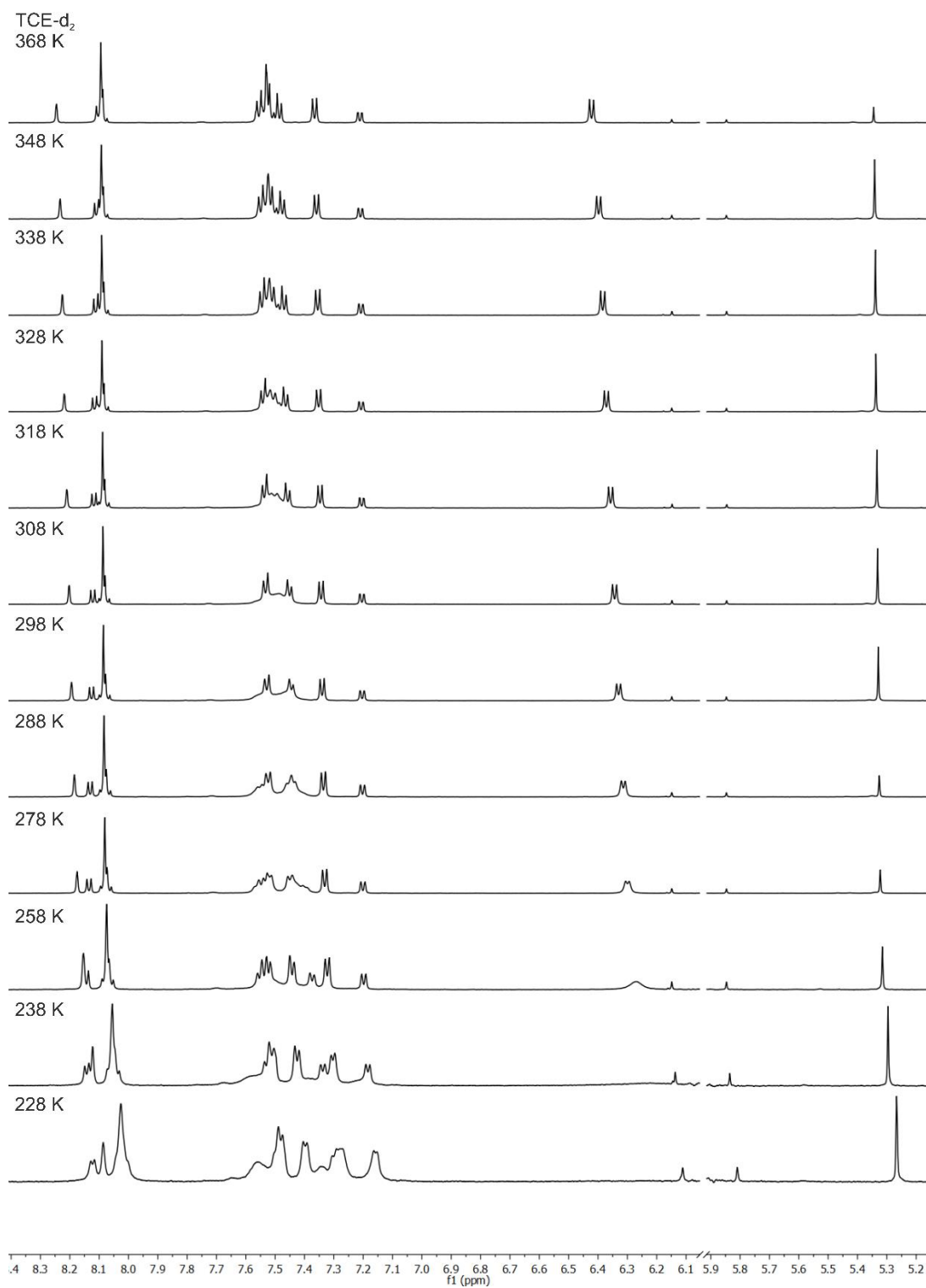


**Figure S52.** <sup>1</sup>H-NMR (600 MHz, TCE-d<sub>2</sub>) spectra of **1** at variable temperature.

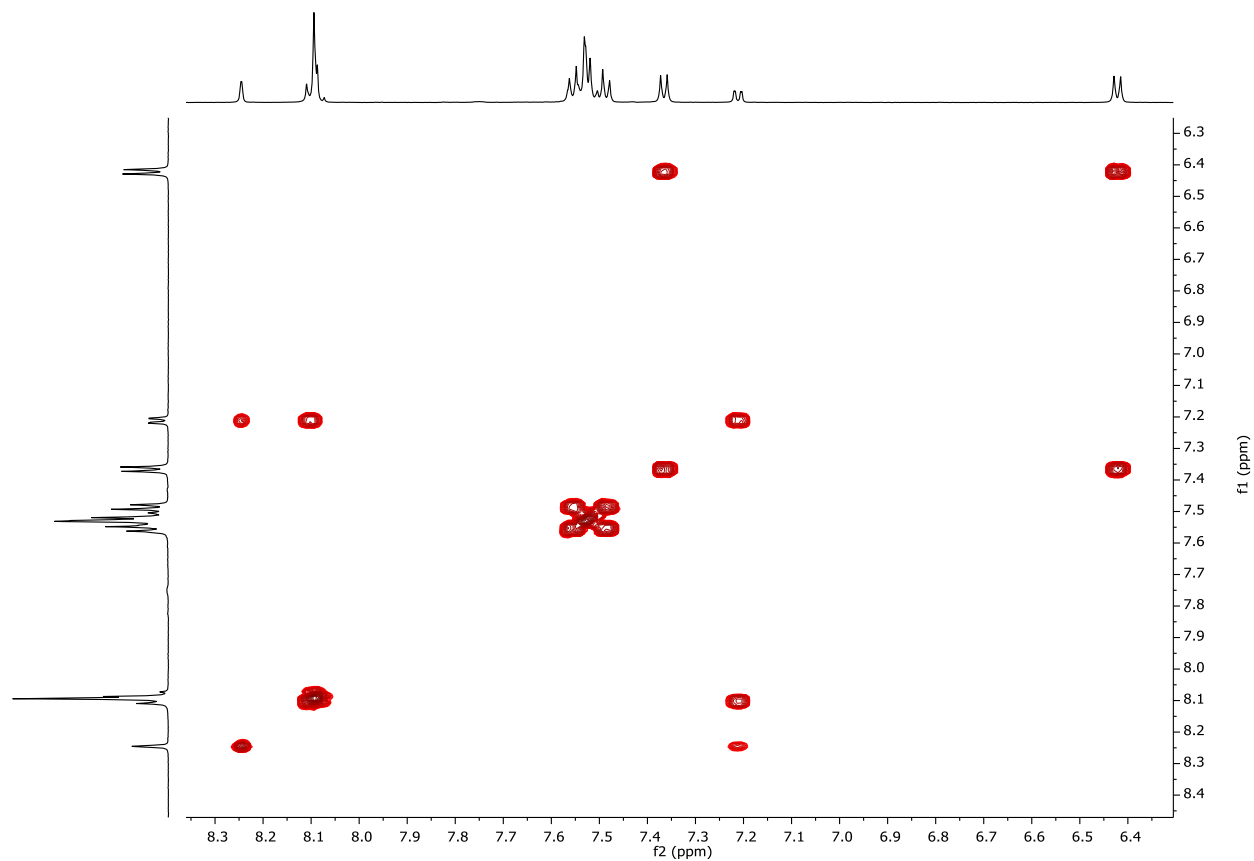
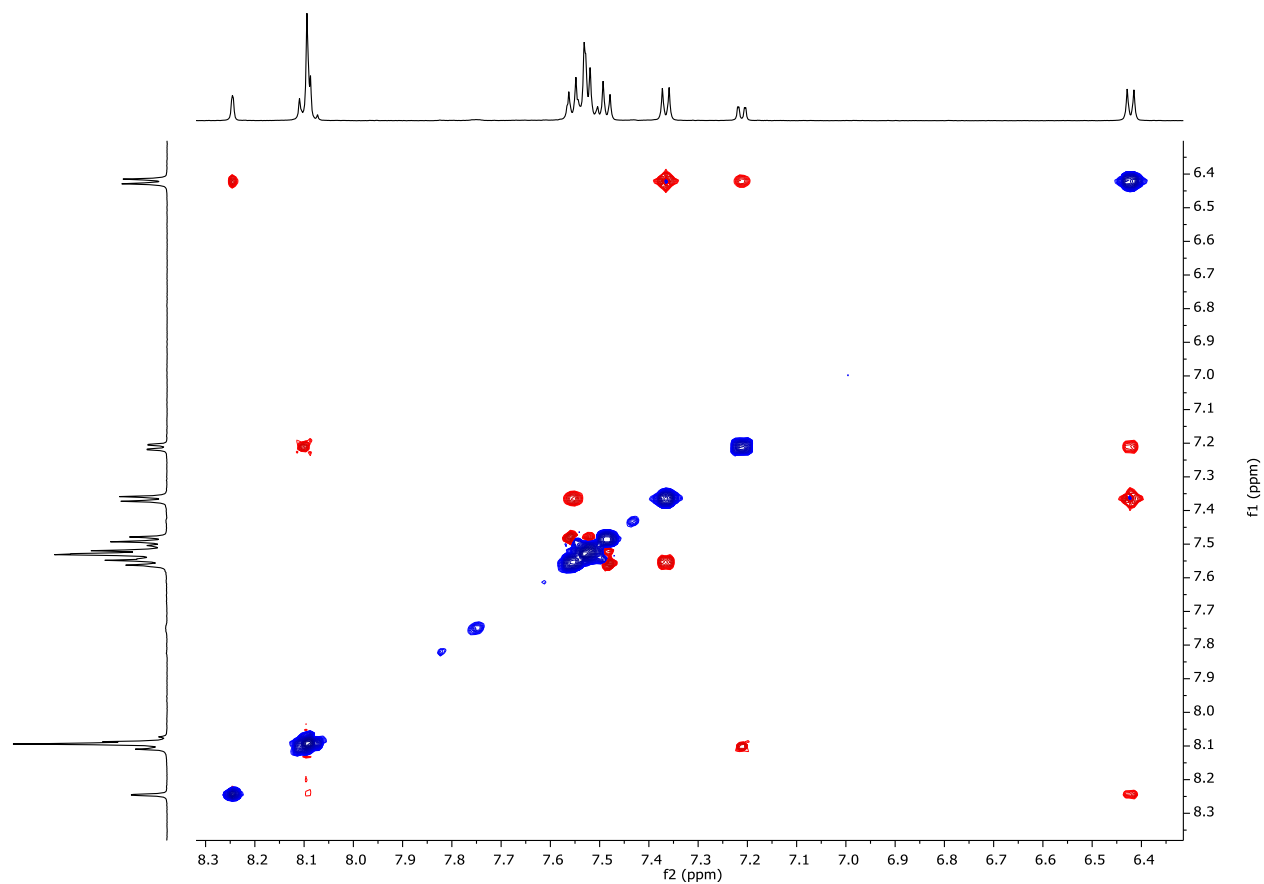
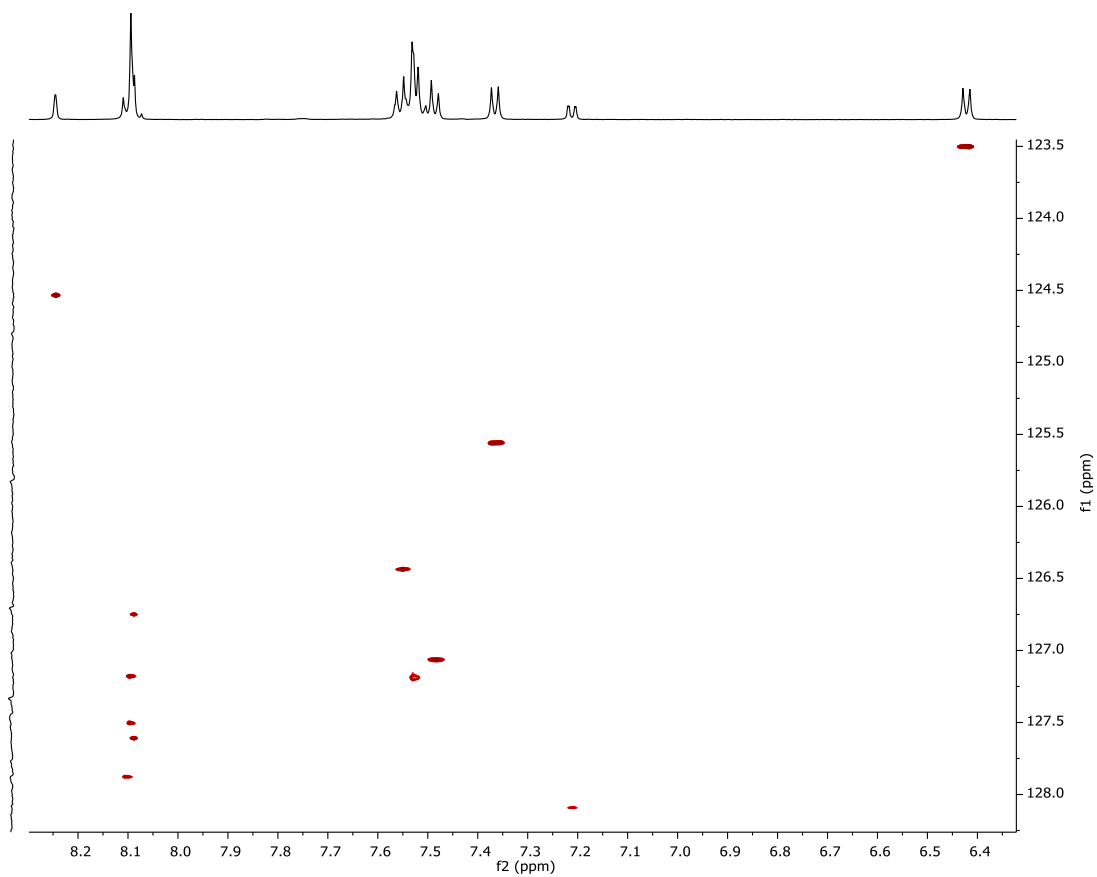


Figure S53. Aromatic region of the <sup>1</sup>H-<sup>1</sup>H COSY spectrum of compound **1** (14.1 T, TCE-*d*<sub>2</sub>, 368 K).



**Figure S54.** Aromatic region of the <sup>1</sup>H–<sup>1</sup>H NOESY spectrum of compound **1** (14.1 T, TCE-*d*<sub>2</sub>, 368 K).



**Figure S55.** Aromatic region of the  $^1\text{H}$ - $^{13}\text{C}$  HSQC spectrum of compound **1** (14.1 T,  $\text{TCE-}d_2$ , 368 K).



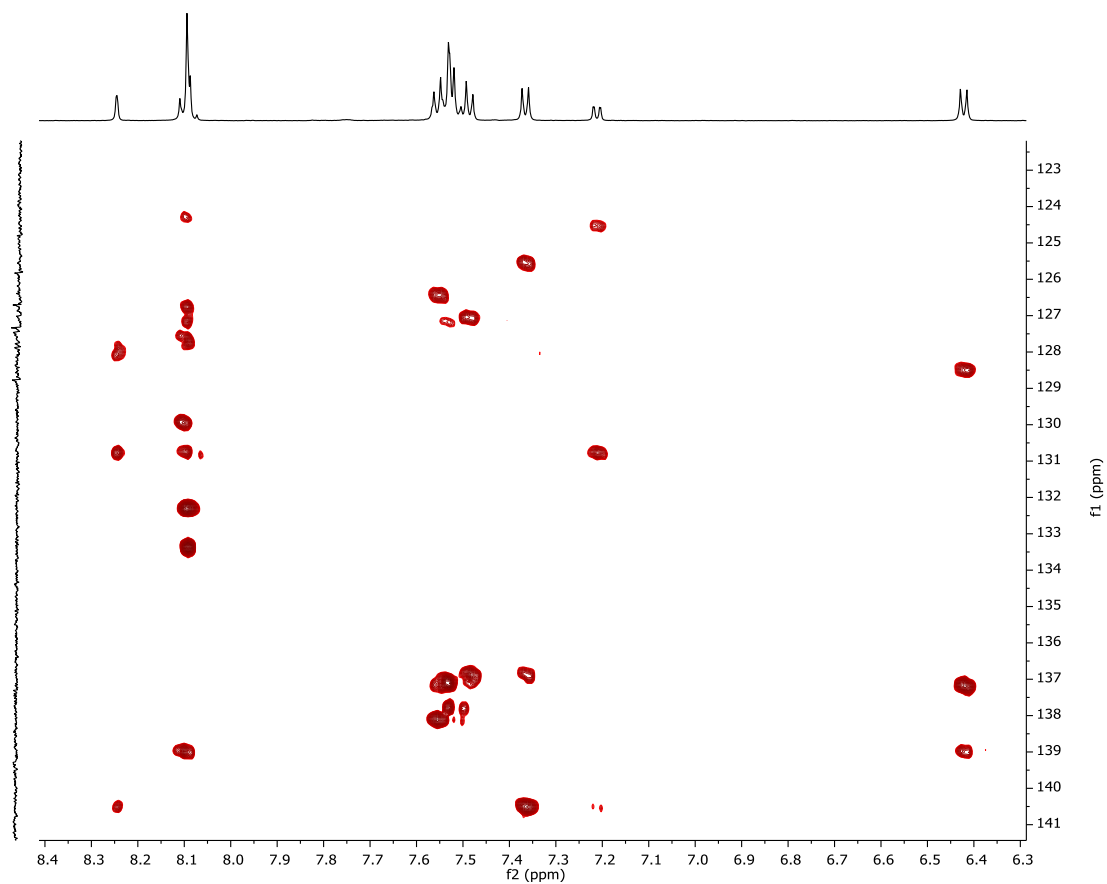


**Figure S56.** Aromatic region of the  $^1\text{H}$ - $^{13}\text{C}$  HMBC spectrum of compound **1** (14.1 T,  $\text{TCE-}d_2$ , 368 K).

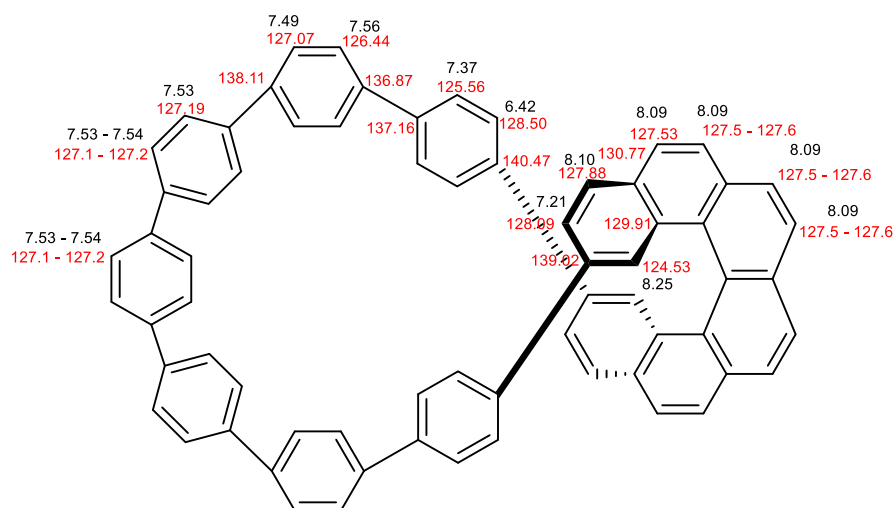


**Figure S57.** Complete assignment of  $^1\text{H}$  (black) and partial assignment of  $^{13}\text{C}$  (red) chemical shifts of **1** in  $\text{TCE-}d_2$  at 368 K.

Appendix

$^1\text{H}$  NMR (600 MHz, THF) $\delta$  8.34 – 8.16 (m, 12H), 7.87 – 7.58 (m, 16H), 7.58 – 7.46 (m, 4H), 7.46 – 7.23 (m, 8H), 5.38 (s, 2H).

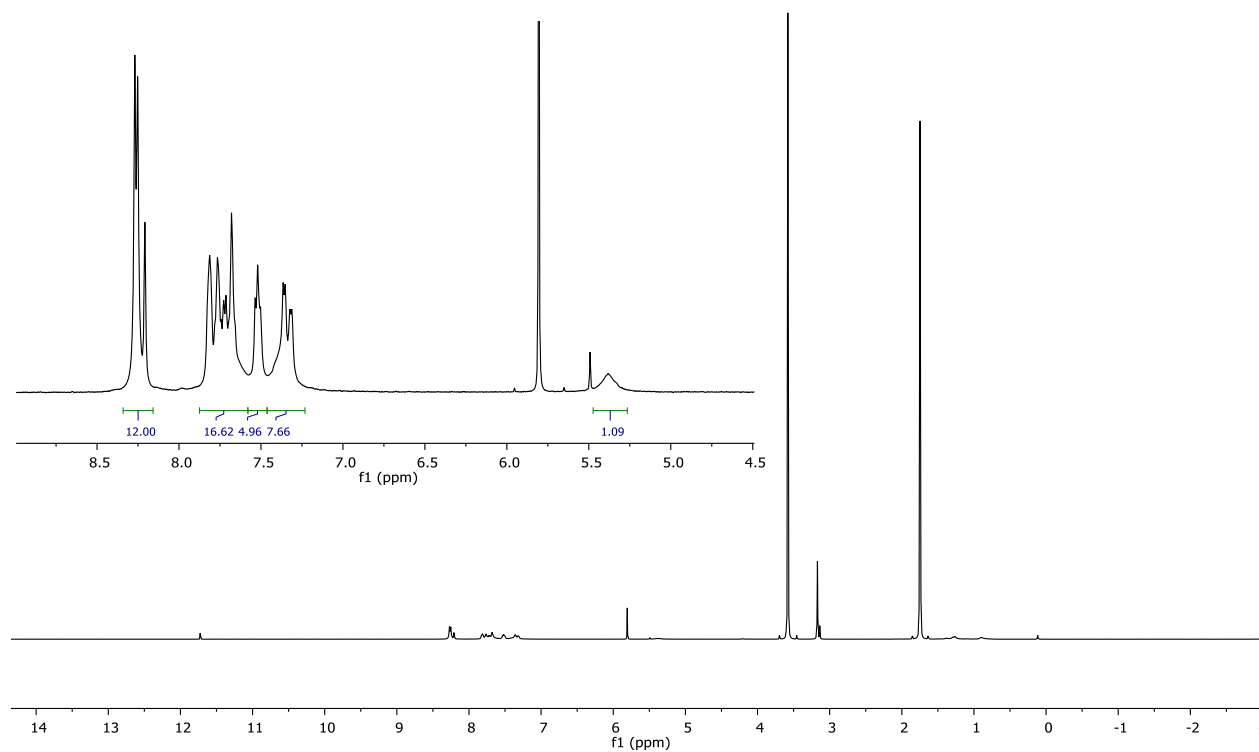


**Figure S58.**  $^1\text{H}$ -NMR (600 MHz, THF- $d_6$ , 168 K) spectrum of **1**.

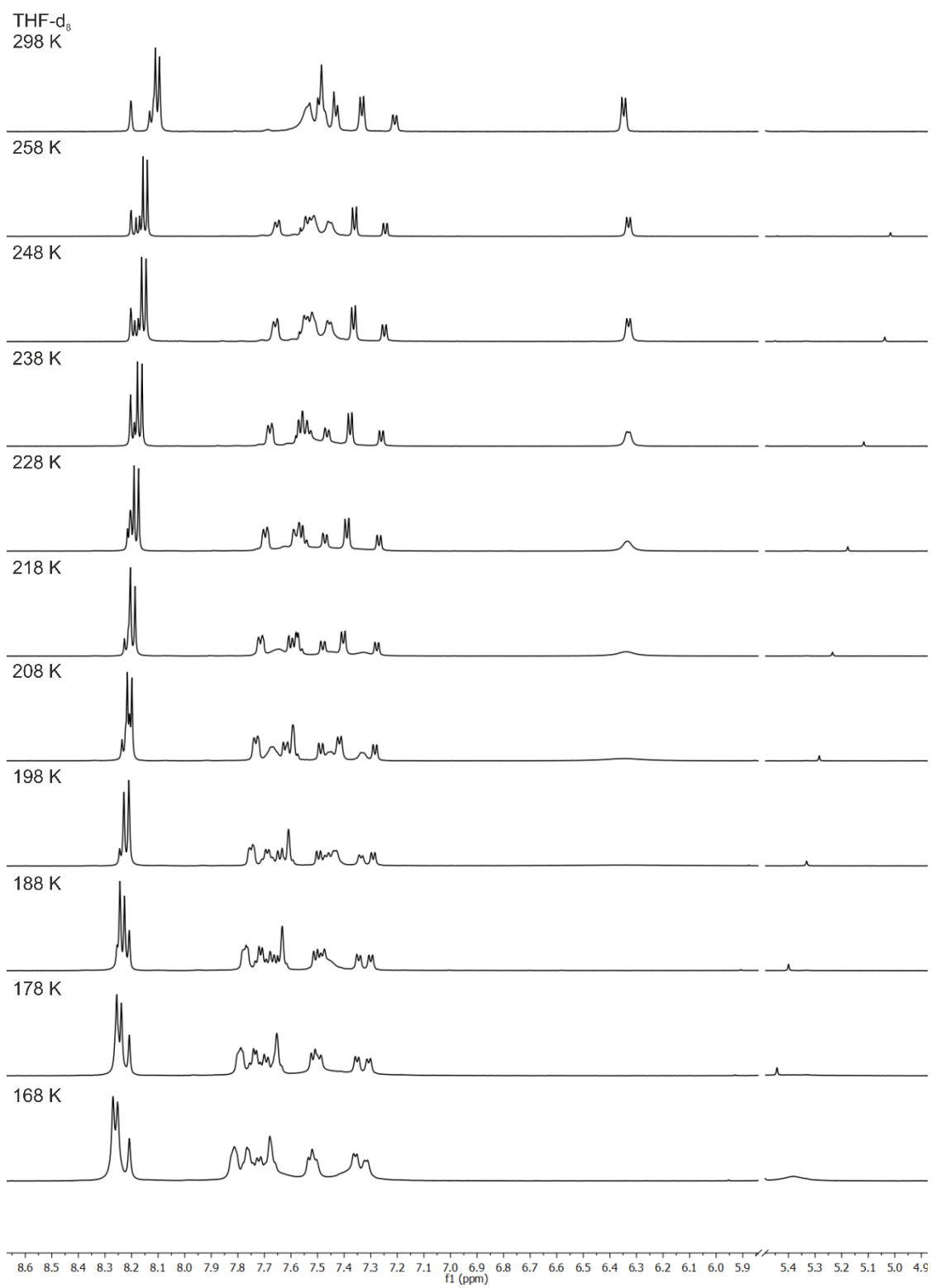


**Figure S59.**  $^1\text{H-NMR}$  (600 MHz, THF- $d_6$ ) spectra of **1** at variable temperature.

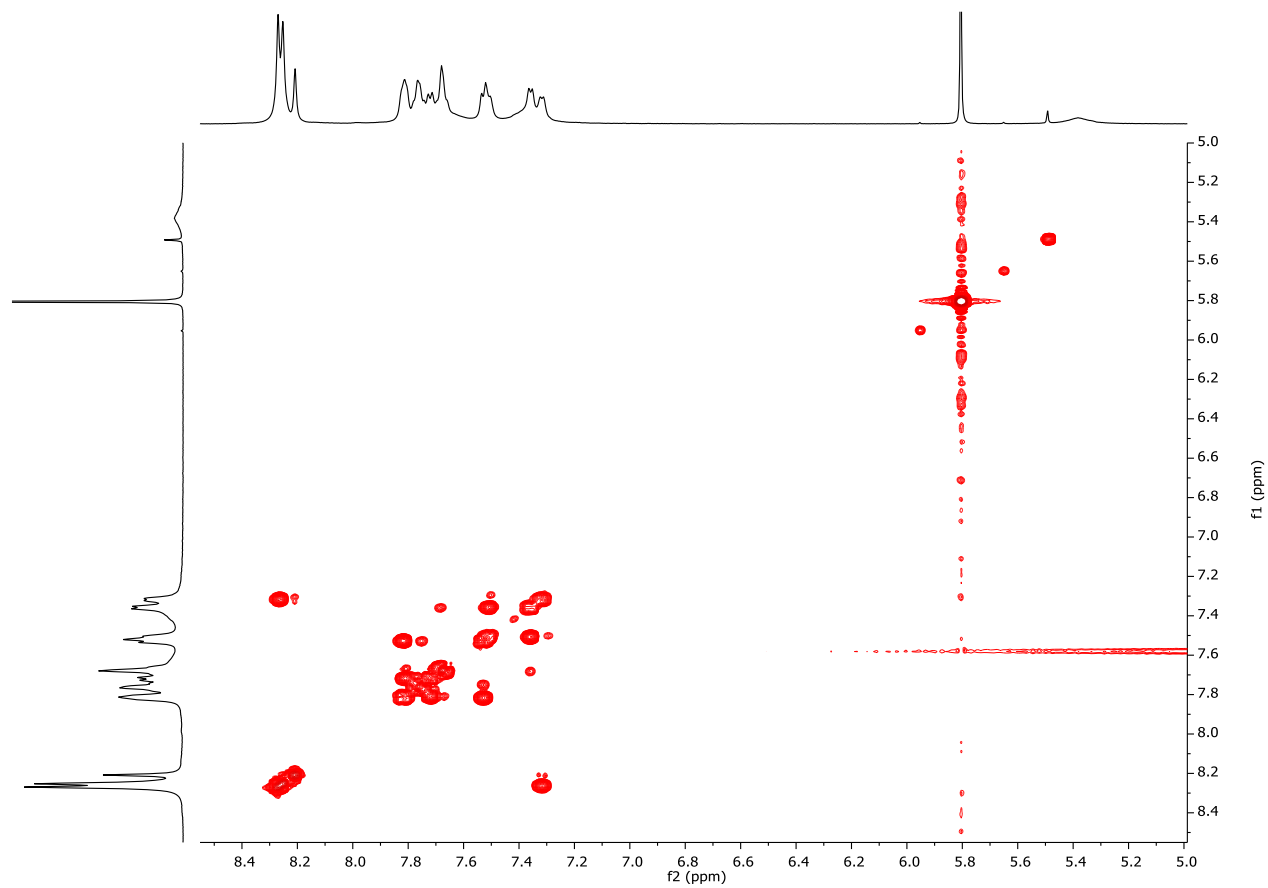


**Figure S60.** Aromatic region of the  $^1\text{H}$ - $^1\text{H}$  COSY spectrum of compound **1** (14.1 T,  $\text{THF-}d_8$ , 168 K).

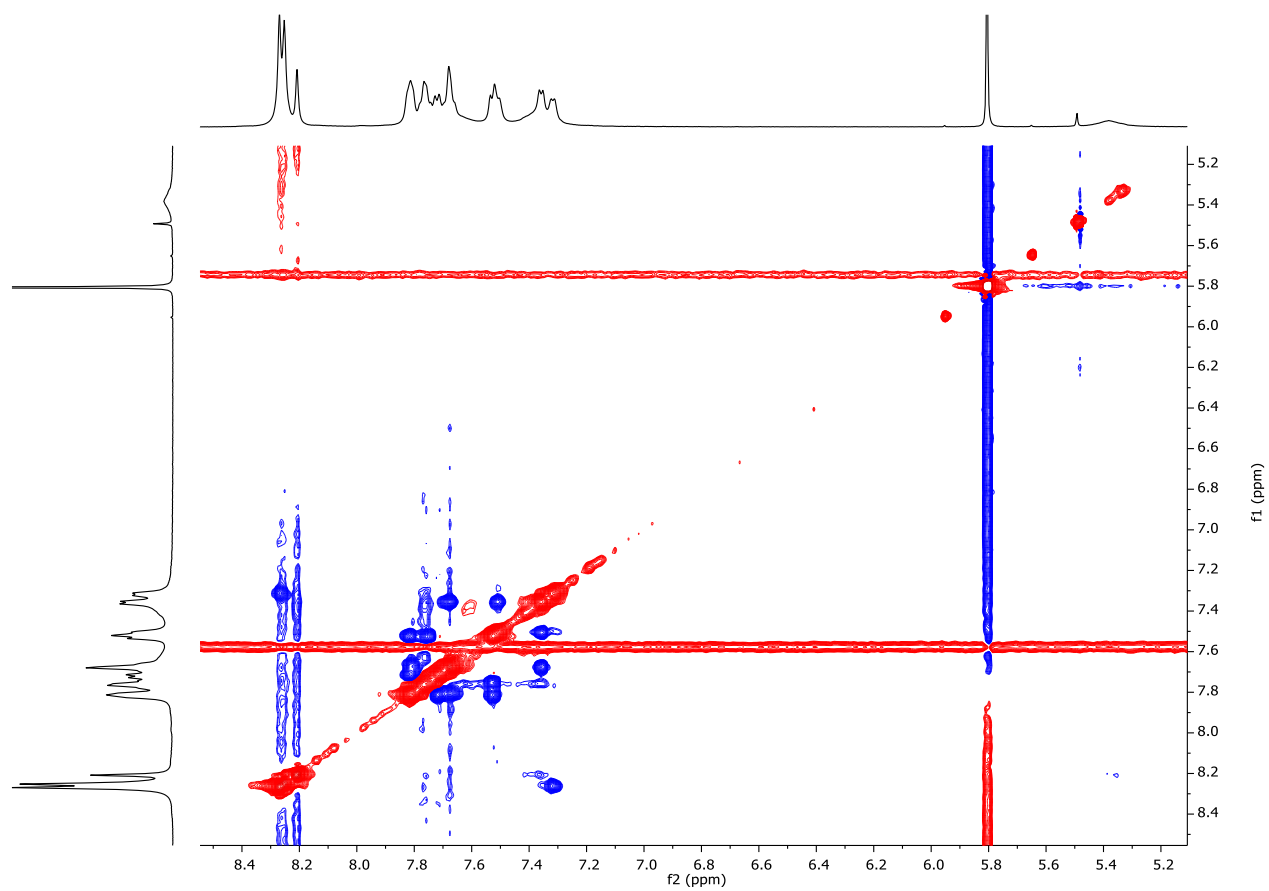


**Figure S61.** Aromatic region of the  $^1\text{H}$ - $^1\text{H}$  ROESY spectrum of compound **1** (14.1 T,  $\text{THF-}d_8$ , 168 K).

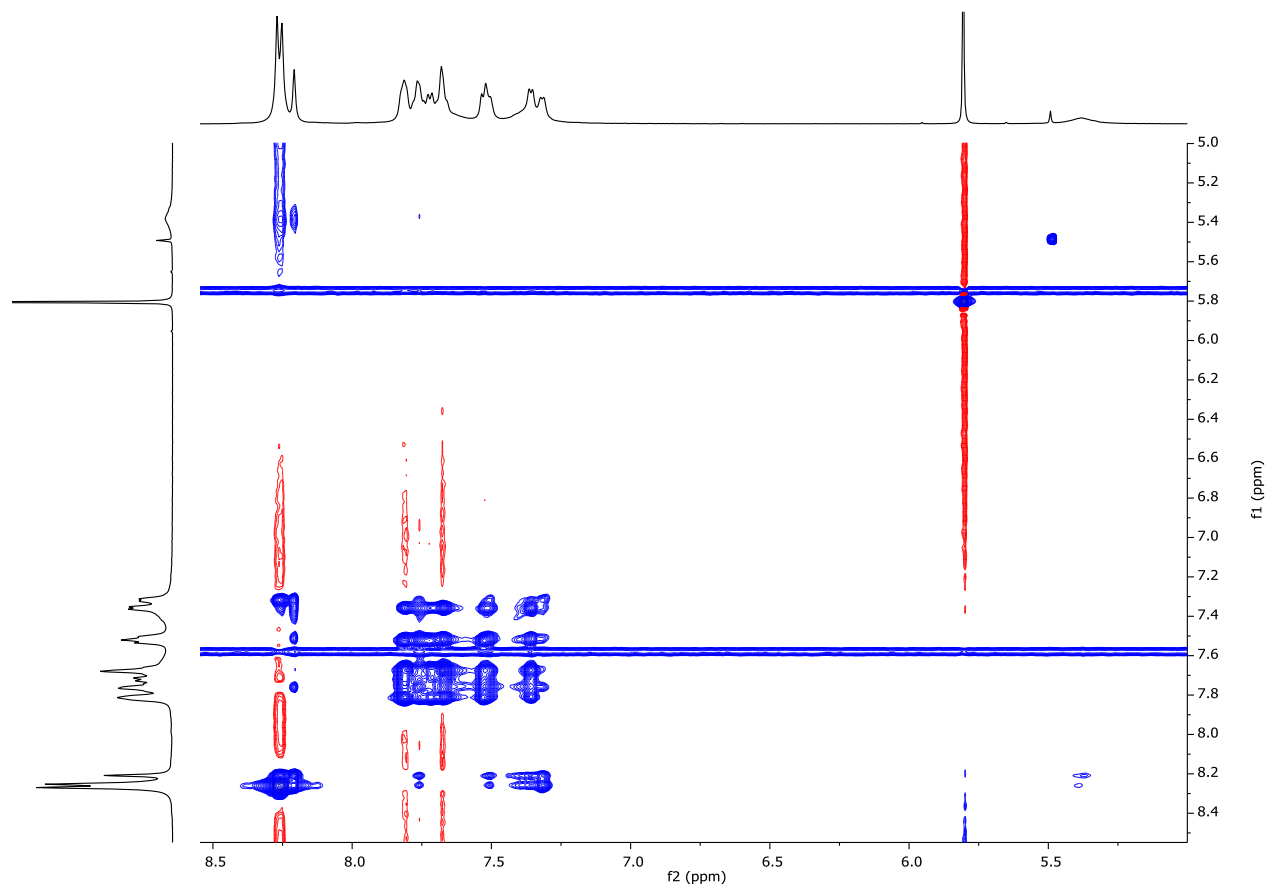


**Figure S62.** Aromatic region of the  $^1\text{H}$ - $^1\text{H}$  NOESY spectrum of compound **1** (14.1 T,  $\text{THF-}d_8$ , 168 K).

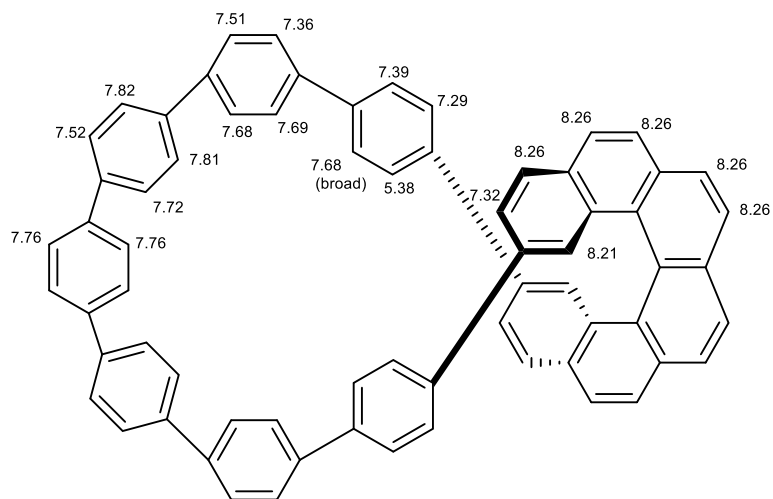


**Figure S63.** Complete assignment of  $^1\text{H}$  chemical shifts of **1** in  $\text{THF-}d_8$  at 168 K.

## A.2.4. HR-MS Spectra

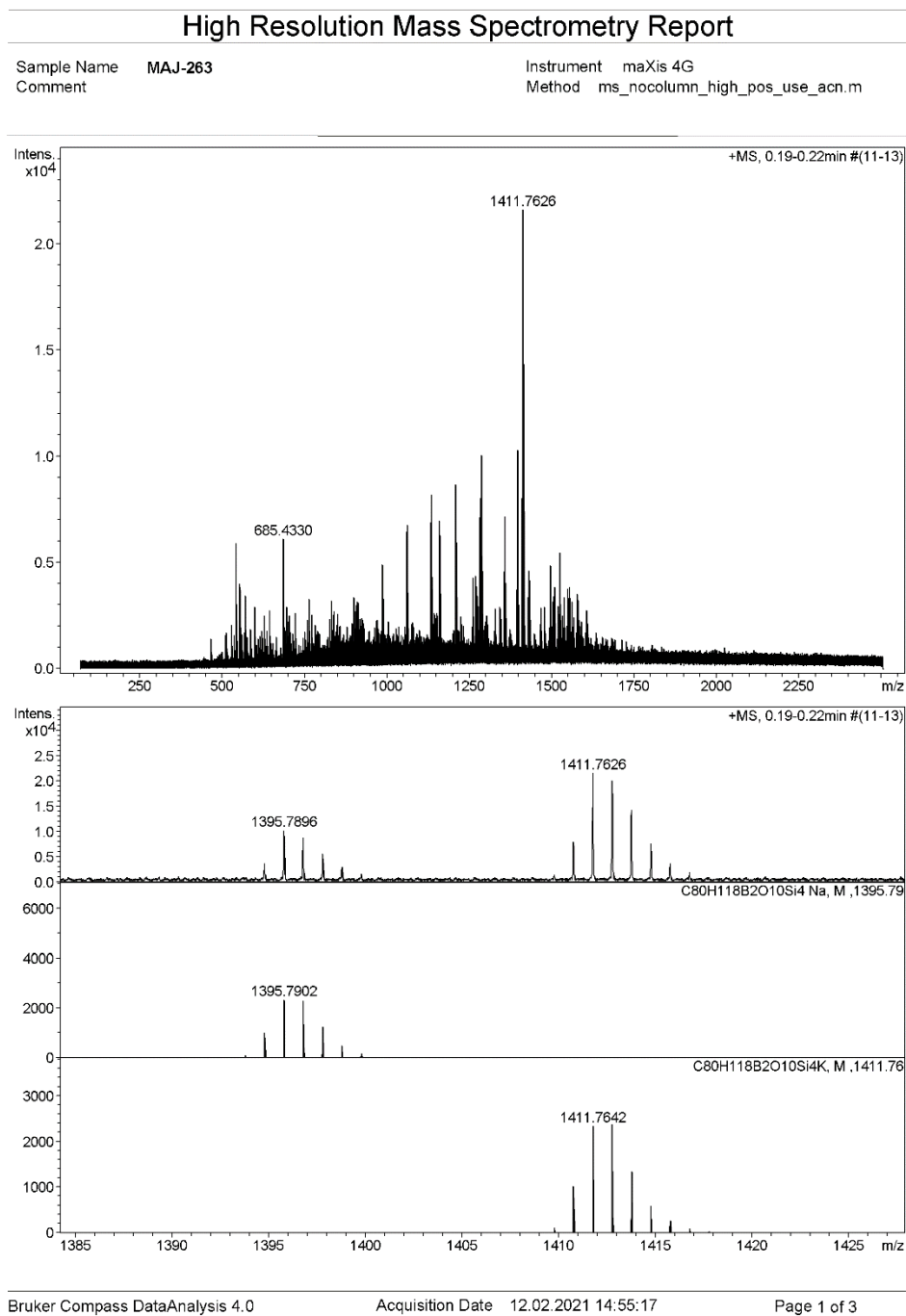
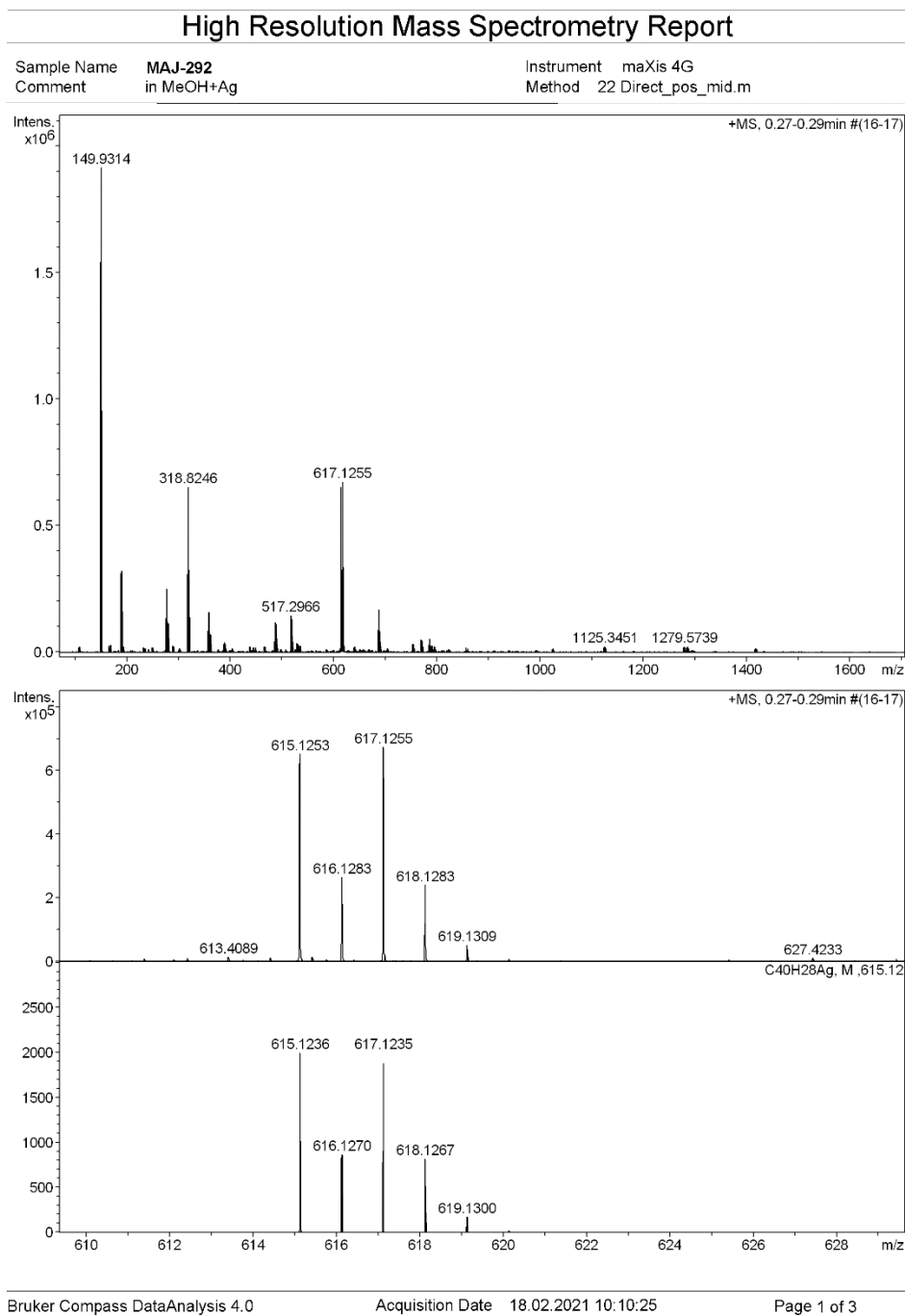
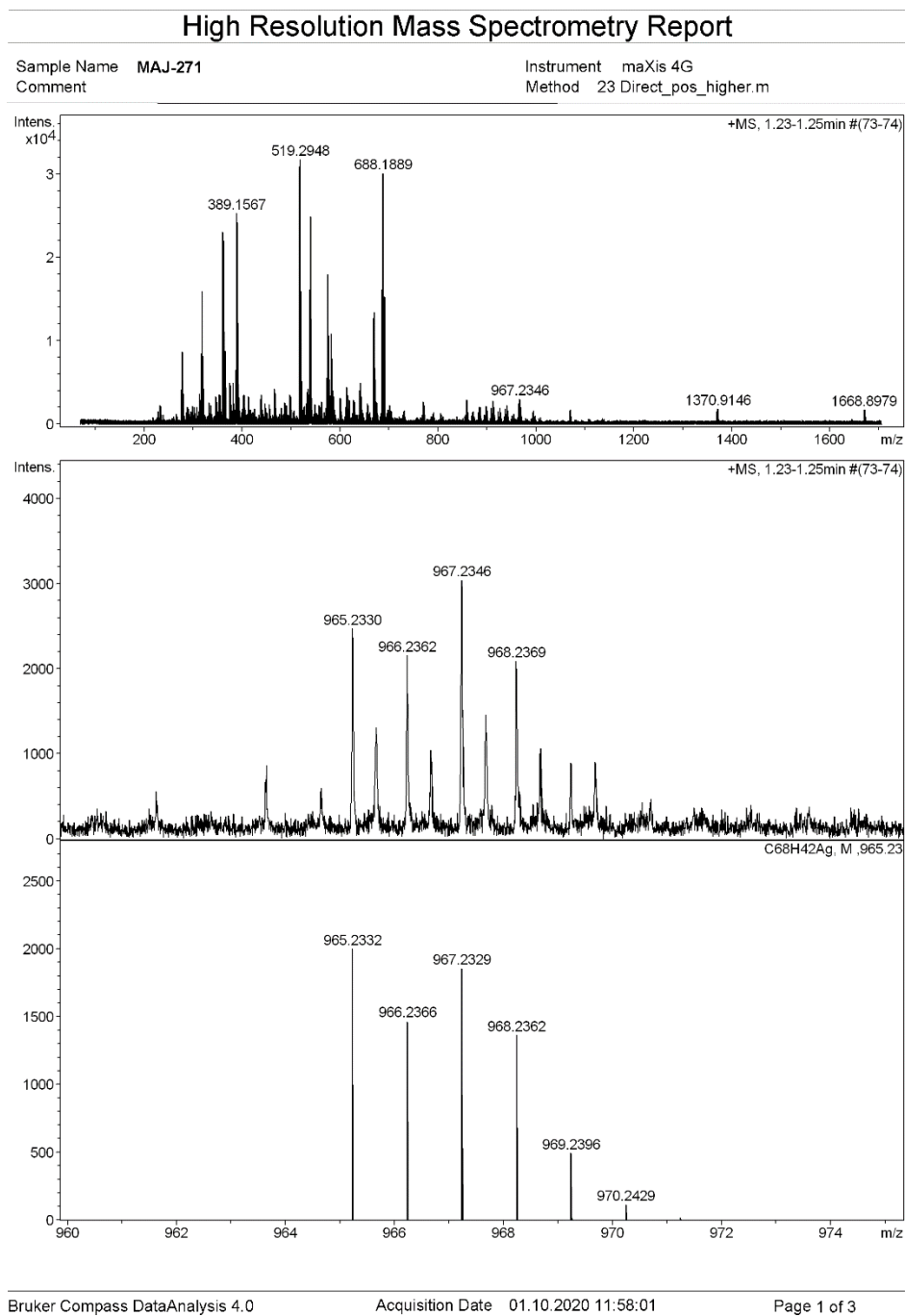


Figure S64. HR-MS (ESI, +) spectrum of 4.



**Figure S65.** HR-MS (ESI, +) spectrum of **5**.





**Figure S66.** HR-MS (ESI, +) spectrum of **1**.

## A.2.5. XYZ Atomic Coordinates

### (P)-1-A<sub>Möbius</sub>

$$E = -2616.69467521$$

C	-2.236439	1.957518	1.606688	C	-1.80279	-2.89271	2.65572	H	0.30562	-4.33721	3.15918
C	-2.137718	2.391783	0.274630	C	-0.89935	-3.13430	0.04225	H	2.14146	-1.99233	-1.49121
C	-1.367595	2.535627	2.547586	H	-2.41318	-1.69659	-0.45847	C	1.29510	2.58992	-2.43945
C	-1.122980	3.259036	-0.120789	C	-0.75241	-3.75371	2.35920	C	2.02035	2.40627	-0.15398
H	-2.803135	1.976556	-0.473450	C	-2.15044	-2.80167	3.68169	C	0.28571	3.46123	-2.05292
C	-0.353280	3.399771	2.151384	C	-0.21880	-3.82960	1.05843	H	1.39625	2.32437	-3.48833
H	-1.451216	2.258231	3.959541	H	-0.15959	-3.15921	-0.97513	C	1.00966	3.28615	0.23113
C	-0.162168	3.723243	0.795726	C	-0.20562	-4.33721	3.15918	H	2.66855	1.97300	0.60215
H	-1.037703	3.523879	-1.171370	C	-2.14146	-1.99233	-1.49121	C	0.07581	3.77986	-0.69857
H	0.362033	3.748374	2.890709	C	-1.29510	2.58992	-2.43945	H	-0.40918	3.82347	-2.80422
C	-2.248626	-1.869760	-1.672820	C	-2.02035	2.40627	-0.15398	H	0.91075	3.54349	1.28232
C	-2.112110	-2.371763	-0.367760	C	-0.28571	3.46123	-2.05292	C	-1.13036	-4.39814	0.81004
H	-1.037703	3.523879	-1.171370	H	-1.39625	2.32437	-3.48833	C	-2.248626	-4.29428	1.81465
H	0.362033	3.748374	2.890709	C	-1.00966	3.28615	0.23113	C	-2.112110	-4.83894	-0.45497
C	-2.248626	-1.869760	-1.672820	H	-2.66855	1.97300	0.60215	C	-2.112110	-4.83894	-0.45497
C	-2.112110	-2.371763	-0.367760	C	-0.07581	3.77986	-0.69857	H	-1.82809	-3.95331	2.80600
H	-1.037703	3.523879	-1.171370	H	0.40918	3.82347	-2.80422	C	-2.91682	-5.00052	-0.74112
H	0.362033	3.748374	2.890709	H	-0.91075	3.54349	1.28232	H	-0.83281	-5.00748	-1.24249
C	-2.248626	-1.869760	-1.672820	C	1.13036	-4.39814	0.81004	C	1.30349	-4.73051	0.22553
C	-2.112110	-2.371763	-0.367760	C	2.10891	-4.29428	1.81465	C	2.10891	-4.29428	1.81465
H	-1.037703	3.523879	-1.171370	C	1.56252	-4.83894	-0.45497	H	-3.21465	-5.28328	-1.74757
H	0.362033	3.748374	2.890709	C	3.45789	-4.45847	1.53137	H	-5.31210	-4.40364	-0.11171
C	-2.248626	-1.869760	-1.672820	H	5.57847	-3.68996	-1.28759	C	-5.31210	-4.40364	-0.11171
C	-2.112110	-2.371763	-0.367760	C	2.91682	-5.00052	-0.74112	H	-5.07847	-3.68996	-1.28759
H	-1.037703	3.523879	-1.171370	C	0.83281	-5.00748	-1.24249	C	-6.34839	-4.47664	0.84000
H	0.362033	3.748374	2.890709	C	3.90349	-4.73051	0.22553	C	-6.70459	-2.87147	-1.39065
C	-2.248626	-1.869760	-1.672820	H	4.18223	-4.23512	2.30850	H	-4.81849	-3.61444	-2.06056
C	-2.112110	-2.371763	-0.367760	H	3.21465	-5.28328	-1.74757	C	-7.47357	-3.66366	0.73952
H	-1.037703	3.523879	-1.171370	C	5.31210	-4.40364	-0.11171	H	-6.22766	-5.10693	1.71718
H	0.362033	3.748374	2.890709	H	5.7847	-3.68996	-1.28759	C	-7.47357	-3.66366	0.73952
C	-2.248626	-1.869760	-1.672820	C	6.34839	-4.47664	0.84000	H	-6.78369	-2.19652	-1.23770
C	-2.112110	-2.371763	-0.367760	C	6.70459	-2.87147	-1.39065	H	-8.20511	-3.66735	1.54367
H	-1.037703	3.523879	-1.171370	H	4.81849	-3.61444	-2.06056	C	-1.22045	-4.38608	-0.30176
H	0.362033	3.748374	2.890709	H	4.1849	-3.61444	-2.06056	H	-4.01814	-4.76476	0.04979
C	-2.248626	-1.869760	-1.672820	C	7.47357	-3.66366	0.73952	H	-3.73734	3.62961	1.86268
C	-2.112110	-2.371763	-0.367760	H	6.22766	-5.10693	1.71718	H	-3.87703	5.96181	-1.74364
H	-1.037703	3.523879	-1.171370	C	7.60942	-3.20229	-1.74757	H	-5.46670	4.44501	-0.00772
H	0.362033	3.748374	2.890709	H	6.78369	-2.19652	-1.23770	C	-5.98449	3.97068	1.30166
C	-2.248626	-1.869760	-1.672820	C	8.20511	-3.66735	1.54367	H	-7.96427	4.24876	1.39388
C	-2.112110	-2.371763	-0.367760	C	1.22045	-4.38608	-0.30176	C	-8.75129	-0.68236	-2.09398
H	-1.037703	3.523879	-1.171370	C	1.87514	3.93133	0.85594	H	-7.92483	2.71734	-0.06695
H	0.362033	3.748374	2.890709	C	1.96016	5.20988	-1.17263	H	-7.33232	2.63962	-2.19334
C	-2.248626	-1.869760	-1.672820	C	3.24189	4.12073	1.03016	H	-9.02646	1.27294	-2.09598
C	-2.112110	-2.371763	-0.367760	H	1.34300	3.29951	1.56084	C	-8.38194	1.38297	-0.20966
H	-1.037703	3.523879	-1.171370	C	3.33024	5.38993	-1.00551	H	-8.24133	0.159601	0.59601
H	0.362033	3.748374	2.890709	H	1.46869	5.65882	-2.03207	H	-8.78745	0.70743	-1.19955
C	-2.248626	-1.869760	-1.672820	C	4.01814	-4.04979	1.54367	C	-8.22002	-0.79117	1.05739
C	-2.112110	-2.371763	-0.367760	H	3.73734	3.62961	1.86268	H	-7.96461	1.06056	2.06917
H	-1.037703	3.523879	-1.171370	C	3.88703	5.96181	-1.74364	H	-7.37161	3.41518	1.10655
H	0.362033	3.748374	2.890709	C	5.46670	4.44501	-0.00772	H	-7.92483	2.71734	-0.06695
C	-2.248626	-1.869760	-1.672820	C	5.98449	3.97068	-1.22549	H	-7.33232	2.63962	-2.19334
C	-2.112110	-2.371763	-0.367760	C	6.22766	4.24876	1.39388	H	-9.02646	1.27294	-2.09598
H	-1.037703	3.523879	-1.171370	C	7.08439	3.12163	-1.25331	H	-8.38194	1.38297	-0.20966
H	0.362033	3.748374	2.890709	H	5.42037	4.12348	-2.14101	H	-8.24133	0.159601	0.59601
C	-2.248626	-1.869760	-1.672820	H	7.37161	3.41518	1.10655	H	-8.78745	0.70743	-1.19955
C	-2.112110	-2.371763	-0.367760	H	5.94277	4.67925	2.08688	C	-8.22002	-0.79117	1.05739
H	-1.037703	3.523879	-1.171370	H	7.2483	2.71734	-0.06695	H	-7.96461	1.06056	2.06917
H	0.362033	3.748374	2.890709	C	7.33232	2.63962	-2.19334	H	-7.37161	3.41518	1.10655
C	-2.248626	-1.869760	-1.672820	H	9.02646	1.27294	-2.09598	H	-7.33232	2.63962	-2.19334
C	-2.112110	-2.371763	-0.367760	C	8.32935	-1.45544	-0.17761	H	-9.02646	1.27294	-2.09598
H	-1.037703	3.523879	-1.171370	H	7.92764	-1.34955	1.94158	C	-8.38194	1.38297	-0.20966
H	0.362033	3.748374	2.890709	H	8.95005	-1.16589	-2.22900	H	-8.24133	0.159601	0.59601
C	-2.248626	-1.869760	-1.672820	C	-1.81266	-0.22773	3.45061	H	-8.78745	0.70743	-1.19955
C	-2.112110	-2.371763	-0.367760	C	-2.75893	-0.02306	2.95876	H	-8.22002	-0.79117	1.05739
H	-1.037703	3.523879	-1.171370	C	-3.25596	-0.94387	2.00322	C	-7.96461	1.06056	2.06917
H	0.362033	3.748374	2.890709	C	-3.45226	1.13152	3.22962	C	-7.37161	3.41518	1.10655
C	-2.248626	-1.869760	-1.672820	H	-3.07615	1.83807	3.96586	H	-7.33232	2.63962	-2.19334
C	-2.112110	-2.371763	-0.367760	C	-4.45350	-0.66797	1.35609	H	-9.02646	1.27294	-2.09598
H	-1.037703	3.523879	-1.171370	H	-4.45352	-1.40505	0.66437	C	-8.38194	1.38297	-0.20966
H	0.362033	3.748374	2.890709	H	-4.63275	-1.43248	2.56376	H	-8.24133	0.159601	0.59601
C	-2.248626	-1.869760	-1.672820	C	-5.18473	0.52704	1.58144	H	-8.78745	0.70743	-1.19955
C	-2.112110	-2.371763	-0.367760	C	-5.37822	2.61650	2.91193	C	-8.22002	-0.79117	1.05739
H	-1.037703	3.523879	-1.171370	H	-4.93730	3.30308	3.63015	H	-7.96461	1.06056	2.06917
H	0.362033	3.748374	2.890709	C	-6.61878	2.83516	2.40397	H	-7.37161	3.41518	1.10655
C	-2.248626	-1.869760	-1.672820	C	-6.44986	0.84695	0.91982	H	-7.33232	2.63962	-2.19334
C	-2.112110	-2.371763	-0.367760	C	-7.20130	1.93101	1.46194	H	-9.02646	1.27294	-2.09598
H	-1.037703	3.523879	-1.171370	H	-7.20646	3.69269	2.72161	C	-8.38194	1.38297	-0.20966
H	0.362033	3.748374	2.890709	C	-5.03693	-0.51634	-1.66488	H	-8.24133	0.159601	0.59601
C	-2.248626	-1.869760	-1.672820	C	-6.38590	-0.74984	-1.15249	H	-8.78745	0.70743	-1.19955
C	-2.112110	-2.371763	-0.367760	C	-5.19714	-2.61741	-2.97882	H	-8.22002	-0.79117	1.05739
H	-1.037703	3.523879	-1.171370	C	-6.50426	-2.74465	-2.63047	C	-7.96461	1.06056	2.06917
H	0.362033	3.748374	2.890709	C	-4.45601	-1.47422	-2.55825	H	-7.37161	3.41518	1.10655
C	-2.248626	-1.869760	-1.672820	C	-7.13679	-1.79042	-1.77401	H	-7.33232	2.63962	-2.19334
C	-2.112110	-2.371763	-0.367760	H	-8.57749	2.10122	1.40661	H	-9.02646	1.27294	-2.09598
H	-1.037703	3.523879	-1.171370	C	-5.03693	-0.51634	-1.66488	H	-8.24133	0.159601	0.59601
H	0.362033	3.748374	2.890709	C	-3.15211	-1.26339	-0.06362	H	-8.78745	0.70743	-1.19955
C	-2.248626	-1.869760	-1.672820	C	-8.49225	0.11823	-0.23721	H	-8.22002	-0.79117	1.05739
C	-2.112110	-2.371763	-0.367760	H	-4.71586	-3.34540	-3.62687	H	-7.96461	1.06056	2.06917
H	-1.037703	3.523879	-1.171370	C	-8.54934	-1.86566	-1.61676	C	-7.37161	3.41518	1.10655
H	0.362033	3.748374	2.890709	C	-2.43114	-0.14349	-2.72807	H	-7.33232	2.63962	-2.19334
C	-2.248626	-1.869760	-1.672820	C	-2.72459	-2.01269	-3.72568	H	-9.02646	1.27294	-2.09598
C	-2.112110	-2.371763	-0.367760	H	-9.22374	1.15850	0.40104	H	-8.38194	1.38297	-0.20966
H	-1.037703	3.523879	-1.171370	H	-7.10386	-3.56733	-3.01166				

H	2.253352	3.247389	-1.500732	H	-2.139279	4.926111	2.399824	H	-5.871780	4.048823	2.132448
C	-0.528806	2.370312	1.878555	C	-4.668652	4.874054	0.140423	C	-7.228428	3.336113	-1.400725
H	-1.252064	-2.363029	1.873855	H	-4.324891	-1.766236	-2.029005	H	-5.685325	4.603469	-2.128193
H	0.553444	4.964459	-1.040744	H	-4.571777	5.146177	2.251459	C	-7.741463	2.590204	-0.317538
C	-0.413082	-4.155827	1.302454	C	-6.057880	4.349004	0.016241	H	-7.702454	2.480218	1.843653
C	-1.488097	-4.252360	2.202939	C	-6.552519	3.564622	1.074535	H	-7.613040	3.153316	-2.403998
C	-0.665838	-4.506610	-0.036446	C	-6.760944	4.268628	-1.203777	C	-0.972475	-4.147369	0.904352
C	-2.781571	-4.490232	1.757351	C	-7.492130	2.565916	0.852074	C	-1.506147	-4.077528	-0.389836
H	-1.318153	-4.060511	3.258720	H	-6.076444	3.606413	2.048674	C	-1.776768	-4.697797	1.914416
C	-1.962252	-4.754205	-0.481580	C	-7.692018	3.258773	-1.422245	C	-2.851924	-0.357199	-0.620602
H	0.148760	-4.477741	-0.756046	H	-6.501428	4.934005	-2.022568	H	-0.897541	-3.671280	-1.193762
C	-3.064657	-4.659287	0.389104	C	-7.974190	2.298521	-0.442232	C	-3.116416	-4.998581	1.678864
H	-3.596014	-4.433422	2.472741	H	-7.707212	1.870303	1.657593	H	-1.370712	-4.805665	2.916851
H	-2.125895	-4.951045	-1.537551	H	-8.124463	3.151903	-2.2423985	C	-3.709831	-4.742214	0.432933
C	-4.452852	-4.435360	-0.090764	C	-0.334053	-4.391666	1.062662	H	-3.268552	-4.143224	-1.600843
C	-4.658651	-3.733811	-1.291950	C	-0.571084	-4.264492	-0.271609	H	-3.730601	-5.398169	2.500127
C	-5.578071	-4.614614	0.737598	C	-1.267864	-4.890471	1.987439	C	-5.166887	-4.461518	0.296255
C	-5.852200	-3.066281	-1.540350	C	-2.086724	-4.441564	-0.624785	C	-5.830675	-3.838997	1.369324
H	-3.828444	-3.575735	-1.973370	H	-0.046841	-3.900437	-1.014652	C	-5.841532	-4.481459	-0.938757
C	-6.770028	-3.940704	0.495857	C	-2.596194	-5.092736	1.628901	C	-6.973730	-3.067821	1.162474
H	-5.496205	-5.236400	1.627772	H	-0.956471	-5.066468	3.013822	H	-5.363571	-3.813511	2.348836
C	-6.893287	-3.059679	-0.594227	C	-3.058049	-4.477348	0.337423	C	-6.983382	-3.711188	-1.145731
H	-5.911622	-2.409067	-2.402773	H	-2.396318	-4.191767	-1.635321	H	-5.418349	-5.038884	-1.773813
H	-7.586512	-4.030659	1.207984	C	-3.299003	-5.439202	2.381466	H	-7.494674	-2.981110	-0.128137
H	-1.816017	-4.925163	0.820523	H	-4.492515	-2.800130	0.047076	H	-7.338939	-4.399476	1.986944
C	-2.718455	4.466918	1.463699	C	-2.880141	-3.954009	1.096117	H	-7.420215	-3.678512	-2.139141
C	-2.321119	0.513148	-0.831335	C	-5.046690	-4.491251	-1.227491	C	-8.202942	-1.605466	-0.409910
C	-4.086281	4.613278	1.261739	C	-6.449282	-3.258234	0.819451	C	-7.846468	-0.901086	-1.573709
C	-2.361329	4.189196	2.451480	C	-4.903400	-3.941652	2.113900	C	-8.886473	-0.874322	0.582564
C	-3.687375	5.190325	-1.027528	C	-6.219428	-3.792345	-1.058839	C	-7.905442	0.485403	-1.618827
H	-1.655896	5.127748	-1.684114	H	-4.517984	-4.979100	-2.042180	H	-7.344195	-1.419474	-2.384556
H	-4.613488	4.850371	-0.022683	C	-6.891357	-3.068002	-0.502373	C	-8.946645	0.516182	0.536593
H	-4.756329	-4.396337	2.088304	C	-6.934610	-2.725920	1.639954	H	-9.282334	-1.389104	-1.454211
H	-4.041034	5.476934	-2.014012	H	-6.574258	-3.745200	-2.532151	C	-8.324528	1.235705	-0.503562
C	-5.977343	4.355982	-0.346387	C	-7.747974	-1.887255	-0.783844	H	-7.446392	0.985372	-2.465130
C	-6.171415	3.716058	-1.584813	C	-7.419445	-1.066085	-1.877134	H	-9.390461	1.049881	1.372935
C	-6.972780	4.145016	0.629095	C	-8.617185	-1.340394	0.181436	H	0.987896	-0.271691	-2.431246
H	-7.125430	2.719505	-1.739046	C	-7.708561	0.293921	-1.863127	C	0.246051	-0.400785	-2.226005
H	-5.455713	3.862429	-2.386933	H	-6.775039	-1.448920	-2.662797	C	2.781266	0.680490	-1.675611
H	-7.930206	-1.165666	0.474371	H	-8.901738	-0.021362	-0.493954	C	2.658912	-2.658912	0.000000
H	-6.938009	4.697174	1.564610	H	-8.988616	-1.967747	0.987536	C	2.098470	-2.429636	-2.900650
H	-7.939397	2.311714	-0.662293	C	-8.333023	0.890375	-0.752283	C	4.122221	0.498738	-1.366931
H	-7.108095	2.134104	-2.652667	H	-7.277360	0.923515	-2.635726	C	4.678915	1.338934	-0.972008
H	-8.614637	2.943207	1.294206	H	-9.481267	0.432163	1.022551	C	0.245056	-1.801193	-2.162140
C	-8.367319	0.890080	-0.623105	H	0.360410	-0.292167	-0.644402	C	4.779956	-0.744172	-1.558957
C	-8.232944	0.186942	0.588394	C	1.415345	-0.306324	-0.899352	C	6.648717	-3.039893	-2.496561
H	-8.503561	0.112864	-1.791512	C	2.212386	0.835810	-0.620847	H	4.042807	-3.831737	-2.920307
H	-7.965552	-1.177593	0.400404	H	-1.951428	-2.725920	1.639954	C	5.991484	-3.184312	-2.347135
H	-8.150957	0.734218	1.522304	H	-1.321359	-2.219610	-1.845732	C	6.176818	-0.984687	-1.205088
H	-8.224311	-1.250335	-1.781996	C	3.565551	0.804757	-0.923958	C	6.784289	-2.150627	-1.757902
H	-8.723187	0.597819	-2.739351	H	4.177768	1.668757	-0.691457	H	6.494456	-0.488970	-2.679380
C	-7.815591	-1.895473	-0.599368	C	3.316515	-1.404955	-1.926298	C	7.020591	-0.087328	-0.420023
H	-7.691261	-1.645159	1.541303	C	4.169484	-0.330671	-1.522154	C	6.601133	0.847878	0.623590
H	-8.221139	-1.798467	-2.720852	C	3.893656	-2.471102	-2.721789	C	5.934106	2.892547	2.537888
C	3.589066	-0.190843	4.391544	C	3.167328	-2.280786	-3.009801	H	7.111396	-2.947394	1.863300
C	0.241513	0.037112	3.524615	C	5.115283	-2.421809	-3.176832	C	5.079569	1.763042	-2.384343
C	4.176905	-0.820009	2.396182	C	5.599698	-0.436622	-1.775706	C	7.491472	1.914577	0.950299
C	5.009033	1.147492	3.528634	C	6.009419	-1.388797	-2.751702	C	8.199798	-2.291195	-1.789644
H	5.046066	1.793496	4.402477	H	5.492671	-3.176645	-3.862194	C	5.401987	0.720855	1.454888
C	5.037529	-0.548675	1.337745	C	6.621626	0.397929	-1.160845	C	3.920756	1.651685	3.187650
H	5.054720	-1.241544	0.513676	C	6.572865	0.101226	0.162287	C	8.426891	-0.150680	-0.690572
C	5.793401	1.942834	2.402895	C	6.567475	2.479271	2.639460	H	5.647175	3.178496	3.231826
C	5.803619	-1.638986	0.474371	H	7.405684	0.820362	-0.627625	H	8.818176	-1.949377	-0.429753
C	6.587561	2.674967	2.437322	C	5.707000	1.304468	2.513799	C	3.065430	0.584754	3.065627
H	6.545531	3.310959	3.317911	C	7.466542	2.099944	0.413029	C	3.716632	2.435084	3.913642
C	7.414129	2.967705	1.399932	C	7.301934	-1.303547	-3.341128	C	8.991812	-1.267536	-1.368245
C	6.586439	1.027188	0.074658	C	5.777179	0.545453	1.299148	H	7.802618	3.771839	2.018264
C	7.467584	2.138524	0.236279	C	4.997663	0.859443	3.612098	C	4.526657	-0.392532	1.414883
H	8.067517	3.835629	1.438892	C	7.817464	0.591042	-1.924567	C	9.297671	0.895593	-0.279800
C	6.628805	0.313642	-1.502833	H	6.523565	3.047449	3.565205	C	3.339717	-0.452622	2.137140
H	5.619111	-1.623398	-1.487776	H	8.497358	-4.298856	-0.218455	H	6.627354	-1.863828	-2.237535
C	3.900978	-2.722145	-2.568890	C	4.210785	-0.263074	3.529600	C	2.186269	0.528527	3.698517
C	5.179105	-2.666661	-3.030083	H	5.034937	1.431764	4.535950	H	9.461437	2.782692	0.706584
C	3.361338	-1.626842	-1.831915	C	8.131786	-0.273378	-3.012119	H	10.344052	0.844175	-0.567849
C	6.046157	-1.587539	-2.670199	H	8.064899	3.700450	1.743404	H	10.070342	-1.302546	-1.498558
H	8.480049	2.421840	-0.723476	C	5.015431	-0.647418	1.291606	H	4.758752	-1.211070	0.753856
C	4.185871	-0.507326	-1.491612	C	8.732342	1.638159	-1.597384				
C	1.996746	-1.623398	-1.487776	C	4.178187	-0.620342	-0.493954				
C	0.7812861	0.479421	-1.993806	H	7.578563	-2.025078	-4.105530				
C	3.253922	-3.562870	-2.806704	H	3.626426	-0.570041	4.390837				
C	7.330478	-1.513206	-3.277492	H	9.153873	3.265653	-0.285327				
C	1.433147	-0.536541	-0.850262	H	9.583405	1.802218	-2.241494				
H	1.388819	-2.493347	-1.702150	H	9.073512	-0.125405	-3.534499				
C	8.703390	1.562164	-1.754219	H	5.034086	-1.263002	0.409117				
H	5.574963	-3.449462	-3.672256								
C	3.558989	0.633140	-0.936700								
C	8.138673	-0.446411	-3.025207								
C	2.200097	0.635612	-0.613649								
H	9.124407	3.282281	-0.563206								
H	0.379213	-0.545527	-0.593512								
H	7.615558	-2.276805	-3.996522								
H	9.072142	-0.310955	-3.565406								
H	9.550576	1.695577	-2.422119								
H	4.139958	1.521199	-0.737168								

**(P)-1-D**Hückel

**E = -2616.68508398**

C	1.486105	2.032807	-0.123843

Appendix

Table of numerical data with multiple columns of values ranging from -4.19361 to 1.700932.

1-TS<sub>enant</sub>

E = -2616.62694778

f<sub>i</sub> = -40.9539

Table of numerical data for 1-TS<sub>enant</sub> with multiple columns of values ranging from -2.398152 to -0.923939.

(P)-1-TS [B → D]

E = -2616.68467694

f<sub>i</sub> = -24.5290

Table of numerical data for (P)-1-TS [B → D] with multiple columns of values ranging from 1.588007 to -0.397334.

(P)-1-TS [A → C]

E = -2616.68246040

f<sub>i</sub> = -24.5290

Table of numerical data for (P)-1-TS [A → C] with multiple columns of values ranging from 3.195031 to -1.763826.

H	4.307697	-2.342312	1.840754	C	-3.386636	1.22362	-3.17554	C	-6.44462	-2.69946	2.64902
H	4.374791	-2.613397	-2.002491	H	-3.00152	1.95573	-3.98012	C	-6.35348	-0.74528	1.12172
H	1.987159	-3.755064	-2.290205	C	-4.40837	-0.63394	-1.38951	C	-7.08480	-1.81541	1.74689
H	1.939884	-1.803038	1.540244	H	-4.81055	-1.39435	-0.73455	H	-7.01120	-3.54554	3.02677
H	-6.060367	3.326463	-3.327969	C	-4.63788	1.46552	-2.57358	C	-7.01648	-0.01906	0.62641
H	-3.676900	2.728667	-3.155164	C	-5.16527	0.53877	-1.63134	C	-6.40637	0.72305	-1.01712
C	-5.701191	2.760613	-2.471629	C	-5.37551	2.62248	-2.95529	C	-5.31869	2.49366	-2.98340
H	-6.211956	-3.784635	-2.842644	H	-4.92333	3.32547	-3.64857	C	-6.58889	2.68057	-2.53128
C	-4.366629	2.434684	-2.369708	C	-6.63868	2.78953	-2.51149	C	-4.58525	1.34371	-2.59203
H	-3.848855	-3.103527	-2.941839	C	-6.47281	0.80738	-1.03142	C	-7.18094	1.77878	-1.61434
H	-8.142380	3.865571	-2.103019	C	-7.22771	1.85848	-1.60302	C	-8.47024	-1.97361	1.52154
C	-5.817817	-3.080680	-2.113523	H	-7.24520	3.62401	-2.85055	C	-5.11736	0.43148	-1.62360
C	-4.493198	-2.705391	-2.163736	C	-7.11561	-0.00011	-0.00001	C	-3.33692	1.08094	-3.18818
C	-7.812807	3.237479	-1.279553	C	-6.47276	-0.80754	1.03142	C	-8.47047	-0.03550	0.08652
C	-6.592086	2.503877	-1.404512	C	-5.37535	-2.62257	2.95530	H	-4.87119	3.18205	-3.69294
H	-8.152774	-4.221845	-1.386000	C	-6.63850	-2.78972	2.51147	C	-8.56166	1.90401	-1.34432
C	-6.640651	-2.694564	-1.030248	C	-4.63780	-1.46555	2.57361	C	-2.62508	-0.04694	0.35060
C	-3.860007	1.877801	-1.168995	C	-7.22759	-1.85870	1.60300	H	-2.94531	1.79754	-3.90488
C	-7.802952	-3.457366	-0.697234	C	-8.62174	1.98165	-1.35964	C	-9.15901	-1.04747	0.78640
C	-3.929894	-1.955096	-1.102529	C	-5.16525	-0.53882	1.63137	H	-7.18555	3.51524	-2.88753
C	-8.428886	3.278682	-0.065614	C	-3.38632	-1.22355	3.17560	C	-4.36652	-0.73909	-1.36114
C	-6.156412	1.676944	-0.321374	C	-8.53693	-0.00017	-0.00002	C	-9.20451	0.96080	-0.58938
C	-4.766897	1.466935	-0.197308	H	-4.92312	-3.32553	3.64857	C	-3.13880	-0.98893	-1.95851
C	-6.172013	-1.691695	-0.122901	H	-8.62159	-1.98139	1.35958	H	-8.98786	-2.79768	2.01453
C	-9.255203	-2.248760	-2.193248	C	-2.10650	-2.06604	2.32188	H	-1.64705	-0.27849	3.23036
C	-4.789279	-1.416131	-0.147673	H	-3.00144	-1.95564	3.88018	H	-9.11383	-2.70994	-1.81782
C	-8.325090	-3.337596	0.554206	C	-9.26980	1.01585	-0.66914	H	-10.28431	0.97506	-0.47804
C	-7.101832	1.349241	0.740765	H	-7.24496	-3.62425	2.85051	H	-10.24127	-1.08675	0.71052
H	-9.095806	-4.019042	0.905701	C	-4.40843	0.63394	1.38956	H	-4.77280	-1.48061	-0.68589
C	-8.069325	2.364677	0.979968	C	-9.26972	-1.01624	0.66907				
C	-7.060612	-1.240337	0.950420	C	-3.17494	0.85968	1.97827				
C	-7.953772	-2.248760	1.411541	H	-9.16054	2.80343	-1.82119				
H	-4.391652	1.067528	0.736102	C	-1.68588	0.04648	3.32188				
H	-7.234952	0.106172	1.508692	H	-9.16033	-2.80382	1.82112				
H	-4.366322	-0.861677	0.676925	H	-10.35185	-1.01640	0.57918				
H	-8.722484	2.443414	2.240984	H	-10.35192	1.01591	-0.57927				
C	-8.555032	-2.141404	2.695979	H	-4.81065	1.39433	0.73460				
H	-9.342100	3.309768	2.458159								
C	-8.006530	0.197351	2.716803								
C	-8.584204	1.430479	-0.89945								
H	-9.102330	-2.993304	3.091712								
C	-8.484771	-0.968133	3.384000								
H	-9.081583	1.470008	4.106992								
H	-8.967263	-0.858180	4.351614								

**(P)-1-B**Möbius  
1st excited state  
 $E = -2615.01570070$

C	-2.29467	-2.00063	-1.63405
C	-2.13339	-2.42966	-0.31207
C	-1.44785	-2.55884	-2.59935
C	-1.08478	-3.26388	0.04441
H	-2.78376	-2.03752	0.46272
C	-0.39836	-3.38564	-2.24262
H	-1.57923	-2.29364	-3.64387
C	-0.14217	-3.69954	-0.99945
H	-0.96408	-3.52910	1.08983
H	-0.29066	-3.71355	-3.01324
C	-2.29481	2.00075	1.63410
C	-2.13353	2.42972	0.31210
C	-1.44804	2.55908	2.59938
-1.08494	3.26395	-0.04442	
H	-2.78387	-2.03752	-0.46268
C	-0.39856	-3.38589	2.24262
H	-1.57943	-2.29395	3.64392
C	-0.14235	3.69970	0.89942
H	-0.96423	3.52910	-1.08986
H	0.29041	3.71388	3.01323
C	1.17263	-4.24686	-0.51431
C	1.99881	-4.93457	-1.42228
C	1.75130	-3.89121	-0.71407
C	3.35321	-5.07941	-1.19858
H	1.57717	-5.32118	-2.34479
C	3.10286	-4.04432	0.94685
H	1.15654	-3.36943	1.45571
C	3.96882	-4.54776	-0.04512
H	3.95805	-5.57361	-1.95218
C	3.51674	-3.63936	1.86085
C	5.39559	-4.06386	0.24328
C	6.02846	-3.90758	1.24958
C	6.15240	-4.04864	-1.14335
C	7.16984	-3.14822	1.26871
H	5.56893	-4.18509	2.19283
C	7.28875	-3.27955	-1.13328
H	5.76359	-4.38306	-2.09913
C	7.78570	-2.65483	0.06220
H	7.56473	-2.83338	2.22770
H	7.76715	-3.05556	-2.07960
C	1.17245	4.24699	0.51427
C	1.75112	3.89129	-0.71410
C	1.99863	4.93470	1.42223
C	3.10268	4.04436	-0.94687
H	1.15636	3.36951	-1.45573
C	3.35304	-5.07951	-1.19854
H	1.57700	-5.32133	-2.34473
C	3.96865	-4.54781	0.04510
H	3.51657	-3.63996	-1.86084
H	3.95789	-5.57372	1.95212
C	5.39542	-4.26386	-0.03329
C	6.15217	-4.04857	1.14335
C	6.02831	-3.90762	-1.24958
H	7.28852	-3.27947	-1.13327
H	5.76332	-4.38290	2.09914
C	7.16969	-3.14825	-1.26872
H	5.56880	-4.18516	-2.19284
C	7.75053	-2.65483	-0.06222
H	7.76684	-3.05536	2.07961
H	7.56459	-2.83347	-2.22772
H	8.47266	-1.41956	-0.03594
C	8.69774	-0.65111	-1.22339
C	8.70285	-0.71322	-1.18901
C	8.70288	-0.71315	-1.18899
H	8.77070	-1.14837	-2.18444
C	8.69781	-0.65105	1.22341
H	8.77432	-1.25647	2.12453
C	8.47276	-1.41951	0.03597
H	8.77432	-1.25641	-2.12451
H	8.77086	-1.14831	-2.18445
H	-1.68575	-0.04630	-3.32178
C	-2.66600	0.10104	-2.88254
C	-3.17485	-0.85959	-1.97820

**(P)-1-B**Möbius  
2nd excited state  
 $E = -2615.02781455$

C	-2.25360	2.19450	1.55278
C	-2.12921	2.58741	0.21627
C	-1.40918	2.80671	2.48624
C	-1.10802	3.43751	-0.18440
H	-2.78103	2.15245	-0.53443
C	-0.38770	3.65039	2.08485
H	-1.51510	2.56855	3.54008
C	-0.16444	3.92405	0.72965
C	-1.00479	3.67084	-1.23975
H	0.30923	4.02135	2.82906
C	-2.27805	-2.14569	-1.61511
C	-2.13051	-2.59425	-0.29855
C	-1.44155	-2.71120	-2.58427
C	-1.10097	-3.45825	0.04975
H	-2.77313	-2.19647	0.48057
C	-0.40884	-3.56284	-2.23378
H	-1.56487	-2.43246	-3.62603
C	-0.16737	-3.90043	-0.89643
H	-0.98670	-3.73903	1.09206
H	0.27791	-3.89402	-3.00517
C	1.14780	4.46560	0.30500
C	1.94449	5.27089	1.13273
C	1.74874	3.96208	-0.85440
C	3.30639	5.40582	0.91175
H	1.50220	5.75316	1.99931
C	3.10686	4.09645	-1.07640
H	1.17255	3.33793	-1.52885
C	3.94087	4.73885	-0.14874
H	3.89574	5.89954	1.61264
C	3.54445	3.56759	-1.91533
H	5.39377	4.42424	-2.23378
C	6.02499	3.93876	-1.31240
C	6.08250	4.27631	1.04991
H	7.12678	3.11014	-1.22084
H	5.59025	4.12269	-2.28962
C	7.19572	3.46211	1.14059
H	5.67077	4.69303	1.96320
C	7.65432	2.73087	0.02823
H	7.49195	2.63829	-2.25076
C	7.64116	3.30108	2.11657
C	1.14807	-4.47177	-0.51622
C	1.74333	-4.09345	0.69245
C	1.94939	-5.18164	-1.42286
C	3.10245	-4.24982	0.90424
H	1.16427	-3.54694	1.42883
C	3.31276	-5.32687	-1.21874
H	1.51143	-5.57315	-3.35755
C	3.93683	-4.78003	-0.08863
C	3.54435	-3.81906	1.79652
H	3.91302	-5.81767	-1.97933
C	5.37599	-4.44457	-0.04120
C	5.99208	-3.95819	-1.20247
C	6.07218	-4.26705	1.16524
C	7.09083	-3.12094	-1.13131
H	5.50804	-4.10125	-2.16310
C	7.17870	-3.44053	1.23548
H	5.68980	-4.71793	2.07639
C	7.62997	-2.72980	0.10595
H	7.42431	-2.63629	-2.04189
H	7.64133	-3.27084	2.20235
C	8.29797	-1.42042	0.21951
H	8.13862	-2.67823	1.39889
C	8.76905	-0.70929	-0.90305
C	8.14586	0.70758	1.37884
H	7.83433	-1.16537	2.31479
C	8.77352	0.67200	-0.92450
H	9.04416	-1.24452	-1.80643
C	8.30921	1.42040	0.17671
H	7.84775	-1.22894	2.28072
C	9.05102	1.17705	-1.84440
H	-1.54683	0.30232	3.27424
C	-2.53289	0.11613	2.86416
C	-3.08995	1.03557	1.94624
C	-3.21257	-1.02319	3.20201
H	-2.78682	-1.72488	3.91398
C	-4.33002	0.75738	1.38840

# Appendix

C	5.75177	-0.40921	-1.73774
C	4.06777	-2.39228	-2.89512
C	5.39814	-2.30952	-3.20952
C	3.49324	-1.33844	-2.14121
C	6.25063	-1.36458	-2.70458
C	8.55213	2.40673	-0.23386
C	4.31916	-0.28783	-1.61673
C	2.10201	-1.29953	-1.93204
C	7.99886	-0.59295	-1.71892
C	3.41986	-3.17688	-3.27423
C	7.57465	-1.28463	-3.17843
C	1.51428	-0.24026	-1.29389
H	1.49563	-2.11706	-2.31142
C	8.40044	1.65894	-1.34399
H	5.82252	-3.12399	-3.86548
C	3.67017	-0.81839	-1.02340
C	8.39516	-0.26475	-2.76396
C	2.29215	0.85860	-0.86185
H	9.17904	3.24837	0.04480
H	0.43892	-0.21172	-1.15916
H	7.90872	-2.00123	-3.92273
H	9.37750	-0.12433	-3.20356
H	9.71652	1.86886	-1.94887
H	4.26823	1.65176	-0.67308

## (M)-5

$$E = -2616.69431404$$

H	-0.36059	-2.63916	3.06567
C	-0.16126	-1.63804	2.69499
C	-1.10052	-1.00966	1.83937
C	-0.99537	-0.98527	3.05399
H	1.69894	-1.45539	3.73720
C	-0.80060	0.24889	1.33211
H	-1.54083	0.74340	0.71760
C	1.29699	0.30594	2.55686
C	0.40829	0.92320	1.62084
C	2.45029	1.01017	3.01796
H	3.12769	-0.51297	3.70789
C	2.64617	2.30843	2.65930
C	-0.73964	2.23642	1.07880
C	1.77200	2.96327	1.73412
H	3.47206	2.87991	3.07557
C	0.01950	2.89577	-0.00072
C	-0.70993	2.24578	-1.07969
C	-2.43806	1.04208	-3.01747
C	-2.61556	2.34330	-2.65991
C	-1.29467	0.32208	-2.55602
C	-1.73205	2.98654	-1.73547
C	1.91152	4.36501	1.52220
C	-0.39715	0.92760	-1.62072
C	-1.01141	-0.97369	-3.05203
C	0.02956	4.32529	-0.00129
H	-3.12253	0.55389	-3.70684
C	-1.85178	-4.39028	-1.52469
C	0.13611	-1.64230	-2.69289
H	-1.72180	-1.43453	-3.73451
C	1.00030	5.03619	0.76095
H	-3.43339	2.92600	-3.07650
C	0.80217	0.23659	-1.33169
C	-0.93111	5.04918	-0.76406
C	1.08438	-1.02635	-1.83824
H	2.70117	4.89693	2.04662
H	0.32109	-2.64648	-3.06270
H	-2.63393	4.93287	-2.04944
H	-0.93732	6.13407	-0.69517
H	1.02179	6.12083	0.69119
H	1.54935	0.72092	-0.71746
H	2.36167	-1.06062	0.56191
C	-2.89302	-1.61915	-0.20071
C	4.08101	-2.26686	0.12590
H	4.47031	-2.18355	1.13862
H	4.47031	-2.18355	1.13862
C	-0.39715	0.92760	-1.62072
C	-1.01141	-0.97369	-3.05203
C	0.02956	4.32529	-0.00129
H	-3.12253	0.55389	-3.70684
C	-1.85178	-4.39028	-1.52469
C	0.13611	-1.64230	-2.69289
H	-1.72180	-1.43453	-3.73451
C	1.00030	5.03619	0.76095
H	-3.43339	2.92600	-3.07650
C	0.80217	0.23659	-1.33169
C	-0.93111	5.04918	-0.76406
C	1.08438	-1.02635	-1.83824
H	2.70117	4.89693	2.04662
H	0.32109	-2.64648	-3.06270
H	-2.63393	4.93287	-2.04944
H	-0.93732	6.13407	-0.69517
H	1.02179	6.12083	0.69119
H	1.54935	0.72092	-0.71746
H	2.36167	-1.06062	0.56191
C	-2.89302	-1.61915	-0.20071
C	4.08101	-2.26686	0.12590
H	4.47031	-2.18355	1.13862
H	4.47031	-2.18355	1.13862
C	-0.39715	0.92760	-1.62072
C	-1.01141	-0.97369	-3.05203
C	0.02956	4.32529	-0.00129
H	-3.12253	0.55389	-3.70684
C	-1.85178	-4.39028	-1.52469
C	0.13611	-1.64230	-2.69289
H	-1.72180	-1.43453	-3.73451
C	1.00030	5.03619	0.76095
H	-3.43339	2.92600	-3.07650
C	0.80217	0.23659	-1.33169
C	-0.93111	5.04918	-0.76406
C	1.08438	-1.02635	-1.83824
H	2.70117	4.89693	2.04662
H	0.32109	-2.64648	-3.06270
H	-2.63393	4.93287	-2.04944
H	-0.93732	6.13407	-0.69517
H	1.02179	6.12083	0.69119
H	1.54935	0.72092	-0.71746
H	2.36167	-1.06062	0.56191
C	-2.89302	-1.61915	-0.20071
C	4.08101	-2.26686	0.12590
H	4.47031	-2.18355	1.13862
H	4.47031	-2.18355	1.13862
C	-0.39715	0.92760	-1.62072
C	-1.01141	-0.97369	-3.05203
C	0.02956	4.32529	-0.00129
H	-3.12253	0.55389	-3.70684
C	-1.85178	-4.39028	-1.52469
C	0.13611	-1.64230	-2.69289
H	-1.72180	-1.43453	-3.73451
C	1.00030	5.03619	0.76095
H	-3.43339	2.92600	-3.07650
C	0.80217	0.23659	-1.33169
C	-0.93111	5.04918	-0.76406
C	1.08438	-1.02635	-1.83824
H	2.70117	4.89693	2.04662
H	0.32109	-2.64648	-3.06270
H	-2.63393	4.93287	-2.04944
H	-0.93732	6.13407	-0.69517
H	1.02179	6.12083	0.69119
H	1.54935	0.72092	-0.71746
H	2.36167	-1.06062	0.56191
C	-2.89302	-1.61915	-0.20071
C	4.08101	-2.26686	0.12590
H	4.47031	-2.18355	1.13862
H	4.47031	-2.18355	1.13862
C	-0.39715	0.92760	-1.62072
C	-1.01141	-0.97369	-3.05203
C	0.02956	4.32529	-0.00129
H	-3.12253	0.55389	-3.70684
C	-1.85178	-4.39028	-1.52469
C	0.13611	-1.64230	-2.69289
H	-1.72180	-1.43453	-3.73451
C	1.00030	5.03619	0.76095
H	-3.43339	2.92600	-3.07650
C	0.80217	0.23659	-1.33169
C	-0.93111	5.04918	-0.76406
C	1.08438	-1.02635	-1.83824
H	2.70117	4.89693	2.04662
H	0.32109	-2.64648	-3.06270
H	-2.63393	4.93287	-2.04944
H	-0.93732	6.13407	-0.69517
H	1.02179	6.12083	0.69119
H	1.54935	0.72092	-0.71746
H	2.36167	-1.06062	0.56191
C	-2.89302	-1.61915	-0.20071
C	4.08101	-2.26686	0.12590
H	4.47031	-2.18355	1.13862
H	4.47031	-2.18355	1.13862
C	-0.39715	0.92760	-1.62072
C	-1.01141	-0.97369	-3.05203
C	0.02956	4.32529	-0.00129
H	-3.12253	0.55389	-3.70684
C	-1.85178	-4.39028	-1.52469
C	0.13611	-1.64230	-2.69289
H	-1.72180	-1.43453	-3.73451
C	1.00030	5.03619	0.76095
H	-3.43339	2.92600	-3.07650
C	0.80217	0.23659	-1.33169
C	-0.93111	5.04918	-0.76406
C	1.08438	-1.02635	-1.83824
H	2.70117	4.89693	2.04662
H	0.32109	-2.64648	-3.06270
H	-2.63393	4.93287	-2.04944
H	-0.93732	6.13407	-0.69517
H	1.02179	6.12083	0.69119
H	1.54935	0.72092	-0.71746
H	2.36167	-1.06062	0.56191
C	-2.89302	-1.61915	-0.20071
C	4.08101	-2.26686	0.12590
H	4.47031	-2.18355	1.13862
H	4.47031	-2.18355	1.13862
C	-0.39715	0.92760	-1.62072
C	-1.01141	-0.97369	-3.05203
C	0.02956	4.32529	-0.00129
H	-3.12253	0.55389	-3.70684
C	-1.85178	-4.39028	-1.52469
C	0.13611	-1.64230	-2.69289
H	-1.72180	-1.43453	-3.73451
C	1.00030	5.03619	0.76095
H	-3.43339	2.92600	-3.07650
C	0.80217	0.23659	-1.33169
C	-0.93111	5.04918	-0.76406
C	1.08438	-1.02635	-1.83824
H	2.70117	4.89693	2.04662
H	0.32109	-2.64648	-3.06270
H	-2.63393	4.93287	-2.04944
H	-0.93732	6.13407	-0.69517
H	1.02179	6.12083	0.69119
H	1.54935	0.72092	-0.71746
H	2.36167	-1.06062	0.56191
C	-2.89302	-1.61915	-0.20071
C	4.08101	-2.26686	0.12590
H	4.47031	-2.18355	1.13862
H	4.47031	-2.18355	1.13862
C	-0.39715	0.92760	-1.62072
C	-1.01141	-0.97369	-3.05203
C	0.02956	4.32529	-0.00129
H	-3.12253	0.55389	-3.70684
C	-1.85178	-4.39028	-1.52469
C	0.13611	-1.64230	-2.69289
H	-1.72180	-1.43453	-3.73451
C	1.00030	5.03619	0.76095
H	-3.43339	2.92600	-3.07650
C	0.80217	0.23659	-1.33169
C	-0.93111	5.04918	-0.76406
C	1.08438	-1.02635	-1.83824
H	2.70117	4.89693	2.04662
H	0.32109	-2.64648	-3.06270
H	-2.63393	4.93287	-2.04944
H	-0.93732	6.13407	-0.69517
H	1.02179	6.12083	0.69119
H	1.54935	0.72092	-0.71746
H	2.36167	-1.06062	0.56191
C	-2.89302	-1.61915	-0.20071
C	4.08101	-2.26686	0.12590
H	4.47031	-2.18355	1.13862
H	4.47031	-2.18355	1.13862
C	-0.39715	0.92760	-1.62072
C	-1.01141	-0.97369	-3.05203
C	0.02956	4.32529	-0.00129
H	-3.12253	0.55389	-3.70684
C	-1.85178	-4.39028	-1.52469
C	0.13611	-1.64230	-2.69289
H	-1.72180	-1.43453	-3.73451
C	1.00030	5.03619	0.76095
H	-3.43339	2.92600	-3.07650
C	0.80217	0.23659	-1.33169
C	-0.93111	5.04918	-0.76406
C	1.08438	-1.02635	-1.83824
H	2.70117	4.89693	2.04662
H	0.32109	-2.64648	-3.06270
H	-2.63393	4.93287	-2.04944
H	-0.93732	6.13407	-0.69517
H	1.02179	6.12083	0.69119
H	1.54935	0.72092	-0.71746
H	2.36167	-1.06062	0.56191
C	-2.89302	-1.61915	-0.20071
C	4.08101	-2.26686	0.12590
H	4.47031	-2.18355	1.13862
H	4.47031	-2.18355	1.13862
C	-0.39715	0.92760	-1.62072
C	-1.01141	-0.97369	-3.05203
C	0.02956	4.32529	-0.00129
H	-3.12253	0.55389	-3.70684
C	-1.85178	-4.39028	-1.52469
C	0.13611	-1.64230	-2.69289
H	-1.72180	-1.43453	-3.73451
C	1.00030	5.03619	0.76095
H	-3.43339	2.92600	-3.07650
C	0.80217	0.23659	-1.33169
C	-0.93111	5.04918	-0.76406
C	1.08438		

C	-3.043624	-2.437165	0.846055
C	-1.409147	-1.543048	+1.209463
C	-1.816013	-2.864910	-1.173483
C	-2.580898	-3.338428	-0.093609
H	-3.742615	-2.754876	1.616224
H	-0.910777	-1.165758	-2.088864
H	-1.555241	-3.530366	-1.991732
H	-2.870195	-4.384461	-0.041648
C	2.311609	3.025466	-0.160275
C	1.201987	3.547680	-0.758455
C	2.339066	1.667509	0.223799
C	1.316143	0.774898	-0.208122
C	3.387451	1.211857	1.091650
C	3.474797	-0.090170	1.474668
C	2.704745	-1.066481	0.767691
C	1.727022	-0.628975	-0.184619
H	3.176590	3.658718	0.052166
H	1.156600	4.593839	-1.049143
H	4.073983	1.956723	1.486602
H	4.213898	-0.418553	2.200769
C	3.043270	-2.437585	0.846057
C	1.408902	-1.543235	-1.209449
C	1.815566	-2.865153	-1.173463
C	2.580399	-3.338782	-0.093595
H	3.742222	-2.755395	-1.616223
H	0.910595	-1.165864	-2.088855
H	1.554679	-3.530579	-1.991699
H	2.869531	-4.384853	-0.041630

## 11,15-diphenyl[6]helicene

$E = -1462.6332933$

H	2.88343	0.14144	3.08529
C	1.88166	-0.02714	2.70141
C	1.25917	0.97011	1.90985
C	1.22178	-1.20135	2.98208
H	1.68714	-1.95158	3.61716
C	-0.00021	0.71243	1.38243
H	-0.48928	1.49476	0.81770
C	-0.07110	-1.46104	2.46597
C	-0.68251	-0.50855	1.59088
C	-0.78286	-2.63783	2.84998
H	-0.29023	-3.36268	3.49331
C	-2.08241	-2.80076	2.47982
C	-1.99795	-0.79451	1.02884
C	-2.73163	-1.86290	1.61498
H	-2.65929	-3.64859	2.84080
C	-2.65265	0.00001	-0.00001
C	-1.99793	0.79453	-1.02886
C	-0.78280	2.63784	-2.84997
C	-2.08235	2.80079	-2.47983
C	-0.07105	1.46105	-2.46596
C	-2.73159	1.86293	-1.61501
C	-4.13436	-1.97851	1.39539
C	-0.68248	0.50856	-1.59088
C	1.22183	1.20135	-2.98205
C	-4.08215	0.00002	-0.00002
H	-0.29014	3.36270	-3.49329
C	-4.13432	1.97856	-1.39542
C	1.88170	0.02713	-2.70138
H	1.68721	1.95158	-3.61712
C	-4.79949	-1.01417	0.69683
H	-2.65921	3.64863	-2.84091
C	-0.00020	-0.71243	-1.38243
C	-4.79947	1.01422	-0.69688
C	1.25918	-0.97012	-1.90983
H	-4.67154	-2.79754	1.86665
H	2.88347	-0.14146	-3.08525
H	-4.67149	2.79749	-1.86669
H	-5.88425	1.02357	-0.62676
H	-5.88427	-1.02351	0.62676
H	-0.48929	-1.49476	-0.81771
H	1.29768	-2.39041	0.40301
C	1.84621	-2.88114	-0.39327
C	2.48172	-4.09673	-0.14762
H	2.40249	-4.55276	0.83600
C	3.22573	-4.71918	-1.15228
C	3.32825	-4.11382	-2.40463
H	3.89869	-4.59293	-3.19818
C	2.69145	-2.89823	-2.65345
H	2.75590	-2.44801	-3.64042
C	1.93808	-2.26318	-1.65175
C	3.22578	4.71913	1.15228
C	3.32826	4.11380	2.40665
H	3.89869	4.59291	3.19821
C	2.69144	2.89821	2.65347
H	2.75587	2.44800	3.64044
C	1.93809	2.26315	1.65176
C	1.84624	2.88111	0.39328
H	1.29773	2.39037	-0.40301
C	2.48177	4.09668	0.14763
H	2.40256	4.55270	-0.83601
H	3.72251	-5.66641	-0.95986
H	3.72257	5.66636	0.95986

## Biphenyl

$E = -463.321368667$

H	0.74791	2.01451	-0.92498
C	0.40532	1.13541	-1.46389
C	0.40469	1.13617	-2.85807
H	0.72982	2.02314	-3.39565
C	0.00000	0.00000	-3.56176
H	0.00000	0.00000	-4.64842
C	-0.40469	-1.13617	-2.85807
H	-0.72982	-2.02314	-3.39565
C	-0.40532	-1.13541	-1.46389
H	-0.74791	-2.01451	-0.92498
C	0.00000	0.00000	-0.74229
H	-0.72982	2.02314	3.39565
C	-0.40469	1.13617	2.85807
C	-0.40532	1.13541	1.46389
H	-0.74791	2.01451	0.92498
C	0.00000	0.00000	0.74229
H	0.72982	-2.02314	-3.39565
C	0.00000	0.00000	3.56176
H	0.00000	0.00000	4.64842

## Terphenyl

$E = -694.389341890$

H	-3.08959	-2.09888	0.46248
C	-3.62799	-1.18069	0.24428
C	-5.02204	-1.18128	0.24343
H	-5.55962	-2.10471	0.44261
C	-5.72580	0.00000	0.00000
H	-6.81243	0.00000	0.00000
C	-5.02204	1.18128	-0.24343
H	-5.55962	2.10471	-0.44261
C	-3.62799	1.18069	-0.24428
H	-3.08958	2.09888	-0.46248
C	-2.90600	0.00000	0.00000
H	1.22845	-1.90502	-0.99315
C	0.69562	-1.07508	-0.53735
C	-0.69562	-1.07508	-0.53735
H	-1.22845	-1.90502	-0.99315
C	-1.42297	0.00000	0.00000
C	-0.69562	1.07508	0.53735
H	-1.22845	1.90502	0.99315
C	0.69562	1.07508	0.53735
H	1.22845	1.90502	0.99315
C	1.42297	0.00000	0.00000
H	5.55962	-2.10471	0.44261
H	3.08959	-2.09888	0.46248
C	5.02204	-1.18128	0.24343
C	3.62799	-1.18069	0.24428
C	5.72580	0.00000	0.00000
H	6.81243	0.00000	0.00000
C	2.90600	0.00000	0.00000
C	5.02204	1.18128	-0.24343
C	3.62799	1.18069	-0.24428
H	5.55962	2.10471	-0.44261
H	3.08958	2.09888	-0.46248





### A.3. SI [5,*n*]Helicene *para*-phenylenes

#### A.3.1. Experimental part

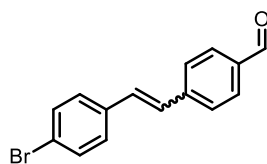
##### General remarks

All commercially available chemicals were purchased from Acros, Alfa Aesar, Apollo Scientific, Fluorochem and Sigma-Aldrich and used without further purification. KOAc was dried in an oven at 130 °C overnight prior to use. Anhydrous solvents were purchased from Acros and stored over molecular sieves (4 Å). Column chromatography was performed on silica gel P60 (40–63 μm) from Silicycle™. Celite® 545 (0.02–0.1 mm) from Supelco was used. Automated flash chromatography was performed using Biotage Isolera One. TLC was performed with silica gel 60 F254 aluminium plates purchased from Merck. High resolution mass spectra (HRMS) were measured on a maX-is™4G instrument from Bruker for HR-ESI-ToF MS. UV-Vis absorption were measured using Jasco V-770 with Jasco ETCR-762 Peltier thermostatted cell holder at 25 °C in 1 cm cuvette. Excitation and emission spectra and quantum yield (using nitrogen purged integrating sphere and 0.5 cm cuvette) were recorded using Jasco FP-8600 with Jasco ETC-815 Peltier thermostatted cell holder at 25 °C in 1 cm cuvette. Circular dichroism was measured using Jasco J-1500 with Jasco PTC-517 Peltier thermostatted cell holder at 25 °C in 1 cm cuvette. Time-correlated single photon counting (TCSPC)-based emission lifetime measurements were performed on a LifeSpec II spectrometer (Edinburgh Instruments) employing a picosecond pulsed diode laser (ca. 60 ps pulse width). Circularly polarized luminescence (CPL) was recorded in an Olis DSM172 spectrophotometer equipped with a xenon lamp of 150 W. NMR experiments were performed on Bruker Avance III NMR spectrometers operating at 400, 500 or 600 MHz proton frequencies. The instruments were equipped with a direct-observe 5 mm BBFO smart probe (400 and 500 MHz), an indirect-detection 5 mm BBI probe (600 MHz). All probes were equipped with actively shielded z-gradients (10 A). The chemical shifts are reported in ppm relative to tetramethylsilane or referenced to residual solvent peak and the J values are given in Hz (±0.1 Hz). Standard Bruker pulse sequences were used, and the data was processed on Topspin 3.6 (Bruker) using twofold zero-filling in the indirect dimension.

##### Synthetic procedures

9,12-Dibromo-[5]helicene **9a** was prepared according to a modified procedure by Moorthy et al.<sup>[18]</sup> Compounds **10b–d** were kindly provided to me by my colleague Remigiusz Kręcijasz. **10b** was prepared according to a procedure by Jasti *et al.*<sup>[19]</sup> **10c** and **10d** were prepared according to a procedure by Jasti *et al.*<sup>[1]</sup>

6



Terephthalaldehyde (804 mg; 5.87 mmol; 1 eq.) and (4-bromobenzyl)-triphenylphosphonium bromide (3.0 g; 5.87 mmol; 1 eq.) were dissolved in DCM (100 mL) and cooled to 0 °C. NaOH (5 g) was dissolved in H<sub>2</sub>O (5 mL) and approximately 4 mL of the resulting viscous NaOH solution was added. The reaction immediately changed color to orange. The bath was removed and the reaction was stirred at r.t. for 3 h upon which the orange color had disappeared. H<sub>2</sub>O (100 mL) was added, the phases were separated and the aqueous phase was extracted with DCM (3 times 30 mL) and dried with Na<sub>2</sub>SO<sub>4</sub>. The crude product was purified using automated flash chromatography (SiO<sub>2</sub>, 25% EtOAc in cyclohexane) affording a mixture of two diastereomers of **6** as a slightly yellow solid (878 mg; 96%).

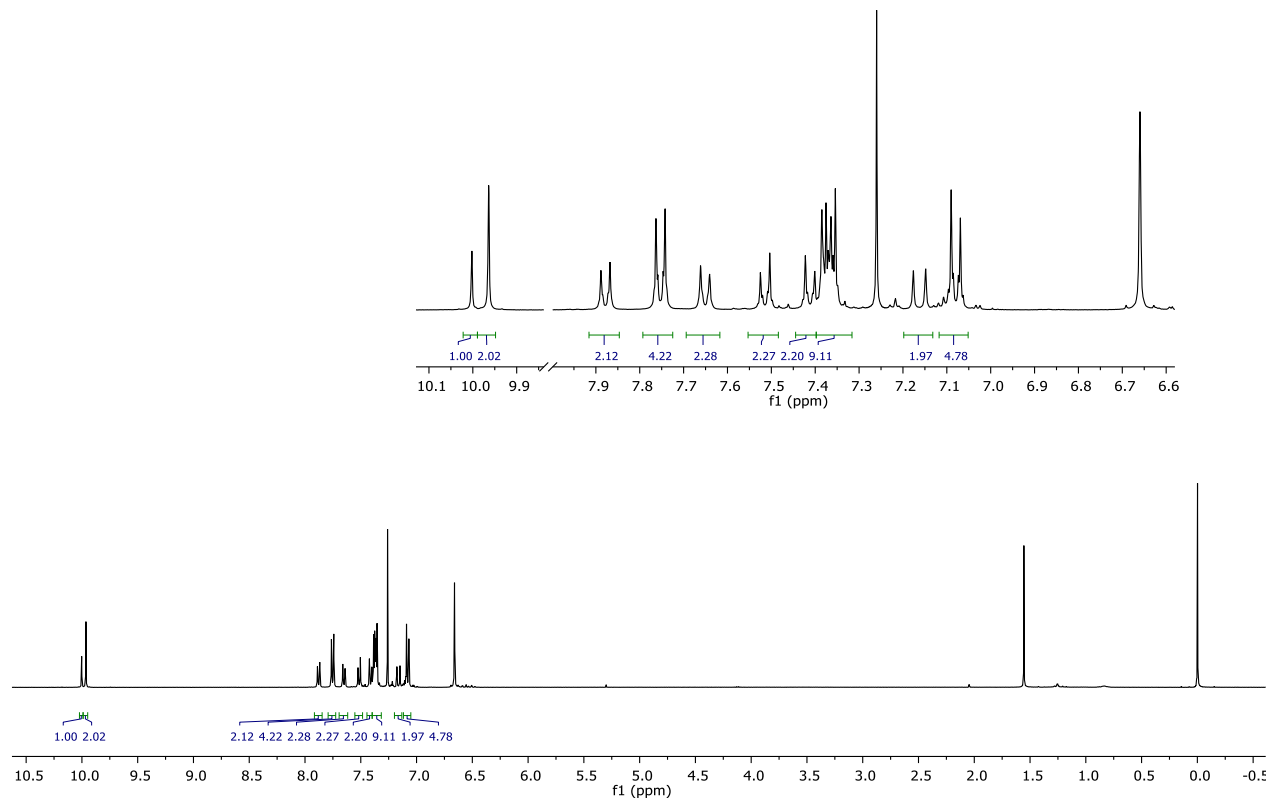
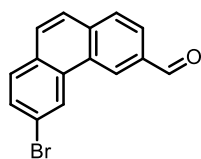


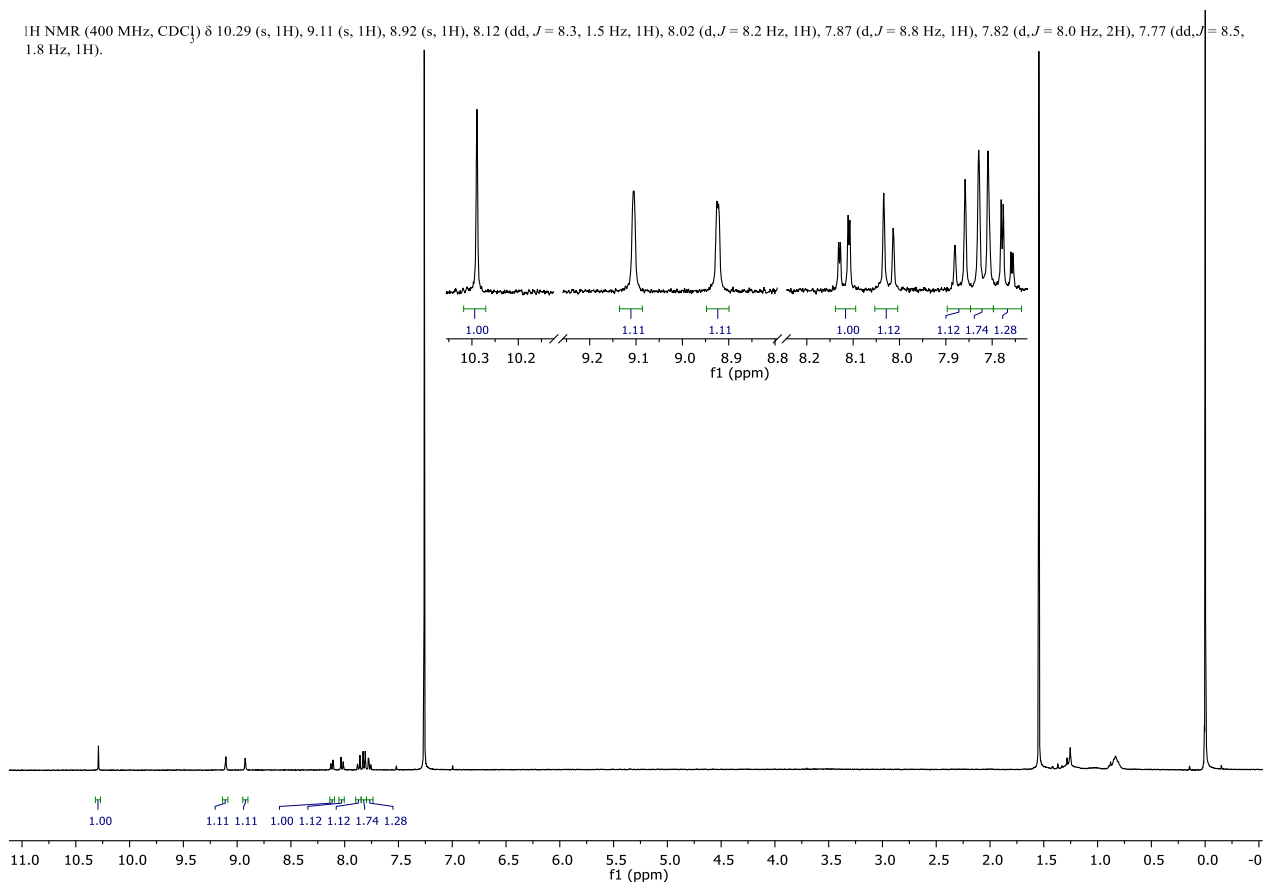
**Figure A11.**  $^1\text{H-NMR}$  (500 MHz,  $\text{CDCl}_3$ , 298 K) spectrum of a mixture of (*E*)-**7** and (*Z*)-**7**.

**7**



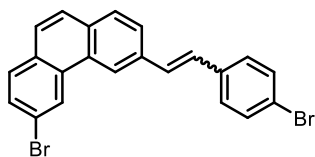
Alkene **6** (582 mg; 2.03 mmol; 1 eq.) was dissolved in toluene (500 mL) and degassed by bubbling with Ar for 1 h. Iodine (514 mg; 2.02 mmol; 1 eq.) and propylene oxide (14.1 mL; 202 mmol; 100 eq.) were added and the reaction was vigorously stirred and irradiated (370 nm LED) for 16 h. The reaction mixture was concentrated under reduced pressure to around  $\frac{1}{4}$  of volume and washed with sat. aq.  $\text{Na}_2\text{S}_2\text{O}_3$  (50 mL),  $\text{H}_2\text{O}$  (50 mL) and dried with  $\text{Na}_2\text{SO}_4$ . Volatiles were evaporated and the crude product was purified by recrystallization from dioxane. Crystals were filtered off and washed with cold dioxane and cyclohexane affording **7** as yellowish fluffy needles (316 mg; 55%).

$^1\text{H-NMR}$  (500 MHz,  $\text{CDCl}_3$ , 298 K,  $\delta/\text{ppm}$ ): 10.29 (s, 1H), 9.11 (s, 1H), 8.92 (s, 1H), 8.12 (dd,  $J = 8.3, 1.5$ , 1H), 8.02 (d,  $J = 8.2$ , 1H), 7.87 (d,  $J = 8.8$ , 1H), 7.82 (d,  $J = 8.0$ , 2H), 7.77 (dd,  $J = 8.5, 1.8$ , 1H).



**FigureA 12.** <sup>1</sup>H-NMR (500 MHz, CDCl<sub>3</sub>, 298 K) spectrum of **7**.

## 8



Aldehyde **7** (599 mg; 2.1 mmol; 1 eq.) and (4-bromobenzyl)-triphenylphosphonium bromide (1.18 g; 2.3 mmol; 1.1 eq.) were dissolved in DCM (60 mL) and cooled to 0 °C. NaOH (5 g) was dissolved in H<sub>2</sub>O (5 mL) and approximately 3.3 mL of the resulting viscous NaOH solution was added.

The reaction immediately changed color to orange. The reaction was stirred for 16 h while warming up to r.t. upon which the orange color had disappeared. H<sub>2</sub>O (50 mL) was added, the phases were separated and the aqueous phase was extracted with DCM (3 times 25 mL) and dried with Na<sub>2</sub>SO<sub>4</sub>. The crude product was purified using automated flash chromatography (SiO<sub>2</sub>, 0 to 100% DCM in cyclohexane) affording a mixture of two diastereomers of **8** as a white solid (878 mg; 96%).

Analytically pure samples of (*E*)- and (*Z*)-diastereomers were obtained during flash chromatography:

### (*E*)-**8**

<sup>1</sup>H-NMR (500 MHz, CDCl<sub>3</sub>, 298 K, δ/ppm): 8.85 (d, *J* = 1.8, 1H), 8.62 (s, 1H), 7.88 (d, *J* = 8.3, 1H), 7.86 – 7.82 (m, 1H), 7.78 – 7.65 (m, 4H), 7.53 (d, *J* = 8.6, 2H), 7.47 (d, *J* = 8.6, 2H), 7.37 (d, *J* = 16.3, 1H), 7.25 (d, *J* = 16.3, 1H).

**(Z)-8**

<sup>1</sup>H-NMR (500 MHz, CDCl<sub>3</sub>, 298 K, δ/ppm): 8.54 (d, *J* = 1.9, 1H), 8.45 (s, 1H), 7.75 – 7.63 (m, 5H), 7.46 (dd, *J* = 8.3, 1.6, 1H), 7.38 (d, *J* = 8.5, 2H), 7.17 (d, *J* = 8.4, 2H), 6.87 (d, *J* = 12.1, 1H), 6.68 (d, *J* = 12.1, 1H).

<sup>1</sup>H NMR (400 MHz, CDCl<sub>3</sub>) δ 8.85 (d, *J* = 1.8 Hz, 1H), 8.62 (s, 1H), 7.88 (d, *J* = 8.3 Hz, 1H), 7.86 – 7.82 (m, 2H), 7.78 – 7.65 (m, 4H), 7.53 (d, *J* = 8.6 Hz, 1H), 7.47 (d, *J* = 8.6 Hz, 1H), 7.37 (d, *J* = 16.3 Hz, 1H), 7.25 (d, *J* = 16.3 Hz, 1H).

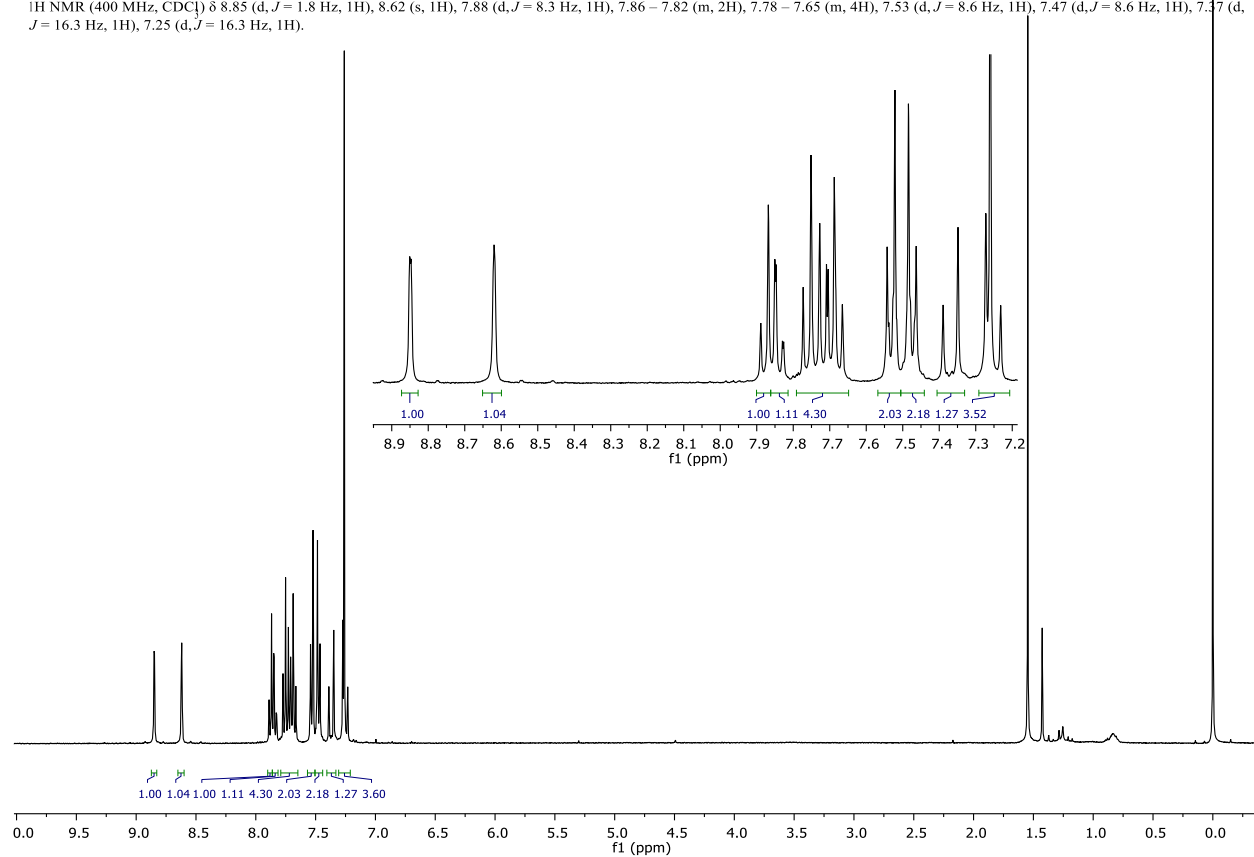


**Figure A13.** <sup>1</sup>H-NMR (500 MHz, CDCl<sub>3</sub>, 298 K) spectrum of (*E*)-8.

$^1\text{H-NMR}$  (400 MHz,  $\text{CDCl}_3$ )  $\delta$  8.54 (d,  $J = 1.9$  Hz, 1H), 8.45 (s, 1H), 7.75 – 7.63 (m, 5H), 7.46 (dd,  $J = 8.3, 1.6$  Hz, 1H), 7.38 (d,  $J = 8.5$  Hz, 2H), 7.17 (d,  $J = 8.4$  Hz, 2H), 6.87 (d,  $J = 12.1$  Hz, 1H), 6.68 (d,  $J = 12.1$  Hz, 1H).

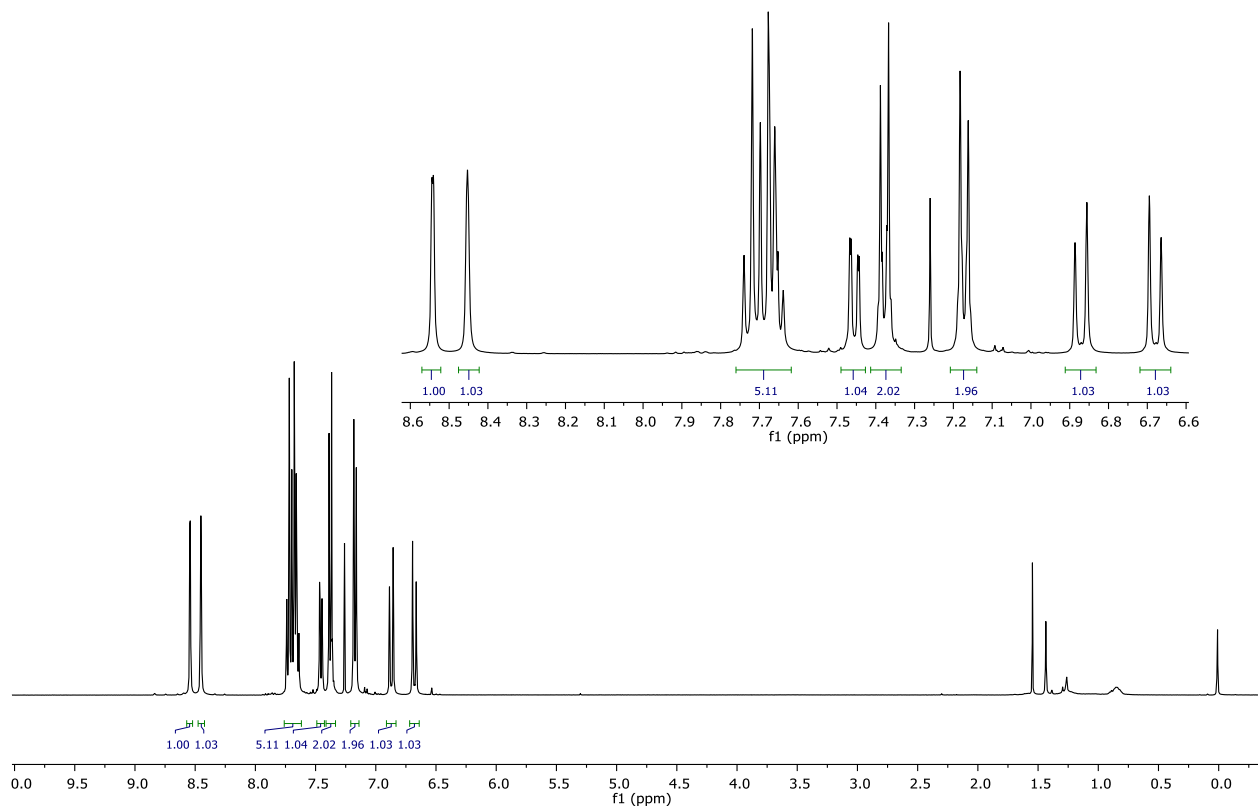
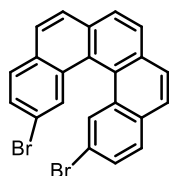


**Figure A14.**  $^1\text{H-NMR}$  (500 MHz,  $\text{CDCl}_3$ , 298 K) spectrum of (Z)-**8**.

### 9a



Alkene **8** (879 mg; 2.01 mmol; 1 eq.) was dissolved in toluene (500 mL) and degassed by bubbling with Ar for 1 h. Iodine (509 mg; 2.01 mmol; 1 eq.) and propylene oxide (11.6 mL; 200 mmol; 100 eq.) were added and the reaction was vigorously stirred and irradiated (370 nm LED) for 3 h. The reaction mixture was concentrated under reduced pressure to around  $\frac{1}{4}$  of volume and washed with sat. aq.  $\text{Na}_2\text{S}_2\text{O}_3$  (50 mL),  $\text{H}_2\text{O}$  (50 mL) and dried with  $\text{Na}_2\text{SO}_4$ . Volatiles were evaporated and the crude product was purified using automated flash chromatography ( $\text{SiO}_2$ , 10% DCM in cyclohexane) affording **9a** as a white solid (825 mg; 95%).

$^1\text{H-NMR}$  (500 MHz,  $\text{CDCl}_3$ , 298 K,  $\delta$ /ppm): 8.69 (d,  $J = 1.9$ , 2H), 7.89 (s, 6H), 7.84 (d,  $J = 8.5$ , 2H), 7.65 (dd,  $J = 8.6, 1.9$  Hz, 2H).

$^1\text{H-NMR}$  (400 MHz,  $\text{CDCl}_3$ )  $\delta$  8.69 (d,  $J = 1.9$  Hz, 1H), 7.89 (s, 3H), 7.84 (d,  $J = 8.5$  Hz, 1H), 7.65 (dd,  $J = 8.6, 1.9$  Hz, 1H).

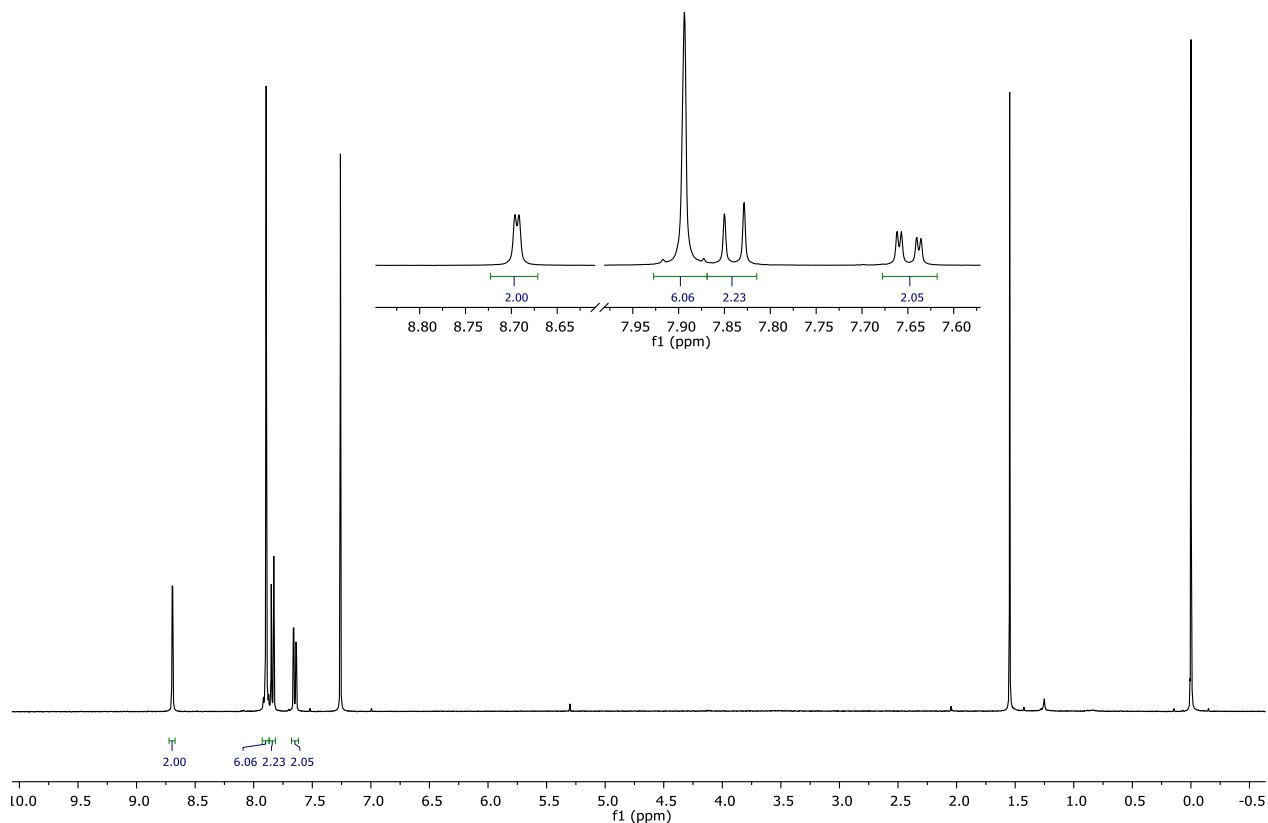
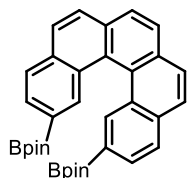


**Figure A15.**  $^1\text{H-NMR}$  (500 MHz,  $\text{CDCl}_3$ , 298 K) spectrum of **9a**.

### 9b

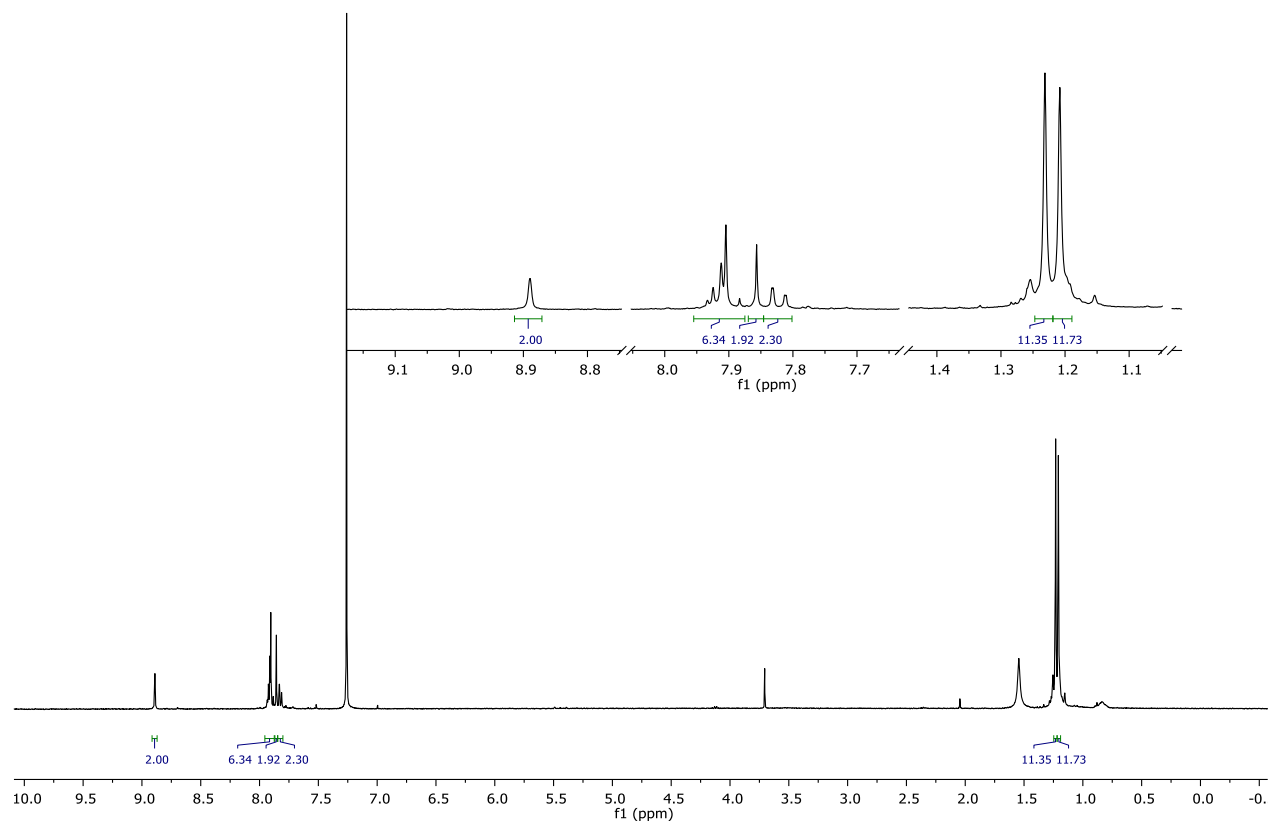


**9a** (488 mg; 1.12 mmol; 1 eq.) was dissolved in THF (35 mL) and cooled to  $-78$  °C. *n*-BuLi (1 mL; 2.46 mmol; 2.2 eq.) was added and the reaction was stirred at  $-78$  °C for 1 h. *i*-PrOBin (0.6 mL; 2.8 mmol; 2.5 eq.) was added and stirring was continued at  $-78$  °C for 1 h after which the bath was removed and the reaction was allowed to warm up to r.t. over 3 h. The reaction was poured into  $\text{H}_2\text{O}$  (50 mL), extracted with EtOAc (3 times 20 mL) and dried with  $\text{Na}_2\text{SO}_4$ . Volatiles were evaporated and the crude product was recrystallized from dioxane. Crystals were filtered off, washed with cold dioxane and dried in vacuo affording **9b** as a white crystalline solid (300 mg; 51%).

$^1\text{H-NMR}$  (500 MHz,  $\text{CDCl}_3$ , 298 K,  $\delta$ /ppm): 8.89 (s, 1H), 7.95 – 7.88 (m, 3H), 7.86 (s, 1H), 7.82 (dd,  $J = 8.0, 1.0$  Hz, 1H), 1.23 (s, 7H), 1.21 (s, 7H).

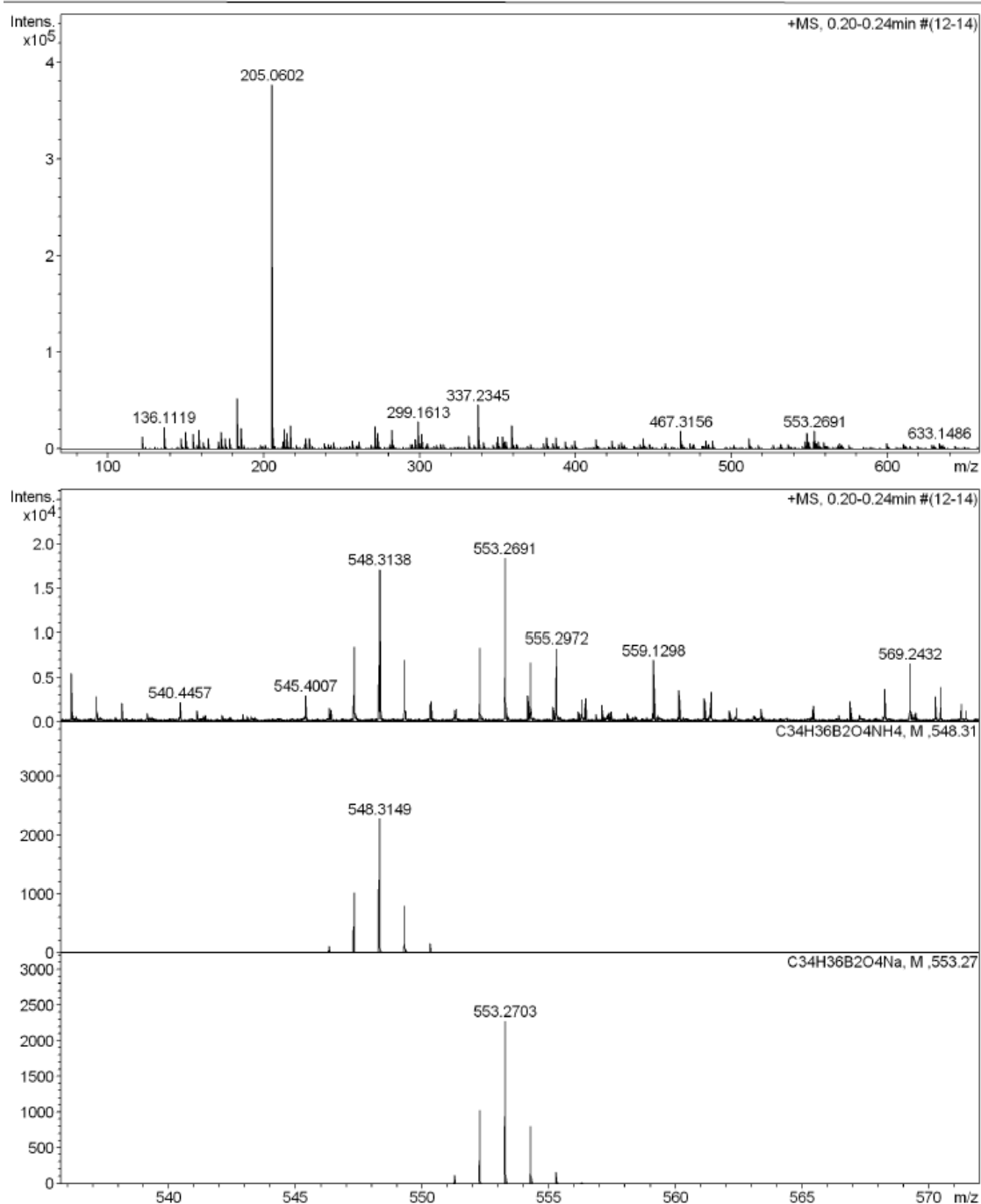
**HRMS (ESI, +):**  $m/z$  calcd. for  $\text{C}_{34}\text{H}_{41}\text{B}_2\text{NO}_4$   $[\text{M}+\text{NH}_4]^+$ : 548.3149, found: 548.3138;  $\text{C}_{34}\text{H}_{36}\text{B}_2\text{NaO}_4$   $[\text{M}+\text{Na}]^+$ : 553.2703, found: 553.2691.

$^1\text{H NMR}$  (400 MHz,  $\text{CDCl}_3$ )  $\delta$  8.89 (s, 1H), 7.95 – 7.88 (m, 3H), 7.86 (s, 1H), 7.82 (dd,  $J = 8.0, 1.0$  Hz, 1H), 1.23 (s, 7H), 1.21 (s, 7H).



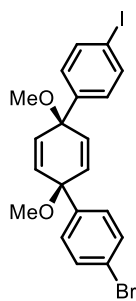
**Figure A16.**  $^1\text{H-NMR}$  (500 MHz,  $\text{CDCl}_3$ , 298 K) spectrum of **9b**.

## High Resolution Mass Spectrometry Report

Sample Name MAJ-333  
CommentInstrument maXis 4G  
Method ms\_nocolumn\_mid\_pos.mFigure A17. HR-MS (ESI, +) spectrum of **9b** [M+NH<sub>4</sub>]<sup>+</sup> and [M+Na]<sup>+</sup>.



## 10a



A round-bottom flask was charged with 1,4-diiodobenzene (522 mg; 1.55 mmol; 1.1 eq.) and dry THF (40 mL) was added. The solution was cooled down to  $-78\text{ }^{\circ}\text{C}$ . *n*-BuLi (2.4 M; 0.65 mL; 1.55 mmol; 1.1 eq.) was added dropwise and the reaction was stirred at  $-78\text{ }^{\circ}\text{C}$  for 1 h. A solution of **1b** (535 mg; 1.41 mmol; 1.00 eq.) in dry THF (5 mL) was added via cannula and the reaction was stirred and left to warm to r.t. over 16 h.  $\text{H}_2\text{O}$  (25 mL) and brine (20 mL) were added and the resulting mixture was extracted with EtOAc (3 times 25 mL). Combined organic phases were washed with brine (20 mL) and dried with  $\text{Na}_2\text{SO}_4$ . Volatiles were evaporated. Resulting solid was dissolved in MeOH (100 mL) and  $\text{K}_2\text{CO}_3$  (1.95 g; 14.1 mmol; 10 eq.) was added and the reaction was stirred at  $70\text{ }^{\circ}\text{C}$  for 16 h. Reaction was quenched with sat. aq.  $\text{NH}_4\text{Cl}$  (50 mL) and the resulting mixture was concentrated under reduced pressure until a precipitation was observed. EtOAc (50 mL) was added to dissolve the precipitate, the phases were separated and the organic phase was extracted with EtOAc (3 times 25 mL), washed with brine (40 mL) and dried with  $\text{Na}_2\text{SO}_4$ . Volatiles were evaporated and the afforded solid was dried in vacuo. Dried solid was dissolved in THF (40 mL) and cooled to  $0\text{ }^{\circ}\text{C}$ . NaH (226 mg; 60% in oil; 5.64 mmol; 4 eq.) was added, stirred for 30 min and MeI (0.88 mL; 14.1 mmol; 10 eq.) was added and the reaction was stirred while warming to r.t. for 16 h. The reaction was quenched with  $\text{H}_2\text{O}$  (50 mL). Brine (50 mL) was added and the resulting mixture was extracted with EtOAc (3 times 30 mL). Combined organic phases were washed with brine (30 mL) and dried with  $\text{Na}_2\text{SO}_4$ . Volatiles evaporated. The crude product was purified using column chromatography (50% DCM in cyclohexane). The product was isolated as a white solid (495 mg; 71%)

$^1\text{H-NMR}$  (400 MHz,  $\text{CDCl}_3$ , 298 K,  $\delta$ /ppm): 7.64 (d,  $J = 8.6$ , 2H), 7.44 (d,  $J = 8.7$ , 2H), 7.24 (d,  $J = 8.6$ , 2H), 7.11 (d,  $J = 8.6$ , 2H), 6.07 (s, 4H), 3.41 (s, 6H).

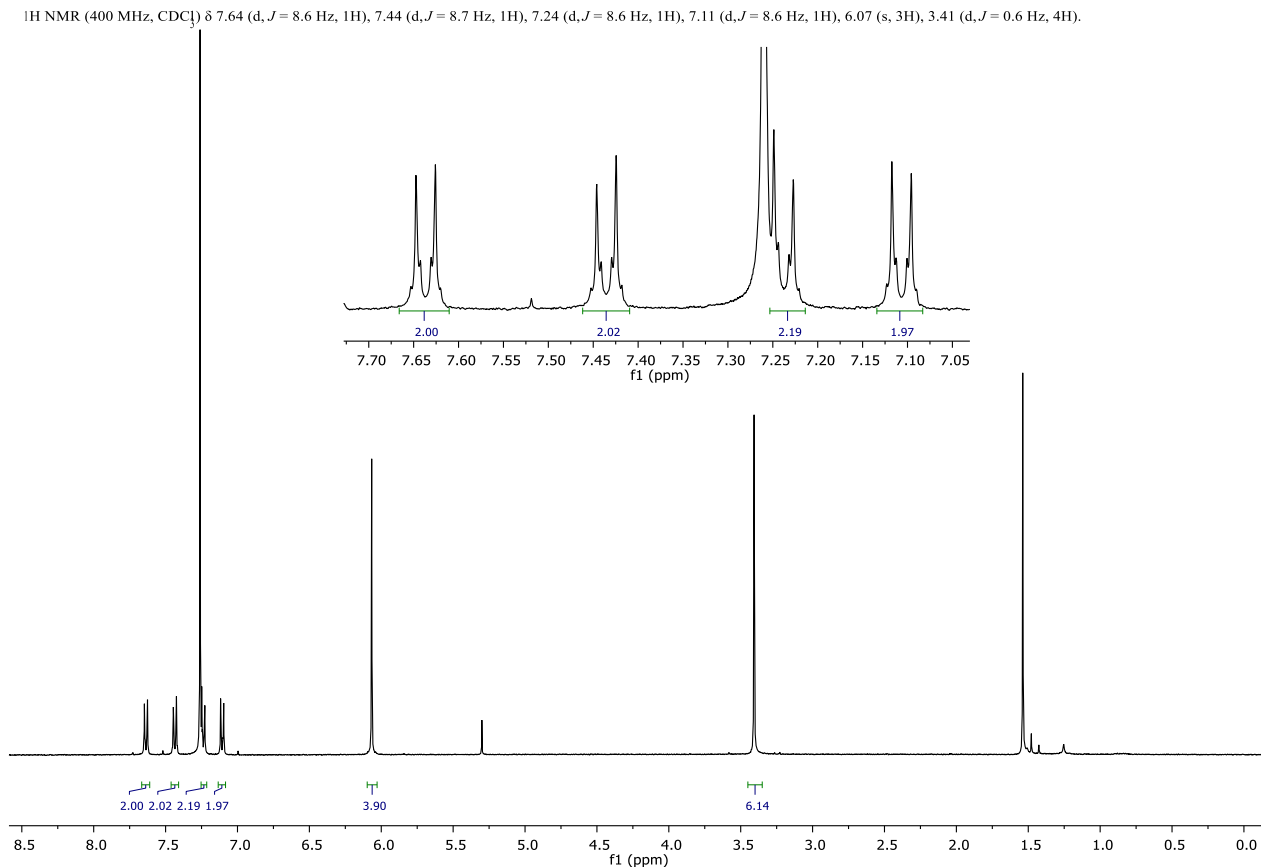
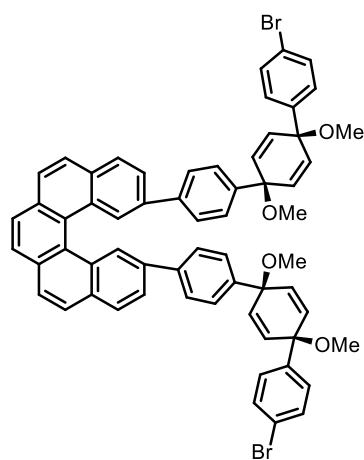


**Figure A18.** <sup>1</sup>H-NMR (500 MHz, CDCl<sub>3</sub>, 298 K) spectrum of **10a**.

### 11a

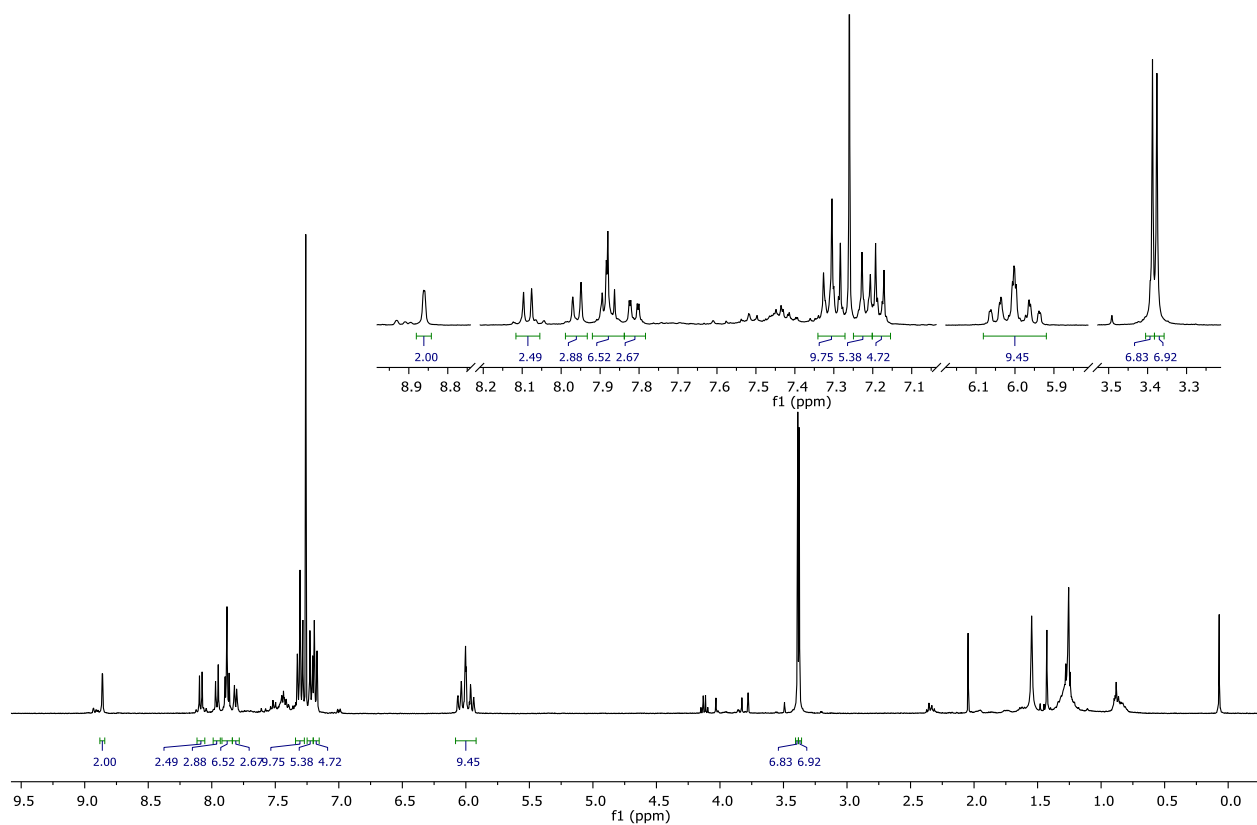


Helicene **9a** (10 mg; 18.9 μmol; 1.00 eq.) and **10a** (20 mg; 39.7 μmol; 2.10 eq.) were added to a Schlenk flask followed by THF (15 mL) and water (1 mL). The solution was degassed by bubbling with Ar for 1 h. KOH (17 mg; 0.3 mmol; 16 eq.) and Pd(PPh<sub>3</sub>)<sub>3</sub>Cl<sub>2</sub> (1 mg; 1.9 μmol; 0.1 eq.) were added and the degassing was further continued for 15 min. The Schlenk flask was sealed and stirred at room temperature for 16 h. The reaction mixture was filtered through celite, the flask and celite were rinsed with EtOAc and the volatiles were evaporated. The crude product was purified using column chromatography (SiO<sub>2</sub>, 10% EtOAc in cyclohexane). The product was isolated as a white solid (5 mg; 26%).

<sup>1</sup>H-NMR (400 MHz, CDCl<sub>3</sub>, 298 K, δ/ppm): 8.86 (d, *J* = 1.7, 2H), 8.09 (d, *J* = 8.4, 2H), 7.96 (d, *J* = 8.4, 2H), 7.91 – 7.85 (m, 4H), 7.81 (dd, *J* = 8.4, 1.8, 2H), 7.30 (t, *J* = 8.6, 8H), 7.22 (d, *J* = 8.4, 4H), 7.18 (d, *J* = 8.6, 4H), 6.08 – 5.92 (m, 8H), 3.39 (s, 6H), 3.38 (s, 6H).

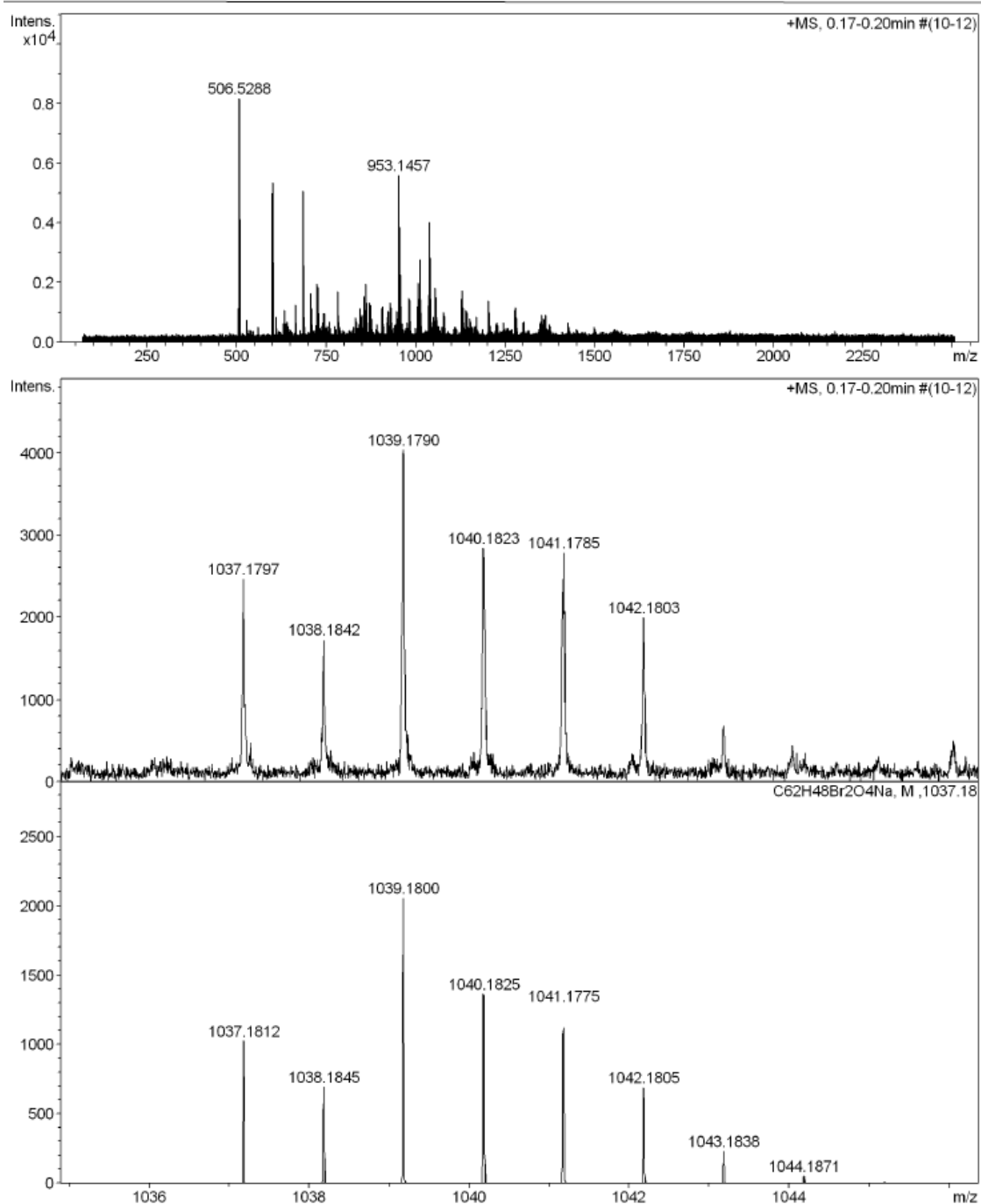
**HRMS (ESI, +):** *m/z* calcd. for C<sub>62</sub>H<sub>48</sub>Br<sub>2</sub>NaO<sub>4</sub> [M+Na]<sup>+</sup>: 1037.1812, found: 1037.1797.

$^1\text{H}$  NMR (400 MHz,  $\text{CDCl}_3$ )  $\delta$  8.86 (d,  $J = 1.7$  Hz, 2H), 8.09 (d,  $J = 8.4$  Hz, 2H), 7.96 (d,  $J = 8.4$  Hz, 2H), 7.91 – 7.85 (m, 4H), 7.81 (dd,  $J = 8.4, 1.8$  Hz, 2H), 7.30 (t,  $J = 8.6$  Hz, 6H), 7.22 (d,  $J = 8.4$  Hz, 3H), 7.18 (d,  $J = 8.6$  Hz, 3H), 6.08 – 5.92 (m, 8H), 3.39 (s, 6H), 3.38 (s, 7H).

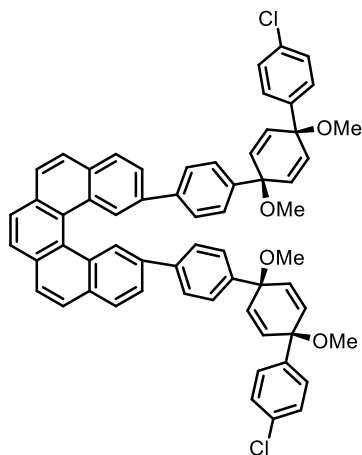


**Figure A19.**  $^1\text{H}$ -NMR (500 MHz,  $\text{CDCl}_3$ , 298 K) spectrum of **11a**.

## High Resolution Mass Spectrometry Report

Sample Name maj-343  
CommentInstrument maXis 4G  
Method ms\_nocolumn\_high\_pos\_use\_acn.mFigure A20. HR-MS (ESI, +) spectrum of **11a** [M+Na]<sup>+</sup>.

## 11b



Helicene **9a** (100 mg; 0.23 mmol; 1.00 eq.) and **10c** (207 mg; 0.46 mmol; 2.00 eq.) were added to a Schlenk flask followed by dioxane (100 mL) and water (10 mL). The solution was degassed by bubbling with Ar for 1 h.  $K_3PO_4$  (389 mg; 1.83 mmol; 8.00 eq.) and SPhos Pd G3 (18 mg; 22.9  $\mu$ mol; 0.1 eq.) were added and the degassing was further continued for 20 min. The Schlenk flask was sealed and stirred at room temperature for 24 h. The reaction mixture was filtered through celite, the flask and celite were rinsed with EtOAc and the volatiles were evaporated. The crude product was purified using column chromatography (10% EtOAc in cyclohexane). The product was isolated as a white solid (170 mg; 80%).

$^1H$ -NMR (400 MHz,  $CDCl_3$ , 298 K,  $\delta$ /ppm): 7.70 (d,  $^3J_{HH} = 8.2$  Hz, 4H), 7.33 (d,  $^3J_{HH} = 8.2$  Hz, 4H), 7.33-7.25 (m, 8H), 6.12 (d,  $^3J_{HH} = 10.2$  Hz, 4H), 5.97 (s, 4H), 5.94 (d,  $^3J_{HH} = 10.2$  Hz, 4H), 3.34 (s, 6H), 1.32 (s, 24H), 1.00-0.90 (m, 36H), 0.71-0.55 (m, 24H).

HRMS (ESI, +):  $m/z$  calcd. for  $C_{62}H_{48}Cl_2NaO_4$   $[M+Na]^+$ : 949.2822, found: 949.2819;  $C_{62}H_{48}Cl_2KO_4$   $[M+K]^+$ : 965.2561, found: 965.2552.

$^1H$  NMR (400 MHz,  $CDCl_3$ )  $\delta$  8.86 (d,  $J = 1.7$  Hz, 0H), 8.07 (d,  $J = 8.4$  Hz, 0H), 7.96 (d,  $J = 8.5$  Hz, 0H), 7.90 – 7.85 (m, 1H), 7.80 (dd,  $J = 8.3, 1.8$  Hz, 0H), 7.31 (d,  $J = 8.5$  Hz, 0H), 7.25 – 7.20 (m, 1H), 7.13 (d,  $J = 8.7$  Hz, 0H), 6.08 – 5.91 (m, 1H), 3.39 (s, 1H), 3.38 (s, 1H).

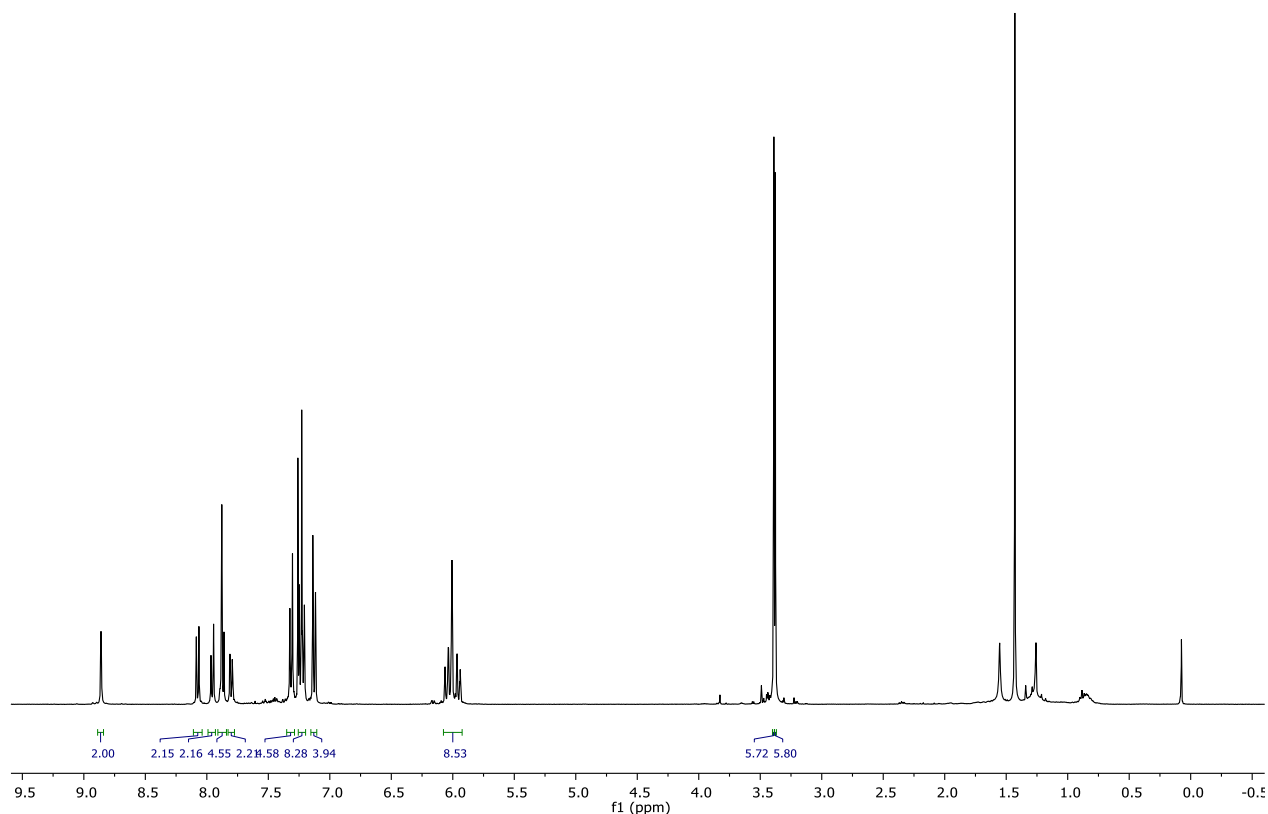
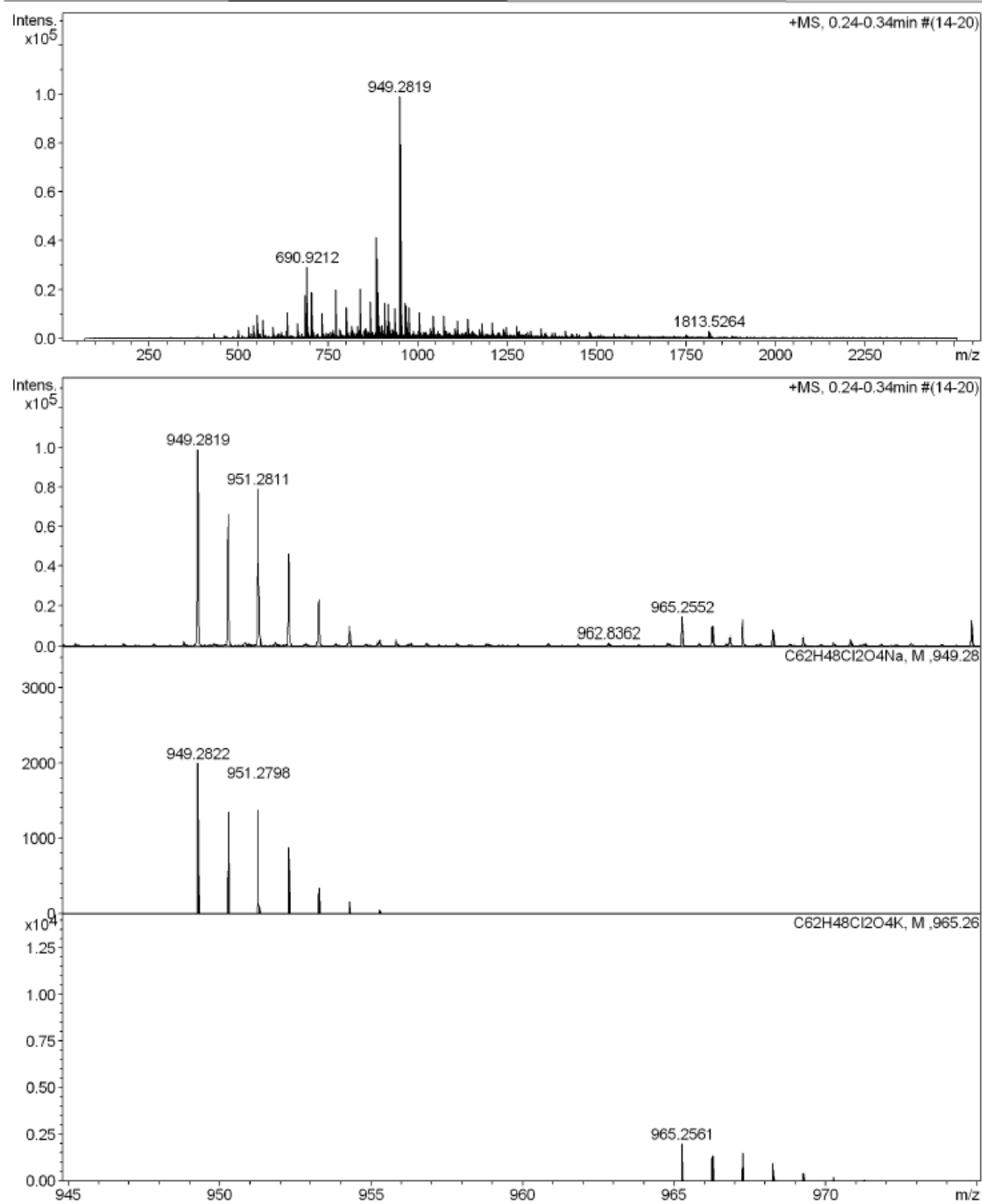
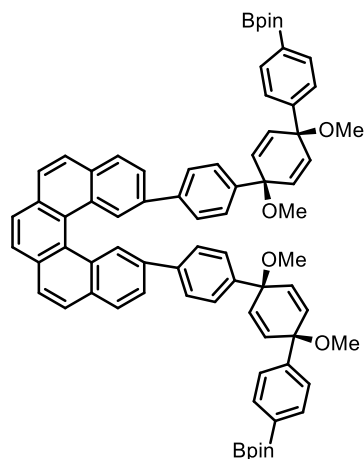


Figure A21.  $^1H$ -NMR (500 MHz,  $CDCl_3$ , 298 K) spectrum of **11b**.

## High Resolution Mass Spectrometry Report

Sample Name maj-344  
CommentInstrument maXis 4G  
Method ms\_nocolumn\_high\_pos\_use\_acn.m**Figure A22.** HR-MS (ESI, +) spectrum of **11b** [M+Na]<sup>+</sup> and [M+K]<sup>+</sup>.

## 11c



KOAc (7 mg; 0.713 mmol; 6.6 eq.) was weighed while still hot into a dry Schlenk flask, the flask was evacuated and placed into an oil bath at 130 °C for 1 h after which it was cooled down to r.t. under Ar. Afterwards, **11b** (10 mg; 10.8  $\mu$ mol; 1.00 eq.), (Bpin)<sub>2</sub> (12 mg; 43  $\mu$ mol; 4 eq.), XPhos (1 mg; 2  $\mu$ mol; 0.2 eq.) and Pd<sub>2</sub>dba<sub>3</sub> (1 mg; 2  $\mu$ mol; 0.2 eq.) were added. The flask was evacuated and filled with Ar 3 times. In a separate dry flask, dioxane was degassed by bubbling with Ar for 1 h. Degassed dioxane (1 mL) was added to dissolve all components. The Schlenk flask was sealed with a glass stopper and placed into an oil bath pre-heated to 100 °C. The reaction was stirred for 16 h at 100 °C. and The reaction mixture was filtered through celite, the flask and celite were rinsed with EtOAc and the volatiles were evaporated. The crude product was precipitated with EtOH, filtered off and washed with EtOH. Crude product was used without further purification.

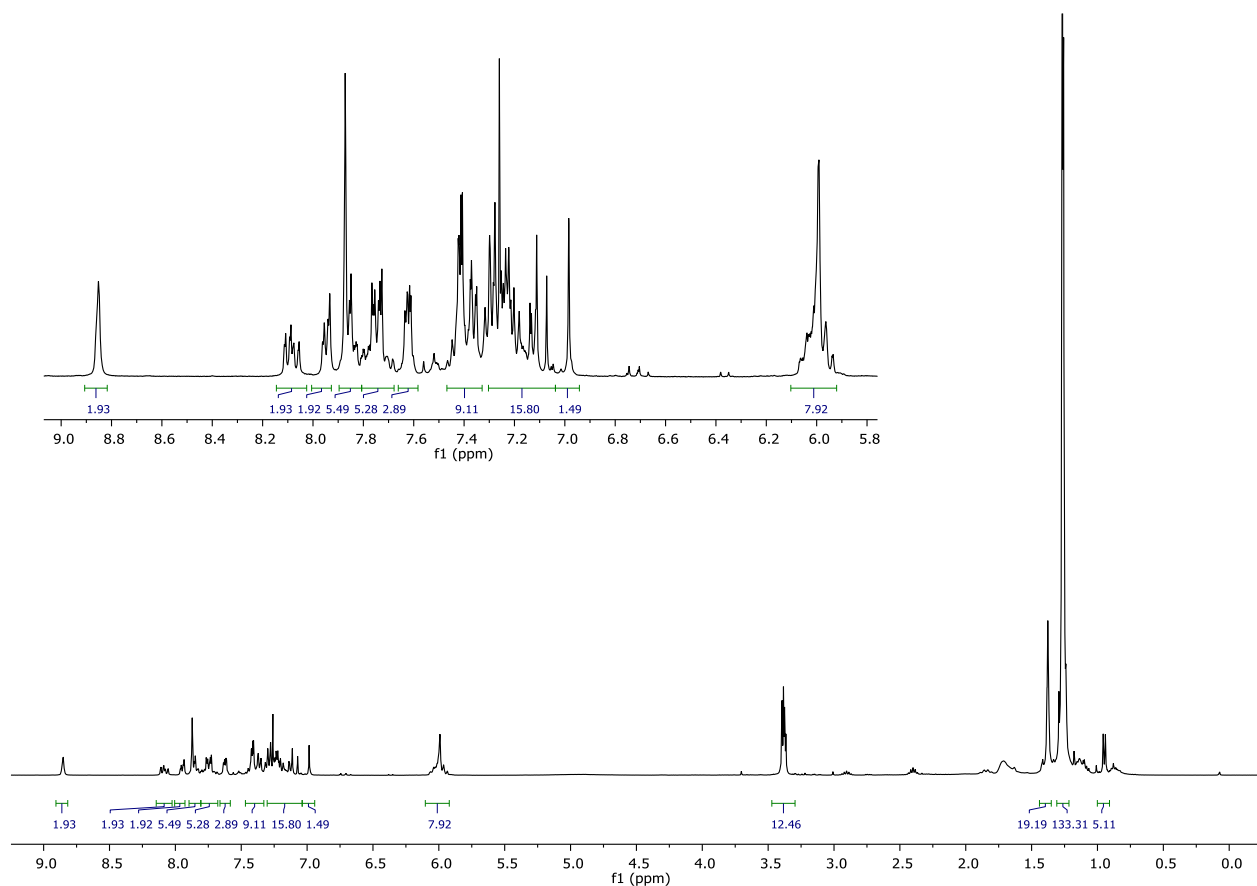
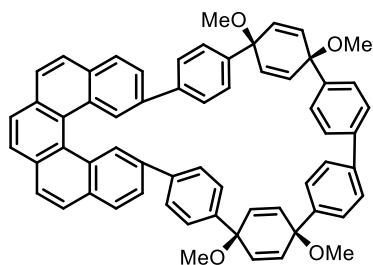


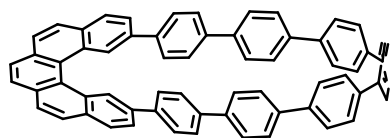
Figure A23. <sup>1</sup>H-NMR (500 MHz, CDCl<sub>3</sub>, 298 K) spectrum of crude **11c**.

12



To a crude **11c**, Pd(PPh<sub>3</sub>)<sub>2</sub>Cl<sub>2</sub> (1 mg; ~0.2 eq.) and B(OH)<sub>3</sub> (3 mg, ~5 eq.) were added. The solids were dissolved in THF (18 mL) and stirred vigorously for 10 min. KF (1 mg; ~2 eq.) was dissolved in H<sub>2</sub>O (1 mL) and added. The reaction was stirred at 40 °C open to air for 16 h. The next day, the mixture was filtered through celite, flask and celite were washed with EtOAc and concentrated to give a yellow-orange solid which was analyzed using MALDI-MS (see Section 4).

## [5,7]HPP

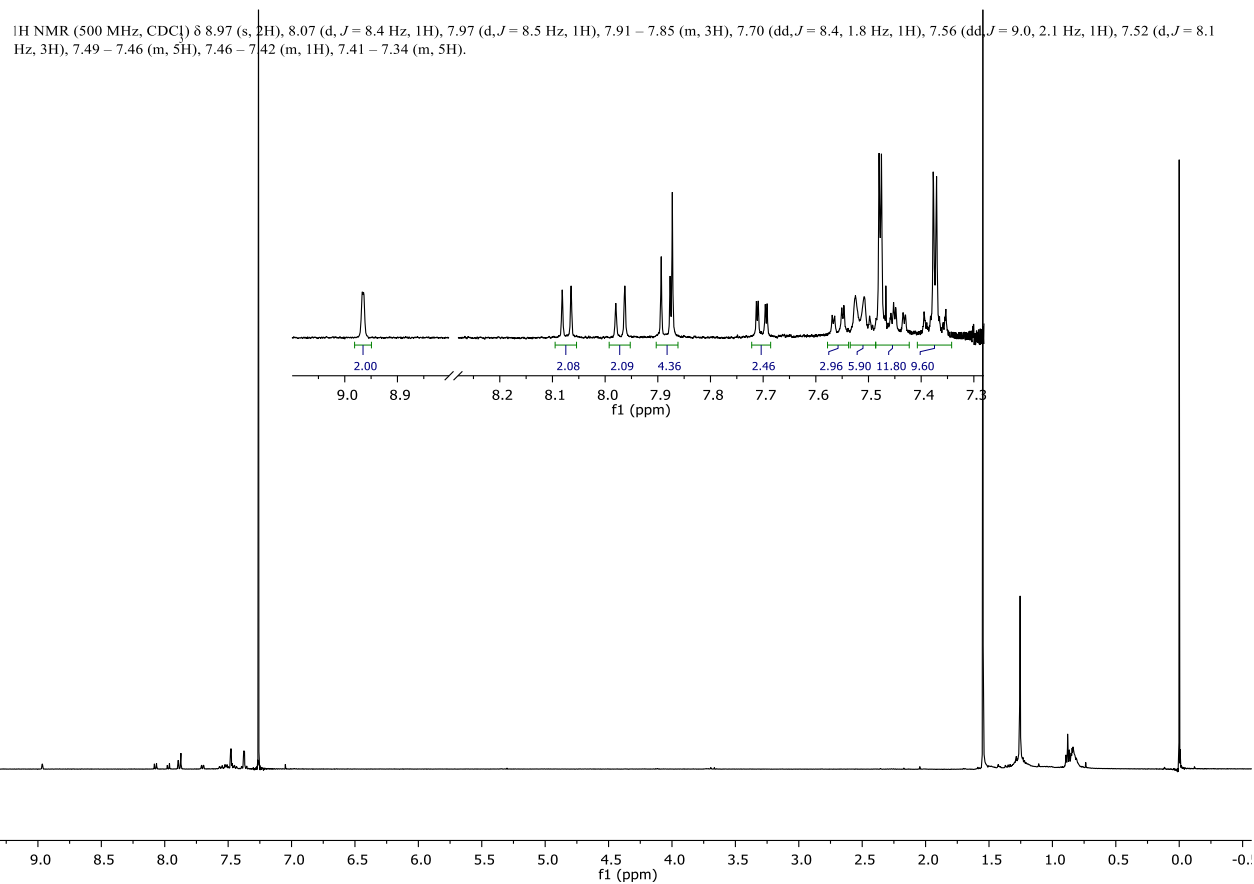


**9a** (56 mg; 0.13 mmol; 1.00 eq.) and **3b** (193 mg; 0.14 mmol; 1.10 eq.) were weighed in a Schlenk flask and dissolved in dioxane (100 mL) and H<sub>2</sub>O (10 mL). The resulting solution was degassed by bubbling with Ar for 1 h. K<sub>3</sub>PO<sub>4</sub> (217 mg; 1.02 mmol; 8.00 eq.) and SPhos Pd G3 (20 mg; 25.6 μmol; 0.2 eq.) were added and the degassing was further continued for 30 min. The Schlenk flask was sealed and placed into an oil bath pre-heated to 80 °C. The reaction was stirred for 16 h at 80 °C. The reaction mixture was filtered through celite, the flask and celite were rinsed with EtOAc and the volatiles were evaporated and crude product dried in high vacuum. The residue was dissolved in dry THF (3 mL) and TBAF (1 M in THF; 0.77 mL; 768 μmol; 6.00 eq.) was added and the reaction was stirred for 1 h at room temperature and quenched with H<sub>2</sub>O (5 mL). The resulting mixture was concentrated on rotavap (40 °C; 160 mbar). Formed precipitate was filtered off, washed with DCM (2 times 5 mL) and dried in high vacuum. The residue was dissolved in THF (10 mL) and H<sub>2</sub>SnCl<sub>4</sub> (127 mM in THF; 3.3 mL; 420 μmol; 3.3 eq.) was added. The reaction was stirred for 4 h at room temperature and quenched with 10% aqueous NaOH (2.5 mL). The resulting mixture was diluted with H<sub>2</sub>O (50 mL) and extracted with DCM (4 times 25 mL). The combined organic phases were washed with brine (25 mL) and dried with Na<sub>2</sub>SO<sub>4</sub>. Volatiles were evaporated. The crude product was purified by column chromatography (50% toluene in *n*-heptane). The product was isolated as yellow solid (7.2 mg; 7%).

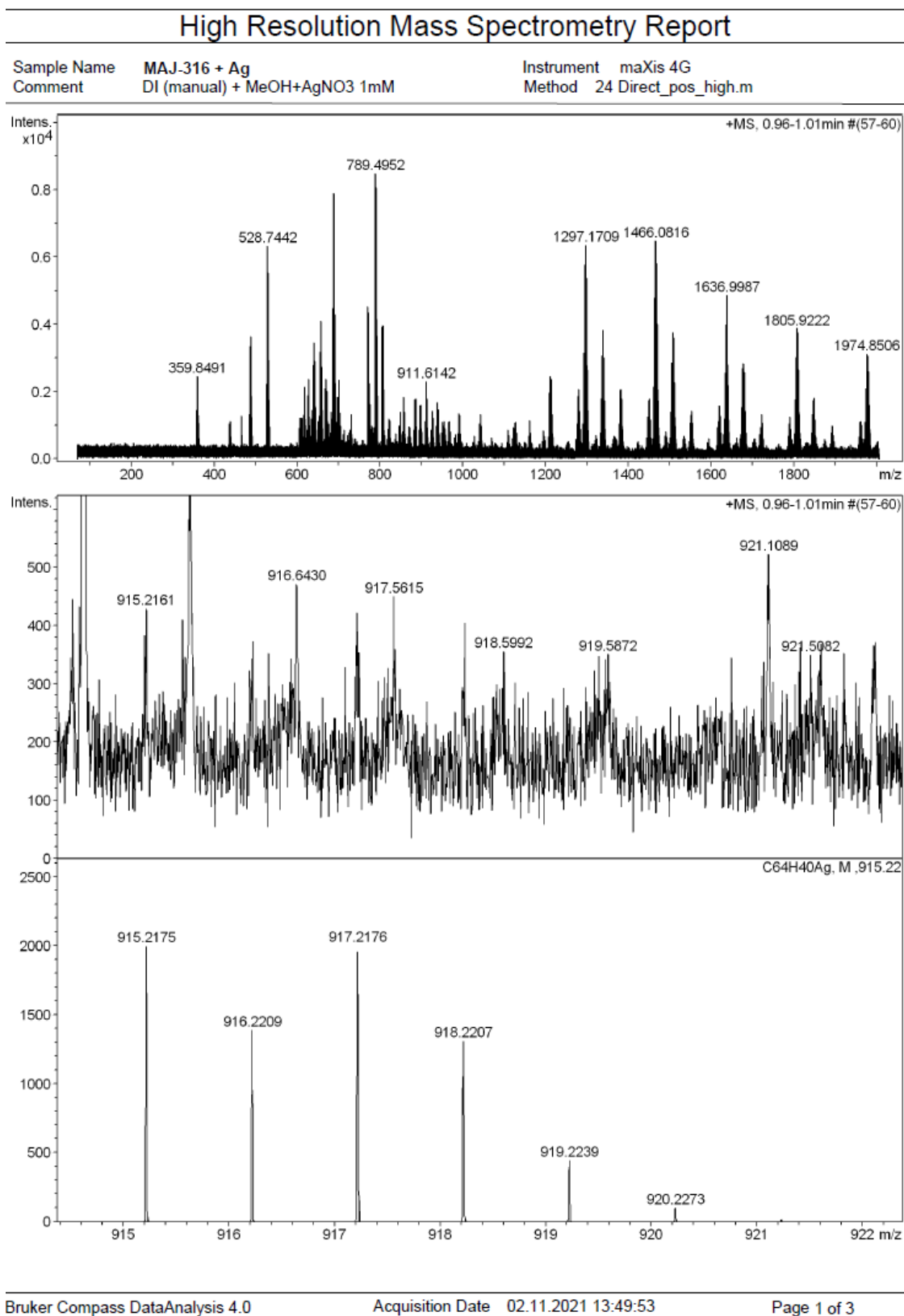
<sup>1</sup>H-NMR (500 MHz, CDCl<sub>3</sub>, 298 K, δ/ppm): 8.97 (s, 2H), 8.07 (d, *J* = 8.4 Hz, 1H), 7.97 (d, *J* = 8.5 Hz, 1H), 7.91 – 7.85 (m, 3H), 7.70 (dd, *J* = 8.4, 1.8 Hz, 1H), 7.56 (dd, *J* = 9.0, 2.1 Hz, 1H), 7.52 (d, *J* = 8.1 Hz, 3H), 7.49 – 7.46 (m, 5H), 7.46 – 7.42 (m, 1H), 7.41 – 7.34 (m, 5H).

HRMS (ESI, +): *m/z* calcd. for C<sub>58</sub>H<sub>42</sub>Ag [M+Ag]<sup>+</sup>: 915.2175, found: 915.2161.

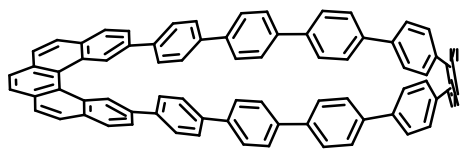




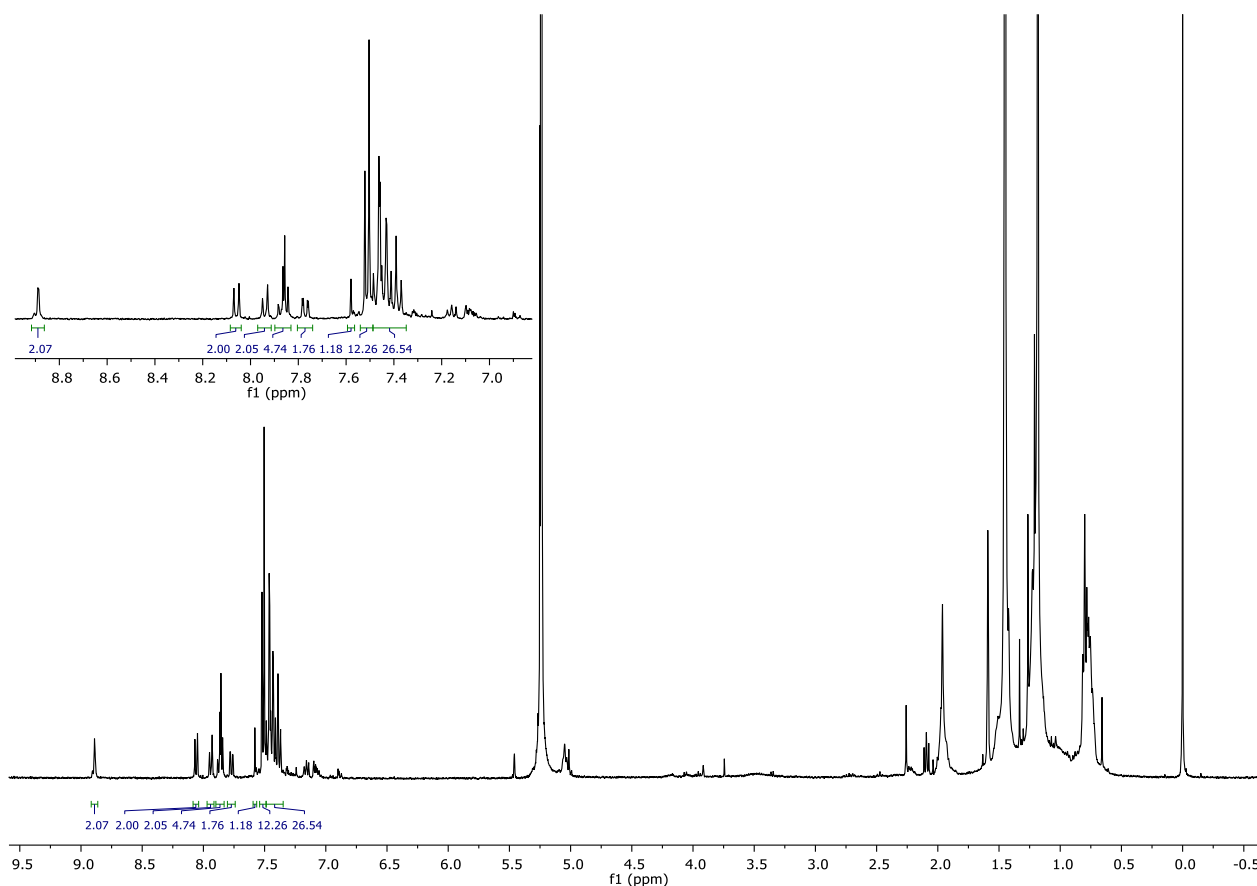
**Figure A24.**  $^1\text{H}$ -NMR (500 MHz,  $\text{CD}_2\text{Cl}_2$ , 298 K) spectrum of [5,7]HPP.



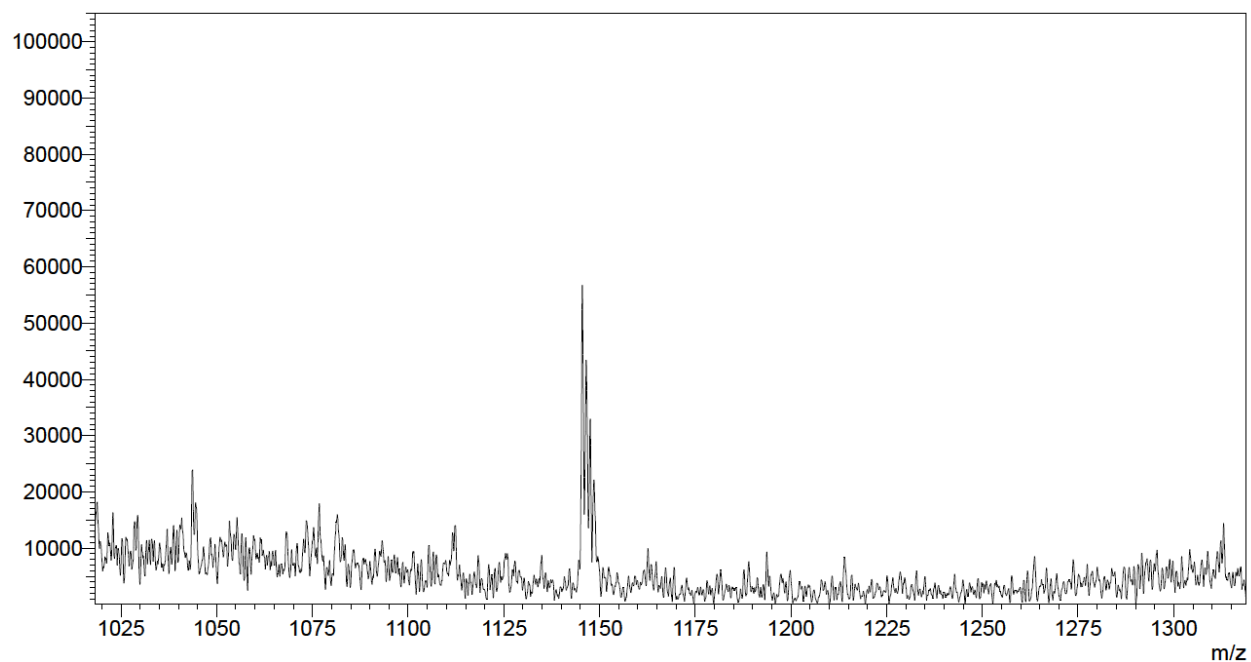
**Figure A25.** HR-MS (ESI, +) spectrum of [5,7]HPP [M+Ag]<sup>+</sup>.

**[5,9]HPP**

**11b** (57 mg; 61.4  $\mu\text{mol}$ ; 1.00 eq.) and **10d** (33 mg; 61.4  $\mu\text{mol}$ ; 1.10 eq.) were weighed in a Schlenk flask and dissolved in dioxane (50 mL) and  $\text{H}_2\text{O}$  (5 mL). The resulting solution was degassed by bubbling with Ar for 1 h.  $\text{K}_3\text{PO}_4$  (104 mg; 0.491 mmol; 8.00 eq.), XPhos (6 mg; 0.12 mmol; 0.2 eq.) and  $\text{Pd}_2\text{dba}_3$  (3 mg; 3  $\mu\text{mol}$ ; 0.05 eq.) were added and the degassing was further continued for 15 min. The Schlenk flask was sealed and placed into an oil bath pre-heated to 100  $^\circ\text{C}$ . The reaction was stirred for 16 h at 100  $^\circ\text{C}$ . The reaction mixture was filtered through celite, the flask and celite were rinsed with EtOAc and the volatiles were evaporated and crude product dried in high vacuum. The residue was dissolved in THF (10 mL) and  $\text{H}_2\text{SnCl}_4$  (127 mM in THF; 1.6 mL; 0.203 mmol; 3.3 eq.) was added. The reaction was stirred for 16 h at room temperature and quenched with 10% aqueous NaOH (0.5 mL). The resulting mixture was diluted with  $\text{H}_2\text{O}$  (25 mL) and extracted with DCM (3 times 25 mL). The combined organic phases were washed with brine (25 mL) and dried with  $\text{Na}_2\text{SO}_4$ . Volatiles were evaporated. Crude product was partially purified by column chromatography ( $\text{SiO}_2$ , 50% toluene in *n*-heptane) and using GPC ( $\text{CHCl}_3$ ).

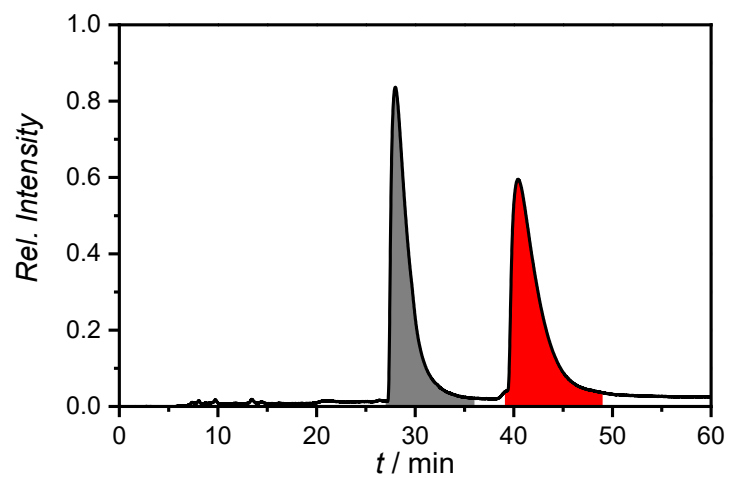


**Figure A26.**  $^1\text{H}$ -NMR (500 MHz,  $\text{CD}_2\text{Cl}_2$ , 298 K) spectrum of partially-purified [5,9]HPP.

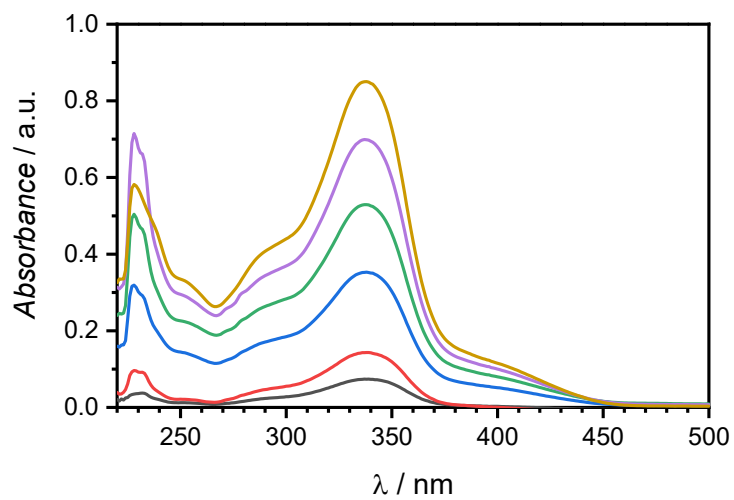
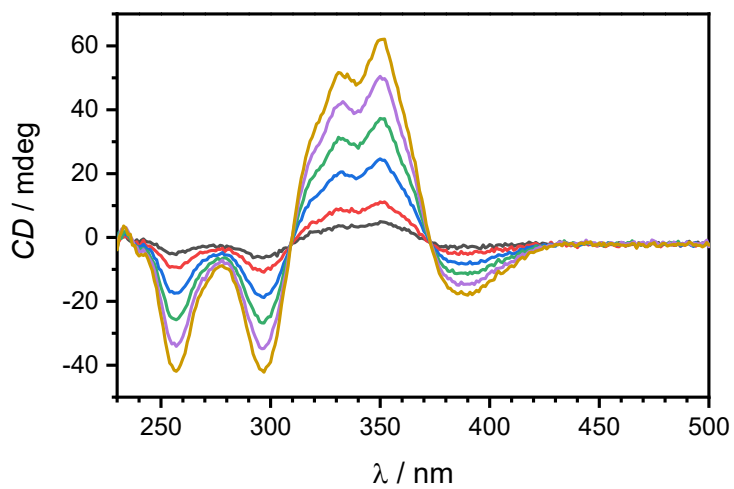


**Figure A27.** ESI-MS spectrum of macrocycle **13** [M]<sup>+</sup>.

### HPLC



**Figure A28.** HPLC chromatogram of [5,7]HPP with (*M*)-enantiomers (grey) eluting first followed by (*P*)-enantiomers (red).

**Optical properties****Figure A29.** Absorption dilution series of [5,7]HPP.**Figure A30.** Circular dichroism dilution series of [5,7]HPP.

### A.4.2. DFT calculations

Calculations were performed with Gaussian 09<sup>[7]</sup> (release D.01) software. Molecular geometries were optimized at D3-B3LYP/6-31g(d) level of theory. Stationary points were confirmed by a subsequent vibrational frequencies calculations. All vibrational frequencies were real. UltraFine integration grid was used in all calculations. The single point energies were then calculated at D3-B3LYP/cc-pVTZ level of theory. We used StrainViz software developed by Jasti group<sup>[15]</sup> to visualize local strain of [5,*n*]HPPs (*n* = 6,7,9). NICS values were calculated using GIAO at B3LYP/6-31G(d)/gas phase level of theory. AICD plots were obtained by first calculating NMR shielding tensor using CSGT at B3LYP/6-31G(d) level of theory and then using AICD program developed by Herges *et al.* on the Gaussian output file.<sup>[20]</sup>

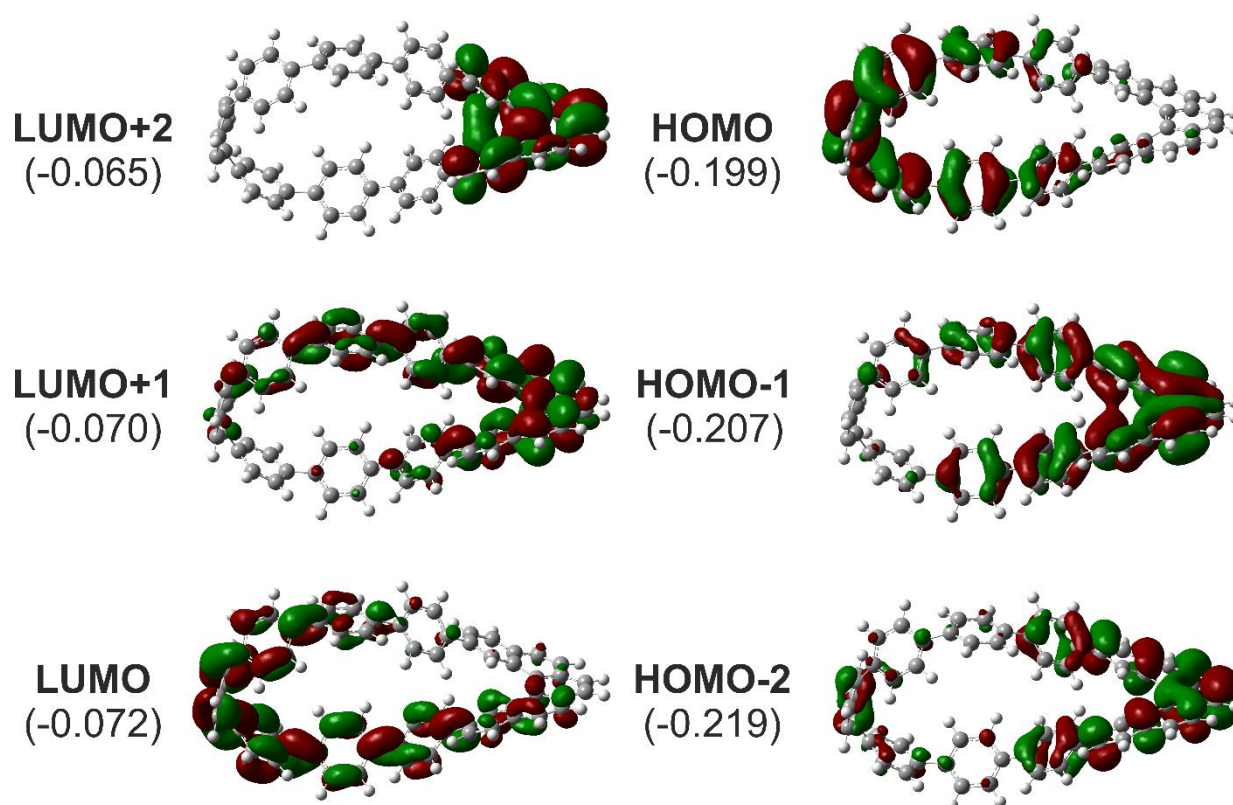


**Figure A31.** Frontier molecular (canonical) orbitals of [5,7]HPP with their energies in eV in brackets calculated at D3-B3LYP/6-31G(d) level of theory.

**TD-DFT**

The CD spectra were obtained calculating first 50 singlet excitations on ground state geometries at CAM-B3LYP/6-31g(d) level of theory.

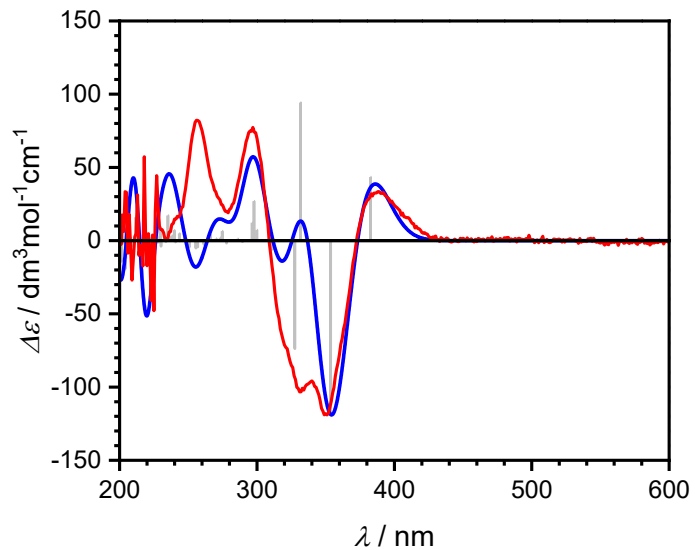


**Figure A32.** Experimental (red) and calculated (blue) CD spectra of (*M*)-[5.7]HPP with excitation transitions (grey lines) in DCM.

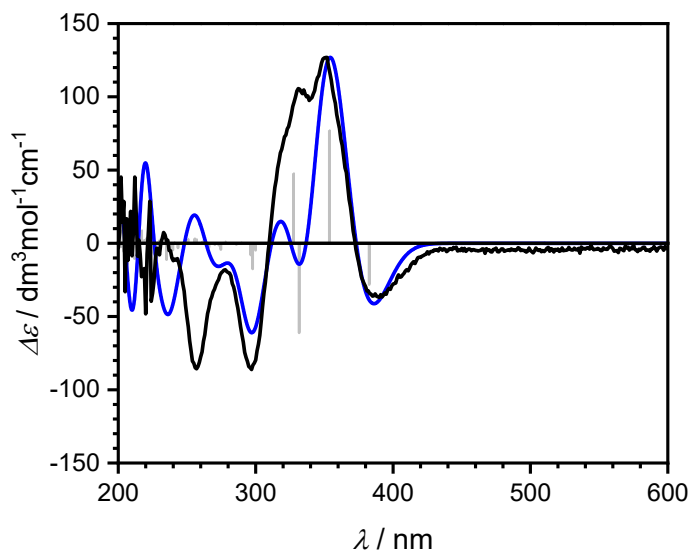


**Figure A33.** Experimental (black) and calculated (blue) CD spectra of (*P*)-[5.7]HPP with excitation transitions (grey lines) in DCM.

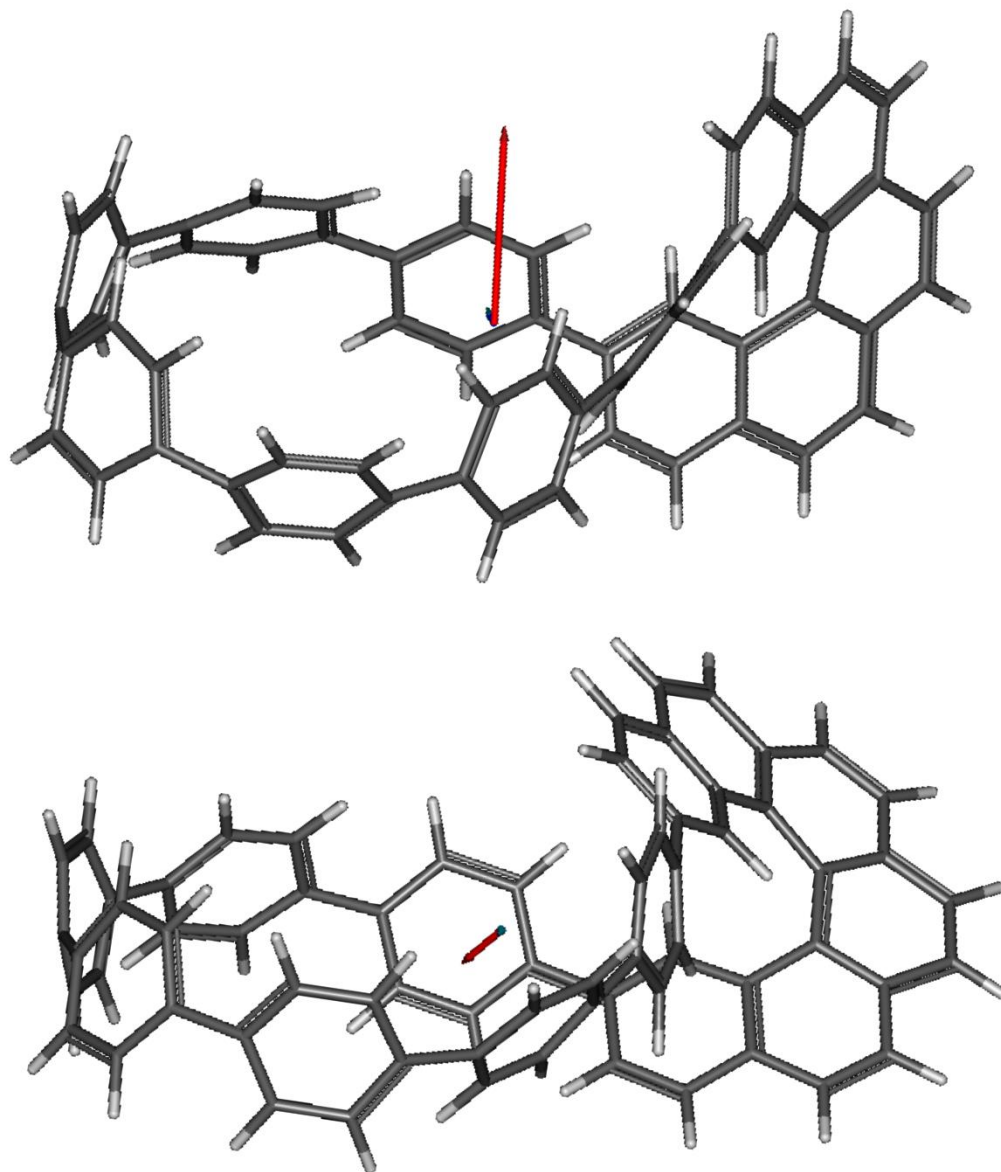


**Figure A34.** Electric (blue) and magnetic (red) transition dipole moments of the  $S_0 \rightarrow S_1$  transitions for [5,7]HPP (top) and [6,7]HPP (bottom). The vectors were scaled up by a factor of 2 due to the small length of  $\mu$ .



## A.4.3. XYZ atomic coordinates

[5.6]HPP

neutral

 $E = -2232.69950871$ 

C	-1.79278	-2.51316	-0.63204
C	-1.19506	-1.85743	0.45700
C	-1.19037	-3.69929	-1.08999
C	0.01033	-2.31108	0.98966
H	-1.63420	-0.93941	0.83870
C	0.00758	-4.15469	-0.55345
H	-1.66619	-4.26571	-1.88573
C	0.66484	-3.43946	0.46237
H	0.49836	-1.72636	1.76438
H	0.45532	-5.06493	-0.94326
C	-1.79260	2.51323	0.63172
C	-1.19029	3.69936	1.08974
C	-1.19487	1.85751	-0.45731
C	0.00768	4.15481	0.55324
H	-1.66620	4.26569	1.88548
C	0.01051	2.31120	-0.98993
H	-1.63401	0.93948	-0.83898
C	0.66495	3.43961	-0.46259
H	0.45541	5.06506	0.94302
H	0.49857	1.72656	-1.76467
C	2.07870	-3.71565	0.81349
C	2.98580	-4.02027	-0.21544
C	2.61723	-3.48446	2.09179
C	4.35631	-3.90158	-0.02540
C	2.61313	-4.21755	-1.21629
C	3.99261	-3.38555	2.28661
H	1.94771	-3.32482	2.93311
C	4.89312	-3.48082	1.20611
H	5.00249	-3.99525	-0.89186
H	4.36291	-3.14859	3.28015
C	6.22002	-2.80918	1.20566
C	6.40964	-1.68804	2.03401
C	7.13724	-2.96063	0.14359
C	7.21176	-0.62884	1.62795
H	5.77579	-1.54002	2.90235
C	7.93193	-1.89611	-0.27188
H	7.13600	-3.87259	-0.44717
H	7.84589	-0.64510	0.37060
H	7.15884	0.29906	2.18904
H	8.51205	-1.99484	-1.18615
C	2.07892	-2.71575	-0.81359
C	2.61757	3.48459	-2.09183
C	2.98586	4.02024	0.21549
C	3.99295	3.38563	-2.28649
H	1.94815	3.32511	-2.93326
C	4.35642	3.90145	0.02562
H	2.61305	4.21736	1.21632
C	4.89335	3.48083	-1.20587
H	4.36341	3.14866	-3.27995
H	5.00248	3.99498	0.89216
C	6.22026	2.80908	-1.20548
C	7.13755	2.96032	-0.14338
C	6.40988	1.68813	-2.03402
C	7.93218	1.89573	0.27186
H	7.13649	3.87230	0.44733
C	7.21186	0.62873	-1.62807
H	5.77611	1.54031	-2.90245
C	7.84596	0.64476	-0.37075
H	8.51245	1.99425	1.18606
H	7.15877	-0.29906	-2.18932
H	-2.15981	-2.44917	-3.30042
C	-3.00476	-2.02692	-2.76502
C	-2.96268	-1.94737	-1.34735
C	-4.10680	-1.58431	-3.45637
H	-4.15260	-1.68941	-4.53782
C	-4.01912	-1.33443	-0.68451
H	-3.99942	-1.29765	-0.39772
C	-5.21775	-1.02326	-2.78265
C	-5.14959	-0.81787	-1.36914
C	-6.43069	-0.75752	-3.48788
H	-6.45115	-0.85975	-4.56596
C	-7.56407	-0.44574	-2.80102
H	-6.29971	-0.55978	-1.38651
C	-7.53726	-0.23485	-1.38629
H	-8.51661	-0.35027	-3.31639
C	-6.29961	0.23794	0.68350
C	-5.14935	0.81789	1.36918
C	-3.00423	2.02674	2.76481
C	-4.10616	1.58408	3.45633
C	-2.96242	1.94731	1.34713
C	-5.21725	1.02326	2.78271
C	-8.76105	-0.06187	-0.67955
C	-4.01897	1.33447	0.68439
H	-7.53706	0.23509	1.38661
H	-2.15916	2.44894	3.30007
C	-6.43013	0.75748	3.48809
C	-8.76096	0.06226	0.68002
H	-4.15179	1.68906	4.53778
C	-7.56365	0.44585	2.80136
H	-9.69419	-0.09681	-1.23609
H	-6.45042	0.89574	4.56618
H	-8.51613	0.35051	3.31686
H	-9.69403	0.09730	1.23668
H	-3.99946	1.29780	-0.39785

[5.6]HPP

2+

 $E = -2231.33922131$ 

C	-1.78679	2.49204	0.56144
C	-1.25167	1.82290	-0.56249
C	-1.11090	3.65047	1.01373
C	-0.05191	-2.22196	-1.12271
H	-1.74841	0.93701	-0.94538
C	0.07703	4.05787	0.44555
H	-1.54376	4.24019	1.81395
C	0.68078	3.32081	-0.60380
C	0.36583	1.62356	-1.92393
H	0.54511	4.96171	0.81754
C	-1.78680	-2.49204	-0.56145
C	-1.11090	-3.65046	-1.01375
C	-1.25168	-1.82291	0.56248
C	0.07703	-4.05786	-0.44557
H	-1.54376	-4.24019	-1.81397
C	-0.05192	-2.22197	1.12270
H	-1.74842	-0.93702	0.94538
C	0.68078	-3.32082	0.60379

H	0.54511	-4.96170	-0.81757
H	0.36582	-1.62357	1.92393
C	2.05944	3.55980	-1.00504
C	2.94641	4.29310	-0.16985
C	2.63196	2.94417	-2.14986
C	4.31036	4.19974	-0.31713
H	2.55948	4.86187	0.66637
C	3.99639	2.85770	-2.30655
H	1.99147	2.48759	-2.89538
C	4.88697	3.36866	-1.31826
H	4.94388	4.71866	0.39250
H	4.38363	2.30120	-3.15147
C	2.61920	2.79083	-1.15912
C	6.73198	1.85762	-2.10109
C	2.94641	2.86245	0.09796
C	7.52858	0.82417	-1.68127
H	6.42656	1.89789	-3.14020
C	7.66157	1.82276	0.52418
H	6.66476	3.66950	0.78849
C	7.92049	0.65666	-0.28918
H	7.81356	0.06065	-2.39528
H	8.05707	1.84278	1.53311
C	2.05943	-3.55980	1.00503
C	2.63195	-2.94418	2.14985
C	2.94641	-4.29309	0.16984
C	3.99638	-2.85771	2.30655
H	1.99146	-2.48760	2.89538
C	4.31036	-4.19973	0.31712
H	2.55948	-4.86186	-0.66638
C	4.88697	-3.36867	1.31826
H	4.38363	-2.30121	3.15147
H	4.94388	-4.71865	-0.39251
C	6.19919	-2.79083	1.15912
C	6.87652	-2.86245	-0.09795
C	6.73197	-1.85762	2.10110
H	7.66157	-1.82277	-0.52419
H	6.66477	-3.66951	-0.78849
C	7.52857	-0.82417	1.68128
H	6.42654	-1.89789	3.14021
C	7.82048	-0.65666	0.28919
H	8.05708	-1.84278	-1.53309
H	7.81355	-0.06065	2.39529
C	-2.19681	2.65057	3.21942
C	-3.02699	2.89578	2.69742
C	-2.95666	1.99229	1.28611
C	-4.13243	1.78254	3.39414
H	-4.20036	1.95512	-4.14038
H	-4.00289	1.32792	0.64356
H	-3.96958	1.22809	-0.43318
C	-5.23451	1.17654	2.73562
C	-5.14751	0.87354	1.33567
C	-6.44776	0.96169	3.44699
H	-4.75980	1.16996	4.51175
C	-7.57358	0.60885	2.76610
C	-6.29308	0.26839	0.67012
C	-7.53392	0.31245	1.36497
H	-8.53137	0.54912	3.27429
C	-6.29309	-0.26839	-0.67011
C	-5.14752	-0.87354	-1.33567
C	-3.02701	-2.18785	-2.69743
C	-4.13245	-2.89578	-3.39414
C	-2.95667	-1.99229	-1.28612
C	-5.23453	-1.17653	-2.73561
C	-4.20037	-0.10240	0.67033
H	-4.00289	-1.32792	-0.64356
C	-7.53393	-0.31245	-1.36495
H	-2.19682	-2.65057	-3.21943
C	-6.44777	-0.96169	-3.44698
C	-8.75980	-0.10240	-0.67032
H	-4.20038	-1.95511	-4.46408
C	-7.57360	-0.60884	-2.76608
H	-9.68774	0.16699	1.23039
H	-6.47982	-1.16996	-4.51174
H	-8.53139	-0.54913	-3.27427
H	-9.68775	-0.16698	-1.23037
H	-3.96958	-1.22809	0.43317

[5.6]HPP

2+

reoptimized with UB3LYP

 $E = -2231.34097901$ 

C	-1.83146	2.75584	0.38097
C	-1.20464	1.99964	-0.62713
C	-1.23840	3.98701	0.73571
C	0.02108	2.38935	-1.15247
H	-1.63446	1.05256	-0.94061
C	-0.02420	4.38416	0.19808
H	-1.73888	4.63943	1.44433
C	0.67310	3.56125	-0.71136
H	0.51945	1.72643	-1.85177
H	0.39472	5.33888	0.49952
C	-1.83153	-2.75590	-0.38037
C	-1.23861	-3.98732	-0.73447
C	-1.20462	-1.99923	0.62733
H	-0.02447	-4.38423	-0.19861
H	-1.73916	-4.64000	-1.44280
C	0.02108	-2.38878	1.15282
H	-1.63435	-1.05195	0.94031
C	0.67297	-3.56101	0.71235
H	0.39432	-5.33927	-0.49754
C	0.51954	-1.72549	1.85169
C	2.09306	3.78926	-1.04367
C	2.94561	4.44746	-0.12728
C	2.70304	3.20022	-2.17265
C	4.32116	4.32302	-0.20844
H	2.52464	4.97561	0.72145
C	4.07879	3.07460	-2.25738
H	2.08947	2.78397	1.85169
C	4.92555	3.52668	-1.21275
H	4.92733	4.78773	0.56165
H	4.49248	2.52579	-3.09582
C	6.23307	2.90159	-1.01846
C	6.81751	2.04914	-1.99935
C	6.81749	2.84512	0.27872
C	7.58709	0.97223	-1.62371
H	6.57853	2.18137	-3.04909
H	7.58563	1.76787	0.65799
H	6.54337	3.57197	1.03453
C	7.80922	0.68333	-0.24152
H	7.91881	0.27934	-2.38886
H	7.89666	1.69393	1.69382
C	2.09294	-3.78893	1.04475

[5.6]HPP

2-

 $E = -2231.84104593$ 

C	-1.79734	2.47874	0.40772
H	-1.12988	1.65804	-0.51603
C	-1.12982	3.37082	0.71937
C	0.09020	2.04532	-1.06194
H	-1.52433	0.67074	-0.74017
C	-0.02988	4.13441	1.10442
H	-1.75827	4.41384	1.35298
H	0.70476	3.27250	-0.72718
H	0.62794	1.32848	-1.68984
H	0.37000	5.11640	0.35331
C	-1.85433	-2.50967	-0.64275
C	-1.07540	-3.54851	-1.21916
C	-1.35862	-1.98622	0.58025
H	0.112373	-3.96127	-0.24232
H	-1.44686	-4.05587	-2.10622
C	-0.14598	-2.38741	1.10961
H	-0.18609	-1.18508	0.74661
H	0.69346	-3.35993	0.48085
H	0.65680	-4.76637	-1.17861
H	0.21568	-1.87227	1.99409
C	2.10284	3.54381	-1.09671
C	2.95072	4.28392	-0.24227
C	2.73993	2.89815	

# Appendix

C	-5.19971	1.24395	2.74514
C	-5.17024	0.12506	1.25450
C	-6.39183	1.05048	3.51281
H	-6.37667	1.28800	4.57400
C	-7.54541	0.69334	2.87948
C	-6.34910	0.29244	0.73761
C	-7.56661	0.36661	1.49347
H	-8.48743	0.65028	3.42447
C	-6.39766	-0.27981	-0.58024
C	-5.26342	-0.89989	-1.28294
C	-3.16396	-0.12420	-0.72675
C	-4.29034	-1.71880	-3.38855
C	-3.04276	-2.00372	-1.30803
C	-5.40193	-1.15741	-2.69702
C	-8.18396	0.13835	0.85062
C	-4.11008	-1.36200	-0.63426
C	-7.67351	-0.33305	-1.24197
H	-2.53036	-2.53036	-3.29129
C	-6.63399	-0.95684	-3.34687
C	-8.86725	-0.11434	-0.48769
H	-4.36755	-1.84630	-4.46765
C	-7.76323	-0.62337	-2.62288
H	-9.72476	0.22174	1.44167
H	-6.69497	3.12525	4.14325
H	-8.74144	-0.58601	-3.09811
H	-9.82285	-0.21429	-0.99965
H	-4.05040	-1.27644	0.44321

## [5.7]HPP neutral

$$E = -2463.85180194$$

C	2.79758	2.14141	-1.30712
C	2.21787	1.80252	-0.07275
C	2.18647	3.16057	-2.05849
C	1.04045	2.41022	0.35546
H	2.65604	1.00985	0.52706
C	1.01538	-1.77193	-1.01538
H	2.64190	3.48235	-2.99110
C	0.39410	3.38525	-0.42542
H	0.57493	2.06814	1.27545
H	0.57159	4.55921	-2.22895
C	2.59281	-0.07393	-1.19549
C	1.76885	-2.89104	1.98858
C	2.24206	-1.92855	-0.15905
C	0.26102	-3.47398	1.47598
H	2.06709	-3.06539	3.02916
C	1.09949	-2.53211	-0.67645
H	2.84573	-1.30051	-0.80851
C	0.23479	-3.29054	0.13503
H	-0.02264	-4.03949	2.14632
H	0.86487	-2.38750	-1.72693
C	-0.96207	3.86488	-0.06625
C	-1.92887	4.02348	-1.07184
C	-1.38477	4.02348	1.26577
C	-3.27026	4.21542	-0.75932
H	-1.64474	3.91176	-2.11301
C	-2.72831	4.21366	1.57909
H	-0.56402	3.96608	2.06816
C	-3.71443	4.24190	0.57534
H	-3.99754	4.21698	-1.56536
H	-3.02147	4.29489	2.62244
C	-5.15344	4.00277	0.84963
C	-5.51307	3.11642	1.87941
C	-4.16589	-4.36288	-4.06173
C	-6.12278	2.43286	1.84543
H	-4.77611	2.82700	2.62252
C	-3.67768	3.67765	-0.09775
H	-5.96776	5.12539	-0.81037
C	-7.62339	2.60173	-0.77683
H	-6.88173	1.62769	2.55615
H	-8.09373	3.90910	-0.88169
C	-1.09697	-3.75216	-0.32995
C	-1.79612	-3.03450	-1.31602
C	-1.78631	-4.90558	-0.30260
C	-3.14709	-3.26104	-1.55143
H	-1.31146	-2.21024	-1.83006
C	-3.14438	-5.01976	0.08315
H	-1.26309	-5.44189	1.01054
C	-3.87144	-4.20364	-0.79949
H	-3.67955	-2.60755	-2.23641
H	-3.65992	-5.79813	0.64017
C	-5.34709	-4.05670	-0.75018
C	-5.95508	-3.90481	0.50721
C	-6.11710	-3.71449	-1.87634
H	-7.14000	-7.14000	-0.64413
H	-5.40899	-4.19092	1.40183
C	-7.31736	-3.02403	-1.73851
H	-5.72401	-3.90630	-2.87161
C	-7.77504	-2.60900	-0.47023
H	-7.46771	-2.53837	1.64720
H	-7.83829	-2.70356	-1.63887
C	-8.51562	-1.33101	-0.28170
C	-8.40567	-0.34210	-1.27770
C	-8.93369	-0.88557	0.99046
C	-8.37305	1.00673	-0.94792
H	-8.14184	-0.61911	-2.29291
C	-8.88897	0.46480	1.32531
H	-9.16831	-1.60665	1.76857
C	-8.44363	1.42328	0.39399
H	-8.08198	1.71655	-1.71622
H	-9.07747	0.76011	2.35448
C	3.23229	1.35715	-3.87069
C	4.06023	1.10227	-3.21575
C	3.97939	1.41678	-1.83334
C	5.18142	0.49034	-3.72592
C	5.25867	0.23960	-4.79270
H	5.02135	-0.49974	-1.02116
H	4.97637	1.30300	0.04286
C	6.26819	0.13227	-2.89131
C	6.15999	0.32977	-1.47998
C	7.49560	-0.33488	-3.45326
H	7.55155	-0.49174	-2.52652
H	6.60009	-0.47037	-2.66758
C	7.27386	-0.05824	-0.62083
C	8.52890	-0.28751	-1.25001
H	9.56273	-0.72397	-3.10474
H	7.21904	-0.12752	0.82278
C	6.02195	1.36925	1.59746
C	3.72588	-0.96793	3.15242
C	4.83585	-0.40982	3.74166
C	1.37065	-1.37069	1.78919
C	6.02099	-0.17577	3.00295
C	9.72380	-0.29740	-0.47502
C	4.89553	-1.08769	1.04664
C	8.43263	0.03422	1.54641
H	2.82290	-1.11512	3.73653
C	7.22807	-0.22278	3.65401
C	9.68137	-0.04267	0.86642
H	4.82374	-0.15876	4.79972

C	8.40138	0.24822	2.96134
H	-10.44139	-0.98139	-0.32424
H	7.20653	0.42238	4.72244
H	9.34112	0.44569	3.47124
H	10.59727	0.04766	1.44500
H	4.94215	-1.41713	0.01651

## [5.7]HPP

2+

$$E = -2462.41068627$$

C	2.73855	2.10557	-1.29309
C	2.21043	1.82635	-0.01578
C	2.06466	3.05823	-2.08654
C	1.03461	2.41996	0.41594
H	2.69964	1.09310	0.61731
C	0.89273	3.65160	-1.65613
H	2.48505	3.34810	-3.04344
C	0.32187	3.32171	-0.40655
H	0.62155	2.12423	1.37442
H	0.42134	4.39683	-2.28742
C	2.63657	-2.06730	1.21733
C	1.78688	-2.87307	2.01028
C	2.30346	-1.92339	-0.15153
C	0.65045	-3.45301	1.48635
H	2.03578	-3.05382	3.04956
C	1.15700	-2.49279	-0.67199
H	2.92914	-1.31565	-0.79675
C	0.27395	-3.25125	0.13650
H	0.01507	-4.03127	2.14654
C	0.93799	-2.34547	-1.72358
C	-1.01607	3.78409	-0.03581
C	-1.95710	4.12886	-1.03386
C	-1.47038	3.79602	1.30597
C	-3.29002	4.31378	-0.73179
H	-1.65389	4.15586	-2.07374
C	-2.80382	3.98043	1.61069
C	-0.76022	2.64522	2.11324
C	-3.77553	4.16209	0.59146
H	-3.98201	4.47710	-1.98546
H	-3.10454	3.96329	2.65216
C	-5.19421	3.94087	0.82078
H	-5.64610	-1.26518	1.98546
C	-6.16515	4.15490	-0.19977
H	-6.83814	2.57796	1.98760
H	-4.99447	3.16684	2.84500
C	-7.35304	3.46568	-0.20388
H	-5.94548	4.82105	-1.02588
C	-7.65026	2.51652	0.81954
H	-7.07531	1.96368	2.84752
H	-8.03223	3.59504	-1.03875
C	-1.03307	-3.69460	-0.33470
C	-1.65204	-3.08795	-1.45482
H	-4.80333	-4.80333	-1.38842
C	-2.98904	-3.28321	-1.72802
H	-1.10120	-2.37616	-2.05785
C	-3.14324	-4.83570	0.11958
H	-1.34052	-5.23799	1.16513
H	-3.80418	-4.08065	-0.89005
H	-3.44015	-2.71256	-2.53100
C	-5.69796	-5.55589	0.71114
C	-5.24444	-3.92045	-0.92231
C	-6.02034	-4.12212	0.25242
C	-5.90535	-3.30504	-2.02123
H	-7.21352	-3.46099	-4.43097
H	-5.61276	-4.69071	1.08013
C	-7.10542	-2.65830	-1.85031
H	-5.42885	-3.28289	-2.99479
C	-7.70815	-2.56480	-0.56030
H	-7.71818	-3.55057	-1.38546
H	-7.52629	-2.11849	-2.68982
C	-8.46472	-1.38802	-0.20169
C	-8.74611	-0.36563	-1.15700
C	-8.61321	-1.01523	1.16950
H	-8.73532	-0.95673	-0.78764
H	-8.85364	-0.61296	-2.20657
C	-8.59177	0.30635	1.53822
H	-8.60730	-1.77074	1.94588
C	-8.42930	1.32956	0.55617
H	-8.80857	1.71274	-1.56012
H	-9.58922	0.55733	2.59267
H	3.18147	1.35994	-3.85818
C	4.01164	1.14486	-3.20424
C	3.92631	1.40934	-1.81399
C	5.14014	0.52814	-3.71931
H	5.22179	0.34186	-1.78615
C	4.97520	1.02970	-0.98368
H	4.93318	1.30557	0.06126
C	6.23624	0.19191	-2.88739
C	6.12873	0.17193	-1.47316
C	7.47000	-0.23986	-3.46721
C	7.51961	-0.39048	-5.41222
C	8.58087	-0.35280	-2.69281
C	7.25612	0.00799	-0.62721
C	8.51315	-0.18505	-1.26982
H	9.54677	-0.57508	-3.13619
C	7.21722	-0.08259	0.81015
C	6.03683	-0.41294	1.59546
C	3.78993	-1.07195	3.20395
C	4.89799	-0.51517	3.78139
C	3.78790	-1.39187	1.81270
C	6.06352	-0.22691	3.01795
C	9.71411	-0.18414	-0.51538
C	4.90745	-1.04819	1.04635
C	8.43832	0.06835	1.52311
H	2.91023	-1.26728	3.80624
C	7.26563	0.15670	3.66246
H	9.68174	0.03615	-4.44764
C	4.91507	-0.30823	4.84733
C	8.42799	0.22900	2.94137
C	10.65926	-0.30404	-1.03579
H	7.26754	0.30808	4.73732
H	9.37382	0.41766	3.44624
H	10.60011	0.13198	1.40667
H	4.93252	-1.33577	0.00469

## [5.7]HPP

2-

$$E = -2462.91527923$$

C	2.76926	2.19092	-1.14959
C	2.14705	1.74406	0.02760
C	2.19192	3.28447	-1.81652
C	0.96247	2.32489	0.47263
H	2.55375	0.88697	0.55687
C	1.01818	3.87248	-1.36283

H	2.68004	3.67824	-2.70499
C	0.34445	3.32812	-0.32284
H	4.05981	1.89402	1.33317
H	6.60515	4.72144	-1.90086
C	2.69635	-2.15204	1.21631
C	1.81949	-2.91406	2.02958
C	2.34082	-2.06845	-0.15469
C	0.86654	-3.48664	1.53646
H	2.06170	-3.05948	3.07896
C	1.18081	-2.64030	-0.64633
H	2.96539	-1.49259	-0.83276
C	0.26933	-3.35282	0.17995
H	0.01945	-4.01617	2.23024
H	0.95657	-2.51441	-1.70155
C	-1.00503	3.85247	0.13158
C	-1.91413	4.24941	-0.87052
C	-1.51847	3.78501	1.44260
H	-3.26194	4.42760	-0.60813
H	-1.57374	4.30926	-1.90090
C	-2.86519	3.97816	1.71134
H	-0.84614	3.54875	2.26419

C	1.59501	-4.95897	-0.11805
H	1.99538	-4.59242	-2.20439
H	0.82004	-5.22794	1.87883
C	7.24281	-4.61129	0.49705
C	7.97086	-4.32817	1.66759
C	7.76806	-4.12856	-0.71388
C	9.03769	-3.43370	1.65113
H	7.65066	-4.75537	2.61442
C	8.82628	-3.22859	-0.72889
H	7.24676	-4.33451	-1.64397
C	9.41306	-2.77221	0.46561
H	9.52867	-3.18155	2.58733
H	9.08996	-2.75790	-1.67098
C	-0.88496	3.95579	0.27978
C	-0.12132	3.46595	-0.79371
C	-0.35196	5.03281	1.01259
C	1.14855	3.96616	-1.06247
H	-0.48858	2.62480	-1.37434
C	0.92414	5.52318	0.75404
H	-0.94002	5.48358	1.80694
C	1.72049	4.97030	-0.26240
H	1.74574	3.50676	-1.84519
H	1.31900	6.33507	1.25938
C	7.38698	4.54013	-0.59413
C	8.27448	4.62560	0.49662
C	7.73708	3.65381	-1.62803
C	9.31277	3.71137	0.65388
H	8.10269	5.36519	1.27392
C	8.78018	2.74971	-1.47770
H	7.09582	3.55953	-2.49867
C	9.51600	2.67985	-0.28110
H	9.91916	3.74577	1.55551
H	8.91406	1.97885	-2.23169
C	10.12802	1.37363	0.07024
C	10.66188	0.49811	-0.89400
C	9.81727	0.82495	1.32697
C	10.63745	-0.87977	-0.69877
H	11.00645	0.89394	-1.84605
C	9.78905	-0.55144	1.51732
H	9.42441	1.66920	2.10884
C	10.06537	-1.43745	0.46197
H	10.97256	-1.53194	-1.50093
H	9.36321	-0.93264	2.44298
H	-5.08608	-0.53771	-4.03219
C	-5.91300	-0.42530	-3.33709
C	-5.82410	-1.00873	-2.04565
C	-7.04275	0.26455	-3.71214
H	-7.12712	0.66826	-4.71842
C	-6.86649	-0.80209	-1.15156
H	-6.81649	-1.28507	-0.18459
C	-8.12886	0.43947	-2.81959
C	-8.01099	-0.03283	-1.47625
C	-9.36451	0.99662	-3.27089
H	-9.43063	1.36793	-4.29052
C	-10.46376	0.96584	-2.46648
C	-9.11886	0.17164	-0.54952
C	-10.38024	0.51108	-1.11193
H	-11.43146	1.29239	-2.83937
C	-9.04941	-0.03966	0.87950
C	-7.84425	0.11000	1.68495
C	-5.52741	0.34412	3.28619
C	-6.63234	-0.31535	3.77222
C	-5.57260	0.99528	2.02359
C	-7.82651	-0.40659	3.01605
C	-11.56734	0.36402	-0.33868
C	-6.72344	0.86175	1.25673
C	-10.25479	-0.24213	1.57047
H	-4.61730	0.38125	3.87697
C	-9.02684	-0.92458	3.59153
C	-11.51042	-0.14269	0.92889
H	-6.60903	-0.76139	4.76378
C	-10.20748	-0.82183	2.91838
H	-12.52264	0.60197	-0.79976
H	-8.99418	-1.32411	4.60206
H	-11.14124	-1.11656	3.39097
H	-12.42031	-0.34680	1.48767
H	-6.78122	1.38413	0.31055
H	5.38159	-4.09841	2.37134
H	2.95690	-4.21793	2.10243
C	4.97368	-4.63346	1.51881
C	3.59292	-4.69695	1.36342
C	5.84240	-5.10071	0.51629
C	3.01817	-5.22936	0.19743
C	5.26474	-5.77939	-0.57206
C	3.88355	-5.83990	-0.72876
H	5.90619	-6.21702	-1.33253
H	3.46796	-6.32916	-1.60565
H	5.91471	5.06787	1.61313
H	3.48735	5.24537	1.74882
C	5.34978	5.18799	0.69403
C	3.96492	5.28124	0.77361
C	6.06636	5.08525	-0.54604
C	3.16923	5.25970	-0.38949
C	5.21709	5.24121	-1.70178
C	3.82935	5.31233	-1.62318
H	5.68959	5.24780	-2.68008
H	3.24363	5.36585	-2.53727



## A.4. References

- [1] E. R. Darzi, T. J. Sisto, R. Jasti, *J. Org. Chem.* **2012**, *77*, 6624–6628.
- [2] V. K. Patel, E. Kayahara, S. Yamago, *Chem. – Eur. J.* **2015**, *21*, 5742–5749.
- [3] T. C. Lovell, C. E. Colwell, L. N. Zakharov, R. Jasti, *Chem Sci* **2019**, *10*, 3786–3790.
- [4] L. Bondarenko, I. Dix, H. Hinrichs, H. Hopf, *Synthesis* **2004**, *2004*, 2751–2759.
- [5] G. Meyer-Eppler, E. Vogelsang, C. Benkhäuser, A. Schneider, G. Schnakenburg, A. Lützen, *Eur. J. Org. Chem.* **2013**, *2013*, 4523–4532.
- [6] Y. Wu, G. Zhuang, S. Cui, Y. Zhou, J. Wang, Q. Huang, P. Du, *Chem. Commun.* **2019**, *55*, 14617–14620.
- [7] M. J. Frisch, G. W. Trucks, H. B. Schlegel, G. E. Scuseria, M. A. Robb, J. R. Cheeseman, G. Scalmani, V. Barone, B. Mennucci, G. A. Petersson, H. Nakatsuji, M. Caricato, X. Li, H. P. Hratchian, A. F. Izmaylov, J. Bloino, G. Zheng, J. L. Sonnenberg, M. Hada, M. Ehara, K. Toyota, R. Fukuda, J. Hasegawa, M. Ishida, T. Nakajima, Y. Honda, O. Kitao, H. Nakai, T. Vreven, J. A. Montgomery, J. E. Peralta, F. Ogliaro, M. Bearpark, J. J. Heyd, E. Brothers, K. N. Kudin, V. N. Staroverov, R. Kobayashi, J. Normand, K. Raghavachari, A. Rendell, J. C. Burant, S. S. Iyengar, J. Tomasi, M. Cossi, N. Rega, J. M. Millam, M. Klene, J. E. Knox, J. B. Cross, V. Bakken, C. Adamo, J. Jaramillo, R. Gomperts, R. E. Stratmann, O. Yazyev, A. J. Austin, R. Cammi, C. Pomelli, J. W. Ochterski, R. L. Martin, K. Morokuma, V. G. Zakrzewski, G. A. Voth, P. Salvador, J. J. Dannenberg, S. Dapprich, A. D. Daniels, Ö. Farkas, J. B. Foresman, J. V. Ortiz, J. Cioslowski, D. J. Fox, *Gaussian 09 Revision D.01*, **2009**.
- [8] M. D. Hanwell, D. E. Curtis, D. C. Lonie, T. Vandermeersch, E. Zurek, G. R. Hutchison, *J. Cheminformatics* **2012**, *4*, 17.
- [9] J. M. Fox, D. Lin, Y. Itagaki, T. Fujita, *J. Org. Chem.* **1998**, *63*, 2031–2038.
- [10] A. Granzhan, E. Largy, N. Saettel, M.-P. Teulade-Fichou, *Chem. – Eur. J.* **2010**, *16*, 878–889.
- [11] R. Balasaravanan, K. Duraimurugan, J. Sivamani, V. Thiagarajan, A. Siva, *New J. Chem.* **2015**, *39*, 7472–7480.
- [12] G. M. Sheldrick, *Acta Crystallogr. Sect. Found. Adv.* **2015**, *71*, 3–8.
- [13] O. V. Dolomanov, L. J. Bourhis, R. J. Gildea, J. a. K. Howard, H. Puschmann, *J. Appl. Crystallogr.* **2009**, *42*, 339–341.
- [14] G. M. Sheldrick, *Acta Crystallogr. Sect. C Struct. Chem.* **2015**, *71*, 3–8.
- [15] C. E. Colwell, T. W. Price, T. Stauch, R. Jasti, *Chem. Sci.* **2020**, *11*, 3923–3930.
- [16] T. Bruhn, A. Schaumlöffel, Y. Hemberger, G. Bringmann, *Chirality* **2013**, *25*, 243–249.
- [17] K. Dhbaibi, L. Abella, S. Meunier-Della-Gatta, T. Roisnel, N. Vanthuyne, B. Jamoussi, G. Pieters, B. Racine, E. Quesnel, J. Autschbach, J. Crassous, L. Favereau, *Chem. Sci.* **2021**, *12*, 5522–5533.
- [18] S. Jhulki, A. K. Mishra, T. J. Chow, J. N. Moorthy, *Chem. – Eur. J.* **2016**, *22*, 9375–9386.
- [19] T. J. Sisto, M. R. Golder, E. S. Hirst, R. Jasti, *J. Am. Chem. Soc.* **2011**, *133*, 15800–15802.
- [20] D. Geuenich, K. Hess, F. Köhler, R. Herges, *Chem. Rev.* **2005**, *105*, 3758–3772.



**A.5. List of abbreviations**

AFM	Atomic force microscopy
AICD	Anisotropy of induced current density
BET	Brunauer-Emmet-Teller surface area
CNS	Carbon nanoscroll
CNT	Carbon nanotube
CPP	Cycloparaphenylene
CVD	Chemical vapor deposition
ECD	Electronic circular dichroism
HOMO	Highest occupied molecular orbital
HPLC	High-performance liquid chromatography
HPP	Helicene <i>para</i> -phenylene
LUMO	Lowest unoccupied molecular orbital
MWCNT	Multi-walled carbon nanotubes
NICS	Nucleus-independent chemical shift
NIR	Near-infrared
NMR	Nuclear magnetic resonance
OPP	Oligo- <i>para</i> -phenylene
PMMA	Poly(methyl methacrylate)
SFC	Supercritical fluid chromatography
SPP	Spiral <i>para</i> -phenylene
STM	Scanning tunneling microscopy
STM-BJ	Scanning tunneling microscope–break junction
SWCNT	Single-walled carbon nanotube
TEM	Transmission electron microscopy
TES	Triethylsilyl
TGA	Thermo-gravimetric analysis

## Juraj Malinčík

---

Birth date: 21.04.1994

Nationality: Slovak

E-mail: [malincik.juraj@gmail.com](mailto:malincik.juraj@gmail.com)

### Education

---

- 2018 – 2023 University of Basel, Basel, Switzerland  
PhD in Organic Chemistry, *Magna cum laude*
- 2013 – 2018 University of Chemistry and Technology, Prague, Czech Republic  
Master of Science in Organic Chemistry, *Summa cum laude*  
Bachelor of Science in Chemistry, *Magna cum laude*

### Research Experience

---

- 2018 – 2023 Department of Chemistry, University of Basel, Basel  
Group of Topological Organic Materials  
Advisors: Assist. Prof. Tomáš Šolomek; Prof. Marcel Mayor  
Research topics: Chiral carbon nano hoops; Shape-persistent redox-active macrocycles
- 2013 – 2018 Department of Organic Chemistry, University of Chemistry and Technology, Prague  
Group of Heterocyclic and Material Chemistry  
Advisors: Assoc. Prof. Michal Kohout; Prof. Jiří Svoboda  
Research topics: Liquid crystalline materials; Stationary phases for liquid chromatography; Metal nanoparticles applications
- 2017 Internship at research company APIGENEX s.r.o., Prague  
Advisor: Dr. Miroslav Havránek  
Research topics: Non-standard amino acid peptides; Peptide nucleic acids

### Selected Oral and Poster Presentations

---

- 2022 28th Lecture Conference on Photochemistry, Düsseldorf, Germany  
*Circularly Polarized Luminescence in a Möbius Helicene Carbon Nano hoop* (oral)
- The 19th International Symposium on Novel Aromatic Compounds, Warszawa, Poland  
*Circularly Polarized Luminescence in a Möbius Helicene Carbon Nano hoop* (poster)
- Fall Meeting of Swiss Chemical Society 2022, Zürich, Switzerland  
*Emissive Properties of Helicene Carbon Nano hoops* (poster)
- Central European Conference on Photochemistry 2022, Bad Hofgastein, Austria  
*Emissive Properties of Helicene Carbon Nano hoops* (oral)
- 2021 Fall Meeting of Swiss Chemical Society 2021, online  
*Möbius Carbon Nano hoops* (oral)
- Organic pi-Electron Molecules and Materials Meetings, online  
*Möbius Carbon Nano hoops* (oral)
- RSC virtual Macrocylic and Supramolecular Chemistry Seminars, online  
*Möbius Carbon Nano hoops* (oral)

### Awards

---

- 2022 Best poster presentation, Runner-up Award  
Fall Meeting of Swiss Chemical Society 2022
- 2021 Journal of Physical Organic Chemistry award for best lecture  
Organic pi-Electron Molecules and Materials Meetings
- 2018 Rector's prize for highest marks during Master's degree
- 2016 Dean's prize for study excellence during Bachelor's degree



## List of Publications

---

- 11.) X. Wu, **J. Malinčík**, A. Prescimone, C. Sparr:  
X-Ray Crystallographic Studies of Quasi-Racemates for Absolute Configuration Determinations  
*Helvetica Chimica Acta* **2022**, *105*, e202200117.
- 10.) **J. Malinčík**, S. Gaikwad, J. P. Mora-Fuentes, M.-A. Boillat, A. Prescimone, D. Häussinger, A. G. Campaña, T. Šolomek:  
Circularly Polarized Luminescence in a Möbius Helicene Carbon Nano hoop.  
*Angewandte Chemie International Edition* **2022**, *61*, e202208591.
- 9.) A. D'Addio, **J. Malinčík**, O. Fuhr, D. Fenske, D. Häussinger, M. Mayor:  
Geländer Molecules with Orthogonal Joints: Synthesis of Macrocyclic Dimers.  
*Chemistry – A European Journal* **2022**, *28*, e202201678.
- 8.) **J. Malinčík**, M. Kohout, J. Svoboda, S. Stulov, D. Pocięcha, Z. Böhmová, V. Novotná:  
Photochromic spiropyran-based liquid crystals.  
*Journal of Molecular Liquids* **2022**, *346*, 117842.
- 7.) **J. Malinčík**, S. Gaikwad, M.-A. Boillat, D. Häussinger, A. Prescimone, T. Šolomek:  
Figure-of-Eight Helicene Carbon Nano hoop with Möbius Topology.  
*ChemRxiv*. **2021**, preprint. DOI: 10.26434/chemrxiv.13817498.v1
- 6.) E. Sidler, **J. Malinčík**, A. Prescimone, M. Mayor:  
Induced axial chirality by a tight belt: naphthalene chromophores fixed in a 2,5-substituted cofacial *para*-phenylene–ethynylene framework.  
*Journal of Materials Chemistry C* **2021**, *9*, 16199.
- 5.) H. Dekkiche, **J. Malinčík**, A. Prescimone, D. Häussinger, M. Mayor:  
An *Ortho*-Tetraphenylene-Based “Geländer” Architecture Consisting Exclusively of 52 sp<sup>2</sup>-Hybridized C Atoms.  
*Chemistry – A European Journal* **2021**, *27*, 13258.
- 4.) R. Mannancherry, T. Šolomek, D. Cavalli, **J. Malinčík**, D. Häussinger, A. Prescimone, M. Mayor:  
Sulfone “Geländer” Helices: Revealing Unexpected Parameters Controlling the Enantiomerization Process. *Journal of Organic Chemistry* **2021**, *86*, 5431.
- 3.) P. Zwick, K. J. Weiland, **J. Malinčík**, D. Stefani, D. Häussinger, H. S. J. van der Zant, D. Dulić, M. Mayor:  
Mechanical Fixation by Porphyrin Connection: Synthesis and Transport Studies of a Bicyclic Dimer.  
*Journal of Organic Chemistry* **2020**, *85*, 118.
- 2.) M. Guricová, J. Pinc, **J. Malinčík**, J. Rak, M. Kuchař, V. Bartůněk:  
Rare earth nanofluorides: synthesis using ionic liquids.  
*Reviews in Inorganic Chemistry* **2019**, *39*, 77.
- 1.) K. Dobrovolný, P. Ulbrich, M. Švecová, S. Rimpelová, **J. Malinčík**, M. Kohout, J. Svoboda, V. Bartůněk:  
Copper nanoparticles in glycerol-polyvinyl alcohol matrix: In situ preparation, stabilisation and antimicrobial activity.  
*Journal of Alloys and Compounds* **2017**, *697*, 147.

## References

---

- |   |   |
|---|---|
| 1. Prof. Marcel Mayor<br>University of Basel<br>+41 61 207 10 06<br><a href="mailto:marcel.mayor@unibas.ch">marcel.mayor@unibas.ch</a>  | 3. Assoc. Prof. Michal Kohout<br>University of Chemistry and Technology, Prague<br>+420 220 44 3688<br><a href="mailto:michal.kohout@vscht.cz">michal.kohout@vscht.cz</a> |
| 2. Assist. Prof. Tomáš Šolomek<br>University of Amsterdam<br>+41 31 684 42 31<br><a href="mailto:t.solomek@uva.nl">t.solomek@uva.nl</a> | 4. Assist. Prof. Michal Juríček<br>University of Zürich<br>+41 44 635 31 43<br><a href="mailto:michal.juricek@chem.uzh.ch">michal.juricek@chem.uzh.ch</a>                 |